NEW FLAVOURS
AND HADRON SPECTROSCOPY

XVIth Rencontre de Moriond - Second Session
Les Arcs - Savoie - France, March 21-27, 1981

NEW FLAVOURS AND HADRON SPECTROSCOPY

ISBN 2-86332-012-2

1981 Editions Frontières 7 avenue Kennedy
28100 DREUX - France

Proceeding of the

SIXTEENTH RENCONTRE DE MORIOND

Les Arcs - Savoie - France, March 15-27, 1981

VOL. II

NEW FLAVOURS AND HADRON SPECTROSCOPY

edited by

J. TRAN THANH VAN

The second session of the Sixteenth Rencontre de Moriond on
New Flavours and Hadron spectroscopy
was organized by

L. MONTANET
and J. TRAN THANH VAN

with the active collaboration of

R. BLANKENBECLER
A. CAPELLA
J. PEOPLES

Associate Editor: Mrs. O. LEBEY

FOREWORD

The XVIth Rencontre de Moriond was held at Les Arcs - Savoie (France) from March 15 to March 27.

The first such meeting was at Moriond in the French Alps in 1966. There, experimental as well as theoretical physicists, not only shared their scientific preoccupations but also the household chores. The participants at the first meeting were mainly French physicists interested in electromangetic interactions. In subsequent years, a session on high energy strong interactions was also added.

The main purpose of these meetings is to discuss recents developments in contemporary physics and also to promote effective collaboration between experimentalists and theorists in the field of elementary particle physics. By bringing together a relatively small number of participants, the meeting helps to develop better human relations as well as a more thorough and detailed discussion of the contributions.

This concern for research and experimentation of new channels of communication and dialogue which from the start animated the Moriond Meetings, inspired us, starting eleven years ago, to organize a simultaneous meeting of biologists on Cellular Differentiation and to create this year the Moriond Astrophysics meeting. Common meetings between biologists, astrophysicists and high energy physicists are organized to study the implications of the advances in one field into the others. We hope that these conferences and lively discussions may give birth in the future to new analytical methods or new mathematical languages.

The first session of the XVIth Rencontre de Moriond (March 15 - March 21, 1981) was devoted to the electroweak interactions and unified theories. One day common session with astrophysicists on Cosmology and Particles was organized.

The second session (March 15 - March 21, 1981) was devoted to the study of low Q phenomena. Particular emphasis was put on the spectroscopy of heavy quark systems, non perturbative QCD and

lattice gauge theories.

I thank M. DAVIER, F. HAYOT and R. TURLAY for the first session. R. BLANKENBECLER, A. CAPELLA, L. MONTANTET and J. PEOPLES for the second session and the conferences secretaries, J. BORATAV, L. BRONDERS, O. LEBEY, B. LELOUP, N. MATHIEU and L. NORRY who have devoted much of their time and energy to the success of this Rencontre.

I am also grateful to Mr VITRE the Hotel Director, Mr TOURAILLE and Ms FERRANDON, who contributed through their hospitality and cooperation to the well-being of the participants enabling them to work in a relaxed atmosphere.

J. TRAN THANH VAN.

CONTENTS

GLUE IN THE LATTICE

V. Alessandrini
Laboratoire de Physique Théorique et Hautes Energies
Université de Paris-Sud, 91 405 Orsay

ABSTRACT

A simple qualitative discussion is given of the lattice approach to the confinement problem in QCD.

We have witnessed in the last few years the process of Quantum Chromodynamics (QCD) reaching maturity as a fundamental theory of the strong interactions. For high Q^2 processes asymptotic freedom allows in principle a direct confrontation of the theory with experiments,since perturbative techniques are applicable to such processes[1]. On the other side, QCD-motivated models (like quark models, bags, ...) are rather successful in describing the gross features of low Q^2 hadron physics. It is therefore extremely important to confirm that the theoretical prejudices about confinement which provide the main ingredients of QCD-motivated models are indeed correct, namely, that long-wavelength phenomena taking place in QCD behave in the way we expect.

What we exepct is, of course, the coexistence of asymptotic freedom and confinement, namely, the fact that the very same physical system that reveals itself as made of weakly interacting quarks and gluons at short distances will be such that in fact only color singlet states occur as energy eigenstates. The lattice approach to QCD has provided in the last few years an impressive amount of evidence that this is indeed the case, and the purpose of this talk is to give a simple introduction to these developments, in order to help non-experts to better appreciate what has been accomplished.

There are two outstanding long-wavelength phenomena of non perturbative nature in QCD :

a) Gluon and heavy quark confinement, when light quarks are ignored.

b) Spontaneous breaking of chiral invariance, when light quarks are taken into account.

In the absence of light quarks, or even in the absence of quarks at all (in a pure Yang-Mills theory) there is a confinement problem because massless gluons, being color octets, should not occur as energy eigenstates in a confining phase. The correct energy eigenstates should rather be massive color singlets made out of coherent states of gluons. They are referred to as glueballs.

We know that in scale invariant quantum field theories (as pure Yang-Mills theories) the dilatation symmetry is always broken by quantum fluctuations, and that consequently the true independent parameter of the theory is not the dimensionless coupling constant but some rather some characteristic mass scale. In a confining phase such a free parameter can be taken to be, for example, the mass of the lowest-lying glueball. We then expect to find in QCD, in a quarkless world, color singlets having a typical mass or, what is the same, a typical size. We don't know yet what the ground state of pure Yang-Mills theory in a confining

phase is, but we can clearly think of a glueball at rest as some disturbance of the chromoelectric vacuum fields extending over a region of the order of the size of a hadron.

The confinement of heavy quarks, introduced as external sources, is a closely related problem. Heavy quark confinement is believed to be a consequence of gluon confinement, or confinement of the chromoelectric flux (see fig. 1). The chromoelectric field created by the external sources will not spread over all space but will rather stay confined in a tube (string) joining the external sources[2]. The energy stored in such a field configuration will obviously be proportional to the distance R between the q and the $\bar{q}$, so a linearly rising $q\bar{q}$ potential is obtained. We notice the appearance in this mechanism of a fundamental unit of length L measuring the width of the string or, what is the same, the confinement distance of the chromoelectric fields. Such a unit of length will obviously be related to the size of a glueball.

Finally, when light dynamical quarks are included in the theory a new non perturbative phenomenon must happen : the fermionic content of the ground state must be such that $\bar{\psi}\psi$ develops a non-vanishing vacuum expectation value even in the absence of a quark mass term. Chiral invariance will then be spontaneously broken and the pion will emerge as the corresponding Goldstone boson. There have been recently interesting developments concerning the possible relationship between the spontaneous breaking of chiral symmetry and the confining properties of the underlying gauge theory[3].

1. YANG-MILLS THEORIES ON A LATTICE

Lattice gauge theories have been invented by Wilson and Polyakov[4], as a clever way of performing a gauge invariant regularization of gauge theories. Instead of starting from the continuum theory and introducing an ultraviolet cutoff Λ, (which in general breaks gauge invariance) one starts from a coarse grained structure (for example, a hypercubical lattice) in space-time and then one defines a quantum field theory having a local (gauge) symmetry. The advantage of this procedure is that degrees of freedom are discrete, that the lattice spacing a acts as an ultraviolet cutoff, and that gauge invariant is preserved at all stages of the calculations. Lattice gauge theories are therefore cutoff field theories where there is a fundamental length, the lattice spacing a. There will be of course a dimensionless coupling constant g in the Lagrangian, which plays the role of the bare coupling constant of the quantum field theory.

Since the motivation for studying gauge theories on the lattice is not to do coarse-grained physics butto understand the properties of the continuum theory, one must make sure that all relevant phenomena occur at wavelengths L much bigger than the lattice spacing a. The bigger the scale (in units of a) in which these phenomena take place, the less they will be distorted by the presence of the lattice. Forcing the typical scales L to diverge for a given lattice spacing a is clearly equivalent to forcing $a \to 0$ for a given scale L. This is the way in which the continuum theory will eventually be reached.

Before entering into the details of QCD in a lattice, let us briefly discuss the physics that emerges. Once QCD has been formulated on a lattice, it turns out that the physics of the theory can be extracted in a very simple way in the strong coupling regime, namely, for very large values of the bare coupling g. Gluon confinement shows up as a kinematical consequence of the compacteness of the gauge group. The spectrum of the theory consists of massive glueballs, and if heavy quarks are introduced, there is confinement by a linear potential. Glueballs are of a size of the order of the lattice spacing a, and the strong coupling theory is therefore heavily cutoff dependent. The confinement problem reduces to proving that glueballs stay glueballs when they are forced - in a way to be discussed later on - to become much bigger than the lattice spacing a, and that in this case ordinary QCD with its asymptotic freedom properties is recovered.

Lattice gauge theories can be formulated in two equivalent ways. In the Lagrangian formulation[4], a lattice is introduced in euclidean space-time, and path integral quantization methods are then employed. This is the method used by many people, and in particular those involved in lattice Monte Carlo calculations[5]. Since this subject will be covered by other speakers, I have decided to concentrate on the Hamiltonian formulation first introduced by Kogut and Susskind[6]. In this case time is left continuous and a lattice is introduced only in space. This formulation can of course be obtained as the time-continuous limit of the previous one, when the lattice spacing in the time direction a_t goes to zero.

Rather than going through an extensive derivation of the QCD Hamiltonian on a lattice, I will simply motivate the result by briefly reviewing the basic physics contained in the Hamiltonian formulation of continuum QCD[7]. Let us for the moment ignore the presence of quarks and work in the $A_o^{\alpha} = 0$ gauge. In this case the QCD Hamiltonian is[7] :

$$H = \frac{1}{2} \int d\vec{x} \{ \vec{E}^{\alpha} \cdot \vec{E}^{\alpha} + \vec{B}^{\alpha} \cdot \vec{B}^{\alpha} \} \qquad (1)$$

where $\alpha = 1, \ldots, 8$ is a color index. The canonical variables are the space components of the vector potential, $A_i^{\alpha}(\bar{x})$, which play the role of generalized coordinates, and the chromoelectric fields $E_i^{\alpha}(\bar{x},t)$ which are the corresponding conjugate momenta. The chromoelectric energy density is therefore a "kinetic energy", and the chromomagnetic energy density a "potential energy" since the chromomagnetic fields B_i^{α} are defined in terms of the coordinates A_i^{α} by :

$$B_i^{\alpha} = \frac{\partial A_k^{\alpha}}{\partial x_j} - \frac{\partial A_j^{\alpha}}{x_j} + g f^{\alpha\beta\gamma} A_j^{\beta} A_k^{\gamma} \qquad (2)$$

where (i,j,k) is a cyclic permutation of (1,2,3) and $f^{\alpha\beta\gamma}$ are the structure constants of the gauge group. Now the basic physics of the Hamiltonian (1) that has to be underlined is the local invariance of the potential energy $\bar{B}^{\alpha}\bar{B}^{\alpha}$ with respect to time independent Gauge transformations. This symmetry of the potential energy implies the existence of constants of the motion in very much the same way as the rotational invariance of the potential energy in particle mechanisms implies the conservation of angular momentum. The constants of the motion are nothing butthe non-abelian version of Gauss Law

$$D_i E_i^{\alpha} = \frac{\partial Ei^{\alpha}}{\partial x_i} + g f^{\alpha\beta\gamma} A_i^{\beta} E_i^{\gamma} (\bar{x},t) = \text{indep. of time} \qquad (3)$$

which expresses the local conservation of electric flux. The Gauss operator $D_i E_i^{\alpha}$ is taken to be zero in the gauge invariant sector, namely, in the absence of external sources. Since the constants of motion are respected by quantum fluctuations, their presence effectively reduces the number of fluctuating degrees of freedom from three to two polarization degrees of freedom.

Let us now discuss how the same physics can be realized in a cubic lattice. Sites are labelled by a position vector $\vec{r}$,and links joining two neighbouring sites by $(r,\hat{n})$:the site from which they start and an oriented unit vector $\hat{n}$ indicating its direction in space (see fig. 2). Clearly, $(\vec{r},\hat{n}) \equiv (\bar{r}+\hat{n}a,-\hat{n})$. Vectors variables like the vector potential are most naturally defined on links : $A^{\alpha}(\bar{r},\hat{n}_x)$ implies that

$$A^{\alpha}(\bar{r}+\hat{n}a,-\hat{n}) = -A(\bar{r},\hat{n}) \qquad (4)$$

Rather than working with the vector potentials , it is much more convenient to take as fundamental dynamical variables SU(3) matrices defined on links,

denoted by $U(\vec{r},\hat{n})$ and related to the vector potentials by

$$U(\vec{r},\hat{n}) = e^{\frac{1}{2} ag\lambda_\alpha A^\alpha(\vec{r},\hat{n})} \tag{4}$$

In so doing the vector potentials become compact variables : they play the role of generalized Euler angles that parametrize the group element $U(\vec{r},\hat{n})$. In the case of SU(2), the resulting theory can then be thought as a quantum mechanical many-body system made out of a rigid rotator at each link (since the dynamical variables are SU(2) group element, half integer values of the spin of the rigid rotator are not rejected). From Eq. (4) one immediately obtains that

$$U(\vec{r} + a\hat{n}, -\hat{n}) = U^+(\vec{r},\hat{n}) \tag{5}$$

Let us now define what we mean by time-independent gauge transformations in our spacial lattice : they correspond to SU(3) matrices defined on sites :

$$V(\vec{r}) = e^{\frac{1}{2} \lambda_\alpha \omega^\alpha(\vec{r})} \tag{6}$$

the $\omega^\alpha(\vec{r})$ being the parameters of the SU(3) transformation that is performed at the site $\vec{r}$. Under the gauge transformation $V(\vec{r})$ the U matrices transform as follows :

$$U(\vec{r},\hat{n}) \rightarrow V(\vec{r})U(\vec{r},\hat{n})\ V^+(\vec{r}+\hat{n}a) \tag{7}$$

and the lattice Hamiltonian must be invariant under this local symmetry operation. Finally, we can introduce the operators $E^\alpha(\vec{r},\hat{n})$ which generate the gauge transformations in the link $(\vec{r},\hat{n})$ in the sense that their commutator with $U(\vec{r},\hat{n})$ reproduces the effect of an infinitesimal gauge transformation $V(\vec{r}) \simeq [1 + i\ \frac{\lambda\alpha}{2}\ \delta\omega^\alpha(\vec{r})]$ at the site $\vec{r}$:

$$[E^\alpha(\vec{r},\hat{n}),\ U(\vec{r}',\hat{n})] = \frac{\lambda\alpha}{2} U(\vec{r},\hat{n})\ \ \delta_{\vec{r}\vec{r}'}\delta_{\hat{n}\hat{n}'} \tag{8}$$

They obviously satisfy the commutation relations

$$[E^\alpha(\vec{r},\hat{n}),\ E^\beta(\vec{r}',\hat{n}')] = i\ f^{\alpha\beta\gamma}\ \ E^\gamma(\vec{r},\hat{n})\ \ \delta_{r\vec{r}}\ \ \delta_{\hat{n}\hat{n}'} \tag{9}$$

We are now prepared to write the QCD Hamiltonian on the lattice :

$$H = \frac{g^2}{2a} \sum_{\vec{r},\hat{n}} E^{\alpha}(\vec{r},\hat{n})\, E\,(\vec{r},\hat{n}) - \frac{1}{4ag^2} \sum_{pl} \{ \mathrm{Tr}\,[UUUU] + h.c \} \qquad (10)$$

where g is a dimensionless coupling constant. The first and second terms represent the chromoelectric and chromomagnetic energies, respectively. The notation for the magnetic energy is the following :Tr [UUUU] is a shorthand for the trace of the ordered product of U matrices along an elementary closed loop in the lattice, the boundary of a plaquette:

$$\mathrm{Tr}\,[U(\vec{r},\hat{n})\, U(\vec{r}+\hat{n},\hat{n}')U(\vec{r}+\hat{n}+\hat{n}',-\hat{n})U(\vec{r}+\hat{n}',-\hat{n}')] \qquad (11)$$

where $\hat{n}' \neq \hat{n}$. The sum extends over all plaquettes in the lattice. Under the gauge transformation (7), the expression (11) transforms as

$$\mathrm{Tr}\ [UUUU] \rightarrow \mathrm{Tr}\,[V(\vec{r})UUUU\ V^{+}(\vec{r})] \equiv \mathrm{Tr}\,[UUUU] \qquad (12)$$

The potential energy is therefore invariant under the local symmetry operation (7). The associated constants of the motion are clearly the generators of such a symmetry transformation, namely

$$\sum_{\hat{n} = \pm\hat{n}_x,\ \pm\hat{n}_y,\ \pm\hat{n}_z} E^{\alpha}(\vec{r}_0,\hat{n}) \qquad (13)$$

which is the lattice version of the Gauss operator. The generators $E^{\alpha}(\vec{r},\hat{n})$ are then identified with the electric flux operator. In the gauge invariant sector (absence of external sources) the Gauss operator is zero at every site $\vec{r}$. The ultimate justification of the Hamiltonian (10) is that it reproduces on the lattice the physics of the continuum QCD Hamiltonian. Moreover, if one naively takes the limit $a \rightarrow 0$ and expands Eq.(4) in powers of (ag) the continuum QCD Hamiltonian is reproduced. Indeed, the powers of the coupling constant in Eq. (10) have been tailored for this to happen.

Let us go back to SU(2) and its interpretation in terms of rigid rotators sitting on links. In this case the electric flux operators $E^{\alpha}(\vec{r},\hat{n})$ (α = 1,2,3)

are the three components of the angular momentum operator $\vec{J}$ of the rigid rotator sitting at $(\vec{r},\hat{n})$. The electric energy is additive, and each rotator contributes $(g^2/2a)\ \vec{J}^2$. The magnetic energy couples the neighbouring degrees of freedom. Gauss law imposes severe correlations on the wave functions of the system : the angular momenta of all rotators sitting on links attached to the same site must be coupled to zero, and this is true at all sites.

It is instructive to discuss how ordinary quantum electrodynamics looks on a lattice. In this case the basic degree of freedom is just a phase :

$$U(\vec{r},\hat{n}) = e^{i\phi(\vec{r},\hat{n})} \quad ; \quad \phi(\vec{r},\hat{n}) = agA(\vec{r},\hat{n}) \tag{14}$$

so we have to deal with a quantum mechanical many body system made out of axial rotators at each link. The electric flux operator $E(\vec{r},\hat{n})$ plays the role of the third component of angular momentum, L_z. In the expression of the magnetic energy there is of course no trace to take. The lattice QED Hamiltonian is

$$H = \frac{g^2}{2a} \sum_{\text{links}} E^2(\vec{r},\hat{n}) - \sum_{\text{pl}} \frac{1}{g^2 a} \cos(\Sigma\phi) \tag{15}$$

where

$$\begin{aligned} \Sigma\phi &= \phi(\vec{r},\hat{n}) + \phi(\vec{r}+\hat{n},\hat{n}') + \phi(r+\hat{n}+\hat{n}',-\hat{n}) + \phi(\vec{r}+\hat{n}',-\hat{n}') \\ &= g\, a^2\, B(\text{plaquette}) \end{aligned} \tag{16}$$

is g times the magnetic flux across the plaquette under consideration Gauss law reduces to the conservation of electric flux at each site.

2. THE STRONG COUPLING SPECTRUM

The quantum mechanical many-body system described by the Hamitonians (10) (for QCD) and (15) (for QED) on a lattice, can be easily handled in the strong-coupling $g \to \infty$ limit. In this case the magnetic energy is a small perturbation and standard Raleigh-Schrödinger perturbation theory can be applied, by taking as the unperturbed Hamiltonian H_0 the electric energy of the system. Since H_0 is additive, its eigenvalues and eigenfunctions are easily found. In order to simplify the presentation I shall concentrate on QED. It will be clear to the reader that the physics of strong-coupling QCD is essentially the same.

In order to find the strong-coupling spectrum we have to diagonalize the

electric flux operator $E(\vec{r},\hat{n})$ on each link. Since the basic dynamical variable is the angle $\phi(\vec{r},\hat{n})$, $E(\vec{r},\hat{n})$ behaves like the third component of angular momentum and has discrete eigenvalues 0, ±1, ..., ±n, ... Therefore, the compacteness of the gauge group leads to quantization of electric flux. The strong-coupling ground state $|\psi_0>$, namely, the lowest eigenstate of the electric Hamiltonian H_0, satisfies

$$E(r,n)|\ \Psi_0> = 0 \qquad \text{for all } (\vec{r},\hat{n}) \tag{17}$$

This ground state is very different from the usual perturbative vacuum found in weak-coupling perturbation theory. In this case the QED Hamiltonian is diagonalized by collective excitations corresponding to free photons, and the electric and the electric and magnetic energies play an equivalent role. Both electric and magnetic fields fluctuate by equal amounts. In the strong coupling vacuum (17) there are no electric fluctuations, since the electric flux has been exactly diagonalized. Such a state has perfect electric order, and consequently complete magnetic disorder.

Excited states, satisfying the constraints unposed by Gauss law, are closed loops of quantized electric flux. The first excited state is a unit of electric flux circulating around a plaquette (see fig. 3). This state is highly degenerate because such an elementary electric flux loop can be placed everywhere in the lattice. It has an energy (or mass)

$$M = \frac{g^2}{2a}\ 4.\ 1 \tag{18}$$

where $(\frac{g^2}{2a})$ is the basic energy unit, 4 is the number of links and 1 is the eigenvalue of E^2. The spectrum is made out of massive neutral objects, which we shall call abelian glueballs. Notice that the existence of a finite mass is directly related to the quantization of electric flux.

Higher excited states can be easily imagined : they correspond to a unit of electric flux encircling more than one plaquette, or two units of electric flux around a plaquette, and so on. We therefore find in the strong coupling limit that the theory confines in a very natural way, due to the compactness of the gauge group and the consequent quantization of electric flux. Electric flux is confined because its costs energy to spread it on the lattice.

The confinement of heavy quarks, considered as external sources, can be easily understood in terms of the confinement of electric flux. If external charges (quantized in the same units as the electric flux) are introduced at

a distance R in the lattice, the lowest energy eigenstate of H_o compatible with Gauss law is a state where an electric string is formed on the lattice along the shortest path joining the two opposite charges. The energy stored in such a field configuration is proportional to R, so we have confinement by a linear potential. The tension T of the string, which is defined as the energy per unit length, is given for lattice QED by

$$T = \frac{g^2}{2a^2} \tag{19}$$

as $g \to \infty$.

The above picture applies in the $g^2 \to \infty$ limit. At large but finite g^2, straightforward application of Raleigh-Schrödinger perturbation theory allows one to compute the eigenvalues and eigenstates of the full Hamiltonian H[7]. The magnetic perturbation Tr [UUUU] adds - or substracts - one unit of closed electric flux along the boundary of the plaquette on which it acts. Therefore, to order g^{-2} the eigenstates of H_o begin to mix. The vacuum state becomes at large but finite g^2 a dilute soup of glue, since to order g^{-2} its wave function develops components on states where there is one elementary Wilson loop somewhere in the lattice, to order g^{-4} it develops components on states when there are two elementary Wilson loops or one elementary Wilson loop with two units of electric flux, and so on and so forth. The first excited state - the glueball - which was at $g = \infty$ the state shown in fig. (3), namely, an elementary Wilson loop, develops at finite g components on states where there are two or more Wilson loops, as well as components on states where the original electric flux spreads over two or more lattice spacings. Once vacuum fluctuations are subtracted out, the glueball wave function can be regarded as a state of the form

$$|\text{glueball}) = \sum_n C_n \, g^{-2n} \, \psi_n^{(0)} \tag{20}$$

where the $\psi_n^{(0)}$ are eigenstates of Ho containing a unit of electric flux spreading over (n+1) lattice spacings, as well as higher and higher units of electric flux - up to n units - spreading over shorter and shorter distances. To the extent that strong-coupling perturbation theory is convergent - which seems to be the case - [7] one can safely conclude that at large values of g the glueball wave function will have prominent components on states where the electric flux spreads over a few lattice spacings. A typical glueball size L

will then be of the order of a few lattice spacings a.

As for as the string is concerned, its wave function will also acquire components on states where the electric flux spreads in the transverse direction over a distance of the same order of magnitude as the glueball size L, namely, a few lattice spacings. What is going on in strong coupling perturbation theory is that the electric field is no longer "frozen" : as soon as g is decreased from the limiting $g = \infty$ value, the magnetic term in the Hamiltonian switchs on electric fluctuations : the system exhibits a bit less of electric order (and of magnetic disorder). The glueball size - or the transverse dimension of the string - measure the strength of the electric fluctuations. However, to the extent that the mass gap M and the tension of the string are finite the qualitative physics is unchanged : electric order is still dominant and the theory confines.

I have discussed here the case of QED on a lattice, but the strong-coupling physics of lattice QCD is qualitatively the same. For example, strong coupling calculations of the tension of the string for lattice QCD - in the Hamiltonian formulation that we are discussing - have been performed by Kogut, Pearson and Shigemtsu[8]. They obtained

$$T = \frac{g^2}{2a^2} \cdot \frac{4}{3} \left[1 - 0{,}053921569\ x^2 - 0{,}0280\,3388\ x^3 - 0{,}00953362635\ x^4 - 0{,}00230039064\ x^5 - \ldots \right] \qquad (21)$$

where $x = 2/g^4$. Strong coupling series seem to have in general a finite radius of convergence.

3. THE CONTINUUM LIMIT.

We have seen that confinement is an almost trivial affair for lattice gauge theories based on a compact gauge group in the strong-coupling limit. Both QED and QCD confine in this case. However, at very large g the typical scales L - like the glueball sizes - are of the order of a few lattice spacings, so this is not yet long-wavelength physics. The strong coupling results are still cut-off dependent. The real difficult problem in proving confinement in the lattice appraoch lies in being able to control their stability when the continuum limit is taken. It is at this point that physical phenomena will occur that will distinguish QED from QCD.

How to take the continuum limit ? Let us consider any physical observable, like the mean square radius L of a glueball or its mass M. Since we have only one dimensionful parameter, namely, the lattice spacing, they can be expressed

as

$$L = a\, l(g) \tag{22}$$

$$M = \frac{1}{a}\, m(g) \tag{23}$$

where the functions $l(g)$ and $m(g)$ can eventually be computed in terms of strong-coupling series. Clearly, taking $a \to 0$ at fixed g is not what we want to do : if a glueball spreads over three lattice spacings at a given value of g, and a is scaled its size L is also scaled in such a way that in the new lattice the glueball still spreads over three lattice spacings. Physics is unchanged, since all we have done is to change the unit of length.

The only way to reach long-wavelength physics is to allow dimensionless ratios to change, which forces us to vary the bare coupling constant. Therefore the continuum limit is taken by fixing some renormalized physical observable, like L, M or T. This defines a "running" bare coupling constant $g(a)$ which varies with the cutoff a so as to keep fixed the physical observable that has been chosen to renormalize the theory. This procedure is sketched in fig. (4).

One can easily understand some qualitative features of the function $g(a)$. Taking $a \to 0$ at fixed L (or at fixed M) means that $L \to \infty$ (or $M \to 0$) in lattice units a (or $1/a$). Therefore, in going to the continuum limit electric fluctuation must be enhanced in the lattice scale, which means that the bare coupling $g(a)$ will be driven away from the strong coupling regime. Let us imagine that we take the continuum limit by fixing the glueball mass M to a given value. Then, the coupling $g(a)$ will start decreasing from $g = \infty$ and, as $a \to 0$, it will tend to a limiting value g_c such that

$$m(g_c) = 0 \tag{24}$$

The critical value g_c corresponds to a second order phase transition point, characterized by the fact that the mass gap vanishes, or that the correlation length L is infinite. It is for values of g in the immediate neighborhood of this second-order phase transition point g_c, when length scales are much bigger then a, and mass scales much smaller than $\frac{1}{a}$, that the theory becomes cutoff independent and the continuum limit is reached. We have shown in fig. (5) a typical behavior of the mass gap $m(g) = aM$. For values of $g < g_c$ the physics is entirely different : a new ground state has replaced the confining vacuum and the system is in a non-confining phase.

It is rather well established that lattice QED undergoes a diconfining phase transition at a finite value of g_c of the order of unity[9]. In other words, lattice QED in the weak coupling region $g < g_c$ is a non-confining Coulomb phase, the one realized in nature.

The case of QCD is entirely different. Our theoretical prejudices lead us to expect that the continuum theory obtained from the lattice in the strong-coupling confining phase matches continuum QCD as we know it, with its asymptotic properties. A necessary condition for this to happen is that $g_c = 0$. Indeed, asymptotic freedom implies that :

$$g(a) \to 0$$
$$a \to 0$$

If asymptotic freedom is to arise in the confining phase of lattice QCD nothing must prevent the running bare coupling g(a) from reaching $g = 0$ when it is driven from the strong coupling region to the strong-coupling region as the lattice spacing goes to zero. This means that no deconfining phase transition must occur in lattice QCD at any $g \neq 0$. Neither the glueball mass M nor the tension of the string T must vanish in lattice QCD at any finite value of the bare coupling g. They should only vanish as $g \to 0$, and in a way compatible with the predictions of asymptotic freedom. If this is the case, heavy quark and gluon confinement in continuum QCD would be proven.

There is growing empirical evidence, coming from Monte Carlo analysis, that this is indeed the case for lattice QCD[5]. This subject is beyond the scope of this talk. In order to give the reader a feeling of the beautiful results arising from the lattice approach to QCD, I shall discuss the work of Kogut, Pearson, and Shigemitsu [8] based on the strong coupling series for T given by Eq. (21). Let us imagine that the theory is renormalized by fixing T.

$$T = \frac{1}{a^2} F(g) = \text{constant} \tag{25}$$

which defines $g(a^2T)$. Once a renormalization condition like (25) is given, one can define the Gell-Mann-Low β function

$$\beta(g) = -a \frac{dg}{da} \tag{26}$$

which is obtained from

$$\frac{dT}{da} = 0 = -\frac{2}{a^3} F(g) + \frac{1}{a^2} F'(g) \frac{dg}{da} \tag{27}$$

namely

$$\beta(g) = -\frac{2F(g)}{F'(g)} \tag{28}$$

Notice that $\beta(g)$ inherits the zeros of $F(g)$, that is to say, of T. So if no phase transition occurs in going from the strong coupling regime to the weak coupling limit where one recovers the continuum theory, $\beta(g)$ should have no zeros at finite g. From the known coupling expansion for $F(g)$ it follows that $\beta(g)$ behaves as $(-g)$ for large g. Therefore $(-\beta(g)/g)$ is positive at large g and tends to 1 as $g \to \infty$. This behavior is sketched in fig. (6). On the other hand, asymptotic freedom predict that $(-\beta(g)/g$ is also positive near $g \simeq 0$. Indeed, in the weak coupling limit one obtains :

$$-\beta(g) = b_0 g^3 + b_1 g^5 + O(g^7) \tag{29}$$

where
$$b_0 = \frac{11}{16\pi^2} \quad , \quad b_1 = \frac{34}{3}\left(\frac{3}{16\pi^2}\right) \tag{30}$$

Equation (29) follows from the well-known fact that the first two coefficients in the weak coupling expansion of the β function are universal in the sense that they are independent of the renormalization scheme. Therefore they also apply to the renormalization scheme defined by Eq. (25). One then obtains

$$-\frac{\beta(g)}{g} \simeq \frac{11}{16\pi^2} g^2 + \ldots \tag{31}$$

This behavior is also sketched in fig. (6). We therefore know the limiting behavior of $(-\beta(g)/g)$ at weak and strong coupling in the spatial lattice regularisation of QCD. It is rewarding to discover that both limiting values have the same sign, so they are compatible with the absence of zeros of $\beta(g)$. In fact, if there is no deconfining phase transition in going from strong to weak cou-

pling, the intermediate coupling β function should smoothly interpolate between both limiting behaviors without changing its sign. From Eqs. (28) and the known strong coupling expansion for F(g)(see Eq. (21)), a strong coupling series for β(g) can be obtained[8]. This series can then be extrapolated to the weak coupling regime by using Padé approximants[8]. The result is shown in fig. (7) : different Padé extrapolations of the strong-coupling β function are seen to match the weak coupling result in a way consistent with the absence of a deconfining phase transition.

There is a subtlety involved in the previous analysis : the tension of the string T is a physical observable which undergoes a phase transition of its own at a finite value of g - called roughening transition - This roughening transitions is not a bulk property of the system but rather a peculiar phenomenon arising by the presence of a one-dimensional string of electric flux in a three-dimensional medium. It is not a deconfining phase transition because T stays finite, but it is clear that the strong-coupling series for T cannot be extrapolated beyond the roughening transition point g_R. It has been pointed out by the authors of Ref.(8) that in the spatial lattice regularisation the roughening transition point g_R is well inside the weak-coupling region, so that its presence should not affect too much the analysis of the matching of the strong-coupling results with the weak-coupling limit. In any case, this is a problem only for strong-coupling analysis based on T. The same analysis could be carried out by computing the strong-coupling β function from the strong-coupling expansion for the glueball mass M, which is unfortunately harder to compute. There is nevertheless some evidence, obtained from simpler lattice gauge theories, of the fact that strong-coupling expansions for glueball masses are free of the pathologies associated to the roughening transition[11].

To sum up, we may say that there is convincing evidence that lattice QCD has only one (confining) phase. The important problem ahead is the understanding of the role played by light fermions.

Fig. 1. The confinement mechanism for heavy quarks

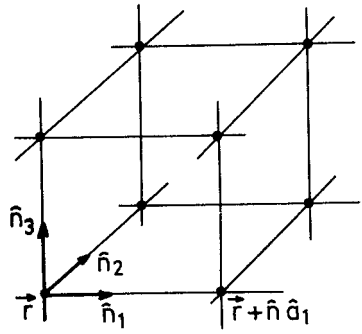

Fig. 2. The spacial lattice

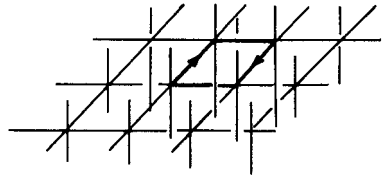

Fig. 3. The lowest-lying glueball in the strong coupling limit. The heavy lines indicate a unit of quantized electric flux on the corresponding links.

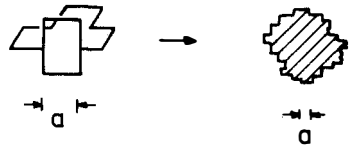

Fig. 4. A schematic view of the continuum limit. When the lattice spacing is scaled to 1/2 of its original value, the electric flux spreads in the average twice as far in the new lattice units.

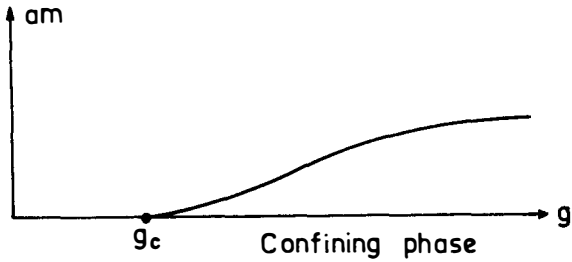

Fig. 5. Qualitative behavior of the mass gap.

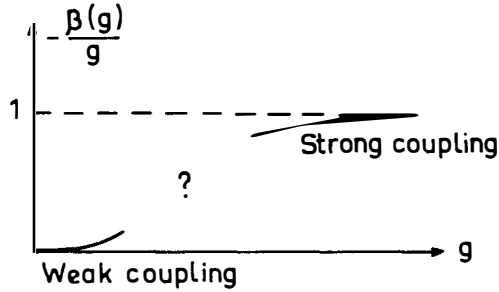

Fig. 6. The weak and strong-coupling behavior of the β-function of QCD, in the spacial lattice regularisation

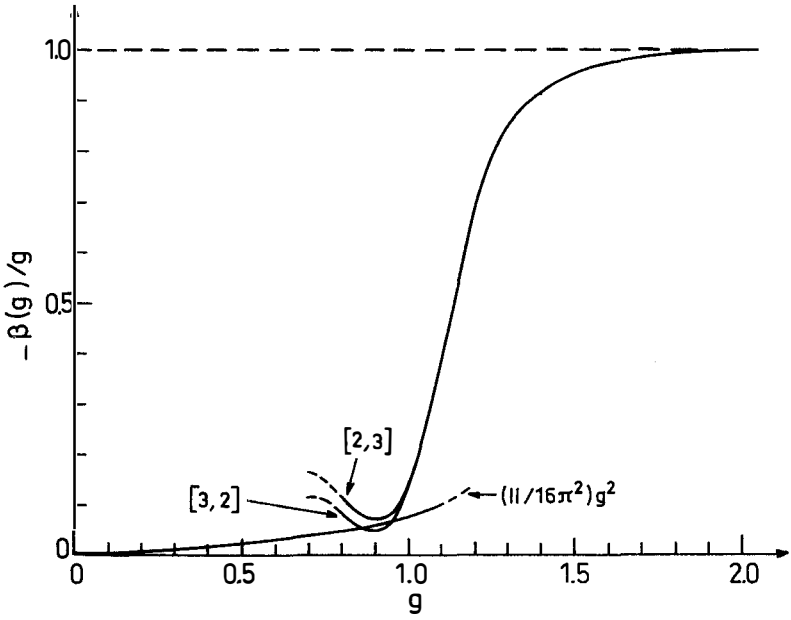

Fig. 7. [2,3] and [3,2] Padé approximants of the SU(3) β function strong coupling series [taken from ref. (8)] .

REFERENCES

1. H. D. Politzer, Phys. Rev. Lett. 30, 1346, (1973)
   D.J. Gross and F. Wilczek, Phys. Rev. Lett. 30, 1343 (1973) ;
   Phys. Rev.
   G't Hooft, unpublished
2. This picture has been emphasized by L. Susskind et al. See, for example, A. Casher and L. Susskind, Phys. Rev. D9, 436 (1974)
3. G't Hooft, in "Recent Developments in Gauge Theories" Cargèse Summer Institute 1979, Plenum Press, New York (1980), pag. 135.
4. K. Wilson, Phys. Rev. D10, 2445 (1974)
   A.M. Polyakov, Phys. Lett. 59B, 82 (1975)
   For a general introduction to lattice gauge theories, see J. Kogut, Rev. Mod. Phys. 51, (1979), 659
5. For a discussion of Monte Carlo methods in the Lagrangian formulation, see the talk of R. Sugar at this Meeting.
6. J. Kogut and L. Susskind, Phys. Rev. D11, 395 (1975)
7. See, for example, J.D. Bjorken "Elements of Quantum Chromodynamics, SLAC PUB 2372 (1979)
8. J.B. Kogut, R.B. Pearson and J. Shigemitsu, Phys. Rev. Lett. 43, 484 (1979) ; J.B. Kogut, "Progress in Lattice Gauge Theory" Santa Barbara preprint NSF-ITP-80-16 (Les HMuches lectures, 1980)
9. K. Osterwalden and E. Seiler, Ann. Phys. (NY) 110, 440 (1978) ; A. Guth, Phys. Rev. D21, 2291 (1980)
10. C. Itzykson, M. Peskin, and J.B. Zuber, Phys. Lett. 95B (1980) 259
    A.E. and P. Hansenfratz, CERN-TH-2890 (1980)
    M. Lüscher, G. Münster and P. Weisz, DESY 80/63
11. V. Alessandrini, V. Hakim, A. Krzywicki, preprint LPTHE 81/6, to be published.

MONTE CARLO CALCULATIONS OF LATTICE FIELD THEORIES

Robert L. Sugar
Department of Physics
University of California
Santa Barbara, California 93106

ABSTRACT

Monte Carlo calculations of lattice field theories are described. Recent work on lattice gauge theories is summarized, and preliminary results of calculations for coupled boson-fermion systems are presented.

I have been asked to summarize recent work on the use of Monte Carlo calculations to study lattice gauge theories. I would also like to briefly describe some ideas for future work in this field.

If our present ideas about the strong interactions are correct and they are indeed described by a non-Abelian gauge theory of quarks and gluons, then it will be necessary to develop reliable non-perturbative techniques for studying them. The problems of quark confinement and of calculating the properties of physical hadrons are inherently non-perturbative in gauge theories. Monte Carlo calculations are a very promising means of studying such theories.

The starting point of the Monte Carlo calculations is the path integral formulation of field theory. The expectation value of an operator, O, can be written in the form

$$\langle O \rangle = \int e^{iS} O / \int e^{iS} \tag{1}$$

where the action S, is related to the Lagrangian density $\mathcal{L}$ by

$$S = \int dt d^3x \, \mathcal{L} \tag{2}$$

The integral in Eq. (1) is over all possible configurations of the fields on which S depends.

Eq. (1) is not convenient for numerical calculations for a number of reasons. One is that the integrand is complex and can oscillate rapidly. It is therefore customary to work with Euclidean field theory in which the time variable, t, is taken to be pure imaginary. Eq. (1) then becomes

$$\langle O \rangle = \int e^{-S_E} O / \int e^{-S_E} \tag{3}$$

where the Euclidean action S_E is obtained from S by the substitution $t \rightarrow -i\tau$.

Eq. (3) is still not tractable because functional integrals are notoriously difficult, and because it contains all the usual infinities of quantum field theory. We meet these difficulties by placing the theory on a lattice in both space and imaginary time.

To this end we divide the space-imaginary time continuum into four-dimensional cubes of length Δ on a side. We assign a lattice point to the center of each cube. Each matter field is replaced by its average over the cube and associated with the corresponding

lattice point. Derivatives of matter fields become finite differences, and functional integrals become products of ordinary integrals, one integration for each lattice point.

This procedure must be modified slightly for gauge theories. Let us start by considering quantum electrodynamics. Under a gauge transformation the electromagnetic potential $A_\mu(x) \to A_\mu(x) - \partial_\mu \Lambda(x)$. A matter field $\psi(x) \to e^{ie\Lambda(x)}\psi(x)$. On the lattice this translates into $\psi_i \to e^{ie\Lambda i}\psi_i$. A quantity such as $\bar{\psi}\gamma_\mu \partial_\mu \psi(x)$ or its lattice equivalent $\bar{\psi}_i \gamma_\mu \psi_{i+\mu}$ is not gauge invariant. (ψ_i is the field at the lattice point i and $\psi_{i+\mu}$ at the point point one lattice spacing from i in the direction μ.) In the continuum theory we know we must replace ∂_μ by the covariant derivative $\partial_\mu - ieA_\mu$ to obtain a gauge invariant quantity. On the lattice, the appropriate gauge invariant quantity is

$$\bar{\psi}_i \gamma_\mu e^{i\int_{x_i}^{x_i+\Delta\mu} A_\nu dx_\nu} \psi_{i+\mu} \equiv \bar{\psi}_i \gamma_\mu U_\mu(i) \psi_{i+\mu} \tag{4}$$

since under a gauge transformation $U_\mu(i) \to e^{i\Lambda_i} U_\mu(i) e^{-i\Lambda_{i+\mu}}$. For a non-Abelian theory the generalization is

$$U_\mu(i) = e^{i\int_{x_i}^{x_i+\Delta\mu} \vec{\lambda}\cdot\vec{A}_\nu dx_\nu} \tag{5}$$

where $\vec{\lambda}$ are the generators of the gauge group in the representation of the matter field, ψ. The pure gauge action, which reduces to $-\frac{1}{4}\int d\tau d^3x\, F^2_{\mu\nu}$ in the limit of zero lattice spacing can be written in terms of products of U's around elementary squares or plaquettes on the lattice. Thus, the fundamental ingredients of a lattice gauge theory are the matter fields which are associated with the lattice points, and the unitary matrices $U_\mu(i)$ which link neighboring lattice points. On the lattice the functional integrals reduce to ordinary integrals over the matter fields and the gauge variables, $U_\mu(i)$. This procedure for constructing lattice gauge theories was set down by Wilson in 1974.[1]

The final step in making the functional integrals of Eq. (3) tractable is to limit the lattice to a finite extent in both space and imaginary time. In the space directions we impose periodic boundary conditions. By limiting the imaginary time variable to a finite range we are in effect study a finite temperature field

theory. The appropriate boundary conditions are that the boson fields be periodic in imaginary time and that the fermion fields be anti-periodic.

We are now left with a set of integrals of large, but finite dimension. We evaluate these integrals by Monte Carlo methods. The basic idea is to generate a sequence of field configurations, Σ_i, i=1,...N, such that the probability of a particular configuration occurring is given by

$$P(\Sigma_i) = e^{-S_E(\Sigma_i)} / \sum_{j=1}^{N} e^{-S(\Sigma_j)} \quad . \tag{6}$$

Then

$$\langle O \rangle = \lim_{N\to\infty} \sum_{i=1}^{N} O(\Sigma_i) \quad . \tag{7}$$

Of course in practice we cannot take N to infinity so the theorists who play this game are faced with the problems so familiar to all experimentalists of analyzing statistical and systematic errors. In fact this subject can be thought of as theoretical experimental physics or experimental theoretical physics. I am not sure which ordering is more appropriate.

In order to generate the different field configurations one repeatedly sweeps through the lattice making random changes in each matter field at one lattice point at a time and in each gauge field on one link at a time. One accepts or rejects a particular field change according to an algorithm, such as the Metropolis algorithm,[2] which insures that Eq. (6) is satisfied once the system reaches equilibrium. The important point about the Monte Carlo algorithms is that they require us to compute the change in the action corresponding to each field change. Because we are dealing with a local field theory this calculation only requires a knowledge of the fields in the immediate vicinity of the lattice point or link on which a field change is being made. This is why the calculations can be carried out with a reasonable amount of computer time.

The work of Creutz and his collaborators[3] has indicated that Monte Carlo calculations may be a very useful way of studying lattice gauge theories and it has inspired considerable work by many authors during the last two years. The main effort has gone into the study of pure gauge theories, that is theories without dynamical fermions. It is known from the strong coupling expansion

that these theories confine heavy quarks for large values of the lattice coupling constant.[1] From perturbation theory one knows that the non-Abelian lattice gauge theories are asymptotically free in the weak coupling domain. The first question is whether confinement and asymptotic freedom occur in the same phase or if there is a phase transition at some finite value of the lattice coupling constant. The Monte Carlo calculations for SU(2) and SU(3) lattice gauge theories give strong evidence that the only phase transition is at zero value of the lattice coupling constant. This result is important for understanding the continuum limit. This limit will exist if the lattice theory has a critical point for which all physical length scales become infinitely larger than the lattice spacing. Had such a critical point existed for a finite value of the lattice coupling constant, then it would have been possible to have one continuum theory with confinement and a separate one with asymptotic freedom.

The potential between the static quarks has been calculated and the string tension (the coefficient of r in the heavy quark potential) has been extracted.[3,4] The most ambitious calculation of which I am aware is by Bhanot and Rebbi who study SU(2) theory on a 16^4 lattice, that is on a four dimensional lattice with 16 lattice points in each direction. They obtain the above quantities as well as the glue ball mass in terms of the string tension.

Another interesting type of calculation is to study the theory at finite temperature. It is expected that when the temperature is increased from zero, there will eventually be a phase transition to a state in which the quarks and gluons are unbound. Strong evidence for such a phase transition has been found in SU(2) lattice gauge theories.[5]

Considerable work has also gone into the study of Abelian U(1) gauge theory,[3,6,7] which is the lattice analogue of quantum electrodynamics. This theory is of great interest in its own right, and it serves as a valuable check of our understanding of the non-Abelian theories. It also confines static fermions in the strong coupling limit, but there is a phase transition for finite lattice coupling constant. There appears to be a line of fixed points in the weak coupling phase. This merely means that for each value of the lattice coupling constant, there is a continuum theory with a different fine structure constant. The heavy fermion potential in the weak coupling phase is simply the lattice version of

the Coulomb potential.[7]

The Monte Carlo calculations have provided considerable insight into the structure of non-Abelian gauge theories; however, they cannot yet be used to make reliable calculations of the detailed properties of these theories. I would like to briefly describe two promising ideas for improving the Monte Carlo calculations.

It would clearly be very desirable to collect data for Monte Carlo experiments more rapidly. The greatest fraction of time spent in a Monte Carlo calculation is in updating the fields. Even after the system has reached equilibrium so that Eq. (6) is satisfied, it is necessary to sweep through the lattice a number of times updating the fields at each lattice point or on each link between taking data. This is essential in order that the field configurations at which one takes data be statistically independent. Pearson, Richardson and Toussaint have recently suggested[8] that this updating could be done much faster than on a standard computer if one built a micro-processor which was especially designed for the purpose. They are presently building a prototype which will Monte Carlo the three dimensional Ising model on a $(64)^3$ lattice. They estimate that their processor will update spins a factor of fifty times faster than an array processor and/or a fast computer. They also believe that their ideas can be extended to the study of lattice gauge theories and many other systems of physical interest. One of the chief advantages of building an inexpensive processor dedicated to performing a specific calculation is that it can be run indefinitely without having to worry about the costs of computer time.

The calculations I have described so far are for pure gauge theories with no dynamical fermions. However, it is clear that fermions must be included if we are to make realistic calculations of QCD. A parallel situation exists in condensed matter physics. Monte Carlo simulations have been useful in studying a variety of problems with boson degrees of freedom, but it would be very useful to be able to extend these calculations to the study of interacting boson-fermion systems. There has recently been considerable interest in this problem.[9]

The difficulty is easy to state. In the path integral formulation of field theory bosons are represented by c-number fields. However, fermions are represented by anti-commuting fields which are in fact operators. The path integrals are

therefore not directly susceptible to numerical calculations.

In most cases of interest the Euclidean action can be written in the form

$$S_E = S_B + \int_0^\beta d\tau \int d^D x \psi^+(\vec{x},\tau)\left[\frac{\partial}{\partial\tau} + H\right]\psi(\vec{x},\tau) \qquad (8)$$

where S_B is the pure boson action, $\psi(\vec{x},\tau)$ is the fermion field, H is a single particle operator which contains both the fermion kinetic energy and its coupling to the boson fields, and β is the inverse temperature. It was emphasized by Fucito et. al.[9] that in such cases the fermion degrees of freedom could be integrated out exactly leaving an effective boson action defined by

$$e^{-S_{eff}} = e^{-S_B} D \quad , \qquad (9)$$

where

$$D = \det\left[\frac{\partial}{\partial\tau} + H\right] \quad . \qquad (10)$$

The suggestion is that one can perform standard Monte Carlo calculations with this effective action. Recently Blankenbecler, Scalapino and I have shown[9] that D can be written as a determinant of an operator acting on space coordinates only,

$$D = \det\left[I + Te^{-\int_0^\beta d\tau H(\tau)}\right] \quad , \qquad (11)$$

where T is the time ordering operator. We believe that this form is useful for numerical studies.

At first glance it would appear that the effective action defined by Eqs. (9)-(11) will not be susceptible to Monte Carlo calculations because of the long time required to compute the determinant. However, only the change in the determinant arising from a local change in the boson fields is required, and this has proven to be a tractable problem. A number of groups have been studying simple models using these ideas.[9]

Scalapino and I have studied two simple models. One is the quantum mechanics model of a fermion interacting with a harmonic oscillator. The Euclidean action is given by

$$S_E = \int_0^\beta d\tau \left[\left(\frac{\partial\varphi}{\partial\tau}\right)^2 + \Omega^2\varphi^2 + \psi^+\left(\frac{\partial}{\partial\tau} + \omega + \lambda\varphi\right)\psi\right] \quad . \qquad (12)$$

Monte Carlo results for the fermion Green's function are given in Table I along with the exact results for the lattice and continuum

theories.

A more interesting model is the one space one time field there given by the action

$$S_E = \int_0^\beta d\tau \int dx \left[\left(\frac{\partial\varphi}{\partial\tau}\right)^2 + \left(\frac{\partial\varphi}{\partial x}\right)^2 + \Omega^2\varphi^2 + \psi^+\left(\frac{\partial}{\partial\tau} - \frac{\partial^2}{\partial x^2} + \omega + \lambda\varphi\right)\psi \right] . \qquad (13)$$

This model is relevant to the study of problems in polymer physics as well as to the polaron problem. If one drops the $\left(\frac{\partial\varphi}{\partial x}\right)^2$ and $\left(\frac{\partial\varphi}{\partial\tau}\right)^2$ terms in S_E, the model can be solved exactly. Results of the Monte Carlo calculation for this case are compared with the exact answers in Tables II and III. There is no added difficulty in including the $\left(\frac{\partial\varphi}{\partial x}\right)^2$ and $\left(\frac{\partial\varphi}{\partial\tau}\right)^2$ terms in the Monte Carlo calculations and we are in the process of analyzing the data for these cases.

Of course this two dimensional model even though it is of interest in its own right is a long way from a four dimensional lattice gauge theory. Extending these ideas to gauge theories is a challenging problem for the future.

References

1. K.G. Wilson, Phys. Rev. D10, 2445 (1974).
2. N. Metropoulis, A. Rosenbluth, M. Rosenbluth, A.H. Teller and E. Teller, J. Chem Phys. 21, 1087 (1953).
3. M. Creutz, L. Jacobs and C. Rebbi, Phys. Rev. Lett. 42, 1390 (1979); Phys. Rev. D20, 1915 (1979); M. Creutz, Phys. Rev. Lett. 42, 533 (1979); Phys. Rev. D21, 2308 (1980); C. Rebbi, Phys. Rev. D21, 3350 (1980).
4. G. Bhanot and C. Rebbi, CERN preprint TH. 2979.
5. J. Kuti, J. Polonyi and K. Szlachanyi, Central Research Institute for Physics, Budapest, preprint; L.D. McLerran and B. Svetitsky, SLAC preprint.
6. B. Lautrop and M. Nauenberg, Phys. Lett. 95B, 63 (1980); T. DeGrand and D. Toussaint, Phys. Rev. D22, 2478 (1980).
7. T. DeGrand and D. Toussaint, Phys. Rev. D, to be published.
8. R. Pearson, J. Richardson, and D. Toussaint. To be published.
9. F. Fucito, E. Marinari, G. Parisi and C. Rebbi, CERN preprint TH-2960; D.J. Scalapino and R.L. Sugar, Phys. Rev. Lett. 46, 519 (1981); R. Blankenbecler, D.J. Scalapino and R.L. Sugar, to be published; D. Weingarten and D. Petcher, Phys. Lett. 99B, 333 (1981); A. Duncan and M. Furman, Columbia preprint CU-TP-194; H. Hamber, Phys. Rev., to be published.

Table I

τ	$G_M(\tau)$	$G_{LAT}(\tau)$	$G_{CONT}(\tau)$
0	$.999969 \pm .15\times10^{-4}$	.999957	.999955
1	.412 ± .001	.4107	.4092
2	.197 ± .002	.1964	.1955
3	.104 ± .002	.1030	.1026
4	.057 ± .001	.0572	.0570
5	.033 ± .001	.0328	.0328
9	.0038 ± .0003	.0041	.0041

The fermion Green's function $G(\tau)$ for the model of Eq. (12) with $\lambda = \Omega = .5$, $\omega = 1$, $\beta = 20$. G_M is the Monte Carlo result, G_{LAT} the exact answer on the lattice and G_{CONT} the exact continuum value.

Table II

$\tau = 0$

x	$G_M(x,0)$	$G_{LAT}(x,0)$
0	.4993 ± .0003	.4999
1	-.3180 ± .0003	-.3181
2	$(6.7\pm2) \times 10^{-4}$	-5.6×10^{-8}
3	.1093 ± .0002	.1095
5	-.0823 ± .0002	-.0827

$\tau = 5$

0	.0903 ± .006	.0900
1	$-(7.3\pm3)\times10^{-4}$	-3.35×10^{-9}
2	-.0628 ± .0004	-.0625
3	.0014 ± .0004	.00128
5	$-(1.7\pm.5)\times10^{-4}$	-2.5×10^{-8}

The fermion Green's function $G(x,\tau)$ for the model of Eq. (13) with the φ^2 and $(\frac{\partial\varphi}{\partial x})^2$ terms omitted. $G_M(x,\tau)$ is the Monte Carlo result, and $G_{LAT}(x,\tau)$ the exact answer on the lattice. The lattice and continuum results are virtually indistinguishable.

Table III

k	$n(k)_M$	$n(k)_{LAT}$
0	1.000	1.000
2	.958	.956
3	.046	.044
4	.000	.000

The fermion occupation number as a function of momentum, k for the model of Eq. (13). $n(k)_M$ is the Monte Carlo result and $n(k)_{LAT}$ the exact result.

LATTICE PREDICTIONS FOR THE INTERQUARK POTENTIAL

Eve Kovacs
Stanford Linear Accelerator Center
Stanford University, Stanford, California 94305

Abstract: The measured values of Wilson loops in Monte Carlo simulations of SU(3) lattice gauge theories are used to predict the $q\bar{q}$ potential. The relationship between Λ_0 and the short distance scale of the $q\bar{q}$ potential is also calculated. The predictions are in agreement with theoretical expectations but indicate that fermions must be incorporated into the lattice calculations before any realistic results relevant to QCD can be derived.

1. Introduction

The behaviour of Wilson loops on the lattice has been extensively studied in recent Monte Carlo simulations[1] of pure SU(3) lattice gauge theories.[2] In continuum QCD the potential between two static colour sources separated by a distance R is evaluated from the expectation values of Wilson loops, $\mathrm{Tr}\ \mathbf{P}\ \exp\{ig\oint_C A_\mu^a T^a\, dx^\mu\}$, and is given by

$$V(R) = \lim_{T\to\infty}\left[-\frac{1}{T}\,\ell n\left(\mathrm{Tr}\ \left\langle 0\left|P\left[\exp\left\{ig\oint_C A_\mu^a T^a\, dx^\mu\right\}\right]\right|0\right\rangle\right)\right] \quad . \tag{1}$$

Here **P** denotes path ordering and A_μ^a and T^a denote the colour gauge fields and group generators respectively, a being the colour index. Assuming that the weak coupling limit and the continuum limit of the lattice theory are identical, we can use (1) and the measured values of rectangular Wilson loops to obtain a lattice prediction for the $q\bar{q}$ potential in the absence of light quarks.[3]

We expect that at short distances perturbative calculations should be valid, so that (1) is dominated by single gluon exchange. Hence for SU(3) the $q\bar{q}$ potential is given by

$$V\left(\bar{q}^2\right) \sim -\frac{\frac{4}{3}\,\alpha_s\left(\bar{q}^2\right)}{\bar{q}^2} \quad , \qquad \alpha_s = \frac{g^2}{4\pi} \quad . \tag{2}$$

At long distances, potential models for heavy $q\bar{q}$ systems and string models imply a linearly confining potential $V(R) \sim KR$, where K is the string tension. The string model also predicts[4] that an additional contribution, proportional to 1/R, will be present as a consequence of string dynamics.

We note that lattice gauge theories are known to exhibit confinement naturally in the strong coupling limit. Furthermore, since the string tension is an undetermined parameter which must be chosen in order to set the QCD scale,[5] any calculation of the $q\bar{q}$ potential using lattice results is guaranteed to exhibit the desired behaviour at large R. The areas of interest lie in the short distance region where the lattice potential should exhibit Coulomb-like behaviour and in the comparison with phenomenologically determined potentials.

2. The Static $q\bar{q}$ potential at Short Distances

Incorporating the lowest order behaviour of $\alpha_s(\bar{q}^2)$ into (2) and taking the Fourier transform we obtain[6]

$$V(R) = \frac{8\pi}{33R\,\ell n\,(\Lambda R)} \quad , \qquad \Lambda R \ll 1 \quad . \tag{3}$$

Unfortunately, Λ is a scheme dependent quantity and is ambiguous in lowest order. In order to make a useful prediction for short distance behaviour of the lattice $q\bar{q}$ potential, we need to evaluate the perturbative expansion for the energy between two static colour sources to the one loop level, using as an expansion parameter $g_0(a)$, the coupling constant defined in the presence of the lattice cutoff. Since we know how to relate expansions in different renormalization schemes, the evaluation of this quantity in any scheme will suffice, provided all finite terms to a given order in g^2 are retained.

Using the minimal subtraction scheme (MS) in the Feynman gauge ($\alpha = 1$) we find the potential is given by[7)]

$$V_{MS}\left(\bar{q}^{-2}\right) = -\frac{g^2_{MS}\left(\mu^2\right)C_2(R)}{\bar{q}^2}\left[1 + \frac{g^2_{MS}\left(\mu^2\right)C_2(G)}{16\pi^2}\left(\frac{11}{3}\,\ell n\,\frac{\mu^2}{\bar{q}^2} - \frac{11}{3}\,\gamma + \frac{31}{9}\right)\right] \quad , \qquad (4)$$

where $C_2(R)$ and $C_2(G)$ are the usual Casimir factors for SU(N) and γ is Euler's constant.

The relationship between $g_0(a)$ and $g_{MOM}(\mu^2)$, the coupling constant defined in the momentum subtraction scheme, is given by[8)]

$$g^2_{MOM}\left(\mu^2\right) = g^2_0(a)\left[1 + g^2_0(a)\left(\frac{11C_2(G)}{48\pi^2}\,\ell n\,\frac{\pi^2}{a^2\mu^2} + R(N)\right) + \ldots\right] \quad , \qquad (5)$$

where R(N) is a finite number depending on the gauge group SU(N).

Expressing $g_{MS}(\mu^2)$ in terms of $g_{MOM}(\mu^2)$ we obtain[9)]

$$g^2_{MS}\left(\mu^2\right) = g^2_{MOM}\left(\mu^2\right)\left[1 + A\left(\alpha, n_f\right)\frac{g^2_{MOM}\left(\mu^2\right)}{4\pi} + \ldots\right] \quad , \qquad (6)$$

where the $A(\alpha,n_f)$ are calculated[13)] for various values of α and n_f. Using (4), (5) and (6), we obtain

$$V_0\left(\bar{q}^{-2}\right) = -\frac{C_2(R)g^2_0(a)}{\bar{q}^2}\left[1 + \frac{g^2_0(a)C_2(G)}{16\pi^2}\left(\frac{11}{3}\,\ell n\,\frac{\pi^2}{a^2\bar{q}^2} - J\right)\right] \quad , \qquad (7)$$

where

$$J = \frac{11\gamma}{3} - \frac{31}{9} + \frac{4\pi A(1,0)}{C_2(G)} + \frac{16\pi^2 R(N)}{C_2(G)} \quad .$$

We can rewrite (7) by absorbing J into the logarithm and expressing $g^2_0(a)$ in terms of a and the QCD scale, Λ_0.[10)]

If we take the Fourier transform of the resulting expression in the short distance limit and as usual, absorb terms of $O[(1/\ell nR)^2]$ into the definition

of Λ, we obtain a prediction for the short distance behaviour of the lattice potential given by

$$V_0(R) = \frac{4\pi C_2(R)}{11R\ell n\left(\Lambda_P R\right)^2} \quad , \tag{8}$$

where

$$\Lambda_P = 82.07\Lambda_0 \text{ for SU(3)} , \quad n_f = 0 \quad ,$$

$$= 56.47\,\Lambda_0 \text{ for SU(2)} , \quad n_f = 0 \quad .$$

The determination of Λ_P from the measured values of Wilson loops thus provides a consistency check on lattice calculations.

3. Calculation of the $q\bar{q}$ Potential from the Numerical Data

The Monte Carlo procedure measures the lattice average of a rectangular Wilson loop, $\langle W(I,J)\rangle$, as a function of the coupling constant, with I and J denoting the side lengths of the loop in fundamental lattice units. If we suppose for the moment that J corresponds to the time direction and convert (1) into lattice variables we obtain the potential

$$V(Ia) = \lim_{Ja\to\infty} \left\{ \frac{1}{Ja} \left[-\ell n\langle W(I,J)\rangle \right] \right\} \quad . \tag{9}$$

For SU(3), the total lattice size is only 6^4 and the values of I and J are restricted to lie in the range, $1 \le I,J \le 3$. Finite size effects could thus be important and it may be necessary to include terms in (9) for finite J, that drop out in the limit $J\to\infty$. For example, correction terms involving powers of the cutoff and an important perimeter dependent contribution due to the self-energy of the static sources must be considered.

Two simple parametrizations of $\langle W(I,J)\rangle$ which include these additional contributions come to mind: (i) $\langle W(I,J)\rangle$ asymmetric in I,J and (ii) $\langle W(I,J)\rangle$ symmetric in I,J. Consider first the asymmetric case given by

$$-\ell n\,\langle W(I,J)\rangle = V(Ia)\cdot Ja + P_I(a)\cdot Ia + P_J(a)\cdot J(a) + C(a) \quad , \quad I \le J \quad , \tag{10}$$

where $P_I(a)$, $P_J(a)$ and $C(a)$ are a dependent constants to be determined. The condition $I \le J$ is imposed with the idea that an $I \times J$ Wilson loop approximates (9) if J is chosen to be the time direction. Since there is nothing to distinguish the time direction, the Monte Carlo data for SU(3) is actually symmetric in I and J. In (10) we note that the self-energy contribution $P_J(a)$ can never be separated from V(Ia). This means that the potential is determined only up to an arbitrary a dependent constant.

For the values of I and J that are available, (10) generates an overdetermined system of equations. The extra equation is used to obtain an additional estimate of the value of one of the potentials which, in the absence of finite size effects and statistical fluctuations, would be equal to the other estimates.

The magnitude of finite size effects can also be estimated from (10) by observing that the perimeter dependent and constant terms can be eliminated to give

$$\left[V(Ia) + P_J(a)\right] = \frac{1}{a}\left\{-\ell n\langle W(I,J+1)\rangle + \ell n\langle W(I,J)\rangle\right\} \quad . \tag{11}$$

The larger value of J, the better we expect the estimate (11) of V(Ia) to be. For example, for $I,J \leq 3$, $[V(a) + P_J(a)]$ can be chosen to be

$$\frac{1}{a}\left\{-\ell n\langle W(1,3)\rangle + \ell n\langle W(1,2)\rangle\right\} \quad , \tag{12}$$

or

$$\frac{1}{a}\left\{-\ell n\langle W(1,2)\rangle + \ell n\langle W(1,1)\rangle\right\} \quad . \tag{13}$$

We expect (12) to give a better estimate of V(a) than (13). The spread in the values obtained using (12) and (13) also gives an indication of the errors involved in using small sized Wilson loops.

Next we consider the case of W(I,J) symmetric in I,J, which is given by

$$-\ell n\langle W(I,J)\rangle = \tfrac{1}{2}\left\{\left[V(Ia)+P(a)\right]Ja + \left[V(Ja)+P(a)\right]Ia + C(a)\right\} \quad . \tag{14}$$

Here we have adopted the idea that the lattice results average each of the possible interpretations of the time direction for an $I \times J$ loop. Again, for $I,J \leq 3$, the system is overdetermined. As before, we can estimate finite size effects by choosing some subset of the equations generated by (14) to determine our potentials. The two possibilities chosen for illustration are:

$$\text{(a)} \qquad \{I,J\} = \{1,2\}$$

$$\text{(b)} \qquad \{I,J\} = \{1,3\} \quad .$$

Both sets of SU(3) data analysed here are measured with $g_0^2 < 1$. Hence the distance between the sources may be calculated using the known weak coupling behaviour.[11] It turns out that the distance scales differ by a factor of two, so that the unknown normalization due to the self-energy contribution can be removed by choosing $V(a_1) = V(2a_2)$, with $a_1 = 2a_2$.

4. Discussion

The results of the calculations described in Section 3 using parametrizations (10) and (14) are shown in Figures 1 and 2, respectively. Both figures

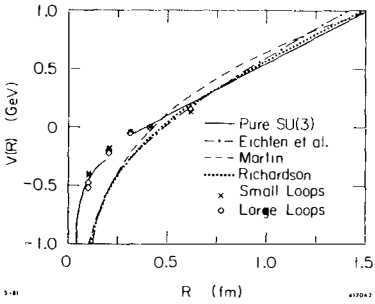

Fig. 1. The evaluation of the $q\bar{q}$ potential from lattice measurements of Wilson loops using parametrization (10). The calculated points are compared with various phenomenological potentials and with the prediction (15) for the $q\bar{q}$ potential in the absence of light quarks. The points labelled "large loops" and "small loops" correspond to choosing V(a) given by (12) and (13), respectively.

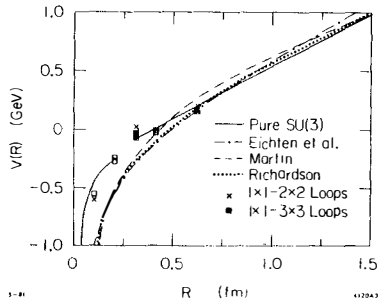

Fig. 2. As for Figure 1, but using parametrization (14) to evaluate the potential. The points labelled "1 × 1 - 2 × 2 loops" and "1 × 1 - 3 × 3 loops" correspond to alternatives (a) and (b) respectively, as discussed in Section 3.

include for comparison several phenomenological potentials determined from heavy $q\bar{q}$ bound state spectra.[6,12] The solid lines in each figure are plots of

$$V(R) = \frac{16\pi}{33R \ln\left(\Lambda_p R\right)^2} \quad , \quad R < 0.2 \text{ fm} \quad ,$$

and (15)

$$V(R) = KR \quad , \quad R > 0.3 \text{ fm} \quad .$$

These curves exhibit the expected long and short distance behaviour of the lattice $q\bar{q}$ potential. We see that in both cases the data points give a reasonable description of the short distance behaviour calculated in Section 2. It is also reassuring to note that the results are not very dependent on the detailed method of extraction of V(R) since there is reasonable agreement between the results for different methods of estimating the potential. In Figure 1, the values determined from (12) are in marginally better agreement with the prediction (15), but more data would be required to see a definite trend.

Presumably due to the absence of light fermions in the lattice analysis, the lattice potential is in poor agreement with the phenomenological potentials and consequently does not give a good fit to $c\bar{c}$ and $b\bar{b}$ spectra. These results thus indicate the need to include fermions in the lattice analysis before we can determine any realistic values for quantities relevant to QCD.

Acknowledgement

It is a pleasure to thank L. Montanet and J. Tran Thanh Van for organizing this meeting.

References and Footnotes

1. M. Creutz, Phys. Rev. Lett. 45, 313 (1980); M. Creutz, Bad Honnef Lectures, preprint BNL-27981 (1980); M. Creutz, Copenhagen Lectures, preprint BNL-27995 (1980).

2. These results are obtained using the Wilson form of the action.

3. See E. Kovacs, SLAC-PUB-2755 for a detailed discussion of the work outlined in this report.

4. M. Lüscher, Nucl. Phys. B180, 317 (1981).

5. Note that the numerical value used for K is determined in the presence of light quarks. Due to screening effects this value is expected to be somewhat smaller than the string tension for pure QCD.

6. J. L. Richardson, Phys. Lett. 82B, 272 (1979).

7. W. Fischler, Nucl. Phys. B129, 157 (1977).

8. A. Hasenfratz and P. Hasenfratz, Phys. Lett. 93B, 165 (1980).

9. W. Celmaster and R. Gonsalves, Phys. Rev. D20, 1420 (1979).

10. Recall that Λ_0 has been determined in Monte Carlo simulations of SU(2) and SU(3) lattice gauge theories. For SU(3) the value is given by $(5 \pm 1.5) \times 10^{-3} \sqrt{K}$.

11. These values are subject to a 30% uncertainty due to the uncertainty in Λ_0. There is also a systematic error in Λ_0 arising from using the value of K determined in the presence of light quarks instead of that for pure QCD.

12. E. Eichten, K. Gottfried, T. Kinoshita, K. D. Lane and T. M. Yan, Phys. Rev. D21, 203 (1980); A. Martin, Phys. Lett. 93B, 338 (1980); A. Martin, CERN-TH-2980 (November 1980).

13. Note that in the MS scheme used in Ref. 7, $\ell n\, 4\pi$ terms are also subtracted. The values calculated for $\Lambda_{MOM}/\Lambda_{MS}$ in Ref. 9 must therefore be divided by $\sqrt{4\pi}$ to obtain the correct ratios for the MS scheme of Ref. 7. In particular for $\alpha = 1$ and $n_f = 0$, $\Lambda_{MOM}/\Lambda_{MS} = 2.170$.

A BRIEF REVIEW OF THE STATUS OF CHARMED MESON DECAYS

George H. Trilling
Department of Physics and Lawrence Berkeley Laboratory
University of California, Berkeley, California 94720

ABSTRACT

The present experimental information on the spectroscopy and decay properties of charmed mesons is summarized.

I. INTRODUCTION

Since I have just submitted a detailed review of charmed particle decays to Physics Reports,[1] I shall confine myself in this paper to a brief summary of the present experimental situation. The interested reader can find further details, figures and references in the Physics Report. Because of limited time and space, my summary will only deal with a few selected topics in the area of charmed meson decay.

II. D MESON DECAYS

A. Studies of Decay Modes From e^+e^- Annihilation Experiments

The $\psi''(3770)$ resonance, through its decays into $D^0\bar{D}^0$ and D^+D^-, has provided a "D meson factory" from which considerable information on D decay modes has been extracted. We can summarize the results in the following way.

(i) About 26% of the D^0 and 30% of the D^+ decay rates are accounted for in fully reconstructed Cabibbo-favored hadronic decay modes. Table I summarizes measured branching ratios, from the Mark II group at SPEAR, for pseudoscalar-pseudoscalar and pseudoscalar-vector decay modes. The $\bar{K}^0\eta$, $\bar{K}^0\eta'$, $\bar{K}^0\rho^+$, $\bar{K}^0\omega$ and $\bar{K}^0\varphi$ modes have not been measured because of the combination of low detection efficiency and limited statistics. It may be noted that "color suppression" of $\bar{K}^0\pi^0$ or $\bar{K}^{*0}\pi^0$ does not seem to occur. Indeed those two modes occur at roughly half of the $K^-\pi^+$ and $K^{*-}\pi^+$ rates, as expected if the final state is predominantly isospin 1/2, and the corresponding D^+ decay rates are suppressed. Such suppression for these two modes is compatible with the quoted branching ratios and a lifetime ratio $\tau(D^+)/\tau(D^0)$ significantly greater than unity (see Section IIB). The $\bar{K}\rho$ modes, with very small $\bar{K}^0\rho^0$ branching ratio, do not seem to follow this picture but the data are statistically weak and need confirmation.

(ii) Both the Mark II and Lead-Glass-Wall (LGW) groups have determined inclusive branching ratios for decays of the Cabibbo-allowed forms $D^0 \to \bar{K} + X$, $D^+ \to \bar{K} + X$, by using fully reconstructed D decay modes as tags for production of the associated $\bar{D}$. The Mark II results can be summarized as follows:

$$B(D^0 \to \bar{K}^0 + X) = 13 \pm 13\%$$
$$B(D^0 \to K^- + X) = 47 \pm 12\%$$
$$B(D^+ \to \bar{K}^0 + X) = 40 \pm 20\%$$
$$B(D^+ \to K^- + X) = 13 \pm 7\% \ .$$

Here the X are either multipion states or $\mu^+\nu$, $e^+\nu$ combinations with additional pions. Thus Cabibbo-favored branching fractions for D^0 and D^+ are $(60 \pm 18)\%$ and $(53 \pm 21)\%$ respectively, and appear to be lower than the naive expectation of about 90% based on the size of the Cabibbo angle. The uncertainties are substantial, however, and confirmation is needed.

(iii) The Mark II group has measured the Cabibbo-suppressed $D^o \to \pi^+\pi^-$, $D^o \to K^+K^-$ decay mode branching ratios. The results,

$$\frac{B(D^o \to \pi^+\pi^-)}{B(D^o \to K^-\pi^+)} = 0.033 \pm 0.015 \quad \text{and} \quad \frac{B(D^o \to K^+K^-)}{B(D^o \to K^-\pi^+)} = 0.113 \pm 0.030$$

are to be compared with $\tan^2\theta_c = 0.05$, the theoretical expectation based on SU(3) symmetry and the simple 4-quark model. The general magnitude of the observed effect agrees with theory, but the quantitative agreement is not very good. Branching ratio upper limits for other Cabibbo-suppressed modes have been measured but are mostly too large to be terribly meaningful.

B. Status of D Lifetime Information

Semileptonic decay modes of D^+ and D^o produced in ψ'' decays have been studied by the DELCO and Mark II groups at SPEAR. If one assumes that the observed rates arise almost exclusively from Cabibbo-favored modes, it follows from the $|\Delta\vec{I}| = 0$ selection rule that,

$$\frac{\tau(D^+)}{\tau(D^o)} = \frac{B(D^+ \to e^+ + X)}{B(D^o \to e^+ + X)} \equiv \frac{B_e^+}{B_e^o} .$$

Measurements by the DELCO and Mark II groups give the following results:

$$\frac{B_e^+}{B_e^o} \to \begin{cases} > 4.3 \ (95\% \ \text{C.L.}) & \text{-- DELCO} \\ = 3.1^{+4.6}_{-1.4} & \text{-- Mark II} \end{cases}$$

The best estimate of B_e^+ based principally on the DELCO data with some input from Mark II and direct lifetime measurements (see below) is $19^{+4}_{-3}\%$. The corresponding B_e^o depends on the value of the above ratio which is still quite uncertain. These results give evidence that $\tau(D^+)$ is significantly larger than $\tau(D^o)$.

Several experiments have been attempting to measure charmed-particle lifetimes through measurement of decay path lengths in high-spatial-resolution detectors. We quote here the results with the greatest statistical significance, namely those of the E531 group working at Fermilab with incident neutrinos, emulsion and a downstream spectrometer. The D lifetimes reported by J. Prentice at this Conference,[2] based on the most recent statistics, are as follows:

$$\tau(D^o) = (3.1^{+1.1}_{-0.7}) \times 10^{-13} \text{ sec} \qquad (18 \text{ events})$$

$$\tau(D^+) = (9.5^{+6.5}_{-3.3}) \times 10^{-13} \text{ sec} \qquad (6 \text{ events})$$

In summary, the semileptonic branching ratio data and the direct lifetime measurements agree in giving a D^+ lifetime about 3-5 times longer than the D^o lifetime. The statistics on each of these experiments are rather limited, but the totality of the evidence makes a convincing case. The D^+ semileptonic rate

determined from $\tau(D^+)$ and B_e^+, is about 2×10^{11} sec^{-1} in good agreement with theoretical expectation.

III. F MESON DECAYS

Evidence for decay modes of the form $F^+ \to \eta + X^+$ produced in e^+e^- annihilation at the 4400 MeV resonance was presented several years ago by the DASP group at DORIS. A recent study of inclusive η production between 3.68 and 5.2 GeV by the Crystal Ball group at SPEAR has indicated production of η at all these energies, but has not confirmed the DASP group interpretation in terms of F decay. The η data from the Crystal Ball, expressed in terms of

$$R_\eta \equiv \frac{\sigma(\eta + X)}{\sigma(\mu^+\mu^-)} ,$$

show a value of R_η which remains roughly constant at 0.4 - 0.6 between 3.68 and 5.2 GeV, rather than a large peak at 4.4 GeV as reported by DASP. At 4.4 GeV the 90% C.L. upper limit for $R(e^+e^- \to F\bar{F}X)B(F \to \eta X)$ is given as 0.19 by the Crystal Ball to be compared with a measured value of 0.46 ± 0.09 reported by DASP. Upper limits for this quantity for the other energies studied by the Crystal Ball range from 0.14 to 0.32. These results do not contradict possible observations of exclusive F^+ decay modes containing η, such as $\eta\pi^+$ (reported by DASP and by a photoproduction experiment at the Ω spectrometer) and $\eta(3\pi)^+$, $\eta(5\pi)^+$ (also reported in the Ω spectrometer). However these observations are all rather weak in statistics and need confirmation.

Experiments aimed at charmed particle lifetime measurements in emulsions, with incident ν and $\bar{\nu}$, have yielded several convincing reconstructed events. Two of these are of the form $\pi^\pm\pi^+\pi^-\pi^0$ with none of the $\pi^+\pi^-\pi^0$ combinations representing an η decay. This absence of $s\bar{s}$ quark content suggests mechanisms other than the simple free-spectator-quark model, for example W annihilation. The best lifetime estimates for the F^+, also reported by Prentice at this Conference[2] is $(1.8^{+1.2}_{-0.6}) \times 10^{-13}$ sec. This value is comparable to $\tau(D^0)$ and substantially smaller than $\tau(D^+)$. This result is expected for interpretations of $\tau(D^+)/\tau(D^0) > 1$ in terms of either non-spectator-quark diagrams or SU(4) 20-dominance.

IV. SOME OUTSTANDING PROBLEMS

It is clear from the above remarks that the experimental situation on charmed particles is still rather fragmentary. Therefore I complete this report with a short and non-exhaustive list of experimental topics requiring much more study:

1) Improved measurements of lifetimes and lifetime ratios.

2) D and F branching ratio determinations for all pseudoscalar-pseudoscalar and vector-pseudoscalar final states.

3) Quantitative studies of Cabibbo-suppressed decays.

4) Studies of semileptonic final states of D, F and charmed baryons.

5) Identification of the large number of undiscovered charmed baryon states unstable only to weak decay.

Some of these questions will probably be answered by experiments run in the next few years.

REFERENCES

1. G. H. Trilling, The Properties of Charmed Particles (LBL-12283), submitted to Physics Reports for publication.

2. J. Prentice, Invited Talk at the XVIth Rencontre de Moriond (1981).

Table I. D decay branching ratios into simple final states.

Decay mode	Branching ratio (%)
$K^-\pi^+$	3.0 ± 0.6
$\bar{K}^0\pi^0$	2.2 ± 1.1
$\bar{K}^0\pi^+$	2.3 ± 0.7
$K^{*-}\pi^+$	3.6 ± 1.3
$\bar{K}^{*0}\pi^0$	$1.4^{+2.3}_{-1.4}$
$\bar{K}^{*0}\pi^+$	< 3.7
$K^-\rho^+$	7.2 ± 3.0
$\bar{K}^0\rho^0$	$0.1^{+0.6}_{-0.1}$

NONLEPTONIC DECAYS OF D- AND K-MESONS

Christoph Schmid
Institut für theoretische Physik
Eidgenössische Technische Hochschule
8093 Zürich, Switzerland

ABSTRACT

Exclusive nonleptonic decays ($D\text{-}K\pi, K\text{-}\pi\pi$) are discussed. The old standard model used factorization with vacuum insertion and disagrees with the $D\text{-}K\pi$ experiments. Two proposed remedies, the annihilation model and the interference model are compared. We prove that annihilation graphs with arbitrary numbers of gluons, which were proposed to enhance $D^0\text{-}\bar{K}\pi$ and $K^0_S\text{-}\pi\pi$, are zero for $K\text{-}\pi\pi$ at the physical point, if the amplitudes are taken to be linear in the kinematic invariants. As a new tool we use valence quark topology in conjunction with soft π limits and current algebra.

1. Valence quark topology (flavour topology)

Flavour flow topology turns out to be a very useful tool. Consider the exclusive nonleptonic decay of a meson into two mesons, $M_i \to M_a + M_b$. Let us follow the flavour flow. We begin with the quarks entering or leaving the elementary weak interaction vertex H_w . These quark lines must either close on themselves or end up as valence quarks in the external mesons*. If all 4 quark lines from H_w close to form 2 loops, we cannot have flavour change. If 2 quarks from H_w close to form 1 loop, we obtain a penguin topology, which is Cabibbo suppressed. If all 4 quarks from H_w end up as valence quarks in external mesons we obtain the topologies shown in fig. 1: Quark annihilation (M_i-annihilation) and quark decay (M_a- or M_b annihilation).

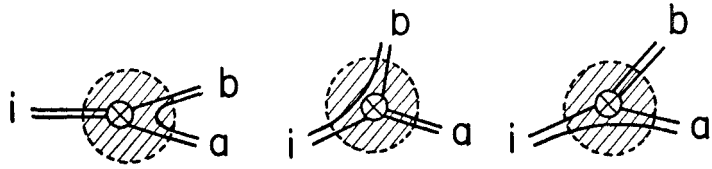

a) b) c)

Figure 1. Valence quark topologies for Cabibbo favoured decays. Shaded blob: Gluons and quark-antiquark sea.
(a) Quark annihilation (i-annihilation),
(b) Quark decay (a-annihilation),
(c) Quark decay (b-annihilation).

These are the only possibilities for Cabibbo favoured decays (e.g. $D\text{-}\bar{K}\pi$). This is a general and unique decomposition according to flavour flow. Gluons and $q\bar{q}$-sea-loops are irrelevant for this classification.

*) Since we are only interested in flavour flow, we do not draw gluons. Therefore the $q\bar{q}$-sea-pairs in a meson are not drawn connected to the valence quarks of that meson. If they end up in H_w or as valence quarks in other mesons, they are drawn. Otherwise they belong to a disconnected closed loop and are not drawn.

2. The old standard model

Let me briefly remind you of the old standard model[1,2] for nonleptonic decays, which dramatically disagrees with the new experiments of the summer 1979. Hard gluons are included using perturbative QCD and the renormalization group equations. They produce a renormalized effective 4 fermion point interaction[1]. Since the quark masses are neglected, the (V-A)(V-A) structure is unchanged. But the strengths are renormalized, for s-decays the $\Delta I=1/2$ operator gets enhanced, the $\Delta I=3/2$ operator gets suppressed. However, these effects are too small to explain the experimental $\Delta I=1/2$ rule in K-decays.

Soft gluons are contained in the matrix elements of H_w^{eff}, e.g. $\langle \bar{K}\pi | H_w^{eff} | D \rangle$. For the evaluation of these matrix elements the one and only assumption of the old standard model[2,3] for exclusive decays is factorization with vacuum insertion. This is equivalent to neglecting those soft gluons (and soft $\bar{q}q$-sea pairs) which connect the two sides of the effective weak 4-fermion vertex as shown in fig. 2.

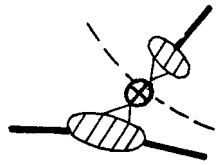

Figure 2. Factorization with vacuum insertion in the example of the quark decay topology. Vacuum saturation means that no soft gluon crosses the dashed line. Hard gluon effects are contained in H_w^{eff}, which is denoted by a cross.

With vacuum saturation the nonleptonic problem is reduced to a product of two semileptonic problems, e.g. for the quark decay topology:

$$\langle \bar{K}\pi | H_w^{eff} | D \rangle \propto \langle \pi | A_\lambda | 0 \rangle \langle \bar{K} | V_\lambda | D \rangle \qquad (1)$$

The semileptonic matrix elements are known up to form factors, which can be obtained from experiment. (In ref. 2 the unrealistic

assumption of exact SU_4 for $f_+^{DK}(0)$ was made, but this form factor drops out in ratios.) With vacuum saturation the annihilation topology (fig. la) is zero for D-$\bar{K}\pi$ in the SU_3 limit, because of CVC (conserved vector current):

$$\langle \bar{K}\pi |\, V_\lambda | 0 \rangle \langle 0 |\, A_\lambda | D \rangle \;\alpha\; f_D \;\langle \bar{K}\pi |\, \partial_\lambda V_\lambda | 0 \rangle \;=\; 0 \qquad (2)$$

It is well known that this model[2], i.e. vacuum saturation, is in dramatic disagreement with experiment[4]:

$$\frac{\Gamma(D^o \to K^- \pi^+)}{\Gamma(D^+ \to \bar{K}^o \pi^+)} \;=\; \begin{cases} 13 & \text{exp.} \\ 1.7 & \text{old std. model} \end{cases} \qquad (3)$$

$$\frac{2\Gamma(D^o \to \bar{K}^o \pi^o)}{\Gamma(D^o \to K^- \pi^+)} \;=\; \begin{cases} 1.5 \pm 0.7 & \text{exp.} \\ = 1/2 & \text{old std. model} \end{cases} \qquad (4)$$

This is a direct measure of the failure of the vacuum saturation assumption. In order to solve the D-$\bar{K}\pi$ puzzle, one must introduce soft gluons connecting the two sides of the effective 4 fermion interaction vertex (crossing the dashed line in fig. 2).

3. The annihilation model and the interference model

Remedies proposed to solve the D-puzzle fall roughly into two classes. The proponents of the annihilation mechanism[5] introduce soft gluons only for the quark annihilation topology (fig. la). As a result the annihilation amplitude does not vanish. This enhances $D^o \to \bar{K}\pi$, while $D^+ \to \bar{K}^o\pi^+$, where the annihilation topology is forbidden, is left unchanged compared to the old standard model.

In contrast to this, it has been proposed[6,7] that a suppression of $\Gamma(D^+ \to \bar{K}^o\pi^+)$ relative to $\Gamma(D^o \to K^-\pi^+)$ arises as an effect of destructive interference between the two quark decay topologies contributing to $D^+ \to \bar{K}^o\pi^+$, see fig. 3. In the free quark model the ratio is $1 : 1/3$, due to color counting. Inclusion of hard gluons shifts this ratio to $1 : -0.1$. The assumption in the "interference model"[6,7] is that somehow soft gluons further shift this ratio to $1 : -1$, which is the value needed for the $\Delta I = 1/2$ rule (in s-de-

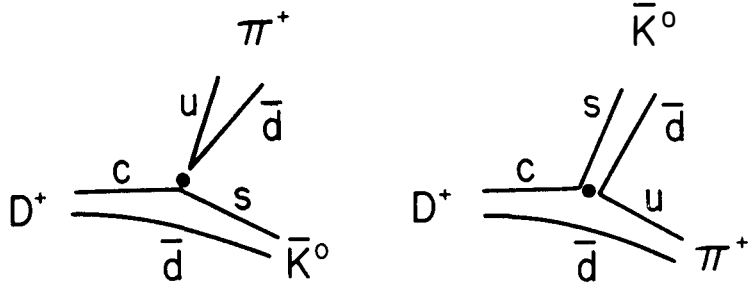

cays) and the 6-rule (in c-decays). In this proposal the annihilation graph is neglected, either by arguing[6] that soft gluons exchanged within the final state are a more important effect, or by assuming[7] $m_q = 0$ in the discussion of soft gluon effects and thereby arriving again at an effective (V-A)(V-A) interaction, which gives zero for the p.v. annihilation amplitude by SU_3 - CVC.

The predictions of the two models are (by construction) identical for the ratios $D^+ - \bar{K}^0\pi^+ : D^0 - K^-\pi^+ : D^0 - \bar{K}^0\pi^0$. But the predictions differ for absolute magnitudes of exclusive nonleptonic rates[8]. In the annihilation model $D^+ - \bar{K}^0\pi^+$ is left unchanged compared to the old standard model, which used vacuum saturation and predicted (Fakirov + Stech, ref. 2)

$$\frac{\Gamma(D^+ - \bar{K}^0\pi^+)_{\text{vac sat}}}{\Gamma(D^+ - \bar{K}^0 e^+\nu)} = 0.99 \qquad (5)$$

In this nonleptonic to semileptonic ratio the form factor $f_+^{DK}(0)$ drops out. Therefore the semileptonic calculation becomes essentially free of assumptions, and in the nonleptonic calculation the one and only remaining assumption is vacuum saturation. The experimental value for the inverse of this ratio is:

$$\frac{BR(D^+ - \bar{K}^0 e^+\nu)}{BR(D^+ - \bar{K}^0\pi^+)} = \frac{(12.5 \pm 3.1)\%}{(2.3 \pm 0.7)\%} = 5.4 \pm 2.1 \qquad (6)$$

Since the semileptonic prediction is essentially free of assumptions, it can be identified with the experimental value. Multiplying the two ratios we obtain[8]:

$$\frac{BR_{vac\ sat}(D^+ - \bar{K}^o\pi^+)}{BR_{exp}(D^+ - \bar{K}^o\pi^+)} = 4.8 \pm 1.9 \qquad (7)$$

We conclude: Assuming vacuum saturation in quark decay graphs, as is done by the proponents of the annihilation model, is in clear disagreement with experiment, it overestimates $\Gamma(D^+ - \bar{K}^o\pi^+)$ by a factor 5. The same test in the interference models shows an overestimate of $\Gamma(D^+ - \bar{K}^o\pi^+)$ by a factor of 2.0 ± 0.8 in both models[6,7].

4. The vanishing of the annihilation amplitude in $K_S^o - \pi\pi$

The flavour structure of the three channels in $K - \pi\pi$ and in $D - \bar{K}\pi$ are identical, except for an overall factor $\sin\theta_c$ resp. $\cos\theta_c$ and except for the possibility of penguins in $K - \pi\pi$. Soft gluon effects may be different in the two cases, they are expected to be stronger for $K - \pi\pi$. Any solution to the $D-\bar{K}\pi$ puzzle will automatically be a candidate for explaining the $\Delta I = 1/2$ rule in $K - \pi\pi$ either fully or partially. Indeed some authors of the annihilation mechanism (Fritzsch and Minkowski, Bernreuther, Nachtmann and Stech, ref. 5) have proposed that this mechanism also explains the $\Delta I = 1/2$ rule in $K - \pi\pi$ (without involving penguins).

But the following theorem has been proved by M. Bonvin and myself[9]: The annihilation amplitude for $K_S^o - \pi\pi$, in the presence of an arbitrary number of soft gluons and $q\bar{q}$-sea-pairs, is zero, if the amplitudes are taken linear in the kinematic invariants.

In order to prove this, we decompose the nonpenguin part of the $K - \pi\pi$ amplitude according to flavour topology (see section 1):

$$A_{iab}(p_i,p_a,p_b) = \sum_{t=i,a,b} F_{iab}^{(t)} D^{(t)}(p_i,p_a,p_b) \qquad (8)$$

The superscript t runs over the three topologies shown in fig 1. The subscripts i,a,b identify the flavours of the external mesons. The flavour factors $F^{(t)}_{iab}$ are simple, they contain $\sin\theta_c$ and Clebsch-Gordons like $\langle \pi^o | u\bar{u} \rangle = 1/\sqrt{2}$, but they are independent of momenta. The dynamical factors $D^{(t)}(p_i, p_a, p_b)$ contain all strong interaction effects and are difficult to estimate, but they are independent of flavour (except for mass factors), since gluons are flavour blind.

When taking a soft π limit, some momentum in $D^{(t)}(p_i,p_a,p_b)$ will go to zero, but the flavour factors $F^{(t)}_{iab}$ will be unchanged. This implies that the flavour topologies cannot change in the process of taking a soft pion limit.

For a discussion of soft π limits and current algebra it is advantageous not to make the (somewhat arbitrary) separation between hard and soft gluons, but rather to take for H^W_{NL} the elementary (V-A)(V-A) four-fermion vertex. With H^W_{NL} α (V-A)(V-A) we have $\left[Q^5_b, H^W_{NL} \right] = - \left[Q_b, H^W_{NL} \right]$ and

$$\lim_{p_b \to 0} A_{iab} = \frac{\sqrt{2}}{f_\pi} \langle M_a | \left[Q^+_b, H^W_{NL} \right] | M_i \rangle \qquad (9)$$

Now we can draw the flavour flow graphs for this expression (again leaving out penguin topologies). Note that Q_b acting on M_a has no dynamical effect, but it does create a flavour change, see fig. 4.

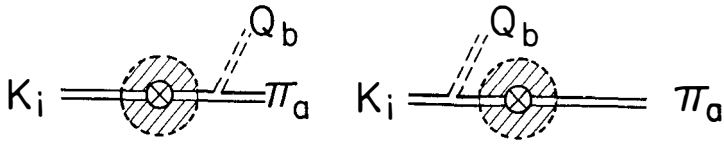

a) b)

Figure 4. Soft π_b limit of $M_i \to M_a + \pi_b$.

Observe that the first half of the commutator, $\langle M_a | Q^+_b H^W_{NL} | M_i \rangle$, has a flavour topology, fig. 4a, which is exactly the same as the one of fig. 1a. The second half of the commutator has the flavour topology of figs 4b and 1b. The topology of fig. 1c is missing in the

soft π_b limit.* Since the flavour topology cannot change when taking the soft π_b limit, we have:

$$\lim_{p_b \to 0} A^{(i)}_{iab} = \frac{\sqrt{2}}{f_\pi} \langle M_a | Q_b^+ H | M_i \rangle$$

$$\lim_{p_b \to 0} A^{(a)}_{iab} = -\frac{\sqrt{2}}{f_\pi} \langle M_a | H Q_b^+ | M_i \rangle \qquad (10)$$

$$\lim_{p_b \to 0} A^{(b)}_{iab} = 0$$

Comparing the soft π_a with the soft π_b limit for the annihilation topology

$$\left(\frac{\text{soft } \pi_b \text{ limit}}{\text{soft } \pi_a \text{ limit}} \right)_{\substack{\text{annihil.} \\ \text{topology}}} = \frac{\langle \pi_a | Q_b^+ H | K_i \rangle}{\langle \pi_b | Q_a^+ H | K_i \rangle} = -1 \qquad (11)$$

we obtain -1, because of the antisymmetry of the structure constants ε_{abc} of SU_2.

How do we get from the soft π points to the physical point? If we identify A_{phys} with $A_{soft\ \pi}$, then we obtain zero for all topologies, because the two soft π limits are unequal. Using a linear approximation in the kinematic invariants and using the theorem that A vanishes in the SU_3 limit[10] one can show[9] that the physical amplitude is proportional to the sum of the two soft π limits. For the annihilation topology this sum is zero, because of eq.(11). This completes our proof.

We conclude that in the linear approximation the annihilation mechanism (including arbitrary numbers of gluons) cannot contribute to $K\text{-}\pi\pi$ at the physical point. This means that the explanation[5] of $\Gamma(K^0_S\text{-}\pi\pi >> \Gamma(K^+ - \pi\pi)$ by the dominance of the annihilation graph is untenable.

*) Note that we are talking about Q_b, and not Q_b^5. The latter can create $q\bar{q}$-pairs from the vacuum, the former cannot do this. Therefore $\langle M_a | Q_b^{5+} H^w_{NL} | M_i \rangle$ does not have a definite flavour topology.

The situation for hyperon-decays is very different. Initial baryon "annihilation" (where 2 quarks in the initial baryon get transformed into 2 new quarks by H^{W}_{NL}) is allowed, dominant, but final baryon "annihilation" is of comparable dynamical weight (exactly equal weight in the soft π limit) and cannot be neglected. On the other hand meson annihilation is zero in the soft meson limit, but presumably important for physical pion momenta (as in K-decays).

References

(1) M.K. Gaillard and B.W. Lee, Phys.Rev.Letters 33, (1974) 108;
G. Altarelli and L. Maiani, Phys. Letters 52B, (1974) 351.

(2) D. Fakirov and B. Stech, Nucl.Phys. B133, (1978) 315;
N. Cabibbo and L. Maiani, Phys. Letters 73B, (1978) 418;
see also J. Ellis, M.K. Gaillard and D. Nanopoulos, Nucl.Phys. B100, (1975) 313.

(3) M.A. Shifman, A.I. Vainshtein and V.I. Zakharov,
Zh. Eksp. Theor. Fiz. 72, (1977) 1275
[Sov.Phys.JETP 45, (1977) 670];
M.K. Gaillard, Proceedings of Summer Institute on Particle Physics, SLAC Report No 215, November 1978.

(4) W. Bacino et al., Phys.Rev.Letters 45, (1980) 329;
Phys.Rev.Letters 43, (1979) 1073;
R.H. Schindler et al. SLAC-PUB-2507 and LBL-10905, Mai 1980 and R.H. Schindler, Ph.D. thesis, SLAC-219 (1979);
Ushida et al. Phys.Rev.Letters 45, (1980) 1049 and 1053.

(5) M. Bander, D. Silverman and A. Soni, Phys.Rev.Letters 44, (1980) 7 and 962 (E);
H. Fritzsch and P. Minkowski, Phys.Letters 90B, (1980) 455;
Nucl.Phys. B171, (1980) 413;
W. Bernreuther, O. Nachtmann and B. Stech, Z. Physik C4, (1980) 275.

(6) N. Deshpande, M. Gronau and D. Sutherland, Phys. Letters 90B, (1980) 431;
G. Eilam and M. Gronau, Phys.Letters 69B, (1980) 391;
M. Gronau and D. Sutherland, preprint Technion Haifa and Glasgow University.

(7) B. Guberina, S. Nussinov, R.D. Peccei and R. Rückl, Phys. Letters 89B, (1979) 111.

(8) M. Bonvin and C. Schmid, ETH preprint, May 1981.

(9) M. Bonvin and C. Schmid, ETH preprint, November 1980.

(10) N. Cabibbo, Phys.Rev.Letters 12, (1964) 62;
M. Gell-Mann, Phys.Rev.Letters 12, (1964) 155;
S. Pakvasa, S.P. Rosen and E.C.G. Sudarshan,
Phys.Rev. 146, (1966) 1118;
D.G. Boulware and L.S. Brown, Phys.Rev.Letters 17, (1966) 772.

EMULSION-SPECTROMETER MEASUREMENTS OF CHARMED HADRON WEAK DECAY LIFETIMES

J.D. Prentice
Department of Physics
University of Toronto
Toronto M5S 1A7
Canada

ABSTRACT

Recent results on the weak decay lifetimes of the Λ_c^+, F^+, $D^\mp$ and D° charmed hadrons from Fermilab E531 are presented and compared with other charmed hadron lifetime measurements. A probable example of the weak decay of a neutral charmed baryon is presented.

A new observation of the decay of a photoproduced $D^\circ\bar{D}^\circ$ pair from the CERN Omega prime-emulsion collaboration (WA 58) is briefly discussed.

Introduction

The active current interest in the lifetimes of weakly decaying charmed hadrons has been well documented in the review of George Trilling [1] in these proceedings and in the flood of recent theoretical attempts to interpret the first measurements of them. It is clear that an understanding of the hadronic partial widths requires careful application of not only electroweak interaction theory but also the corrections of Q.C.D. Charmed hadron spectroscopy has already provided us with many branching ratios [2] but it is only with measured lifetimes that these can be converted to the partial decay widths that confront theory directly.

Initial expectations of nearly equal lifetimes for all charmed hadrons [3] were based on a model in which the heavy charmed quark lifetime was almost unaffected by the much lighter spectator quarks that were bound to it. As early as 1979, however, substantial differences between the semi-leptonic branching ratios of the charged and neutral D mesons were used to infer an equivalent difference in lifetimes [4]. At the same conference direct lifetime measurements[5] confirmed this difference and indicated that the Λ_c^+ and F^+ were also much shorter lived than the D^+. Published values of these 4 lifetimes,[6] based on modest statistics have sufficiently wide error margins to accommodate almost all the host of recent predictions which now include the relevance of W exchange and quark annihilation diagrams, the importance of gluon radiation from both initial and final states, colour effects and final state interactions.

Preliminary results reported here, based on a larger sample of events from the same experiment, indicate that not only better statistics but also a clear understanding of scanning efficiencies

and improved particle identification will be necessary to produce the accurate values required to evaluate the many and varied current theoretical models.

Recent results from Fermilab E531

Further analysis of the data obtained in an exposure of 23 litres of emulsion to the Fermilab broad band neutrino beam[6] has produced an enlarged sample of charm decay candidates. Events were located in the emulsion and the production and decay particles were anlaysed in the spectometer shown schematically in fig. 1. and described in ref[6].

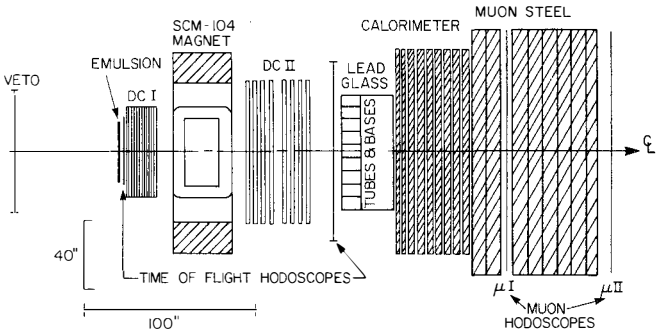

Fig.1. E531 Spectrometer

The horn focussed neutrino beam was incident on the emulsion target from the left. In the first run exposure a total of 7×10^{18}, 350 GeV/c protons were incident on the production target. Neutrino interactions in or near the emulsion target were identified by a simple neutral trigger requiring two or more charged particles in each of the time of flight scintillator planes and no accompanying pulse in the veto counters, thus accepting both charged and neutral current interactions. The momenta of the 80% of the charged

secondaries that traversed the spectrometer were measured with an accuracy $\Delta p = \pm [(0.005p^2)^2 + (0.013p)^2]^{1/2}$ by 12 and 8 drift chambers placed respectively upstream and downstream of a wide aperture analyzing magnet. For particles seen in the upstream drift chambers only, the magnet fringe field gave a resolution of $\Delta p = \pm 0.34p^2$ while still wider angle charged particle momenta were obtained from multiple scattering measurements in the emulsion. Neutral momenta were measured in a 68 element array of lead glass shower counters and a 5 plane steel-scintillator hadron calorimeter. Particle identification, which was particularly important in fitting the charmed particle decays, was provided by a 30 element time of flight hodoscope with a resolution of $\pm$120 p sec. This gave a 1σ separation of pions and kaons up to 3 GeV/c and kaons and protons up to 6 GeV/c. Emulsion ionization measurements on wide angle particles gave π-K separation below 0.8 GeV/c and K-p identifications up to 1.5 GeV/c. Electrons were identified in the lead glass and muons by their penetration to two hodoscopes behind 1.2m and 2.9 m of steel respectively. The hadron calorimeter was very coarse grained being divided only into 4 vertical strips each 75cm wide but was occasionally able to reveal the presence of a n or K_L^o in regions where there was not too much overlap with charged tracks.

The success of this experiment was largely dependent on a technique developed to trace individual tracks from the spectrometer to the emulsion, in the presence of a large integrated background of beam associated muons. the fiducial sheet, shown in fig. 2. covered the downstream face of all the emulsion modules and was changed every two days and immediately developed to limit the background of both beam and cosmic ray muons.

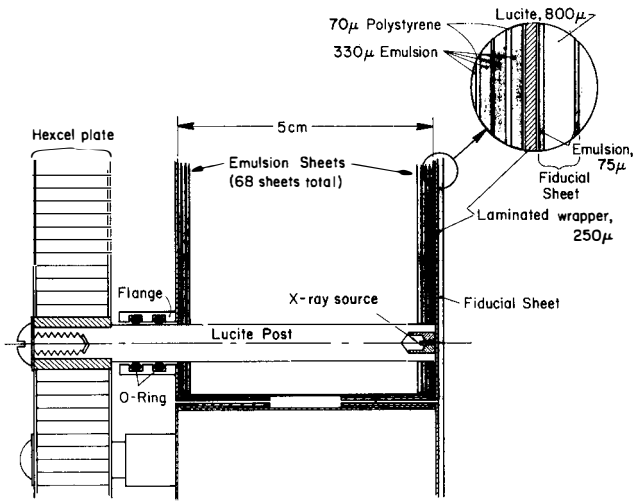

Fig.2. Arrangement of vertical emulsion and fiducial sheet.

Constructed of 75 μm layers of emulsion on both sides of a 0.8 mm thick lucite sheet, it provided high resolution angle and position measurements as close to the main emulsion stacks as possible. It was located relative to them to better than 100 μm accuracy by the marks made on the fiducial sheet emulsion by collimated Fe^{55} X-ray sources mounted integrally in the main emulsion stacks.

Over 85% of the events searched for by track following were located in the emulsion providing 726 of the 1235 neutrino interactions that were found. The combined finding efficiency of the track following and volume scanning near the predicted vertex was 1235/1800=69%.

The search for charmed particle decay candidates was accomplished by following all charged particles with angles of less than 0.2 rad to the beam direction downstream for 6 mm from the production vertex. A cylinder of 300 μm radius and 1000 μm length along

the beam direction was scanned at high magnification for neutral decays. Finally, over half of all tracks found in the spectrometer with momentum > 0.7 GeV/c and which extrapolated back to within 2mm of the production vertex but could not be associated with any of the emulsion tracks seen at the vertex, were followed back. This procedure located several decay candidates lying outside the limits of the other two searches. Almost equally importantly it contributed to the understanding of the variation of finding efficiency with distance from the primary vertex.

The charm search located a total of 43 multiprong decay candidates of which 23 were charged and 20 neutral. In addition 26 single prong kinks with a transverse momentum change of > 0.1 GeV/c were found. Five of these that have p_t >0.25 GeV/c are considered to be decay candidates.

Using the measurement data from the spectrometer and the emulsion, decay tracks were identified, where possible, and kinematic fits to the decays were attempted.

For events in which the observed charged and neutral particles balanced transverse momentum about the decay direction 2 constraint fits were obtained which determined the mass and error of the decaying particle corresponding to each hypothesis for the decay products. Assigning known charmed particle masses to the parent particles allowed three constraint fits to be made and the associated confidence levels to be calculated. Particle Data Table values were used for the D^+ and D^o and 2030 MeV and 2285 MeV for the F^+ and Λ_c^+ respectively.

For the semi-leptonic decays with a neutrino in the final state and for a few other events where an assumed missing π° or K° that would have missed the detector could provide transverse momentum balance, a zero constraint calculation was made. For these decays only $\Delta S = \Delta C$ (Cabbibo favoured) decays were considered. In most cases this gave two possible values for the parent momentum and proper decay time. In some zero constraint events one set is ruled out by the absence of a signal in the detector or the kinematics only allow a unique solution at the minimum of the curve of missing momentum versus mass.

The results of these fits are shown in table I. For each event the length of the decay track, the decay hypothesis, the mass obtained from the two constraint-fit, the confidence level for the three constraint fit, the momentum of the decaying particle and the proper decay time, are given.

Table I: Charmed Hadron Decays The particles underlined in the decay hypothesis were identified by ionization, range or time of flight in the emulsion or spectrometer. The presence of the particles in parentheses was assumed to obtain transverse momentum balance about the decay direction. Masses used in the 3C fits were 2285, 1868, 2030 and 1863 MeV/c^2 for the Λ_c^+, D^+, F^+ and D^o respectively.

Λ_c^+ DECAYS

DECAY LENGTH (μm)	DECAY HYPOTHESIS	2C FIT MASS (MeV/c^2)	3C FIT C.L.	Pch (Gev/C)	DECAY TIME (10^{-13})
41	$\Lambda_c^+ \to \Lambda^o \pi^+ \pi^+ \pi^-$	2131$\pm$63	.27	5.73	0.54
175	$\Lambda_c^+ \to \underline{p}\, K_L^o$	2204$\pm$200	.97	5.80	2.30
180	$\Lambda_c^+ \to \Lambda^o \pi^+ \pi^+ \pi^-$	2274$\pm$41	.41	8.40	1.63
221	$\Lambda_c^+ \to \Lambda^o \pi^+ \pi^+ \pi^-$	2374$\pm$63	.05	4.67	3.60
21	$\Lambda_c^+ \to \underline{p\pi^+ K^-} (\pi^o)$	-	-	1.9 2.7	0.60 0.40
28	$\Lambda \to \underline{p\pi^+ \pi^-} (\bar{K}^o)$	-	-	2.9 5.0	0.73 0.42

		$D^{\pm}$ DECAYS			
457	$*D^{+}\rightarrow K^{-}\pi^{+}\pi^{+}\pi^{o}$	1829±35	.07	10.0	2.85
1802	$D^{+}\rightarrow K^{-}K^{+}\pi^{+}\pi^{o}$	1862±25	.52	17.4	6.44
2150	$*D^{+}\rightarrow K^{-}\pi^{+}\mu^{+}(\nu_{\mu})$	(AT MIN)	-	16.6	8.06
2203	$D^{+}\rightarrow\pi^{+}\pi^{+}\pi^{-}(K_{L}^{o})$	(AT MIN)	-	11.0	12.5
13,000	$*D^{+}\rightarrow K^{-}\pi^{+}e^{+}(\nu_{e})$	(AT MIN)	-	111.	6.9
2307	$D^{-}\rightarrow\underline{K}^{+}\pi^{-}\underline{e}^{-}(\bar{\nu}_{e})$				
		$F^{\pm}$ DECAYS			
130	$F^{+}\rightarrow\underline{K}^{+}\pi^{+}\pi^{-}K_{L}$	2057±111	.68	9.33	0.94
132	$F^{+}\rightarrow\underline{K}^{+}\underline{K}^{-}\underline{\pi}^{+}\underline{\pi}^{o}$	2050±45	.46	5.93	1.51
670	$F^{-}\rightarrow\underline{\pi}^{+}\underline{\pi}^{-}\pi^{-}\underline{\pi}^{o}$	2026±56	.51	12.25	3.90
		D^{o} DECAYS			
6.5	$D^{o}\rightarrow K^{-}\underline{\pi}^{+}\underline{\pi}^{+}\pi^{+}\underline{\pi}^{-}\underline{\pi}^{-}$	1923±46	.06(ic)	19.2	0.021
125	$D^{o}\rightarrow\underline{\pi}^{+}\underline{\pi}^{+}\pi^{+}\underline{\pi}^{-}\pi^{-}\pi^{-}(\pi^{o})$(AT MIN)		-	8.85	0.88
27	$\bar{D}^{o}\rightarrow K^{+}\pi^{+}\underline{\pi}^{-}\pi^{-}\underline{\pi}^{o}$	1766±48	.05	9.18	0.18
42	$D^{o}\rightarrow K^{-}\underline{\pi}^{+}\underline{\pi}^{+}\pi^{-}\underline{\pi}^{o}$	1855±43	.99	15.43	0.17
256	$D^{o}\rightarrow K^{-}\pi^{+}\pi^{+}\pi^{-}$	1816±40	.12	12.3	1.29
749	$D^{o}\rightarrow K^{-}\pi^{+}\pi^{+}\pi^{-}$	1876±122	.78	13.53	3.23
4053	$D^{o}\rightarrow K^{-}\underline{\pi}^{+}\pi^{+}\pi^{-}\pi^{o}$	1859±38	.45	23.6	10.69
5472	$D^{o}\rightarrow K^{-}\pi^{+}\mu^{+}\pi^{-}(\nu_{\mu})$	-	-	36/59	9.5/5.8
116	$D^{o}\rightarrow K^{-}\pi^{+}\pi^{o}\pi^{o}$	1939±117	.88	30.08	0.24
184	$\bar{D}^{o}\rightarrow\pi^{+}\pi^{-}\pi^{o}\pi^{o}$	1857±76	.99	20.89	0.52
326	$D^{o}\rightarrow\pi^{+}\pi^{-}K_{L}^{o}$	1911±76	.94	11.23	1.80
703	$D^{o}\rightarrow\pi^{+}\underline{\pi}^{-}\underline{K}_{3}^{o}\ ^{o}$	1859±34	.30	12.35	3.54
67	$D^{o}\rightarrow\pi^{+}\pi^{-}(\bar{K}^{o})$	-	-	11.3	0.37
187	$\bar{D}^{o}\rightarrow K^{+}\pi^{-}(\pi^{o})$	-	-	6.8/9.5	1.7/1.2
2646	$D^{o}\rightarrow K^{-}\mu^{+}(\nu_{\mu})$	-	-	23/39	7.2/4.2
4374	$D^{o}\rightarrow K^{-}\underline{e}^{+}(\nu_{e})$	-	-	30/70	9.2/4.3
		Two Decay Event			
590	$D^{o}\rightarrow K^{-}\pi^{+}\pi^{o}$	2000±130	.61	13.23	2.77
3170	$X^{o}\rightarrow ?$	-	-	-	-

Scanning efficiencies, for short decay lengths, were measured by examining the region of confusion near the vertex for 200 typical events and for long distances by comparing results of the track following and neutral scan with those of the scan back of extra spectrometer tracks. The efficiency of the neutral charm search is shown in fig. 3.

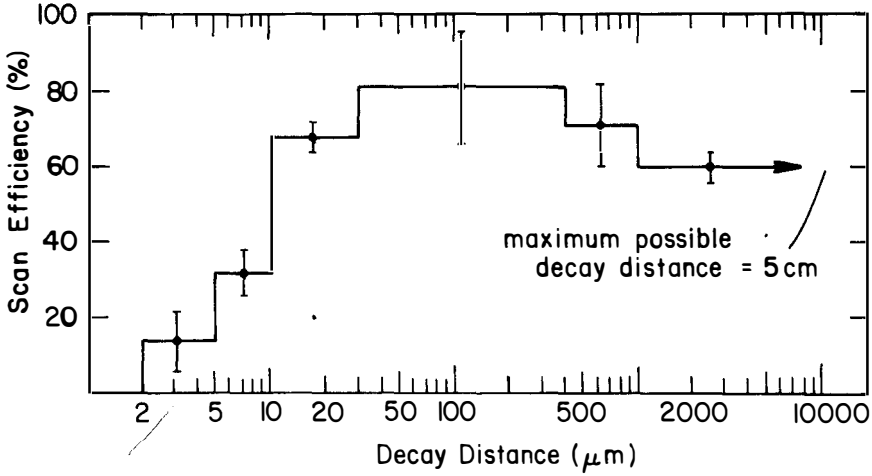

Fig.3. Scanning efficiency for neutral decays.

With this detailed understanding of the dependence of event finding efficiency on track length maximum likelihood fits to the lifetimes were possible. The results for the Λ_c^+, $F^\pm$ and $D^\pm$ are shown in Table II together with the weighted means of the masses determined by the two constraint fits and the number of events in the sample; these results are preliminary as the analysis of some of the events is still in progress.

Table II: fitted lifetimes and masses for charged charmed hadrons

Particle	Fitted Lifetime (10^{-13}s)	Fitted Mass (MeV/c^2)	Number of Events
Λ_c^+	$1.7^{+0.9}_{-0.5}$	2263 ± 27	6
$D^\pm$	$9.5^{+6.5}_{-3.3}$	1851 ± 20	6
$F^\pm$	$2.0^{+1.8}_{-0.8}$	2042 ± 33	3

Two other hybrid emulsion experiments (CERN WA 17 and WA 58) have each obtained a well fitted Λ_c^+ event. The first [7] using BEBC as a downstream detector and the CERN broad band neutrino beam found a $\Lambda_c^+ \to pK^-\pi^+$ decay with a proper time of 7.3×10^{-13} sec and a mass of 2.26 ± 0.02 GeV/c^2. A $\Lambda_c^+ \to \Lambda^\circ\pi^+$ decay [8] with mass of 2.33 ± 0.05 GeV/c^2 and proper decay time 0.57×10^{-13} sec was photoproduced in emulsion by the CERN tagged photon beam and analysed by the Omega prime spectrometer in the arrangement shown in fig 4. These results are clearly consistent with the mass and lifetime shown in Table II.

A Fermilab experiment (E 564) with cryogenic emulsions in the 15 foot D_2 bubble chamber, exposed to the broad band neutrino beam found an $F^+ \to \pi^+\pi^+\pi^-\pi^\circ$ decay [9] with proper time 1.5×10^{-13} sec and fitted mass 2017 $\pm$25 MeV. Including this event with the 3 from Table I gives a weighted average $M_{F^+} = 2026\pm20$ and $\tau = 1.8^{+1.2}_{-0.6}\times10^{-13}$sec. It is interesting to note that in the F^+

event, one $\pi^+\pi^-\pi^\circ$ combination has a mass consistent with that of an ω° and that none of the 2π or 3π sub-masses for this event or for the F^- event in Table I is consistent with a known meson with a substantial $s\bar{s}$ component in its state vector. This apparent absence of $s\bar{s}$ quarks in the F decay products in two out of four events suggests a possibly important contribution from $c\bar{s}$ annihilation to the hadronic decays of the F. This in turn is one of the possible explanations that has been advanced for the small ratio of its lifetime to that of the D^+, for which such annihilation channels are Cabbibo unfavoured.

While none of the F events in Table I has a D decay hypothesis with confidence level > 1%, there is some possibility of F contamination in our D sample. The entries marked with * have acceptable F decay hypotheses $\Delta S=\Delta Q$ but they are less favoured because of time of flight information or OZI rule suppression of a $F\to\pi^+\pi^-e^+\nu_e$ final state.

The D° was not included in Table II. Although the mean fitted mass obtained from the events of table I ($M_{D^\circ}=1856\pm15$) is in excellent agreement with the establlished value and a maximum likelihood fit gives a lifetime of $\langle\tau\rangle = 3.1^{+1.1}_{-0.7}$ with a confidence level for the events being a statistical sample of a single lifetime >30%, nevertheless there are a number of reasons for concern about accepting this figure uncritically. Firstly, the first seven events found in this experiment[6] gave $\langle\tau\rangle=1.00^{+0.52}_{-0.31}\times10^{-13}$sec. Secondly three of the four longest lived events are semi-leptonic decays and the mean life for those three events, giving equal weight to both solutions in each case, is $8.5^{+0.8}_{-3.6}\times10^{-13}$s.

If we conlcude that there is some indication of two lifetime components in our D° sample, to what should we attribute them? Although much has been written theoretically about $D^\circ\bar{D}^\circ$ mixing there is no experimental evidence for it from e^+e^- collisions [2] and even if it were strong it is hard to devise a scheme to cause a substantial lifetime difference between D_1° and D_2° since most of the final states resulting from D° decay have S=-1 and are therefore not eigen states of CP.

A more likely scenario is that the sample is contaminated with weakly decaying neutral charmed strange baryons or charmed strange exotic mesons[10] or baryons[11]. Although there are theoretical predictions for the masses of possible weakly decaying neutral hadrons with quark content such as (cds)[12], $(cs\bar{u}d)$[10] and $(c\bar{s}ddd)$[11] there is no experimental evidence for their existence. Kinematic fits of the events of table I to such decays as $(cds) \rightarrow K^-\pi^+pK^-\pi^\circ$ are at best speculative. This is, however, a consistent interpretation of the longest lived entry in the D° section, giving a fitted mass of 2583 ± 26 MeV/c^2. Futhermore one neutral decay candidate (not shown in Table I) has a well identified proton in its final state and fits $(cds) \rightarrow p\pi^-K_s^\circ$ (m=2459 MeV/c^2) or $(css) \rightarrow pK^-K_s^\circ$ (m = 2658 MeV/c^2) if one is willing to accept Cabbibo unfavoured decays. It has also been pointed out[11] that assuming the K_s° to be a K° instead of $\bar{K}^\circ$ permits a Cabibbo favoured decay $(c\bar{s}ddd) \rightarrow pK^-K^\circ$. This event has a very long proper time $\sim 80\times10^{-13}$s which might suggest that it is not a decay; but an estimate of the probabililty that it results from a neutral particle interaction gives $<10^{-4}$.

The last two entries in Table I refer to an event which appears to involve two high momentum decaying neutral particles. The first is reasonably well fitted to a D° decay and a preliminary fit to the second was consistent with a $\bar{D}^\circ$. This event is currently being remeasured but at present there is no acceptable fit for the second 2 prong candidate to the weak decay of a D° or $\bar{D}^\circ$. As there is no identified muon in the event it initially appeared to be a candidate for associated production of a $c\bar{c}$ pair by the weak neutral current.

Photoproduction of a $D^\circ\bar{D}^\circ$ pair

Analysis of the first 2000 of 160,000 hadronic events expected from an exposure of 6000 emulsion pellicles to photons of energy 20-70 GeV in the CERN tagged photon beam has already yielded 6 events each containing two charmed particle decay candidates the analysis of which has been published [8) 13)].

The experimental set up is shown schematically in fig. 4.

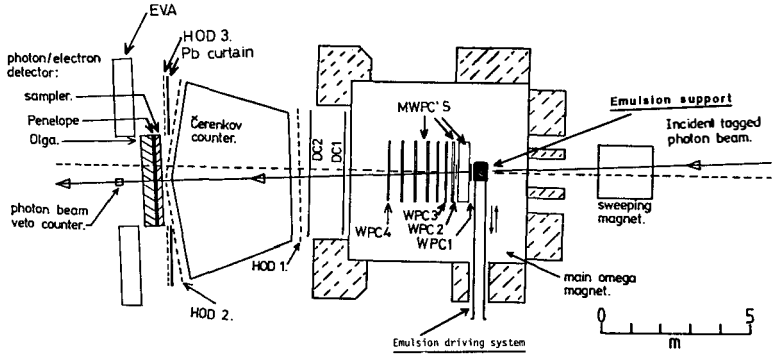

Fig.4. The emulsion- Ω′ experiment (CERN WA 58)

A recently observed event contains two neutral decays which appear to fit $D^{\circ} \rightarrow K_s^{\circ} \pi^- e^+ \nu_e$ and $\bar{D}^{\circ} \rightarrow K^+ \pi^+ \pi^- \pi^-$. The low energy e^+ is identified in the emulsion. The remaining tracks, including the decay products of the K_s°, are observed in the spectrometer. It is expected that this example of photoproduction and decay of a $D^{\circ}\bar{D}^{\circ}$ pair can be fully reconstructed. Analysis of this run is continuing. With more than 95% of the expected events still to be examined, the physics prospects are excellent.

Conclusions

As more events are analysed from the hybrid emulsion charm lifetime experiments the substantial difference between the lifetimes of the shorter lived Λ_c^+, F^+ and D° and the longer lived D^+ is being confirmed.

It is clear that a detailed knowledge of scanning efficiency is required to convert a small set of decay times to a reliable lifetime estimate.

Even with tens of events the presence of two lifetime components in a sample of decays is difficult to detect solely from the distribution of decay times. It is therefore essential to obtain a sample of well fitted unambiguous events. In view of the many possible weakly decaying states identification of the individual decay products is becoming increasingly important.

Both Fermilab experiments E531 and E564 are just completing their second data taking runs with improved detectors and higher expected yields of reconstructed charmed hadron decays. The continuing analysis of the large body of data from CERN (WA 58) is already producing further events. Substantial further contributions to the understanding of charmed particle decays can be expected from hybrid emulsion experiments in the coming year.

References

1) G. Trilling Review of Charmed particle decays these proceedings.

2) See for example R.H. Schindler "Charmed Meson Production and Decay Properties at the ψ (3770)" Thesis, SLAC 219 unpublished and R.H. Schindler et al Phys. Rev. D to be published.

3) See for example M.K. Gaillard, B.W. Lee and J.L. Rosner Rev. Mod. Phys. 47 (1975) 277; N. Cabbibo and L. Maiani Phys. Lett. 73B (1978) 418.

4) V. Luth, "Proceedings of the 1979 International Symposium on Lepton and Photon Interactions at High Energies" Fermilab (1979), p. 78.
J. Kirkby, ibid, p. 107.

5) J. Prentice, ibid, p. 563.

6) N. Ushida, T. Kondo, G. Fujioka, H. Fukushima, Y. Takahashi, S. Tatsumi, C. Yokoyama, Y. Homma, Y. Tsuzuki, S. Bahk, C. Kim, J. Park, J. Song, D. Bailey, S. Conetti, J. Fischer, J. Trischuk, H. Fuchi, K. Hoshino, M. Miyanishi, K. Niu, K. Niwa, H. Shibuya, Y. Yanagisawa, S. Frrede, M. Gutzwiller, S. Kuramata, N.W. Reay, K. Reibel, T.A. Romanowski, R. Sidwell, N.R. Stanton, K. Moriyama, H. Shibata, T. Hara, O. Kusumoto, Y. Noguchi, M. Teranaka, H. Okabe, J. Yokota, J. Harnois, C. Hebert, J. Hebert, S. Lokanathan, B. McLeod, S. Tasaka, P. Davis, J. Martin, D. Pitman, J.D. Prentice, P. Sinervo, T.-S. Yoon, H. Kimura, and Y. Maeda Phys. Rev. Lett. 45 (1980) 1049, 1053.

7) D. Allasia et al., Nucl. Phys. 176B (1980) 13.

8) A. Fiorini et al., Lett. Nuovo Cimento 30 (1981) 166.

9) R. Ammar et al., Phys. Lett. 94B (1980) 118.

10) H.J. Lipkin Phys. Lett. 70B (1977) 113;
N. Isgur and H.J. Lipkin Phys. Lett. 99B (1981) 151.

11) J. Rosner private communication.

12) K. Maltman and N. Isgur Phys. Rev. D22 (1980) 1701.

13) M.I. Adamovich et al., Phys. Lett. 99B (1981) 271.

OBSERVATION OF A FULLY RECONSTRUCTED $D^0\bar{D}^0$ PAIR WITH LONG LIFETIMES IN A HIGH RESOLUTION HYDROGEN BUBBLE CHAMBER AND THE EUROPEAN HYBRID SPECTROMETER

Amsterdam-Brussels-CERN-Madrid-Mons-Nijmegen-Oxford-Padova-Paris-Roma-Rutherforf Lab.-Serpukhov-Stockholm-Strasbourg-Torino-Trieste-Vienna Collaboration

(Presented by J. LEMONNE)

ABSTRACT

In an experiment with a 360 GeV/c π^- beam at the CERN SPS using the high resolution hydrogen bubble chamber LEBC and the European Hybrid Spectrometer, an event has been observed of the type $\pi^- p \to \bar{D}^0 D^0$ + 8 prongs. The fully reconstructed decay modes are $D^0 \to K^- \pi^+ \pi^0 \pi^0$ and $\bar{D}^0 \to K^+ \pi^+ \pi^- \pi^-$, with all six charged tracks being detected in the spectrometer and all four photons from the π^0 decays detected in the lead glass gamma detection system. The D^0 has momentum 119.0 ± 0.6 GeV/c, x_F = 0.31, length 4.1 ± 0.1 mm and proper lifetime 2.1 ± 0.1 x 10^{-13}s. The $\bar{D}^0$ has momentum 78.5 ± 0.3 GeV/c, x_F = 0.19, length 7.5 ± 0.1 mm and proper lifetime 5.9 ± 0.1 10^{-13}s.

Direct measurements of the D° lifetime using the emulsion technique with ν beam [1,2] or γ beam [3] indicate a value $< 1 \times 10^{-13}$s. We report here the observation of an exceptionally clean, fully reconstructed, unambiguous hadronic event containing a $D^\circ\bar{D}^\circ$ pair. If one accepts the value of the D° lifetime quoted above, then both D° and $\bar{D}^\circ$ in this event are rather long-lived.

The small rapid cycling liquid hydrogen Lexan Bubble chamber LEBC was specially designed and built for the study of short-lifetime particle properties [4]. In a prototype experiment at the CERN SPS, the hadronic production of charm was detected via a topological signal [5]. In order to more fully investigate the production and decay properties of charm particles, LEBC was coupled with the European Hybrid Spectrometer (EHS) [6,7,8] and during several SPS periods immediately prior to the SPS shutdown of June 1980, LEBC was exposed to beams of 360 GeV/c π^- and 360 GeV/c protons. Approximately 1.3 million pictures were taken (equally divided into pion and proton data) with the bubble chamber flash tubes fired by the interaction trigger described elsewhere [5]. This consists of scintillators upstream and downstream of LEBC which detect the incoming beam particle, veto upstream interactions and identify interactions in LEBC by detecting an outgoing multiplicity > 2.

LEBC was equipped with two stero views, both giving spatial resolution $\sim 40\mu$m. The beam included a kicker magnet to avoid background in the pictures coming from early tracks. The spectrometer, a preliminary version of EHS consists of a charged particle momentum analysis stage [6], γ detection using the lead glass walls [8] and a single module of the pictorial drift chamber ISIS (referred to as ISIS1) giving ionisation data for charged particle identification [7]. The triggered pictures are being double scanned and all multi-vertex events checked by a physicist.

In order to set up and test the analysis program chain [9] and to provide data for checking and calibration purposes a small sample of multi-vertex events has been measured using the CERN ERASME system [10]. From this sample, 71 V° decays have been identified as either K°, Λ or $\bar{\Lambda}$. The percentage of V° decays with one or more tracks hybridized(+) is in agreement with that predicted by a Monte-Carlo calculation assuming 100 % hybridization efficiency. The mass distribution for the identified K° events is shown in fig.1(a) and the $p\pi^+$ (and $\bar{p}\pi^+$) mass distribution for the identified Λ(and $\bar{\Lambda}$) in fig.1(b). The K° and Λ ($\bar{\Lambda}$) masses are found to be 498.0 ± 1.0 MeV/c^2 and 1116.5 ± 1.5 MeV/c^2, respectively. For K° and $\Lambda(\bar{\Lambda})$ decays having both tracks hybridized the full

(+) When a track is successfully reconstructed using information from the bubble chamber and from the spectrometer it is said to be hybridized.

widths at half maximum (FWHM) are 6 MeV/c^2 and 4 MeV/c^2, respectively. For decays in which only one track is accepted by the spectrometer for hybridization (the shaded events in fig.1), the momentum of the second track is found by balancing the transverse momentum about the direction of the V°. In this case the resolution deteriorates to 10 MeV/c^2 and 8 MeV/c^2. These values of the measured resolution are consistent with the EHS design measurement precision of $\Delta p/p \sim 1$ % [6]. The γ detection system resolution is also in good agreement with design values [8]. The two photon mass distribution accumulated throughout the experiment shows a clear π° signal with FWHM $\sim$ 20 MeV [11].

The event of interest was selected for the detailed analysis described here because the topological information alone makes it a highly probable charm candidate. It has been measured on three independent measuring devices and all measurements give compatible results. Fig. 2 (a) shows a diagram of the event based on the ERASME digitizations. The event is a 360 GeV/c $\pi^- p$ interaction giving 8 charged tracks and two neutral particles which materialise as 2-prong decay (V2) and 4-prong decay (V4), respectively. Of the six decay tracks, 5 are successfully matched between bubble chamber and spectrometer, the sixth being connected to a spectrometer track with the assumption of a small angle scatter (7.2 ± 0.6 mr) in the bubble chamber exit window which leaves the momentum of the track unchanged, within the error. There are no ambiguities in associating the tracks reconstructed in the spectrometer with those observed in the bubble chamber. Three of the tracks from the production vertex are also successfully hybridized. The momenta and space angles of all these tracks are summarized in table 1.

Four of the six charged decay particles (those labelled A, C, D and E in table 1) reach one of the γ detectors. Their energy release is significantly smaller than the momentum measured in the spectrometer, indicating that none of them are electrons. In addition, the γ detectors identify six showers which are also given in table 1. These can be associated to give three clear π°'s with reconstructed masses of 130 ± 9 MeV/c^2, 134 ± 11 MeV/c^2 and 140 ± 20 MeV/c^2 (+). The momenta and angles of these are also given in table 1. No other $\gamma\gamma$ combination has a recognizable meson mass.

The ISIS1 particle identification information for this event is indicated in table 1. For each track a maximum likelihood fit was performed to the ionisation distribution [12]. The results were then compared with the expected ionisations and computed as a number of standard deviations for each mass hypo-

(+) This π° is composed of 75 and 50 GeV photons. The position of the 75 GeV shower is uncertain because of the late development of the electromagnetic cascade in the lead glass converter. This uncertainty is then reflected in the large error.

thesis. Fig. 2(b) shows the pictorial information from ISIS1 for this event. The labels correspond to those given in table 1. The track information is excellent. All tracks seen in this figure are clearly identified in the spectrometer, without ambiguity. The module used in this experiment is a prototype version of the full ISIS [7]. It has < 60 active sense wires as compared with the 320 wires of the final chamber. The ionisation resolution is thus limited by sampling statistics and should be taken as corroborating evidence for mass assignments derived from kinematic hypotheses rather than definitive identification. This is reflected in the data of table 1.

If the 92.5 GeV/c negative particle from the V2 is a K^-, the 18.0 GeV/c positive particle is a π^+ and the 5.3 GeV/c π° and 3.2 GeV π° are associated with the decay, then the combination $K^-\pi^+\pi^\circ\pi^\circ$ gives a mass of 1.857 ± 0.022 GeV/c^2 in good agreement with the D° mass. Furthermore, the vector sum of outgoing momenta points, well within errors, at the production vertex. The ISIS1 data is consistent with this solution. The decay length and momentum of the D° are 4.1 ± 0.1 mm and 119.0 ± 0.6 GeV/c, respectively.

If the 16.1 GeV/c positive particle from the V4 is a K^+ and the other three particles are pions, the combination $K^+\pi^+\pi^-\pi^-$ gives a mass of 1.862 ± 0.009 GeV/c^2, also in excellent agreement with the D° mass. Again the vector sum of the four charged particles points at the production vertex and the ISIS1 data is consistent with their assigned mass. The decay length and momentum of the $\bar{D}^\circ$ are 7.5 ± 0.1 mm and 78.5 ± 0.3 GeV/c, respectively.

No other combinations (i.e. assuming different mass assignments and with and without associated π°'s) give any recognizable strange or charm masses. Table 1 gives the momenta and angles of all measured particles in the event.

The production characteristics are as follows : for the D°, x_F = 0.31 and p_T = 0.64 GeV/c; for the $\bar{D}^\circ$, x_F = 0.19 and p_T = 0.63 GeV/c. Neither D° nor $\bar{D}^\circ$ can be associated with any reconstructed production π to make a D^* mass. It is noteworthy that 90 % of tha available energy of the event is contained in the three particles D°, $\bar{D}^\circ$, π°. The effective mass of this $D^\circ\bar{D}^\circ\pi^\circ$ system is 5.11 GeV/c^2 and the 3 two-body masses are $M(\bar{D}^\circ D^\circ)$ = 3.96 GeV/c^2, $M(D^\circ\pi^\circ)$ = 2.86 GeV/c^2, $M(\bar{D}^\circ\pi^\circ)$ = 3.04 GeV/c^2.

We conclude that the event contains the decays $D^\circ \to K^-\pi^+\pi^\circ\pi^\circ$ and $D^\circ \to K^+\pi^+\pi^-\pi^-$ with lifetimes of (2.1 ± 0.1) x 10^{-13}s and (5.9 ± 0.1) x 10^{-13}s, respectively. Previous direct measurements of the D° mean lifetime give $0.53 \,^{+\,0.57}_{-\,0.25}$ x 10^{-13}s [1], $1.01 \,^{+\,0.43}_{-\,0.27}$ x 10^{-13}s [2] and $0.58 \,^{+\,0.8}_{-\,0.2}$ x 10^{-13}s [3]. The emulsion technique used in [1,2,3] is quite different from the present technique and scanning biasses and event losses are not the same. In particular, our detection efficiency for particle lifetimes < 10^{-13}s is small [5].

Nevertheless, the present event is hardly consistent with the previous lifetime measurements and suggests that a longer mean lifetime applies for the D°.

ACKNOWLEDGEMENTS

We would like to acknowledge the SPS operating team, the invaluable assistance of Niels Doble and the EA group, and the support and understanding of Jurgen May - the SPS coordinator. We are grateful for the technical assistance of the entire LEBC/EHS team. In an experiment such as this the importance of the scanning work cannot be overstated; we would like to thank the scanners in all the collaborating laboratories. We also acknowledge the initial help in data taking from those of our colleagues who have not participated in the analysis.

REFERENCES

[1] D. Allasia et al., Nucl. Phys. B176 (1980) 13

[2] N. Ushida et al., Phys. Rev. Lett. 45 (1980) 1049
K. Niu, "Charmed particle production and decay lifetimes". Communication to the International Conference on High Energy Physics, Madison, U.S.A. (1980)

[3] M.I. Adamovitch et al., CERN/EP 80-197 (Rev), submitted to Phys. Lett. B (Dec. 1980).

[4] A. Hervé et al., "A rapid cycling hydrogen bubble chamber with high spatial resolution to visualise charm decays", Proceedings of the Conference on Miniaturization in High Energy Physics, Pisa (1980)

[5] W. Allison et al., Phys. Lett. 93B (1980) 509

[6] W. Allison et al., EHS Part A; Proposal CERN/SPSC 76-43

[7] W. Allison et al., EHS Part B; Proposal CERN/SPSC 78-91;
W. Allison et al., CERN/EP/EHS/PH 78-10

[8] G.A. Akopjianov et al., EHS Part C, Proposal CERN/SPSC 77-44

[9] F. Bruyant et al., GEOHYB EHS Software Notes (1979, 1980, 1981)

[10] W. Krischer, "Scanning and Measuring of EHS film at CERN", Proceedings of Second Vezelay Workshop on EHS, CERN/EP/EHS/PH 80-2

[11] B. Powell et al., The EHS lead glass calorimeters and their laser based monitoring system, to be submitted to Nucl. Instrum. and Meth. (1981).

[12] W. Allison et al., to be submitted to Nucl. Instrum. and Meth.

TABLE 1

Summary of all reconstructed particle parameters, ISIS1 ionization data exposed as a number of standard deviations (σ) for each mass hypothesis and D^0, $\bar{D}^0$ parameters (see text). All angles are given with respect to the incident beam direction and transverse momenta, p_T, with respect to the appropriate incident particle. The π^0 quantities are the result of kinematic fits.

Track Label	Particle	P (GeV/c)	P_T (GeV/c)	λ (mr)	ϕ (mr)	ISIS1 particle identification			
						< 2σ	2-3σ	3-4σ	> 4σ
A	K^-	92.5 ± 0.5	0.297 ± 0.015	− 3.1 ± 0.1	7.0 ± 0.1	e,π,K,p	−	−	−
B	π^+	18.0 ± 0.2	0.113 ± 0.006	− 9.2 ± 0.3	0.6 ± 0.1	e,π	−	−	K,p
	Y	4.75 ± 0.12	0.040 ± 0.002	6.9 ± 0.3	− 7.5 ± 0.2	−	−	−	−
	Y	0.48 ± 0.06	0.037 ± 0.005	73.7 ± 1.5	47.3 ± 2.0	−	−	−	−
	π^0	5.28 ± 0.11	0.096 ± 0.004	13.4 ± 0.4	− 2.2 ± 0.3	−	−	−	−
	Y	2.89 ± 0.15	0.042 ± 0.004	− 19.5 ± 1.0	− 71.2 ± 1.0	−	−	−	
	Y	0.34 ± 0.05	0.041 ± 0.006	− 25.3 ± 2.0	63.7 ± 1.5	−	−	−	−
	π^0	3.23 ± 0.13	0.203 ± 0.010	− 20.1 ± 0.3	− 56.8 ± 1.6	−	−	−	−
C	K^+	16.1 ± 0.2	0.387 ± 0.007	22.5 ± 0.3	− 15.6 ± 0.1	e,π,K	p	−	−
D	π^+	7.6 ± 0.1	0.206 ± 0.004	23.2 ± 0.4	− 18.9 ± 0.2	π	e,K	p	−
E	π^-	35.7 ± 0.1	0.193 ± 0.008	5.6 ± 0.2	8.2 ± 0.1	π	K	p	−
F	π^-	19.2 ± 0.3	0.412 ± 0.010	− 8.1 ± 0.5	18.1 ± 0.1	e,π,K	p	−	−
G	$\pi^+/K^+/p$	12.9 ± 0.1	0.400 ± 0.004	2.9 ± 0.3	− 31.7 ± 0.2	π,K,p	−	e	−
H	π^-	6.4 ± 0.1	0.256 ± 0.004	− 24.5 ± 0.5	31.4 ± 0.3	π	e	K	p
I	π^-	6.4 ± 0.1	0.333 ± 0.004	47.6 ± 0.5	− 21.4 ± 0.3	π	e	K	p
	Y	75.0 ± 3.0	0.070 ± 0.041	4.2 ± 0.5	5.0 ± 0.2	−	−	−	−
	Y	50.5 ± 3.0	0.068 ± 0.015	4.1 ± 0.2	7.3 ± 0.2	−	−	−	−
	π^0	125.2 ± 4.1	0.907 ± 0.049	4.2 ± 0.3	5.9 ± 0.1	−	−	−	−

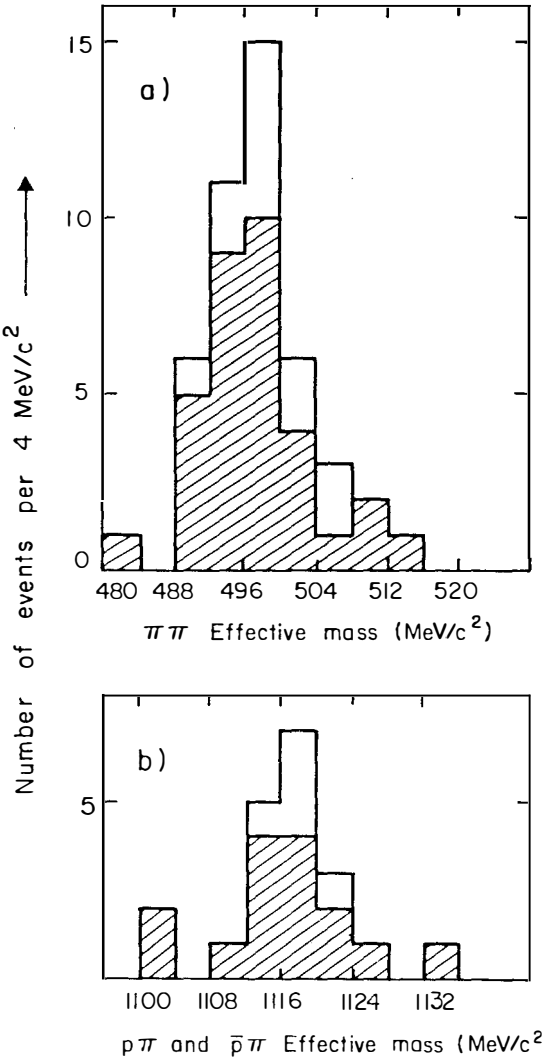

FIG. 2

Fig. 1a : ππ effective mass distribution for the V° sample described in the text. The shaded region shows events for which only one of the two decay tracks has been successfully reconstructed (see text).

Fig. 1b : $p\pi^-$ and $\bar{p}\pi^+$ effective mass distribution for the V° sample described in the text. The shaded region shows events for which only one of the two decay tracks has been successfully reconstructed (see text).

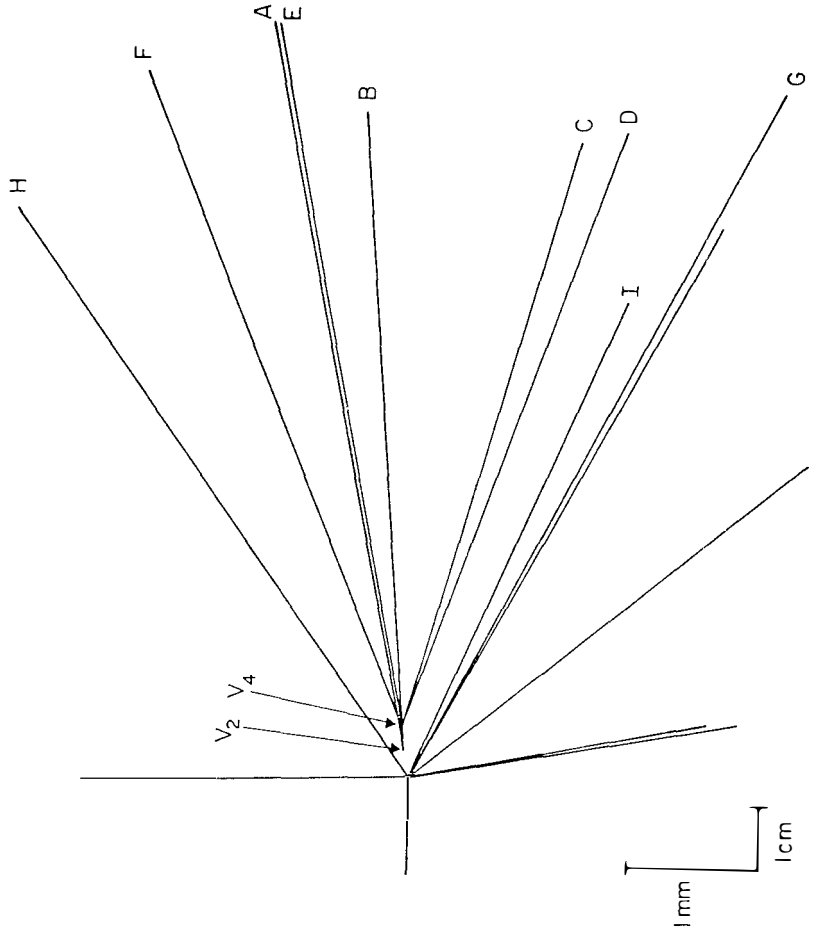

FIG. 1a

Fig. 2 : The event discussed in the text.The track labels are common to fig. 1(a), (b) and to table 1.

Fig. 2a : Sketch of the event based on the measuring machine digitizations. It should be noted that the transverse scale is greatly magnified.

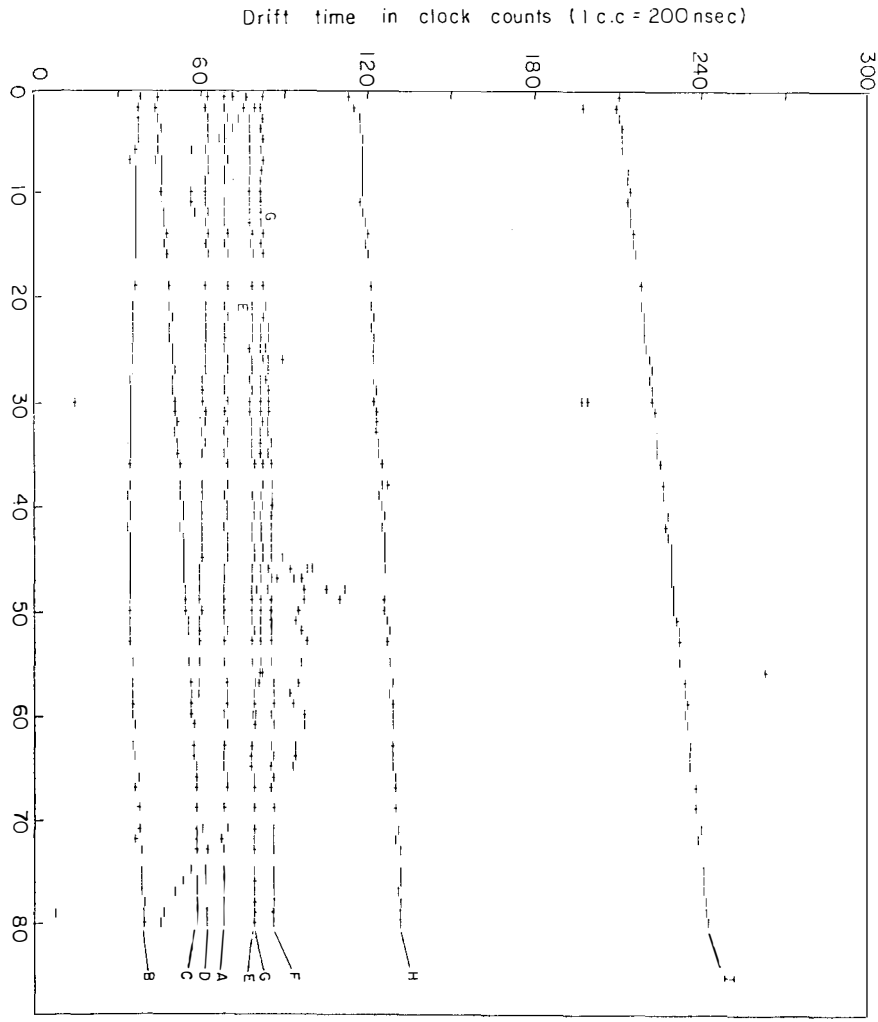

Fig. 2b : The ISIS1 pictorial information for the event. The vertical axis is drift time and the horizontal axis gives the sense wire number.

CHARM PRODUCTION IN HADRONIC INTERACTIONS*

Stanley G. Wojcicki†
CERN, Geneva, Switzerland and Section Physik der Universität, München, FRG.

ABSTRACT

The status of bound and unbound charm production in hadronic interactions is reviewed. The J/ψ production data is now quite extensive and can be understood reasonably well in terms of the gluon-gluon fusion mechanism. On the other hand the experimental situation on the production of open charm is still relatively confused. The lower energy data, $\sqrt{s} \lesssim 30$, is reasonably consistent with central production that one might expect from standard lst order QCD diagrams. The ISR data, however, indicate a much more forward production and a cross section that is larger by more than an order of magnitude from what might be expected on the basis of SPS and Fermilab measurements.

†Alexander von Humboldt fellow, on sabbatical leave from Stanford University.

INTRODUCTION

This review attempts to summarize the status of bound and unbound charm production in hadronic interactions. The data on bound states (mainly J/ψ production) is now quite rich and lends itself well to detailed comparison with various phenomenological models. This is mainly due to the fact that the decay modes $J/\psi \to e^+e^-$ or $\to \mu^+\mu^-$ give a relatively clean signature, have a relatively high branching ratio, and are capable of being observed with high detection efficiency.

This situation should be contrasted with the unbound charm production. There the experimental problems are numerous and severely limit one's ability to form a coherent picture out of the existing data. The most serious problem is the very poor signal to noise ratio, necessitating frequently severe cuts on the data and restrictions to a limited kinematical region to pick out the charm signal out of the dominant hadronic background. This in turn makes the subsequent interpretation of the data in terms of total cross-section or different production models rather difficult. Because of the importance of these experimental problems, I would like to start this review with a brief discussion of experimental techniques and theoretical uncertainties that limit our understanding of the data.

We can distinguish between 3 different classes of experimental techniques that can be used to study charm production. They all have their advantages and their limitations, and it is worthwhile to keep these in mind when looking at the data.

a) Invariant mass peak technique. This method certainly provides the cleanest way to identify production of specific states (e.g. Λ_c, F^+, D^o, etc.) but suffers generally from poor signal to noise ratio due mainly to the rapidly growing number of combinatorials as the masses increase and hence multibody decays become more prevalent. Furthermore these experiments for a variety of reasons explore only a very limited region of phase space.

b) Study of charm production through its semileptonic decay modes by detecting one of the leptons. This method is capable of high statistics (if μ is detected) or very good signal to noise ratio (beam dump experiments), but the interpretation of the data is more difficult. Not only production features are somewhat washed out, but one effectively integrates over all charm production weighed by their semileptonic branching ratio.

c) Search for short tracks. The big shortcoming here so far has been low event rate due mainly to the necessity of using visual scanning techniques. The vigorous development work in electronic techniques that is going on at present might, however, improve this considerably in the future. The method

is potentially capable of bias-free identification of short lived particles over a full 4π solid angle.

I should finally mention limitations on interpretation of the data due to our lack of knowledge about other relevant input. The first one concerns the different lifetimes[1] (and hence different semi-leptonic branching ratios) of charmed particles. Due to this difference (which appears to be close to an order of magnitude for D^o and $D^{\pm}$) one must know which charm particles are produced, before one can unambigously translate the lepton experimental results into total cross-sections. The second point concerns the A dependance. That dependance must be known before heavy target experiments can be compared with the hydrogen experiments. It has been traditional (and this procedure will be followed in this review) to assume $A^{1.0}$ dependance for charm production, in analogy with J/ψ production. The question cannot be resolved definitively, however, except by direct measurements which so far have not been performed.

CHARM PRODUCTION AT SPS AND FERMILAB ENERGIES

Most of the information in this energy region comes from 3 sources, i.e.

a) Beam dump experiments observing neutrinos via their interactions.

b) Single prompt charged lepton experiments.

c) Short track experiments.

We shall summarize next the results from each set of these experiments. The neutrino beam dump experiments have now gone through two generations, and a third generation of experiments is at present being planned. Very briefly, these experiments dump the primary proton beam in a heavy target, so that the effective decay path for π's and K's is reduced as close to zero as possible. The majority of neutrino interactions observed downstream of the dump can then be expected to come from prompt sources, i.e. decays of particles whose decay length is short compared to the interaction length. The signal of electron neutrinos is almost totally free of contamination because of relatively low $\pi \to e$ and $K \to e$ branching ratios; the signal of muon neutrinos from prompt sources, however, must be observed by extrapolation, i.e. performing the experiment with several target densities and extrapolating to infinite density. Alternatively, one can attempt to calculate the non-prompt ν_μ contamination by using the known π and K yields.

The most recent experimental results come from 3 different groups, all running simultaneously with their detectors arranged serially one behind the other. The results can be summarized as follows:

1) All 4 kinds of prompt ν's have been observed (ν_μ, ν_e, $\bar{\nu}_\mu$, $\bar{\nu}_e$)

2) Production features are reasonably consistent with central production, i.e.,

$$\frac{d\sigma}{dx} \propto (1-x)^n \quad \text{with} \quad 3 \lesssim n \lesssim 5$$

3) The total charm production cross section estimates[2] from the 3 groups are:

BEBC	$11 < \sigma_{TOT} < 22\mu b$
CDHS	$7 < \sigma_{TOT} < 14\mu b$
CHARM[3]	$\sigma_{TOT} = 12 \pm 4\mu b$

A 8% average semi-leptonic branching ratio was assumed.

4) Some anomalies in ν_μ/ν_e and $\nu_\mu/\bar{\nu}_\mu$ ratios have been observed but situation here is confused. More will be said on this subject a little later.

A series of experiments studying presumably the same kind of physics, but using quite different experimental techniques have been performed at Fermilab. This program is still in progress and most recent results have been presented at this Moriond Conference by J. Ritchie. The technique here is to study production of prompt muons from a hadron beam incident on an instrumented beam dump. The density of the beam dump can be varied to allow extraction of the prompt signal by extrapolation to infinite density. The other important features of the experimental apparatus are its very large solid angle, allowing rejection of most of the $\mu^+\mu^-$ and calorimetry capability in the target, permitting a measurement of average energy carried off by the neutrinos. The results of this program can be summarized as follows:

1) production features reasonably consistent with central production.
2) no evidence for diffractive production.
3) reasonable agreement with neutrino beam dump experiments.
4) the reported total cross sections from several different subsets of the data are (assuming 8% average muonic branching ratio)

High p_T, single μ[4]	$\sigma_T = 30 \pm 8\mu b$
High p_T, 2μ + missing energy[5]	$\sigma_T = 15 \pm 5\mu b$
$P > 8$ GeV/c, no p_T cut[6]	$\sigma_T = 22 \pm 9\mu b$
High p, no p_T cut[7]	$\sigma_T = 25 \pm 10\mu b$

Essentially all of the data from the short track experiments came from "engineering" runs designed to test the feasibility of these new experimental techniques. Much better experiments are in progress or planned for the near

future. Even these first results, however, provide some new and interesting insight into charm production by hadrons. The total cross section estimates from the different experiments are:

a) high resolution streamer chamber[8]
   400 GeV neutrons - $\sigma \lesssim 40\mu b$
b) emulsion, 400 GeV protons[9] - $\sigma = 30 \pm 20\mu b$
c) emulsion, 400 GeV protons[10] - $\sigma = 160 \pm 40\mu b$
d) high resolution bubble chamber[11] (LEBC)
   350 GeV π^- - $\sigma \lesssim 35\text{-}40\mu b$
e) emulsion chamber,[12] 340 GeV π^- - $\sigma \lesssim 44 \pm 22\mu b$.

As can be seen from above, all of these experiments, although quite limited in statistics, seem to be consistent with a cross section of about 40μb. Whether the difference between this number, and a value of 15-20μb, indicated by previously discussed experiments, is significant remains an open question at this time.

We should finally mention 3 other experiments that observe a positive charm signal, namely:

a) observation of single prompt electrons[13] in TST in BEBC with a beam of 70 GeV π^- yields $\sigma \lesssim 19 \pm 11\mu b$.

b) observation of D^* production[14] by 200 GeV π^-, coupled with some assumptions about the dynamics of charm production gives $\sigma \lesssim 10 \pm 4\mu b$.

c) finally a forward production experiment observes a $D^\pm$ production[15] in the $K\pi\pi$ mode with a $\sigma \lesssim (6 - 10) \pm 4\mu b$. More recent results from this experiment have been presented at this Conference by Cooper.

To summarize the data discussed so far, all the experiments are quite consistent with central $D\bar{D}$ production with σ in the range of 15 - 40μb, the last experiment being the only one to indicate sizable forward production. In addition, within the framework of the limited statistical accuracy discussed above, there appears no need for any significant cross section difference between nucleons and pions.

However, several recent results cast some doubt as to whether this simple picture is sufficient to account for all the experimental data. I would like to discuss next three of these results, which though far from definitive and often in disagreement with other data, throw some question on the simple interpretation put forth above.

a) The CHARM collaboration[3] in their beam dump experiment sees a 2.5σ excess of no-μ events for shower energies $2 < E_{SH} < 20$ GeV, above what one would expect from the $D\bar{D}$ central production model. (Fig. 1) The other beam dump

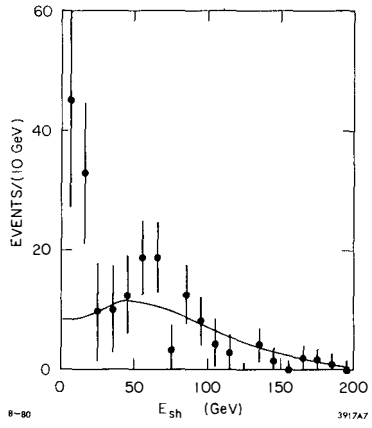

Fig. 1. Visible energy distribution of no-μ events from CHARM experiment. The curve gives the expected contribution to electron neutrino interactions from $D\bar{D}$ decay.

experiments are unable to investigate this low shower energy region and thus are able neither to support nor contradict this result. There is no obvious mechanism to explain this phenomenon, if true.

b) All the beam dump experiments appear to favor a ν_e/ν_μ ratio lower than unity. These results are summarized in Table I. Different collaborations can obtain slightly different values for this ratio, depending on whether they use the extrapolation technique to obtain the ν_μ rate, or whether they obtain it by subtracting from the observed rate the calculated non-prompt background. One should emphasize, here, however the probability that systematic errors in all 3 experiments are quite similar and thus results are not really completely independent.

c) The final question concerns the point whether the lepton antilepton ratio is consistent with unity. The results from all the beam dump experiments and the prompt muon experiments are summarized in Table II. Clearly, the most significant departure from unity occurs for the CDHS extrapolation result. The discrepancy between the various beam dump experiments is due mainly to the low density μ^+ point as can be seen from Fig. 2.

Table I

ν_e/ν_μ Ratios from CERN Beam-Dump Experiments

Group	ν_e/ν_μ Ratio	Statistical Error	Systematic Error	Method
CDHS	0.77	±0.18	±0.24	Extrapolation
CDHS	0.58	±0.07	±0.19	Subtraction
CHARM	0.48	±0.12	±0.10	Subtraction ($CC\nu_e$ from prod model)
CHARM	0.49	±0.21		Extrapolation ($CC\nu_e$ from prod model)
CHARM	0.44	±0.11	±0.10	Subtraction ($CC\nu_e$ directly identified)
BEBC	0.59	$^{+0.35}_{-0.21}$		Subtraction

Table II
Lepton charge ratio from different experiments

Group	Ratio	Value	Statistical Error	Systematic Error	Method
CDHS	ν_μ/ν_μ	0.12	±0.20	±0.12	Extrapolation
CDHS	$\bar{\nu}_\mu/\nu_\mu$	0.56	±0.09	±0.13	Subtraction
CHARM	$\bar{\nu}_\mu/\nu_\mu$	1.3	±0.5	$^{+0.4}_{-0.2}$	Subtraction
CHARM	$\bar{\nu}_\mu/\nu_\mu$	1.8	±1.1		Extrapolation
BEBC	$\bar{\nu}_\mu/\nu_\mu$	0.75	±0.32		Subtraction
BEBC	$\bar{\nu}_e/\nu_e$	0.76	±0.35		Subtraction
CIT-Stanford	μ^-/μ^+	1.3	±0.4		Extrapolation
CCFRS	μ^-/μ^+	0.8	±0.3		Extrapolation

I should point out that the departure of ν_e/ν_μ ratio from unity would indicate something new that is quite fundamental. On the other hand, lepton/anti-lepton ratio could depart from unity for a variety of rather simple reasons, like Λ_c production or unequal D^+/D^- production cross-section. Clearly, experiments of higher accuracy are needed to answer some of these questions.

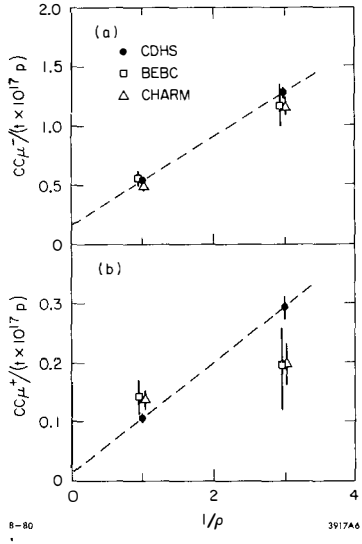

Fig. 2. Comparison of charged current μ event rates as a function of density for the 3 CERN beam dump experiments: a) μ^-, b) μ^+.

CHARM PRODUCTION IN THE ISR ENERGY RANGE

According to the standard QCD diagrams,[16] the charm production should increase by only a modest factor (∿ 3) between Fermilab/SPS energies and the ISR energies. This is illustrated in Fig. 3 where we show the gluon-gluon and quark-antiquark fusion mechanism predictions as a function of incident energy for both protons and antiprotons. In addition we show the combined contributions of both mechanisms for protons, π's, and K's. The surprising thing about ISR results discussed below is that they give a cross section that is

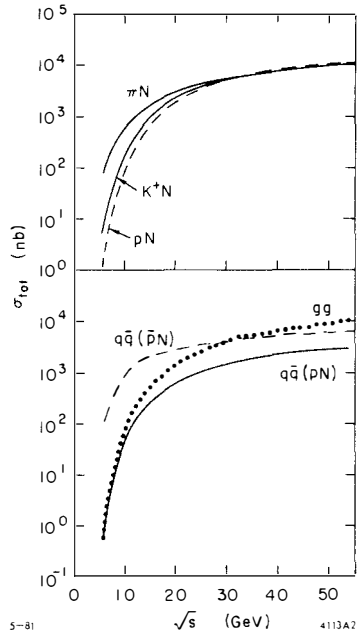

Fig. 3. Prediction of the charm cross-section as a function of energy on the basis of gluon-gluon and quark-anti-quark fusion mechanisms.

significantly larger than expected and the x dependance that is considerably flatter than one would expect from central production.

I shall start out by reviewing the data on Λ_c production. There are basically 7 experimental measurements on this topic, i.e.

a) 3 measurements by groups who trigger on a relatively central electron and identify the Λ_c by its decay mode into $K^-p\pi^+$. In all cases a signal is seen in association with the e^-, but no Λ_c peak is seen when one triggers on e^+. A couple of those measurements are illustrated in Figs. 4 and 5.

b) 3 measurements by groups[20, 21, 22] who look at a relatively fast K^- and then reconstruct the mass of the $K^-p\pi^+$ system. These measurements obtain the Λ_c cross section at rather large values of x. A typical spectrum (from the Lamp Shade Magnet experiment) is illustrated in Fig. 6.

c) Finally the UCLA-Saclay collaboration[22] has observed a peak in the $\Lambda 3\pi$ system in the region of the Λ_c mass.

The first 6 of these measurements can be compared directly (Fig. 7), since they all observe the same decay mode, i.e. $K^-p\pi^+$, and thus the uncertainty in the branching ratio drops out. There is still considerable model dependance involved in displaying these points because of finite Δx region explored and the requirement of an electron trigger for some of these data. In the case of electron-associated points, the assumptions made are that the electrons come from a centrally produced $\bar{D}$ with a branching ratio of 8-10% (the exact values used in the 3 experiments are 10, 8, and 8.5%). An assumption of $\frac{d\sigma}{dx}(\bar{D})$ = constant tends to raise the calculated cross-section by close to an order of magnitude.

It should be clear from Fig. 6 that any total cross-section for Λ_c

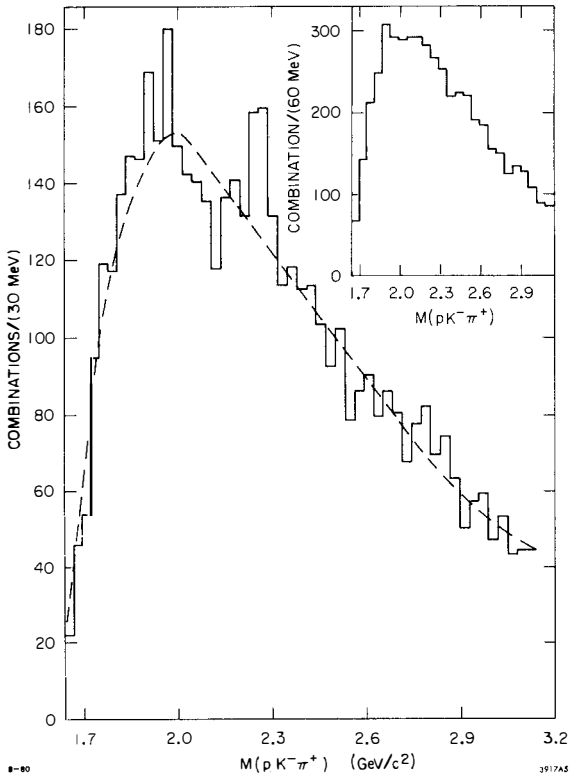

Fig. 4. $K^-p\pi^+$ spectrum from the SFM experiment obtained with the e^- trigger. Insert shows the data obtained with the e^+ trigger.

production extracted from these data will be subject to great uncertainties. To obtain some quantitative estimate, however, we shall assume a flat x dependance up to $x \approx 0.7$ with $B \frac{d\sigma}{dx} \approx 5\mu b$. σ_{TOT} will then be given by $\sigma_{TOT} = 2 \cdot 0.7 \cdot B \frac{d\sigma}{dx}/B \approx 320$ μb if we take $B = 2.2 \pm 1\%$ for the $K^-p\pi^+$ mode.

We thus appear to have a rise in the total charm cross-section due to Λ_c alone (D and F contributions are still to be added) of at least an order of magnitude between $\sqrt{s} \gtrsim 27$ and $\sqrt{s} \approx 60$, considerably more then predicted by the fusion mechanisms. On the other hand, one cannot emphasize too strongly the many uncertainties involved in this comparison. Probably the two most important questions deal with the A dependance, which could be considerably flatter for the diffractive production, and with the Λ_c semileptonic branching ratio. A low value for this last parameter would decrease proportionally the

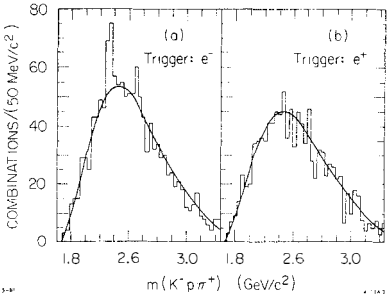

Fig. 5. $K^-p\pi^+$ spectra from the Bologna-CERN-Frascati experiment for both the e^- and e^+ triggers.

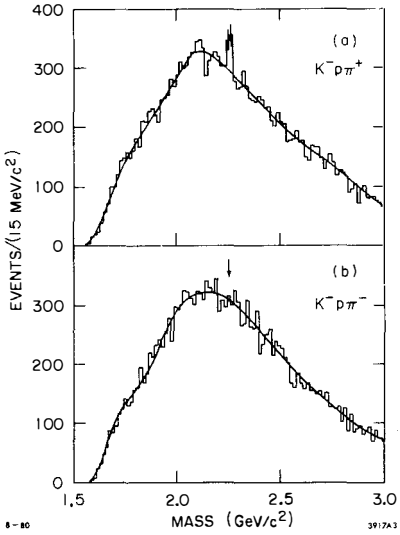

Fig. 6. $K^-p\pi^+$ and $K^-p\pi^-$ mass spectra from the LSM experiment obtained with the K^- trigger.

sensitivity of the CERN beam-dump and Fermilab prompt muon experiments.

The other piece of evidence, however, that argues for some new phenomenon at high energy is the x dependance of the data. The predictions of the fusion mechanisms are displayed in Fig. 8. They are clearly steeper as a function of x by several orders of magnitude than the data, and within the framework of that model cannot be reconciled by a mere adjustment of parameters. Thus it appears that one must invoke new mechanism(s) at the ISR energies to account for the large cross-sections and relatively flat x-dependance.

I would like to finally summarize the data relevant to D production in the ISR energy domain. The SFM group[24] has obtained a positive $D^+ \to K^-\pi^+\pi^+$ signal in forward production by utilizing the K^- trigger, and a positive $D^o \to K^-\pi^+$ signal near x = 0 (Fig. 9) by looking at events associated with an electron.[25] The LSM group has also looked for various signatures of D mesons,[26] but no statistically significant effect has been found. Their most stringent 95% confidence upper limits, the 2 positive D signals from the SFM experiment, as well as the value extracted from an older eμ/ee coincidence experiment,[27] are all displayed in Fig. 10. The last experiment assumed an equal 10% semileptonic branching ratio for both neutral and charged D's. Unequal values, as indicated by recent data, and/or predominant $D^o(\bar{D}^o)$ production in the x region investigated, could however, significantly alter the interpretation of the data. Extraction of total D cross section is clearly

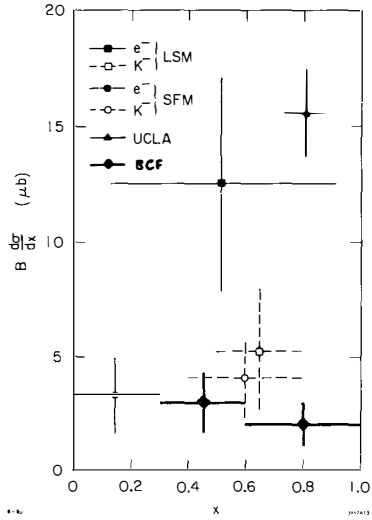

Fig. 7. Summary of the ISR $\Lambda_c \to Kp\pi^+$ production cross-section data.

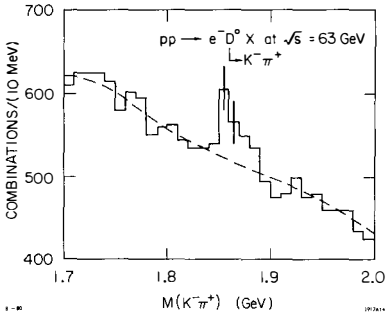

Fig. 9. $K^-\pi^+$ mass spectrum from the SFM experiment obtained with the e^- trigger. The smooth curve shows the background estimate obtained with the e^+ trigger.

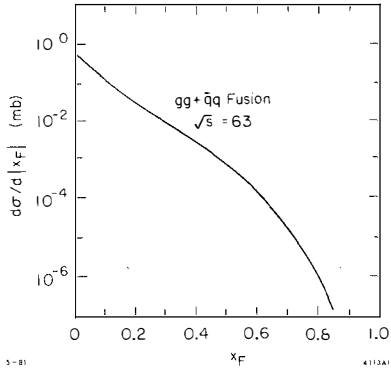

Fig. 8. Prediction of the x-dependance for charm production from the gluon gluon fusion mechanism.

beset with all kinds of uncertainties; if we take the 2 SFM points literally, however, we obtain a total D production cross-section of about 500 μb.

In conclusion, we can state that the total charm production cross-section in the ISR range is in the vicinity of 1 mb, but that number is probably uncertain by at least a factor of 2 or 3. The x dependance, especially for Λ_c, is quite flat, and these 2 factors argue for new production mechanisms in addition to the fusion processes. We might finally end by remarking that the "anomalously high" e/π ratio observed at the ISR in the low x and low p_T region, would have difficulty accommodating a charm cross section higher than several hundred microbarns.

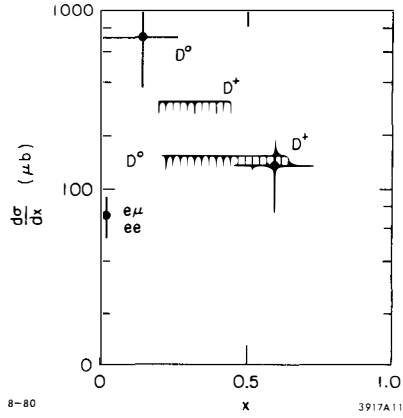

Fig. 10. Summary of the ISR D^0 and D^+ data. The shaded bars correspond to the upper limits from the LSM experiment.

J/ψ HADROPRODUCTION

The existence of the $\psi \to \mu^+\mu^-$ and $\psi \to e^+e^-$ decay modes with a relatively large branching ratio has provided the experimentalists with a rather straightforward and easy (as compared to open charm) means of studying the production of J/ψ particles. The strong constraint imposed by the 2 body decay mode, lack of combinatorial problem, and the high possible acceptance for this decay mode, have all been quite helpful in accumulation of a great deal of data on J/ψ hadroproduction and subsequent J/ψ decay. The data by now is quite extensive and lends itself readily to detailed comparisons with the various phenomenological models. These comparisons have been extensively summarized in a recent review article by Phillips.[28] Accordingly, I shall limit myself here only to a brief discussion of various experimental results that have a bearing on the production mechanism. Specifically, I would like to discuss production cross sections as function of energy and incident particle, x dependance, information on possible intermediate states, and finally the decay angular distributions.

The dependance of the cross section on the nature of the incident beam is interesting because it can provide information on the relative importance of the gluon-gluon vs quark-antiquark mechanisms. In general, the gluon spectrum is expected to be softer than the valence quark spectrum, and since $M^2 = sx_1x_2$, we would expect production through valence quark fusion to be the dominant mechanism at low energy. Since that mechanism can contribute to the J/ψ production in $\bar{p}p$ collisions, but not in pp collisions, we would expect the latter to have a significantly lower cross section at lower energies. The ratio of these 2 cross-sections[29] is plotted in Fig. 11. It shows the anticipated behavior at the lowest energy and a slow rise in the relative importance of the proton production cross section. The latter feature can be interpreted as the growing importance of the gluon-gluon fusion mechanism with the rising energy.

The same conclusions can be reached by comparing various meson nucleon J/ψ production cross sections. At 40 GeV,[29] $\sigma_{K^+}/\sigma_{K^-} = 0.29 \pm 0.07$, which can

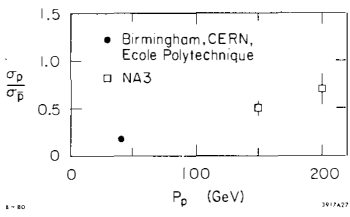

Fig. 11. Ratio of proton induced to antiproton induced inclusive J/ψ production as a function of incident energy.

be understood by the inability of $\bar{s}$ antiquark in K^+ to annihilate with any of the nucleon quarks; on the other hand, the antiquark in K^-, $\bar{u}$, can give rise to the process $\bar{u}u \to J/\psi$. As might be expected from these arguments, the π^+/π^- cross section ratio on nucleons is consistent with unity.

The x_F distributions in J/ψ production provide another interesting insight into the production mechanism. Those distributions have been studied by the WA11 collaboration[30] at CERN for 150, 175, and 185 GeV π^-p interactions, and are displayed in Fig. 12. For the quark-antiquark fusion mechanism, we

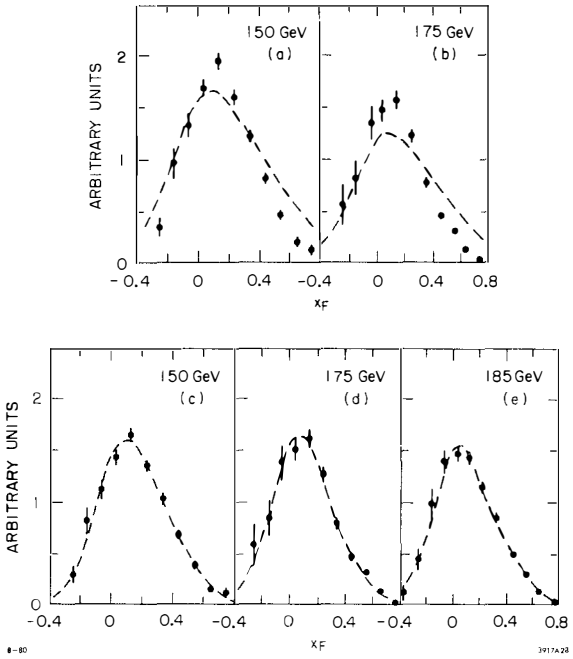

Fig. 12. x_F distribution for J/ψ production compared with the quark-antiquark fusion predictions (a and b) and gluon-gluon fits (c, d, e).

have very specific predictions, determined entirely by the pion and nucleon structure functions. Those predictions are compared with the data in the top two histograms in Fig. 12 and show that the agreement is quite poor. On the other hand if one fits the data to the gluon-gluon fusion mechanism, with gluon distribution having a functional form

$$ng_{\pi}(\eta) \approx (1-x)^{m}$$

$$ng_{N}(\eta) \approx (1-x)^{n}$$

one obtains quite good agreement (see bottom three histograms) and reasonable values for the exponents, i.e. $m = 2.3 \pm 0.3$ and $n = 5.1 \pm 0.6$.

An interesting question associated with the J/ψ production, is what fraction of these states are produced via intermediate χ state, followed subsequently by the radiative decay $\chi \rightarrow J/\psi + \gamma$. The gluon-gluon fusion mechanism would tend to favor intermediate χ production. In addition if a substantial fraction of J/ψ is produced via this intermediate state, this would partly explain the very high ψ/ψ' production ratio that has been observed experimentally.

Several experiments have looked for γ rays associated with the J/ψ particle with a view to answering the question posed above. The results of the most recent experiments are summarized in Table III. Except for the earliest

Table III
Results on searches for γ's associated with J/ψ

Group	Reference	Reaction	Energy ($\sqrt{s}$)	Observed fraction
A. G. Clark et al.	31	pp	55 GeV	$15\ ^{+10}_{-15}\%$
C. Kourkoumelis et al.	32	pp	62 GeV	$47 \pm 8\%$
T. B. W. Kirk et al.	33	$\pi^- p$	20 GeV	$70 \pm 28\%$
WA11 (calorimeter)	34	$\pi^- p$	17 GeV	$36 \pm 5\%$
WA11 (spectrometer)	34	$\pi^- p$	17 GeV	$31 \pm 6\%$

measurement, the agreement is reasonable and indicates a fraction in the neighborhood of 40%. Furthermore, different energies and different kinematical regions explored in different experiments, can certainly influence this comparison. The majority of these experiments observe only a broad peak in the vicinity of the 3.5 GeV for the mass of the $J/\psi + \gamma$ system and are unable to resolve the 3 potentially contributing χ states, i.e. 0^{++} (3.415 GeV), 1^{++} (3508 GeV), and 2^{++} (3.554 GeV). Because of its low $\chi \rightarrow J/\psi + \gamma$ branching ratio, the first state is not expected to contribute strongly; furthermore, the 2^{++} production is strongly favored on theoretical grounds over the 1^{++} production.

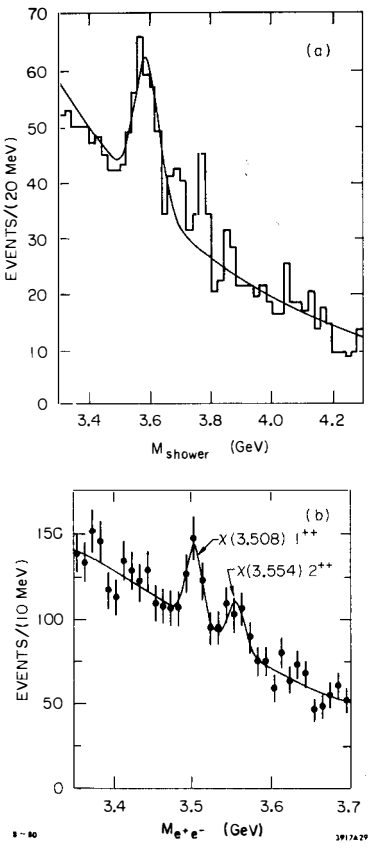

Fig. 13. Mass spectrum of the $J/\psi + \gamma$ system from the WA11 experiment. The photon measurements came from $\gamma \to e^+e^-$ conversions.

The first successful separation of the peaks was achieved by the WA11 collaboration (Fig. 13) by studying the e^+e^- pairs produced by conversion of the γ's either in the production target or the downstream scintillators and chambers. From the observed production rates and the known radiative branching ratios, they conclude that the production cross section rate is

$$\sigma_{2^{++}}/\sigma_{1^{++}} = 1.4 \pm 0.9$$

The decay angular distribution of the J/ψ particle can provide additional information on the production process. On general grounds, this distribution has to be of the form

$$\frac{d\sigma}{d\cos\theta} = 1 + \lambda \cos^2\theta$$

and it is the value of λ that sheds light on the production mechanism. Thus for example, the light quark annihilation directly into J/ψ must give a value of λ around unity in contrast with experimental observations that generally find λ to be consistent with 0, i.e. an isotropic angular distribution. A detailed study of this decay was performed by the NA3 collaboration[35] in π^-p interactions at 150 GeV. They find $\lambda = 0.05 \pm 0.07$; thus light quark annihilation is either relatively unimportant at these energies, or else proceeds via an intermediate state, with a resultant washout of the original helicity information.

SUMMARY AND CONCLUSIONS

One can hope that the relatively large mass of the charmed quarks will make QCD perturbative calculations meaningful. Accordingly there has been great interest in comparing the predictions obtained from the simplest QCD diagrams with the actual data on bound and unbound charm production. The J/ψ data allow

meaningful comparisons and the emerging picture is quite consistent with the calculations. The quark-antiquark annihilation is important at low energies but as $\sqrt{s}$ increases, the gluon-gluon fusion mechanism becomes dominant, with the production via intermediate state playing an important role.

Experimentally, the open charm situation is in much worse shape. The data are much more meager, frequently contradictory, often come from very limited kinematical regions, and on the whole do not lend themselves readily to a thorough phenomenological analysis. The general conclusions that can be drawn are that the QCD simple diagrams can account for most of the data in the lower energy region ($\sqrt{s} \lesssim 30$ GeV) but some leading particle mechanism appears to dominate at the ISR energies. The cross sections there appear much higher and much broader in x than QCD would predict and new mechanism must be invoked to explain the data.

REFERENCES

1) W. Bacino et al., Phys. Rev. Lett. 45, 228 (1980); N. Ushida et al., Phys. Rev. Lett. 45, 1049 (1980) and Phys. Rev. Lett. 45, 1053 (1980).

2) For a review of these experiments see H. Wachsmuth, Proc. of the Lepton-Photon Symposium, Fermilab (1979).

3) M. Jonker et al., Phys. Lett. 96B, 435 (1980).

4) K. W. Brown et al., Phys. Rev. Lett. 43, 410 (1979).

5) A. Diamant-Berger et al., Phys. Rev. Lett 43, 1774 (1979).

6) J. Ritchie et al., Phys. Rev. Lett. 44, 230 (1980).

7) K. W. B. Merritt, Ph.D. thesis, California Institute of Technology, Pasadena, Cal.

8) J. Sandweiss et al., Phys. Rev. Lett. 44, 1104 (1980).

9) H. Fuchi et al., Phys. Lett. 85B, 135 (1979).

10) T. K. Malhotra, paper presented at the 1980 International Conference on High Energy Physics in Madison, Wis.

11) W. Allison et al., Phys. Lett. 93B, 509 (1980).

12) H. Fuchi et al., DPNU-42-80, December 1980, submitted to Lettere al Nuovo Cimento.

13) Bologna, Glasgow, Rutherford, Saclay, Torino Collaboration, paper submitted to the 1980 International Conference on High Energy Physics in Madison, Wis.

14) V. L. Fitch et al., Phys. Rev. Lett. 46, 761 (1981).

15) L. J. Koester, paper presented at the 1980 International Conference on High Energy Physics in Madison, Wis.

16) C. E. Carlson and S. Suaya, Phys. Rev. D18, 760 (1978).

17) Annecy, CERN, College de France, Dortmund, Heidelberg, Warsaw Collaboration, paper presented at the 1980 International Conference on High Energy Physics in Madison, Wis.

18) J. Irion et al., Physics Letters 99B, 495 (1981).

19) M. Basile et al., CERN-EP/80-214 and CERN-EP/81-22, submitted to Nucl. Phys. B.

20) D. Drijard et al., Phys. Lett. 85B, 452 (1979).

21) K. L. Giboni et al., Phys. Lett. 85B, 437 (1979).

22) W. Lockman et al., Phys. Lett. 85B, 443 (1979).

24) D. Drijard et al., Phys. Lett. 81B, 250 (1979).

25) G. Sajot, paper presented at the 1980 International Conference on High Energy Physics in Madison, Wis.

26) F. Muller, paper presented at the 1980 International Conference on High Energy Physics in Madison, Wis.

27) A. Chilingarov et al., Phys. Lett. 83B, 136 (1979).

28) R. J. N. Phillips. rapporteur talk at the 1980 International Conference on High Energy Physics, Madison, Wis; also available as RL-80-050.

29) Papers presented to the 1980 International Conference on High Energy Physics, Madison, Wis., by the Birmingham, CERN, Ecole Polytechnique Collaboration and the NA3 Collaboration.

30) J. G. McEwen, paper submitted to the 1980 International Conference on High Energy Physics, Madison, Wis.

31) A. G. Clark et al., Nucl. Phys. B142, 29 (1978).

32) C. Kourkoumelis et al., Phys. Lett. 81B, 405 (1979).

33) T. B. W. Kirk et al., Phys. Rev. Lett. 42, 619 (1979).

34) Papers presented by the WA11 Collaboration to the 1980 International Conference on High Energy Physics, Madison, Wis.

35) P. Delpierre, paper presented to the 1980 International Conference on High Energy Physics, Madison, Wis.

HADRONIC CHI PRODUCTION AND DIFFRACTIVE CHARM MESON PRODUCTION

John W. Cooper
University of Pennsylvania
Philadelphia, Pa. 19104 (USA)

Abstract

Preliminary results are presented on χ production in 225 GeV/c π^-Be interactions at Fermilab using the Chicago Cyclotron Particle Spectrometer (CYCLOPS). The eye of CYCLOPS is a 147 element Lead Glass array for detection of χ's via the decay $\chi \rightarrow \psi + \gamma$. Results on diffractive charmed D meson production from an earlier experiment in the same apparatus are also reported. Hadronic decays of D mesons were detected in coincidence with a prompt muon and a recoil proton from a hydrogen target. D mesons are seen in the channels $K\pi$ and $K\pi\pi$ with identified K_s^o or $K^{\pm}$.

This is a preliminary report of results from Fermilab Experiment E610 on hadronic χ (3.5) production at 225 GeV/c. The people involved in this Fermilab-Illinois-Pennsylvania-Purdue-Tufts collaboration are listed in reference 1.

The experiment used the Chicago Cyclotron Particle Spectrometer (CYCLOPS) shown in Fig. 1 to detect χ's via

$$\pi^- Be \rightarrow \chi + X$$
$$\chi \rightarrow \psi + \gamma$$
$$\psi \rightarrow \mu^+\mu^-$$

The Chicago Cyclotron magnet (7.5 T-m) serves as the analyzing magnet in the CYCLOPS apparatus. Charged tracks are detected with 25 planes of MWPC's and 4 X-Y Drift Chambers. An 18 cell threshold Cerenkov counter separates π's from K's in the range 8-30 GeV/c. Particles which penetrate a 3m steel shield are identified as μ's and the apparatus is triggered on a high mass $\mu^+\mu^-$ pair. The eye of CYCLOPS is a 147 element Lead Glass array shown in detail in Fig. 2. The eye consists of a 2.3 radiation length active converter followed by three planes of proportional tubes (8 mm spacing) for shower position measure-

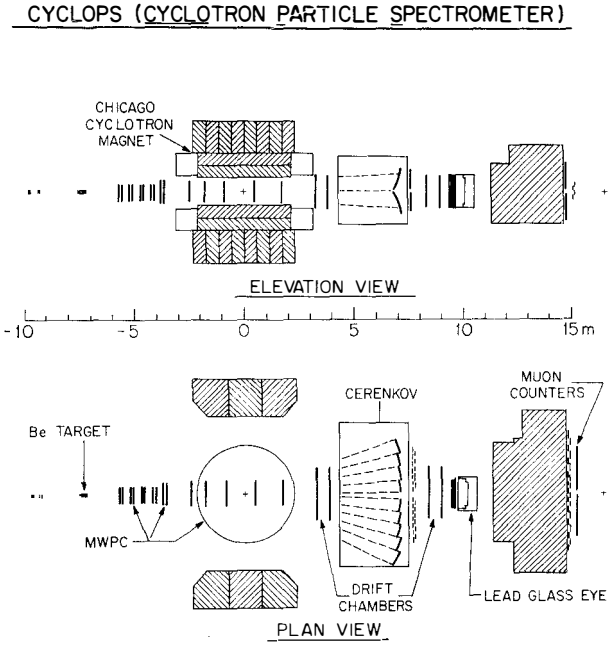

Fig. 1. The CYCLOPS apparatus (elevation view and plan view).

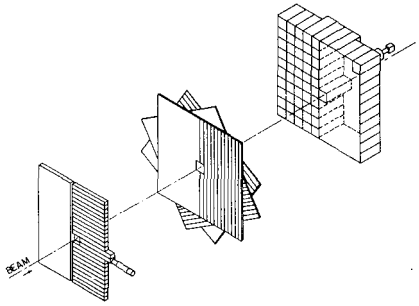

Fig. 2. An exploded view of the CYCLOPS "eye". The active preconverter contains 48 Lead Glass blocks. The proportional tube array (center) has 60° geometry and each plane contains 208 tubes. The final Lead Glass array is 1.5m x 1.5m and contains 99 blocks.

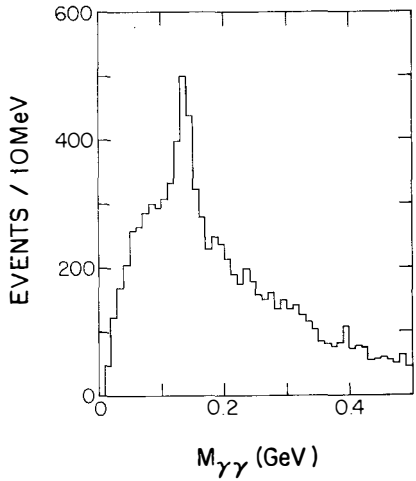

Fig. 3. $\gamma\gamma$ invariant mass

ment and by 18.0 radiation lengths of Lead Glass for the primary energy measurement. In a calibration electron beam this detector achieved a position resolution of $\Delta x=\Delta y\approx 9$mm (FWHM) and an energy resolution of $\Delta E/E\approx 15\%/\sqrt{E}$ (FWHM). With this resolution we expect a reconstructed π^o width of 10 MeV (FWHM) and a $\chi(3.5)$ width of 25 MeV (FWHM).

Our present understanding of the CYCLOPS eye is indicated by the γ-γ invariant mass plot in Fig. 3. There is a clear π^o peak at 0.135 GeV, but the FWHM is 30 MeV. This larger than expected π^o width is due to run to run energy calibration problems which are being intensively studied.

The $\mu^+\mu^-$ mass spectrum above 2.0 GeV is shown in Fig. 4. There is a ψ peak of about 760 events above background. We take all events in the range 2.95 - 3.25 GeV as ψ events and fix the $\mu^+\mu^-$ mass at 3.1 GeV. The $\psi + \gamma$ invariant mass for these "ψ's" is then formed and the result is shown in Figure 5. Photons with $M_{\gamma\gamma}$ in the π^o mass range (0.1 - 0.2 GeV) are not used in $\psi\gamma$ combinations, and all the photons used have energies in the range 1-30 GeV. The background curve in

Fig. 5 is formed by taking events with $2.5 < M_{\mu\mu} < 2.75$ GeV. We then set $M_{\mu\mu} \equiv 3.1$ GeV and form the $M_{\mu\mu} + \gamma$ invariant mass. This background is normalized absolutely by the ratio of "ψ" events to $2.5 < M_{\mu\mu} < 2.75$ GeV events.

Fig. 5 shows a clear excess of 50 events above background at ~3.5 GeV. Based on our π^o width (Fig. 3) we expect a χ mass resolution of about 50 MeV (FWHM) in this preliminary analysis. Our Monte Carlo determined acceptance is 0.4 for the γ once the ψ is detected. We estimated our γ pattern recognition efficiency to be less than 70%. We therefore conclude that the fraction of ψ's produced via an intermediate χ state is greater than 0.29. We do not quote an error due to the preliminary nature of this report.

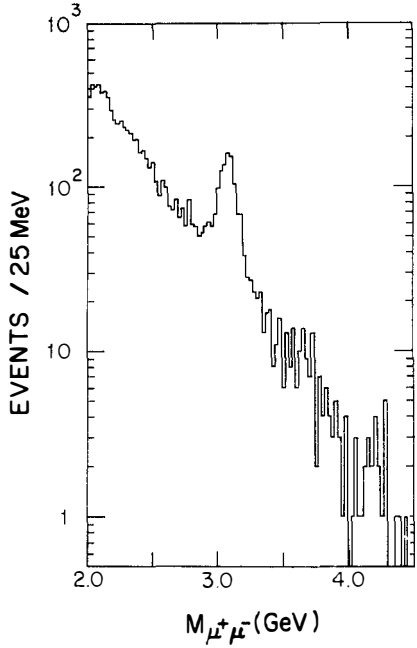

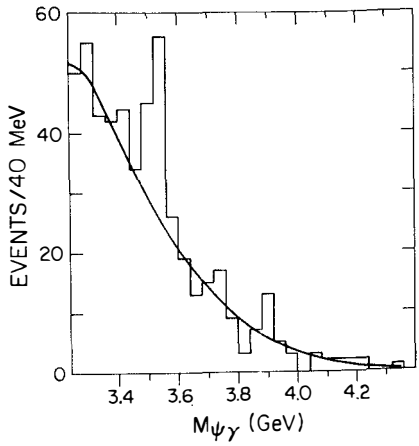

Fig. 5. The $\psi + \gamma$ invariant mass.

Fig. 4. The $\mu^+\mu^-$ invariant mass.

Now I turn to the subject of diffractive charm production in the reaction $\pi^- p \to M_x^- + p$ at 217 GeV/c. Using an early version of the apparatus in Fig. 1 with a hydrogen target and a recoil proton arm, we restricted the recoil mass M_x^- to the range 2.5 - 7.0 GeV. We then triggered on a single prompt muon to detect charmed D mesons via

$$M_x^- \to D + \bar{D} + X, \quad \bar{D} \to \mu + X, \quad D \to K\pi \text{ or } K\pi\pi$$

The people involved in this Fermilab-Harvard-Illinois-Oxford-Tufts experiment are listed in reference 2.

At the Madison conference we reported[3)] 23 ± 8 D^+ meson events in the channel $K^-\pi^+\pi^+$ and 26 ± 10 events in the channel $K^+\pi^-\pi^-$ with identified $K^\pm$. These mass plots are shown in Fig. 6. Fig. 7 shows the non-exotic $K\pi\pi$ mass where no signal is seen. Our mass resolution in all these plots is 36 MeV, so the D signals appear in a single bin. Since Madison we have also looked for D decays containing a K_s^o. Fig. 8 shows our K_s^o signal and Fig. 9 shows the $K_s^o\pi^+\pi^-$ mass spectrum where we see a peak of 26 ± 8 D^o events at ~1.86 GeV.

In the reaction $\pi^- p \to M_x^- + p \to D\bar{D}\, X\, p$, there are four production cross sections, D^+D^-, $D^o\overline{D^o}$, $D^+\overline{D^o}$, and D^-D^o. We have measured only three numbers, the amounts of D^+ production, D^- production, and $D^o + \overline{D^o}$ production. Therefore we must make one additional assumption to extract a diffractive charm D meson cross

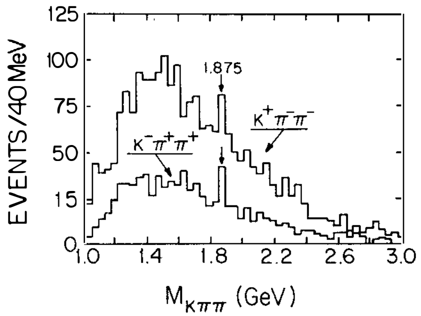

Fig. 6. The exotic $K^+\pi^-\pi^-$ and $K^-\pi^+\pi^+$ invariant mass.

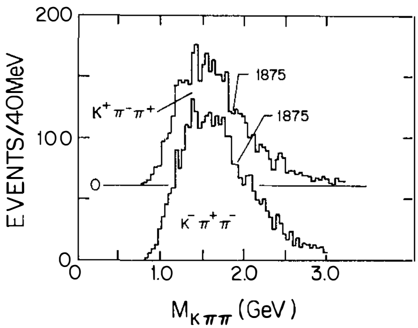

Fig. 7. The non-exotic $K^\pm\pi^+\pi^-$ invariant mass.

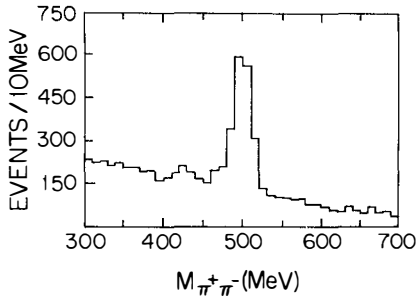

Fig. 8. The $\pi^+\pi^-$ invariant mass distribution for tracks not associated with the primary event vertex.

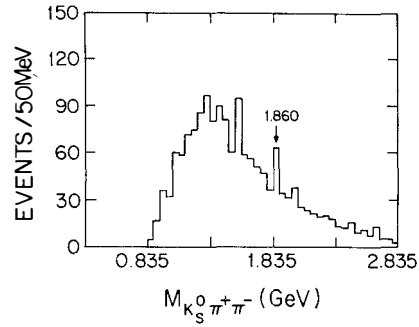

Fig. 9. The $K^0_S\pi^+\pi^-$ invariant mass.

section. If we try various values for the ratio of $D^0\bar{D}^0$ production to D^+D^- production, we find[4,5,6] the total diffractive $D\bar{D}$ production cross section limits shown in Figure 10. For a wide choice of the ratio $D^0\bar{D}^0/D^+D^-$ the total diffractive $D\bar{D}$ production cross section is 40-50 μb.

As a final check on our results we have examined the 2-body decay channels. Since we see 49 ± 13 $D^\pm \to K^\mp\pi^\pm\pi^\pm$ events, we expect to see 6 ± 3 events in $D^\pm \to K^0_S\pi^\pm$ and we do find 13 ± 5 events. We also see 26 ± 8 $D^0 \to K^0_S\pi^+\pi^-$ events, so we expect to see 25 ± 12 events in $D^0 \to K^\pm\pi^\mp$, but we find no events in this channel. We are re-examining our analysis of $D \to K^{ch}$ channels in an attempt to resolve this discrepancy.

References

1. Fermilab: D. Bauer, D. Judd, T. Kirk, S. Pordes. R. Raja, and A. Wehmann; Illinois: G. Alverson, H. Budd, T. Graff, S. Hahn, L. Holloway, L. Koester, U. Kruse, W. Li, P. Lukens, R. Sard, and P. Schoessow; Pennsylvania: J. Cooper; Purdue: V. Barnes, C. Davis, A. Garfinkel, and A. Laasanen; Tufts: S. Hossain, R. Milburn, W. Oliver, and R. Thornton.

2. Fermilab: T. Kirk and R. Raja; Harvard: M. Goodman, A. Loomis, A. Sessoms, R. Wilson, C. Tao; Illinois: G. Alverson, G. Ascoli, D. Bender, J. Cooper, L. Holloway, L. Koester, U. Kruse, W. MacKay, R. Sard, M. Shupe, E. Smith; Oxford: J. Davis and T. Quirk; Tufts: R. Milburn and R. Thornton.

3. L.J. Koester et al., High Energy Physics - 1980 (XX International Conference, Madison, Wisconsin), edited by L. Durand and L. Pondrom, A.I.P. Conference Proceedings No. 68, Particles and Field Subseries No. 22, New York, 1981, pg. 190.

4. To extract cross sections we evaluate the $D \to K\pi$ or $K\pi\pi$ acceptance and the $D \to \mu$ acceptances via Monte Carlo. These acceptances are relatively independent of whether the D's are produced by $M_X \to D\bar{D}$ or $M_X \to D\bar{D}X \to D$. We also take into account the probability that our prompt muon trigger came from a $\pi \to \mu$ decay.

5. We used the branching ratios for $D \to$ hadrons as reported by R.L. Kelly et al., Rev. Mod. Phys. 52, S1 (1980).

6. We take the $D^{ch} \to \mu$ and $D^o \to \mu$ branching ratios from DELCO: W. Bacino et. al., Phys. Rev. Letters 45, 329 (1980).

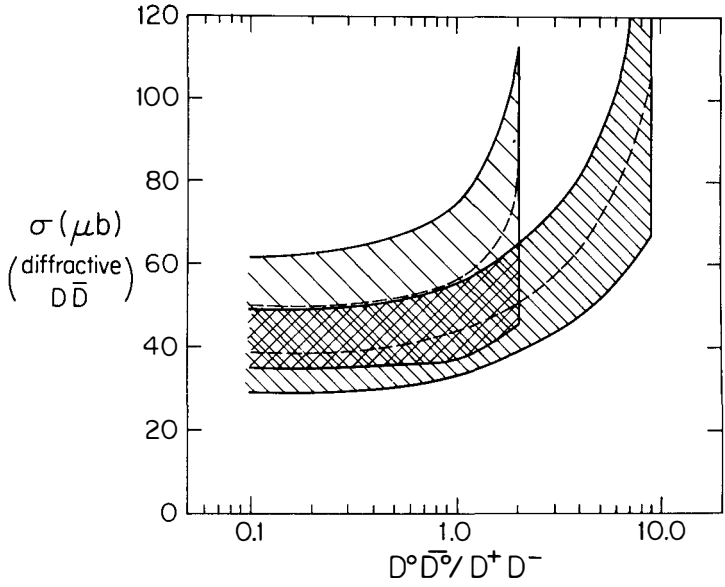

Fig. 10. The total diffractive DD cross section versus the ratio of the D^oD^o cross section to the D^+D^- cross section. The double-shaded curve follows from the DELCO result of $D^{ch} \to \mu$ branching ratio = 22%, $D^o \to \mu$ B.R. = 0%. The single-shaded curve follows the DELCO 2σ limit $D^{ch} \to \mu$ BR = 18%, $D^o \to \mu$ BR = 4%. The bands represent $\pm$ one std. dev. limits.

PROMPT SINGLE MUON PRODUCTION BY PROTONS ON IRON

A. Bodek , R. Breedon, R.N. Coleman, W. Marsh, S. Olsen, and J.L. Ritchie
University of Rochester, Rochester, New York 14627

B.C. Barish, R.L. Messner, M.H. Shaevitz , and E.J. Siskind
California Institue of Technology, Pasadena, California 91125

F.S. Merritt
University of Chicago, Chicago, Illinois 60637

H.E. Fisk, P.A. Rapidis, and Y. Fukushima
Fermilab, Batavia, Illinois 60510

G. Donaldson and S.G. Wojcicki
Stanford University, Stanford, California 94305

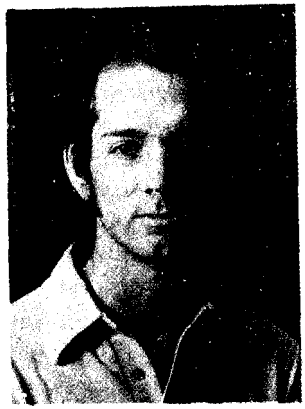

ABSTRACT

A new experiment has been performed at Fermilab to measure the hadronic production of prompt single muons. A preliminary analysis of a sample of the data indicates approximately equal production of prompt single μ^+'s and μ^-'s in 350 GeV p-Fe interactions. The observed momentum distributions of prompt single μ^+'s and μ^-'s can satisfactorily be fit by the hypothesis of central production of D mesons with a cross section of 16 ± 4 μb/nucleon.

We have performed an experiment at Fermilab to measure the production of prompt single muons in hadronic interactions. Data were taken with both 350 GeV protons and 280 GeV π^-s incident on an iron "beam dump" instrumented with scintillation counters. The density extrapolation technique was employed to separate prompt muons from non-prompt muons originating from decays of long-lived particles such as π's, k's, and hyperons. Prompt dimuons were identified with a very large acceptance muon identifier.

Data were taken in two different triggering configurations. One required only that the produced muon have momentum greater than 8 GeV. This corresponds, for the 350 GeV proton data, to most of the forward hemisphere, allowing a fairly model-independent determination of the charm cross section, if prompt single muons are interpreted as the products of the semi-leptonic decays of charmed hadrons. The other triggering configuration was more restrictive. It required a minimum muon momentum of 20 GeV.

Results are reported here only for the proton data taken with the 20 GeV trigger. (We have analyzed about one-half of this data sample.) Results from the full data set will i) extend the prompt single muon distributions to lower p, ii) reduce the size of the errors, which are dominated by statistics, and iii) allow a comparison between proton induced and pion induced charm production.

The detector[1)] consisted of a beamline spectrometer to measure the momentum of each incoming hadron, a target-calorimeter which served as a variable density "beam dump", a muon identifier and an iron toroid spectrometer. See Figure 1.

The target-calorimeter consisted of 49 steel plates with a scintillation counter on the downstream face of each. The plates were mounted independently on rails so that the spacing between the plates could be varied. Of the 2.4 meters of steel comprising the target-calorimeter, the density of the upstream most 1.7 meters was varied. Data were taken at three different effective densities, ρ, in the ratio 1:2/3:1/2. The most compact density of the target-calorimeter was about 3/4 that of steel.

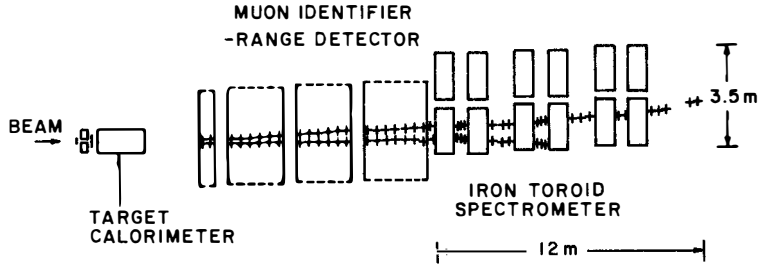

Figure 1. Plan view of the apparatus.

The muon identifier consisted of 42 3mx3m scintillation counters and 21 3mx3m spark chambers sandwiched periodically throughout 4.5 meters of steel. This device allowed identification of muons down to 5 GeV/c in momentum.

The toroid spectrometer, composed of 24 magnetized iron disks of radius 3.6 meters and interspersed with scintillation counters and spark chambers, allowed a determination of muon sign and momentum (with resolution of about 12%). It should be noted that the toroid spectrometer was placed "off-axis" (i.e., displaced laterally from beam center by one-half radius) to avoid a hole in the acceptance for low p_T muons.

Each event was required to pass selection criteria which consisted of a beamline PWC requirement of one and only one incoming hadron with momentum within 2% of beam momentum, a hadronic interaction in the upstream 25cm of the calorimeter, a requirement that muons originate in the target-calorimeter (to remove triggers from halo muons in time with hadrons) and a requirement that the triggering muon traverse the entire toroid system.

Events passing these selection criteria were placed in one of four categories: (i) a single triggering μ^+, (ii) a single triggering μ^-, (iii) dimuon with a triggering μ^+, and (iv) dimuon with a triggering μ^- (note that an event with two muons of opposite sign both of which trigger will fall into both iii and iv). Figure 2 shows the trigger rates of these types of events versus density. The intercepts at $1/\rho = 0$ of the lines drawn through the single μ^+ and μ^- rates are the prompt single μ^+ and μ^- signals, respectively. The difference in the slopes of these two lines is a result of more π^+'s than π^-'s being produced in proton interactions.

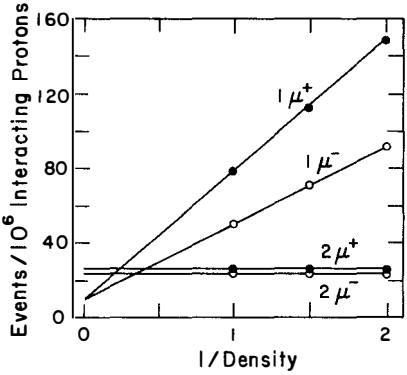

Figure 2. Event rates versus 1/density.

There was a contamination in the single muon sample from highly asymmetric dimuon events because muons of momentum less than 5 GeV were not identified. This background was subtracted with the aid of a Monte Carlo calculation which was normalized to the observed number of identified dimuon events. The resulting prompt single muon distributions versus p are shown in Figure 3a and 3b. The data indicate equal rates for the production of μ^+ and μ^- events. The efficiency corrected prompt single muon rates for $p > 20$ GeV/c are $(12.2 \pm 3.8)\times10^{-6}$ μ^+'s per interacting proton and $(10.1 \pm 2.6) \times 10^{-6}$ μ^-'s per interacting proton.

A possible source of additional background has not been subtracted in this preliminary analysis. Decays from non-prompt sources which take place in the unexpanded region of the target-calorimeter (recall that 10 interaction lengths are expanded), or in the drift space following the calorimeter, would result in a false prompt single muon signal. In an earlier experiment[2] with a significantly smaller target-calorimeter, this background was calculated to be small.

The prompt single muon distributions in Figure 3 have been compared with two models of $D\bar{D}$ production. In model A, D's were produced independently according to

$$E \frac{d^3\sigma}{d^3p} = (1 - x)^{\alpha} e^{-\beta p_T}$$

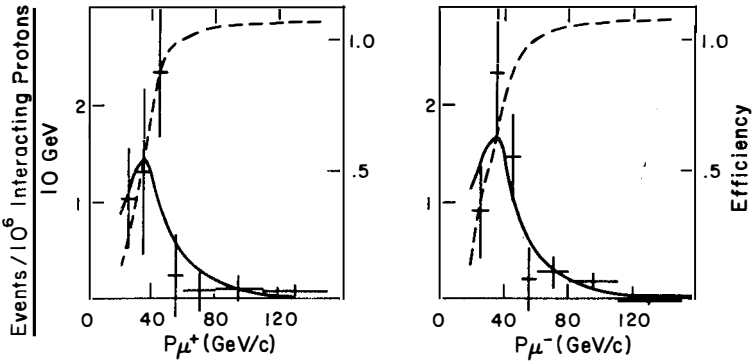

Figure 3. Prompt single muon rates versus momentum for μ^+ (a) and μ^- (b). The rates are not corrected for trigger efficiency. The dashed line is the efficiency. It can be greater 1.0 because it includes resolution smearing effects. The solid line is from the best fit $D\bar{D}$ production model A (see text).

In model B, $c\bar{c}$ pairs were produced with a mass m according to

$$E\frac{d^3\sigma}{d^3p} = \frac{1}{m^3}(1-x)^{\alpha} e^{-\beta p_T} e^{-\gamma m/\sqrt{s}}$$

and the composite $c\bar{c}$ systems decayed into $D\bar{D}$ pairs. For both models, we have assumed that the semi-leptonic decay modes of the D are $D \rightarrow K\mu\nu$ (60%) and $D \rightarrow K^*\mu\nu$ (40%). Both of these models adequately fit the data. The best fit with model A was achieved with $\alpha = 4.7 \pm 1.0$ and $\beta = 2.5$ (β was kept fixed). The best fit with model B was achieved with $\alpha = 2 \pm 1.2$, $\beta = 2.5$, and $\gamma = 15$ (β and γ were kept fixed).

It is instructive to plot the rate for producing single muons with momentum p greater than p_{min}. This plot, Figure 4, was obtained by correcting the data in Figure 3 for efficiency and adding the μ^+ and μ^- rates. The corresponding curves calculated from models A and B, discussed above, are similar (the curve for model A is shown in Figure 4). The intercept of these curves at $p_{min}=0$ is simply the total prompt single muon rate. For model A this rate is $(1.9 \pm 0.4) \times 10^{-4}$ and from model B it is $(1.8 \pm 0.6) \times 10^{-4}$. If we assume an 8% average branching ratio and linear A-dependence, these rates correspond to total charm production cross sections of 16 ± 4 μb/nucleon and 15 ± 5 μb/nucleon, respectively. Here the errors are only statistical, and mainly come from the uncertainty in α.

Also shown in Figure 4 is a measurement of the total prompt muon production rate above 8 GeV from an early test run of this experiment[3] When our new low momentum data is analyzed, it will provide a substantial improvement in this region.

In conclusion the data indicate approximately equal production of prompt μ^+'s and μ^-'s in 350 GeV p-Fe interactions. The data do not confirm results[4] from beam dump experiments which indicate unequal prompt ν_μ and $\bar{\nu}_\mu$ rates. The momentum distribution are adequately described by a central $D\bar{D}$ production model with a cross section of 16 ± 4 μb/nucleon. The data do not indicate a large diffractive charm production cross sections of the magnitude reported[5] by ISR experiments ($\sqrt{s}$ = 60 GeV).

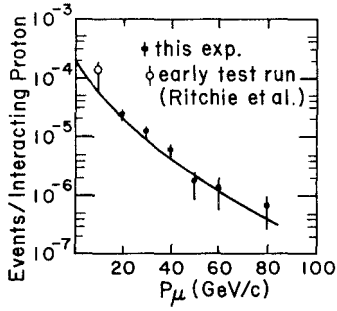

Figure 4. Total prompt single μ rates ($\mu^+ + \mu^-$) with p greater than p_{min}.

REFERENCES
1. Parts of the detector have been used in neutrino experiments by the Caltech-Fermilab-Rochestar-Rockerfeller group.
2. K.W. Brown, Ph.D. thesis, Caltech, 1980.
3. J.L. Ritchie, et al., Phys. Rev. Lett. 44 230 (1980).
4. K. Kleinknecht, Proceedings of the XXth International High Energy Physics Conference, Madison, June 1980, p. 237, L. Durand and L.G. Pondrom editors.
5. G. Sagot ibid p. 193, also S. Wojcicki ibid p. 1430.

A SEARCH FOR SINGLE e± -PRODUCTION IN $p\bar{p}$ INTERACTIONS AT 70 GeV/c

(presented by J.LEMONNE)

J.J. DUMONT, J. LEMONNE, G. VANHOMWEGEN, F. VERBEURE, J. WICKENS
IIHE (ULB-VUB), Brussel, Belgium

V.M. HAGMAN, V. KARIMAKI, J. TUOMINIEMI, K. VALTONIN
Department of High Energy Physics, University of Helsinki, Finland

J.A. ESTRUCH, W.H. EVANS, P. MASON, H. MUIRHEAD
Department of Physics, University of Liverpool, U.K.

J.F. BALAND, F. GRARD, P. HERQUET, J. KESTEMAN
Faculté des Sciences, Université de l'Etat à Mons, Belgium

G. EKSPONG, B. SELLDEN, L. SZILLY, N. YAMDAGNI
Institute of Physics, University of Stockholm, Sweden

ABSTRACT

A search for single $e^{\pm}$-production in 70 GeV/c $\bar{p}p$ interactions was performed at the CERN-SPS using the BEBC bubble chamber, equipped with a H_2 filled TST surrounded by a H_2-Ne blanket. No candidates for single $e^{\pm}$-production of momentum p_e greater than 500 MeV/c were found in a sample of $\sim$ 66 000 primary interactions. This result places an upper limit of 2.5 μb on single $e^{\pm}$-production at the 90 % confidence limit. The corresponding estimate of the upper limit for the charm production cross section is 14 μb.

I. INTRODUCTION

Although it has been advocated[1] that the bulk of the prompt $e^{\pm}$ production observed at SPS energies could be due to associated $e^{+}e^{-}$ production, single electron production should arise from the leptonic decays of charmed particles. Beam dump experiments[2] have suggested and recent experiments[3] have confirmed that charmed particles are produced in hadronic interactions in the 300 to 400 GeV energy range with cross sections amounting to several tens of μb. In particular, from a bubble chamber study of $\pi^{-}p$ interactions at incident momenta as low as 70 GeV/c performed in experimental conditions almost identical to those of this experiment, a charmed particle cross section of (19 ± 11) μb has been reported[4]. On the other hand, this cross section (assumed to be $A^{1.}$ dependent) was estimated to be (5 ± 4) μb per nucleon from a p-Fe beam dump experiment[3] also performed at the same incident momenta. In the present experiment the same phenomena will be investigated for the first time with high energy antiprotons.

II. EXPERIMENTAL PROCEDURE

The data stem from an exposure at the CERN SPS of the bubble chamber BEBC equipped with a Track Sensitive Target (TST) and with an External Muon Identifier (EMI) to an RF seperated beam of antiprotons (S3 beam) with a momentum of 70 GeV/c.

According to the results of continuous beam monitoring measurements performed with Cerenkov counters the beam was known to be remarkably pure ($\sim$ 95 % $\bar{p}$), the bulk of the background being due to muons. The chamber, with a diameter of 3.7m was placed in a 3.5 T magnetic field. The TST of dimensions (1.0 x 1.4 x 2.4)m^3 was filled with H_2 and surrounded by a 25/75 mole % H_2-Ne mixture with a radiation length of 40 cm. The exposure took place in mid 1978 and a total of 188.000 pictures were taken, $\sim$ 30 % of which were of rather poor quality due to important parasitic boiling in the chamber. The results presented in this paper come from the analysis of $\sim$ 125.000 pictures mainly belonging to the better quality portion of the film. The frames were scanned and partially rescanned (25 %) for all $\bar{p}p$ interactions occuring inside the TST within a 2m long fiducial volume. A total of 65.908 $\bar{p}p$ interactions were recorded whose secondary tracks were followed over their entire length and all possible track signatures (interactions, stops, decays, leaving tracks, tracks disappearing in the TST walls) and in particular the $e^{\pm}$ signatures (bremsstrahlung, Comptons, tridents, annihilation, curvature change and spiralization) were noted. All $\bar{p}p$ inter-

actions for which at least one $e^{\pm}$ candidate track was recorded at scanning were entirely re-examined by physicists. As a result of this inspection $\sim$ 4 % of all $\bar{p}p$ interactions were submitted to measurement on high magnification ($\sim$ life size) devices and subsequently reconstructed using a TST-version of the HYDRA-geometry. For e^+e^- "Dalitz pair" candidates without an additional single electron or positron, the measurements were restricted to the beam and e^+e^- tracks. When an unpaired electron was present, all leaving tracks or tracks of opposite charge disappearing in the TST walls were measured in addition. The contribution of high mass pairs to the "Dalitz decay" like events will be discussed elsewhere and in the following we will concentrate on the results of a search for single direct $e^{\pm}$ production.

III. SELECTION AND STUDY OF $e^{\pm}$ CANDIDATES

In order to establish the presence of a prompt $e^{\pm}$ signal it is important to specify a number of selection criteria which eliminate or reduce the contribution of competing background processes to the measured sample. Some of these selections were straightforward to apply and the necessary corrections were easy to estimate. But others needed independent background studies to decide on the cuts and Monte Carlo simulations to correct for the loss of the signal. Each of these selections, which reduce the background but also affect the genuine prompt $e^{\pm}$ detection efficiency, is discussed below and estimates of the ensuing corrections to the potential prompt electron signal are given in table I. The remaining backgrounds are discussed in section IV.

To reduce the possible background from delta rays, Compton electrons and electrons (positrons) from very assymmetric Dalitz pairs or from gammas converting near the vertex the analysis was restricted to events with even number of prongs i.e. the charge balance was required. This cut removes 2 % of the events.

For low momentum tracks which are trapped inside the TST the electron identification is difficult and the π-μ-e decays without visible decay points give a background which is impossible to control. For this reason only those single $e^{\pm}$ candidates were retained which had enough track length in H_2-Ne mixture to allow a positive identification. A momentum cut at 500 MeV/c was chosen for this purpose. The effect of this cut on the $e^{\pm}$ signal was estimated with a Monte Carlo calculation. The production and subsequent semileptonic V-A decay of D particles were simulated according

to different models allowing for central as well as diffractive D-meson production. The fraction of electrons lost was found to be rather insensitive to the model used and was estimated to be (15 ± 3) %.

In order to further reduce the background, only tracks with at least two independent electron signatures were accepted with the first signature occuring either inside the TST or within 50 cm track length in the H_2-Ne mixture. In addition, tracks for which the only signatures were a change in curvature followed by spiralization were rejected. These conditions drastically reduce any background of hadronic origin without strongly reducing the electron signal. Indeed, from a study of 1500 $e^{\pm}$ tracks from $\gamma \to e^+e^-$ conversions occuring within the fiducial volume of the TST, it was found that the fraction of electrons satisfying the above criteria is (.80 ± .02) for electrons with $p_e > 500$ MeV/c.

As part of the single $e^{\pm}$ signal could also arise from Dalitz-like e^+e^- pairs in which one of the electron tracks remains unrecognized all candidates with an invariant mass below m_{π^0} in combination with a track of opposite charge leaving the chamber or disappearing within the TST-wall were discarded. The possible loss due to this invariant mass cut on single $e^{\pm}$ particles, produced in semi-leptonic charmed particle (D-meson) decays, was again estimated by Monte-Carlo methods and found to be (5 ± 3) %. This estimate takes into account hadron e combinations in which the hadron and e both arise from D-decay, as well as combinations with directly produced pions. In the latter case, the pions were assumed to have the same production characteristics as those observed in K^+p interactions at 70 GeV/c[5].

Secondary hadrons which pass through the TST supports have a significant probability to interact and give an aligned electron track with the same charge due to a γ conversion within the obscured region. To remove this background, a geometrical cut was applied. Using the same Monte-Carlo calculation as explained above, it was estimated that the reduction in the electron signal for $e^{\pm}$ with momentum larger than 500 MeV/c was 2 ± 1 %.

For single $e^{\pm}$ candidates passing the above cuts, the largest remaining source of background is due to K_{e3} decays having a small decay angle between the kaon and electron. In order to reduce the contribution of this background, all surviving candidates were carefully remeasured to detect any angular deviation (kink) of the supposed electron track. The following quantities were studied on the basis of these measurements :

1° The change in projected angle on the film plane at each measured point. This was obtained from sliding circle fits to the raw measurements on each of the four views.

2° The change in dip and azimuth of the track between successive arcs reconstructed by the HYDRA geometry program. By adjusting the geometry constants and making several runs, the transition points between the arcs can be moved along the tracks.

3° The change in dip and azimuth of the track at break points introduced in the mass dependent fit by the HYDRA geometry[6].

In order to decide the selection criteria on changes in dip and azimuth angles in hydrogen, in the TST wall and in the H_2-Ne mixture, a similar study was made on genuine electrons coming from γ conversions inside the TST. On the basis of these tests it was decided to reject any candidate with dip $\Delta\lambda$ or azimuthal angle $\Delta\phi$ change larger than the limits given in the following table

	$\Delta\lambda$	$\Delta\phi$
H_2	2°	2°
TST wall	3°	3°
H_2-Ne	3°	3°

Furthermore, the point at which the first electron signature arose was carefully studied and candidates were rejected if a γ ray was observed within one conversion length compatible with being produced at this point with an angle larger than 5° relative to the electron candidate track. From the study of genuine electron tracks it was estimated that the cuts remove 10 ± 3 % of the single electron signal.

The scanning efficiency for detecting single $e^{\pm}$ was obtained by rescanning the sequences of films which contained single $e^{\pm}$ events with $p_e > 500$ MeV/c for which a low invariant mass combination (< 135 MeV/c^2) was found with a particle of opposite charge producing an unsigned track. Effort was made to do this rescan in as unbiassed a manner as possible. The scanning efficiency was found to be (85 ± 6)%. As can be seen from table I the overall detection efficiency of genuine single electrons after applying all cuts amounts to (47 ± 8)%.

IV. BACKGROUND ESTIMATES

A Monte-Carlo estimate of the importance of K_{e3} background has been performed by generating samples of $K^{\pm}$-mesons originating in the fiducial volume of the BEBC-TST with Feynman x_F and p_T^2 distributions in accordance with the characteristics of K°-production in 69 GeV/c pp interactions[7]. The total inclusive cross sections for charged and neutral kaons were assumed to be equal and the latter was taken to be 8 mb from an interpolation of existing data. Each generated K-particle has been traced through the various media (H_2, Lexan, H_2-Ne) and the path lengths for decays up to 50 cm from the exit of the TST-wall were determined taking into account the reduction from secondary interactions and stopping particles. It was assumed that γ-rays arising from Ke3-decay could only be correlated to the $K^{\pm}$-decay point if converting within 1 conversion length of H_2-Ne. Cuts were applied on the space angle θ_γ between the direction of flight of the kaon at the K_{e3} decay point and that of each observable and on the differences in dip and azimuth between the $K^{\pm}$ and $e^{\pm}$ laboratory momentum. For K momenta above 500 MeV/c, rates for unobservable K_{e3} decays were computed following the study described in the previous section allowing for minimum detectable values of $\theta_\gamma = 5°$, $\Delta\lambda = \Delta\phi = 2°$ in H_2 and $\Delta\lambda = \Delta\phi = 3°$ in lexan and H_2-Ne. With these angular cuts, undetected K_{e3} decays would result in a background of 2.8 single electrons with momentum p_e greater than 500 MeV/c. This and other sources of background amounting to an additional 0.8 single electrons are listed in table II. The remaining backgrounds for $p_e > 500$ MeV/c, normalized to the total number of events and applying none of the other cuts discussed in section 3 unless stated, are respectively :

1. The decay $K_L^\circ \to \pi\ e\ \nu$ close to the primary vertex. It was found from the experimental decay length distribution that 40 % of V°s decaying within 6 cm of the primary vertex were not detected at the scanning level leading to an upper limit of 0.26 events assuming that no such K_L° decays are detectable due to their decay configuration.
2. Compton electrons and delta rays within 4 cm of the primary vertex are unlikely to be detected as such. If produced in an odd topology event with a missing negative track they will simulate charge balanced events. These two effects amount to about 0.28 events.
3. Asymmetric Dalitz pairs or gammas converting into an asymmetric e^+e^- pair within 4 cm of the primary vertex can combine with an odd topology event and may result in a charge balanced event. Assuming that the momentum of the undetected track of the pair is less than 5 MeV/c an estimate of 0.02

background events was found by Monte-Carlo simulation of π° production and decay.

4. π^- (π^+)-charge exchange giving a converted γ close to the interaction point and without visible positron (proton) can simulate an electron if the deviation between the π and the e falls within the angular cuts previously defined. A similar effect can be obtained for a pion interacting in the TST wall if the secondary tracks of the interaction do not emerge from the Lexan and if only one same sign track of a converted gamma emerges. These backgrounds amount to 0.02 events in H_2, 0.05 events in Lexan and 0.17 events in H_2-Ne.
5. Background from π-μ-e decay is expected to be completely eliminated due to the 500 MeV/c momentum cut and the requirement that the electron has at least two signatures taking the combination of curvature change and spiral as 1 signature.

V. RESULTS AND CONCLUSIONS

None of the candidates for direct single $e^\pm$-production survived the selection criteria described in section III. Assuming that those event selection criteria not applied when estimating the contribution of a background process (see table II) affect equally this process and the signal, the overall expected background is reduced to 2 events, a number compatible with zero. It should be noted that the bulk of the background arises from $K^\pm_{e3}$ decay, for which the estimation requires a series of uncertain assumptions regarding the inclusive production cross sections. The fact that no event was found to satisfy the single $e^\pm$ selection criteria allows for a maximum observable signal of 2.3 events at the 90 % confidence level. The latter event number is increased to 4.8 single electron events after correction for the overall electron detection efficiency.

The corresponding upper limits on the cross section for direct single $e^\pm$ production σ_e and the $(\frac{e}{\pi})$ ratio R are $\sigma_e = 2.5$ μb and $R = 1.5 \times 10^{-5}$ respectively. The microbarn equivalent per event applying to our data was computed by normalizing the estimated total cross section for events with charged topology ≥ 4 to the corresponding number of recorded events.

Assuming semi-leptonic decay branching ratios of charmed particles into electrons of about 10 %, our result imposes an upper limit of 14 μb at the 90 % C.L. on the cross section for the associated production of charmed particles in $\bar{p}p$ interactions at 70 GeV/c.

It should be noted that as the Serpukhov beam dump result could only increase from (5 ± 4) μb to ∿ 20 μb if an $A^{.67}$ dependence of the cross section is assumed instead of A^{1}, our result suggests that similar charmed particle production cross sections apply to $\bar{p}p$ and pp interactions at 70 GeV/c. Such an observation tends to favour gluon fusion over quark annihilation processes as the dominant charmed particle production mechanisms effective at this energy.

REFERENCES

[1] : For recent reviews of this subject see for example : R. Stroynowski: SLAC-PUB-2650 (1980); H. Bodek : University of Rochester preprint, Rochester-N.Y. : UR-730 (1979) and N.S. Craigie, Physics Reports 47 (1978) 1

[2] : P. Alibran et al., Phys. Letters 74B (1978) 134;
T. Hansl et al., Phys. Letters 74B (1978) 139;
P. Bosetti et al., Phys. Letters 74B (1978) 143;
A.E. Asratyon et al., Phys. Letters 79B (1978) 497;
D. Treille, Hadro and photoproduction of new flavours, International Conference on High Energy Physics, Geneva (1979) 569;
H. Wachsmuth, International Symposium on Lepton and Photon Interactions, FNAL, (1979) : also CERN/EP 79-115.

[3] : J.L. Ritchie et al., Phys. Rev. Letters 44 (1980) 230;
J. Sandweiss et al., Phys. Rev. Letters 44 (1980) 1104;
W. Allison et al., Phys. Letters 93B (1980) 509

[4] : R. Barloutaud et al., Nucl. Phys. B172 (1980) 25

[5] : M. Barth et al., Z. Physik C 7 (1981) 187

[6] : D.J. Crenell, Break Point Method for Electron Fitting, Proceedings of the Topical Conference on Neutrino Physics at Accelerators, 1978 (Ruth. Lab. RL 78-081) 386.

[7] : H. Blumenfeld et al., Phys. Letters 45B (1973) 528.

TABLE I

Expected reduction of the genuine prompt electron signal as a result of cuts applied to the data.

Selection criteria	Fraction of the signal affected
Even topology	.98
Electron momentum .5 GeV/c	.85 ± .03
Signatures requirement	.80 ± .02
Mass combination .135 GeV/c^2	.95 ± .03
Geometrical cut (TST supports)	.98 ± .01
Angular cuts on electron tracks	.90 ± .03
Scanning efficiency	.85 ± .06
Overall detection efficiency	.47 ± .08

TABLE II

Estimated background to the single electron signal with $p_e > 500$ MeV/c (only partly corrected for cuts as described in text).

Background	single electron		
	per event		for the experim.
K_{e3}	4.2	10^{-5}	2.8
$K_L^o \to \pi$ e γ	0.40	10^{-5}	0.26
Compton electron	0.25	10^{-5}	0.17
Delta ray	0.16	10^{-5}	0.11
Asymmetric Dalitz pair	0.03	10^{-5}	0.02
Asymmetric γ conversion	0.003	10^{-5}	0.002
$\pi^{\pm}$ interaction in TST wall	0.07	10^{-5}	0.05
$\pi^{\pm}$ charge exchange in H_2	0.02	10^{-5}	0.02
$\pi^{\pm}$ charge exchange in Ne	0.25	10^{-5}	0.17
Total	5.38	10^{-5}	3.6

CHARMED MESON PAIR COHERENT PHOTOPRODUCTION OFF ACTIVE SILICON TARGET

M.A. Giorgi
INFN - Sezione di Pisa, Italy

ABSTRACT

The preliminary results of CERN NA1 photoproduction experiment are presented 46 charmed pair have been found so far in a sample of 670000 events analysed out of 1.8 million collected. A first indication of charged D lifetime is also given.

RESUME

Les résultats préliminaires de l'expérience de photoproduction cohérente NA1 au CERN sont présentés. 46 paires de mésons charmés ont été trouvés parmi 670000 évènements analysés sur un total de $1.8 \cdot 10^6$ enregistrés. On donne aussi une première indication de la durée de vie moyenne du méson D chargé.

I report here the preliminary results coming from 670000 out of 1.8 million events collected in the NA1 experiment performed by FRAMM Collaboration [1] at SPS using the 150 GeV H4/E4 beam in electron mode.

During the experiment a bremsstrahlung photon beam radiated by electrons in a 0.1 radiation length lead converter, was interacting in a Silicon target (0.15 radiation length).

The aim of the experiment is to study the diffractive excitation of the photon into heavy states $J^P = 1^-$ and, in particular, to measure with electronic technique the decay path of charmed mesons produced in pairs with such a mechanism. The physical processes are illustrated in fig. 1.

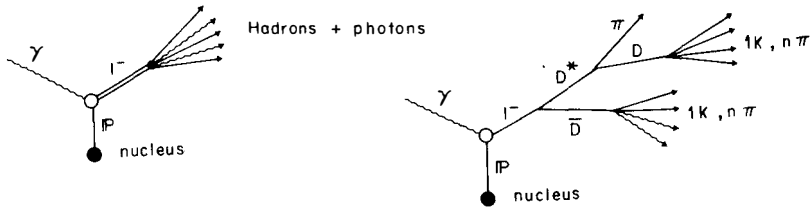

Fig 1. Coherent photoproduction of $D\bar{D}$ pairs.

1. THE APPARATUS

The experimental apparatus, as shown in fig. 2, is composed of a tagging system, a vertex detector including target and a forward spectrometer [2]. The tagging system is a hodoscope for momentum measurement of the electron bent by a magnet positioned after the converter where the photon is radiated. Since the bremsstrahlung of high energy electrons is always dominated by multiphoton emission, in order to reconstruct the energy of the photon interacting in the target, the information given by the tagging hodoscope is used together with the measurement of the energy of extra photons produced in the converter. The energy of photons non interacting in the target is measured in the last electromagnetic calorimeter. The energy of interacting photons is eventually determined in intervals of $DE_\gamma/E_\gamma = 5\%$.

The target, 1.6 cm long, is a telescope of 40 silicon detectors 300 μm thick and 100 μm apart, its granularity along the beam being 400 μm. The telescope has been expressely designed to detect the decay of charmed mesons [3], it takes into account the fact that in coherent photoproduction on

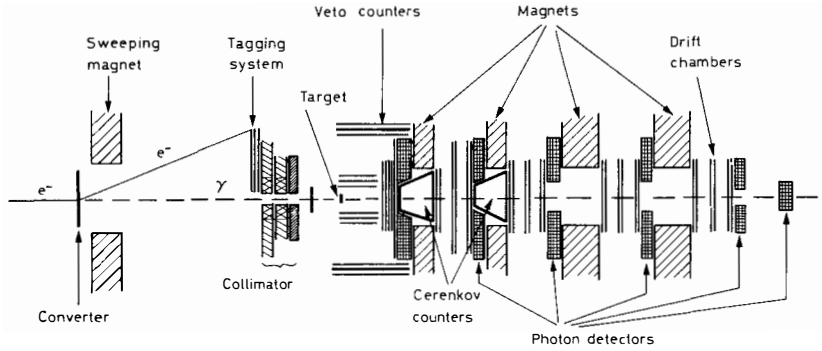

Fig. 2 Experimental apparatus.

silicon nucleus the photon energy (typically above 60 GeV) flows almost entirely into the charmed meson pair. The short decay path of D mesons can therefore be stretched by a large Lorentz γ-factor up to the order of a millimeter or more (several silicon layers). Since the signal amplitude in a single detector is proportional to the multiplicity of transversing minimum ionizing particles, we look for steps in pulse height produced by the increase of the multiplicity of charged particles after the charm decay. In fig. 3 a pulse height pattern of an expected DD event in the target is shown.

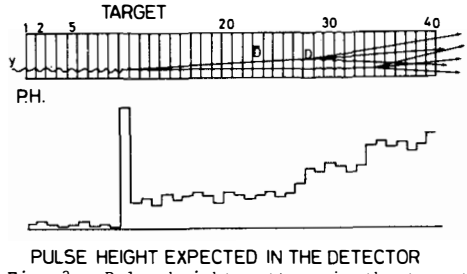

Fig. 3. Pulse height pattern in the target.

A set of magnets interspaced with MWPC and drift chambers[4] measures the momentum of all particles with momentum larger than 0.5 GeV/c and produced within a cone of 90 mrad half-aperture. This system provides a rather uniform resolution between 1 and 150 GeV/c, generally better than 1%. A set of counters positioned around the target vetoes all events in which particles are produced at large angles. However, to accept events where the π from the D^* decay goes outside the magnetic spectrometer acceptance, a single particle is allowed to be detected in a cone up to 30^o.

Two multicell Cerenkov counters are installed inside the first two magnets to select kaons from pions in the momentum interval 4-20 GeV/c. Five shower detectors subdivided with a very fine granularity measure all photons and electrons produced within ± 30. They provide standard energy and a very good space (± 1.5mm) resolutions. Their information is also used at the trigger level.

2. TRIGGER

The experiment was run with the following trigger conditions:

a) At least 2 hadrons or 1 hadron and 1 photon in the forward spectrometer.
b) Nothing outside experimental acceptance.
c) No geometrical cut in the horizontal plane.
d) The trigger efficiency was then > 70% for 4 hadrons, nearly 100% for photons.

1.8 Million events have been collected using the 150 GeV electron beam of $3 \cdot 10^6$ electrons pulse. About 1/3 of the full statistics has been processed so far, in this sample 50 charm pairs coherently photoproduced are expected to be visible in FRAMM apparatus (Montecarlo calculations).

3. ANALYSIS CRITERIA

a) Removal of e^+e^- pairs, using the momentum measured in the magnetic spectrometer and the energy measured in electromagnetic detectors.
b) π^0 reconstruction.
c) Take events with total energy measured in the forward spectrometer $E_{TOT} > 80$ GeV and ask for them a match within an uncertainty of ± 30% between photon energy given by the tagging and E_{TOT}.
d) Check on total P_T according to the silicon form factor to insure the coherence of the event.
e) Use Cerenkov information for positive identification of pions in the interval $4 \leqslant P \leqslant 20$ GeV/c to have kaons candidates.
f) Ask for multiplicity at the end of target less or equal to the charged multiplicity in forward spectrometer. In addition only events with a spectrometer charged multiplicity $\geqslant 6$ have been accepted.
g) Require at least 1 visible step in the target corresponding to a multiplicity variation $\Delta n \geqslant 2$ (from 2 to 4 or more, from 4 to 6 or more, etc.).

e) Allow K^0 short when $\pi^+\pi^-$ invariant mass is ≃ 500 MeV.
Combination are then built to form the individual D's of the pair using 2 further criteria:

i) To build combinations only 1 K or K^0, chosen among candidates, for each of the two mass states (D and $\bar{D}$) is assigned in building combinations.

ii) Exoticity condition according to Cabibbo's selection rule is imposed in combinations giving charged D's.

All the events where no combination gives a total invariant mass above DD threshold have been rejected (to be safe the software thereshold has been set at 3.5 GeV). In our selection we have events with even number of charged prongs 6 or 8 and events with an odd number of charged prongs 7 or 9 reconstructed in momentum, these latter have been kept, because of the possibility of 1 pion from $D^* \to \pi D$ decay gone out of magnetic acceptance. For each event several combinations have been built giving the masses M_1 and M_2 of the two states charm and anticharm to be identified.

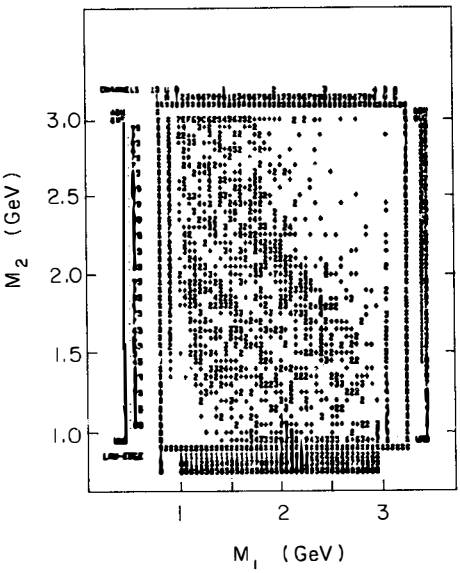

Fig. 4. M_1 vs. M_2 scatter plot

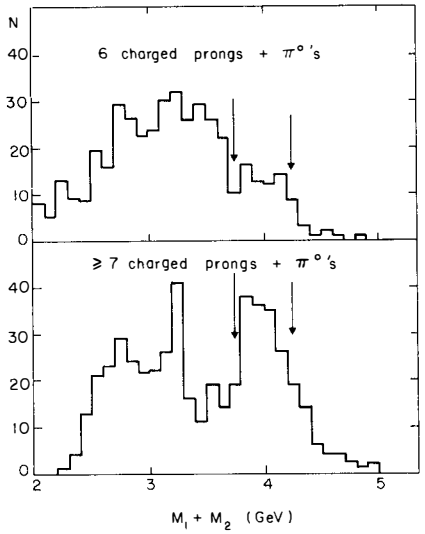

Fig. 5. Sum of the two mesons masses

Fig. 4 shows a scatter plot M_1 versus M_2 where combinations have been entered, a transverse band more populated than outside is well visible in it. Separate projections for 6 and > 7 prong events along the principal diagonal corrisponding to plot combinations versus $(M_1 + M_2)$ are presented in fig. 5, in the higher multiplicity sample of events a clear bump is shown in the 4 GeV region [(2 M_D), (M_D* + M_D), 2 M_D*] allowing to select a window, marked by the arrows where charmed mesons have to be searched . In fig. 6 is reported the mass of one state M_2 when the other state mass M_1 is contained in the interval 1.9 to 2.1 GeV, a signal corresponding to charmed meson mass is clearly visible, the arrows mark the nominal values of D and D^* masses.

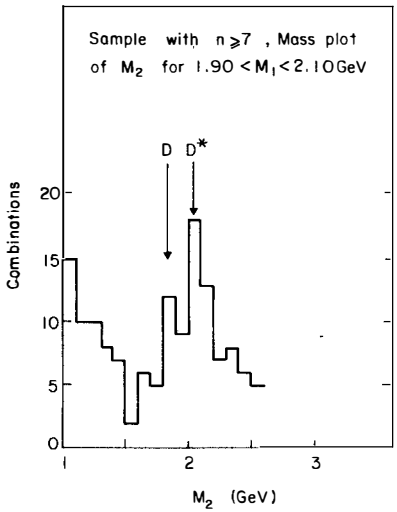

Fig. 6. Mass plot for D and $\bar{D}$.

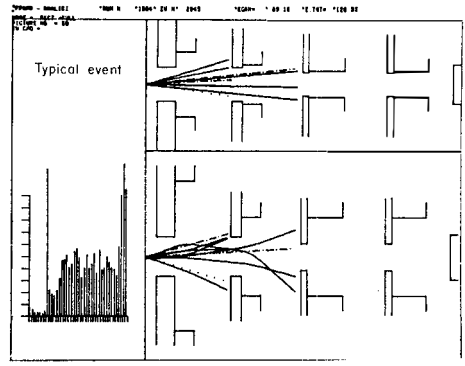

Fig. 7. Typical event.

Therefore for the events giving at least one combination inside a region where both states have their masses, M_1 and M_2, simultaneously in the range between 1.85 and 2.15 GeV, a more accurate scanning of pulse height patterns of the target was done looking for steps and levels.

46 events (∿1/3 of selected) inside the mass window present steps, levels and multiplicity compatible with charmed meson pair decays, most of them present also a high energy release in the silicon layer where the production accured, compatible with the recoil of silicon nucleus.

The computer display of one of these events reconstructed in the spectrometer is shown in fig. 7. In the left hand side of the figure the

pulse height pattern of the target is shown, where the first spike is due to the recoil of silicon nucleus, the following 4 layers show a pulse height compatible with the energy released by 2 minimum ionizing particles, and then a long level corresponding to 4 particles, the last jump heing not incompatible with 8 particles. The event is interpreted as D^+D^-, one of D's decaying into 3 charged prongs, the other into 5 charged prongs, seven charged particles and three π^0 have been fully reconstructed in the forward spectrometer. 10 events out of 46 have been positively identified as D^+D^- pairs with both decays measured inside the telescope target. In the remaining 36 events, 40 decays have been measured, one of two mesons often decays either immediately in the production layer or outside the telescope. For all these events the identification between D^oD^o, D^+D^-, $D^oD^\pm\pi^\pm$ still remains ambiguous, therefore at this stage we have given up in recognizing the fine structure of the event namely:

i) discriminate D^+D^- versus $D^o\bar{D}^o$ channels
ii) attribute energy to the individual D meson

4. CONCLUSIONS

All the decays observed have been entered in the same plot and individual decay paths have been corrected for the finite lenght of the target. The stretching γ Lorentz factor has been therefore appoximately attributed to D mesons in the following way:

$$\gamma_D = \gamma_{\bar{D}} = E_{TOT}/2M_D$$

where E_{TOT} is the total energy of $D\bar{D}$ pair.

Since the hadron collision length of the target is 5%, a nuclear interaction of pions (for instance a coherent production of A_1) can produce steps corresponding to variations in charged multiplicity and a normal hadronic event with a high number of pions could simulate a decay event. The plot of fig. 8 shows the decay path distribution of the 46 events identified as a pair of charmed mesons. In the low part of the figure is shown the background extracted from a sample of hadronic events with 4 charged prongs and no photons in the spectrometer. The target pattern of the events entered in the plot presents a step from 2 to 4 minimum ionizing particles, due to interaction of one pion. Real decay and background events are treated in the same way and both are corrected for the finite length of the target. The distribution of background events is flat whereas the $D\bar{D}$ events show a clear exponential decrease.

Making use of the average γ factor, the plot of the number of charmed mesons with a life longer than t versus t is built and displayed in fig.9 in logarithmic scale. Points are in agreement with a straight line. I have to remark again that this plot contains $D^{\pm}$ and D^{o}s well.

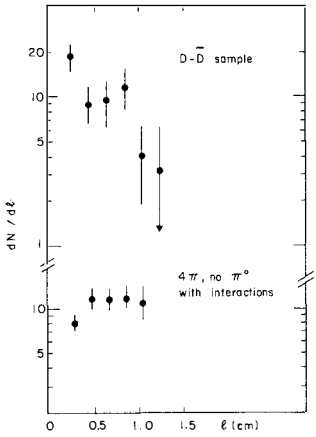

Fig. 8. Living path plot.

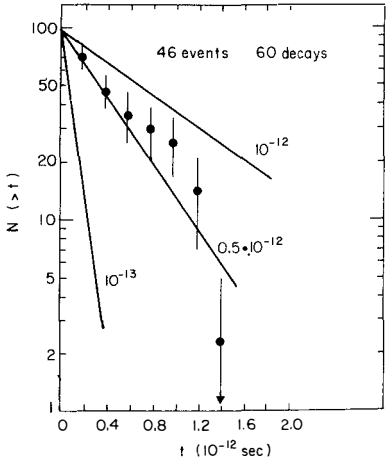

Fig. 9. Lifetime plot.

A statistical treatment of 18 measured decays in the sample of 10 events positively identified as $D^{+}D^{-}$ pairs, gives a mean lifetime between $5 \cdot 10^{-13}$ and 10^{-12} sec.

REFERENCES

[1] FRAMM Collaboration: Frascati, Milano, Pisa, Roma, Torino, Trieste.

[2] Status Report on NA1 experiment 5 September 1980, CERN/SPSC/80-85, SPSC/M 247

[3] S.R. Amendolia et al., Nucl. Instr. and Methods, 176(1980), 449
G. Bellini et al., to be published on Proceedings of "Meeting on Miniaturization of High Energy Physics Detectors". Pisa 18-20 Sept. 1980.
P.F. Manfredi, to be published on Proceedings of "Meeting on Miniaturization of High Energy Physics Detectors". Pisa 18-20 Sept. 1980.

[4] S.R. Amendolia et al., Nucl. Instr. and Methods, 176(1980), 461

RECENT RESULTS ON THE TAU LEPTON

Kenneth G. Hayes
CERN - EP Division
1211 Geneva 23
Switzerland

We review recent experimental results on the tau lepton: the new measurements of the tau pair production cross section in e^+e^- annihilations; the observation of the decay $\tau^- \to K^{*-}(892)\nu_\tau$; the searches for lepton number violating tau decays; and recent results with neutrino beams.

I. INTRODUCTION

In the six years since the discovery of the tau lepton[1], many of its properties have been measured. All results have confirmed our understanding of the tau as being a point-like, spin 1/2, charged sequential lepton, associated with its own neutrino, and which obeys conventional electro-weak theory with V-A coupling to the intermediate vector bosons[2]. The recent experimental results on the tau, which we shall reiew here, continue to support this view.

II. TAU PRODUCTION CROSS SECTION IN e+e- ANNIHILATION

The pair production cross section for spin 1/2 point particles in e+e- annihilations is given by equation (1)

$$\sigma=4\pi\alpha^2\beta(3-\beta^2)/6S \qquad (1)$$

where S is the square of the center of mass energy (E_{cm}), β is the particle velocity in units of the speed of light, and α is the fine structure constant. For center of mass energies which are large relative to the particle's mass, σ approaches the limiting form

$$\sigma \rightarrow \sigma_{muon}=4\pi\alpha^2/3S \qquad (2)$$

known as the muon pair production cross section. Several experiments at PETRA have recently published new measurements on the tau pair production cross section σ_{tau}. Figure 1 shows the MARK J measurement of σ_{tau} for E_{cm} between 12 and 36.4 GeV.

It is customary to parameterize possible deviations of the measured cross section from the point cross section by including a form factor in equation 1:

$$\sigma=\sigma_{point}\cdot|F(S)|^2 \qquad (3)$$

with the usual choice for F(S) given by

$$F(S)=1\pm S/(\Lambda_{\pm}^2-S). \qquad (4)$$

The most recent 90% confidence level lower limits on $\Lambda_{\pm}$ set by the PETRA experiments are listed in Table 1. Note that these limits

are typically only a factor of two smaller than the limits on $\Lambda_{\pm}$ for the muon pair production cross section measured in the same experiments.

TABLE 1

90% confidence level lower limits on $\Lambda_{\pm}$ for tau pair production.

Experiment	Λ_+	Λ_-	Reference
MARK-J	100	127	3
PLUTO	79	63	4
TASSO	67	74	5

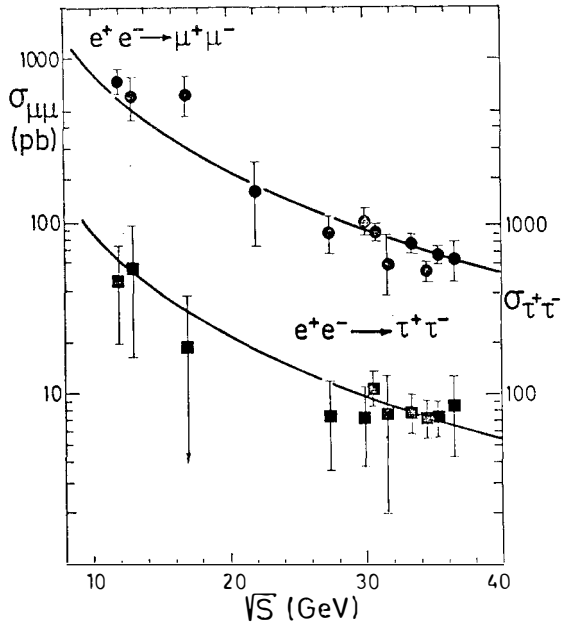

Figure 1. MARK J measurement of $\sigma(e^+e^-\to\mu^+\mu^-)$ and $\sigma(e^+e^-\to\tau^+\tau^-)$ compared to the point QED cross section.

III. MEASUREMENT OF THE DECAY $\tau^-\to K^{*-}(892)\nu_\tau$

The MARK II collaboration, using data collected at SPEAR, has recently added a new member to the list of measured tau decay modes with their measurement[6] of the decay $\tau^-\to K^{-*}(892)\nu_\tau$. This is the

first measurement of a Cabibbo suppressed tau decay, and gives further evidence for the conventional nature of the tau's weak interactions. The rate for this decay can be simply calculated from the rate for $\tau^- \to \rho^- \nu_\tau$ by multiplying by the $\tan^2$ of the Cabibbo angle, and including a kinematic factor[7]:

$$\Gamma(\tau^- \to K^{*-} \nu_\tau) = \Gamma(\tau^- \to \rho^- \nu_\tau) \cdot \tan^2 \vartheta_c \cdot .93 \qquad (5)$$

Using the measured branching ratio for the decay $\tau^- \to \rho^- \nu_\tau$ of 20.5±4.1%[8], the predicted branching ratio for the decay $\tau^- \to K^{*-} \nu_\tau$ is approximately 1.0%.

In the analysis, the decay chain listed in reaction 6 was used.

$$\begin{array}{l} e^+e^- \to \tau^{+(-)} + \tau^{-(+)} \\ \qquad\qquad\quad \tau^{-(+)} \to l^{-(+)} \nu\nu \qquad (l = e \text{ or } \mu) \\ \qquad\quad \tau^{+(-)} \to K^{*+(-)} \nu \\ \qquad\qquad\quad K^{*+(-)} \to K_s \pi^{+(-)} \\ \qquad\qquad\qquad\quad K_s \to \pi^+\pi^- \end{array} \qquad (6)$$

This has a very clean event signature as vertex constraints allow a pure sample of neutral kaons to be selected, while the lepton tag helps to insure the tau origin of the events. There is negligible background from conventional physics, including charm particle production and decay, in the K*+lepton events.

Figure 2 shows the K_s-π invariant mass distribution for all events satisfying the topology of reaction 6. A clean K*(892) is observed. Using the number of K* events in this distribution, the MARK II collaboration calculates a branching ratio for the decay

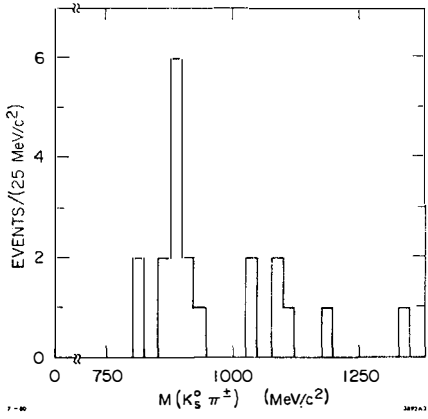

Figure 2.

$-\to K^{*-}(892)\nu_\tau$ of 1.7±.7%, consistent with theoretical expectations.

IV. A SEARCH FOR LEPTON NUMBER VIOLATING TAU DECAYS

The MARK II collaboration has also obtained new limits[9] on the branching ratio for many tau decays which would violate lepton number conservation in the sequential lepton model. In this model, each lepton generation (e-ν_e, μ-ν_μ, τ-ν_τ) has a unique, conserved lepton number. Thus, we expect all decays of the $\tau^-(\tau^+)$ to include a $\nu_\tau(\overline{\nu}_\tau)$ in the decay products. The possibility of non-zero neutrino masses and neutrino mixing leading to lepton number violating processes has recently generated much interest. Tau decays provide a new area in which to test our understanding of lepton number conservation.

Searches were made for the tau decay modes listed in 7a which are analogous to the long sought lepton number violating muon decays $\mu\to e\gamma$ and $\mu\to eee$, and for the tau decays to a charged lepton and neutral hadron listed in 7b.

$$\begin{array}{cccc} & \tau\to\mu\gamma & & \tau\to e\gamma \\ \tau\to ee^+e^-, & \tau\to\mu e^+e^-, & \tau\to e\mu^+\mu^-, & \tau\to\mu\mu^+\mu^- \end{array} \qquad (7a)$$

$$\begin{array}{ccc} \tau\to e\pi^0, & \tau\to eK^0, & \tau\to e\rho^0 \\ \tau\to\mu\pi^0, & \tau\to\mu K^0, & \tau\to\mu\rho^0 \end{array} \qquad (7b)$$

Since these are all neutrinoless decays, evidence for them can be found in the invariant mass plot of the decay products. The fact that each tau is produced with the beam energy provides a constraint on the energies of the decay products which can be used to reduce background, and to dramatically improve the detector's mass resolution by exploiting the constraint in a fitting procedure. Using this technique, the constrained mass resolution was sufficient so that with a data sample which contained 48,000 produced tau pairs, the search sensitivity was not limited by backgrounds.

As an example of the analysis methods, I shall briefly review the search for the decay $\tau \to \mu\gamma$. In this search, events satisfying the topology of the reaction

$$e^+e^- \to \tau^{+(-)} + \tau^{-(+)} \quad \begin{cases} \to X^{-(+)} + \text{neutrals} \\ \to \mu^{+(-)} + \gamma \end{cases} \tag{8}$$

were used. One tau is assumed to decay via a conventional mode to one charged particle X (roughly 70% of all tau decays) where X must be detected but need not be identified, while the other decays via the lepton number violating mode $\tau \to \mu\gamma$. Cuts were applied to insure consistency of the measured muon and photon energies with the beam energy constraint, and to remove obvious backgrounds such as events from the purely electromagnetic processes $e^+e^- \to \mu^+\mu^-\gamma$ and $e^+e^- \to \mu^+\mu^-\gamma\gamma$, or background photons arising from π^0 decays or electron bremsstrahlung. Figure 3 shows the beam constrained μ-γ invariant mass spectrum obtained after applying all cuts. No evidence is observed for any pair produced particle with mass between .3 and 3.2 Gev/c^2 which decays to a muon and photon. Figure 4 shows the data in the region near the tau mass with an expanded scale and with the expected resolution function for

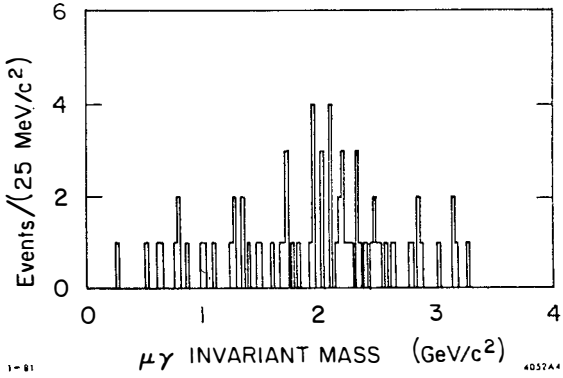

Figure 3. The $\mu\gamma$ invariant mass spectrum with all cuts.

the decay $\tau \to \mu\gamma$ calculated with Monte Carlo methods. The one event found inside the mass resolution function is consistent with the background, and can be used to set a 90% confidence level upper limit on the branching ratio for the decay $\tau \to \mu\gamma$ of 5.5×10^{-4}.

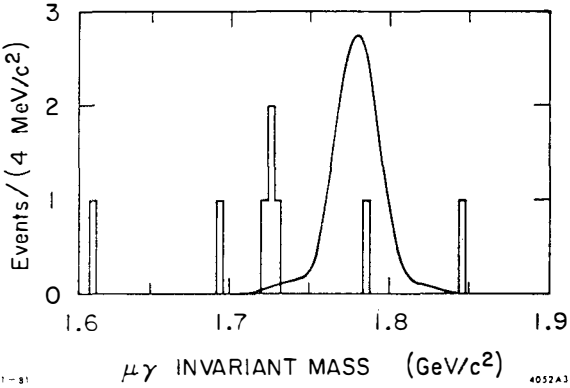

Figure 4. The $\mu\gamma$ invariant mass spectrum in the neighborhood of the tau mass. The smooth curve shows the expected τ mass resolution.

Similar methods were used to search for all of the modes listed in equation 7. Table II lists the 90% confidence level upper limits on the branching ratio for each mode, the average detector efficiency, and the number of events detected within the mass interval used to define the acceptance.

No evidence for any of the decay modes was seen, with all modes (except $\tau \to e + \pi^0$) having at most 1 event in the acceptance window. Thus the search sensitivity is not limited by background, but instead by the number of produced taus in the data sample. This sample represents roughly one year of running at SPEAR, and as it is difficult to increase the detector acceptance by more than a factor of two, further increases in the search sensitivity will require the accumulation of a still larger data sample.

TABLE II

Listed here are the detector efficiency, the number of events consistent with the tau mass, and the 90% confidence level upper limits on the branching fraction for the tau decays listed in column 1.

Decay mode τ^+	Detector efficiency(%)	#Events at tau mass	Upper limit on branching ratio
$\mu\gamma$	7.3	1	5.5×10^{-4}
$e\gamma$	6.3	1	6.4×10^{-4}
$\mu\mu^+\mu^-$	4.9	0	4.9×10^{-4}
$e\mu^+\mu^-$	7.3	0	3.3×10^{-4}
μe^+e^-	9.3	1	4.4×10^{-4}
ee^+e^-	10.1	1	4.0×10^{-4}
$\mu\pi^0$	2.9	0	8.2×10^{-4}
$e\pi^0$	3.5	3	$21.\times10^{-4}$
μK^0	2.4	0	$10.\times10^{-4}$
eK^0	3.1	1	$13.\times10^{-4}$
$\mu\rho^0$	5.5	0	4.4×10^{-4}
$e\rho^0$	6.5	0	3.7×10^{-4}

V. NEUTRINO EXPERIMENTS

Although the tau neutrino has still to be directly observed, there have been several recent results which tighten the upper limits on the coupling of the old neutrinos to the τ-ν_τ system. The first experiment of this type searched for production of taus by a muon neutrino beam in the 15 foot bubble chamber at Fermilab[10]. The observed absence of tau production enabled a 90% confidence level upper limit to be set on the coupling strength between ν_μ and $\tau^{+(-)}$ of less than .025 of the conventional Fermi coupling constant:

$$G_{tau}/G_F < .025 \qquad \text{(90\% C.L.)}. \qquad (9)$$

Two recent experiments have given improved upper limits for this coupling although the results are expressed in the language of neutrino oscillations. At Fermilab, the USA-Canada-Korea-Japan collaboration working with a tagged emulsion spectrometer in the wide-band neutrino beam, used the observed absence of tau production in their emulsions to set an upper limit of[11]

$$P(\nu_\mu \to \nu_\tau)/P(\nu_\mu \to \nu_\mu) < 1.1\% \qquad \text{(90\% C.L.)}. \qquad (10)$$

on the probability that the muon neutrino oscillates into a tau neutrino before reaching their detector. Another 15 foot bubble chamber experiment, the FNAL-Serpukhov-Moscow-Michigan collaboration, obtained a similar limit[12]:

$$P(\nu_\mu \rightarrow \nu_\tau)/P(\nu_\mu \rightarrow \nu_\mu) < .75\% \qquad (90\%\ \text{C.L.}). \qquad (11)$$

The Aachen-Bonn-CERN-London-Oxford-Saclay collaboration recently published the first result by a neutrino experiment on the electron neutrino--tau coupling. Using the BEBC detector with the CERN beam dump, they set an upper limit on the probability that an electron neutrino oscillates into a tau neutrino while traversing the 1200 meter path between the beam dump and BEBC of[13]

$$P(\nu_e \rightarrow \nu_\tau) < .35 \qquad (90\%\ \text{C.L.}). \quad (12)$$

Although this result is much less sensitive than the results using muon neutrinos, it is the first measurement of this type and will undoubtedly be improved in the next generation of beam dump experiments.

VI. CONCLUSIONS

We see that the most recent experimental results on the tau continue to support the conventional picture. The tau is known to be point-like to at least 10^{-16} cm; the weak current responsible for its decay has the same Cabibbo structure as the conventional weak current; and there is no evidence for any lepton number violating tau decays, or tau neutrino oscillations. In the foreseeable future, the possibility of directly observing the tau neutrino looks hopeful either in the new CERN beam dump experiments, or at the Tevetron. Besides directly observing tau production by neutrino beams, these experiments have a good chance of measuring the tau lifetime. In e+e- annihilations, the high resolution vertex detectors to be installed at PEP and PETRA also provide a very good opportunity to measure the tau lifetime.

References:

1. M.L. Perl, Proc. of Summer Institute on Particle Physics, SLAC-191, Stanford Linear Accelerator Center, Stanford University, Stanford, California, (1975) p.333; M.L. Perl et al., Phys. Rev. Lett 35:1489, (1975).
2. For recent reviews of the tau lepton see: M.L. Perl, Ann. Rev. Nucl. Part. Sci., 30:299 (1980). G. Flugge, Z. Phys. C1:121 (1979). G. Wolf, DESY Report DESY 80/13 (1980).
3. D.P. Barber et al., Massachusetts Institute of Technology Report MIT-LNS-TR 113 (1980).
4. Ch. Berger et al., DESY Report DESY 81-001 (1981).
5. R. Brandelik et al., DESY Report DESY 80-12 (1980).
6. J.M. Dorfan et al., Phys. Rev. Lett. 46:215 (1981).
7. Y.S. Tsai, Phys. Rev. D4:2821 (1971).
8. G.S. Abrams, et al., Phys. Rev. Lett. 43:1555 (1979).
9. K.G. Hayes, Ph.D. Thesis, Stanford Univ. (1981), unpublished.
10. A.M. Cnops et al., Phys. Rev. Lett. 40:144 (1978).
11. K. Niu, Nagoya Report DPNU 28-80 (1980), and XXth Int. Conf. on High Energy Physics (Madison) 1980.
12. B.P. Roe, quoted in V. Barger, K. Whisnant, and R.J.N. Phillips, Wisconsin Preprint DOE-ER/00881-151 (1980).
13. P. Fritze et al., Oxford Preprint OUNP 80-71 (1980).

RESONANCE PARAMETERS OF Υ AND Υ' AND INCLUSIVE SPECTRA MEASURED AT DORIS

DESY - Dortmund - Heidelberg - Lund - Moscow - Collaboration

W. Schmidt-Parzefall
Deutsches Elektronen-Synchrotron DESY, Hamburg.

ABSTRACT

Results on measurements of the Υ and Υ' resonances by the DASP2 collaboration obtained at the DORIS storage ring are reported. From the cross sections for $e^+e^- \to \mu^+\mu^-$ and $e^+e^- \to$ hadrons we obtain a branching ratio for the $\Upsilon(9.46)$ of $B_{\mu\mu} = (2.9 \pm 1.3 \pm 0.5)$ %, a leptonic width $\Gamma^{\Upsilon}_{ee} = (1.35 \pm 0.11 \pm 0.22)$ keV and a total width of $(47 \,^{+\,37}_{-\,15})$ keV. We studied inclusive particle production and observed an excess of antiprotons produced on the Υ and Υ' resonances.

RESUME

Les résultats présentés sur les résonances Υ et Υ' ont été obtenus par la collaboration DASP2 auprès de l'anneau de stockage DORIS. A partir des sections efficaces $e^+e^- \to \mu^+\mu^-$ et $e^+e^- \to$ hadrons, nous obtenons un rapport de branchement $B_{\mu\mu} = (2.9 \pm 1.3 \pm 0.5)$ % pour la résonance $\Upsilon(9.46)$, une largeur leptonique $\Gamma^{\Upsilon}_{ee} = (1.35 \pm 0.11 \pm 0.22)$ keV et une largeur totale de $(47 \,^{+\,37}_{-\,15})$ keV. Nous avons également étudié des productions inclusives et observé un excès d'antiprotons produits sur les résonances Υ et Υ'.

RESONANCE PARAMETERS

The Υ and Υ' were first seen in e^+e^- collisions [1] at DORIS in 1978. Then DORIS had to serve PETRA as injector. After construction of the positron accumulation ring PIA, high energy physics could resume at DORIS. New data were taken during a run from December 1979 until Easter '80. Fig. 1 shows the energy range covered by DORIS so far. Note the small statistical errors on the peaks of the resonances. Recently, detailed acceptance calculations have been performed [2] and the absolutely normalized resonance cross sections have been obtained, as shown in Fig. 2. The observed shape of a resonance is dependent upon the beam energy spread of the storage ring and on radiative effects. However the area under a resonance gives its electronic width, Γ_{ee} ($\Upsilon \to ee$)

$$\Gamma_{ee} = \frac{M^2}{6\pi^2(1-3B_{\mu\mu})} \int \sigma_h \, d\sqrt{s}$$

where M denotes the resonance mass and $B_{\mu\mu}$ ($\Upsilon \to \mu\mu$) its branching ratio into muon pairs. Our preliminary result is $\Gamma_{ee} = (1.35 \pm 0.11 \pm 0.22)$ keV.

The total width of the Υ can be determined indirectly using

$$\Gamma_{tot} = \frac{\Gamma_{ee}}{B_{ee}} = \frac{\Gamma_{ee}}{B_{\mu\mu}}$$

The branching ratio $B_{\mu\mu}$ ($\Upsilon \to \mu\mu$) has recently been measured by DASP2 [3] and LENA [4]. In order to reduce a large background counting rate due to cosmic muons, time-of-flight measuring equipment was added. Thus muon pairs from e^+e^- annihilation could be safely identified over a large solid angle. We obtained $B^{\Upsilon}_{\mu\mu} = (2.9 \pm 1.3 \pm 0.5)\%$, and, finally, for the total width $\Gamma^{\Upsilon}_{tot} = (47\ ^{+\ 37}_{-\ 15})$ keV.

Whereas in 1978 at DORIS just the first evidence for the Υ' resonance was obtained, it has been precisely measured by now. For the mass difference between Υ' and Υ we obtain ΔM ($\Upsilon' - \Upsilon$) = (556 ± 10) MeV and for the ratio of the electronic widths $\Gamma_{ee}(\Upsilon) / \Gamma_{ee}(\Upsilon') = 0.45 \pm 0.1$.

The resonance parameters are summarized in Table I. The average for DORIS is computed by taking into account also the results of the LENA [4] and PLUTO [5] collaborations. From these figures some important results can be deduced. Each of them is connected with interesting physics.

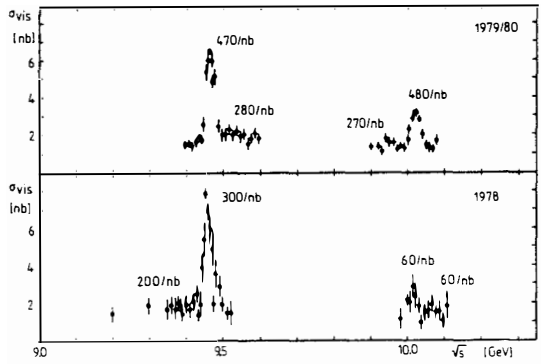

Fig. 1 DASP2 visible cross section and luminosity for all energies in the T and T' region scanned at DORIS.

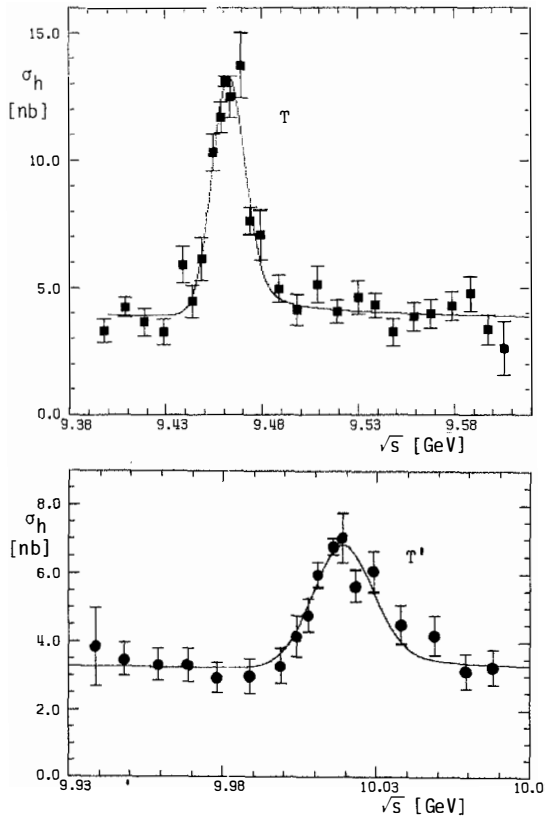

Fig. 2 Cross section for e^+e^- → hadrons showing the T and T' resonance.

TABLE I

Resonance parameters of the T and T' (preliminary)

		DASP2	DORIS average
$\Gamma_{ee}(T)$	[keV]	1.35 ± 0.22	1.29 ± 0.13
$B_{\mu\mu}(T)$	[%]	2.9 ± 1.3	3.0 ± 0.8
$\Gamma_{tot}(T)$	[keV]	47^{+37}_{-15}	43^{+20}_{-11}
$\Delta M(T',T)$	[MeV]	556 ± 10	556 ± 10
$\Gamma_{ee}(T') / \Gamma_{ee}(T)$		0.45 ± 0.1	0.45 ± 0.04

Γ_{ee} gives the charge e_b of the b-quark. To lowest order

$$\Gamma_{ee}(T \to e^+e^-) = 16\pi\alpha^2 e_b^2 \frac{|\psi(o)|^2}{M^2}$$

holds, where $\psi(o)$ denotes the quark wave-function at the origin and α the electromagnetic coupling constant. Though the wave function is unknown, it can be shown experimentally, Fig. 3, and also argued theoretically using quark potentials, that $|\psi(o)|^2/M^2$ does not vary strongly as a function of quark mass. Assuming then that Γ_{ee}/e_Q^2 is roughly constant, one obtains the result that the b-quark charge is $|e_b| = 1/3$.

$B_{\mu\mu}$ is connected to the strong coupling constant α_s. According to QCD a T state decays into 3 gluons just as orthopositronium decays into 3 photons. The first order expression for the width is [6]

$$\Gamma_{3g}(T \to 3g) = \frac{160}{81}(\pi^2 - 9)\alpha_s^3 \frac{|\psi(o)|^2}{M^2} \quad .$$

Using the above expression for Γ_{ee}, the unknown wave function cancels

$$\Gamma_{3g} = \frac{10(\pi^2 - 9)\alpha_s^3}{9\pi\alpha^2} \Gamma_{ee} \quad .$$

The unknown width Γ_{3g} can be approximated noting that the dominant decays of the T go into 3 gluons and into lepton- or quark-pairs, and neglecting other decay modes,

$$\Gamma_{tot} = \Gamma_{3g} + (R + 3)\Gamma_{ee} + \ldots .$$

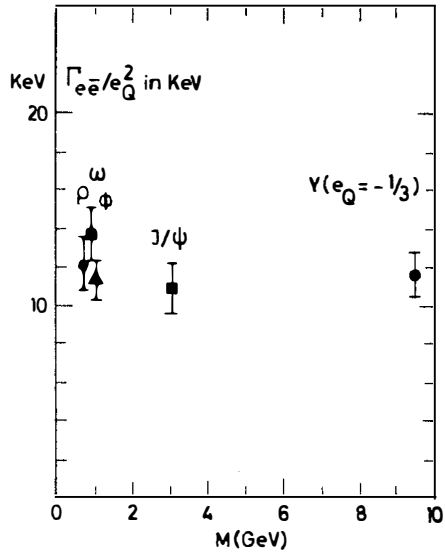

Fig. 3 The ratio of the electronic width Γ_{ee} over the square of the e_Q^2 for radial ground state vector mesons as a function of mass.

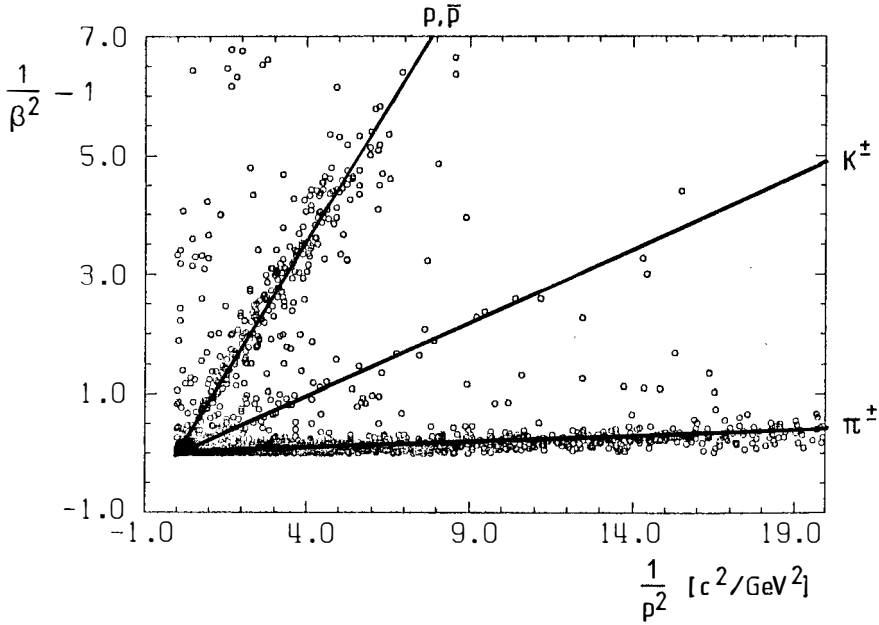

Fig. 4 The particle separation properties of the DASP detector.

where $R = \sigma_h/\sigma_{\mu\mu}$ denotes the ratio of the cross sections for hadron to muon production in the continuum below the Υ. Finally the strong coupling constant α_s is given by

$$\alpha_s = 0.0557 \sqrt[3]{1/B_{\mu\mu} - (R+3)} \quad ,$$

which leads to

$$\alpha_s(\Upsilon) = 0.17 \pm 0.02 \quad , \quad \text{to be compared with}$$

$$\alpha_s(J/\psi) = 0.19 \pm 0.02 \quad , \quad \text{obtained the same way.}$$

Experimentally the reaction $\Upsilon \to \mu\mu$ determines α_s with a maximum of precision. This should be a challenge to theory, to compute the higher order corrections to the now available first order expressions.

$\Gamma_{tot}(\Upsilon)$ has almost the same size as $\Gamma_{tot}(J/\psi) = (67 \pm 12)$ keV. This suggests that the nature of the two mesons is indeed very similar, and is in fact the strongest proof that the Υ is a bound state of b-quarks, carrying the fifth flavour.

$\Delta M(\Upsilon',\Upsilon)$, the mass difference between the Υ' and the Υ resonance, gives evidence for the flavour independence of the quark force. Over the range, where the quark potential is probed by the J/ψ and Υ states, it is well described by a logarithmic shape. For a logarithmic potential the level spacing is independent from the quark mass. Thus, the observation of about equal level spacing for the Υ- and the J/ψ-states is evidence for the flavour independence of the quark force.

INCLUSIVE SPECTRA

It is believed that e^+e^- annihilation proceeds via an initial quark-antiquark pair fragmenting into hadrons in the continuum. In contrast, intermediate quarkonium states such as J/ψ or Υ decay predominantly into three gluons, which again fragment into hadrons. Hence one might expect to find differences in the particle spectra from quarkonium decay and from non-resonant production.

The inclusive spectra of $\pi^\pm$, $K^\pm$ and $\bar{p}$ produced at the Υ, the Υ' and the nearby continuum have been measured [7]. The DASP detector is ideally suited for these measurements due to its excellent particle identification properties, as can be seen in Fig. 4.

Fig. 5 shows the invariant cross section $E\, d^3\sigma/dp^3$ as a function of the hadron energy E in the three regions of interest. The on-resonance cross sections refer

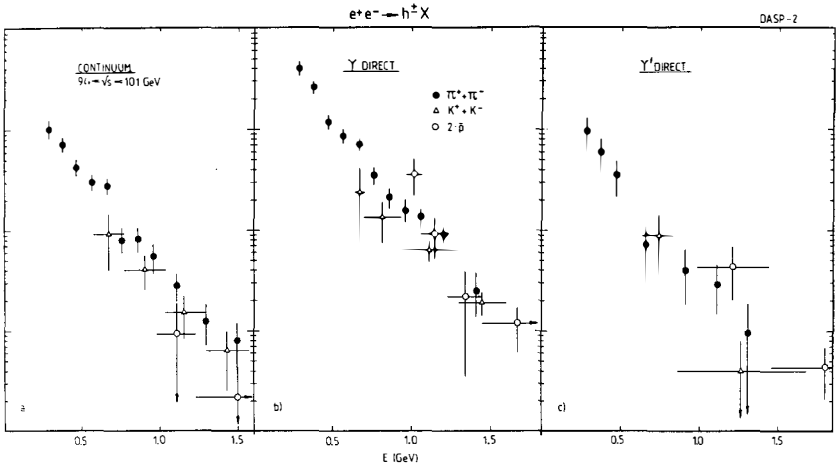

Fig. 5 Invariant cross sections $E\,d\sigma^3/dp^3$ as a function of particle energy E for the sum of π^+ and π^-, K^+ and K^- and twice the $\bar{p}$ production in the continuum (a), and for direct decays of Υ(b) and Υ' (c).

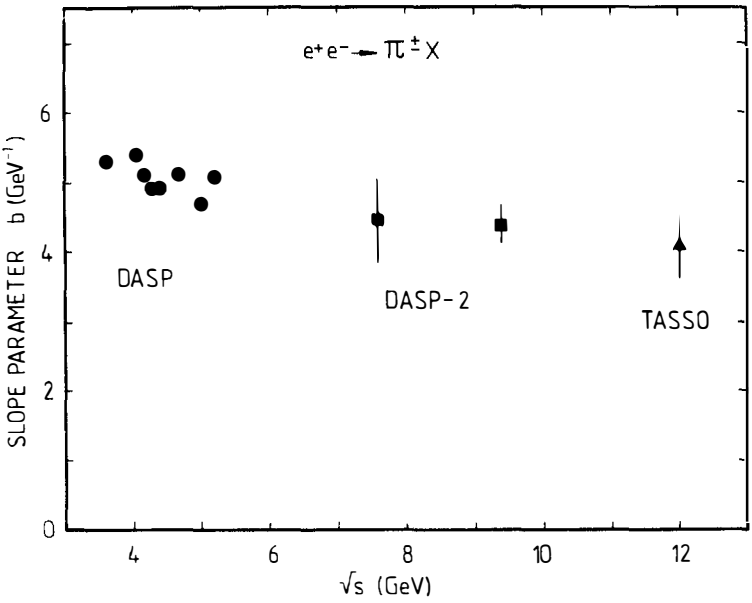

Fig. 6 Slope parameter b versus $\sqrt{s}$ for non-resonant $\pi^\pm$ production obtained from exponential fits to the invariant cross sections, $Ed\sigma^3/dp^3 \propto \exp(-bE)$. Data points are from DASP, Ref. 8, TASSO, Ref. 9 and this experiment, where the point of 7.6 GeV was obtained from unpublished data.

to the direct decays only. Contributions from non-resonant background and vacuum polarization have been subtracted.

The invariant cross sections can be approximated by an exponential, $Ed^3\sigma/dp^3 \propto \exp(-bE)$. From the least-squares fit we get $b = (4.4 \pm 0.3)$ GeV^{-1} for non-resonant pion production. This value agrees with the slope parameters for pion production in the continuum measured at other energies [8,9], as shown in Fig. 6. The slope appears to fall slightly, weaker than $1/\sqrt{s}$, with the centre of mass energy.

The pion spectrum from direct Υ decay has a slope which is practically equal to the continuum value, if fitted over the entire measured energy range. However, its lower part ($E < 1$ GeV) falls off faster, with $b = (4.9 \pm 0.2)$ GeV^{-1}

The average number of charged pions, kaons and antiprotons can be calculated by a numerical integration of the measured spectra. Using $R = \sigma_h/\sigma_{\mu\mu} = 3.6 \pm 0.2$ and the exponential fits described above in order to extrapolate to zero energy, we find a total charged hadron multiplicity of 6.9 ± 0.6 in the continuum and 7.9 ± 0.6 for direct Υ decay, in agreement with other experiments [10,11]. This observation is in contrast to early speculations, which predicted a much higher multiplicity from gluon fragmentation. The average fraction of the centre of mass energy carried by the charged hadrons was calculated in the same way as the multiplicity. We obtain $\langle E_{ch}\rangle_{off}/\sqrt{s} = (51.8 \pm 8.0)\%$ in the continuum and $\langle E_{ch}\rangle_{on}/\sqrt{s} = (48.0 \pm 3.6)\%$ for direct Υ decays. Again this result is in contrast to speculations, which expected an excess of neutral particles produced by gluon fragmentation.

The invariant cross sections of the three types of hadrons in the continuum and on the Υ resonances are close together (cf. Fig. 5). However, antiproton production appears to be more abundant on resonance than off resonance. The ratio between the yields of $2\bar{p}$ and all charged hadrons is indeed as high as $(8.1 \pm 2.1)\%$ for direct Υ decay compared to $(1.5 \pm 1.1)\%$ in the continuum. This increase of $(6.6 \pm 2.4)\%$ has a statistical significance of 2.8 standard deviations. A similar effect of 2.5 standard deviations is found for direct Υ' decays.

The fractions of the various charged particles are summarized in Table II Using the mean charged multiplicity as determined above, the average number o antiprotons per event comes out to be $\langle\bar{p}\rangle = 0.32 \pm 0.08$ on the Υ, and $\langle\bar{p}\rangle = 0.05 \pm 0.03$ in the continuum.

TABLE II

Particle ratios in the momentum range $0.3 < p < 1.5$ GeV/c

	$2\bar{p}$	$K^{\pm}$	$\pi^{\pm}$
continuum	0.015 ± 0.011	0.183 ± 0.039	0.802 ± 0.059
T	0.081 ± 0.021	0.154 ± 0.027	0.765 ± 0.048
T'	0.189 ± 0.069	0.119 ± 0.072	0.692 ± 0.129

It is interesting to note that a similar rise in the antiproton yield has been seen on the J/ψ [8]. In the continuum, a large production of (anti)baryons has recently been reported by PETRA groups around 30 GeV [12]. Since it is believed that gluon emission processes become appreciable at this energy and that, on the other hand, the J/ψ and T states decay primarily via three gluons, one may wonder whether more copious baryon production is connected with gluon fragmentation. This effect of about three standard deviations deserves a more thorough investigation both theoretically and experimentally.

OUTLOOK

A workshop on DORIS experiments was held at DESY in February 1981. Potential improvements of the storage ring and experiments with an upgraded DORIS were discussed. Dr. K. Wille proposed an improvement programme for DORIS, which foresees the following achievements :

An increase of the luminosity at T energies from 10^{30} to 10^{31} $cm^{-2}s^{-1}$.
An increase of the maximum centre of mass energy from 10.2 to 11.2 GeV.
A reduction of the power consumption to one half of the present value.

This upgraded machine would be an excellent tool with which to study the T-region, including B-mesons. Preparations have been started to have this improvement programme completed in the summer of 1982.

Two detectors will be available at this time. A magnetic universal detector called ARGUS is under construction. In addition a complementary, Crystal Ball type detector will be installed. It could be an upgraded LENA detector or even the famous Crystal Ball itself, which is now running at SPEAR.

The discussion of possible experiments at the Workshop showed that a large number of important but difficult experiments are possible at DORIS.

REFERENCES

1) C.W. Darden et al., Phys.Lett. 76B (1978) 246
Ch. Berger et al., Phys.Lett. 76B (1978) 243.

2) H. Hasemann, thesis, University of Hamburg, (1981)

3) M. Albrecht et al., Phys.Lett. 93B (1980) 500

4) J. Bienlein et al., Phys.Rev.Lett. 46 (1981) 92

5) Ch.Berger et al., Phys.Lett. 93B (1980) 497

6) T. Appelquist and A.D. Politzer, Phys.Rev.Lett 34 (1975) 43
V.A. Novikov et al., Physics Reports 41 (1978) 1

7) H. Albrecht et al., DESY 81-011, submitted to Physics Letters;
E. Steinmann, thesis, University of Hamburg, (1981)

8) R. Brandelik et al., Nucl. Phys. B148 (1979) 181

9) The slope parameter b at 12 GeV was calculated from data in Ref. 12

10) Ch. Berger et al., (PLUTO collaboration), DESY 80/117 (Dec. 1980), Zeitschrift für Physik C 8 (1981) 101

11) B. Niczyporuk et al. (LENA collaboration), DESY 81/8 (Jan. 1981) submitted to Zeitschrift für Physik C.

12) D. Pandoulas, rapporteur talk at the 20th International Conference on High Energy Physics, Madison, Wisconsin, 1980, and Imperial College Preprint IC/HENP/80/5 (1980).

RESULTS FROM LENA

LENA collaboration

U. Volland
Physikalisches Institut der Universität Erlangen-Nürnberg,
Glückstraße 10, D-8520 Erlangen

Abstract:

We report the observation of the decay $\Upsilon' \to \Upsilon \pi^+\pi^- \to l^+l^- \pi^+\pi^-$ using the LENA detector at the DORIS e^+e^- storage ring. From the 7 events seen and from the charged multiplicities of the Υ and Υ' decays we obtain a branching ratio $B(\Upsilon' \to \Upsilon \pi^+\pi^-)=(21\pm7)\%$. Using this B value we deduce $\Gamma_{tot}(\Upsilon')=(31\pm10)$ keV and $B_{ee}(\Upsilon')=(1.8\pm0.5)\%$. The estimated two gluon partial width ($\Upsilon' \to gg\Upsilon$) is in agreement with the QCD prediction using vector gluons. Results on the jet structure of the Υ and Υ' direct decays are also presented. The polar angular distribution of the jet axis behave like $1+\alpha(T)\cos^2\theta$ with $\langle\alpha(T)\rangle_\Upsilon = 0.7\pm0.3$ and $\langle\alpha(T)\rangle_{\Upsilon'} = 0.6\pm0.4$. The $\langle\alpha(T)\rangle_\Upsilon$ value is in agreement with the QCD vector gluon assignment.

Introduction

I want to report on an experiment using the LENA detector (Lead glass NaI) at the DORIS e^+e^- storage ring at DESY. The LENA detector was initially constructed by the DESY-Heidelberg group, but is now used and further developed by a Carnegie-Mellon/Cracow/DESY/Erlangen-Nürnberg/Hamburg/Michigan State/Nijmegen/Saclay/Tel-Aviv/Würzburg collaboration *).

The aim of the experiment was to get improved values of the resonance parameters of the Υ and Υ', to observe transitions from the Υ' to the Υ and to obtain first results on the topology of the Υ' decays. The study of the decay modes of the Υ' and the analysis of the topology of the charged hadron production at the Υ and Υ' resonances are of great interest since several crucial QCD features (e.g. the strong coupling constant α_s and the spin of the gluon) can be determined from these properties. Furthermore theoretical work carried out in the study of the J/ψ family can be applied and tested in the study of the Υ family.

The LENA detector

The LENA detector [1,2] is shown in Fig.1 in a view along the beam direction. Its main components are a track detector, an energy detector and a muon detector. The track detector consists of three cylindrical drift chambers and two cylindrical scintillation hodoscopes for triggering and timing. The track detector is surrounded by the energy detector (178 blocks of lead glass and NaI). It covers 72% of the solid angle 4π and is used to measure the energy of photons and electrons and the energy loss of hadrons and muons. The energy detector is then followed by the time of flight counters, a steel absorber, muon drift chambers and outer scintillation hodoscopes. The time-of-flight measurement enables us to clearly separate cosmic ray muons from muons produced in e^+e^- reactions. The luminosity was measured by large angle Bhabha scattering within the detector and also by small angle Bhabha scattering at

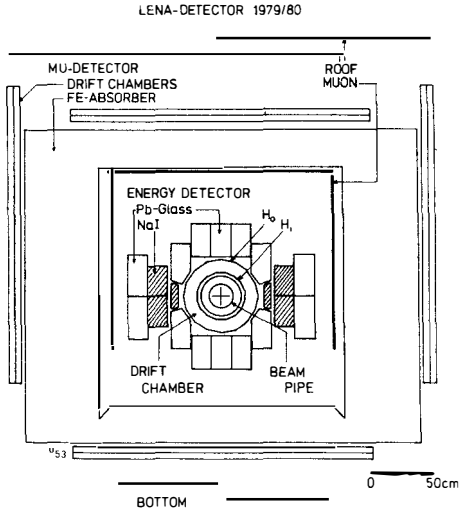

Fig.1 The LENA detector shown along the beam direction.

130 mrad scattering angle in a separate monitor.

Resonance Parameters

In 1979/80 we accumulated an integrated luminosity of about 2400nb^{-1}. The luminosity taken was nearly equally distributed among the Υ and Υ' resonances and the nearby continua. The corrected hadronic cross sections at the Υ and Υ' energies are shown in Fig.2. The fitted curves include the continuum cross section and a convolution of a radiatively corrected Breit-Wigner resonance cross section with a Gaussian machine energy distribution. From the fits one obtains M, the mass of the resonance and $\tilde{\Gamma}_{ee} := \Gamma_{ee} \cdot \Gamma_h / \Gamma_{tot}$, where Γ_{ee} is the electronic width, Γ_h the hadronic width and Γ_{tot} the total width. In order to obtain Γ_{ee} and Γ_{tot} one has to measure the muonic branching ratio $B_{\mu\mu} := \Gamma_{ee} / \Gamma_{tot}$. In the case of the Υ' resonance only an upper limit of $B_{\mu\mu}(\Upsilon')$ was obtained. The results are summarized in Table 1.

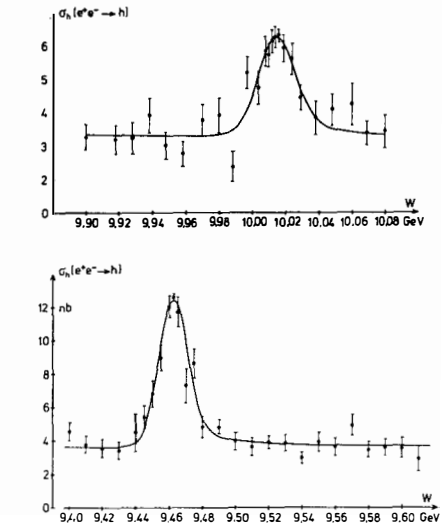

Fig.2 Hadronic cross sections at the Υ (top) and Υ' (bottom) energy regions.

Table 1: Results on the Υ and Υ' resonance parameters

	Υ	Υ'
Mass (MeV)	9461.6±0.6±10.0	10 013.6±1.2±10.0
$\tilde{\Gamma}_{ee}$ (keV)	1.10±0.07±0.11	0.53±0.07±0.06
$B_{\mu\mu}$ (%)	3.5 ±1.4 ±0.4	< 4.5 (95% c.l.)
Γ_{ee} (keV)	1.23±0.10±0.14	0.56±0.07±0.06

The Decay $\Upsilon' \to \Upsilon \pi^+ \pi^-$

The observation of the decay $\Upsilon' \to \Upsilon \pi^+ \pi^-$ constitutes a direct evidence for a tran-

sition linking two states of the bottonium system. To identify the decay $\Upsilon' \rightarrow \Upsilon + \pi^+\pi^-$ we have searched for the reaction $e^+e^- \rightarrow l^+l^-\pi^+\pi^-$ (l=μ or e). In scanning our data for such events we required the following cuts.

- 4 tracks from the interaction region
- 2 opposite tracks within 25° in the polar angle Θ and 12° in the azimuthal angle Φ for $\mu^+\mu^-$ or e^+e^- candidates. For a μ-pair both tracks have to penetrate the steel absorber and to hit outer muon detectors with the proper time of flight. The total deposited energy had to be less than 1.8 GeV, which is far above the typical energy deposit for two minimum ionizing muons and two charged pions. For the e^+e^- sample a minimum deposited energy of 3 GeV with at least 1.2 GeV behind each track was required.
- the 2 (pion) tracks had to deposit less than 0.6 GeV.

With these cuts we arrived at a final sample:

- 3 events of the type $\mu^+\mu^-\pi^+\pi^-$
- 5 events of the type $e^+e^-\pi^+\pi^-$.

Fig.3 shows one event of each type. One event of the type $\mu^+\mu^+\pi^+\pi^-$ could not be

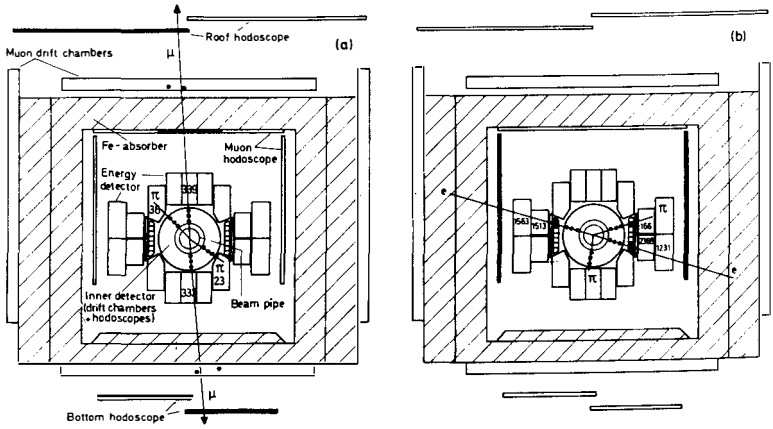

Fig.3 Two events of the type $e^+e^- \rightarrow l^+l^-\pi^+\pi^-$ in the LENA detector. The numbers in the blocks give the deposited energy in MeV. The almost collinear lepton tracks either penetrate the Fe-absorber and hit outer muon chambers a) or shower in the energy detector b).

kinematically reconstructed and was therefore rejected. It should be mentioned that none resonant higher order QED processes may look in the LENA-detector like a $l^+l^-\pi^+\pi^-$ event. That none of our seven events were found off the Υ' resonance strongly indicates that the contribution of these higher order processes to our $\Upsilon' \rightarrow \Upsilon\pi^+\pi^- \rightarrow l^+l^-\pi^+\pi^-$ sample can be neglected.

The branching ratio $B(\Upsilon' \rightarrow \Upsilon\pi^+\pi^-)$ was calculated by the relation

$$B(\Upsilon' \rightarrow \Upsilon \pi^+\pi^-) = \frac{N(ll\pi\pi)\ \varepsilon(\Upsilon' \rightarrow X)}{N(\Upsilon' \rightarrow X)\ \varepsilon(ll\pi\pi)} \cdot \frac{1}{B_{ll}(\Upsilon)} \qquad (1)$$

Where the N's and ε's denote the numbers and the detector efficiencies of the indicated events ($N(\Upsilon' \rightarrow X)=1680\pm110$, $\varepsilon(\Upsilon' \rightarrow X)=0.77$, $\varepsilon(e^+e^-\pi^+\pi^-)=0.375$, $\varepsilon(\mu^+\mu^-\pi^+\pi^-)=0.15$). The efficiencies were determined by Monte Carlo calculations. $B_{ll}(\Upsilon)$ is the leptonic branching ratio of the Υ. Using the world average value $B_{ll}(\Upsilon)=(3.2\pm0.8)\%$ [2,3] we obtained $B(\Upsilon' \rightarrow \Upsilon \pi^+\pi^-)$ values of (19+10)% and (19±14)% for the decay modes $e^+e^-\pi^+\pi^-$ and $\mu^+\mu^-\pi^+\pi^-$, respectively. An independent value of this branching ratio of (26±13)% was determined by comparing the charged multiplicity of the Υ and Υ' decays [4]. The weighted average is $B(\Upsilon' \rightarrow \Upsilon \pi^+\pi^-)=(21\pm7)\%$.

Deduced Results: $\Gamma_{tot}(\Upsilon')$, $B_{ee}(\Upsilon')$, $\Gamma_{2g}(\Upsilon' \rightarrow gg\Upsilon)$

Using the above result some estimates concerning the total and partial width of Υ' can be made. Isospin symmetry requires the decay $\Upsilon' \rightarrow \Upsilon \pi^\circ\pi^\circ$ to have half the probability of the $\pi^+\pi^-$ mode. Hence, the total branching ratio is $B(\Upsilon' \rightarrow \Upsilon \pi\pi)=(31\pm10)\%$.

Neglecting decay modes of the Υ' with very small branching ratios the total width of Υ' is given by

$$\Gamma_{tot}(\Upsilon') \approx \Gamma_{3g}(\Upsilon') + \Gamma_{2g}(\Upsilon') + \Gamma_{P\gamma}(\Upsilon') + \Gamma_{"\gamma"}(\Upsilon') \qquad (2)$$

The subscripts indicate: 3g: $q\bar{q}$ annihilation into three hard gluons; 2g: hadronic transition to the Υ by emission of two soft gluons which fuse into a pion pair; P_γ: electric dipole transition to the P-states; "γ": $q\bar{q}$ annihilation via a virtual photon into leptons and hadrons (vacuum polarisation). For the Υ the decay channels 2g and P_γ are absent.

Therefore:

$$\Gamma_{tot}(\Upsilon) \approx \Gamma_{3g}(\Upsilon) + \Gamma_{"\gamma"}(\Upsilon) \qquad (3)$$

Γ_{3g} and $\Gamma_{"\gamma"}$ are directly proportional to Γ_{ee}, the width for annihilation into an e^+e^- pair [5].

Using this proportionality (the same for Υ and Υ') and the definition of $B_{ee} := \Gamma_{ee}/\Gamma_{tot}$ one obtains

$$\Gamma_{3g}(\Upsilon') + \Gamma_{"\gamma"}(\Upsilon') = \Gamma_{ee}(\Upsilon') \cdot \frac{\Gamma_{tot}(\Upsilon)}{\Gamma_{ee}(\Upsilon)} = \frac{\Gamma_{ee}(\Upsilon')}{B_{ee}(\Upsilon)} \qquad (4)$$

From the branching ratio $B(\Upsilon' \rightarrow \Upsilon \pi\pi)$ one gets the relation

$$\Gamma_{2g}(\Upsilon') = B(\Upsilon' \rightarrow \Upsilon \pi\pi) \cdot \Gamma_{tot}(\Upsilon') \tag{5}$$

Combining eq.(2), (4) and (5) yields

$$\Gamma_{tot}(\Upsilon') = \left[\Gamma_{ee}(\Upsilon')/B_{ee}(\Upsilon) + \Gamma_{P\gamma}(\Upsilon')\right] / \left[1 - B(\Upsilon' \rightarrow \Upsilon \pi\pi)\right] \tag{6}$$

The only not yet measured quantity of eq.(6) is the width $\Gamma_{P\gamma}(\Upsilon')$. Therefore we estimate it by scaling the corresponding charmonium value [6,7] using the logarithmic quarkonium potential

$$\Gamma_{P\gamma}(\Upsilon') = \left[e_b/e_c\right]^2 \cdot \left[m_c/m_b\right] \cdot \Gamma_{P\gamma}(\psi') \approx 4.2 \text{ keV} \tag{7}$$

(e and m are the charge and the mass of the quarks indicated). We finally obtain: $\Gamma_{tot}(\Upsilon')=(31^{+10}_{-7})$keV, $B_{ee}(\Upsilon')=\Gamma_{ee}(\Upsilon')/\Gamma_{tot}(\Upsilon')=(1.8\pm0.5)\%$ and $\Gamma_{2g}(\Upsilon')=(10\pm5)$ keV. At last we compare the hadronic width Γ_{2g} of the Υ' and ψ' [7]. The measured ratio

$$\frac{\Gamma_{2g}(\Upsilon')}{\Gamma_{2g}(\psi')} = \frac{(10 \pm 5) \text{ keV}}{(110 \pm 22) \text{ keV}} = 0.09 \pm 0.05 \tag{8}$$

is in agreement with the expected mass scaling behaviour of QCD dipole radiation [8]

$$\Gamma_{2g}(\Upsilon')/\Gamma_{2g}(\psi') = \left(m_c/m_b\right)^2 = \left(M_{J/\psi}/M_\Upsilon\right)^2 = 0.11 \tag{9}$$

For scalar gluons this ratio is expected to be near unity [9]. This is incompatible with our experimental result.

Hadron Jet Analysis

Off resonance the event topology is expected to be of a two jet structure due to quark-antiquark fragmentation. The direct decay, however, is expected to be mediated by three gluons which lead to three hadron jets. In the case of the Υ' the jet structure is somewhat more complex due to several additional decay channels. In general the three jets are not resolved, due to relatively small CM-energies. Nevertheless, there should be a difference in the space configuration of the direct decay events and the two jet structure of the continuum. The cross feature of the angular structure of the continuum and the resonance direct decays was studied by the $\cos\delta$ distribution, where δ is the opening angle between pairs of tracks.[10] In Fig.4 the experimental $\cos\delta$ distributions with the Monte Carlo (MC) calculations are compared. Off resonance the distributions are strongly enhanced at values $\cos\delta = \pm 1$ and well described by $q\bar{q}$ Monte Carlo calculation. The Υ and Υ' distributions in $\cos\delta$ are essentially the same but less

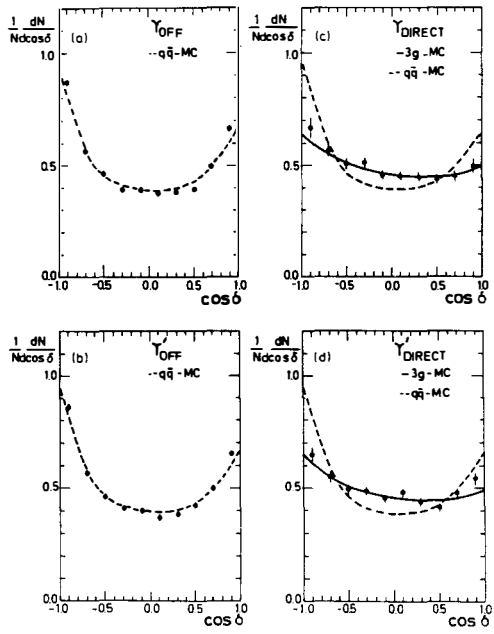

Fig.4 The normalized $\cos\delta$ distributions for Υ_{off} (a), Υ'_{off} (b) and Υ direct (c) and Υ' direct (d) data.

enhanced than the continuum. The data are well described by the 3 gluon Monte Carlo calculation. For a quantitative measure of the jet structure a thrust like quantity was used. It is defined by:

$$T' = \max\left\{\frac{\sum_{i=1}^{N}|\cos\vartheta_i|}{N}\right\}$$

where ϑ_i is the angle between the track i and the axis which maximizes $\sum_{i=1}^{N}|\cos\vartheta_i|$ and N is the number of charged particle tracks in a given event.

The normalized experimental thrust distributions and the predicted curves from $q\bar{q}$ and 3 gluon Monte Carlo calculations are shown in Fig.5. The $q\bar{q}$ MC fits the continuum data adequately well whereas the direct decay data of Υ and Υ' are better described by the 3 gluon MC prediction.

The average thrust of the Υ and Υ' direct decays are nearly equal ($\langle T'(\Upsilon)\rangle = 0.718 \pm 0.035$, $\langle T'(\Upsilon')\rangle = 0.722 \pm 0.026$) but are significantly lower than those corresponding to the nearby continua ($\langle T'_{cont}(\Upsilon)\rangle = 0.777 \pm 0.004$; $\langle T'_{cont}(\Upsilon')\rangle = 0.771 \pm 0.003$). The angular distributions of the thrust axis with respect to the beam axis are shown in Fig.6. The angular distributions of the thrust axis were fitted with a $1+\alpha\cdot\cos\Theta$ function and the α values are compared with the predictions from theory. The continuum data yield a value of $\alpha = 0.7 \pm 0.1$. This value is smaller than that one expected from theory for spin 1/2 pointlike quarks ($\alpha_{th} = 1$). The theoretical curve is indicated by the dashed line.

From the fits of the Υ and Υ' direct decay data the averaged values $\langle\alpha_{\Upsilon}(T)\rangle = 0.7 \pm 0.3$ and $\langle\alpha_{\Upsilon'}(T')\rangle = 0.6 \pm 0.4$ are derived. Fig.6b), c) also contains the theoretical expectation for scalar gluons [12] $\langle\alpha(T)\rangle = -0.995$ (dashed-dotted lines) and for vector gluons [11] $\langle\alpha(T)\rangle = 0.39$ (dashed lines). The vector gluon prediction is in good agreement with the experimental data, whereas scalar

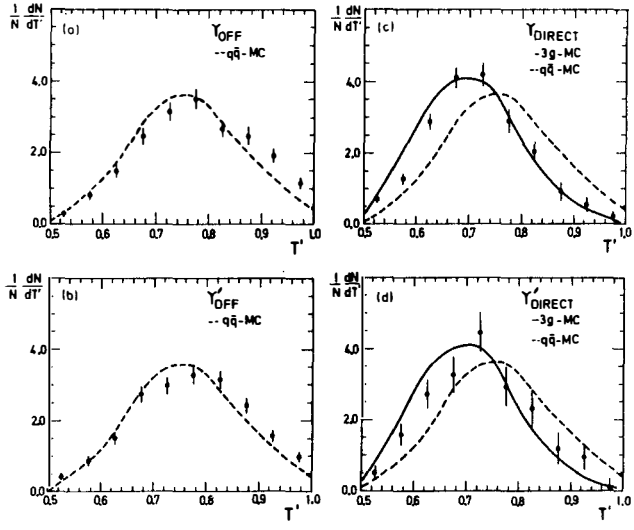

Fig.5 The thrust T' distributions for the Υ_{off} (a), Υ'_{off} (b) and Υ(c) and Υ' direct decay (d) data.

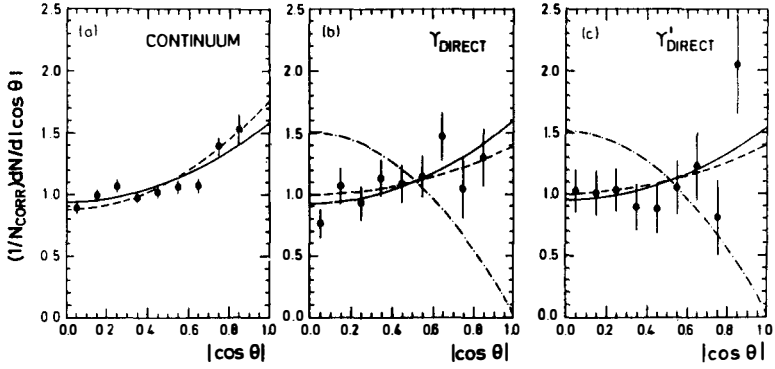

Fig.6 The thrust angular distribution for (a) the combined continuum data between 9 and 10 GeV, (b) the Υ direct and (c) the Υ' direct data.

gluons are rejected by more than four standard deviations.

References:

*) The members of the collaboration are: M. Coles, A. Engler, R.W. Kraemer, D. Marlow, F. Messing, C. Rippich, B. Stacey, S. Youssef/B.Niczyporuk, T. Zeludziewicz/J.K. Bienlein, R. Graumann, J. Krüger, M. Leißner, M. Schmitz, H.J. Trost/G. Folger, B. Lurz, H. Vogel, U. Volland, H. Wegener/F.H. Heimlich, R. Nernst, A. Schwarz, U. Strohbusch, P. Zschorsch/K.W. Chen. R. Hartung/ A. König, M. Raymakers, J. Schotanus/A. Fridman/G. Alexander, A. Av-Shalom, G. Bella, Y. Gnat, J. Grunhaus/E. Hörber, W. Langguth, M. Scheer/

1) W. Bartelt et al., Phys.Lett. 64B (1976) 483, 77B (1978) 331
   LENA Collab., B. Niczyporuk et al., Phys.Lett. 99B (1981) 169
2) LENA Collab., B. Niczyporuk et al., Phys.Rev.Lett. 46 (1981) 92
3) PLUTO Collab., Chr. Berger et al., Phys.Lett. 93B (1980) 497
   DASP Collab., H. Albrecht et al., Phys.Lett. 93B (1980) 500
4) LENA Collab., B. Niczyporuk et al., Phys.Lett. 100B (1981) 95
5) E. Eichten et al., Phys.Rev. D17 (1978) 3090, D21 (1980) 203
6) K. Gottfried, The Spectroscopy of the new particles, in:
   Proc. 1977, Intern. Symp. on Lepton and Photon Interaction at
   High Energies, ed. F. Gutbrod (DESY Hamburg, 1977)
7) Particle Data Group, Rev.Mod.Phys. 52 (1980) No.2
8) K. Gottfried, Phys.Rev.Lett. 40 (1978) 598
9) T.-M. Yan, Phys.Rev. D22 (1980) 1652
10) LENA Collab., B. Niczyporuk et al., Charged hadron production in
    e^+e^- annihilation in the Υ and Υ' region, DESY report 81/008 (1981)
11) K. Koller, H. Krasemann, and T.F. Walsh, Z. Physik C1 (1979) 71
12) K. Koller and H. Krasemann, Phys.Lett. 88B, 119 (1979)

E(G)(1420): $s\bar{s}$ VERSUS GG

Ted Barnes
Rutherford Laboratory
Theory Division
Chilton, Didcot, Oxon. Oxll OQX
England

ABSTRACT

The E(G)(1420) may be an $s\bar{s}$ state, a glueball, or both. We study the spectrum of $s\bar{s}$ and transverse gg states in potential models to see if the alternatives can easily be distinguished. We conclude that either identification is possible; the models require $M_{s\bar{s}}(1^{++}) \simeq 1.45$ GeV and $M_{gg}(0^{-+}) \sim 1.3$ GeV. The glueball option predicts a degenerate 0^{++} gg state. We also discuss the masses and quantum numbers of other $s\bar{s}$ and gg states.

The Mark II detector at SPEAR recently studied the decay $\psi \to X\gamma$ in a search for gg resonances. An unexpectedly large signal is seen at $M_X = 1.44$ GeV[1]. It has been suggested that this X(1.44) state is an $s\bar{s}$ 1^{++} strangeonium state E(1420)[2], or alternately, that it is a 0^{-+} gg state, called the G(1440)[3].

To explain the puzzling experimental status of $I^G = 0^+$ states in this mass region (reviewed by S.U. Chung at this conference[4]), Chanowitz[3] suggested the existence of both $s\bar{s}$(E) and gg(G) resonances at $\sim$ 1.45 GeV, which are accidentally degenerate. This alternative can account for some otherwise puzzling aspects of the production of the E(G)[3,4].

To help clarify the situation, we shall consider two questions regarding the spectrum of these states in the context of potential models. The questions and answers are as follows:

1. Within a plausible range of potential model parameters, is an $s\bar{s}$ 1^{++} unavoidably predicted near 1.45 GeV? Yes.

2. What spectrum of transverse gg states do we expect? A (0^{++}, 0^{-+}) degenerate pair at M_0; a 2^{++} at $\sim 1.8\ M_0$; a (0^{++}, 0^{-+})' radial excitation at $\sim 2.0\ M_0$; many states above $\sim 2.4\ M_0$; no exotics. M_0 is estimated to be $\sim$ 1.3 GeV.

1. $s\bar{s}$

We fit the $s\bar{s}$ system with the conventional vector Coulomb plus linear scalar potential used to treat charmonium by Eichten et al[5] and Krammer and Krasemann[6], and we use the complete $O(v^2/c^2)$ hyperfine hamiltonian as a first order perturbation. The hyperfine terms[7] are derived from the general results of Gromes[8].

$$V_0 = \underbrace{-\frac{4\alpha_s}{3r}}_{\text{vector}} + \underbrace{ar}_{\text{scalar}} \qquad (1)$$

$$V_{hfs} = \underbrace{-\frac{\vec{p}^4}{4m^3}}_{\text{Rel.K.E.}} + \underbrace{\frac{4\pi\alpha_s}{3m^2}\left(1 + \frac{8}{3}\vec{S}_1\cdot\vec{S}_2\right)\delta(\vec{r})}_{\text{Contact + Spin-Spin}} + \underbrace{\frac{4\alpha_s}{m^2 r^3}\left(\vec{S}_1\cdot\hat{r}\vec{S}_2\cdot\hat{r} - \frac{1}{3}\vec{S}_1\cdot\vec{S}_2\right)}_{\text{Tensor}}$$

$$+ \underbrace{\frac{1}{m^2}\left(\frac{2\alpha_s}{r^3} - \frac{a}{2r}\right)\vec{L}\cdot\vec{S}}_{\text{(Vector + Scalar) Spin-Orbit (note relative sign)}} \underbrace{- \frac{a}{m^2 r}\left(1 + \tfrac{1}{2}\vec{L}^2\right)}_{\text{Scalar Shift}} \underbrace{- \frac{2\alpha_s}{3m^2 r}\left(\vec{p}^2 + \hat{r}(\hat{r}\cdot\vec{p})\vec{p}\right)}_{\text{Magnetic}} \qquad (2)$$

Typical parameter values for charmonium[5-7] are $\alpha_s = 0.4$ and $a = 0.18\ \text{GeV}^2$.

The problem with fitting the $s\bar{s}$ system is the lack of data, as there are only two solid $s\bar{s}$ states, the $\phi(1.019)\ 1^{--}$ and the $f'(1.516)\ 2^{++}$; the $E(1.42?)$ and $\phi'(1.64?)$[9] are not yet well enough established to be used

Erratum

T.BARNES "E(G)(1420) : $\bar{s}s$ versus gg" p.175

The gg matrix element of $\vec{L}.\vec{S}$ given in this paper is incorrect, which changes the spectrum of gg states quoted here. The degeneracy of $J^{PC}=(2n)^{++}$ states is however unchanged. The effect of this change is given in the revised paper "A Transverse Gluonium Potential Model with Breit-Fermi Hyperfine Effects", Z.Phys.C10,275(1981).

ranges from 1.42 → 1.49 GeV. The variation of other levels is discussed in

detail elsewhere[7]. So, we conclude that the potential model in its present form unavoidably predicts an $s\bar{s}$ 1^{++} state near 1.45 GeV.

2.gg

Now we consider the spectrum of gg states predicted by a potential model. As potential models (quite surprisingly!) give a good qualitative description of much of the light meson and baryon[11,12] spectrum, we expect that they will give a resonable zeroth order estimate of the gg spectrum, providing we are not too naive.

As gauge invariance eliminates the longitudinal mode as a physical degree of freedom to lowest order in g, we use asymptotic states constructed from transverse gluon states only. The problem of constructing these states is the same as the two photon problem, discussed by Landau and Jacob and Wick[13,14]. There are two general series of states, helicity singlets (even and odd, $J^{PC} = 0_s^{\pm+}$, $2_s^{\pm+}$, $4_s^{\pm+}$, ...), and helicity doublets ($J^{PC} = 2_d^{++}$, 3_d^{++}, 4_d^{++}, ...). The angular and helicity dependence of these states is shown in Figs.2a, 2b.

The suggestion of using only transverse gluon states to construct glueballs is due to Fritzsch and Minkowski[15].

To obtain the Breit-Fermi gg hamiltonian due to one gluon exchange and the 4-gluon contact term, we Fourier transform the $O(g^2)$ scattering amplitude in the Breit frame, after introducing a gluon mass μ in the energies and polarization vectors and expending to $O(v^2/c^2)$. This procedure, as well as the above states and their matrix elements, is described in detail elsewhere[16]. The resulting potential and Breit-Fermi terms are;

FT 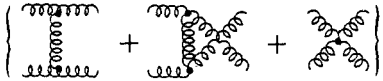

$$= -\frac{3\alpha_s}{r}$$

Coulomb

$$+\frac{\pi\alpha_s}{\mu^2}\,(4 + (8-3)\,\vec{S}_1\cdot\vec{S}_2)\,\delta(\vec{r}) + \frac{9\alpha_s}{\mu^2 r^3}\,(\vec{S}_1\cdot\hat{r}\;\vec{S}_2\cdot\hat{r} - \tfrac{1}{3}\,\vec{S}_1\cdot\vec{S}_2)$$

Contact + (t-channel + 4-gluon) Spin-Spin Tensor

$$-\frac{3\alpha_s}{2\mu^2 r}\,(\vec{p}^2 + \hat{r}\cdot(\hat{r}\cdot\vec{p})\vec{p}) + \frac{9\alpha_s}{4\mu^2 r^3}\,(\vec{S}_1 + \vec{S}_2)\cdot\vec{L}$$

Magnetic Spin-Orbit

$$-\frac{9\alpha_s}{2\mu^2 r^3}\,\left((\vec{\varepsilon}_1\cdot\hat{r}\;\vec{\varepsilon}_1'^{*}\cdot\hat{r} - \tfrac{1}{3}\,\vec{\varepsilon}_1\cdot\vec{\varepsilon}_1'^{*}) + (1\leftrightarrow 2)\right) \qquad (3)$$

Polarization Tensor

FT 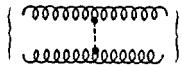

$$= a_g r$$

(input scalar confinement term)

$$-\frac{a_g}{2\mu^2 r}\,(\vec{S}_1 + \vec{S}_2)\cdot\vec{L}$$

Scalar Spin-Orbit

$$+\frac{a_g}{2\mu^2 r}\,\left((\vec{\varepsilon}_1\cdot\hat{r}\;\vec{\varepsilon}_1'^{*}\cdot\hat{r} - \tfrac{1}{3}\,\vec{\varepsilon}_1\cdot\vec{\varepsilon}_1'^{*}) + (1\leftrightarrow 2)\right)$$

Scalar Polarization Tensor

$$+ \ldots \text{ (spin-independent terms } \propto (\vec{\varepsilon}_1\cdot\vec{\varepsilon}_1'^{*})\;(\vec{\varepsilon}_2\cdot\vec{\varepsilon}_2'^{*})) \qquad (4)$$

We have repeatedly used $\vec{S}_i = i\,\vec{\varepsilon}_i \times \vec{\varepsilon}_i'^{*}$ and have dropped factors such as $(\vec{\varepsilon}_1\cdot\vec{\varepsilon}_1'^{*})\;(\vec{\varepsilon}_2\cdot\vec{\varepsilon}_2'^{*})$ which have unit matrix elements between the transverse gg states.

Interesting features of this hamiltonian include the 4-gluon inverted spin-spin term and the new "polarization tensor" interaction, which has no analogue in $(\frac{1}{2}) \times (\frac{1}{2})$.

To estimate the gg state spectrum, we solve the Schrödinger equation numerically for the Coulomb plus linear potential with a constituent gluon mass μ, and treat the Breit-Fermi hamiltonian as a first order perturbation. We take $\alpha_s = 0.6$ as a representative value for light mesons[7], and we choose to let $\mu = \sqrt{a_g}$, so only one mass scale remains in the problem. The choice constituent mass = $\sqrt{}$long range force coefficient is reasonable as the current mass goes to zero, as $a_g(\text{GeV}^2)$ is the only remaining scale in the problem. This choice is acceptable for light quarks, as fitting a_q and m_q independently typically gives $m_q \sim .35$ GeV and $a_q \sim .16$ GeV^2. Note $m_q \simeq \sqrt{a_q}$; .35 GeV $\simeq \sqrt{.16}$ GeV^2 = .4 GeV.

The actual value chosen for the mass scale $\mu = \sqrt{a_g}$ requires knowledge of the octet-octet long-range color force, relative to the approximately known $3 - \bar{3}$ force, $a_q \sim .18$ GeV^2. Several suggestions for this ratio a_g/a_q have been made[17,18]; the most reasonable is probably the bag model result[18], which gives asymptotically $a_g/a_q \sim e_g/e_q = 3/2$. This suggests that we take $a_g = .27$ GeV^2 as a trial value, and hence $\mu = .52$ GeV.

The unperturbed spectrum predicted by the Schrödinger equation with these parameters is given in Fig.3. The ground state is a degenerate pair, $(0^{\pm+})$, at M_0, with a first excited state (2^{++}) at 1.77 M_0 and a radial excitation of the $(0^{\pm+})$ at 2.01 M_0. With the values suggested above for a_g and μ, we find $M_0 = 1.28$ GeV. The 2^{++} and $(0^{\pm+})'$ are estimated to lie at $\sim$ 2.3 GeV and $\sim$ 2.6 GeV, respectively.

When we take matrix elements of the Breit-Fermi hamiltonian, we find two interesting results. First, the matrix elements are numericaly so large for $\alpha_s = 0.6$ that we are left with no reliable prediction of the spectrum; shifts are on the order of M_0. Second, and more important,

although the shifts are numerically large, they do not lift the degeneracy of the $(2n)^{\pm+}$ pairs we found to zeroth order. So, the prediction of an approximately degenerate $(0^{\pm+})$ pair remains at the one gluon exchange level, although it is arguable where this pair of states lies. A reasonable guess is that the zeroth order potential model spectrum is approximately correct, although the levels will show higher order shifts and splittings due to effects such as mixing with $q\bar{q}$ states and multiple gluon exchange.

To summarize, we find that both $s\bar{s}$ and gg states are expected near the X(1.44) mass. If the X is a 0^{-+} gg state, we should also see a 0^{++} gg state nearby in mass in $\psi \to X\gamma$, $X \to K\bar{K}$, $\pi\pi$, $\eta\eta$. The weakness of the 2^{++} signal relative to the expectation of a tree-diagram QCD calculation, reported at this conference by Navelet[19], is accounted for in this picture, as we expect the 2^{++} gg state at $\sim$ 2.5 GeV, which restricts the phase space available in $\psi \to gg(2^{++})\gamma$ considerably.

It is a pleasure to thank Lucien Montanet, Tran Thanh Van, and the staff and participants of this conference for a very enjoyable and useful experience. I would also like to thank the Rutherford Laboratory Theory Group for supporting this work and for making my attendance possible.

REFERENCES

1. D.L. Scharre et al, SLAC-PUB-2514 (May 1980).
2. J. Coyne et al, E(1420): Glueball or Quarkonium?, College of William and Mary preprint (1980).
3. M. Chanowitz, LBL preprint LBL-11977 (Dec.1980).
4. S.U. Chung, 1981 Moriond Conference (these proceedings).
5. E. Eichten et al, Phys. Rev. D21, 203 (1980).
6. M. Krammer, H. Krasemann, XVIII Schladming Conference (1979).
7. T. Barnes, Southampton preprint SHEP 79/80-4.

8. D. Gromes, Nucl. Phys. B131, 80 (1977).

9. J.C. Bizot, 1981 Moriond Conference (these proceedings).

10. H.J. Schnitzer, op. cit.

11. D. Gromes, op. cit.

12. N. Isgur, op. cit.

13. L.D. Landau, Dokl. Akad. Nauk. SSSR, 60, 207 (1948).

14. M. Jacob, G.C. Wick, Ann. Phys. 7, 404 (1959).

15. H. Fritzsch, P. Minkowski, Nuovo Cimento 30A, 393 (1975).

16. T. Barnes, Rutherford preprint RL-81-017 (Feb.1981).

17. H. Suura, Phys. Rev. Lett. 44, 1319 (1980).

18. R.R. Horgan, personal communication.

19. A. Billoire, R. Lacaze, A. Morel, H. Navelet, Phys. Lett. 80B, 381 (1979).

20. A.B. Wicklund, 1981 Moriond Conference (these proceedings).

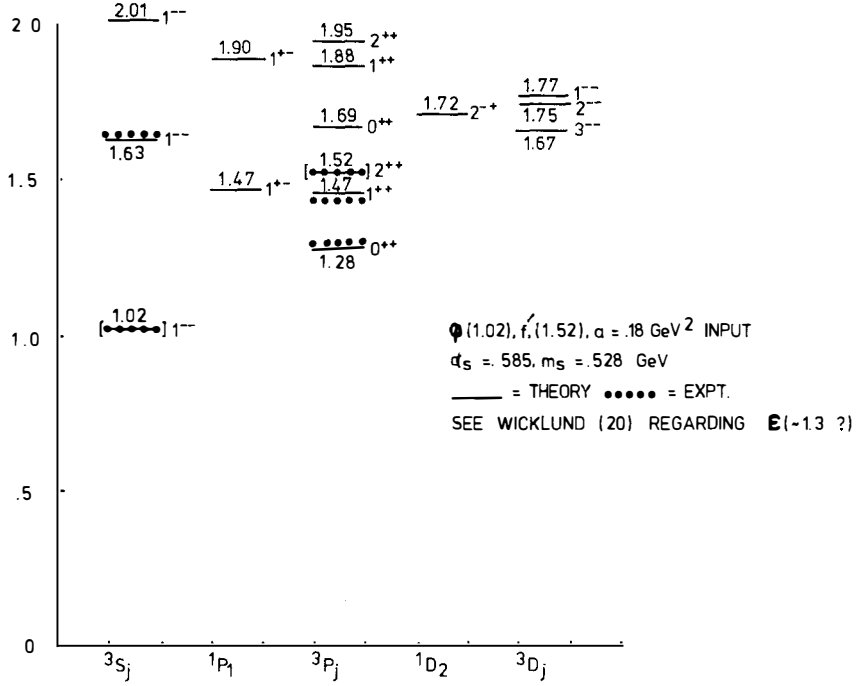

FIG. 1

PREDICTED AND OBSERVED $S\bar{S}$ SPECTRUM

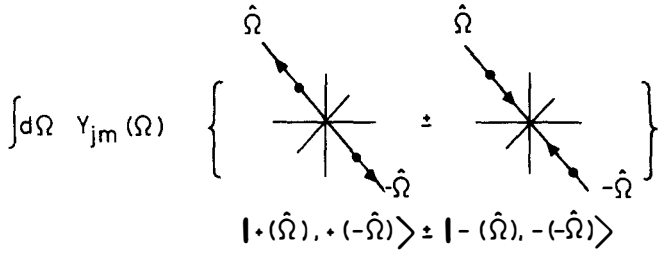

FIG. 2a EVEN / ODD HELICITY SINGLETS

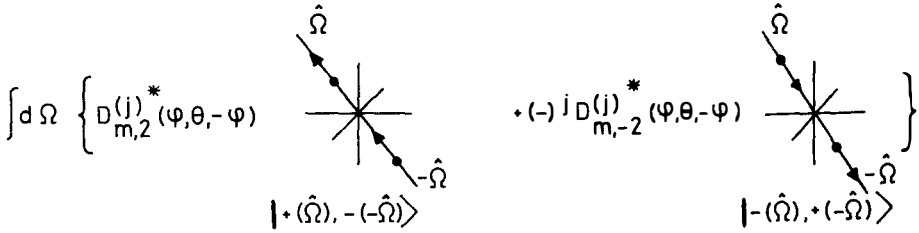

FIG. 2b HELICITY DOUBLETS

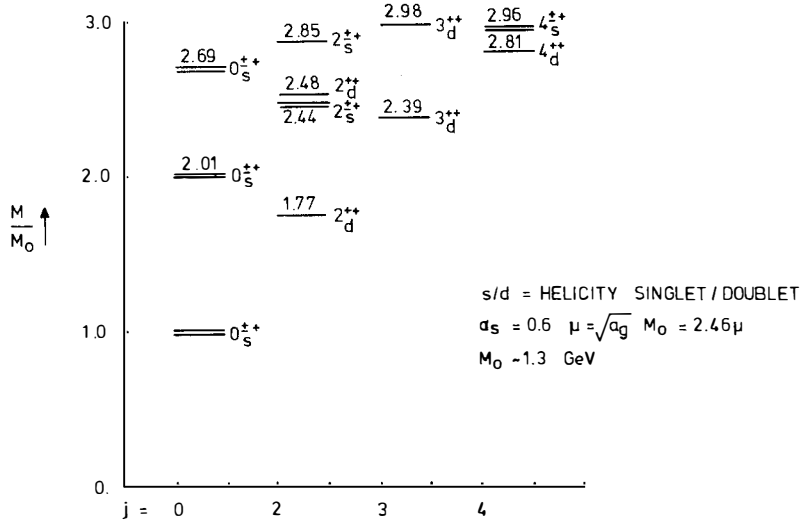

FIG. 3

PREDICTED LOWEST ORDER gg SPECTRUM

QCD, OZI, AND EVIDENCE FOR GLUEBALLS

S.J. Lindenbaum
Brookhaven National Laboratory, Upton, New York 11973*
and
City College of New York, New York, New York 10031+

Abstract

The characteristics expected from low Q^2-QCD for the behavior of glueballs and the OZI rule will be discussed.

The reaction $\pi^- p \to \phi\phi n$ represents an OZI forbidden (hairpin) diagram. It has been observed at the Brookhaven National Laboratory multiparticle spectrometer by the Brookhaven National Laboratory/City College of New York group. The author has shown that the expected OZI suppression is essentially entirely absent and in fact the Isobar Model which does not contain OZI suppression quantitatively explains the observed results. A general evaluation of the special characteristics of the data compared to other related reactions plus the foregoing facts leads the author to conclude that the intervention of glueball resonances is the likely explanation in the context of QCD. Other explanations are shown to be improbable. In particular the hypothesis that decay of a radial excitation of the η' isresponsible for lack of OZI suppression is ruled out. Planned experiments with the purpose of explicitly discovering glueballs will be discussed. The OZI rule peculiarities such as violation of crossing symmetry and unitarity are attributed to color confinement.

Introduction

QCD[1,2] is a non-abelian gauge theory with the following novel characteristics.

I. The gauge bosons are an octet of colored vector massless gluons which self interact.

II. Asymptotic Freedom.

Gluon-gluon and multigluon interactions occur with the same coupling constant as the quark gluon interaction and these interactions become stronger as the energy decreases (and weaker as the energy increases).

Characteristics I and II follow from the nature of the non-abelian gauge theory and do not occur in an abelian gauge theory such as QED.

III. In addition, QCD has color confinement.

Considering the properties of gluon-gluon interactions, which become stronger as the energy becomes lower, and the characteristic of confinement, I believe one would almost inescapably be led to expect to find multigluon glueball resonances at low energies. Glueballs would be the only hadrons in a pure Yame Mills Theory[3] where $SU_c(3)$ was a local symmetry.

In a strict sense there is no gauge invariant separation into 2g, 3g, etc. due to the self couplings of gluons. Any number of gluons can couple together and transform into a different number. However, a gauge invariant description is possible.[4] Nevertheless classification by number of gluons is physically appealing and may well be meaningful judging by the success of quark model classifications. It should be noted that simple confinement arguments, the bag model, the quark potential model, and lattice calculations all predict glueball resonances.[5-12]

Therefore, if glueball resonances are not found, it would be difficult not to conclude QCD is in trouble. On the other hand discovery of real glueballs would be a great triumph for QCD.

Expected Characteristics of Glueball States

Glueball states[5-8] are color singlets with I = 0, B = 0 (u,d,s,c,b = 0), J^{PC} can be either non-exotic or exotic. Manifestly exotic J^{PC} combinations occur naturally in 2g and 3g combinations in contrast to the quark case where for example to obtain an exotic J^{PC} one must go from a $q\bar{q}$ (2 quark state) to a $q\bar{q}q\bar{q}$ (four quark state). So if the J^{PC} is not exotic they could appear as additional singlets resembling the I = 0 singlet of an SU(3) nonet. These states could mix with ordinary $q\bar{q}$ mesons. Exotic J^{PC} states can only mix with the exotic quark sector which appears to be heavily suppressed since no one has discovered an explicitly exotic state. Therefore exotic glueballs which are referred to as oddballs[7] would be purer glueballs.

Glueball Widths

One would expect the full width Γ of a glueball to be reduced compared to the typical hadronic width by $\sim \sqrt{\text{OZI suppression factor}}$ for vector gluons since you go from $q\bar{q}$ to glue only once. The OZI suppression factor was determined for vector particles which require a three gluon intermediate state. For a scalar glueball only two gluons would be involved in the intermediate state, therefore one could expect that the typical hadronic width would be reduced by $\sim \sqrt[3]{\text{OZI suppression factor}}$. Taking the OZI suppression factor of $\sim$ 100 and a typical hadronic width $\sim$ 200 MeV a ballpark figure for the expected glueball widths would be $\Gamma \lesssim 30 \pm 10$ MeV.

Carlson, Coyne, Fishbane, Gross and Meshkov[7] use perturbation theory calculations to conclude that J = 0 and J = 1 2g glueballs are as narrow as a few MeV or less and the exotics have $\Gamma \sim 1$ MeV. The use of perturbation theory in decays of resonant states may not be accurate. Of course 3g glueballs could be wider, with typical widths like those given above.

Glueball Masses

Estimates of glueball masses are somewhat uncertain and to say the least obviously difficult to make. An order of magnitude estimate of the ground states of the glueball spectrum can be made by using a confined size $\sim$ 1 fermi and the uncertainty principle.

This leads to the result that the average energy of a gluon is

$$E_{gluon} > \sqrt{3}/R \sim 350 \text{ MeV}.$$

Hence crudely speaking the 2g spectrum would have $M \gtrsim 700$ MeV. The 3g spectrum would have $M \gtrsim 1$ GeV.

The latest bag model prediction for glueball masses have been made by Donoghue et al.[9] and the mass estimates for the states considered for 2g range from about 0.96 GeV (for 0^{++} and 2^{++}) to 1.3 GeV (for 0^{-+} and 2^{-+}). For 3g ground states (0^{++}, 1^{+-}, 3^{+-}) the mass is estimated to be 1.45 GeV with numerous other states at 1.8 GeV.

Quark potential models can be used to estimate the glueball mass. The coefficient of the term br which is linear in r is multiplied by a factor proportional to $(\text{charge})^2$. Thus going from quark anti-quark to gluon-gluon states the linear term in the potential should be multiplied by $(3/2)^2$. Thus the two gluon glueball masses should be the quark model masses multiplied by a factor of 3/2 and hence could be expected to have their ground states in the range of 1-2 GeV. Fishbane[8] (this paper is a good review reference) uses the fact that the ideas of quantum mechanics and better understanding of low energy tests of QCD such as charmonium decays require an effective mass for the gluons which has been shown by Parisi and Petronzio[10] to be 0 (0.8 GeV). Thus Fishbane[8]

estimates that the low lying two gluon states are at O(1.6 GeV) while the three gluon spectrum begins at O(2.4 GeV). This approach may well be one of the better ways of estimating glueball masses.

Lattice Gauge Theories,[11] String Models,[12] and Effective Lagrangian Models[13] all give glueball ground state estimates of 1-2 GeV. Of course, based on experience with quark spectroscopy the excited state masses should be expected to be roughly a factor of two higher than those of the ground states.

Table I (based on Coyne, Fishbane and Meshkov[7]) shows J^{PC} values through spins of 3 which are allowed (√) or forbidden (X) for $q\bar{q}$ (quark model states) 2g glueballs and 3g (glueballs). Exotic states are indicated by arrows on the side of the table. If the arrow is solid, the J^{PC} is exotic in the quark model, but allowed only for 3g glueballs which allow all J^{PC} combinations. If there is a dotted arrow under the solid arrow the state is allowed for 2g as well as 3g glueballs. Of course $q\bar{q}$, 2g as well as 3g states of the same J^{PC} all mix to a certain extent. However, quark model classification successes, and general considerations, lead one to expect that to a reasonable extent these classifications may hold.

Therefore, if one discovered a flavorless boson state with I = 0 and a relatively narrow width it would make it an excellent candidate for a glueball. If it should turn out to have an exotic J^{PC}, the argument would be even more compelling.

How Would One Find Glueballs?

We have discovered many $q\bar{q}$ meson states and qqq baryon states, but to date no glueball states. From the success of the quark model, it is clear that the hadronization process leads to dominance of particle states built predominantly of q and $\bar{q}$. Therefore, starting from quark-built states, how can we produce glueballs.

It is obvious that the best way is to find a process where there is an intermediate state which contains 2 or more gluons with a variable total effective mass and no quarks (or anti-quarks). Thus the gluons can resonante and form a glueball which is a color singlet if one exists within their effective mass range. Thus an OZI forbidden process with a variable mass for the glue is an excellent candidate for a reaction to make glueballs enhanced relative to the normal OZI allowed hadronic background which is suppressed.

OZI Within the Context of QCD

The OZI rule[14,15] has found a natural explanation in the context of QCD.[16,17] The connected diagrams for OZI allowed processes allow a series of one-gluon exchanges without violating color confinement; on the other hand the disjoint or

TABLE I

List of states (J^{PC}) for quark model and glueballs. √(X) indicates allowed (disallowed). 2g (3g) correspond to glueball state formed from 2 (3) gluons. Solid arrow (→) indicates quark model exotics in 3g states. Dotted arrow (⇢) indicates exotics in 2g states.

State	$q\bar{q}$	2g	3g
0^{++}	√	√	√
$3g \rightarrow 0^{+-}$	X	X	√
0^{-+}	√	√	√
$3g \rightarrow 0^{--}$	X	X	√
1^{++}	√	√	√
1^{+-}	√	X	√
$3g \rightarrow 1^{-+}$	X	√	√
1^{--}	√	X	√
2^{++}	√	√	√
$3g \rightarrow 2^{+-}$	X	X	√
2^{-+}	√	√	√
2^{--}	√	X	√
3^{++}	√	√	√
3^{+-}	√	X	√
$3g \rightarrow 3^{-+}$	X	√	√
3^{--}	√	X	√

hairpin diagrams requires 3 gluon exchange since the ϕ is a vector (2 gluon exchange would be permissible if the ϕ were a pseudoscalar). Therefore, the OZI suppression is attributable to the factor g^6 involved in going from quarks to quarks via 3 gluon exchange.

However, it has been shown[2,18-20] the two OZI allowed processes can be used to eliminate the OZI forbidden diagram and replace it with a sequence of two OZI allowed steps. For example $\phi \to \pi^- + \rho^+$ is an OZI forbidden process. However, $\phi \to K^-K^+ \to \pi^-\rho^+$ is a two step process, each of which is OZI allowed. Thus the OZI rule appears to violate crossing symmetry and unitarity.[2,18-20] Furthermore, this is a quite general phenomenon occurring in production as well as decay.

For example the typical OZI suppression factor ~ 100 has been found[14,15] in the reaction $\pi^-p \to \phi n$. However, this reaction can occur via a two-step process,[17,19] each step of which is allowed, namely, $\pi^-p \to K^+K^-n \to \phi n$.

I have pointed out[18,19] that what is unique here is that by the two steps we have converted a process which requires 3 gluon exchange into one which can go by a series of single gluon exchanges. Since the OZI rule works well, this evidently is not allowed, although it cannot be explicitly demonstrated by calculation, due to the well-known difficulties with strong interaction calculations. Thus, the crossing symmetry and unitarity arguments made without taking into account this QCD fact of life are probably only applicable when one does not change the nature of a gluon exchange. I view this as an added requirement due to color confinement. Thus the OZI rule can be considered reasonable within the context of QCD. Furthermore, it works.

J/ψ Radiative Decay

One suggested way[6,7] of finding glueballs in an OZI forbidden process is in investigating radiative J/ψ decay.[21] Perturbation theory treatments indicate that the important diagram is that shown in Fig. 1. One would expect to find evidence for the glueball by plotting dN/dE as a function of γ-ray energy as shown. The rationale for Fig. 1 allowing enhanced production of glueballs is that the γ can have a variable energy so that the effective mass of the two gluons could sweep over a range of masses and thus if there is a gg resonance corresponding to a glueball, one would favor forming it. Thus the plot of dN/dE vs. E (Fig. 1) might show structure corresponding to glueballs.

In regard to the radiative decay of the J/ψ it has been considered[6,7,21,22] that the E observed in $J/\psi \to \gamma + E(1420)$ may be a glueball. There is considerable controversy and a lack of convincing evidence about this particular interpretation for this low statistics experiment. We will not discuss it in this paper since it has been discussed by other papers in this conference and elsewhere.[6,7,21,22]

The OZI Forbidden $\pi^- p \to \phi\phi n$

Another way suggested by the author[19,20] some time ago is shown by the diagram in Fig. 2.

The $\phi\phi$ system forms a hairpin diagram disjoint from the rest of the quark line diagram, thus it is OZI suppressed. In the context of QCD it proceeds via exchange of 2 gluons (if $\phi\phi$ is a scalar system) or 3 gluons if $\phi\phi$ is a vector system. The key point is to have a multi-gluon intermediate state of variable mass so that if glueball resonances exist they can be produced enhanced relative to other states. This experiment was performed some time ago by the BNL/CCNY collaboration.[23,24]

The quark line diagrams relevant to the BNL/CCNY experiments are shown in Fig. 3. Incident π^- mesons of 22.6 GeV/c interacted with protons to produce the reactions:

a) $\pi^- p \to K^+K^-K^+K^- n$

b) $\pi^- p \to \phi K^+K^- n$

c) $\pi^- p \to \phi\phi n$.

Figs. 3a and 3b are rearrangement diagrams that are expected to have the allowed order of cross section. An explicit check of the assumption that rearrangement diagrams have the OZI allowed order of cross section is obtained by comparing $\pi^- p \to K^+K^-\phi\pi^- p$ corresponding to a planar diagram from a CERN experiment at comparable energies with the BNL $\pi^- p \to K^+K^-\phi n$ which corresponds to a rearrangement diagram. The cross sections obtained for the two reactions are $\sigma \sim .4$ μb and $\sigma \sim .3$ μb respectively which shows there is no essential difference in cross section.[18,19,20]

A scatter plot of the mass of one K^+K^- pair, chosen in a random way, on the x-axis versus the mass of the second K^+K^- pair plotted on the y-axis is shown in Fig. 4. Thus each event is plotted twice. An enhancement over background is seen in each of the two ϕ mass bands. An enormous enhancement over background is seen where the two ϕ mass bands cross. This region (i.e. the $\phi\phi$ region) appears as a very densely populated area which is almost black. When corrections for resolution and double counting are made, the peak intensity in the $\phi\phi$ region is approximately 1500 times the adjoining background level. This clearly implies that the OZI suppression is apparently not working since if OZI suppression were perfect there would be no $\phi\phi$ events at all and thus no enhancement in the $\phi\phi$ region.

To see more quantitatively what is happening we plot in Fig. 5 the mass spectrum of K^+K^- pairs from the reaction $\pi^- p \to K^+K^-K^+K^- n$. Four K^+K^- combinations are plotted for each event. In addition, the shaded curve is the mass spectrum of like sign K pairs, which can be used as an indication of the extra background due to multiple combinations. A very clear ϕ signal is obtained

corresponding to a peak to background ratio of about 4:1. We then correct by a factor of two to allow for multiple combinations which gives 8:1. We then correct for our mass resolution which is about three times the ϕ mass width so the true ϕ peak to background ratio is $\sim$ 25. Hence we see a large enhancement factor $\sim$ 25 at the ϕ mass.

Reaction (c) corresponds to Fig. 3c and is an OZI forbidden reaction. To study reaction (c) we select events with a K^+K^- pair in the ϕ mass band and plot the effective mass of the other K^+K^- pair, and obtain the mass spectra shown in Fig. 6 which exhibits a huge ϕ signal corresponding to reaction (c). The peak to background ratio is about 20:1. When corrected for the resolution, the true peak to background ratio is about 60:1. If the OZI suppression were 100%, no signal would be seen in Fig. 4c. We therefore have the unusual situation that the forbidden reaction (c) produces a higher ϕ enhancement over K^+K^- background than the allowed reaction (b), although equal enhancements cannot be ruled out because of the possible contamination of the data with $\bar{p}p$ pairs, and the errors in corrections for combinational problems.

Figure 7 shows the mass spectra for the effective masses (ϕK^+K^-) and $\phi\phi$ for our published spectrum[23] of $\sim$ 100 $\phi\phi$ events. The ϕK^+K^- mass spectrum shows a broad distribution which occupies most of the available phase space while the $\phi\phi$ mass spectrum has a low effective mass peak and is restricted to relatively low energies. Thus the $\phi\phi$ spectrum has a distinctly different character than the ϕK^+K^-. Furthermore there is some indication that there may possibly be some structure in the neighborhood of 2.4 GeV. If we integrate the two spectra we get a ratio of reaction b to reaction c of less than five which is of the order of the value for background to resonance ratios in allowed reactions.*

Hence we have clear evidence that there is no OZI suppression[24] (perhaps even an enhancement) in our K^+K^- effective mass studies and we find even in comparing total cross sections we are consistent with normal resonance behavior for the second K^+K^- pair (after the first has made a ϕ) with no evidence for OZI suppression for creation of a second ϕ. Therefore we conclude that OZI suppression is absent in these processes.

I shall now proceed to treat the observations from the point of view of the isobar model[25] which we proposed over 2 decades ago. The isobar model never heard of OZI suppression and ignores it. We will shortly find quantitative agreement of the present observations with these isobar model calculations. The agreement will depend on final state K^+K^- resonant interactions built into the isobar model treatment. I have shown[18,19,20] that such final state interactions

---

* For example C. Baltay et al., Phys. Rev. Letts. 40, 87 (1978) find that production accounts for about 5% of the $\pi^+\pi^-\pi^o$ spectrum in the reaction $\pi^-p \to \Delta^{++}\pi^+\pi^-\pi^o$ at 15 GeV/c. Resonance production is typically 1/10 of a reaction.

completely defeat the OZI rule and thus we will show that the OZI rule is inoperative in these reactions.

Let us now calculate the enhancement factor expected from the point of view of the isobar model where the ϕ isobar formation probability is related to the K^+K^- resonant scattering to form a ϕ. We consider the ϕ as an L = 1, I = 0 resonance of the K^+K^- scattering which decays back into K^+K^- with a branching ratio of 0.47 and into K^oK^o with a BR of 0.35. Off resonance we assume the K^+K^- scattering cross section is estimable by using the additive quark model (AQM) to determine $\sigma(K^+K^-) \approx 2/3\ \sigma(K\text{-}N) \approx 8$ mb (non-resonance). The maximum cross section for K^+K^- scattering at the resonance can then be estimated to be:

$$\sigma(K^+K^- \to K^+K^-) \approx 12\pi\lambda^2 \times \underset{\uparrow}{1/2}_{T=0} \times \underset{\text{factor}}{\text{Inelasticity}} \times \text{effective BR} \approx 200 \text{ mb}$$

The estimated enhancement factor at the peak =

$$\frac{200 \text{ mb (peak resonant cross section)}}{8 \text{ mb (non-resonant cross section)}} \approx 25.$$

Thus we predict an enhancement factor over background $\approx$ 25 for the ϕ peak over background. This is indeed what we find for the first ϕ.

For the second ϕ employing the isobar model we would expect the same enhancement factor and as stated observe $\approx$ 60. This treatment from the isobar model viewpoint has no OZI suppression in it and thus the fact that the enhancement found for the second ϕ peak is if anything greater than the first, but at least comparable and thus in general agreement with the isobar model shows clearly that the OZI suppression is effectively absent.[19,20]

Glueballs and Failure of OZI

I would give as the most likely explanation for this complete failure of the OZI suppression in $\pi^- p \to \phi\phi n$ the following:

In an OZI forbidden reaction the intermediate state which connects the two disconnected parts of the diagram is a collection of gluons. If a variable mass of this intermediate state is allowed by the reaction (as in $\phi\phi$) and some part of the mass region covers existing glueball resonances, the resonances may lead to effectively strong coupling and the OZI rule may be defeated. In essence we would be looking at a diagram where exchange of glueballs would occur. This is obviously a very good way to look for glueballs and the complete failure of the OZI rule and different shape of the $\phi\phi$ and ϕK^+K^- effective mass spectra indicates that we may well have seen them in this reaction. It is interesting to note that the peak of the $\phi\phi$ spectrum is at about 2.4 GeV which is the number deduced for the 3g ground state.[8]

In the above treatment we have assumed that the $\phi\phi$ state comes from either a glue system or from a quark system involving only $s\bar{s}$ quarks (i.e. a singlet of

an ideally mixed nonet) so that we truly can represent the process as OZI forbidden (disconnected) diagram. However one could consider for example $\pi^- p \to \eta'^* + n$ where for example the η'^* is the singlet in a nonet which is a radial excitation of the lowest mass 0^- nonet. The η' in the above could be far from ideally mixed and thus could decay via $\phi\phi$ and circumvent the OZI suppression of this process.

This decay from another state which is not $s\bar{s}$ and is heavily mixed with ordinary quarks and thus circumvents OZI suppression could in principle occur. I deem this to be an improbable explanation of what we observe, since there would in general be no correlation between the enhancement factor we observed in producing the second ϕ over the ϕK^+K^- compared to the enhancement factor in producing the first ϕ. We are dealing with a very small cross section ($\sim$ 23 nb) thus the chance that an uncorrelated number of $\phi\phi$ events would give us within errors just the huge ($\sim$ 25) enhancement factor we expect for the isobar model treatment with the absence of OZI suppression is in my opinion small.

Furthermore the η'^* (a radial excitation) of the η is considered the most likely candidate for production of a singlet in a far from ideally mixed nonet. Let us assume our $\phi\phi$ spectrum is due to decays of η'^*. In the case of a pseudoscalar like the η' it has been shown[26,27] that the angle χ between the two planes formed by the decays $\phi \to K^+K^-$ has the angular distribution $1 - \cos 2\chi$. Figure 8 shows the comparison of the χ distribution from our data and that expected from a pseudoscalar.

The angular distribution of our events is such that we obtain a χ^2 of 588 for 4 degrees of freedom which clearly rules out ($\sim 20\sigma$) the possibility that our $\phi\phi$ spectrum comes from decay of an η'^*.

It is obvious that a higher statistics experiment which would allow any visible structure in the $\phi\phi$ spectrum to be definitely established and allow a definite determination of the J^P of the states in the $\phi\phi$ spectrum is clearly required and we plan to do such an experiment shortly.

Figure 9 shows the observed $\phi\phi$ spectrum with the additional (unpublished) events we have obtained by further analysis. Approximately 170 $\phi\phi$ events are plotted in 20 MeV mass bins which is $\sim$ our full width half maximum resolution. This spectrum may well contain glueballs. Although there is some indication (not statistically significant) of possible structure, it is clear we need much more statistics, to form a conclusion.

The BNL/CCNY collaboration has for some time been preparing for a new experiment with MPS II. In MPS II the spark chambers of MPS I are being replaced by narrow gap high space and time resolution drift chambers. This should allow us to obtain $\sim$ 20 times more statistics and thus gather $\sim$ 3,000-4,000 $\phi\phi$ events in the $\pi^- p \to \phi\phi n$.

We expect that with this number of events we can make a significant observation of possible structure in the spectrum and also perform an effective partial wave analysis to determine whether there are resonant states and their J^P. Therefore we hope to be able to demonstrate the existence of glueballs.

Conclusions

1. The most likely explanation in the context of QCD for our observed failure of the OZI rule in $\pi^- p \to \phi\phi n$ is the intervention of glueball resonances. Therefore we believe the $\phi\phi$ system in this experiment is an excellent place to search for glueballs and their effects may well already have been seen.

2. The possibility that our $\phi\phi$ spectrum comes from the decay of a non-ideally mixed nonet particle and thus circumvents the OZI rule is considered improbable. In particular a radial excitation of the η' which is considered to be the most likely candidate for such a particle is ruled out by our angular distribution.

3. Approximately 170 $\pi^- p \to \phi\phi n$ events have been observed in the previous experiment. The BNL/CCNY collaboration for some time has been planning a second experiment to be done in the near future which is expected to provide $\sim$ 20 times more data. With this amount of data we expect to be able to make significant observations of possible visible structure in the $\phi\phi$ spectrum and to do a significant partial wave analysis which would allow an identification of resonances and their J^P. C is known to be + for $\phi\phi$ and I is known to be 0. Hence we expect that all the quantum numbers can be determined. Thus there is an excellent possibility for the explicit discovery of glueballs especially if J^{PC} is exotic.

References

1. H. Fritzch and M. Gell-Mann, XVI Int. Conf. on High Energy Physics, Chicago-Batavia 1972, Vol. 2, p. 135; H. Fritzch, M. Gell-Mann and H. Leutwyler Phys. Lett. 47B, 365 (1973); S. Weinberg, Phys. Rev. Lett. 31, 494 (1973); Phys. Rev. D8, 4482 (1973); D.J. Gross and F. Wilczek, ibid, 3633 (1973).

2. For a review, see W. Marciano and H. Pagels, Physics Reports Vol. 36, 137 (1978).

3. C.N. Yang and R.L. Mills, Phys. Rev. 96, 191 (1954).

4. J.D. Bjorken, SLAC-PUB-2366 (August 79); SLAC Summer Institute on Particle Physics (1979).

5. a) Fritzch and Minkowski, Nuovo Cimento 30A, 393 (1975); b) R.P. Freund and Y. Nambu, Phys. Rev. Lett. 34, 1645 (1975); c) Kogut, Sinclair and Susskind, Nucl. Phys. B114, 199 (1975); d) D. Robson, Nucl. Phys. B130, 328 (1977).

6. J. Donoghue, Proc. VI Int. Conf. on Experimental Meson Spectroscopy, Brookhaven National Laboratory, April 25-26, 1980, AIP Conf. Proc., No. 67, Subseries on Particles and Fields, No. 21, Eds. S.U. Chung and S.J. Lindenbaum, pg. 104.

7. a) J. Coyne, P. Fishbane, and S. Meshkov, Phys. Lett. 91B, 259 (1980); b) Carlson, Coyne, Fishbane, Gross and Meshkov, Phys. Lett. 98B, 110 (1981); also William and Mary Preprint.

8. P. Fishbane, Glueballs, A Little Review, Talk presented at the 1981 ORBIS Scientiae, Ft. Lauderdale, Fla.

9. J. Donoghue, K. Johnson, B. Li, Phys. Lett. B (to be published).

10. G. Parisi and R. Petronzio, Phys. Lett. 94B, 51 (1980).

11. J. Kogut, D. Sinclair and L. Susskind, Nucl. Phys. B114, 199 (1976); B. Borg, Phys. Lett. 97B, 401 (1980).

12. B. Skagerstam and A. Stern, Phys. Lett. 97B, 405 (1980).

13. M. Cornwall, Deeper Pathways in High Energy Physics, A. Perlmutter Ed., Plenum Press, N.Y. (1977); see also Ref. 8 for latest estimate.

14. S. Okubo, Phys. Lett. 5, 165 (1963); G. Zweig, CERN Report TH 401 and 412 (1964); J. Iizuba, Prog. Theor. Phys. Suppl. 37-38, 21 (1966); J. Iizuba, K. Okuda and O. Shito, Prog. of Theoretical Physics 35, 1061 (1966).

15. S. Okubo, A Survey of the Quark Line Rule (U.R. 641, Dept. of Physics and Astronomy, University of Rochester, N.Y. 1977).

16. T. Applequist, K. Kane and M. Barnett, Ann. Rev. Nucl. Sci. 28, 387 (1978).

17. I.J. Muzinich and F.E. Paige, Phys. Rev. D 21, 1151 (1980).

18. S.J. Lindenbaum, Quark Line Diagrams, Rules and Some Recent Data, BNL 50812 (Dec. 1977).

19. S.J. Lindenbaum, Hadronic Physics of $q\bar{q}$ Light Quark Mesons, Quark Molecules and Glueballs, Lecture presented in XVIII Course: The High Energy Limit, 31 July - 11 August 1980, The International School of Subnuclear Physics, Erice (to be published in proceedings) also BNL 28498, October 1980.

20. S.J. Lindenbaum, The OZI Rule and Glueballs, Il Nuovo Cimento (in press).

21. D.L. Scharre et al., Proc. VI Int. Conf. on Experimental Meson Spectroscopy, Brookhaven National Laboratory, April 25-26, 1980, AIP Conf. Proc., No. 67, Subseries on Particles and Fields, No. 21, Eds. S.U. Chung and S.J. Lindenbaum, pg. 329; Phys. Lett. 97B, 329 (1980).

22. M. Chanowitz, Berkeley Preprint LBL-11977.

23. A. Etkin, K.J. Foley, J.H. Goldman, W.A. Love, T.W. Morris, S. Ozaki, E.D. Platner, A.C. Saulys, C.D. Wheeler, E.H. Willen, S.J. Lindenbaum, M.A. Kramer, U. Mallik, Phys. Rev. Lett. 40, 422 (1978).

24. A. Etkin, K.J. Foley, J.H. Goldman, W.A. Love, T.W. Morris, S. Ozaki, E.D. Platner, A.C. Saulys, C.D. Wheeler, E.H. Willen, S.J. Lindenbaum, M.A. Kramer and U. Mallik, Phys. Rev. Lett. 41, 784 (1978).

25. S.J. Lindenbaum and R.M. Sternheimer, Phys. Rev. 105, 1874 (1957); 106, 1107 (1957); 109, 1723 (1958); 123, 333 (1961).

26. N.P. Chang and C.T. Nelson, Phys. Rev. Lett. 40, 1617 (1978).

27. T.L. Trueman, Phys. Rev. D18, 3423 (1978).

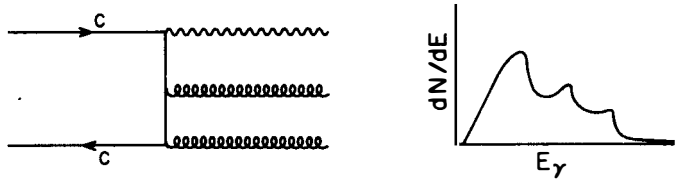

Figure 1 The dominant diagram in radiative J/ψ decay, and to the right of it a plot of dN/dE vs. E_γ.

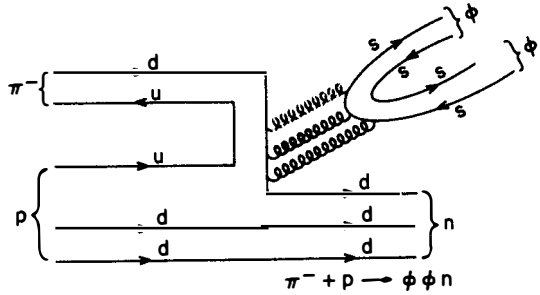

Figure 2 $\bar{\pi}p \rightarrow \phi\phi n$ an OZI forbidden diagram where the multigluon intermediate state (which leads to $\phi\phi$ production) can have a variable mass.

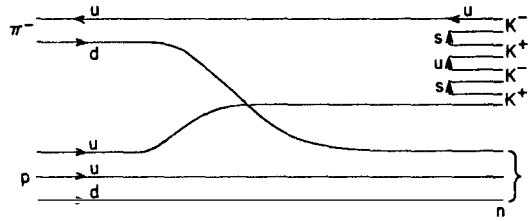

Figure 3a $\pi^- p \to K^+ K^- K^+ K^- n$

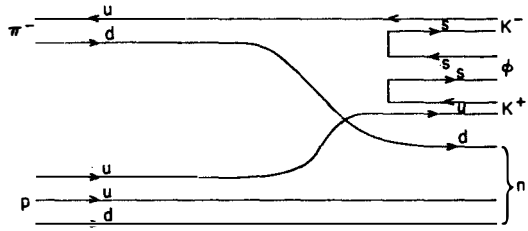

Figure 3b $\pi^- p \to \phi K^+ K^- n$

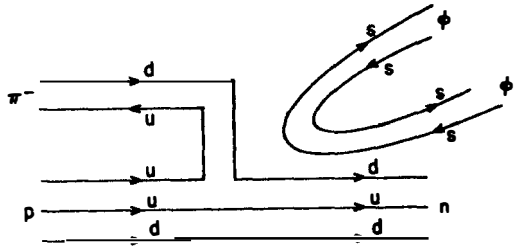

Figure 3c $\pi^- p \to \phi\phi n$

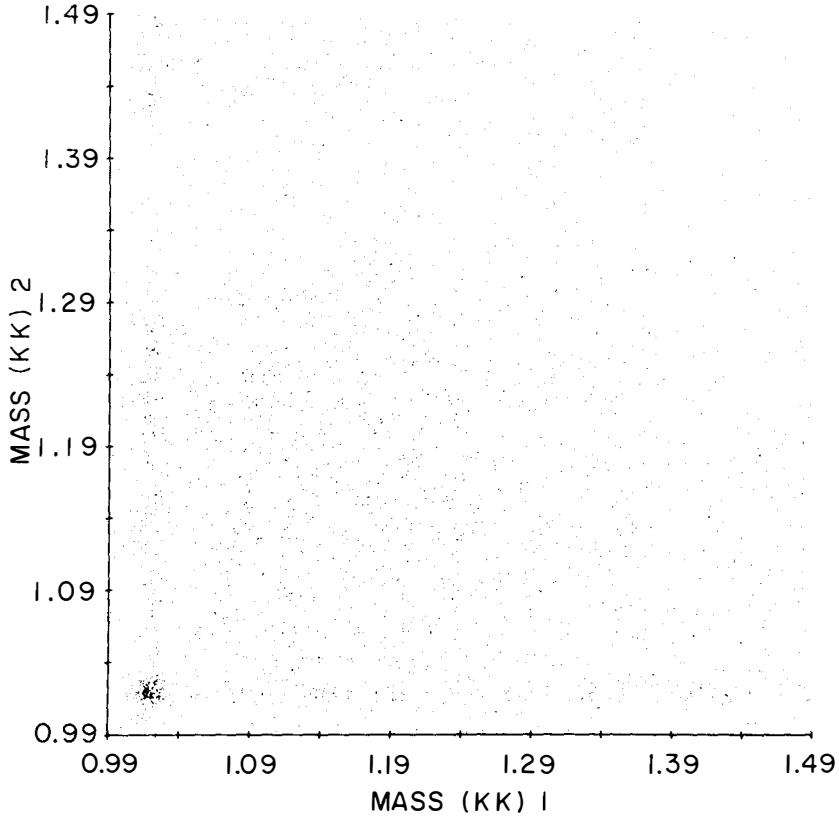

Figure 4 Scatter plot of K^+K^- effective mass for effective masses less than 1.49 GeV/c^2. Two randomly chosen mass combinations are plotted for each event. Clear bands of $\phi(1019)$ are seen with an enormous enhancement where they overlap (i.e. $\phi\phi$).

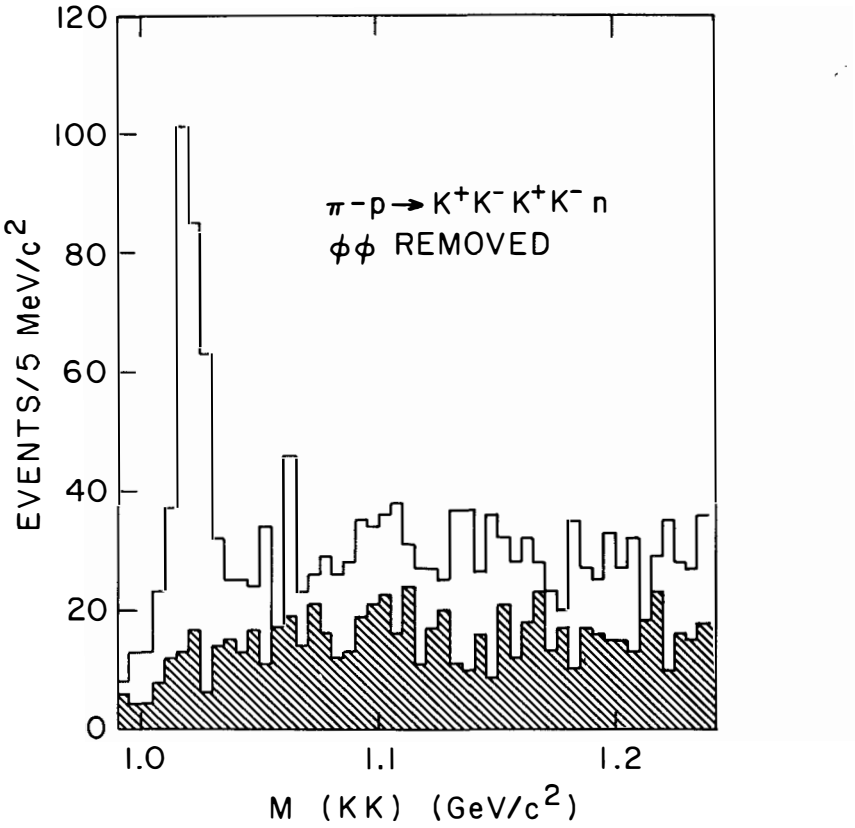

Figure 5 The effective mass spectrum of K^+K^- pairs after removing $\phi\phi$ events. The shaded histogram is the sum of like sign K pairs and is an indication of background due to multiple combinations.

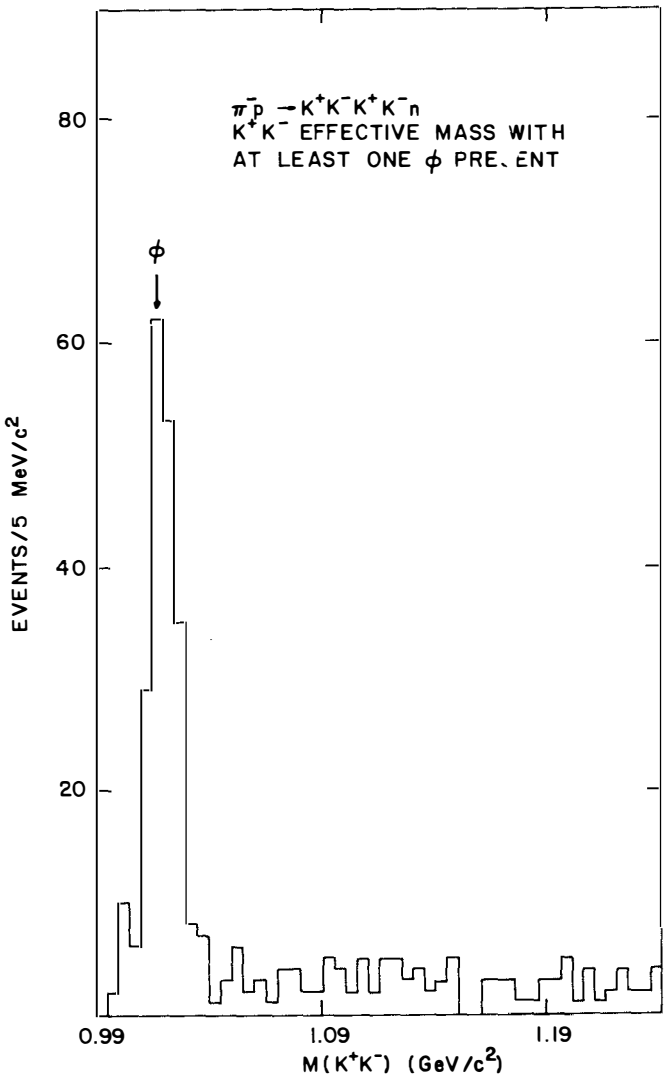

Figure 6 The effective mass of each K^+K^- pair for which the other pair was in the mass band.

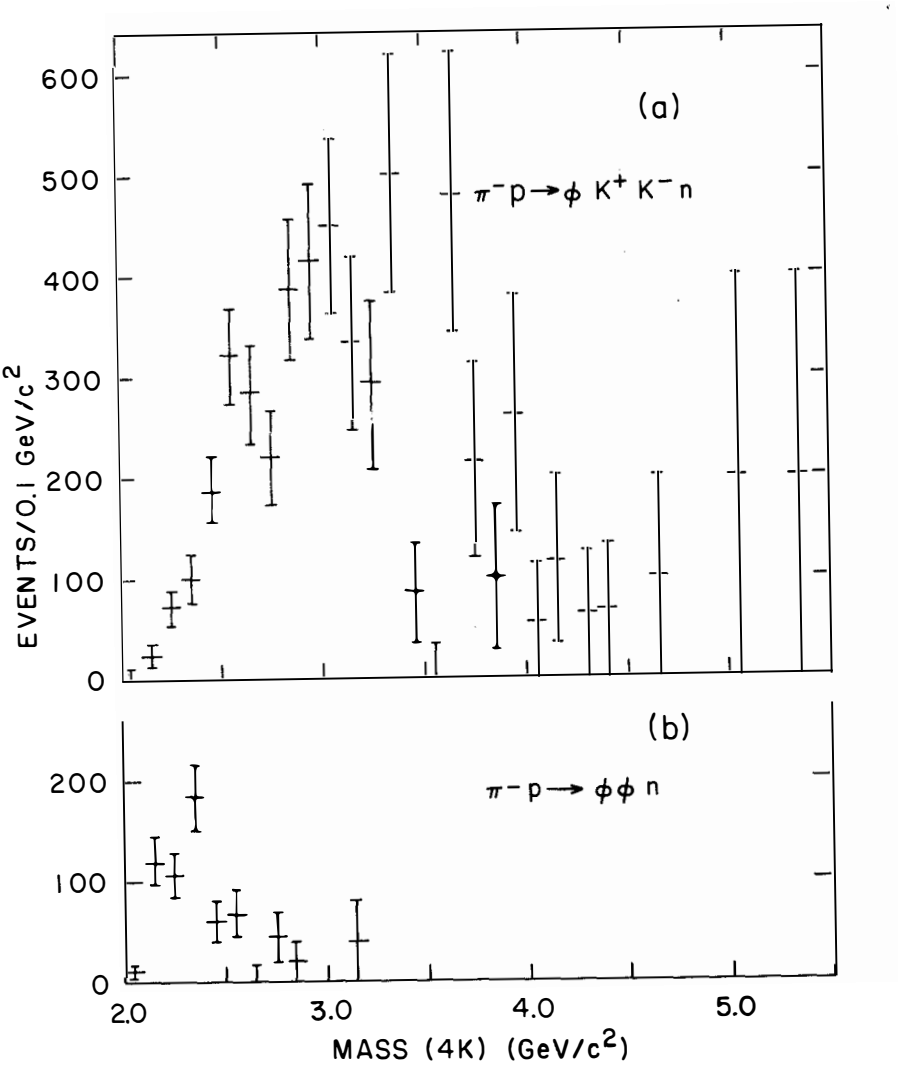

Figure 7 (a) Effective mass spectrum (corrected for acceptance) of the $[\phi K^+ K^-]$ system where the K^+K^- does not lie in the ϕ band.
(b) $\phi\phi$ effective mass spectrum (corrected for acceptance).

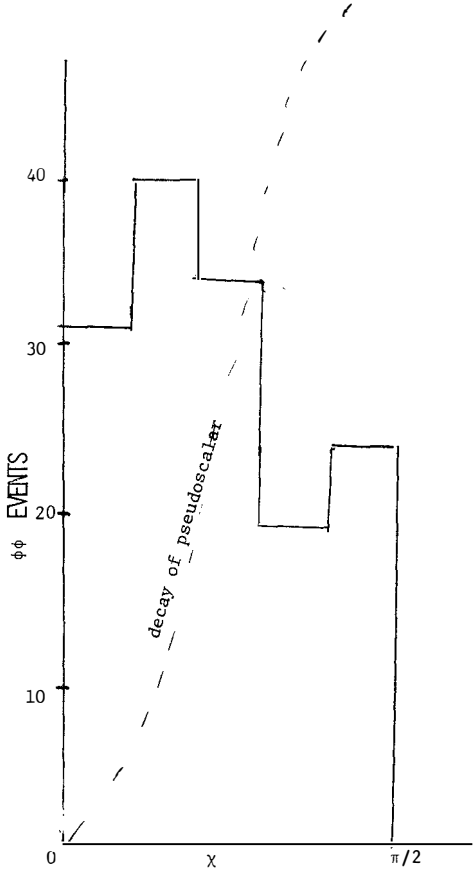

Figure 8 The distribution of $\phi\phi$ events as a function of χ, the angle between the decay planes of the two ϕ's. The dotted curve is the prediction for this distribution if the $\phi\phi$ were the decay products of a pseudoscalar state such as a radial excitation of the η'. This is clearly ruled out (see text for further details).

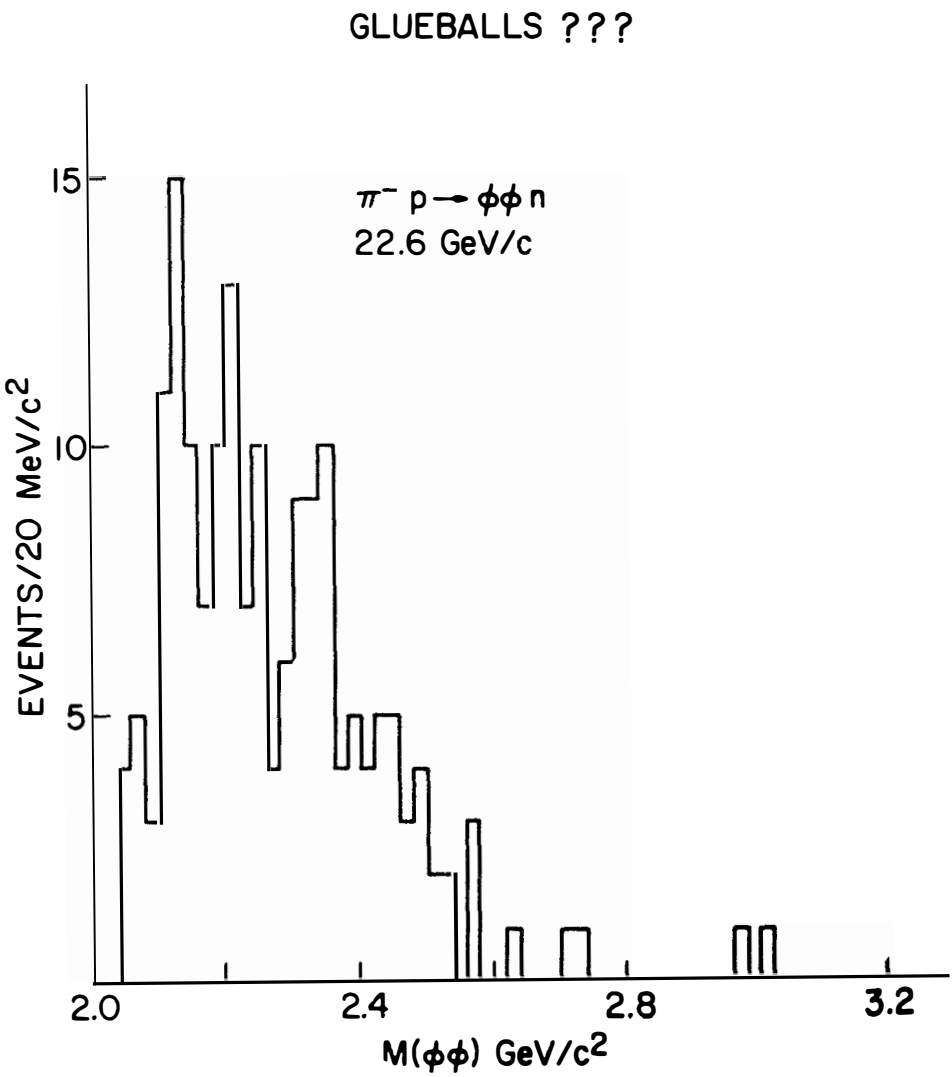

Figure 9 Observed $\phi\phi$ mass spectrum for the final sample $\sim$ 170 $\phi\phi$ events. This spectrum is uncorrected for acceptance.

THE 1^+ NONETS IN LIGHT QUARK MESON SPECTROSCOPY

W. Hoogland

NIKHEF-H
Amsterdam

The status of the 1^+ nonets is shortly reviewed.
Results from recent high statistics experiments, performing a partial wave analysis of 3π and $K\pi\pi$ systems, have given conclusive evidence for the existence of A_1, H, Q_A and Q_B mesons. Some questions remain concerning the assignment of the E-meson.

Introduction.

The naive non-relativistic quark model has been the guiding principle in meson spectroscopy for many years. Until recently, however, the experimental evidence for the existence of the various nonets of the $q\bar{q}$ system, nicely grouped according to the radial excitation number n and the angular momentum L, was meagre. Only for n=L=0 all particles were known (the $J^{PC}=0^{-+}$ and 1^{--} nonets). For values of n or L different from 0, however, few particles were identified. This was already true at the first level of excitation, i.e. for n or L equal to 1. Apart from the ρ' no candidates were known to fill the position of the first radial excitation of the 0^{-+} and 1^{--} nonets. Even more unsatisfactory was the situation for the four L=1 nonets ($J^{PC}=2^{++}$, 1^{++}, 1^{+-}, 0^{++}) of which only the 2^{++} members were fully identified. In particular a lot of confusion existed concerning the isovector member of the 1^{++} nonet and the strange 1^{+} candidates, the famous A_1 and Q enhancements. Similar problems existed for the 0^{+} nonet.

In the last few years there has been much progress in the indentification of the members of the 1^{+} nonets. Evidence has been found for the A_1, for two strange 1^{+} particles Q_a, Q_b and for the H meson ($I\ J^{PC}=01^{+-}$). The spin parity of the I=0, C=+ D meson has been convincingly demonstrated to be 1^{+}, while 1^{+} is also the most probable spin-parity assignment for the E meson. The two 1^{+} nonets are therefore almost complete. Also indications exist for several radial excitations of the L=0 and L=1 $q\bar{q}$ system.

In this talk the experimental evidence is reviewed for the 1^{+} nonets. The status of the 0^{+} nonet and the first radial excitation of the 1^{-} nonet will be discussed by others at this meeting. The progress in this sector of meson spectroscopy comes mainly from a few high statistics experiments which do a partial wave analysis (PWA) of 3π and $K\pi\pi$ systems. The ACCMOR collaboration[1,2] has studied the reactions

$$\pi^- p \to \pi^-\pi^+\pi^- p \text{ at 63 and 94 GeV, and}$$

$$K^- p \to K^-\pi^+\pi^- p$$

$$\to K^-\pi^+\pi^-\pi^0 p \text{ at 63 GeV}$$

$$\pi^0 \to \gamma\gamma$$

A BNL experiment[3] studied

$$\pi^- p \rightarrow \pi^- \pi^+ \pi^o \; p \text{ at } 8.45 \text{ GeV}$$
$$\qquad\qquad\quad \downarrow \rightarrow \gamma\gamma$$

The statistics in these experiments is typically one order of magnitude larger than of previous experiments, having of the order of 1000 events/10 MeV mass bin.

The PWA of the three particle system is done according to the standard isobar model. Partial waves are classified according to $J^P L M^\eta$ (a,b) where the notation is explained by fig. 1. For the analysis of the 3π data of the ACCMOR collaboration the Illinois approach[4] is used; for the other data the LBL-SLAC approach[5] has been chosen.

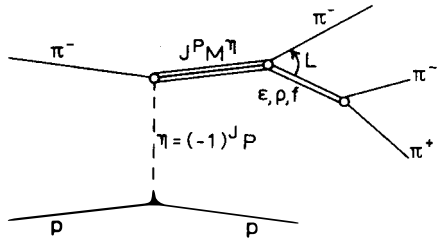

Fig. 1 The 3π system in the isobar model.

The 1^+ mesons.

A complication in the study of the broad enhancements associated with A_1, Q and H particles is the presence of an interfering background due to the Deck process (fig. 2). Bowler[6] formulated a model which corrects the bare Deck amplitude of fig. 2a with a term that accounts for the rescattering through the resonance (fig. 2b). The presence of the coherent amplitude leads to significant shifts in the position of the resonance peak in the invariant mass spectrum. In all experiments discussed here the data have been fitted to this model or a comparable multi Regge model.

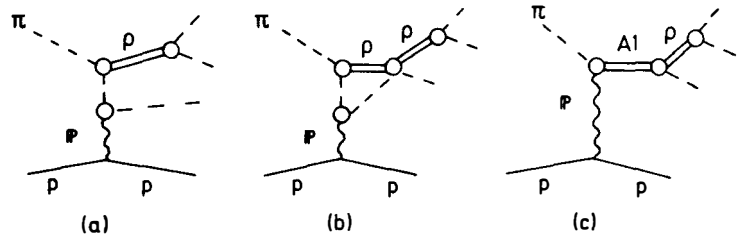

Fig. 2 Three diagrams contributing to the amplitude for diffractive production

a) One-pion exchange Deck mechanism;
b) Deck mechanism with tescattering through $\rho\pi$ final state interactions;
c) Direct diffractive A_1 meson production.

(a) The A_1 meson.

The evidence for the A_1 from the ACCMOR data is shown in fig. 3. The intensity of the 1^+S0^+ $(\rho\pi)$ partial wave is shown for samples with increasing t'. In addition the phase with respect to the A_2 $(2^+D^+1^+)$ $\rho\pi$ wave is shown, after subtracting the phase variation of the 2^+D1^+ wave expected for a BW with resonance parameters of the A_2.

The data clearly demonstrate the forward motion expected for a resonant 1^+S0^+ $(\rho\pi)$ wave. The best values for the mass and width from a fit with the Bowler model are

$$M_{A_1} = 1280 \pm 30 \text{ MeV}$$
$$\Gamma_{A_1} = 300 \pm 20 \text{ MeV}$$

The $\pi^+\pi^-\pi^0$ data from reference [3] confirm the resonant bahaviour of the 1^+S $(\rho\pi)$ wave. The phase of the nucleon helicity flip, natural parity exchange 1^+S wave with respect to an I=2 1^+S $(\rho\pi)$ reference wave, shown in fig. 4, has a large forward motion of $\sim 150^\circ$.

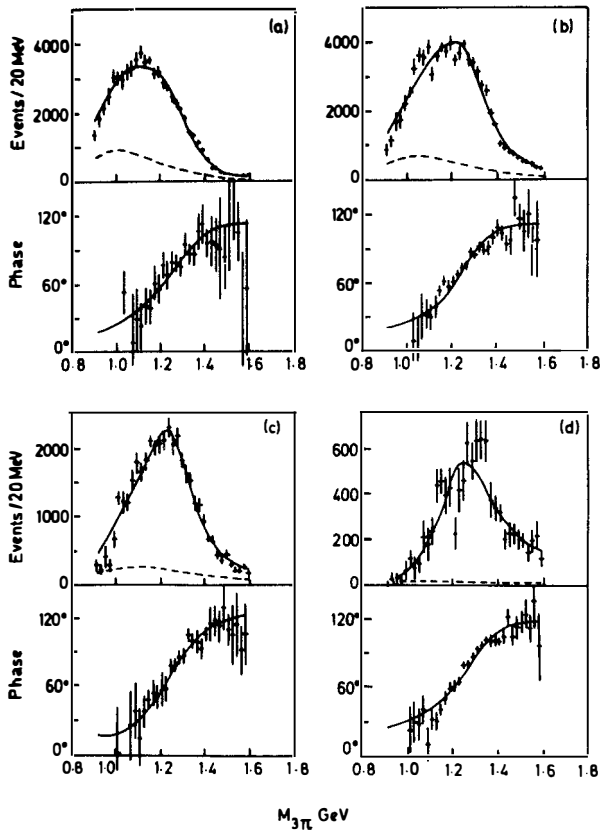

Fig. 3 Results from the ACCMOR collaboration[1] of fitting the 1^+S0^+ intensity and phase measured with respect to the A_2 production amplitude. The solid curves represent the results of a fit with the Bowler model.

a) $0.0 \leq |t'| \leq 0.05$ GeV^2

b) $0.05 \leq |t'| \leq 0.7$ GeV^2

c) $0.16 \leq |t'| \leq 0.3$ GeV^2

d) $0.16 \leq |t'| \leq 0.7$ GeV^2

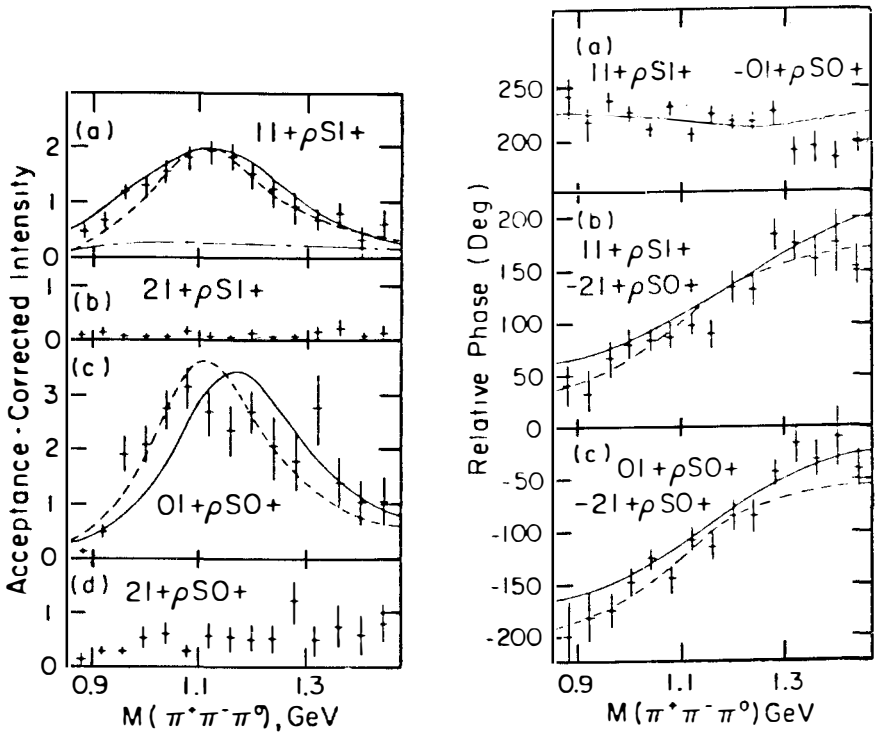

Fig. 4 Results from Dankowych et al.[3] for the $\pi^+\pi^-\pi^0$ system showing the intensity of the nucleon helicity flip, natural parity exchange 1^+S waves and their phases with respect to an I=2 1^+S ($\rho\pi$) reference wave.

If the data are fitted with the model of Bowler the A_1 resonance parameters are found to be

$$M_{A_1} = 1240 \pm 80 \text{ MeV}$$

$$\Gamma_{A_1} = 380 \pm 100 \text{ MeV}$$

in good agreement with the ACCMOR results.

These two experiments not only present convincing evidence for the existence of the A_1 but also indicate that its mass is in the range 1200 - 1300 MeV rather than at 1040 MeV as was determined from an analysis of the 3π system produced backward in the reaction $K^-p \rightarrow \Sigma^- 3\pi$ [7]

This would also better agree with the masses of the other I=1 and I=0 members of the L=1 nonets which are all in the same 1200 - 1300 MeV mass range, indicating that hyperfine splitting effects are small.

(b) The H meson.

Convincing evidence for the H-meson is found in the data of reference [3]. Both the natural parity exchange (NPE), nucleon helicity non-flip I=0 1^+S0^+ ($\rho\pi$) wave and the NPE, flip I=0 1^+S1^+ ($\rho\pi$) wave show resonant behaviour (fig. 4,5). A fit using the Bowler prescriptions gives

$$M_H = 1190 \pm 60 \text{ MeV}$$

$$\Gamma_H = 320 \pm 50 \text{ MeV}$$

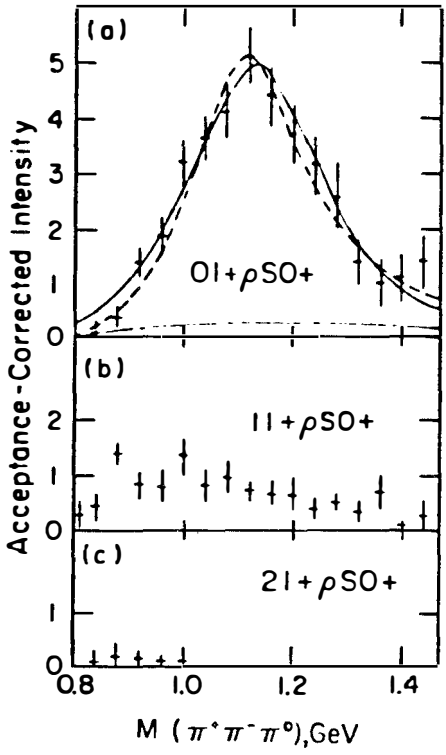

Fig. 5 Results from Dankowych et al.[3] showing the intensities of the nucleon helicity nonflip, natural parity exchange 1^+S waves.

(c) The Q-meson.

In the L=1 $q\bar{q}$ system two strange 1^+ mesons are expected. One belonging to the 1^{++} nonet (Q_A), the other to the 1^{+-} nonet (Q_B). Since strange mesons are not eigenstates of C mixing can occur, especially since the mass difference is expected to be small. Instead of the pure octet states Q_A and Q_B physical states Q_a, Q_b are observed

$$|Q_a> = |Q_A> \cos\Theta_Q + |Q_B> \sin\Theta_Q$$

$$|Q_b> = -|Q_A> \sin\Theta_Q + |Q_B> \cos\Theta_Q$$

The analysis of a 13 GeV $K^-p \to K^-\pi^+\pi^-p$ experiment at SLAC[8] first demonstrated the existence of two Q particles. In the ACCMOR experiment the SLAC results are confirmed with larger statistics. Even the raw mass spectrum shows clearly the two peak structure of the Q bump (fig. 6). In the $K^-\pi^+\pi^-\pi^o$ data the ωK decay channel of the Q_b is demonstrated. A coupled channel analysis was done using two resonances with 6 decay channels [$K^*\pi$ (S-wave), $K^*\pi$ (D-wave), ρK, $\kappa\pi$, εK and ωK (for which the couplings are fixed to $\sqrt{1/3}\rho K$)]. A rescattered Deck amplitude was included, while the mixing of Q_a and Q_b was taken into account to reduce the number of parameters in the fit.

The results are shown in fig. 7. New in these results is the evidence for a d-wave $K^*\pi$ decay.

The best values for mass and width are

$$M_{Q_a} = 1410 \pm 25 \text{ MeV} \qquad \Gamma_{Q_a} = 195 \pm 25 \text{ MeV}$$

$$M_{Q_b} = 1270 \pm 10 \text{ MeV} \qquad \Gamma_{Q_b} = 90 \pm 8 \text{ MeV}$$

The mixing angle Q_a from the fit is 56 ± 3^o which corresponds to mass values for the pure octet states.

$$M_{Q_A} = 1310 \pm 15 \text{ MeV}$$

$$M_{Q_B} = 1370 \pm 20 \text{ MeV}$$

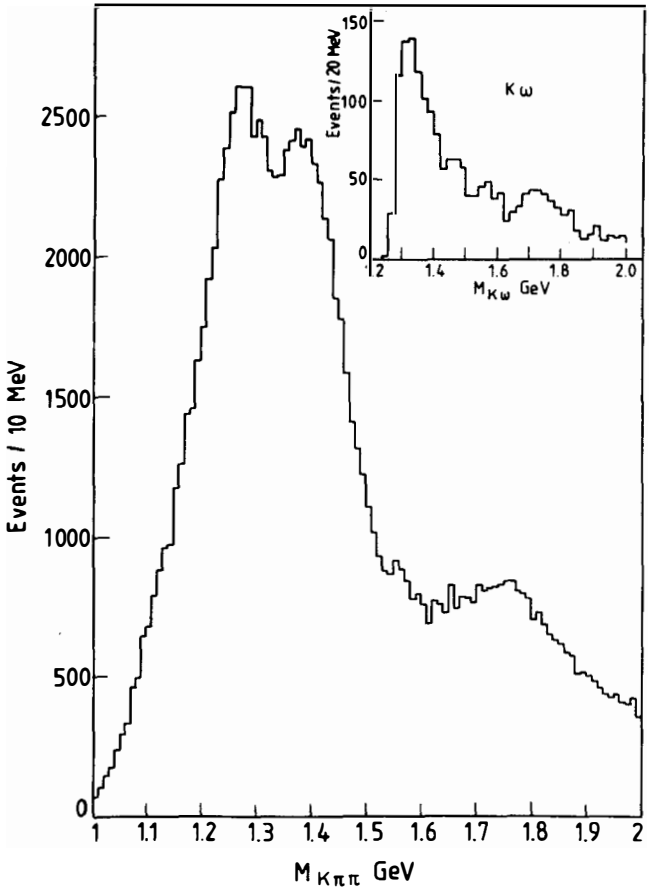

Fig. 6 The $K^-\pi^-\pi^+$ mass spectrum as measured by the ACCMOR collaboration[2]. The raw Kω mass spectrum is shown as an insert.

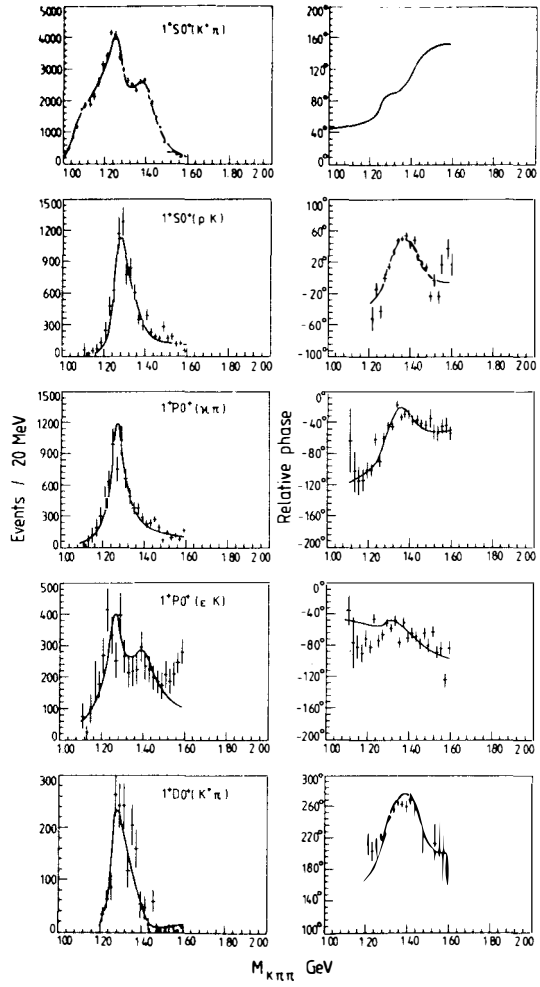

Fig. 7 Results from the ACCMOR collaboration[2] of a partial-wave analysis in the Q region, $1.0 \leq M_{K\pi\pi} \leq 1.6$ GeV, for 1^+0^+ waves, $0 \leq |t'| \leq 0.05$ GeV^2. The phases are measured with respect to 1^+S0^+ $(K^*\pi)$. The curves represent the fits obtained with two Q resonances and coherent background.

(d) The D and E mesons.

If we accept the D and E as its isoscalar members, the 1^{++} nonet is complete. The J^P of the D-meson is well defined as 1^+, in particular by a partial wave analysis of the $\eta\pi\pi$ system by Stanton et al.[9]. The situation for the E-meson is less clear. Dionisi et al.[10] have analyzed the $K^0_S\ K^{\pm}\pi^{\mp}$ system in 3.95 GeV $\pi^- p \to K^0_S\ K^{\pm}\pi^{\mp} n$ interactions and indicate a strong preference for $J^P=1^+$. This, however, is in disagreement with previous $\bar{p}p$ results which favour $J^P=0^-$ [11].

Another problem with the E-meson is its production characteristics. It is generally assumed that the E is the $s\bar{s}$ member of the 1^+ nonet. The near mass degeneracy of A_1 and D is in agreement with that assumption. However, the Dionisi data indicate a rather large cross section of about 10 μb in $\pi^- p$ interactions. On the other hand a comparable cross section is measured for D-production in $K^- p \to Dn$ at 4.2 GeV, while in the same experiment the evidence for the E-meson is hard to find[13]. These results would suggest that the D and E if both belonging to the 1^{++} nonet are far from ideally mixed.

Another possible indication for such an assumption comes from a comparison of the decay widths of the various nonet members assuming SU(3) symmetric couplings. In reference [2] the couplings are determined from a fit to the Q-meson data and are used to predict the width of $A_1 \to \rho\pi$ and $B \to \omega\pi$ decays. These values appear to be in prefect agreement with the observed widths. The predictions for the K^*K partial width of the E-meson depends on the E, D mixing angle. With the couplings from the Q-analysis a mixing angle of 55° is required - significantly larger than the 35° corresponding to perfect mixing - to reproduce the observed width of about 40 MeV. Some care, however, is here required. The E-meson has a mass just above the K^*K threshold. The calculated width therefore becomes very sensitive to the assumptions which are put into the determination of the phase space factor.

In conclusion the situation concerning the E-meson is still rather confused. An isoscalar $s\bar{s}$ member of the 1^{++} nonet is certainly expected at a mass of about 1420 MeV. However, the particle that has been observed at this mass cannot unequivocally be assigned to this state. Possibly the situation is complicated by the presence of

other particles in this mass region, like glueballs and radial excitations of η, and η', which make a clear identification difficult.

Conclusions.

Conclusive evidence now exists for most of the members of the two $J^P=1^+$ nonets expected for a $q\bar{q}$ system with L=1. The A_1 has a mass in the range 1200 - 1300 MeV. This is larger than previous low statistics data seemed to indicate but clearly is in better agreement with the masses of the other L=1 $q\bar{q}$ mesons. Also the I=0, $J^{PC}=1^{+-}$ H-meson has now been firmly established leaving the $s\bar{s}$ member of the 1^{+-} nonet as the only undiscovered particle of the two 1^+ nonets. Using the Gell-Man-Okubo formula its mass is predicted to be ~1.48 GeV.

References.

1) C. Daum et al., CERN-EP/80-219, to be published in Nucl. Phys.
2) C. Daum et al., CERN-EP/81-04, to be published in Nucl. Phys.
3) J.A. Donkowych et al., Phys. Rev. Lett. 46 (1981) 580.
4) G. Ascoli et al., Phys. Rev. D7 (1973) 669.
5) D.J. Herndon et al., Phys. Rev. D11 (1975) 3165, 3183.
6) M.G. Bowler, J. Phys. G5 (1979) 203.
7) P. Gavillet et al., Phys. Lett. 69B (1977) 119.
8) G.W. Brandenburg et al., Phys. Rev. Lett. 36 (1976) 703 and 706; Nucl. Phys. B127 (1977) 509.
9) H.R. Stanton et al., Phys. Rev. Lett. 42 (1979) 346.
10) C. Dionisi et al., Nucl. Phys. B169 (1980) 1.
11) P. Baillon et al. NC 50A (1967) 393.
12) A. Gurtu et al., Nucl. Phys. B151 (1979) 181.

A_3-PRODUCTION IN THE REACTION $\pi^- p \to \pi^- K^+ K^- p$ AT 16 GeV/c

G. Otter
Aachen-Bari-Bonn-CERN-Glasgow-Liverpool-Milan Collaboration

ABSTRACT

A partial wave analysis was performed on the low mass $(K^+K^-\pi^-)$ system produced in $\pi^- p \to \pi^- K^+ K^- p$ at 16 GeV/c using the CERN-Omega spectrometer. A_3-production is found in the waves $2^-S(f\pi)$ and $2^-P(K^*K)$. The A_3 is interpreted as a resonance since the large enhancement $2^-P(K^*K)$ at ∿1700 MeV can certainly not be interpreted as being due to the Deck effect, which is probably responsible for the low mass peak in $1^+S(K^*K)$ around ∿1500 MeV.

The $J^{PC} = 2^{-+}$ nonet for mesons is poorly known. It seems that A_3 (M = 1.66 GeV, Γ = .20 GeV I = 1) is one such particle. Our knowledge of A_3 comes mainly from partial wave analyses (PWA) of the 3-meson system in $\pi^{\pm}p \to \pi^{\pm}\pi^{+}\pi^{-}p$. The results of these experiments [1], listed in table 1, are, however, partly contradictory. Some authors interpret the A_3 peak as a resonance, others as a kinematic threshold effect (Deck effect). Also, the A_3-decay modes are found to be different by different groups. The results of a recent high statistics experiment [2] agree with the resonance interpretation - the corresponding phases of the decay amplitudes vary as expected. They find three decay modes of A_3: $2^{-}S\ f\pi$, $2^{-}P\ \rho\pi$ and $2^{-}D\ \varepsilon\pi$.

We (Aachen-Bari-Bonn-CERN-Glasgow-Liverpool-Milan collaboration) study A_3 in another reaction,

$$\pi^{-}p \to (K^{+}K^{-}\pi^{-})p \qquad (1)$$

The experiment was performed in the CERN-Omega spectrometer (fig. 1) using an incident beam of 16 GeV/c. The following effective trigger system was used to select this channel:

a) interaction trigger (incident π^{-} interact in the target)
b) multiplicity trigger (3 or 4 hits in TS and MWPC1; 2, 3 or 4 hits in MWPC3)
c) matrix trigger (selection of fast K^{-} by requiring correlated hits in the hodoscopes H1/H2 together with no light in the corresponding cells of the Cerenkov counter).
d) π^{o}-veto by using a γ-veto counter.

With these conditions we have 28200 four-prongs and 25200 three-prongs (the low momentum p is missing) of reaction (1) - the highest statistics for this channel!

The following parametrisation of the 2-meson masses in the PWA of the $(K^{+}K^{-}\pi)$-system was used:

$(K^{+}\pi^{-})$-system: S-wave: $(K\pi)$-phaseshifts (κ)
P-wave: Breit-Wigner K^{*}-resonance
D-wave: not necessary

$(K^{+}K^{-})$-system: S-wave: $\bar{K}K$-phaseshifts (S^{*} and ε) denoted in the following as S^{*}
P-wave: not necessary
D-wave: Breit-Wigner f-resonance.

The PWA of the $(K^+K^-\pi^-)$-system was performed in steps of 50 MeV in the mass region $1.3 \leq M(KK\pi) \leq 2.0$ GeV. It took into account the losses due to geometrical acceptance (~40% at 1.3 GeV and decreasing to 15% at 20 GeV), inefficiencies of the various trigger elements and decay and interaction of each track in the spectrometer. Two kinds of solutions with equal probability were found, which differ mainly in the amount of κ-contribution. The results for the 1^+ and 2^- states for one of the two solutions (the other one shows similar results) are seen in fig. 2. The 2^- states are of special interest. $2^-S(f\pi)$ and especially $2^-P(K^*K)$ show peaks in the A_3 mass region (fig. 3, the solid lines are Breit-Wigner curves for A_3 with M = 1.67, Γ = 0.21). This is expected from the PWA of the (3π)-data, since f decays also to K^+K^- ($f^o \to \pi^+\pi^-$ / $f^o \to K^+K^- \simeq 40$) and since, using SU3, the decay $A_3 \to \rho\pi$ predicts other vector plus pseudoscalar particle decay modes of A_3 ($A_3 \to K^*K$). The large $2^-P(K^*K)$ intensity in A_3 can hardly be interpreted by a Deck effect which peaks at lower $(KK\pi)$-masses (the $1^+S(K^*K)$ wave dominating the low $(KK\pi)$-mass peaks around 1.5 GeV and is probably due to this kinematic effect, see fig. 2). We therefore believe that $2^-S(f\pi)$ and $2^-P(K^*K)$ are two decay modes of A_3. In the mass region $1.5 \leq M(KK\pi) \leq 1.8$ GeV we find

$$\frac{A_3^- \to f\pi^- \to K^+K^-\pi^-}{A_3^- \to K^*K^- \to K^+\pi^-K^-} = 0.56 \pm 0.18.$$

No peaks are seen in the A_3 region in the other 2^- states, $2^-D\ f\pi$, $2^-D\ S^*\pi$ or $2^-D\ \kappa K$. The phases of $2^-S(f\pi)$ and $2^-P(K^*K)$ relative to each other and to the background wave $1^+S\ K^*K$ are given in fig. 3. The solid lines are predictions from Breit-Wigner resonance variation and agree quite well with the data (at least for $2^-P\ K^*K$ vs. $1^+S\ K^*K$). The phase between $2^-P(K^*K)$ and $2^-S(f\pi)$ varies slightly which indicates a background contribution under the resonance.

References:

1) G. Ascoli et al., Phys. Rev. D7 (1973) 669
   Yu. Antipov et al., Nucl. Phys. B63 (1973) 153
   G. Thompson et al., Nucl. Phys. B69 (1974) 381
   G. Otter et al., Nucl. Phys. B80 (1974) 1
   J. Pernegr et al., Nucl. Phys. B134 (1978) 436

2) C. Daum et al., Phys. Lett. 89B (1980) 285
   C. Daum et al., CERN-EP/80-219

Table 1

reaction	$\pi^+ p \to \pi^+\pi^+\pi^- p$ [1]	$\pi^+ p \to \pi^+\pi^+\pi^- p$ [1]	$\pi^- A \to \pi^-\pi^+\pi^- A$ [1]	$\pi^- p \to \pi^- K^+ K^- p$
incident momentum GeV/c	13	8, 16, 23	8.9, 12.9, 15.1	16
apparatus	bubble chamber	bubble chamber	spark chamber	Omega spectrometer
nr. of events	40300	∿ 30000	∿ 60000	∿ 53500
acceptance in A_3-region	100%	100%	∿ 72%	∿ 25%
A_3-mass, GeV	2^-SfπM=1.60±.01	not given	M ∿ 1.65	not given
A_3-width, GeV	Γ =.31 ±.04		Γ ∿ .4	
A_3-decay modes	2^-Sfπ 52% 2^-P$\rho\pi$ 48 ± 14%	2^-S fπ ∿ 60% 2^-P $\rho\pi$ ∿ 40%	2^-S fπ 2^-P $\rho\pi$	2^-S(f$\pi\to K^+K^-\pi^-$) 2^-P($K^{*o}K^-\to K^+\pi^-K^-$) ratio .56 ± .18
phases of waves in A_3-region	2^-S vs 1^+P, 1^+S, 2^+D, 3^+P variation 2^-S vs 2^-P no variation	2^-S vs 0^-S, 1^+S 2^-P vs 0^-S, 1^+P variation 2^-P vs 2^-S no variation	2^-S vs 1^+S, 1^+P 2^-P vs 1^+S, 1^+P variation 2^-S vs 2^-P no variation	2^-S vs 1^+S (K^*K) 2^-P vs 1^+S (K^*K) variation 2^-P vs 2^-S weak variation

Table 1 cont.

reaction	$\pi^- p \to \pi^- \pi^+ \pi^- p$ [1]	$\pi^- p \to \pi^- \pi^+ \pi^- p$ [1]	$\pi^- p \to \pi^- \pi^+ \pi^- p$ [2]
incident momentum, GeV/c	5,7,7.5,11,13,16,18.5,20,25	25,40	63,94
apparatus	bubble chamber	CERN-IHEP boson spectrometer	WA3 forward spectrometer
nr. of events	64000	70000	598000
acceptance in A_3-region	100 %	30% (25 GeV/c) 70% (40 GeV/c)	$\sim$ 50 %
A_3-mass, GeV	2^-S $f\pi$ M = 1.66 ± .01	2^-S $f\pi$ M = 1.65 ± .03	2^-S $f\pi$ M = 1.671 ± .002 Γ = .207 ± .010 2^-P $\rho\pi$ M = 1.643 ± .002
A_3-width, GeV	Γ = .27 ± .06	Γ = .30 ± .05 (40 GeV/c data)	Γ = .230 ± .020 2^-D $\varepsilon\pi$ M = 1.655 ± .005 Γ = .228 ± .060
A_3-decay modes	only 2^-S $f\pi$ upper limits: 2^-P $\rho\pi$, 2^-F $\rho\pi$ $\leq$ 10% 2^-D $\varepsilon\pi$, 2^-D $f\pi$ $\leq$ 6%	only 2^-S $f\pi$	2^-S $f\pi$ 57 ± 3 % 2^-P $\rho\pi$ 32 ± 6 % 2^-D $\varepsilon\pi$ 11 ± 5%
phases of waves in A_3-region	2^-S vs 0^-S, 1^+S, 1^+P, 2^-P, 3^+D no variation	2^-S vs 0^-S, 1^+S, 1^+P, 2^-P no variation	2^-S vs 1^+S, 0^-S variation 2^-S vs 2^-P, 2^-D no variation

Fig.1

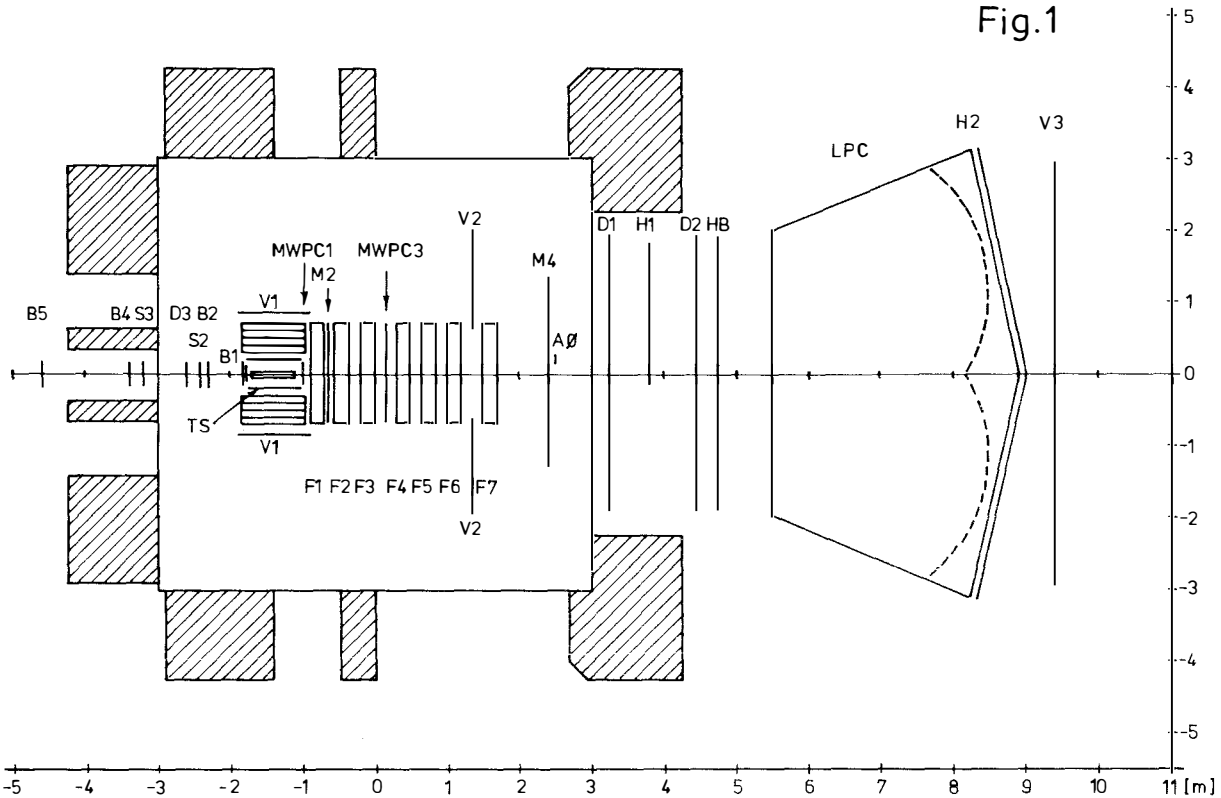
B5
B4 S3
D3 B2
S2
B1
V1
TS
V1
MWPC1
M2
MWPC3
V2
F1 F2 F3 F4 F5 F6 F7
V2
M4
AØ
D1
H1
D2 HB
LPC
H2
V3
5
4
3
2
1
0
-1
-2
-3
-4
-5
-5 -4 -3 -2 -1 0 1 2 3 4 5 6 7 8 9 10 11 [m]

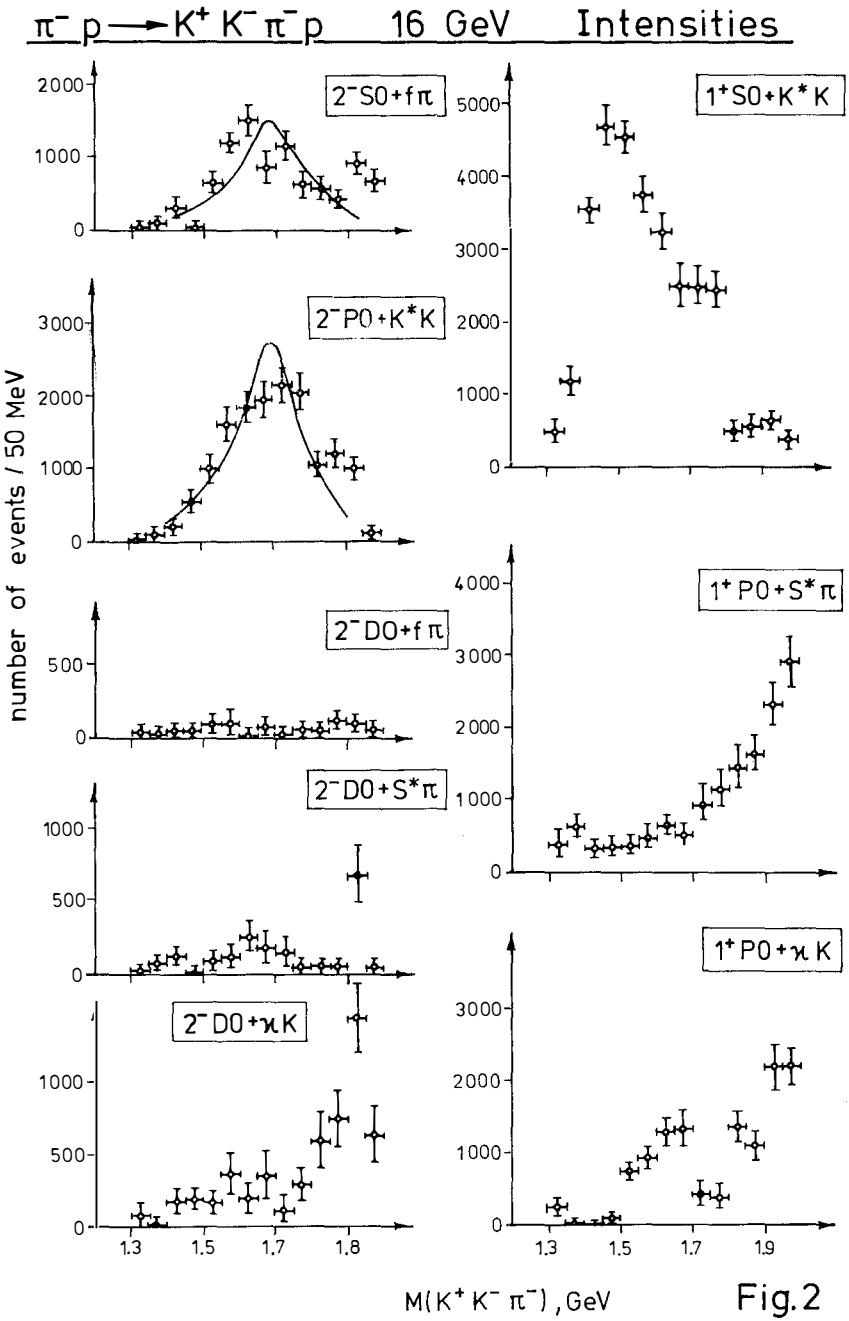
π⁻ p → K⁺ K⁻ π⁻ p 16 GeV Intensities
2⁻S0+fπ
1⁺S0+K*K
2⁻P0+K*K
1⁺P0+S*π
2⁻D0+fπ
2⁻D0+S*π
1⁺P0+κK
2⁻D0+κK
number of events / 50 MeV
M(K⁺ K⁻ π⁻), GeV

Fig.2

$\pi^- p \longrightarrow K^+ K^- \pi^- p$ 16 GeV Phases

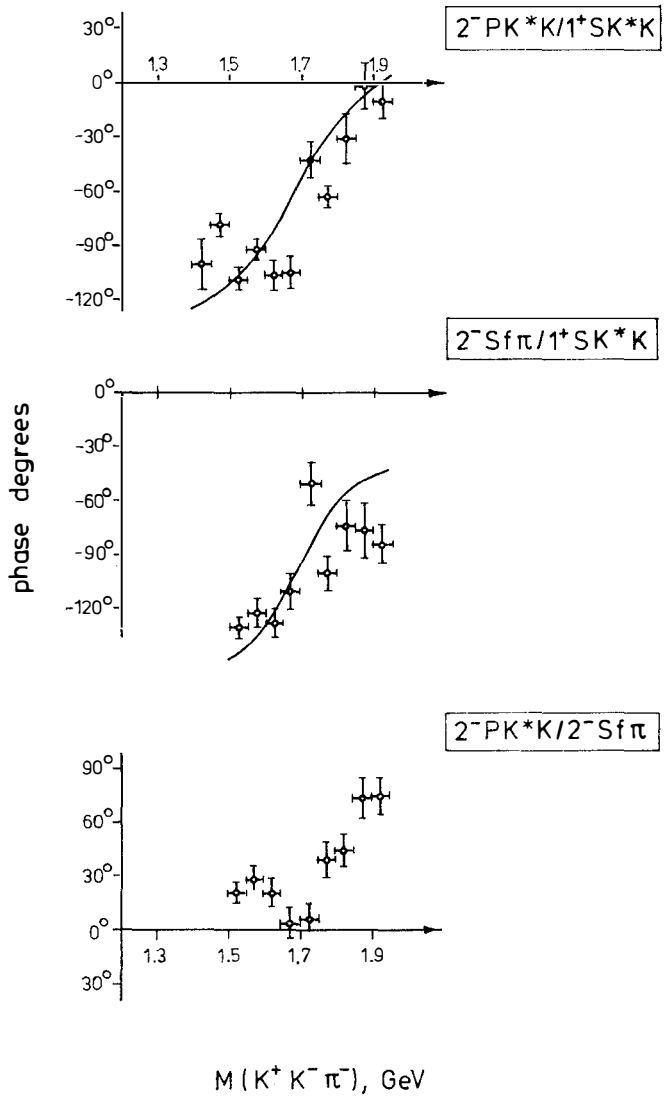

Fig. 3

OBSERVATION OF NEW RESONANCE STRUCTURE IN THE NATURAL SPIN PARITY STRANGE MESON SYSTEM*

(SLAC-Carleton-NRC Canada Collaboration)†

Blair N. Ratcliff
Stanford Linear Accelerator Center
Stanford University, Stanford, California 94305

ABSTRACT

New data from the LASS spectrometer are presented on the reaction $K^-p \to K^-\pi^+n$. An energy independent partial wave analysis of this data yields unique $K^-\pi^+$ elastic scattering partial wave amplitudes in the invariant mass region from 0.7 GeV to 1.8 GeV, and two distinguishable sets of amplitudes between 1.8 GeV and 2.3 GeV. These amplitudes confirm all of the well known $K\pi$ resonances, and display clear evidence for new resonance structure in the S, P and G waves in the mass region above 1.6 GeV.

† D. Aston, R. Carnegie, W. Dunwoodie, S. Durkin, P. Estabrooks, T. Fieguth, R. J. Hemingway, A. Honma, D. Hutchinson, W. B. Johnson, P. Kunz, T. Lasinski, D. W. G. S. Leith, L. Levinson, R. McKee, A. McPherson, W. T. Meyer, G. Oakham, B. N. Ratcliff, R. Richter, S. Shapiro, R. Stroynowski, S. Suzuki, S. Williams, J. Va'Vra.

At the present time, we are engaged in a systematic study of Kp interactions at 11 GeV/c using the LASS spectrometer at SLAC. Broadly stated, the physics goals of this program are to provide a "great leap forward" in our understanding of the strange (e.g., $s\bar{u}$), and strangeonium ($s\bar{s}$) mesons, and of the strangeness -2 and -3 hyperons (e.g., ssu). Even though our general understanding of the hadron spectrum has improved dramatically during the last decade, these areas remain poorly understood. This is largely because nature provides us with no stable meson or strange baryon targets, so that these areas must be studied in production experiments.

The experimental program consists of two separate experiments. In the first, we triggered on essentially the total inelastic cross section and attained a sensitivity of about 1000 ev/μb for K^-p interactions. This experiment was run in 1978 and provides the data sample on which this talk is based. We are presently extending this data sample by a factor of over five in a sequel experiment which uses both K^+ and K^- beams.

The scope of the experimental program is clearly very broad, and I can only discuss a small portion of it here. Today, I would like to focus on our recently completed energy independent partial wave analysis of the Kπ system from the reaction

$$K^-p \rightarrow K^-\pi^+n \qquad (1)$$

at small values of momentum transfer. This reaction is dominated by π exchange, and historically has been an important source of information on Kπ elastic scattering, and the natural spin-parity strange mesons.[1] In a previous analysis of the Kπ system using reaction (1) and several other π exchange dominated reactions at 13 GeV, ($K^+p \rightarrow K^+\pi^+n$, $K^-p \rightarrow K^-\pi^-\Delta^{++}$, $K^+p \rightarrow K^+\pi^-\Delta^{++}$) Estabrooks et al.[2] presented clear evidence for the $J^P = 0^+\kappa(1500)$, as well as evidence for P wave resonance structure in the 1.65 GeV region in two out of four solutions. That analysis was restricted to Kπ masses below 1.8 GeV. In this talk, we present a PWA of new 11 GeV data on reaction (1) which extends the measurements of $K^-\pi^+$ elastic scattering partial waves up to a mass of 2.3 GeV. These partial waves confirm the results of Estabrooks et al.[2] in the low mass region ($M_{K\pi} < 1600$ MeV) while clearly displaying additional resonance structure at higher masses.

Events corresponding to reaction (1) were selected from the charge-zero two-prong sample by requiring the missing mass opposite the outgoing $K^-\pi^+$ system to lie in the range from 0.45 GeV to 1.05 GeV. Events ambiguous with elastic K^-p events and K^0 decay events were explicitly rejected. The final $K^-p \rightarrow K^-\pi^+n$ data sample consisted of ~43,000 events in the Kπ invariant mass range from 0.7 GeV to 2.3 GeV, and the small momentum transfer region, $|t'| < 0.2$ GeV^2. With these cuts, the background to reaction (1) was estimated to be 4 ± 4%.

A maximum likelihood fitting procedure was used to correct the raw data for effects due to spectrometer acceptance, event selection criteria, and other factors. This procedure yields t-channel acceptance corrected $K\pi$ angular moments as a function of the $K\pi$ invariant mass and t'. In these fits the number of L and M moments was limited ($L < L_{max}$, $M < M_{max}$) to the minimum number required to describe the data in each mass region. Because reaction (1) is dominated by π exchange the prominent (M) moments are those with $M = 0$. These are shown in Fig. 1 as a function of $M_{K\pi}$. The most prominent structures in the even L moments are due to the leading K^* resonances (the $J^P = 1^-K^*(892)$, $2^+K^*(1430)$, $3^-K^*(1780)$, and the newly discovered $J^P = 4^+K^*(2090)$ [3] while clear interference effects can be seen in the odd angular moments.

We have performed an energy independent $K\pi$ scattering partial wave analysis using these spherical harmonic moments with an additional cut on the lower vertex ($n\pi$) mass. The $K\pi$ scattering analysis method used is identical to that employed in the previous PWA of the 13 GeV data performed by this group.[2] By extrapolating the π exchange contribution to the pole, this analysis determines the magnitudes and relative phases of the $K\pi \to K\pi$ scattering partial waves (one overall phase cannot be determine). Below 1.2 GeV the S and P waves are known to be elastic,[2] so the imposition of elastic unitarity on the S and P waves is sufficient to fix the overall phase. In the inelastic region above 1.2 GeV we fix the phase of the leading K^* resonance in each mass region near to the Breit-Wigner phase of the associated resonance as is shown in Fig. 3.

There are also discrete ambiguities inherent in any pseudoscalar-pseudoscalar amplitude analysis. These ambiguities are most readily apparent as ambiguities in the sign of the imaginary part of the amplitude zeros described by Barrelet.[4] Requiring the solutions to be smooth, it is possible to switch from one solution to another only when the imaginary part of a particular Barrelet zero approaches zero. Since the Wigner condition combined with the existence of leading resonances requires all of the $Im(Z_i)$ to enter our solutions negatively, elastic unitarity leads to a unique solution below 1.20 GeV. It is seen in Fig. 2 that ambiguities do not arise until $Im(Z_3)$ approaches zero in the 1.86 GeV region. In the region between 1.9 and 2.0 GeV, $Im(Z_1)$ is also nearly zero. Thus, we extract one unique solution below 1.86 GeV, two distinct solutions in the region between 1.86 and 2.02 GeV, and four solutions above 2.02 GeV. The definitions of these four solutions in terms of the signs of the imaginary parts of the amplitude zeros in each mass region can be found in Table I.

The $K^-\pi^+$ partial wave magnitudes and phases are shown in Fig. 3. In general, these results are consistent with, but of higher statistical significance than previous measurements, particularly in the region above the $K^*(1430)$. The four high mass solutions presented actually fall into only two physically distinct

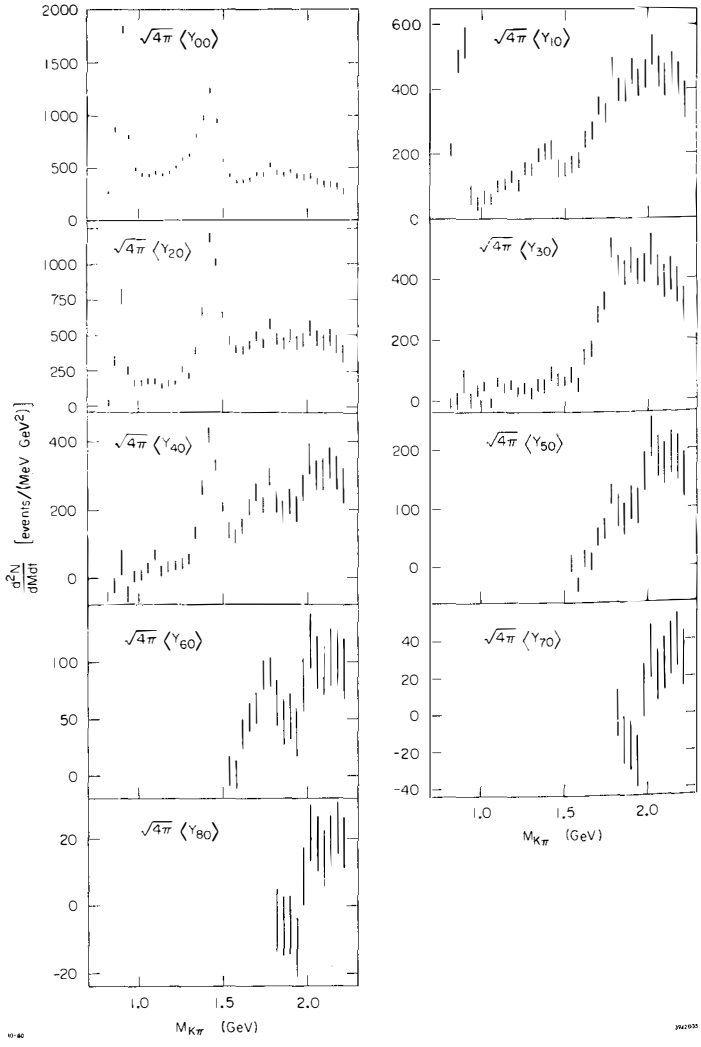

Fig. 1. The final M = 0 acceptance corrected angular moments as a function of mass. These moments are calculated in 40 MeV bins below 1.8 GeV, and 80 MeV overlapping bins above this mass. The moments have been divided by the mass bin and t' bin width.

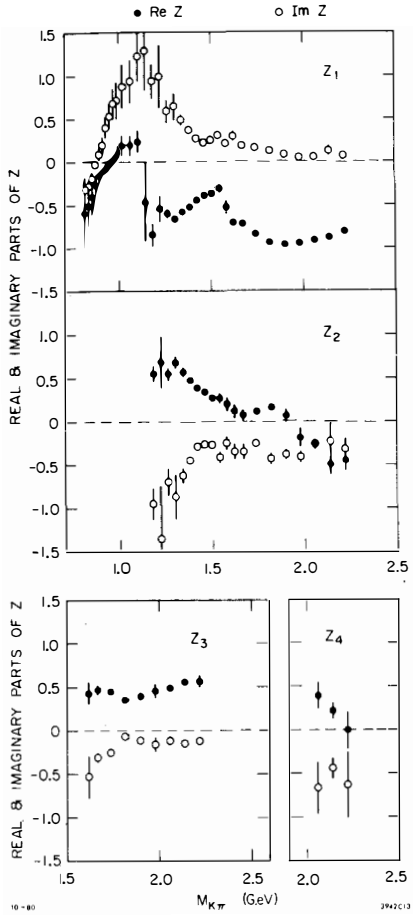

Fig. 2. The amplitude (Barrelet) zeros as a function of mass.

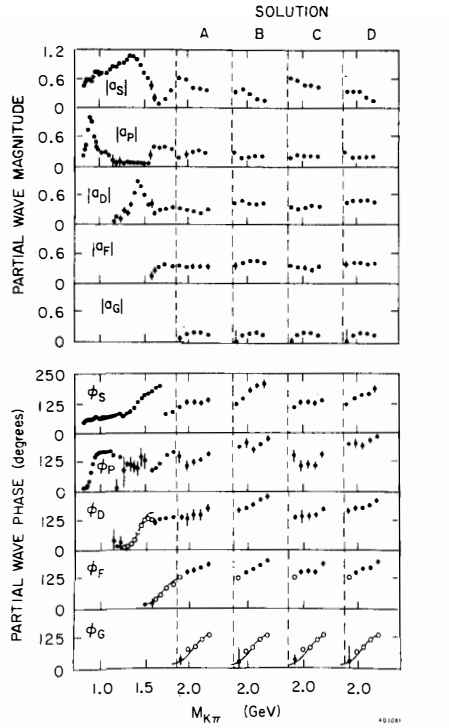

Fig. 3. These data were fit in 20 MeV bins below 1.06 GeV, 40 MeV bins from 1.6 GeV to 1.67 GeV, and 80 MeV bins above 1.67 GeV. The solid line represents the phase predicted by a simple Breit-Wigner fit to the leading resonance in the given mass region. The actual phase in each mass region has been fixed to the phase represented by the symbol o. Where error bars are not shown the size of the points plotted is larger than the statistical error associated with the point.

TABLE I

The Barrelet Zero Solution Classifications

Solution \ Mass (GeV)	1.30 - 1.86			1.86 - 2.02				2.02 - 2.30			
	z_1	z_2	z_3	z_1	z_2	z_3	z_4	z_1	z_2	z_3	z_4
A	+	-	-	+	-	+	-	-	-	+	-
B	+	-	-	+	-	-	-	-	-	-	-
C	+	-	-	+	-	+	-	+	-	+	-
D	+	-	-	+	-	-	-	+	-	-	-

groups (A,C) and (B,D) based primarily on the behavior of the S and P waves. The behavior of the D,F and G waves are essentially independent of the solution. In the ambiguous region the S wave shows relatively similar magnitude peaks coupled with rapid phase motion in all four solutions. Only the P wave above 2 GeV differs substantially between the two solution sets.

All solutions display the leading $J^P = 1^-$, 2^+, 3^- and 4^+ resonances clearly. Additional resonance structure is also seen in the S and P wave solutions. This structure is more easily viewed in the Argand diagrams of Fig. 4 which show the two physically distinct solutions (A,C). In these diagrams, significant departures from the unitary circle can be seen in the S wave solutions at low mass. These departures are due to the fact that the partial waves presented are the sum of the different isospin parts ($a_L = a_L^{1/2} + \frac{1}{2} a_L^{3/2}$). The 3/2 component has been well measured up to 1.6 GeV and contains no significant waves other than the S wave. Above 1.6 GeV, little I = 3/2 information exists. In the S wave plots of Fig. 4, the dotted lines represent our S wave solutions with the isospin 3/2 component subtracted up to 1.6 GeV using the parameterization of Ref. 1. The resulting S wave remains within the unitary circle.

The leading K^* resonances are readily apparent as counter clockwise loops in the appropriate Argand diagrams. In particular, the new $J^P = 4^+ K^*(2090)$ is indicated by the G wave loop in the 2.1 GeV region.

In the S wave Argand plots of Fig. 4, a slow circular motion of the S wave amplitude is seen in the region from 0.80 GeV to 1.35 GeV. Above this mass, the S wave amplitude undergoes a very rapid circular motion with the greatest speed in the 1.420 GeV region. The precise mass of this maximum speed is clearly dependent on our choice of overall phase, as well as nonresonant S wave backgrounds. However, we believe any reasonable choice of phase will exhibit similar resonance behavior. Thus, we conclude that there exists an S wave resonance in this mass region, confirming the $0^+\kappa(1500)$ previously reported.[2)]

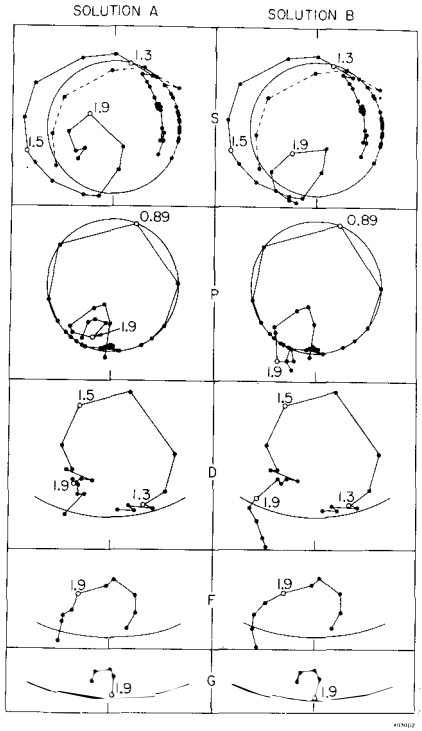

Fig. 4. Argand diagrams of the $K^-\pi^+$ elastic scattering partial waves for solutions A and B. The overall phase has been fixed as in Fig. 3.

In the mass region above 1.60 GeV circular motion is once again seen in the S wave Argand diagrams. Once again the details of this behavior are sensitive to the choice of overall phase, nonresonant backgrounds, as well as in this case, the particular solution being studied. However, all solutions display clear resonance loops at around 1900 MeV. We call this new state the $\kappa'(1900)$.

Figure 4 also shows resonance like behavior in the P wave near 1.65 GeV. Similar behavior was observed by Estabrooks et al. in two of four ambiguous solutions.[2] The precise interpretation of this structure is unclear. It is simplest to assume this behavior is due to a single resonance in the 1700 MeV region, and we will do when presenting parameters below. However, the rapid rise in the P wave amplitude in the 1600 MeV region combined with a very flat magnitude thereafter may indicate other structure in this region as well.

We have extracted resonance parameters for the leading states by fitting the rising edge of the associated partial wave magnitude to a relativistic Breit-Wigner resonance form with a Blatt-Weisskopf barrier factor.[5] In performing these fits, we have assumed that the turn-on of the partial waves associated with these states is resonance dominated. The resulting parameters are given in Table II. The resonance parameters obtained for the $4^+K^*(2090)$ were found to be independent of the solution fitted.

Faced with sizable nonresonant backgrounds, the overall phase uncertainty, and no clear theoretical understanding of the definition of resonance parameters, we have not attempted to determine the parameters of these underlying state precisely. Instead, we have estimated their parameters by ascribing circular motion to the Argand diagram resonance loops. The results are shown in Table II. Within the uncertainties of these estimates, the high mass S and P state parameters

TABLE II

LEADING RESONANCES

J^P	Mass	Width	Elasticity
1^-	894.6 ± 0.8 MeV	49.8 ± 1.2 MeV	---
2^+	1428 ± 3 MeV	98 ± 8 MeV	0.43 ± 0.01
3^-	1753 $^{+25}_{-18}$ MeV	300 $^{+170}_{-80}$ MeV	0.16 ± 0.01
4^+	2070 $^{+100}_{-40}$ MeV	240 $^{+500}_{-100}$ MeV	0.07 ± 0.01

UNDERLYING RESONANCES

J^P	Mass	Width	Elasticity
0^+	~ 1420 MeV	~ 240 MeV	~ 0.85
0^+	~ 1900 MeV	~ 230 MeV	~ 0.35 - 0.45
1^-	~ 1700 MeV	~ 200 MeV	~ 0.35

depend insignificantly on the particular solution chosen.

The resonance states observed in the $K^-\pi^+$ partial waves fit naturally into the framework expected from SU(3) and a simple $q\bar{q}$ quark model. The $K^*(892)$, $K^*(1430)$, $K^*(1780)$ and $K^*(2090)$ form an L-excitation ladder (with $q\bar{q}$ total spin S = 1) with L increasing from 0 to 3. The lower 0^+ state at ~1420 MeV is naturally classified as the lowest lying member of the L = 1, S = 1, $K^*(1430)$ triplet, while the higher 0^+ state can be naturally interpreted as the first radially excited recurrence of the 0^+, L = 1, S = 1 triplet member. The 1^- resonance behavior at 1700 MeV can be either the L = 0, S = 1 radial recurrence of the $K^*(892)$, the lowest lying member of the L = 2, S = 1, $K^*(1780)$ triplet, or perhaps both. Accurate measurements of this invariant mass region in inelastic decay channels should make it possible to establish which of these possibilities is the correct one.

REFERENCES

1. See: R. L. Kelly et al., Particle Data Group, Rev. Mod. Phys. 52, No. 2 (1980) and references therein.
2. P. Estabrooks et al., Nucl. Phys. B133, 490 (1978).
3. D. Aston et al., Phys. Lett. 99B, 503 (1981). Also see W. E. Cleland et al., Phys. Lett. 97B, 465 (1980).
4. E. Barrelet, Nuovo Cimento 8A, 331 (1972).
5. J. Blatt and V. Weisskopf, Theoretical Nuclear Physics, Wiley, New York (1952), p. 361, pp. 409-410.

VECTOR MESONS FROM FRAGMENTATION OF THE REAL PHOTON

A.B. Clegg
Department of Physics, University of Lancaster, Lancaster, U.K.

ABSTRACT

Measurements are presented of vector mesons resulting from fragmentation of photons of energies 25-70 GeV. Particular results include:

(a) the $\rho\pi\pi$ decay of the $\rho'(1600)$ is primarily through the $A_1\pi$ state
(b) indication of a relatively narrow state at a mass $\sim$ 1.65 GeV.
Candidates for nonet mates of the $\rho'(1600)$ are discussed.

1. Introduction

I report recent results on vector mesons produced by diffractive dissociation of photons of energies of 25-70 GeV, primarily from the CERN WA4 experiment with some preliminary complementary information from the CERN WA57 experiment.

A summary of these results is

(i) WA4 results on $\gamma p \to p\pi^+\pi^-\pi^+\pi^-$, particularly relevant to the $\rho'(1600)$.

(ii) Some preliminary, and complementary, indications from the reaction $\gamma p \to p\pi^+\pi^-\pi^0\pi^0$, from early analysis of WA57 results.

(iii) Indication, from WA4 results, of a relatively narrow vector meson with a mass $\sim$ 1.65 GeV, observed to decay into $\pi^+\pi^-\pi^+\pi^-\pi^0$, $\pi^+\pi^-\pi^0$ and K^+K^-.

(iv) Some comments on possible nonet mates of the $\rho'(1600)$ and related matters.

These results are compared with corresponding results from electron-positron annihilation. In particular estimates are presented of total cross-sections for vector mesons colliding with protons, deduced by assuming the diagonal version of the Vector Dominance Model (VDM).

2. The reaction $\gamma p \to p\pi^+\pi^-\pi^+\pi^-$

The results reported in this section are described more fully in a paper submitted for publication[1]. Fig.1 shows the 4π mass spectrum, corrected for acceptance. It is estimated there could be $\sim$ 10% background for $M(4\pi) < 1.8$ GeV and $\sim$ 30% background for $M(4\pi) < 1.8$ GeV, from failure to separate contributions from other reactions. This mass spectrum shows a strong peak at 1.5 GeV, with a tail extending to high masses. Good agreement with $M^2\sigma(e^+e^- \to \pi^+\pi^-\pi^+\pi^-)$ is demonstrated, which would correspond in the VDM to a total cross-section which does not vary with 4π mass.

The tail at higher masses has made for difficulty in fitting the total $e^+e^- \to \pi^+\pi^-\pi^+\pi^-$ cross section with a single resonance. Examination of photoproduction angular distributions shows that this over-simplified interpretation is in error, and indicates a transition at $M(4\pi) \sim 1.9$ GeV between two mechanisms: a ρ' peak at the lower masses, and production of a jet-like structure at the higher masses.

A maximum likelihood analysis has therefore been made, fitting data in 100 MeV bins of 4π mass with linear combinations of intensities of various models. There were some problems in fitting the ρ' peak. $\rho\pi\pi$ phase space and $\rho\varepsilon$ models with s-wave relative motion failed. (The intensity used was the square of the sum of the four amplitudes corresponding to the four possible identifications of the ρ-meson[2]. The ε-meson was described by a Watson final state interaction[3], using the measured s-wave $\pi\pi$ phase shift[4].) Successful fits were obtained with either of two alternative deformations of the $\pi^+\pi^-\pi^+\pi^-$ system:

(i) An $(A_1 \to \rho\pi)\pi$ model with a relatively high mass and wide A_1: M = 1.3 GeV, Γ = 0.3 GeV were the values used in the detailed fits.

(ii) A $\rho\varepsilon$ model with both s and d-wave relative motion, with an amplitude ratio of d/s $\sim$ 0.25. The centrifugal barrier in the d-wave amplitude provides the needed deformation.

Resulting intensities found by the maximum likelihood method for various contributing models assuming the $A_1\pi$ model of the decay of the $\rho'(1600)$ are shown in Fig.2. Similar results are obtained if the $\rho\varepsilon$ s and d-wave model is assumed for decay of the $\rho(1600)$. The conclusions of this analysis are:

(i) A well-separated $\rho'(1600)$ peak with M = 1.52±0.03 GeV, Γ = 0.40±0.05 GeV. As the high mass tail has been separated the discrepancy with the narrower width found[5,6] for the $\pi^+\pi^-$ decay mode of the $\rho'(1600)$ is reduced. The definite peak is not in accord with models which have been proposed[7,8]. At least 80% of production of the $\rho'(1600)$ is by an schc mechanism.

(ii) For masses $\gtrsim$ 2 GeV production of jet-like structures, with $\sim$ 55% $\rho^o\pi^+\pi^-$, dominates. These structures are picked out by p_T-limited phase space models.

(iii) The relative importance of a further contribution is indicated at masses around 1.2 GeV, which is picked out most definitely by 4π p_T-limited phase space.

(iv) Comparison of photoproduction and e^+e^- cross-sections, assuming there is the same fraction of $\rho'(1600)$ in each case and assuming diagonal VDM, indicates

$$\sigma_{TOT}(\rho'(1600) - p) = 16.7\pm3.4 \text{ mbarn}$$

Any correction for variation of the photon-vector meson coupling as the vector meson mass changes from 0 to 1.5 GeV would raise this estimate. From the popular model where $\sigma_{TOT} \sim M_V^{-2}$ one would expect $\sigma_{TOT} \sim 6$ mbarn.

3. The reaction $\gamma p \to p\pi^+\pi^-\pi^o\pi^o$

This section reports preliminary results of the WA57 experiment. Events are selected by requiring two or three charged particles with suitable charged balance (where there are three one has to be consistent with being a recoil proton), two π^o-mesons identified by kinematic fitting of $\gamma\gamma$ pairs, and energy balance. The resulting $\pi^+\pi^-\pi^o\pi^o$ mass spectrum, without acceptance correction, is shown in Fig. 3. Two peaks are seen: it is found that the lower peak particularly corresponds to production of the $\omega^o\pi^o$ state and the upper to production of the $\rho^\pm\pi^\mp\pi^o$ state.

The analysis procedure fitted mass spectra, calculated by Monte Carlo methods, to various projections of the data. In the Monte Carlo calculations mass spectra were calculated both without acceptance corrections and with corrections from a preliminary model of the acceptance. As there was no appreciable change of the shapes of the calculated mass spectra on including these acceptance corrections, it was felt that any further change on developing a more precise model would be small and so would not affect the present level of conclusions. Data in 100 MeV bins of 4π mass were fitted by a sequential procedure:

(i) The $\pi^+\pi^-\pi^o$ mass spectra were fitted with an ω^o-meson peak and a smooth background, to determine the $\omega^o\pi^o$ intensity.

(ii) An $\omega^o\pi^o$ background deduced from this intensity was subtracted from the $\pi^\pm\pi^o$ mass spectrum, and the remainder fitted with $A_1\pi \to \rho^\pm\pi^\mp\pi^o$ (using the same A_1 parameters as in the previous section) and 4π phase space. The sum of the results of these fits for $1.4 < M(4\pi) < 1.8$ GeV is shown in Fig.4(a).

(iii) The results of this latter fit were then compared with the observed $\pi^+\pi^-$ mass spectrum, with the $\omega^o\pi^o$ contribution subtracted. The results of this last comparison are shown in Fig.4(b) for $1.4 < M(4\pi) < 1.8$ GeV. The discrepancy there between calculation and data indicates a weak $\rho^o\pi^o\pi^o$ contribution with $\rho^o\pi^o\pi^o/\rho^\pm\rho^\mp\rho^o \sim 0.1$.

This dominance of $\rho^\pm\pi^\mp\pi^o$ points towards an I=1 $\rho\pi$ state, such as could be due to an A_1 final state interaction, as this would produce all $\rho^\pm\pi^\mp\pi^o$ and no $\rho^o\pi^o\pi^o$, to be contrasted with a $\rho\varepsilon$ mechanism which would produce all $\rho^o\pi^o\pi^o$ and no $\rho^\pm\pi^\mp\pi^o$. This result therefore resolves the ambiguity in the $\rho'(1600) \to \pi^+\pi^-\pi^+\pi^-$ work.

Fig.5(a) shows the yield of $\omega^o\pi^o$ deduced by the above analysis as a function of 4π mass, with preliminary acceptance corrections. A strong peak is seen at a mass of 1.25 GeV and a width of $\sim$ 0.3 GeV, together with a tail to higher masses which may indicate an $\omega^o\pi^o$ decay mode of the $\rho'(1600)$. Fig.5(b) similarly shows the yield of $\rho^\pm\pi^\mp\pi^o$, indicating that this is due to the $\rho'(1600)$.

4. A possible I=0 resonance at 1.65 GeV

Peaking has been reported in $e^+e^- \to$ for X = $\pi^+\pi^-\pi^o$[9], $\pi^+\pi^-\pi^+\pi^-\pi^o$[10], K^+K^-[10,11], $K^o_SK^o_L$[10,12], $K^o_SK^\pm\pi^\mp$[10]. Corresponding mass spectra from photon dissociation to the first three of these states are shown in Fig.6. Fig.6(a) shows the $\pi^+\pi^-\pi^+\pi^-\pi^o$ mass spectrum from $\gamma p \to p\pi^+\pi^-\pi^+\pi^-\pi^o$, with a peak which is fitted with M = 1.657±0.009 GeV, Γ = 0.05±0.03 GeV (to be compared with the corresponding e^+e^- results[10] of M = 1.634±0.009 GeV, Γ = 0.09±0.03 GeV) and an intensity which is 3.7σ from zero. Fig.6(b) shows the $\pi^+\pi^-\pi^o$ mass spectrum from the $\gamma p \to p\pi^+\pi^-\pi^o$ reaction, with a peak which is fitted with M = 1.69±0.02 GeV, Γ = 0.13±0.04 GeV (to be compared with the corresponding e^+e^- result[9] of M = 1.652±0.017 GeV, Γ = 0.042±0.017 GeV) and an intensity which is 4σ from zero. These results indicate a resonance with a mass $\sim$ 1.65 GeV and a width in the range 0.05-0.13 GeV.

Fig.6(c) shows the K^+K^- mass spectrum from the reaction $\gamma p \to pK^+K^-$. This is an extension of work already published[13], including further events with only one of the K-mesons identified by the threshold Cerenkov counter. If fitted assuming no interference one finds for the peak M = 1.748±0.011 GeV, Γ = 0.080±0.033 GeV. However it is easy to find a suitable interference with background to fit with a resonance with M = 1.69±0.01 GeV, Γ = 0.10±0.04 GeV. This latter result is consistent with the 5π and 3π peaks, and with the indication from $e^+e^- \to K\bar{K}$[11,12] of

a peak with M ∿ 1.67 GeV, Γ ∿ 0.1 GeV interfering, in a different way, with background.

Comparing the production of these various states in photoproduction and e^+e^- annihilation one finds consistency with them all being decay modes of the same resonance. Assuming diagonal VDM this comparison indicates $\sigma_{TOT}(Xp) \sim 10.5$ mbarn, and $\Gamma(X \to \pi^+\pi^-\pi^0)/\Gamma(X \to \pi^+\pi^-\pi^+\pi^-\pi^0) \sim 4$.

5. Systematic features of photon dissociation to multimeson states

Various other decay modes of the ρ'(1600) have been indicated: $\pi^+\pi^-$[5,6], $\eta^0\pi^+\pi^-$[14].

A candidate for an ω' member of the same nonet is reported[14] in the $\omega^0\pi^+\pi^-$ state. One sees a broad peak at M ∿ 1.7 GeV with an angular distribution consistent with schc production, together with a continuum with a jet-like structure at masses $\gtrsim$ 2 GeV. This combination of mechanisms is similar to what is seen in $\gamma p \to p\rho^0\pi^+\pi^-$. The ratio of photoproduction of this ω' to that of the ρ'(1600), on making reasonable estimates of other decay modes, is ∿ 0.1 which is consistent with the ratio of 1/9 expected for an ideally mixed nonet.

In the reaction $\gamma p \to p\pi^+\pi^-\pi^+\pi^-\pi^+\pi^-$[15] no vector meson peaks are observed in the 6π mass spectrum, but production of a continuum of jet-like structures is observed for masses $\gtrsim$ 2 GeV. Therefore a transition from production of vector meson states to production of a jet-like continuum at masses $\gtrsim$ 2 GeV is a systematic feature of photoproduction of multipion states, as it also probably is of production of multipion states in electron-positron annihilation.

Candidates for a φ' member of the nonet containing the ρ'(1600) include the relatively narrow peak at 1.65 GeV and a broad peak photoproduced in the K*Kπ state[16]. The ratio of photoproduction cross-sections of these two peaks to that for the ρ'(1600) is consistent with either being a suitable candidate for the φ' member of the nonet.

References

1) D. Aston et al., CERN/EP/81-13.
2) G. Smadja et al., Proceedings of 1972 Meson Resonance Conference, p.349.
3) K.M. Watson, Phys. Rev. 88 (1952) 1163.
4) Particle Data Group, Phys. Lett. 75B (1978) 1.
5) M.S. Atiya et al., Phys. Rev. Lett. 43 (1979) 1691.
6) D. Aston et al., Phys. Lett. 92B (1980) 215.
7) C. Bacci et al., Phys. Lett. 95B (1980) 139.
8) G. Penso and T.N. Truong, Phys. Lett. 95B (1980) 143.
9) G. Cosme et al., Nucl. Phys. B152 (1979) 215.
10) J-C. Bizot et al., reported to International Conference on High Energy Physics (Madison, U.S.A., 1980), summarised in review by L. Montanet at that Conference.
11) B. Delcourt et al., Phys. Lett. 99B (1981) 257.
12) F. Mane et al., Phys. Lett. 99B (1981) 261.
13) D. Aston et al., Nucl. Phys. B172 (1980) 1.
14) D. Aston et al., Nucl. Phys. B174 (1980 269.
15) D. Aston et al., Nucl. Phys. B166 (1980) 1.
16) D. Aston et al., Phys. Lett. 92B (1980) 219.

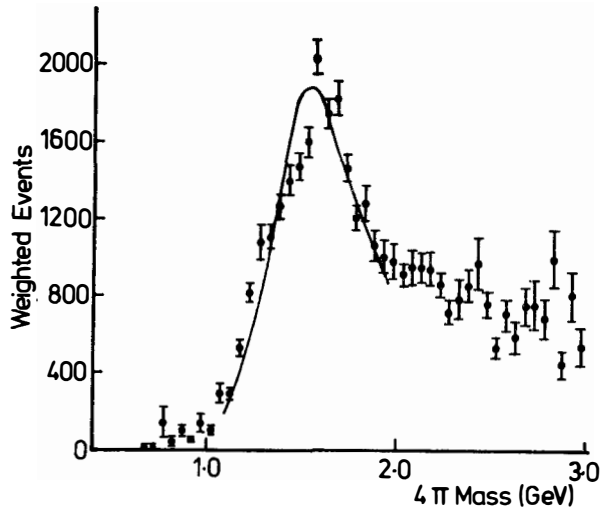

Fig. 1 4π mass spectra from $\gamma p \to p\pi^+\pi^-\pi^+\pi^-$, corrected for acceptance. The curve shows $M^2\sigma(e^+e^- \to \pi^+\pi^-\pi^+\pi^-)$.

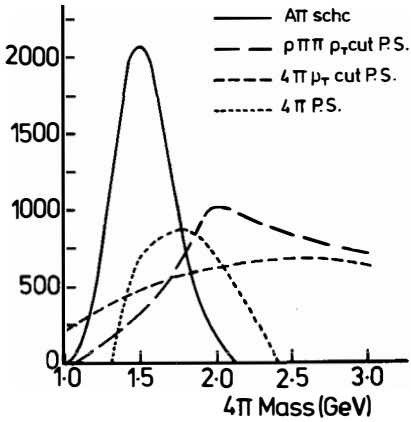

Fig. 2 Results of maximum likelihood fits to $\pi^+\pi^-\pi^+\pi^-$ systems showing contributions of various intensities found as function of 4π mass.

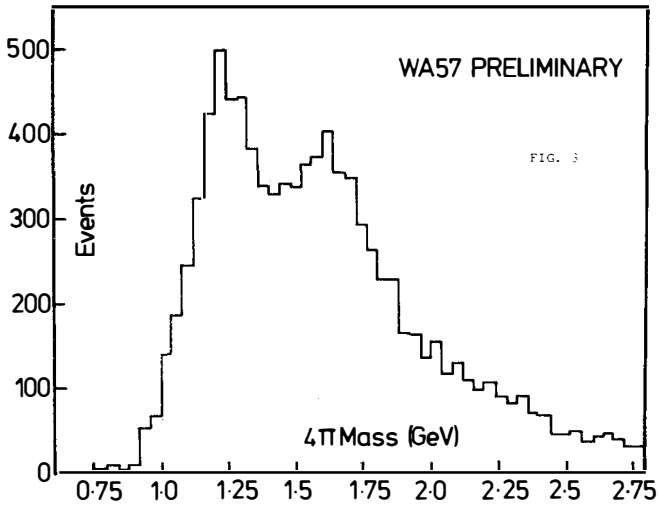

Fig. 3 4π mass spectrum from $\gamma p \to p\pi^+\pi^-\pi^o\pi^o$, not corrected for acceptance.

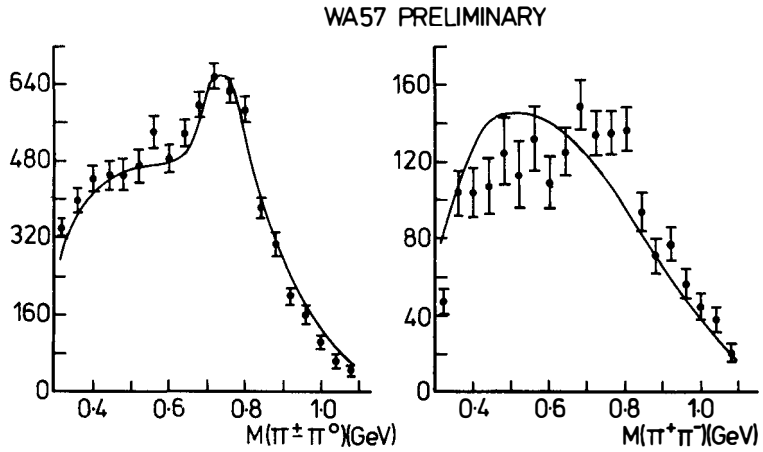

Fig. 4 Measured $\pi\pi$ mass spectra from $\gamma p \to p\pi^+\pi^-\pi^o\pi^o$ for $1.4 < M(4\pi) < 1.8$ GeV, with $\omega^o\pi^o$ contribution subtracted, for (a) $\pi^\pm\pi^o$, (b) $\pi^+\pi^-$. The curves result from a fit to the $\pi^\pm\pi^o$ mass spectrum.

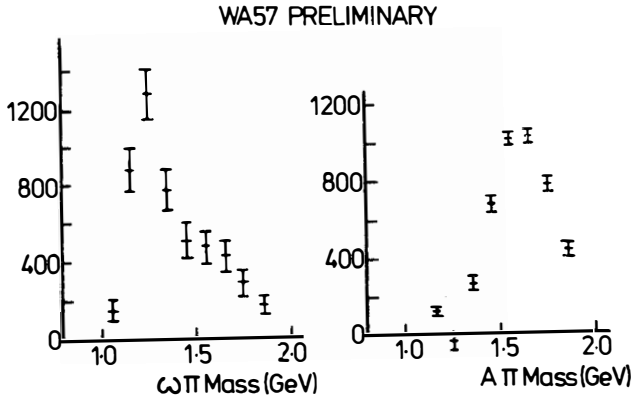

Fig. 5 Yields of (a) $\omega^{o}\pi^{o}$, (b) $A_1^{\pm}\pi^{\mp}$, as a function of 4π mass, found to contribute to $\pi^{+}\pi^{-}\pi^{o}\pi^{o}$ mass spectrum.

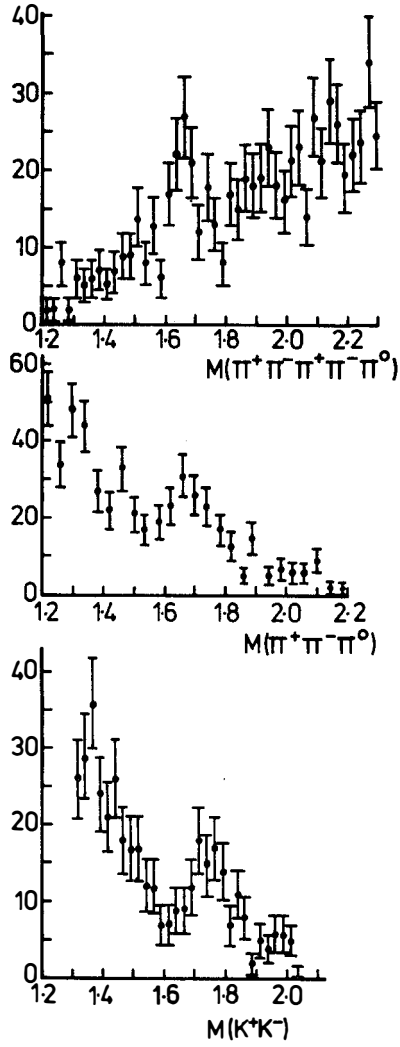

Fig. 6 (a) $\pi^+\pi^-\pi^+\pi^-\pi^o$ mass spectrum from $\gamma p \to p\pi^+\pi^-\pi^+\pi^-\pi^o$
(b) $\pi^+\pi^-\pi^o$ mass spectrum from $\gamma p \to p\pi^+\pi^-\pi^o$
(c) K^+K^- mass spectrum from $\gamma p \to pK^+K^-$.

SOFT QCD : LIGHT QUARK PHYSICS WITH CHROMODYNAMICS

Nathan Isgur
Department of Physics
University of Toronto
Toronto, Canada M5S 1A7

The addition of dynamical ingredients suggested by QCD dramatically improves the ability of quark models to describe soft hadronic phenomena. This approach is discussed in terms of a particularly simple non-relativistic potential model which has been used to study the spectroscopy, decays, and static properties of baryons and mesons. The application of the model to such QCD exotica as multiquark states and glueballs is also mentioned. In addition, an attempt is made to at least partially rationalise the success of the model in terms of more fundamental physics.

I. Introduction to the Model

A. Why Potential Models?

The successes of quarkonium models for the $c\bar{c}$ and $b\bar{b}$ systems, based on a non-relativistic potential model with flavour and spin independent confinement and one gluon exchange, at least raise the question of where, as a function of quark mass, such models become useless. The models I will discuss here are,in response to this question, based on an optimistic extension of the physics expected from QCD for heavy quark systems into the light quark domain. We shall see that the models not only provide a useful framework within which to describe the physics of such systems, but moreover that this extension has, at least at some level, been successful. The reasons for this success are only partly understood; a possible beginning for an interpretation is given below.

While there are many possible variants, I will concentrate on the version of such models that I know best [1,2,3]. It has three main ingredients: confinement, "point-like" constituent quarks, and one gluon exchange.

B. How Do Potentials Confine Colour?

It is non-trivial to construct a potential which will, for example, confine qqq but not qq. One solution[4] is to assume---based on a colour electric flux tube mechanism for confinement---a colour-dependent two body potential between quarks i and j of the form

$$V_{ij}(\vec{r}_{ij}) = -V(r_{ij}) \frac{\vec{\lambda}_i}{2} \cdot \frac{\vec{\lambda}_j}{2} \qquad (1)$$

with $V(r_{ij})$ a flavour and spin independent confining potential and with the prescription that antiquark potentials follow by the replacement $\vec{\lambda} \to \vec{\lambda}^c = (-\vec{\lambda}^*)$. The resulting model allows only colour singlet hadrons to exist[1], but has the property that while the confinement of $q\bar{q}$ and qqq is automatic, the existence of more complicated colour singlet bound states (like $qqq\bar{q}$) becomes a dynamical issue. The model is also very economical in that it relates the physics of baryons, mesons, and multiquark systems; this feature will be discussed below.

C. What Are the Constituent Quarks?

The quarks of the model are not the current quarks of the QCD Lagrangian, but rather a set of "dressed" constituent quarks appropriate to the distance scale of light hadrons. These quarks (which are assumed to be approximately pointlike) have masses which are (in part by their nature and in part because they are at this stage also probably repositories of some of our ignorance about the potential, relativistic corrections, etc.) ill-known, but the values

$$m_u \simeq m_d \simeq 0.33 \text{ GeV} \tag{2}$$

$$m_d - m_u \simeq 6 \text{ MeV} \tag{3}$$

$$m_s \simeq 0.55 \text{ GeV} \tag{4}$$

$$m_c \simeq 1.75 \text{ GeV} \tag{5}$$

etc., are typical. These masses play a crucial role in the model because their differences are the principal origin of flavour symmetry breaking. Note that if we assume that the quarks in a proton are in a Gaussian wave function with the proton's observed charge radius, then with these masses $\frac{p^2}{2m} \simeq 100$ MeV so that these light quark models are probably not hopelessly relativistic.

D. Where Are the Gluons?

The last principal ingredient of the model is one gluon exchange. The most important effects of this type are due to colour hyperfine (magnetic dipole-magnetic dipole) interactions which in lowest order in α_s are given by

$$H_{hyp}^{ij} = A^{ij} \left\{ \frac{8\pi}{3} \vec{S}_i \cdot \vec{S}_j \delta^3(\vec{r}_{ij}) + \frac{1}{r_{ij}^3} \left[\frac{3\vec{S}_i \cdot \vec{r}_{ij} \vec{S}_j \cdot \vec{r}_{ij}}{r_{ij}^2} - \vec{S}_i \cdot \vec{S}_j \right] \right\} \tag{6}$$

where

$$A^{ij} = \begin{cases} \dfrac{2\alpha_s}{3m_i m_j} & \text{in a baryon} \\ \dfrac{4\alpha_s}{3m_i m_j} & \text{in a meson} \end{cases} \tag{7}$$

The first term of H_{hyp}, called the contact term, is, in electromagnetism, responsible for the 21 centimetre line of hydrogen; the second (tensor) term is the usual interaction of a magnetic dipole with a magnetic dipole field. The most important characteristics of H_{hyp} are: 1) it is short range in $\vec{S}_i \cdot \vec{S}_j$, 2) it gives a fixed relation ($\frac{8\pi}{3}$) between the strengths of the contact and tensor terms, 3) it has a strength inversely proportional to the product

of the quark masses, and 4) it violates SU(6) and in particular automatically gives $m_\rho > m_\pi$ and $m_\Delta > m_N$.

One gluon exchange also gives rise to spin-orbit interactions from the interaction of a moving quark colour magnetic moment with colour electric fields. As in the case of electromagnetism, this effect tends to be masked by Thomas precession (the relativistic precession of an accelerated spin), but in this case the suppression of spin-orbit effects is (in the case of $q\bar{q}$ with $m_{\bar{q}} >> m_q$) by a factor of $(1-\frac{1}{2}-f)$ where the "½" and the "f" come from Thomas precession in the Coulomb-like and confinement potentials, respectively. In the light quark hadrons, the quark wave function overlaps very strongly with the confinement region so that f is very large and spin-orbit effects are suppressed[5].

Finally, one gluon exchange gives rise to a variety of spin-independent effects which can normally be absorbed into the unknown confinement potential. Most prominent among these is, of course, the Coulomb-like 1/r potential itself.

II. Baryons First

A. Why Baryons First?

We begin our discussion of the model with the qqq baryon sector even though the $q\bar{q}$ meson sector is simpler to treat theoretically. There are several reasons for doing this; probably the most important of these is that the baryons are much better known experimentally than the corresponding mesons (a consequence of their accessibility as s-channel resonances). Not only are more resonances known, but their masses and widths are better known and there is a wealth of information on their (signed) decay amplitudes. Specifically, the P-wave mesons remain very poorly known (think of the A_1 and the ε), while all seven expected S=0 P-wave baryons are known and have reasonably well measured amplitudes for both electromagnetic and strong channels (typically 5 to 10 amplitudes per resonance). Aside from their being more extensively known, baryons probably have other advantages in practice. For one thing, the quarks in a baryon appear to be somewhat more non-relativistic than those in a meson, making their treatment more reliable. It is also possible that three bodies are sufficient to make the effective potential seen by a quark in a baryon significantly "smoother" than in a meson, thereby making baryons less sensitive to precise knowledge of the potentials. Finally, baryons do not have the isoscalar mixing problem (to be described below) which, while interesting, renders I=0 meson data unreliable for spectroscopic studies and leaves very few

mesons indeed to compare with a potential model.

B. What is the Model for Baryons and Its Solution?

The application of the model to baryons is quite straightforward in its simplest form[6,7]. Building on the pre-QCD analyses[8,9,10] (which were on their own terms already very successful) we take the simple Hamiltonian

$$H = \sum_{i=1}^{3} \left(m_i + \frac{p_i^2}{2m_i} \right) + \sum_{i<j} \left(V^{ij} + H_{hyp}^{ij} \right) \tag{8}$$

and solve it approximately by setting

$$V^{ij} = \frac{1}{2} k r_{ij}^2 + U(r_{ij})$$

and treating H_{hyp} and the anharmonicity U as perturbations. Note that V here contains both the "true" confinement potential and pieces of the one gluon exchange potential (so that U may contain 1/r terms, linear terms, etc.); also note that spin orbit effects have been completely dropped. We have already mentioned that Thomas precession is expected to make spin-orbit effects smaller, but the adequacy of completely neglecting them in baryons is not well understood. Evidence from mesons, where the suppression is more easily studied, does, however, tend to support this approach[5].

The approximate solution of this model Hamiltonian is simple. In the harmonic limit with $m_1 = m_2 \equiv m$ and $m_3 \equiv m'$ (the most general case required for u, d, and s quarks in the approximation $m_u = m_d$),

$$H \to \frac{p_\rho^2}{2m_\rho} + \frac{p_\lambda^2}{2m_\lambda} + \frac{3}{2} k \left(\rho^2 + \lambda^2 \right) \tag{10}$$

where

$$\vec{\rho} = \frac{1}{\sqrt{2}} \left(\vec{r}_1 - \vec{r}_2 \right) \tag{11}$$

$$\vec{\lambda} = \frac{1}{\sqrt{6}} \left(\vec{r}_1 + \vec{r}_2 - 2\vec{r}_3 \right) \tag{12}$$

and

$$m_\rho = m \tag{13}$$

$$m_\lambda = \frac{3mm'}{2m+m'} \tag{14}$$

so that the unperturbed spectra with up to two units of excitation are those of Figure I. One interesting -- and important -- feature is that the solutions of the confinement problem maximally violate SU(6) in excited baryons[6]. For example, the ρ-λ basis $L^P = 2^+$ eigenfunction ρ_+^2 is a 45° mixture of the $[56,2^+]$ wave function $\frac{1}{\sqrt{2}} (\rho_+^2 + \lambda_+^2)$ and the $[70,2^+]$ wave function $\frac{1}{\sqrt{2}} (\rho_+^2 - \lambda_+^2)$

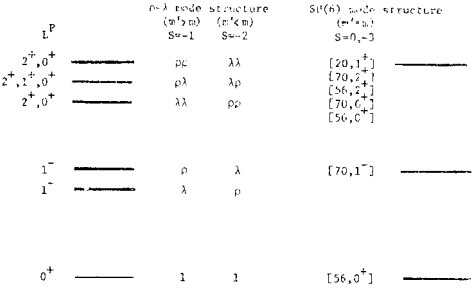

Figure I: the unperturbed solutions to the harmonic confinement problem (with arbitrary scales set to give the same spacing in each sector).

of SU(6). Clearly, to the extent that this phenomenon is important, an SU(6) (or even SU(3)) analysis of excited baryons will fail.

We next take these states and perturb them with the anharmonic term U. It turns out to be unnecessary to actually specify U since one can show that in first order every U gives the same pattern[11], shown in Figure II.

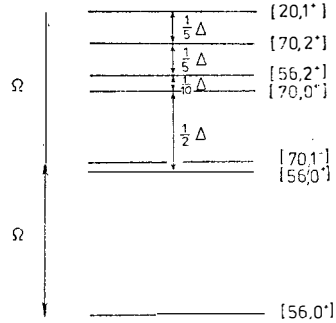

Figure II: the positions of the SU(3)-symmetric supermultiplets under the influence of an arbitrary anharmonic perturbation.

One can therefore take the parameters Ω and Δ of this Figure as describing the potential; the phenomenologically required sign of Δ is, however, consistent with the expected existence of the -1/r anharmonicity. To deal with the case $m_\lambda \neq m_\rho$, the U-perturbed λ excitations are scaled by a factor $(m_\rho/m_\lambda)^{\frac{1}{2}}$ appropriate to the harmonic limit.

The next step in the approximate solution of (8) is to turn on the hyperfine perturbations. These interactions are of crucial importance: they create huge spectroscopic splittings and very strong mixings that destroy almost all vestiges of SU(6) symmetry (except in the ground states).

The final step in the solution is the simplest: one takes the sectors of the Hamiltonian of fixed flavour and J^P and diagonalises the resulting matrices.

C. How Can the Baryon Model Be Compared to Experiment?

There are two crucial elements in the comparison of a model like this with experiment: one is to compare with spectroscopic evidence and the other is to check, via an analysis of decay amplitudes, the predicted internal structure of the eigenstates. The former check is relatively simple; the latter requires the construction of a decay model. We have used for this decay model[12] a slightly generalised form of the single quark emission model[13] that has much in common with more algebraic approaches[14]. It is based on the "elementary" emission processes shown in Figure III.

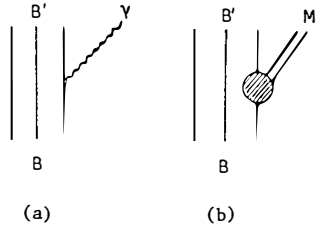

Figure III: (a) photon coupling in the single quark emission model.
(b) meson coupling in the single quark emission model.

As one example of the ways in which a decay analysis can reveal the internal structure of a state, consider the coupling of a uds state with some excitation in the variable ρ to the $\bar{K}N$ channel. As shown in Figure IV, since

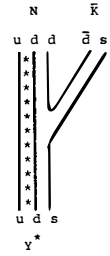

Figure IV: the decoupling of Y^*'s with ρ excitation from the $\bar{N}K$ channel.

the (ud) spectator pair remains excited, it cannot overlap with a nucleonic (ud) pair; the amplitude for this process is therefore zero and the model predicts that such states should not be seen in $\bar{K}N$ partial wave analyses[6].

The full comparison of the baryon model to experiment thus involves comparing not only to an observed spectrum, but also comparing against hundreds of measured decay amplitudes. The flavour of this comparison -- but not its extent -- is reflected in Figures V(a) to V(d) and in Table I.

Figure V(a): the predicted S=0 negative parity baryons compared to experiment; the regions in which the masses of the resonances probably lie are denoted by shaded boxes.

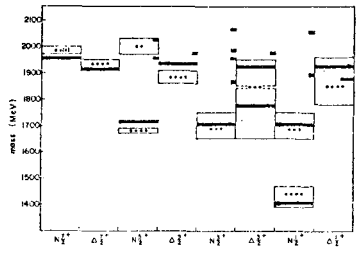

Figure V(b): the predicted S=0 positive parity baryons compared to experiment; states that are predicted to decouple from πN are shown as stubs.

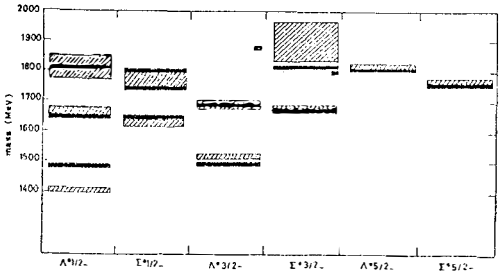

Figure V(c): as in V(a) for the S=-1 negative parity baryons; states that are predicted to decouple from $N\bar{K}$ are shown as stubs.

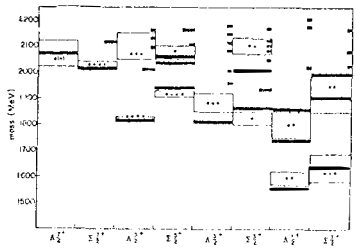

Figure V(d): as in V(b) for S=-1 positive parity baryons; states predicted to decouple from $N\bar{K}$ are shown as stubs.

Table I. The Decay Amplitudes of S11(1535) and S11(1650)

	S11(1535)		S11(1650)	
	theory	experiment	theory	experiment
$N\pi$	5	8±3	9	9±2
$N\eta$	+ 5	+ 9±2	- 2	- 2±1
ΣK	no	no	- 2	± 2±1
ΛK	no	no	- 3	- 4±1
$\Delta\pi$	- 2	(-) 1±1	- 8	- 4±2
γp	+145	+ 80±20	+90	+50±15
γn	-120	-110±35	-35	-45±25

The Figures show a comparison between observed baryons and those predicted to be observable in S=0 and -1 partial wave analyses. (The ground state baryons are not shown since there agreement is to within 10 MeV for all states.) The Table gives the full comparison between predicted and measured decay amplitudes for just two of the observed states. The model is clearly crude and of limited numerical accuracy -- for a few of these hundreds of amplitudes it seems to simply fail -- but it appears nevertheless to have captured the principal features of the physics of baryons.

In particular, the ordering of the multiplets appears to be dominated by a simple anharmonic term, with the ρ-λ splitting effect playing a crucial role in S = -1 and -2 (consider, e.g., the $\Lambda^5/_2^-$ - $\Sigma^5/_2^-$ splitting in the P-waves). Within a given mode, the contact part of the hyperfine interaction produces spin splittings that are comparable to orbital splittings; these forces in turn cause large mixings between SU(6) multiplets like $[56,2^+]$ and $[70,2^+]$. Finally, in certain key places the tensor force produces strong S = 1/2 $\leftrightarrow$ S = 3/2 mixings: the amplitudes of Table I would, for example, be completely wrong were it not for tensor forces.

The net effect of the model is to resolve many old problems with the quark model of baryons. Perhaps the most crucial of these is that the violent SU(6) breaking of the model has the effect, as seen from Figures V, of decoupling large numbers of predicted resonances from s-channel phase shift analyses, thereby resolving the problem of the "missing baryon resonances"[12].

D. What Else Can It Do?

This simple baryon model has also had success in other areas which we will briefly mention:

baryon isomultiplet splittings[15]: After the model succeeds in making the S=0 to S=-1 transition (e.g., uuu $\rightarrow$ uus), it is natural to let it make the transitions through an isospin multiplet (e.g., uuu $\rightarrow$ uud $\rightarrow$ ddu $\rightarrow$ ddd). With $m_d - m_u \simeq 6$ MeV, but no other new parameters, the model gives the isomultiplet splittings of Table II.

Table II. Baryon Isomultiplet Splittings

difference	theory(MeV)	experiment(MeV)
$p - n$	-1.3	-1.3
$\Sigma^+ - \Sigma^o$	-3.3	-3.1 ± 0.1
$\Sigma^- - \Sigma^o$	+4.9	+4.9 ± 0.1
$\Xi^- - \Xi^o$	+6.8	+6.4 ± 0.6
$\Delta^{++} - \Delta^o$	-3.0	-2.6 ± 0.4
$\Delta^{++} - \Delta^-$	-6.9	-5.9 ± 3.1
$\Sigma^{*+} - \Sigma^{*-}$	-5.8	-5.1 ± 0.7
$\Sigma^{*+} - \Sigma^{*o}$	+3.7	+5.4 ± 2.6
$\Xi^{*-} - \Xi^{*o}$	+3.8	+3.2 ± 0.6

configuration mixing in the nucleon[16,17]: The hyperfine interaction also has the effect of distorting the nucleonic wave function: it pushes the two parallel spin quarks toward the periphery and pulls the anti-parallel spin quark into the centre of the nucleon (i.e., it mixes $[70,0^+]$ into the pure $[56,0^+]$ nucleon). This has many observable effects including: a) it gives the neutron a charge radius[16,17], b) it leads to violations of the Moorehouse selection rules[17] $A^p_{3/2}\ (N^{*5}/_2{}^- \to N\gamma) = A^p_{1/2}\ (N^{*5}/_2{}^- \to N\gamma) = 0$, and c) it leads to violations of the Faiman-Plane selection rule[17] $A(\Lambda^5/_2{}^- \to N\bar{K}) = 0$. The predicted effects are in each case in agreement with experiment.

baryon magnetic moments: The constituent quark masses of Section I lead, via their assumed Dirac magnetic moments (compare to equations (6) and (7)), to values for the baryon magnetic moments in good (though not perfect) agreement with the observed values[18].

charmed baryons: The model may easily be extended to the charmed[19] and charmed-strange baryons[20]. The predicted C=1, S=0 ground states seem to be in accord with experiment; there is as yet no information on other sectors. One interesting prediction of the model, however, is that the ρ-λ and $\Sigma_c\,{}^1/_2{}^+ - \Lambda_c\,{}^1/_2{}^+$ splittings will have become sufficiently large to make the lowest-lying orbital excitation $\Lambda_c\,{}^1/_2{}^-$ stable (or nearly stable) against strong decay.

III. Mesons, Too

A. What's New in Mesons?

The mesons have several new features beyond the change from qqq to $q\bar{q}$ constituents. One is that all colour factors in the Hamiltonian change from 2/3 to 4/3 [21]. There are many consequences of this stronger colour coupling: for example, the ρ-π splitting is predicted (and observed) to be about twice the Δ-N splitting. A low pion mass is thus natural in this model and the naive relation $m\,(\text{meson}) \simeq \frac{2}{3}\, m\,(\text{baryon})$ is satisfied by the hyperfine-unperturbed masses: $(\frac{1}{4} m_\pi + \frac{3}{4} m_\rho) \simeq \frac{2}{3} (\frac{1}{2} m_N + \frac{1}{2} m_\Delta)$. Mesons can, in addition to checking meson-baryon connections, play a role all on their own in checking various assumptions of the model. Since the two body problem is easily solved numerically, mesons can provide explicit information on the potential V(r) as well as checks on phenomena like the (near) cancellation of spin-orbit effects via Thomas precession [5]. There is already evidence from the $c\bar{c}$ system for the efficacy of Thomas precession in reducing the strength of the spin-orbit interaction to give the observed $\chi(2^{++}) - \chi(1^{++}) - \chi(0^{++})$ spacings [5]; we shall see below that there may be additional evidence for this mechanism in light mesons.

B. What Is the Model for Mesons and Its Solution?

For mesons we take the same Hamiltonian as for baryons, except that spin-orbit terms are shown explicitly, colour factors are changed, and $q\bar{q}$ annihilation may now occur, so that [22]

$$H = \frac{p_1^2}{2m_1} + \frac{p_2^2}{2m_2} + V^{12} + H_{hyp}^{12} + H_{so}^{12} + H_A \qquad (15)$$

where the potentials are all twice as large as in baryons, where the spin-orbit interaction H_{so}^{12} is given by

$$H_{so}^{12} = H_{so(CM)}^{12} + H_{so(TP)}^{12} \qquad (16)$$

(CM stands for "colour magnetic" and TP for "Thomas precession") where

$$H_{so(CM)}^{12} = \frac{4\alpha_s}{3r^3} \left(\frac{1}{m_1} + \frac{1}{m_2}\right)\left(\frac{\vec{S}_1}{m_1} + \frac{\vec{S}_2}{m_2}\right)\cdot\vec{L}_{12}$$

$$H_{so(TP)}^{12} = -\frac{1}{2r}\frac{dV^{12}}{dr}\left(\frac{\vec{S}_1}{m_1^2} + \frac{\vec{S}_2}{m_2^2}\right)\cdot\vec{L}_{12}$$

and where H_A is the annihilation interaction of Figure VI which must be tacked on to any model of mesons.

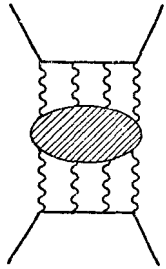

Figure VI: the origin of the annihilation term H_A via gluon intermediate states.

H_A is in principle calculable, but in practice it requires the introduction of a new parameter $A(nJ^{PC})$ for each meson multiplet. This amplitude causes mixing between the $u\bar{u}$, $d\bar{d}$, and $s\bar{s}$ sectors so that after $H\text{-}H_A$ is used to calculate the masses of the excitations with quantum numbers nJ^{PC} in these sectors, H^A creates a mixing matrix of the form (we neglect SU(3) breaking and radial excitations here for simplicity)

$$M(nJ^{PC}) = \begin{vmatrix} m(u\bar{u})+A & A & A \\ A & m(d\bar{d})+A & A \\ A & A & m(s\bar{s})+A \end{vmatrix} \qquad (19)$$

On diagonalisation this matrix gives one eigenvalue (assuming also $m_u = m_d$ for simplicity) $m_{I=1,I_3=0} = m_{u\bar{u}} = m_{d\bar{d}} = m_{u\bar{d}} = m_{d\bar{u}}$ and two I=0 eigenvectors and eigenvalues that depend on A. Phenomenologically, $A(nJ^{PC})$ is normally small (corresponding to nearly "ideal" mixing to $\frac{1}{\sqrt{2}}(u\bar{u} + d\bar{d})$ and $s\bar{s}$, and leading to a nonet with one isoscalar mass just above (below) $m_{I=1}$ if $\theta(nJ^{PC})$ is just below (above) $\theta_{ideal} \simeq 35^o$), though in the pseudoscalar nonet A is very large and leads to nearly "perfect" mixing[23] to the states

$$\eta\ (\eta') = \frac{1}{\sqrt{2}}\left[\frac{1}{\sqrt{2}}(u\bar{u} + d\bar{d}) \mp s\bar{s}\right] \qquad (20)$$

and to $\theta_P \simeq 35^o - 45^o \simeq -10^o$. While this understanding of I=0 mesons is at least partially satisfactory, it makes I=0 mesons much less useful for spectroscopic analyses and makes it clear that it is necessary to focus on the limited number of established I=1 and $^1/_2$ states.

The exact solutions of the meson problem (for I≠0) are most readily

obtained by numerical integration in a given (J,L,S) sector of the Hamiltonian; tensor mixing (e.g., between $^3D_1$ and $^3S_1$) and spin orbit mixing for $m_1 \neq m_2$ can then be treated perturbatively in a (rapidly converging) nearby neighbour mixing expansion. A candidate fit to the I=1 spectrum is shown in Figure VII;

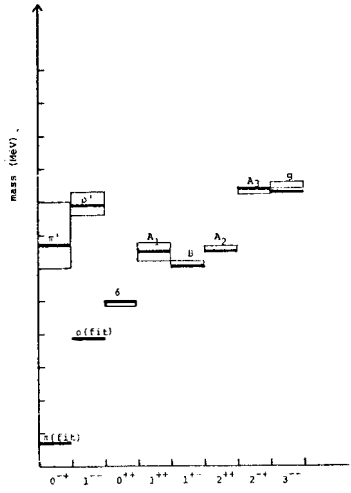

Figure VII: a fit to the I=1 meson spectrum (preliminary).

work is in progress [25] on this problem and our final solution (which may look very different from this early one!) will be reported once we have completed a decay analysis of mesons along the lines of the baryon analysis reported above.

C. What Else Can It Do?

As with the baryon model, the meson model has had success in other areas:

transition magnetic moments: The constituent masses and model wave functions lead (with a simple ansatz for dealing with relativistic ambiguities) to meson magnetic dipole decay rates in quite good (though not perfect) agreement with experiment[26].

annihilation decays: Decays like $\pi \to \mu\bar{\nu}$, $\rho \to e^+e^-$, and $\pi^o \to \gamma\gamma$ proceed through $q\bar{q}$ annihilation and so are sensitive to $\psi(0)$, the $q\bar{q}$ wave function at zero relative coordinate. These processes (once again with a simple ansatz for dealing with relativistic ambiguities) are in reasonable accord with experiment.

charmed mesons: The dominant physical effects in light mesons remain apparent in charmed mesons. For example, the splittings ρ-π, K^*-K, and D^*-D are in roughly the ratios 1 : m_d/m_s : m_d/m_c as expected from (7).

isospin violation: As with the baryons, the model can be applied to the breaking of isospin symmetry[15]. In addition to ordering the observed isomultiplet mass differences, the model predicts dramatic violations of isospin symmetry in certain hadronic decays[27].

IV. Comments on QCD Exotica

A. Do Multiquark States Exist?

It is absolutely certain that multiquark states exist: consider the deuteron, or to be more extreme, a uranium nucleus. This comment is not made flippantly: in potential models there is an analogy between possible "novel" multiquark states and nuclei.

In the bag model the existence of multiquark states[28] is in some sense automatic: the static bag model has stationary states corresponding to any colour singlet combination of quarks and antiquarks. In this approach the "existence" of multiquark states is certain but their widths (and hence observabilities) are determined by the (presently uncalculable) rate at which the bag undergoes fission into a "fall apart mode" (e.g., $\epsilon \to q\bar{q} + q\bar{q}$). Since the bag model was designed to confine, and in view of this problem, it would be prudent (perhaps I should say it would have been prudent) to be wary of drawing the conclusion from the bag model that novel multiquark states (baryonia, five quark baryons, etc.) exist[29], at least without support from other models.

In the potential models the existence of multiquark states is an intrinsically dynamical question[30]. To examine the question one must, to take the simplest example of $qqq\bar{q}$, set up a Schrodinger equation for the four body problem and seek states which exhibit binding in all three relative coordinates. Such states, if they exist, will necessarily be below threshold for falling apart into two $q\bar{q}$ mesons (just as the deuteron is below NN threshold). It is actually straightforward to show that the possible colour and spin recouplings of two pseudoscalar mesons do lead to an attractive potential in certain channels (the cryptoexotic[28] channels); calculations we have just completed[31] in fact have now proved that this effect can lead to a fully bound $qqq\bar{q}$ system under certain conditions. This may well be the reason why the $S^*(980)$ and $\delta(980)$ -- two prime candidates[28] for $ss\bar{d}\bar{d}$ cryptoexotics --

are found just below $K\bar{K}$ threshold[32]. It is also clear that, as with the deuteron, the binding may be SU(3) asymmetric so that there needn't be a full nonet of such cryptoexotic bound states. We hope to report more fully on these investigations shortly, including a report on the quark mass dependence of the effect important for the question of the possible existence of stable charm-strange exotics just below $D\bar{K}$ threshold[30,32].

These questions are, as already stressed, closely related to the problem of the nucleon-nucleon force and preliminary results of an investigation of this old problem along rather new lines look promising[33].

B. Do Glueballs Exist?

As with multiquark states, the existence of glueballs is automatic in the bag[34], and so might be regarded once again with caution. On the other hand, the constituent quark model offers little guidance in this case (apart from suggesting the idea of a massive constituent gluon model[35] with the corresponding sorts of colour dependent potentials) and I can only offer some comments here on possible alternatives.

One alternative to the (basically reasonable!) bag model picture is that glueballs exist but with widths that are very large so that the entire glueball spectrum is smeared into a continuum. A less drastic (but related) possibility is that the low-lying glueballs (assuming that they have non-exotic quantum numbers) have mixed with ordinary $q\bar{q}$ mesons and thereby become "diluted" in the spectrum. We certainly believe (see Section III B and Figure VI) that ordinary $q\bar{q}$ states with I=0 do have a glue component and it is possible that at least the low-lying glueballs can only be disentangled from $q\bar{q}$ spectroscopy once this experimentally difficult subject is itself more clearly resolved[36].

V. Conclusions

A. Why Does It Work At All?[37]

Despite the optimism of Section IA, it is surprising that the non-relativistic potential models work so well. Their phenomenological successes certainly lead one to try to understand the relation of such models to the quark model in its other guises: relativistic quark models like the bag, the quark-parton model, and current quarks.

We have recently examined -- in a very rudimentary exercise which we believe is still revealing -- the question of "relativisation" of the non-relativistic quark model[38]. We took the similarity of the bag model ground

state phenomenology with that of the potential models as a clue that relativistic effects are, for the most part at least, absorbed into the parameters of non-relativistic descriptions, and that as relativistic effects are added to the model, they can mostly be eliminated by a process of "renormalisation" of masses, couplings, etc. (e.g., in the bag the non-relativistic result $\mu_p = \frac{e}{2m}$ becomes $\mu_p \sim \frac{e}{2E}$). To test this idea we took some typical momentum space wave functions for mesons and baryons (which are, as previously mentioned, actually rather relativistic) and calculated various properties (static and transition magnetic moments, G_A/G_V, annihilation amplitudes like f_π, f_ρ, f_{A_1}, etc.) using full Dirac matrix elements instead of the usual static (i.e., non-relativistic) approximations. We found, as hoped, that most of the results of the non-relativistic quark model are practically unchanged with a modest renormalisation of its parameters. The few significant changes that did occur were, in fact, welcome: e.g. , G_A/G_V moved from its naive value of 5/3 to nearly its observed value of 1.25, and f_{A_1}, (the amplitude for the transition $A_1^{\pm} \leftrightarrow W^{\pm}$ via the axial current operative in, e.g., $\tau \to A_1 \nu_\tau$) changed from its naive value of zero to near the current algebra prediction.

The consistency between the constituent quark model and current algebra, exemplified by the cases of G_A/G_V and f_{A_1} just mentioned, leads one to suspect that the massive constituent quark model may be a basis, appropriate for discussing soft phenomena, which is actually equivalent to the current quark picture. The mechanism of this equivalence might be that

a) confinement occurs at $r \sim \Lambda^{-1}$ (where Λ is the QCD scale parameter),

b) α_s at this scale is (by definition) very large, $\alpha_s \sim 1$,

c) $m_{eff} \sim \Lambda$ at this scale (via confinement and/or the dressing of the quarks[37]), and

d) residual interactions of strength $\frac{\alpha_s}{r} \sim \Lambda$ occur.

The net effect is to "conspire" to make $m_\pi^2 \simeq 0$, etc., so that the picture is physically equivalent to the current algebra approach. Of course one picture or the other may certainly be more convenient for discussing particular phenomena: e.g., one would use constituent quarks to discuss baryons, and current quarks for discussing the effects of chiral symmetry.

Such speculations aside, I believe it is now abundantly clear that one reason that the non-relativistic models work is that they provide a simple, calculable framework on which it is possible to hang the dominant physics of the quark model. Most all of the successes of the picture correspond to using

this framework to describe simple physical effects like the repulsion of parallel spins, the smaller chromomagnetic interactions of heavier quarks, and the slower frequencies of heavy quark excitations.

B. What Have We Learned and What Are Some Outstanding Problems?

As just stated, it seems clear that the models, while crude, reflect the dominant physics of the qqq and $q\bar{q}$ states. In particular, we have learned from studying these systems that a) quark colour hyperfine interactions with the expected properties probably exist, b) the confinement potential indeed seems to be flavour independent, c) flavour symmetries are broken (apart from small electroweak contributions) by quark masses, and d) colour factors relate mesons and baryons.

There are, of course, many outstanding questions. The multiquark and glueball sectors remain largely unresolved (including the nucleon-nucleon problem). The many "missing" baryon and meson resonances need to be found by looking at processes where they do not decouple. Finally, but by no means exhaustively, much theoretical work needs to be done on the foundations of the models, and especially on the elucidation of the relations between partons, current quarks, and constituent quarks.

In spite of these outstanding problems, I would conclude that QCD ingredients have dramatically improved the ability of quark models to describe soft phenomena.

Acknowledgements

The work reported here was almost all done in collaboration with others, especially Gabriel Karl, and including Kuang-Ta Chao, Les Copley, Stephen Godfrey, Cameron Hayne, Roman Koniuk, H.J. Lipkin, Kim Maltman, Hector Rubinstein, D.W.L. Sprung, Adam Schwimmer, and John Weinstein.

References

1. For a review, see my lectures at Erice in 1978, in "The New Aspects of Subnuclear Physics", edited by A. Zichichi, Proceedings of the XVI International School of Subnuclear Physics, Erice, 1978 (Plenum, New York, 1980), p. 107. See also refs. (2). This general approach to soft hadron physics flowed from the seminal papers of refs. (3).
2. Gabriel Karl, in Proceedings of the XIX International Conference on High Energy Physics, Tokyo, 1978, edited by S. Homma, M. Kawaguchi, and H. Miyazawa (Phys. Soc. of Japan, Tokyo, 1979), p. 135; O.W. Greenberg, Ann. Rev. of Nucl. and Part. Phys. 28, 327(1978); A.J.G. Hey in Proceedings of the 1979 EPS Conference on High Energy Physics, Geneva, and in Proceedings of Baryon 1980, Toronto, 1980, edited by Nathan Isgur (University of Toronto, 1981), p. 223; Jonathan Rosner, in Proceedings of the Advanced Studies Institute on Techniques and Concepts of High Energy Physics, Virgin Islands, July, 1980; Nathan Isgur, in Proceedings of the XX International Conference on High Energy Physics, Madison, 1980, edited by Loyal Durand and Lee Pondrom (AIP, New York, 1981), p. 30.
3. A. de Rujula, H. Georgi, and S.L. Glashow, Phys. Rev. D12, 147(1975); T. deGrand, R.L. Jaffe, K. Johnson, and J. Kiskis, Phys. Rev. D12, 2060(1975).
4. This solution is very similar to some pre-confinement models considered by Y. Nambu in "Preludes in Theoretical Physics", edited by A. de Shalit, H. Feshbach, and L. van Hove (North Holland, Amsterdam, 1966) and H.J. Lipkin, Phys. Lett. B45, 267(1973). The dynamical basis for the restriction to colour singlets is, however, very different: see ref. (1).
5. See the discussion of this point by Howard J. Schnitzer, in these Proceedings, and the references therein. See also A.B. Henriques, B.H. Kellet, and R.G. Moorhouse , Phys. Lett. 64B, 85(1976); H.J. Schnitzer, Phys. Lett. 65B, 239(1976); 69B, 477(1977); Phys. Rev. D18, 3483(1978); Lai-Him Chan, Phys. Lett. 71B, 422(1977); L.J. Reinders in Proceedings of Baryon 1980, Toronto, 1980, edited by Nathan Isgur (University of Toronto, 1981), p. 203; F.E. Close and R.H. Dalitz in a paper presented to the Workshop on Low and Intermediate Energy Kaon-Nucleon Physics, University of Rome, 1980.
6. Nathan Isgur and Gabriel Karl, Phys. Lett. 72B, 109(1977); 74B, 353(1978); Phys. Rev. D18, 4187(1978); D19, 2653(1979) and D23, 817(E)(1981); D20, 1191 (1979). For related work on baryons, see as examples refs. (7).
7. D. Gromes and I.O. Stamatescu, Nucl. Phys. B112, 213(1976); W. Celmaster, Phys. Rev. D15, 1391(1977); D. Gromes, Nucl. Phys. B130, 18(1977); L.J. Reinders, J. of Phys. G4, 1241(1978).
8. O.W. Greenberg, Phys. Rev. Lett. 13, 598(1964); O.W. Greenberg and M. Resnikoff, Phys. Rev. 163, 1844(1967); D.R. Divgi and O.W. Greenberg, Phys. Rev. 175, 2024(1968); H. Resnikoff, Phys. Rev. D8, 199(1971).
9. R.H. Dalitz, in "High Energy Physics", edited by C. deWitt and M. Jacob (Gordon and Breach, New York, 1966); R.R. Horgan and R.H. Dalitz, Nucl. Phys. B66, 135(1973); R.R. Horgan, Nucl. Phys. B71, 514(1974).
10. G. Morpurgo, Physics 2, 95(1965), reprinted in J.J.J. Kokkedee, "The Quark Model", W.A. Benjamin, New York, 1969 .
11. A general derivation of this rule was given in refs. (1) and (6), but its origin was not understood. Recently K.C. Bowler, P.J. Corri, A.J.G. Hey and P.D. Jarvis, Phys. Rev. Lett. 45, 97(1980), have shown that the rule follows from the Sp(12,R) spectrum generating algebra of the three body oscillator problem and have extended its application to higher excitations.
12. Roman Koniuk and Nathan Isgur, Phys. Rev. Lett. 44, 845(1980); Phys. Rev. D21, 1868(1980) and D23, 818(E)(1981); Roman Koniuk in Proceedings of Baryon 1980, Toronto, 1980, edited by Nathan Isgur (University of Toronto, 1981), p. 217.
13. C. Becchi and G. Morgurgo, Phys. Rev. 149, 1284(1966); 140B, 687(1965); Phys. Lett. 17, 352(1965); A.N. Mitra and M. Ross, Phys. Rev. 158,1630(1967); D. Faiman and A.W. Hendry, ibid. 173,1720(1968); H.J. Lipkin, Phys. Rep. 8C,

173(1973); J.L. Rosner, ibid. 11C, 189(1974); R. Horgan, in Proceedings of the Topical Conference on Baryon Resonances, Oxford, 1976, edited by R.T. Ross and D.H. Saxon (Rutherford Lab., Chilton, Didcot, England, 1976); A. Le Yaouanc et al., Phys. Rev. D11, 1272(1975); L.A. Copley, Gabriel Karl and E. Obryk, Phys. Lett. 29B, 117(1969); L.A. Copley, G. Karl, and E. Obryk, Nucl. Phys. B13, 303(1969); D. Faiman and A.W. Hendry, Phys. Rev. 180, 1572(1969); Kohichi Ohta, Phys. Rev. Lett. 43, 1201(1979); R.G. Moorhouse, Phys. Rev. Lett. 16, 771(1966); R.P. Feynman, M. Kislinger, and F. Ravndal, Phys. Rev. D3, 2706(1971); R.G. Moorhouse and N.H. Parsons, Nucl. Phys. B62, 109(1973).
14. H.J. Lipkin and S. Meshkov, Phys. Rev. Lett 14, 670(1965); D. Faiman and A.W. Hendry, Phys. Rev. 173, 1720(1968); 180, 1609(1969); E.W. Colglazier and J.L. Rosner, Nucl. Phys. B27, 349(1971); W. Petersen and J. Rosner, Phys. Rev. D6, 820(1972); A.J.G. Hey, P.J. Litchfield, and R.J. Cashmore, Nucl. Phys. B95, 516(1975); F. Gilman and I. Karliner, Phys. Rev. d10, 2194(1974); J. Babcock and J. Rosner, Ann. Phys. (N.Y.) 96, 191(1976); J. Babcock et al., Nucl. Phys. B126, 87(1977); D. Faiman and D.E. Plane, Nucl. Phys. B50, 379(1972).
15. Nathan Isgur, Phys. Rev. D21, 779(1980), and D23, 817(E)(1981).
16. R. Carlitz, S.D. Ellis, and R. Savit, Phys. Lett. 64B, 85(1976); Nathan Isgur, Acta. Phys. Pol. B8, 1081(1977); Nathan Isgur, Gabriel Karl, and D.W.L. Sprung, Phys. Rev. D23, 163(1981).
17. Nathan Isgur, Gabriel Karl, and Roman Koniuk, Phys. Rev. Lett. 41, 1269 (1978) and 45, 1738(E)(1980).
18. This issue dates back to M.A.B. Beg, B.W. Lee, and A. Pais, Phys. Rev. Lett. 13, 514(1964); O.W. Greenberg, Phys. Rev. Lett. 13, 598(1964); H.R. Rubinstein, F. Sheck, and R.H. Socolow, Phys. Rev. 154, 1608(1967); Jerrold Franklin, ibid. 172, 1807(1968). The more modern literature can be traced from Nathan Isgur and Gabriel Karl, Phys. Rev. D21, 3175(1980).
19. L.A. Copley, Nathan Isgur, and Gabriel Karl, Phys. Rev. D20, 768(1979) and D23, 817(E)(1981).
20. Kim Maltman and Nathan Isgur, Phys. Rev. D22, 1701(1980).
21. The consequences of this effect have been widely discussed, but see in addition to ref. (1) especially H.J. Lipkin, Phys. Lett. 74B, 399(1978) and I. Cohen and H.J. Lipkin, Phys. Lett. 93B, 56(1980).
22. For related work on mesons see H.J. Schnitzer, Phys. Lett. 65B, 239(1976); 69B, 477(1977); Phys. Rev. D18, 3482(1978); R.H. Graham and P.J. O'Donnell, ibid. 19, 284(1979); B.R. Martin and L.J. Reinders, Nucl. Phys. B143, 309(1978); Phys. Lett. 78B, 144(1978); A.B. Henriques, B. Kellet, and R.G. Moorhouse; Phys. Lett. 64B, 85(1976); L.-Him Chan, Phys. Lett. 71B, 422(1977); R. Barbieri et al., Nucl. Phys. B105, 125(1976); E. Eichten et al., Phys. Rev. D17, 3090(1978); M. Krammer and M. Krasemann, DESY Report No. 79/20, 1979; L.J. Reinders, University College London report, 1979; I. Cohen and H.J. Lipkin, Nucl. Phys. B112, 213(1976); J. Arafune, M. Fukugita, and Y. Oyanagi, Phys. Rev. D16, 772(1977); A. Bradley and F.D. Gault, Durham/Manchester report, 1978; A. Bradley and D. Robson, Manchester report 1979; D.P. Stanley and D. Robson, Phys. Rev. D21, 3180(1980).
23. Nathan Isgur, Phys. Rev. D12, 3770(1975); D13, 122(1976).
24. I. Cohen and H.J. Lipkin, Nucl. Phys. B151, 16(1979) go beyond reference (23) to consider radial mixing and SU(3) breaking. See also in this regard P.J. O'Donnell and R.H. Graham, Phys. Rev. D19, 284(1979).
25. Stephen Godfrey and Nathan Isgur, work in progress.
26. See the review by P.J. O'Donnell in these Proceedings. For a narrower (and more naive) view see Nathan Isgur, Phys. Rev. Lett. 36, 1262(1976).
27. Nathan Isgur, H.R. Rubinstein, A. Schwimmer, and H.J. Lipkin, Phys. Lett. 89B, 79(1979).
28. The bag model discussion of multiquark states, and in particular the discussion of the qqqq sector stems from the work of R.L. Jaffe, Phys. Rev. D15, 267(1977). It is Jaffe who pointed out that the colour hyperfine interactions favour certain qqqq systems which he dubbed cryptoexotic since they had normal qq quantum numbers. See also the talk by J.M. Richard in these Proceedings.

29. The nature of the $qq\bar{q}\bar{q}$ bag states in view of their being unbound against bag fission has been considerably clarified recently by the introduction of a P-matrix analysis of the bag model predictions. See R.L. Jaffe and F.E. Low, Phys. Rev. D19, 2105(1979).
30. For discussion of these dynamics see H.J. Lipkin, Phys. Lett. 74B, 399 (1978) and H.J. Lipkin in "The Whys of Subnuclear Physics", edited by A. Zichichi, Proceedings of the 1977 International School of Subnuclear Physics, Erice, Italy, 1977 (Plenum, New York), p. 11.
31. John Weinstein and Nathan Isgur, in preparation.
32. Nathan Isgur and H.J. Lipkin, Phys. Lett. 99B, 151(1981).
33. Kim Maltman and Nathan Isgur, work in progress.
34. R.L. Jaffe and K. Johnson, Phys. Lett. 34, 1645(1976).
35. See the talk by Ted Barnes in these Proceedings, and also D. Robson, Nucl. Phys. B130, 328(1977); J.J. Coyne, P.M. Fishbane, and S. Meshkov, Phys. Lett. 91B, 259(1980).
36. For a recent look at such a possibility, see Jonathan L. Rosner, "Tests for Gluonium or Other Non-qq Admixtures in the f(1270)", Minnesota preprint, February 1981.
37. For a discussion of these issues see H.J. Lipkin's summary talk in the Proceedings of Baryon 1980, Toronto, 1980, edited by Nathan Isgur (University of Toronto, 1981), p. 461; see also I. Cohen and H.J. Lipkin, Phys. Lett. 93B, 56(1980), and references therein.
38. Cameron Hayne and Nathan Isgur, "Beyond the Wave Function at the Origin: Some Momentum Dependent Effects in the Non-Relativistic Quark Model", University of Toronto report, March 1981.

QCD - HEAVY QUARK BOUND STATES

C. Michael
Department of Applied Mathematics and Theoretical Physics,
University of Liverpool, P.O. Box 147, Liverpool L69 3BX, U.K.

Abstract

The theoretical understanding of heavy quark bound states is reviewed. After an introduction to the non relativistic potential approach, a discussion is presented of relativistic corrections, of higher order QCD corrections and of models for confinement.

INTRODUCTION

The non relativistic quark model of hadrons has a long history and has been relatively successful in correlating information on hadron spectroscopy. It has always been unclear why such a model should be appropriate for light quarks because relativistic and field theoretic effects should be important. As soon as heavy quarks (charm and higher mass flavours are implied by this) were discovered, it was clear that a potential model approach would be more justified in that case since the quark velocities would be much lower. Moreover the asymptotic freedom property of QCD suggested that a bound state of small radius would have a small effective coupling so that field theoretic effects (particle creation, etc) would be suppressed. It appeared that the hadron bound state problem in QCD would be fairly straightforward to solve for heavy quark bound states, and that they would provide the "hydrogen atom" of QCD.

NON-RELATIVISTIC POTENTIAL MODELS

The simplest approach to heavy quark bound states would be to consider one gluon exchange only, in analogy with positronium states bound by one photon exchange. Then the potential would be coulombic with a strength related to α_s, the QCD running coupling; $V(r) = -4\alpha_s/3r$. With a quark mass m_Q, this potential then yields a Bohr radius $a \sim 1/\alpha_s m_Q$, a binding energy $\Delta E \sim \alpha_s^2 m_Q$ and a mean velocity $v \sim \alpha_s c$. Now as $m_Q \to \infty$, $a \to 0$ and hence the distance scale at which α_s is to be evaluated becomes smaller and smaller. Indeed $\alpha_s \to 1/\ln m_Q$ from the naive running coupling expression, and this logarithmic dependence of α_s does not affect the argument that $a \to 0$ as $m_Q \to \infty$. Also $v/c \to 0$ as $m_Q \to \infty$ since $\alpha_s \to 0$. Thus one has a self consistent non relativistic (since $v/c \to 0$) quantum mechanical (since $\alpha_s \to 0$) description as $m_Q \to \infty$: Coulomb bound states. Note that this applies to bound states of a heavy quark and a heavy antiquark, not to systems such as the D or F meson.

This line of reasoning is incomplete since short distance (due to small Bohr radius) does not necessarily imply a short time interval. One could imagine a gluon being absorbed by the bound state at one time and then being re-emitted at a much later time - a long time correlation. The suppression of such correlations follows[1] because the intermediate bound state would be coloured (octet in the example) and coloured states have much higher energy (of order α_s/a) which reduces their contribution. Effectively they live only for a time of order a/α_s which is short in the limit $m_Q \to \infty$.

In practice, a purely coulombic non relativistic bound state will only

apply if ln m_Q is large. Thus the one gluon exchange approximation is inadequate for quark masses of order 1 to 50 GeV and modifications will be needed to the potential, mainly at larger distances r. Conventional phenomenological analyses use a potential of the form

$$V(r) = \frac{A}{r} + Br$$

where the Br term is motivated as due to confinement. The explicit form chosen for V(r) is, however, only relevant for those values of r which are probed by the wave functions considered - smaller r values for heavier quark bound states.

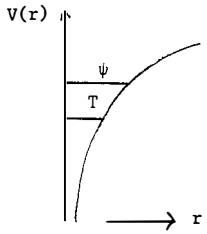

This phenomenology has been widely reviewed[2] and the salient point is that a single potential V(r) can give a satisfactory description of the spectrum of spin triplet charmonium bound states (ψ, centre of gravity of χ states, ψ') and of upsilon states (T, T', T'', T'''). This is a qualitative test of QCD: a flavour independent force between quarks.

Although it is a rough guide, many detailed features are incorrect in this phenomenological picture. In particular, decay widths for electromagnetic transitions (e.g. $\psi \to e^+e^-$, $\psi' \to e^+e^-$, $\psi' \to \chi\gamma$) are found to be a factor of 2 - 3 larger than experiment. Possible explanations are

(i) relativistic effects - since $v^2/c^2 \sim 0.2$ for the ψ meson (though only ~ 0.1 for T)

(ii) $O(\alpha_s)$ QCD corrections since $\alpha_s \sim 0.2$ to 0.4 for charmonium

(iii) a more accurate treatment of the confinement mechanism that is appropriate for larger r.

Let us look at each of these topics in turn.

RELATIVISTIC CORRECTIONS

The standard relativistic bound state treatment is provided by the Bethe-Salpeter equation. This essentially involves a complete solution of the underlying field theory. For QED, where a perturbative expansion is available, this provides the standard treatment for systems such as positronium[3]. For QCD, however, one does not have a systematic means of calculating the relevant Green functions and kernels. Rather, one would be satisfied by a relativistic description in which a phenomenological element (playing the rôle of a

potential) was available and in which spectra and decays could be evaluated. Such a description is provided by the light plane formalism[4].

At its simplest, the light plane formalism involves a wave function which is normalized like a non-relativistic wave function and which satisfies an equation of the form of the Schroedinger equation. In calculating spectra, the only difference from a non-relativistic approach is that the binding energy is to be interpreted as $(M^2 - 4m_Q^2)/4m_Q$ rather than as $M - 2m_Q$. This makes little difference for charmonium or upsilon states. The major change, however, is in the expression for evaluating decays. Here relativistic effects are exactly included. For example for $\psi \to e^+e^-$ (or $\psi' \to e^+e^-$) the decay rate is given (in terms of the conventional non-relativistic expression Γ_{NR}) by

$$\frac{\Gamma_R}{\Gamma_{NR}} = \left| \frac{\int p^2 dp \quad \psi(p) \left\{ \frac{2}{3} \left(1 + \frac{p^2}{m^2}\right)^{-3/2} + \frac{1}{3} \left(1 + \frac{p^2}{m^2}\right)^{-5/2} \right\}}{\int p^2 dp \quad \psi(p)} \right|$$

This yields a suppression of ~ 0.6 for ψ and ~ 0.4 for ψ'. These factors are in the direction required since the non-relativistic theory gave a result 2-3 times too large. Similar explicit expressions have been worked out for other onia decays[4]. There is a qualitative argument for the sign of the relativistic suppression: the non relativistic results involve the wave function at the origin whereas, in a relativistic field theory, decays can occur from a region of size $\sim 1/m_Q$ and, since the wave function in configuration space decreases away from the origin, this will reduce the net result.

Even though annihilation decays ($c\bar{c} \to \gamma$, 2γ, etc) are substantially reduced in this relativistic treatment, the expression for radiative decays ($\psi' \to \chi\gamma$, etc) is little changed. In the case of $\psi' \to \chi\gamma$, however, the non-relativistic result involves a partial cancellation between components of the wave function at small and large distances. Hence the result is rather sensitive to minor changes of the wave function nodes. Thus relativistic effects which modify the wave function would have a relatively pronounced effect[5].

Although the light plane formalism has been presented as a phenomenological approach, it is directly derived from field theory[4]. When calculational techniques exist to evaluate non-perturbative expressions in QCD, then the "potential" in this approach can be evaluated directly and the normalization can be corrected explicitly for components such as ($c\bar{c}$ + glue) in the wave function.

I would recommend that potential theory practitioners who wish to retain the Schroedinger equation nevertheless can still obtain relativistic results if

they supplement this with the decay formulae given in the light plane formalism.

QCD CORRECTIONS OF $O(\alpha_s)$

In a fully relativistic field theory treatment, this topic would be incorporated with the previous one. It is possible to look at field theoretic effects within a non relativistic treatment of the bound state. Thus the non relativistic wave function at the origin (or its derivative as appropriate) is combined with the amplitude for $c\bar{c} \to$ final state at threshold evaluated from conventional Feynman diagrams. This approach neglects intrinsically relativistic bound state effects and also components such as $c\bar{c}$ + glue in the bound state.

Within this framework, there are nevertheless large apparent corrections from diagrams such as that shown which yields a factor $(1 - 16\ \alpha_s/3\pi)$. This is superficially a very large correction but the situation is far from clear. One certain point is that the value of α_s to be used is only known quantitatively if the diagram of next highest order in α_s are calculated. For instance the extraction of α_s from $\psi \to 3$ gluons (extracted from $\psi \to$ hadrons) yields a surprisingly small value of $\alpha_s \sim 0.2$ but one must await calculation of the corrections of next highest order before this α_s value can be compared with that obtained in other processes. Lacking such calculations, one must have recourse to some prejudice as to the choice of renormalization scheme in which to evaluate α_s. Indeed in those schemes in which corrections to other processes are fairly small, then the charmonium corrections are also much reduced[6].

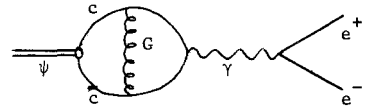

Further uncertainties in $O(\alpha_s)$ corrections come from the fact that the bound state wave function already contains gluon exchanges. Thus only the hard momentum transfer part of one gluon exchange should be included explicitly as a correction since the soft part is already taken into account.

Overall, a relativistic field theoretic treatment of bound states is necessary to analyse rigorously these corrections. Present estimates provide merely an estimate of the inherent uncertainties in the naive approach.

CONFINEMENT

As has been emphasized repeatedly, the non-perturbative or confining force between heavy quarks plays an essential rôle in binding them. Thus a QCD evaluation of heavy quark bound states must face the confinement problem - this

is the root of many of the uncertainties alluded to above.

One direct approach to confinement in QCD is by lattice calculations. Since incorporating fermions on a lattice causes a huge increase in complication, one treats heavy quarks by using static colour sources to represent them. The force between these colour sources at large distances is called the string tension K and this has been successfully related via Monte Carlo simulation to another dimensional parameter of QCD such as Λ, the scale of q^2 evolution[7]. One can try and go further and look at the force between colour sources as they approach closer but then the neglect of light fermions causes α_s to run in an unrealistic fashion[8]. The QCD vacuum is expected to be a complicated system with rampant quarks and gluons. Quantities which would be zero in a perturbation theory approach, such as the vacuum expectation value of the gluon field combination $\langle G^{\mu\nu} G_{\mu\nu} \rangle$, are found to be non-zero. This gluon condensate expression can be extracted using lattice techniques although with little precision[9]. The consequence for heavy quark bound states of this non zero gluon condensate will be discussed later.

Another treatment of confinement is to introduce a bag: a bubble of naive empty vacuum in a world of complicated vacuum. The solution of quark motion inside the bag is relatively straightforward and confinement enters through the bag constant: the "latent heat" to create the bag. One clear consequence of the bag picture is that, although quarks and gluons propagate almost freely inside it, they can be thought of as having an effective mass m since they are confined to a finite region of size R and $m \sim 1/R$. The MIT bag model uses a static picture, the cavity approximation, which is appropriate for spectrum generation but does not allow discussion of decays. Another more recent approach has been to approximate the quarks as static but to find the optimal bag surface for each quark separation[10]. This is appropriate for non-relativistic quarks and leads to a potential between the quarks, given the bag constant. This potential interpolates between coulombic and linear components as might be expected. The approach is still non relativistic, however.

An attempt to relate basic QCD parameters with heavy quark spectroscopy in a relativistic manner has been instigated by Shifman, Vainshtein and Zakharov[11]. To illustrate their approach consider the amplitude for a photon of 4-momentum q to go to a charmed state and then back to a photon: $\langle j_\mu j_\nu \rangle_c$.

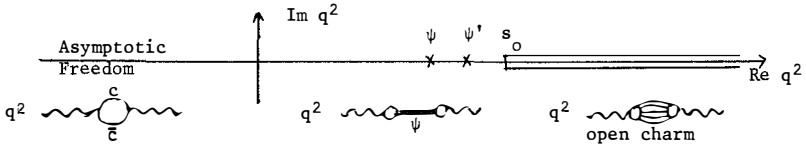

As shown, for $q^2 = m_\psi^2$ there is a big contribution from the ψ, while for $q^2 > s_o$ there is an open charm contribution ($D\bar{D}$ etc) where $s_o \approx 4m_D$. For $q^2 \lesssim 0$, on the other hand, asymptotic freedom implies that the hadronic intermediate state acts like a virtual bare $c\bar{c}$ pair. These two regions of q^2 can be related by dispersion relations. An integral over the ψ, ψ' and open charm region is related to the $c\bar{c}$ bubble contribution which depends only on the charm quark mass m_c. Different weightings can be used in these dispersion integrals so that one can emphasize the ψ region rather than the open charm production for example. In this way quantities such as the partial width $\psi \to e^+e^-$ (given by $\psi \to \gamma$ at $q^2 = m_\psi^2$) have been determined successfully[11].

A naive way to see these results is to remember that the asymptotic freedom expression (the charm quark bubble at $q^2 < 0$) can itself be expressed by a dispersion relation in terms of an integral along the physical region $q^2 > 4m_c^2$ for $c\bar{c}$ quark production. Then one has a "duality" between the quark picture with a $c\bar{c}$ threshold at $4m_c^2$ and the physical picture with ψ and ψ' bound states to be smeared out and with a continuum at s_o, as sketched:

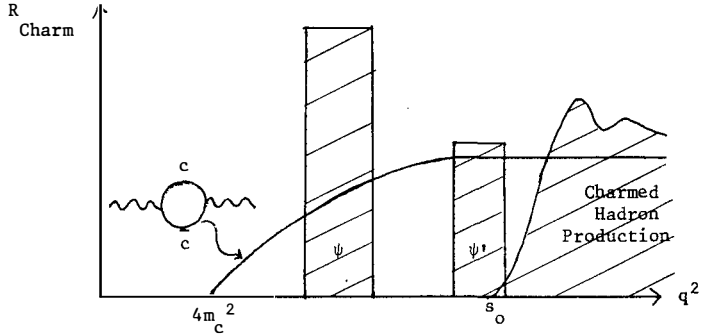

So far no mention has been made of confinement. The refinement emphasized by SVZ[11] is to evaluate the contribution in the asymptotic freedom region ($q^2 < 0$) more completely by taking account of $O(\alpha_s)$ corrections and of a confinement/gluon condensate/higher twist contribution:

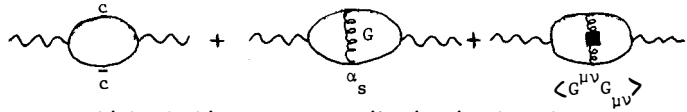

A sloppy way to think of this latter contribution is that the gluon propagator is modified by the presense of gluonic modes in the vacuum.

This more elaborate structure enables more detailed comparison with data, and it can be applied to currents with many different spin-parities. The upshot is that the many parameters involved (m_c, s_o, α_s, $\langle G^{\mu\nu} G_{\mu\nu} \rangle$, and the

moment (n) and q^2 value of the dispersion relation comparison) can be determined and predictions are derivable. It is to their credit that these methods predicted the η_c mass to be close to 3.00 GeV even though experimental evidence at that time indicated 2.86 GeV. The value of $\langle G^{\mu\nu} G_{\mu\nu} \rangle$ obtained is consistent with expectations from the bag model and from lattice estimates. The manner of obtaining this quantity from charmonium spectroscopy is rather indirect but is is nevertheless very remarkable that such fundamental properties of the QCD vacuum are at all relevant.

For upsilon spectroscopy similar methods apply but they give constraints involving several resonances at once since there are several radial excitations close in mass as seen from the q^2 region where asymptotic freedom ideas apply. Thus no direct predictions for single resonances are obtained unlike the case for charmonium.

In summary the SVZ techniques give consistency checks on charmonium spectroscopy and these enable some predictions for masses and decay widths to be made and some estimates of fundamental quantities (α_s, m_c, $\langle G^{\mu\nu} G_{\mu\nu} \rangle$) to be made. There is a subjective element in choosing the appropriate moment and q^2 region to apply the dispersion relations and in selecting the form of the higher twist contribution to be included. These aspects should be checked further in model field theories and in any other way available.

SUMMARY

An understanding of hadronic bound states in QCD is essential. The cleanest starting place is in heavy quark bound states: $(c\bar{c})$, $(b\bar{c})$, $(b\bar{b})$, etc. Current evidence points to a flavour independent potential which is as expected in QCD. A QCD-inspired phenomenological picture with one gluon exchange plus confinement appears to be adequate for an overall description. A more quantitative QCD bound state calculus is needed to substantiate this.

REFERENCES

1. M.E. Peskin, Nucl. Phys. B156, 365 (1979).
2. V.A. Novikov et. al., Phys. Lett. 41C, 1 (1978).
   E. Eichten et. al., Phys. Rev. D21, 203 (1980).
   C. Quigg and J.L. Rosner, FNAL-Pub-81/13-THY (1981).
3. W.E. Caswell and G.P. Lepage, Phys. Rev. A18, 810 (1978); G.P. Lepage SLAC 212 (1978).
4. C. Michael and F. Payne, Phys. Lett. 91B, 441 (1980); Liverpool LTH 63 (1981).
5. H. Krasemann, these proceedings.
6. W. Celmaster, ANL-HEP-CP-80-60, Proc. XXth Int. Conf. on High Energy Physics, Madison 1980.
7. See for example: R. Sugar, these proceedings.
8. E. Kovacs, these proceedings.
9. J. Kripfganz, CERN TH 3020 (1981).
10. P. Hasenfatz, R. Horgan, J. Kuti and J.M. Richard, CERN TH 2837 (1980).
11. M. Shifman, A. Vainshtein and V. Zakharov, Nucl. Phys. B147, 385-448 (1979). L.J. Reinders, H.R. Rubinstein and S. Yazaki, Rutherford RL-80-088 (1980).

BARYONS IN QCD - SOLVED AND UNSOLVED PROBLEMS

Dieter Gromes
Institut für Theoretische Physik
Universität Heidelberg
Philosophenweg 16, D-6900 Heidelberg

ABSTRACT

We briefly review some aspects of baryon spectroscopy within the framework of QCD-inspired potential models. While ground state baryons appear to be well understood, there remain problems for excited multiplets in connection with spin orbit forces. In particular the splitting between $\Lambda(1520)$ and $\Lambda(1405)$ still waits for an explanation.

I. THE MODEL

Potential models have been extremely successful for providing a comprehensive picture of elementary particle spectroscopy[1]. This holds true both for heavy and light mesons as well as for baryons. We shall concentrate on the latter here and, due to time limitation, focus on the spin (and quark mass) dependent splittings within multiplets. The model, inspired from the first successful potential models for charmonium and later extended to the entire field of hadronic spectroscopy in the pioneering work of De Rújula, Georgi and Glashow[2], is very simple: A baryon is visualized as a bound state of three quarks in a color singlet state which interact via some potential arising from the interaction with the gluons. The dynamics is treated nonrelativistically, realistic corrections are taken into account perturbatively.

For short distances between quarks, the interaction, due to asymptotic freedom, is dominated by one gluon (vector) exchange which, taking into account the correct color factors, leads to the potential

$$V(r_{ij}) = -\frac{2}{3}\,\frac{\alpha_s}{r_{ij}} \tag{1}$$

and the Breit-Fermi relativistic corrections (we only keep spin dependent terms here):

$$H_{ss}^{ij} = \frac{16\pi\alpha_s}{9}\,\frac{\delta^{(3)}(\vec{r}_{ij})}{m_i m_j}\,\vec{s}_i\cdot\vec{s}_j \quad \text{(spin spin)} \tag{2}$$

$$H_{so}^{ij} = \frac{2\alpha_s}{3r_{ij}^3}\left\{\frac{(\vec{r}_{ij}\times\vec{p}_i)\cdot\vec{s}_i}{2m_i^2} - \frac{(\vec{r}_{ij}\times\vec{p}_j)\cdot\vec{s}_i}{m_i m_j}\right\} + (i\leftrightarrow j) \quad \text{(spin orbit)} \tag{3}$$

$$H_T^{ij} = \frac{2\alpha_s}{r_{ij}^3}\,\frac{1}{m_i m_j}\left\{\frac{(\vec{s}_i\cdot\vec{r}_{ij})(\vec{s}_j\cdot\vec{r}_{ij})}{r_{ij}^2} - \frac{\vec{s}_i\cdot\vec{s}_j}{3}\right\} \quad \text{(tensor)} \tag{4}$$

We recognize the well-known contact spin-spin interaction, spin orbit and tensor forces and the appearance of the quark masses in the denominators.

As for the long-range confining part, a profound theoretical understanding is still missing, thus the best one can do is to try some ansatz and look for the implications. The most popular ansatz consists of flavor-independent linearly rising two particle potentials[3-7], although logarithmic potentials in baryons have also been advocated for[8]. While the earlier papers on the subject[3,4]

either took the long-range potential as stemming from an effective vector exchange or dropped its spin-dependent contributions completely, there is now good evidence that it must essentially be a scalar. This works well in meson spectroscopy [9], and we shall give good arguments for it in baryons, too. A scalar potential V(r) produces neither spin-spin nor tensor forces but only a spin orbit term due to Thomas procession (for a more detailed discussion of spin-dependent terms and references see e.g. ref. 10).

$$H_{ss} = H_T = 0 \tag{5}$$

$$H_{so}^{ij} = -\frac{1}{2m_i^2}\frac{V'(r_{ij})}{r_{ij}}(\vec{r}_{ij} \times \vec{p}_i)\cdot\vec{s}_j + (i \leftrightarrow j) \tag{6}$$

For an equal mass two-body problem in the c.m.-frame this reduces to

$$H_{so}\ (\text{scalar}) = -(1/3)H_{so}\ (\text{vector}) \tag{7}$$

a relation which is important for understanding suppression of spin orbit forces in mesons. We shall come back to the more subtle problem in baryons later.

All one has to do next is the following: Take the wave functions of the harmonic oscillator model [11] (only for oscillator forces we are able to solve the three body problem), evaluate all the relevant matrix elements, choose a set of parameters, and compare with the data.

II. GROUND STATE BARYONS

The ground state baryons are classified as a totally symmetric 56 under SU(6), i.e. a $^2 8$ and $^4 10$ (notation: $^{2S+1}$SU(3) with S the total quark spin) and they belong to the symmetrical (up to quark mass breaking effects) ground state wave function with L = 0 in the oscillator model. This simplifies the situation considerably since spin orbit and tensor forces are not operative. The spectrum of ground state baryons can therefore be understood solely from an interplay of spin-spin forces and quark mass differences. Rather than presenting a fit (see ref. 12 for a careful study) we concentrate on some important questions and their explanation within the model discussed here:

1) Why is, e.g., $m(\Lambda) > m(p)$? Answer: Because the strange quark is heavier than light quarks, $m_s > m_u \approx m_d$. This explanation is, of course, as old as the quark model and has nothing to do with QCD.

2) Why is $m(\Delta) > m(N)$? Answer: Because the total quark spins are S = 3/2 in the

Δ and $S = 1/2$ in the N, thus the spin-spin force arising from one gluon exchange splits the states. The sign comes out correctly, irrespective of the special choice of parameters.

3) Why is $m(\Sigma^0) > m(\Lambda)$? Answer: This mass difference which was always hard to understand in the old quark model because both particles have identical quark content (uds) as well as identical total quark spin ($S = 1/2$) found a brilliant explanation in ref. 2. The point is that due to the quark mass denominators in eq. (2) the main contribution to the spin-spin force comes from the light quark pair only. Considering the total symmetry of the spatial wave function, the antisymmetry of the color function and the generalized Pauli principle, one finds that spin and isospin must have the same symmetry for the light quark pair, i.e. $I = S = 1$ for Σ^0 , $I = S = 0$ for Λ . Therefore the spin-spin force of the light quarks is repulsive in Σ , attractive in Λ , making the former heavier than the latter. There are several further contributions of various sign which do, however, not essentially change the above reasoning. The argument works also well for the states where the strange quark is replaced by a charmed one (for a more detailed discussion of all these points we refer to ref. 10).

4) Can we understand the magnetic moments? Answer: Essentially yes. The naive static quark model with the three magnetic moments $\mu(u)$, $\mu(d)$, $\mu(s)$ taken as free parameters gives already a rather satisfactory agreement (up to $\approx$ 20 %) with the new precision experiments (for the latter see ref. 13). Inclusion of more sophisticated effects improves the situation, leaves, however, some discrepancies[14].

5) Why does the neutron have a negative charge radius? Answer: Because the two d-quarks are in a $I = 1$, $S = 1$ state and thus repelled by the spin-spin force. The negative charge is therefore somehow concentrated to the outer region[15].

We conclude this section with the pleasant feeling that the properties of ground state baryons appear rather well understood.

III. THE $[70,1^-]_1$ MULTIPLET

We next discuss some details of the first excited SU(6) supermultiplet of negative parity resonances which has $L = 1$ in the oscillator model. It consists of $^2 10$, $^4 8$, $^2 8$, $^2 1$. The 7 nonstrange resonances as well as 10 of the 14 predicted resonances with $S = -1$ are well known experimentally and,what is as important, there are no further negative parity resonances in this energy range which would not fit into the scheme (fig. 1). Since the whole multiplet would be degenerate in the SU(6) limit the observed detailed splitting and mixing pattern provides an excellent test for our understanding of the complicated interplay of spin-spin, spin-orbit, tensor forces and quark mass difference effects. Again we concentrate on some significant points.

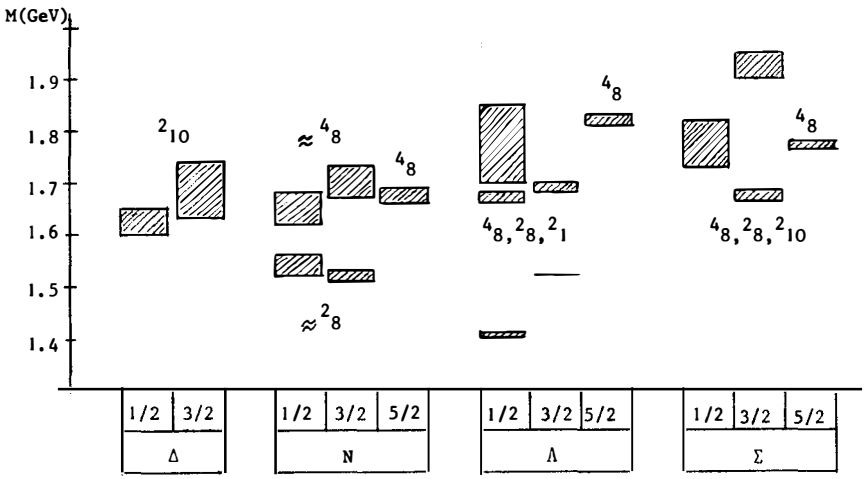

Fig. 1 The $\left[70,\ 1^-\right]_1$ supermultiplet

A first glance on fig. 1 shows that there are significant spin-spin splittings between resonances of different total quark spin while resonances with identical S (and L = 1), but different J, are almost degenerate. Thus we discuss spin-spin splittings first. A calculation of spin-spin splittings from one gluon exchange (in the SU(3) limit for simplicity) gives the following pattern[2]. The $^4_8$ and the $^2_{10}$ become degenerate, the $^2_1$ lies lowest, and the $^2_8$ just half in between. This is in excellent agreement with the experimental situation (note that the two lowest lying Λ-resonances are essentially SU(3) singlets) and explains, in particular, why the singlets, in spite of containing strange quarks, lie below the nucleonic states.

One can go further here and obtain a rather strong argument for the scalar nature of the confining potential[3,16]. Assume e.g. that the long-range potential $V(r_{ik})$ would be due to an effective vector. Then, in contrast to a scalar, it would also contribute to the spin-spin interaction but not with a contact δ-function but proportional to $\Delta V(r_{ik})$. This would immediately destroy the specific pattern described above. Therefore no important spin-spin contribution which is not essentially δ-like can be tolerated.

The next step is, of course, a fit including spin orbit and tensor terms,

but this attempt fails rather drastically unless some violence is done to the original form of the Hamiltonian or to the matrix elements[16-18]. The reason for the failure are difficulties with the spin orbit force which will be discussed below. ThereforeIsgur and Karl[17] proposed to drop spin orbit terms completely from the beginning, since anyhow they appear to be small. Thus they work with the hyperfine terms (spin-spin and tensor) only and obtain quite satisfactory results for spectra and mixing angles if one forgets about some specific details to be discussed immediately. This procedure must of course be criticized (and has indeed also been criticized by the authors themselves from the very beginning) because it puts in by hand what should come out from the calculation. Let us, therefore, now study spin orbit effects in some more detail. Introducing the standard relative coordinates

$$\vec{\lambda} = \frac{1}{\sqrt{6}} (\vec{r}_1 + \vec{r}_2 - 2\vec{r}_3) , \quad \vec{\rho} = \frac{1}{\sqrt{2}} (\vec{r}_1 - \vec{r}_2) , \tag{8}$$

going into the c.m. of the resonance and using some symmetry arguments, one finds[3] that each of the spin orbit terms (3) and (6) contributes two types of terms proportional to

$$(\vec{\rho} \times \vec{p}_\rho) \cdot (\vec{s}_1 + \vec{s}_2) \qquad \text{(symmetric)} \tag{9}$$

and

$$(\vec{\rho} \times \vec{p}_\lambda) (\vec{s}_1 - \vec{s}_2) \qquad \text{(antisymmetric)} \tag{10}$$

respectively. The first of these is a familiar spin orbit term for the 1-2 subsystem, proportional to $\vec{L}_{12} \cdot \vec{S}_{12}$. The second one, however, contains a mixed angular momentum involving all three quarks. Thus, although we started from two-body potentials, the relativistic corrections to these generate a three-body force! The physical meaning of this three-body force is now well understood[19] (and was, by the way, well understood long before, but the relevant literature was not known to the people working in baryon spectroscopy). It is due to the fact that the c.m. of the baryon does not coincide with that of the 1-2 subsystem. The momentum of the third quark influences the boost necessary to go from one to the other and thus also the spin-dependent Wigner rotation (up to the relevant order p^2/m^2) associated with it. The important point is now the following: The "two body" (or "symmetric", with respect to interchange $1 \leftrightarrow 2$, both in position space and in spin) parts (9) give <u>opposite signs</u> for the contributions from one gluon vector exchange and long-range scalar exchange. This is just the same situation as in mesons. Choosing parameters appropriately one can (independent

of the specific form of the long-range potential) achieve exact cancellation for nonstrange and essential cancellation for strange resonances. So far this is a clear justification of the procedure used by Isgur and Karl. For the "three-body" (or "antisymmetric") part (10), however, the contributions from vector and scalar add up which, due to its kinematical character, is not surprising. Many matrix elements vanish for the antisymmetric spin orbit force due to its symmetry properties. There is, however, one important consequence in connection with the two Δ-resonances in the $\left[70,1^-\right]_1$. These resonances are degenerate if only two-body forces are taken into account[20], whereas all recent phase shift analyses find a mass difference of about 100 MeV. Indeed the three-body spin orbit force splits the Δ-resonances and makes $m(\Delta\, 3/2) > m(\Delta\, 1/2)$. The sign is unambiguous and correct. Unfortunately we have now overunderstood the effect because it comes out a factor of three too large.

Finally, we turn to the most terrible problem in this connection, namely the splitting between the two lowest Λ-resonances, $\Lambda^{1/2}(1405)$ and $\Lambda^{3/2}(1520)$. These two resonances which are mostly SU(3) singlets are very well understood experimentally, e.g. they show the smallest uncertainty in the position of the resonance mass. Besides mixing effects with the other Λ-resonances they can be split by spin orbit forces only (tensor does not contribute in diagonal $S = 1/2$ states). In the Isgur-Karl model they are degenerate, inclusion of spin orbit forces leads to a wrong sign. This wrong sign persists even for much mor complicated ansätze for the form or the spin structure of the long-range part[21]. (This incidentally shows that the model at hand is a good model, because it makes definite predictions, even if they are wrong). There is a large splitting in the bag model, but again the sign is wrong[22]. Thus the conclusion in our opinion is quite clear. The two singlet Λ-resonances try to tell us that there is an essential point missing in our understanding and, since the experimental situation is so clear it is up to theoreticians to find the solution. We conclude by a compilation of some of the mathematical approximations we had to perform as well as of some physics which might be missing in the model:

Oscillator wave functions too bad[7]? Perturbative treatment of relativistic effects inadmissible? Other (than linear) form for long-range potential[8]? Genuine three-body potential? More complicated spin structure for long-range potential[21]? Pion cloud corrections[23]? Interaction with decay channels[24]? Gluonic degrees of freedom[25]? Complicated structure of QCD vacuum[26]? Some of the above points have been considered or estimated and appear to have no dramatic effect whatsoever. Due to the many successes of the model which hardly can be thought to be accidental we nevertheless believe that we are on the right way and that a solution to the remaining problems will show up.

REFERENCES

1) N. Isgur, talk given at this meeting.

2) A. De Rújula, H. Georgi, S. L. Glashow, Phys. Rev. D12, 147 (1975)

3) D. Gromes, I.O. Stamatescu, Nucl. Phys. B112, 213 (1976)

4) W. Celmaster, Phys. Rev. D15, 1391 (1977)

5) R. E. Cutkosky, R. E. Hendrick, Phys. Rev. D16, 786, 793 (1977)

6) M. Böhm, Z. Physik C3, 321 (1980)

7) I. M. Barbour, D. K. Ponting, Z. Physik C4, 119 (1980)

8) D. Gromes, I.O. Stamatescu, Z. Physik C3, 43 (1979)

9) H. J. Schnitzer, talk given at this meeting.

10) D. Gromes, Proc. of the IVth International Conference on Baryon Resonances, Toronto 14-16 July 1980, p. 195

11) As introduction to the quark oscillator model see e.g. R. R. Horgan, Proc. Topical Conf. on Baryon Resonances, Oxford 5-9 July 1976, 435

12) N. Isgur, G. Karl, Phys. Rev. D20, 1191 (1979)

13) O. Overseth, talk given at this meeting.

14) N. Isgur, G. Karl, Phys. Rev. D21, 3175 (1980); J. Franklin, Phys. Rev. Lett. 45, 1607 (1980); G. E. Brown, M. Rho, V. Vento, Phys. Lett. 97B, 423 (1980); D. B. Lichtenberg, Z. Physik C7, 143 (1981)

15) R. D. Carlitz, S. D. Ellis, R. Savit, Phys. Lett. 68B, 443 (1977); N. Isgur, G. Karl, R. Koniuk, Phys. Rev. Lett. 41, 1269 (1978); N. Isgur, G. Karl, D.W. L. Sprung, Rutherford Lab. preprint RL-80-053 (August 1980)

16) D. Gromes, Nucl. Phys. B130, 18 (1977)

17) N. Isgur, G. Karl, Phys. Rev. D18, 4187 (1978)

18) L. J. Reinders, J. of Phys. G4, 1241 (1978)

19) L. J. Reinders, Proc. of the IVth International Conference on Baryon Resonances, Toronto 14-16 July 1980, p. 203, and references therein.

20) R. Horgan, Nucl. Phys. B71, 514 (1974)

21) D. Gromes, unpublished useless calculations

22) T. De Grand, Proc. of the IVth International Conference on Baryon Resonances, Toronto 14-16 July 1980, p. 209, and references therein

23) W. N. Cottingham, K. Tsu, J. M. Richard, CERN preprint Ref. TH 2859-CERN (May 1980)

24) D. Gromes, N. Marinescu, Z. Physik C2, 301 (1979); A.K.A. Maciel, J.E. Paton, Oxford preprint Ref. 60/80

25) F. Wagner, talk given at this meeting

26) Y. Chung, H. G. Dosch, M. Kremer, D. Schall, Heidelberg preprint HD-THEP-81-2 (1981)

DUAL-TOPOLOGICAL UNITARIZATION CALCULATION OF HADRON MASSES

Louis A.P. Balázs
Division de Physique Théorique*, IPN Orsay
LPTPE, Université Pierre et Marie Curie, Paris, and
Physics Dept, Purdue University, West Lafayette, IN 47907, U.S.A**

Abstract : A dual-topological unitarization (DTU) approach to the calculation of hadron masses is presented, in which the effect of planar "sea"-quark loops is taken into account. Using techniques based on minimal analyticity and unitarity, we first derive an approximate "generic" Regge-trajectory formula for any given hadronic process and then require simultaneous consistency for entire sets of such processes. This has been applied (largely in collaboration with B. Nicolescu) to a calculation of the masses of all the lowest qq, qqq, qqqq, qqqqq, qqqqqq and qqqqqq ("dibaryon") states for q = u, d, s and the Regge trajectories associated with each of them. The only arbitrary parameters are m_ρ and m_{K^*}, one of which merely serves to fix the energy scale.

Résumé : Nous calculons le spectre de masse des hadrons dans le cadre de l'Unitarisation Duale Topologique. Nous prenons en considération l'effet des boucles planaires de quarks de la mer. En utilisant des techniques basées sur l'analyticité minimale et l'unitarité, nous déduisons une formule générique approximative pour la trajectoire de Regge pour un processus hadronique quelconque. Nous imposons par la suite l'autoconsistance simultanée pour des ensembles de tels processus hadroniques. Nous avons ensuite calculé (en majeure partie, en collaboration avec B. Nicolescu) les masses des hadrons ordinaires (mésons et baryons), ainsi que les masses des hadrons multiquarks qqqq, qqqqq, qqqqqq et qqqqqq ("dibaryons"), où q = u, d, s. Il n'y a que deux paramètres arbitraires dans notre calcul, les masses du ρ et du K*, par exemple ; le rôle d'un de ces paramètres est de fixer l'échelle de masse.

---

* Laboratoire Associé au C.N.R.S.
** Permanent address

In general, calculations of the hadron spectrum can be divided into two basic types :

(A) Semi-Phenomenological, which depend wholly, or in part, on ad hoc phenomenological potentials or bag-boundary conditions parametrized by a number of arbitrary constants which are fitted to the data.

(B) More Fundamental. Here the lattice approach is the one which has recently received the most attention. The usual space-time is replaced by a lattice and light "sea" quarks are generally neglected as a first approximation. The latter assumption is sometimes justified on the basis of an $N_{flavor} / N_{color} \to 0$ limit of quantum-chromodynamics (QCD). However, $N_{flavor} / N_{color} \sim 1$ in the real world and sea quarks are known to play an important role for small fractional quark momenta (x) within hadrons in deep-inelastic lepton-hadron scattering experiments. Since small x corresponds to an important part of the confinement region, there is every reason to expect that a realistic hadronic spectrum will emerge only when the sea-quark loops of Fig. 1 are properly taken into account. The usual difficulties in accounting for the smallness of the pion mass may be a manifestation of this fact.

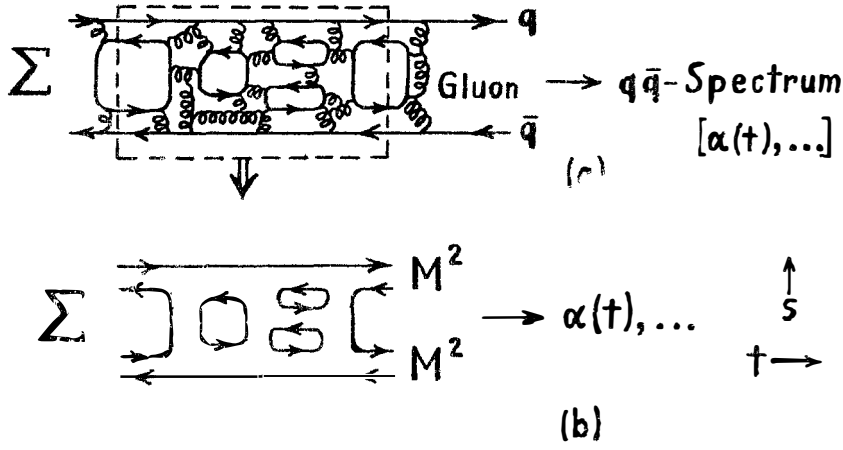

Fig. 1 Generation of $q\bar{q}$ spectrum taking into account quark loops.

The dual-topological unitarization program[1] is a highly promising fundamental approach to the confinement region in which sea quarks, and hence quark loops, are assumed to play an important role form the beginning. Instead of going to the lattice, one uses continuum-space techniques based on minimal analyticity and unitarity - general properties which have been extensively tested for hadronic processes in the past. DTU techniques have, of course, already seen many successful applications[1], particularly in jet and cross-section physics, subjects which are discussed in the talks by Capella, Tran Thanh Van and Nicolescu at this Conference.

In the DTU approach, diagrams of the type shown in Fig. 1 (b) are tackled systematically by starting with (planar) graphs having the simplest topologies. These can be argued to be the most dominant dynamically. Earlier versions of DTU[1], while successful for $q\bar{q}$ mesons (M^2), could not consistently take into account qqq baryons (B^3) and $qq\bar{q}\bar{q}$ baryonium (M^4). Recently, Chew and Poenaru[2] have found a way of doing this in which quarks are treated as purely mathematical objects and in which one or more of the quark lines in Fig. 1 (b) can be replaced by "diquarks" of a certain specified topological structure. One must also introduce "Landau" lines which carry the four-momenta of the hadrons in any given diagram and whose "interactions" with the diquarks can be argued to be weak. This means that it is a good approximation to forbid diquark breakup and formation (in lowest order) in our modified Fig. 1 (b). It also means that $M^4 \leftrightarrow M^2$ transitions are suppressed, so that M^4 states should be narrow below the $B^3\bar{B}^3$ threshold.

The "ordered" fishnet graphs[1] of Fig. 1 (b) have s-t channel crossing where s and t are the usual Mandelstam variables. In addition, since the diagrams are planar, the usual Regge cuts are

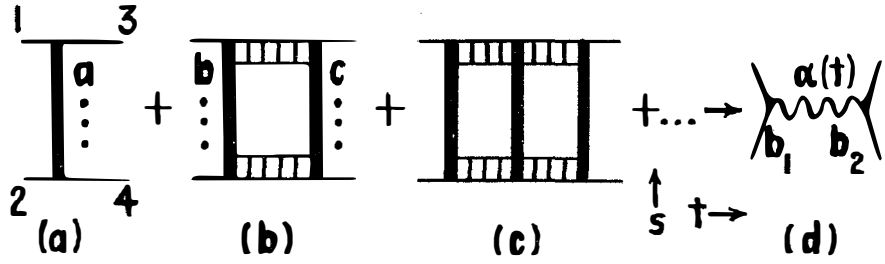

Fig. 2 Dominant contribution to Fig. 1(b) for moderate t.

absent. Together with analyticity, this implies finite-energy sum-rule duality, which can be used to relate Figs. 2(a) and 2(d) through a fixed-t relation of the form

$$\Gamma = b_1 b_2 G(\alpha) \quad , \tag{1}$$

where $\Gamma\delta(s-m_a^2)$ is the lowest nonvanishing contribution (of effective mass m_a) to the s-channel absorptive part of Fig. 2(a).

For moderate values of t, the dominant contribution to the graphs of Fig. 1(b) is expected to come from the generalized infinite ladder sum of Fig. 2, which will be represented by

$$12 \ (a) \ 34 \rightarrow \alpha \tag{2}$$

and in which the masses of the vertical-line clusters (a,...), (b,...), (c,...), ... must be bounded to avoid double-counting. The ladder exchanges in Figs. 2(b), (c), ... themselves have the form of the entire sum of Fig. 2. In previous derivations[3)4)], these were simply approximated by Regge exchanges, which led to spurious Regge-cut effects. A proper high-s cancellation of such effects leads to a peaking (at $s=s_1$) in the s-channel absorptive part of contributions like Fig. 2(b). If we take a generalized Mellin transform of Fig. 2 and sum the resulting series by using Padé approximants, we then obtain an approximate relation of the form

$$b_1 b_2 = \Gamma F(\alpha, s_1) \quad , \tag{3}$$

together with a condition on the internal couplings of Fig. 2.

Eliminating $b_1 b_2/\Gamma$, Eqs.(1) and (3) lead to a relation which can, in general, have up to two solutions for α. If we require s_1 to be such that we have a unique solution, we obtain the simple generic formula

$$\alpha(t) = S_1 + S_2 - \tfrac{1}{2} + 2\hat{\alpha}' \left[m_a^2 + \tfrac{1}{2}\left(t - \sum_{i=1}^{4} m_i^2\right) \right] , \tag{4}$$

where $\hat{\alpha}'$ is a constant, and S_i and m_i are the spins and masses of the external lines i = 1, 2, 3, 4 of Fig. 2, with the initial state defined so that $S_1 + S_2 \geq S_3 + S_4$.

In making actual hadronic-mass calculations we simultaneously apply Eq.(4) to entire sets of processes and require consistency. For a given class (e.g. $q\bar{q}$ or $qq\bar{q}\bar{q}$) of output $\alpha(t)$, we first

order sets of hadronic processes according to increasing quark-mass content in the vertical line of Fig. 2(a) ; this corresponds to decreasing importance of the corresponding horizontal-line channels in Fig. 2. Within each such set we then require (i) that allowed couplings vanish only if this is demanded by consistency, and (ii) that secondary contributions (backgrounds, nondegenerate daughters, etc.., which can shift the effective value of m_a) are minimal ; in other words, we require a simultaneous minimization of m_a for all the processes in the set. We then repeat this procedure until all the possible parameters of our output $\alpha(t)$ class have been extracted.

The above procedure was first applied to q = u, d hadronic states H^n. Here the lowest members can be mesons M_s^n (or dibaryons D_s^n) with spin and isospin S, I = 0, 1, ... n/2, or baryons B_s^n with S, I = 1/2, 3/2, ...n/2 ; in each case n is the total number of quarks plus antiquarks within the hadron and we have complete isospin mass-degeneracy. We can then obtain all of the parameters characterizing M_s^n, B_s^n, D_s^n and their Regge recurrences for $n \leqslant 6$ from the sets of processes

$$M^2M^2(M^2)M^2M^2 \to \alpha_M{}^2 \tag{5}$$

$$B^3\bar{B}^3(M^2)B^3\bar{B}^3 \to \alpha_M{}^4,\ M^4M^4(B^3)B^3\bar{B}^3 \to \alpha_M{}^4 \tag{6}$$

$$M^4M^4(M^2)M^4M^4 \to \alpha_M{}^6 \tag{7}$$

$$B^5\bar{B}^5(M^2)B^5\bar{B}^5 \to \alpha_M{}^8,\ M^6M^6(B^3)B^5\bar{B}^5 \to \alpha_M{}^8 \tag{8}$$

$$M^6M^6(M^2)M^6M^6 \to \alpha_M{}^{10},\ D^6\bar{D}^6(M^2)D^6\bar{D}^6 \to \alpha_M{}^{10}\ . \tag{9}$$

This gives

$$\alpha_{\rho,\omega}(0) = 0.5\ ,\ \alpha_{\rho,\omega}(t) - \alpha_{\pi,\eta}(t) = 1/2 \tag{10}$$

$$\alpha_{\rho,\omega}(t) - \alpha_{\Delta}(t) = 1/4,\ \alpha_{\Delta}(t) - \alpha_N(t) = 1/2 \tag{11}$$

$$\alpha_{\rho,\omega}(t) - \alpha_{M_2}^4(t) = 1,\ \alpha_{M_2}^4(t) - \alpha_{M_1}^4(t) = \alpha_{M_1}^4(t) - \alpha_{M_0}^4(t) = 1/2 \tag{12}$$

$$\alpha_{\rho,\omega}(t) - \alpha_{B_{5/2}}^5(t) = 9/4,\ \alpha_{B_{5/2}}^5(t) - \alpha_{B_{3/2}}^5(t) = \alpha_{B_{3/2}}^5(t) - \alpha_{B_{1/2}}^5(t) = 1/2 \tag{13}$$

$$\alpha_{\rho,\omega}(t) - \alpha_{M_3}^6(t) = 3 \tag{14}$$

$$\alpha_{M_3}^6(t) - \alpha_{M_2}^6(t) = \alpha_{M_2}^6(t) - \alpha_{M_1}^6(t) = \alpha_{M_1}^6(t) - \alpha_{M_0}^6(t) = 1/2 \tag{15}$$

$$\alpha_{D_S}^6(t) = \alpha_{M_S}^6(t),\ S=0,\ 1,\ 2,\ 3 \tag{16}$$

The explicit consideration of unequal-particle channel processes like

$$M^2B^3(M^2)M^2B^3 \to \alpha_B{}^3 \qquad (17)$$

turns out not to affect any of the above results.

Eqs.(10)-(16) are in good agreement with existing experimental data. If we take $m_\rho = 0.775$ GeV, which we use to set our energy scale, we obtain a universal $\alpha'(t) = 0.83\ \text{GeV}^{-2}$ and $m_\pi^2 \approx 0$; a small pion mass thus arises naturally in our approach. We predict baryon Regge intercepts

$$\alpha_\Delta(0) = 0.25,\ \alpha_N(0) = -0.25 \qquad (18)$$

which give $m_\Delta = 1.22$ GeV and $m_N = 0.95$ GeV, and baryonium intercepts

$$\alpha_{M_2^4}(0) = -0.5,\ \alpha_{M_1^4}(0) = -1.0,\ \alpha_{M_2^4}(0) = -1.5, \qquad (19)$$

which should be compared with the average intercept of -0.75 ± 0.2 obtained by Nicolescu[5] from a phenomenological analysis of t-channel exotic (I=2) reactions. Eq.(19) leads to $j^P = 0^+, 1^+, 1^-, 2^-$ baryonium states below the $N\bar{N}$ threshold with masses 1.34, 1.55, 1.73, 1.73 GeV, respectively[4,6]; we have already seen, on very general grounds, that, in contrast to other approaches, M^4 states are expected to be narrow below $N\bar{N}$ in DTU, although they may be broad elsewhere. Possible indications of narrow subthreshold states have been seen by Backenstoss et al[6] at 1.40, 1.56, 1.65 and 1.69 GeV, but clearly any definitive conclusions must await results from the CERN Low-Energy Antiproton Ring (LEAR). We also expect narrow $B^5_{1/2}$ baryon and D^6_0 dibaryon ground states at 1.98 and 2.19 GeV, respectively. Recently, over a year after the completion of our first calculations[6], a narrow dibaryon candidate was observed by a Saclay group at 2.23 GeV[7].

Our approach can be extended to q = u, d, s hadrons H^n, H^n_s, H^n_{ss}, ... containing 0, 1, 2, ... s-quarks plus antiquarks. We find, in all cases,

$$\alpha'_{H^n} = \alpha'_{H^n_s} = \alpha'_{H^n_{ss}} = \ldots = \alpha'_{\rho,\omega} \qquad (20)$$

and

$$m^2_{H^n_s} - m^2_{H^n} = m^2_{H^n_{ss}} - m^2_{H^n_s} = \ldots = \Delta_{H^n}. \qquad (21)$$

Taking $m_{K^*}^2 - m_\rho^2 = 0.20\ \text{GeV}^2$ as input we then obtain

$$\Delta_M 2 = 0.20,\ \Delta_B 3 = 0.50,\ \Delta_M 4 = 1.00,\ \Delta_B 5 = 1.40,\ \Delta_M 6 = 2.00\ (\text{GeV}^2) \tag{22}$$

Eqs.(20)-(22) are in reasonable agreement with present experimental data, as are our preliminary results on $q\bar{q}$ mesons containing c and b quarks.

I would like to express my gratitude to Dr. Nicolescu for numerous helpful discussions and to Profs. Tran Thanh Van and Vinh Mau for their hospitality at this Conference and at IPN, respectively.

References

1) G.F. Chew and C. Rosenzweig, Phys. Rep. 41, 263 (1978) ; L. Montanet, G.C. Rossi and G. Veneziano, Phys. Rep. 63, 149 (1980).

2) G.F. Chew and V. Poénaru, Phys. Rev. Lett. 45, 229 (1980) ; Lawrence Berkeley Laboratory preprint LBL-11433 (1980).

3) L.A.P. Balázs, Phys. Rev. D20, 2331 (1979) ; Phys. Lett. 99B, 481 (1981).

4) L.A.P. Balázs and B. Nicolescu, Z. Phys. C6, 269 (1980).

5) B. Nicolescu, Nucl. Phys. B.134, 495 (1978).

6) Proceedings of the Workshop on Baryonium and Other Unusual States, Orsay, June 1979, edited by B. Nicolescu, J.M. Richard and R. Vinh Mau.

7) P.E. Argan et al, Phys. Lett. 46, 96 (1981).

SPIN STRUCTURE IN MESON SPECTROSCOPY

Howard J. Schnitzer
Physics Department
Brandeis University
Waltham, MA 02254
U.S.A.

Abstract

The spin-dependent structure of mesons is reviewed from a fairly general point of view. It is argued, without reference to detailed potentials or wave-functions, that the spin-splitting of known hadrons is consistent with one-gluon exchange added to a confining potential transforming as a Lorentz scalar. This conclusion is independent of the status of the P-wave scalar meson states. Evidence is given for significant continuum gluon content in the ordinary P-wave I=0 mesons. It is also argued that a search for inverted meson multiplets could provide a decisive test of the non-relativistic quark model of ordinary hadrons.

As a result of the efforts of a great number of people, a concensus appears to have emerged among many workers in hadron spectroscopy that a single non-relativistic (N.R.) quark model is able to correlate a great deal of detailed spectroscopic data of $(q\bar{q})$, $(Q\bar{Q})$, $(q\bar{Q})$, (qqq), and (qqQ) states with very few parameters [Here q represents a light constituent u, d, or s quark and Q a heavy c, b, t,... quark]. The basic assumption of the model is that non-relativistic two-body forces act between pairs of quarks with constituent masses m_i. Since a review of the application of the model to baryon spectroscopy has been given at this meeting by Isgur,[1] I will concentrate on meson spectroscopy with particular emphasis on the ordinary mesons.

It is surprising that the non-relativistic approach works so well for ordinary mesons and baryons, as the average $(v/c)^2$ of the quarks is not small in either case. Nevertheless the Isgur and Karl[1] model is rather successful as a description of baryon spectroscopy even though $(v/c)^2$ is uncomfortably large. The situation for mesons is comparable to baryons in terms of qualitative successes, so that we will proceed in spite of an uneasy feeling about the non-relativistic approach. Later in this paper we will propose a test of the non-relativistic quark model which does not depend on detailed wave-functions or parameters, but rather on the qualitative features of the model. As such, the test should have a decisive role in assessing the future of the model.

If one retains the leading terms correct to $O(v/c)^2$, then the most general $(q\bar{q})$ two-body Hamiltonian is of the form

$$
\begin{aligned}
H = {} & \underbrace{V_c(r)}_{\text{spin-independent}} + \underbrace{\frac{1}{m_1 m_2} V_T(r)\, S_{12}}_{\text{tensor}} + \underbrace{\frac{4}{m_1 m_2} V_S(r)\, \vec{S}_1 \cdot \vec{S}_2}_{\text{spin-spin}} \\
& + \underbrace{\left[\frac{1}{m_1 m_2} V_1(r)\right]}_{\text{spin-orbit}} + \underbrace{1/2\left(\frac{1}{m_1^2} + \frac{1}{m_2^2}\right) V_2(r)}_{\text{Thomas}} \Big] \vec{L}\cdot\vec{S} \\
& + \underbrace{1/2\left[\frac{1}{m_1^2} - \frac{1}{m_2^2}\right] V_2(r)}_{\text{Thomas}}\, \vec{L}\cdot(\vec{S}_1 - \vec{S}_2)
\end{aligned}
\tag{1}
$$

Given Eq.(1) we can obtain a very good understanding of meson spectroscopy with very few additional assumptions. These are:

(1) The matrix elements of V_1, V_2, V_T and V_S are SU(3) invariant, which is very plausible as all light mesons are comparable in size. Therefore the dominant SU(3) breaking is assumed to have its origin in the kinematical factors of constituent quark masses. This assumption allows us to write

$$\langle u\bar{u}|V_i(r)|u\bar{u}\rangle = \langle d\bar{d}|V_i|d\bar{d}\rangle = \langle s\bar{s}|V_i|s\bar{s}\rangle \equiv v_i \text{ for } i = 1, 2, S, T \qquad (2)$$

(2) The meson states are approximately diagonal in the basis

$$\underbrace{1/\sqrt{2}(u\bar{u}+d\bar{d});\ s\bar{s}}_{I=0};\quad \underbrace{1/\sqrt{2}(u\bar{u}-d\bar{d})}_{I=1};\quad \underbrace{s\bar{u},\ u\bar{s}}_{I=1/2}$$

(3) Gluons can mix the I=0 mesons.

We shall neglect possible mixing with $(q\bar{q})(q\bar{q})$ states, which is probably a good approximation except for the $^3P_0$ scalar meson states. The identification of the appropriate $^3P_0$ states is controversial, and we will avoid these states as much as possible in our analysis. In earlier work De Rujula, et al[2] assumed that the $V_i(r)$ in Eq.(1) were given by the one-gluon exchange, which gives relations among the v_i in (2), while Schnitzer[3] assumed that the V_i are obtained from the one-gluon exchange and a Lorentz scalar confining potential. Our approach here is more general, since we need not be specific about the potentials $V_i(r)$, as the data is now good enough to allow us to draw important qualitative conclusions. We now turn to a discussion of meson stationary states using the above assumptions.

S-waves

Here
$$\Delta E = \frac{4}{m_1 m_2} (v_S)_{S\text{-wave}} \langle \vec{S}_1 \cdot \vec{S}_2 \rangle \qquad (3)$$

As emphasized by De Rujula, et al, this implies that

$$[E(K^*) - E(K)]/[E(\rho) - E(\pi)] = m_u/m_s \qquad (4)$$

which is compatible with constituent masses $m_u \sim 330$ Mev and $m_s \sim 500$ Mev. Of course only $(v_S)_{S\text{-wave}}$ is tested by (4), as the expectation values of other terms in (1) vanish for S-waves. In some sense the success of (4) is remarkable, as it

completely ignores the possibility that the pion is the Goldstone boson of broken chiral symmetry. Typical further tests of (3) and the SU(3) invariance of the matrix elements are

$$\frac{[E(K'^*) - E(K')]}{[E(\rho') - E(\pi')]} = \frac{[E(F^*) - E(F)]}{[E(D^*) - E(D)]} = \frac{m_u}{m_s} \qquad (5)$$

where the first ratio involves radial excitations and the second charmed mesons. It is expected that (5) will not involve chiral symmetry breaking to the same extent as (4), so that a test of (5) will provide an interesting confirmation of the basic idea of the model.

The actual value of $(v_s)_{S\text{-wave}} \sim 100 \times 10^6 (\text{Mev})^3$ is a large number; roughly one to two orders of magnitude larger than the corresponding P-wave matrix elements. This is all compatible with a very short ranged spin-spin force whose origin is one-gluon exchange.

P-waves

The growing experimental information encourages analysis of the meson P-wave states along these same lines, while for higher partial waves there is not yet enough data. In Table I we list what we consider reliable meson P-states.[4]

Table I
P-wave meson states

	$^3P_2$	$^1P_1$	$^3P_1$	$^3P_0$
I=1	$A_2(1310)$	B(1235)	$A_1(1200\text{-}1300)$	[δ(980)]
I=1/2	K*(1430)	$Q_B(1355)$	$Q_A(1340)$	
I=0 $(\bar{u}u+\bar{d}d)$	f(1270)	H(1130-1190)	D(1285)	
I=0 $(\bar{s}s)$	f'(1514)		E(1420)	

Note the entry of the H meson taken from a recent report.[5] The states Q_A and Q_B are derived from the SLAC phase-shift analysis,[6] obtained from the experimentally observed Q_1 and Q_2 states. The Q_A and Q_B play a decisive role in fixing the magnitude of the Thomas term, which as we shall see is an important feature

of the $(q\bar{q})$ spin-dependent forces. Notice that D(1285) is approximately 100 Mev more massive than the H-meson and roughly degenerate with f(1270), which is qualitatively different than the analogous I=1 and I=1/2 states. We interpret this to mean that the $(I=0)(\bar{u}u+\bar{d}d)$ states have significant gluon content. Finally we remark that there are no unambiguously identified ^3P_o pure $(q\bar{q})$ states. In spite of this difficulty we are able to ignore the scalar mesons and still draw important general conclusions concerning the spin-dependent forces. We do need to know the mass of at least one scalar $(q\bar{q})$ state in order to separate the tensor force from the P-wave spin-spin force. Tentatively we choose $\delta(980)$, which as an I=1 state can have no gluon admixture. Our uncertainty about this as a pure $q\bar{q}$ state is indicated by the brackets in the table.

It is easy to translate Eq.(1) into mass differences, with the result

$$[E(^3P_2)-E(A)] = 2\left[\frac{1}{m_1 m_2} v_1 + 1/2\left(\frac{1}{m_1^2} + \frac{1}{m_2^2}\right) v_2\right] - \frac{2.4}{m_1 m_2} v_T \tag{6}$$

$$[E(B) -E(A)] = \left[\frac{1}{m_1 m_2} v_1 + 1/2\left(\frac{1}{m_1^2} + \frac{1}{m_2^2}\right) v_2\right] -2v_T/m_1m_2 -4v_s/m_1m_2 \tag{7}$$

$$[E(A) - E(^3P_o)] = \left[\frac{1}{m_1 m_2} v_1 + 1/2\left(\frac{1}{m_1^2} + \frac{1}{m_2^2}\right) v_2\right] + 6\, v_T/m_1m_2 \tag{8}$$

$$M_1 + M_2 = M_A + M_B \tag{9a}$$

$$(M_2 - M_B)(M_B - M_1) = 2\ 1/2\ \frac{1}{m_1^2} - \frac{1}{m_2^2}\ v_2^{\ 2} \tag{9b}$$

where $M_1(M_2)$ is the mass of $Q_1(Q_2)$.

Notice that with the usual constituent quark masses, the I=1/2 states determine the combination of matrix elements $[v_1 + 1.09\ v_2]$ which is not experimentally distinguishable from the combination (v_1+v_2) obtained from the I=0 and I=1 states. Therefore we record information on the spin-orbit force only in the combination (v_1+v_2) even for the I=1/2 states. Equation (9) determines the magnitude of the Thomas term, which underlines the importance of the SLAC phase-shift analysis in this regard. The matrix elements obtained from Table I and Eqs. (6), (7), and (9) are tabulated in Table II.

Table II
Matrix elements obtained from Table I and Eqs. (6) - (9)
Units: 10^6(Mev)^3

	I=1/2	I=1	I=0 ($\bar{u}u$)	I=0 ($\bar{s}s$)
$E(B) - E(A)] \Rightarrow \{v_1+v_2) - 2v_T - 4v_S\}$	2.5	2.7 $A_1(1210)$	-10.3	
$[E(^3P_2) - E(B)] \Rightarrow \{(v_1+v_2) - 0.4v_T + 4v_S\}$	12.4	8.2	8.7 H(1190)	
$[E(^3P_2) - E(A)] \Rightarrow \{2(v_1+v_2) - 2.4v_T\}$	14.9	10.9	-1.6	23.5
$(Q_1,Q_2) \leftrightarrow (Q_A,Q_B) \Rightarrow \lvert v_2\rvert$	14.2	-	-	-

It is to be emphasized that no use is made of any ^3P_o state in completing Table II, so that our conclusions will not depend on the status of these controversial states.

Some observations are in order concerning the results displayed in Table II.

1) The I=1/2 and I=1 matrix elements are in agreement to within factors of 1.5, which indicates the degree of accuracy of our assumption of SU(3) invariant matrix elements.

2) If one considered $A_1(1100)$, the entry for Eq.(7) (I=1) would be 15 x 10^6(Mev)^3, which is a factor of 6 too large, and is incompatible with an approximate SU(3) invariance of the matrix elements. As indicated, the entry in the table uses $A_1(1210)$, but $A_1(1180 - 1250)$ would be satisfactory within the limitations of 50% departure from SU(3) invariance.

3) The (I=0)$\bar{u}u$ multiplet is incompatible with SU(3) invariance. We suggest that this implies a significant admixture of gluon continuum in these states, reminiscent of the gluon admixture in the η and η' mesons.

4) The (I=0)$\bar{s}s$ states, as tested by Eq.(6), is marginally compatible with approximate SU(3) invariance. Table II therefore does not give strong evidence for a gluon admixture in E(1420).

We have yet to use information from the $^3P_0$ scalar states, which we will need in order to separate the P-wave tensor force from the spin-spin force. Suppose we assume $(v_s)_{P\text{-wave}} = 0$. When combined with the results of Table II, we would predict $E(^3P_0)_{I=1/2} = 1030$ Mev, which is a very low mass for a $K\pi$ scalar meson. We conclude that $(v_s)_{P\text{-wave}} \neq 0$. This does not mean $(v_s)_{P\text{-wave}}$ is large, since this matrix element is always accompanied by a large coefficient, and predictions of scalar meson masses are sensitive to small values of this matrix element. Consider the possibility that $\delta(980)$ is the I=1, $^3P_0$ pure $(\bar{q}q)$ state. This state certainly has no gluon admixture, although it might in fact have a substantial $(q\bar{q})(q\bar{q})$ components. Nevertheless, with the assumption that it is a pure $(q\bar{q})$ state we find

$$(v_s)_{P\text{-wave}} = (0.5 \pm 0.25) \times 10^6 \text{ (Mev)}^3$$
$$\ll (v_s)_{S\text{-wave}} \simeq 100 \times 10^6 \text{ (Mev)}^3 \qquad (10)$$

The conclusion is that the spin-spin interaction is very short ranged, and compatible with one-gluon exchange. As a corollary, the pure $(q\bar{q})$ $^3P_0$ states are expected to be in the 1.0 to 1.2 Gev region. The experimental absence of scalar meson states in this mass range therefore remains a puzzle.

Given Eq. (10), we can compute the individual matrix elements which we tabulate in Table III. In the same table we also have added the corresponding matrix elements obtained from charmonium. It is evident that there is significant SU(4) breaking, as the charmonium matrix elements are considerable larger than the correpsonding matrix elements obtained from ordinary mesons. [Recall that kinematical quark mass effects have already been removed before Tables II and III are computed]. The entries in Table III are "typical" values, subject to the 50% variations observed in Table II.

Table III
Summary of matrix elements

Light Mesons	x 10^6 (Mev)^3	Remarks
S-wave v_s	100	spin-spin forces very short-ranged
P-wave v_s	0.5 ± 0.25	
v_T	2.5	spin-orbit force >> tensor force
$v_1 + v_2$	12.0	
$\|v_2\|$	14.2	Thomas term as large as spin-orbit force v_1 [If $v_2>0 \Rightarrow v_1\approx 0$, which is not consistent with baryon spectroscopy]
(Assume $v_2<0$) v_1	26.2	
Charmonium S-wave v_s	225	Matrix elements considerably larger than those of ordinary mesons $\Rightarrow$ significant SU(4) violation
P-wave v_T	23.4	
$v_1 + v_2$	73.1	

It should be emphasized that a single qualitative picture explains all this information, as well as the spin-dependent forces of the baryon model of Isgur and Karl. That is, the spin-dependent forces in (ordinary and new) mesons and baryons are consistent with a short-range one-gluon exchange (transforming as a Lorentz vector) and a confining potential transforming as a Lorentz scalar.[7] This assumption leads to the qualitative picture of the spin-dependent potentials displayed in Fig. 1. Of particular interest is $[V_1(r) + V_2(r)]\vec{L}\cdot\vec{S}$, which is dominated by the (attractive) one-gluon exchange at short distances, and by the (repulsive) Thomas term at large-distances. In Fig. 1 we have also indicated the average sizes of typical hadrons. Since $\langle r\rangle_{\text{baryons}}$ is somewhat larger than $\langle r\rangle_{q\bar{q}}$, one also understands why the coefficient of $\vec{L}\cdot\vec{S}$ is absent in the Isgur-Karl model of baryons, is weakly attractive for ordinary mesons, and more strongly

attractive for charmonium. [Compare Table III]. Fig. 1 also includes $V_T(r)$ and $V_S(r)$, which again are in qualitative agreement with Table III and the baryon model. We see that the behavior of $[V_1(r) + V_2(r)]\vec{L}\cdot\vec{S}$ obtained from Table III and Fig. 1, and $V_2(r)$ obtained from the (Q_A, Q_B) I=1/2 mesons give considerable support to the confining potential transforming as a Lorentz scalar. The possibility that the Thomas term dominates at large distances has some fascinating consequences.

Consider a $(Q\bar{q})$ meson for which $m_2 >> m_1$. From (1) we obtain

$$H \xrightarrow[m_2 >> m_1]{} V_c + \frac{1}{2m_1^2} V_2(r)\,[\vec{L}\cdot\vec{S} + \vec{L}\cdot(\vec{S}_1 - \vec{S}_2)] \tag{11}$$

$$= V_c + \frac{1}{m_1^2} V_2(r)\vec{L}\cdot\vec{S}_1 + O(m_1/m_2)$$

which demonstrates that the Thomas term dominates the spin-dependent forces in limit. Since we argued that $V_2(r) < 0$, we have the prediction[8]

$$E(^3P_2) \underbrace{<\ E(J=1)\ <}_{\text{2 states}} E(^3P_o) \tag{12}$$

That is, we predict inverted <u>P-wave</u> multiplets when $m_2 >> m_1$. Similarly, (11) predicts inverted multiplets for the higher partial waves of the $(\bar{Q}q)$ mesons as well. The P-wave charmed mesons $(D^{**})_{uc}$ and bottom meson $(B^{**})_{bu}$ are leading candidates for a test of the prediction.

Inverted multiplets are also predicted for ordinary (qq) mesons for L sufficiently large, since the size of the $(q\bar{q})$ meson is then large enough for the long-range (repulsive) part of the spin-orbit potential to be dominant. [See Fig. 1]. The question is how large L must be before this occurs, with the minimal value of L required being model dependent. Barnes[9] claims, based on a specific model, that inverted multiplets are expected even for L=2 light mesons. [In order to test the data, one must remember that the tensor force mixes $^3S_1$ with $^3D_1$. Our prediction relates to the <u>unmixed</u> $^3D_1$ state]. A particularly promising place to search for inverted multiplets among the ordinary mesons would be the $K\pi$ I=1/2 states, since these states have no gluon admixture. An extension of the SLAC phase-shift analysis to higher energies might be able to examine these

issues in the forseeable future.[10]

The search for inverted meson multiplets may in fact be a test of the non-relativistic picture itself, as the predictions are not sensitive to the details of parameters and wave-functions, and only depend on qualitative features of the model. At this stage, very few workers would be willing to abandon the idea of a Lorentz scalar confining potential. Therefore, a failure of our prediction would provide a direct attack on the validity of the non-relativistic picture itself, in spite of the numerous successes of the N.R. quark model in light hadron spectroscopy. Given the stakes, one presumes that a search for inverted meson multiplets would be well worth the experimental effort.

A persistent problem in meson spectroscopy is that of the $^3P_0$ scalar meson states. Both the experimental and theoretical situation is still confused, due to possible admixture of $(q\bar{q})(q\bar{q})$ states and the gluon continuum with the pure $(q\bar{q})$ scalar states. As we have emphasized throughout this paper, our over-all understanding of the spin-dependent forces as expressed by Fig. 1, is not sensitive to the ultimate resolution of the scalar meson problem.

In conclusion we claim that the spin-dependent forces in both meson and baryon spectroscopy are compatible with one-gluon exchange and a Lorentz scalar confining potential. Further, the search for inverted multiplets will provide an important test of the non-relativistic picture itself.

Acknowledgements

I wish to thank the conference organizers for providing the excellent physics environment which characterized this meeting. During the course of this work, I benefited from frequent conversations with Professor E. Eichten. Comments by Professor N. Isgur are also appreciated.

References

1) N. Isgur, report to this meeting and references therein. See also the report of D. Gromes at this meeting.

2) A. DeRujula, H. Georgi, and S.L. Glashow, Phys. Rev. D12, 147 (1975).

3) H.J. Schnitzer, Phys. Rev. D18, 3482 (1978).

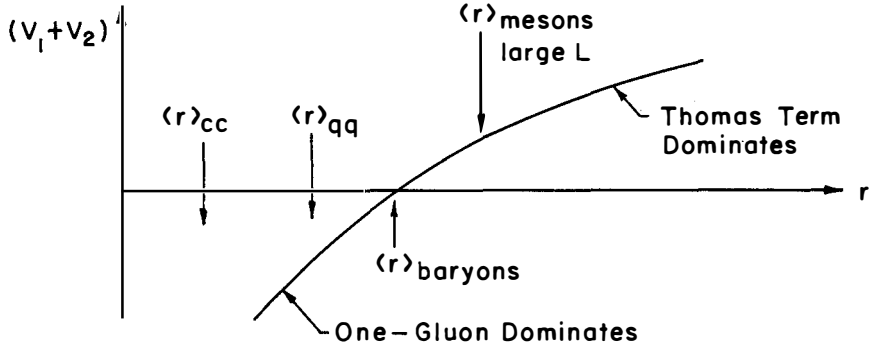

(a) Spin-Orbit Potential

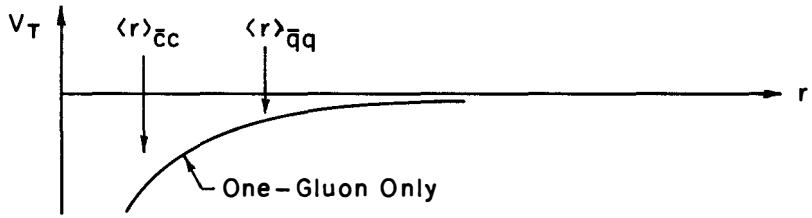

(b) Tensor Potential

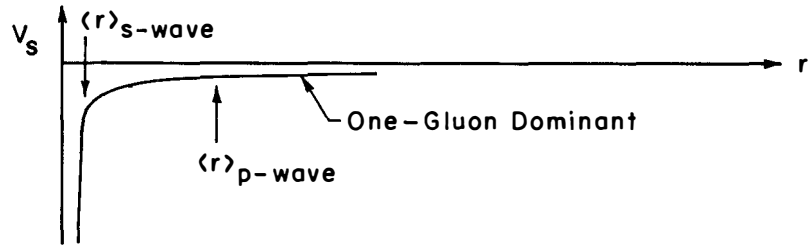

(c) Spin-Spin Potential

FIGURE 1

Qualitative radial dependence of the spin-orbit, tensor, and spin-spin potentials.

4) Particle Data Group, Rev. Mod. Phys. 52, no. 2 (1980).

5) J.A. Dankowych, et al., Phys. Rev. Lett. 46, 580 (1981).

6) D.W.G.S. Leith, Proc. of the 5th International Conference on Experimental Meson Spectroscopy, Boston, MA 1977, pg. 207.

7) The first published report suggesting that the confining potential transforms as a Lorentz scalar is A. Henriques, B. Kellett, and R. Moorhouse, Phys. Lett. 64B, 85 (1976).

8) H.J. Schnitzer, Phys. Lett. 76B, 461 (1978).

9) T. Barnes, report to this meeting and Southampton preprint.

10) B. Ratcliff, report to this meeting.

ψ RADIATIVE DECAYS AND GLUEBALL

R. Lacaze and H. Navelet
DPh-T, CEN Saclay BP n°2, 91191 Gif-sur-Yvette Cedex, France
(Contributed by H. Navelet)

ABSTRACT

It is shown how perturbative QCD at lowest order can be successfully compared with the data for the inclusive J/ψ radiative decays. Our interpretation of the observed γ spectrum allows us to rule out the possibility of gluons having an effective mass and leads to the prediction that the observed E (1440) object has spin 0^-. In the 0^+ sector : glueballs around 1 GeV may contribute, as well as ε and S^* resonances. More accurate data on $\pi\pi$, $K\bar{K}$ and $\eta\eta$ channels would allow to distinguish between these two possibilities for a 0^+ signal which is definitely required by the model.

The radiative decays[1] $\psi \to \gamma X$ are dominated in perturbation theory by $\psi \to \gamma$ + 2 gluons. They thus provide an excellent channel for the search of gluonium states. But the high energy direct photons spectrum casts some doubts about the relevance of the perturbative approach for the inclusive decays. This is clearly shown in Fig.1 curve B which exhibits the discrepancy at large $x(x = \frac{2E_\gamma}{m_\psi})$ between the observed data and the Ore Powell prediction. We have shown[2] that it is possible to reconcile the perturbative approach with the data by taking into account the (non perturbative) hadronization process of the two gluons. Indeed a spin parity analysis[3] of the two gluons system shows that :

i) The 2^+ contribution is dominant.
ii) The $1^\pm$ contribution is forbidden[4].
iii) The $0^+ = 0^-$ contribution is strongly suppressed at W=0 as W^{4Sg+1}[5] where W is the invariant mass of the two gluons and Sg the spin of the gluon. To prove this last point, the argument goes as follow. In the two gluons center of mass, the J=0 configuration corresponds to $\lambda g_1 = \lambda g_2 = \pm$ Sg where λg_i is the gluon i helicity which is invariant under any Lorentz transformation (the gluon is a massless particle). In the ψ system, W near 0 corresponds to $\cos\theta_{12}$ near 1 where θ_{12} is the angle between the two gluons directions ($W^2 \propto (1-\cos\theta_{12})$). The J=0 amplitude is proportional to $D^{Sg}_{\lambda g - \lambda g}(\theta_{12})$ and thus behaves as θ_{12}^{2Sg} or W^{2Sg} near W=0. This J=0 suppression is also responsible for the shape of the spectrum $\psi \to \psi gg \hookrightarrow \pi\pi$[6] because the two pions are produced in an S-wave. Such a suppression does not occur for J=2 because the two configurations $\lambda g_1 = \pm \lambda g_2$ are allowed.

So, naïve Q.C.D. predicts the dominance of the 2^+ contribution at small W or large x $(x=1-(\frac{W}{m_\psi})^2)$. But, as explained in a previous work[3] the two gluons have to materialize at low W mainly into two pions and the short range forces between these pions must lead to the usual threshold behaviour $(W^2-4\mu^2)^{J+1/2}$ in the partial wave cross sections. The 2^+ Q.C.D. width does not exhibit this behaviour which shows that the hadronization in a 2^+ state has to reduce drastically the Q.C.D. width at large x as $(1-x)^{5/2}$. Note that the centrifugal barrier argument does not apply to the J=0$^\pm$ waves. The 0^++0^- Q.C.D. widths can thus be directly compared with the data. As shown in Fig.1 curve A, the $(1-x)^{5/2}$ behaviour fits nicely the large x data ($x \gtrsim .75$ or $W \lesssim 1.6$ GeV) with a rather small value of $\alpha_s \sim .34$. In this region (including the f_o) the actual 2^+ contribution is indeed small. (From experiment the 2^+ contribution at large x is roughly half the pseudoscalar one). Far-away from threshold ($x \lesssim .6$ say) there is no reason that the $J = 2^+$ damping holds. The low energy photon spectrum can thus be described by the Ore Powel formula as it is shown in Fig.1 curve A.

To summarize, the large x region may be described by the 0^+, 0^- and W^5 damped 2^+ contribution, the small x region is well described by the total two gluon contribution. In the transition region the full knowledge of the confinement process would be necessary. The same analysis can be made for the Υ radiative decay from the same spectrum. However the 2^+ damping corresponding to a fixed W range will correspond to a smaller range in x ($x \geq .96$). The inclusive spectrum will thus look like the Ore Powell one.

Another typical prediction of Q.C.D. is the equality between the 0^+ and 0^- production rates. However if η and η'[7] exclusive channel have been observed there is up to now no experimental signal for 2π in an S wave at low energy ($m_{\pi\pi} \lesssim 1$GeV) as in $\psi' \to \psi\pi\pi$. We will return to this point later. In Ref.[2], we have shown that Q.C.D. predictions agree with the observed $\eta+\eta'$ rate with $\alpha_s = .3$. An other exclusive channel has been recently observed $\psi \to \gamma$ E(1440) $\hookrightarrow K\bar{K}\pi$ [8]. If this E is identified with the one E(1420) observed in pp and $\bar{p}p$ collision[9] and known to be a 1^+ state, then the two gluons have to be massive or this single Q.C.D. model has to be abandonned. A non zero mass for the gluons could be interpreted as a confinement effect for the 2g system as is the case for instance in a bag model. We thus study the consequences of an effective gluon mass μ with the three degrees of freedom. (It is possible however that the gluons remain transverse in a bag). We have performed the same spin-parity analysis as before. Now the $1^\pm$ states can be produced provided the helicity 0 is allowed for the massive gluon. The main difference now is that the 0^+ wave is no longer depressed at threshold. (The two massive gluons are now in a relative S wave) even for transverse gluons. Since there is no centrifugal barrier argument for the $J=0^+$ wave, the Q.C.D. 0^+ width in the massive case behaves as $(1-x)^{1/2}$ and, consequently, spoils the $(1-x)^{5/2}$ high x behaviour observed in the massless case. As shown in ref.[1] this rules out the assumption of a gluon effective mass and consequently the 1^+ assignement of this resonance. The $\delta\pi$ decay mode for this resonance forbids a natural parity assignement ($0^+, 2^+, \ldots$) and we are left with the only possibility of 0^-. This 0^- assignment for E(1440) allows one to understand the observed differences with the E(1420). i) No associated D production (spin 1). ii) Dominance of $\delta\pi$ channel (S-wave) over the $K^*\bar{K}$ channel (P-wave) whereas the reverse is true in the case of a pseudovector decay. Identifying from now on the observed E(1440) as a 0^- state, we predict[1] a rate in agreement with experiment for two massless gluons and $\alpha_s = .3$.

The next question is about the 0^+ state, which has not been experimentally observed yet, whereas Q.C.D. predicts that it has to be produced as much as its 0^- partner. We have shown[1] that there is actually room for a non vanishing 0^+

contribution (at a mass around 1 GeV) in the inclusive data when confronted to the sum of all the observed exclusive contributions. A priori the S*(980) and (or) the ε(1300) are good candidates to represent such a 0^+ contribution. However there is still a problem because these S* and ε would decay in $\pi\pi$ and $K\bar{K}$ which have not been seen experimentally yet (all the observed $\pi\pi$ states are compatible with f_o decay products while the $K\bar{K}$ states have been unsuccessfully looked in a search for $\psi \to \gamma f'$ [7], $B(\psi \to \gamma f') * B(f' \to K\bar{K}) < 10^{-3}$). If this experimental situation remains unchanged, there is still the possibility of a 0^+ gluonium state around 1 GeV. Since the $\pi\pi$ and $K\bar{K}$ states are not seen, its main decay channel might be $\eta\eta$ through the η singlet component. Furthermore its 0^- degenerate partner [10] might mix with the η', with possible implications on the mixing problem for the η,η' and E(1440). In this scheme E is not a radial excitation of η-η' but rather a mixture of $q\bar{q}$ and 2g states. Similar conclusions are reached by other authors [11,12].

In conclusion we have been able to obtain semi quantitative agreement between lowest order Q.C.D. prediction and experimental results for radiative J/ψ decay. The shape of the inclusive γ spectrum at high x is understood once one realizes that the $(1-x)^{5/2}$ behaviour of the 0^+ and 0^- production amplitudes, typical of Q.C.D., would also be that of a 2^+ amplitude if non perturbative effects were taken into account. Of course we do not know how to do so in a quantitative way. As far as the exclusive channel are concerned, and since the inclusive γ spectrum behaves as $(1-x)^{5/2}$ at large x, the massive gluon assumption is ruled out and as a consequence the 1^+ assignment for the E(1440) is also excluded. In our scheme the E(1440) resonance has to be a 0^- state and good agreement is obtained for its production rate relative to the other 0^- states η and η'. Finally as the sum of the experimenatlly observed exclusive channels does not saturate the total inclusive spectrum for $x \geq 0.8$, there is room for an expected 0^+ contribution which might be due to a 0^+ glueball around 1 GeV and decaying into $\eta\eta$, unless $\pi\pi$ and $K\bar{K}$ modes are finally discovered. In this latter case, S* and ε production would yield a more conservative interpretation.

The two following experimental investigations are of major interest for definite tests of applications of perturbative Q.C.D. to radiative J/ψ decays. One is to get information on the spin parity of the E(1440) (it should be 0^-). The second is to find evidence for 0^+ states. Apart from the standard yet unseen $\pi\pi$ and $K\bar{K}$, the observation of an $\eta\eta$ state would provide a strong indication for a 0^+ glueball. The E(1440) would be a radial excitation of η,η' if $\pi\pi$ and $K\bar{K}$ happened to be copiously produced, while η,η' and E would be three different mixtures of $q\bar{q}$ (η^1 and η^8) and 2g if $\eta\eta$ final states were observed.

REFERENCES

[1] C.S. Abrams et al., Phys. Rev. Lett. 44 (1980) 114.
[2] R. Lacaze and H. Navelet, Saclay preprint DPh-T 2-81, to be published in Nuclear Physics B.
[3] A. Billoire, R. Lacaze, A. Morel and H. Navelet, Phys. Lett. 80B (1979) 381.
[4] C.N. Yang, Phys. Rev. 77, 242 (1950). The two gluons are in a color singlet.
[5] J.P. Ader, M. Capdeville and H. Navelet, Nuovo Cimento 56A, 315 (1968).
[6] A. Billoire, R. Lacaze, A. Morel and H. Navelet, Nucl. Phys. B155 (1979)493.
[7] a) D.L. Scharre, Proceedings of the XIV Rencontre de Moriond, vol. II (RMIEM Orsay 1979) 219.
b) R. Partridge et al., Phys. Rev. Lett. 44 (1980) 712.
c) W. Braunschweig et al., Phys. Lett. 67B (1977) 243, 74B (1978) 292.
d) G. Alexander et al., Phys. Lett. 72B (1978) 493, 76B (1978) 652.
c) W. Bartel et al., Phys. Lett. 64B (1976) 483, 66B (1977) 489.
[8] D.L. Scharre et al. SLAC, Pub 2514, LBL 10 931, May 1980.
[9] G. Dionisiet al., Nucl. Phys. B169 (1980) 1, see also S.U. Chung's Talk at this meeting.
[10] T. Barnes, Rutherford lab. preprint (1981) RL 81-017, T286 and also Talk at this meeting.
[11] M. Chanowitz, LBL 11 977, Phys. Rev. Lett. 46 (1981) 981.
[12] K. Ishikawa, DESY 80/113, Phys. Rev. Lett. 46 (1981) 978.

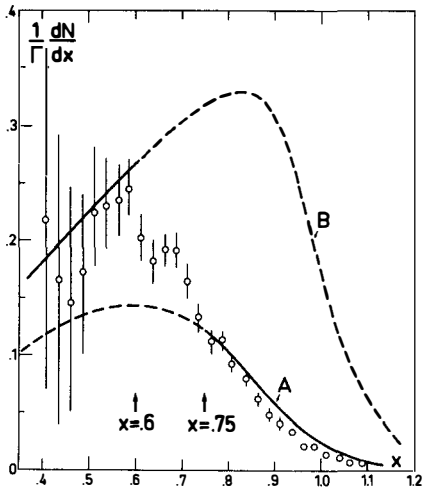

Fig.1 - Inclusive spectrum as a function of $x = \frac{2E_\gamma}{m_\psi}$. Data are from ref.1.
- Curve A $0^+ + 0^-$ contribution for $\alpha_s = .34$ ($\alpha_s = .3$ if a small admixture of the damped 2^+ contribution is allowed).
- Curve B. Total inclusive spectrum for $\alpha_s = .3$.
For curve A and B we have taken into account the photon energy experimental resolution.

BAGS, UNITARITY AND MESON SPECTROSCOPY*

Nils A. Törnqvist
Research Institute for Theoretical Physics
University of Helsinki

ABSTRACT We discuss methods by which one can improve zero width models like the bag model to take into account finite width effects and in particular the associated hadronic mass shifts.

1. Introduction

It is a widely accepted fact that the bag model[1] as well as potential type models[2] generally work to within 20% in predicting masses and static properties of hadrons. However in detailed comparison with experiment there are some obvious difficulties:

i) The strong coupling constant α_s comes out too large (of the order unity) when "hyperfine splittings (ψ-η_c, D^*-K, K^*-K, ρ-π, Δ-N^* etc.) are fitted. Also the Σ-Λ splitting comes out too small.

ii) Meson mixings (ϕ-ω, η-η' etc.) are not fully understood. The simplest gluon annihilation graphs alone give often even the wrong sign for the mixing compared with experiment.

iii) The bag model, as well as the potential model, is really a zero width approximation.

The last point implies that we must in some way take into account the finite hadronic couplings such as $\rho\pi\pi$, $\rho K\bar{K}$, $\rho\omega\pi$, etc. In full generality this is a formidable task since it implies the implementation of unitarity into the model. As extensively discussed already in the early sixties, the mass of any hadron will then, in principle, depend on the masses of all the other hadrons in the theory. In order to compute, say the ρ mass one should include e.g. the loop diagrams $\rho \to \pi\pi \to \rho$, $\rho \to \pi\omega \to \rho$, $\rho \to N\bar{N} \to \rho$, etc. These contributions depend on the masses of π, ρ, ω, N etc.

Unitarity effects are today often neglected. The main motivation for this is that, a posteriori, one finds that effectively they cannot be very big since quark models work reasonably well.

However, unitarity effects do modify any simple zero width prediction to mass spectra and induce violations of the OZI rule. The reason why zero width models work surprisingly well in spite of large hadronic shifts is that the latter are nearly equal and nearly cancel in the off-diagonal elements. Therefore the hadronic shifts can be approximately absorbed by renormalization of the mass parameters in the zero width model. How good is such an approximation? In the following we discuss some recent work related to this question and present some new results from our model calculation.

2. The bag model

In the bag model there are several contributions to the hadron mass matrix. Usually one includes the five terms listed below

M = Bag volume energy ($B \cdot 4\pi R^3/3$)
+ Quark relative kinetic energy (Constant/R)
+ Gluon exchange diagrams (1)
+ Quark masses (m_u, m_d, m_s, m_c, ...)
+ Gluon annihilation diagram.

Let us look in particular at the flavourless states ($u\bar{u}$, $d\bar{d}$, $s\bar{s}$, ...) of a given spin-parity. We can parametrize the contributions of eq. (1) (for four flavours) as:

$$M = \begin{pmatrix} 1 & 0 & 0 & 0 \\ 0 & 1 & 0 & 0 \\ 0 & 0 & 1 & 0 \\ 0 & 0 & 0 & 1 \end{pmatrix} m_0 + 2 \begin{pmatrix} m_u & 0 & 0 & 0 \\ 0 & m_d & 0 & 0 \\ 0 & 0 & m_s & 0 \\ 0 & 0 & 0 & m_c \end{pmatrix} + \begin{pmatrix} 1 & 1 & 1 & 1 \\ 1 & 1 & 1 & 1 \\ 1 & 1 & 1 & 1 \\ 1 & 1 & 1 & 1 \end{pmatrix} a \qquad (2)$$

where the three first terms of eq. (1) are combined in m_0.

3. Finite widths and hadronic shifts

The usual way to introduce finite widths is to introduce an effective coupling constant g_{ABC} describing the break-up of hadron A into two B,C. The width is then given by expressions of the form: $(g_{ABC})^2 \cdot$(phase space)$\cdot$(spin counting factor)$\cdot$(Bose factor). The coupling constants g_{ABC} are related by flavour symmetry predictions such that if we know the quark content of the three mesons A, B and C and their C-parity, then g_{ABC} is obtained through quark line rules:

$$g_{ABC} = \frac{g}{\sqrt{2}} \left[\text{A B C} + C_A C_B C_C \text{ A B C} \right] \qquad (3)$$

On the other hand the widths should also be given by the imaginary part of the mass matrix. This demands that we introduce a sixth term added to eq. (1). For the squared mass matrix we can write:

$$M^2 = M_0^2 + \sum_{ij} \Delta M_{ij}^2 \ , \qquad (4)$$

where ΔM_{ij}^2 is the contribution from a loop diagram with a two particle intermediate state ij

$$(\Delta M^2_{ij})_{AB} =$$ 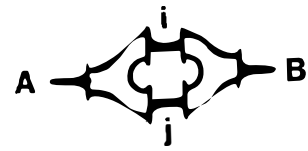

(5)

and which satisfies:

$$(\mathrm{Im}\Delta M^2_{ij})_{AA} = -m_A \Gamma_{A\,ij} \tag{6}$$

The real part $\mathrm{Re}(\Delta M^2_{ij})$ gives the mass shift. For models with hadrons as composite objects of finite size there is an obvious physical reason for a cut-off in the dispersion relation relating the real and imaginary part. Then the mass shift is a finite and computable quantity. Since hadrons are known to have a nearly flavour independent size it is reasonable to, as a first approximation, assume that the cut-off is flavour and spin independent. However, ΔM^2_{ij} will <u>not</u> be flavour-spin independent for kinematical reasons when the thresholds are nondegenerate.

Typical behaviour of $\Delta M^2_{ij}(s)$ for P-wave thresholds are shown in Fig. 1 below.

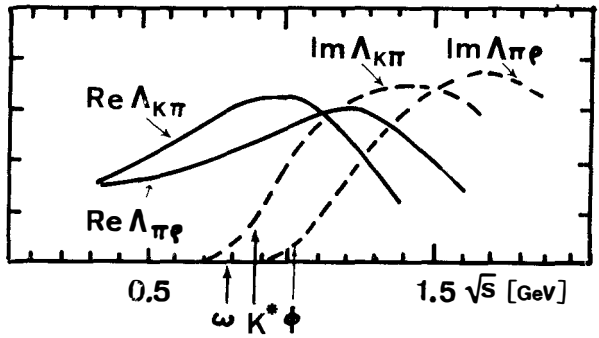

Fig. 1. The behaviour of $\mathrm{Re}\Lambda_{ij}$ and $\mathrm{Im}\Lambda_{ij}$ for the $K\pi$ and $\pi\rho$ threshold.

4. The little and chiral bag

Hadronic shifts due to emission and absorption of pions have been calculated by a Nordita[3] and a CERN[4] group in the little

or chiral bag. Originally in the first paper on the little bag the authors obtained a very large (> 1 GeV) mass shift for the nucleon but more recently using a smaller cut-off they quote a mass shift of -186 MeV for the nucleon and -160 MeV for the delta. This way one can explain a large fraction of the Δ-N mass splitting. The model was motivated by SU(2) x SU(2) chiral symmetry breaking by the confinement mechanism along the lines first discussed by Wilson[5] and Callan, Dashen and Gross [5]. Therefore they only include pions, not kaons nor etas, arguing that the latter are suppressed by the larger energy denominator.

5. The P matrix and hadronic shifts

In a quite different approach Maciel and Pagels[6] recently estimated hadronic shifts by comparing the poles (primitives) of the P matrix of Jaffe and Low[7] with those of the S matrix for a given resonance. In this way they found that the first two particle threshold contributes a mass shift $m_{S\text{-matrix}} - m_{P\text{-matrix}}$ of also typically 100 MeV for the baryons.

6. How many thresholds?

In all models of this kind one encounters the question of how many thresholds should one take into account? The open thresholds must obviously be included in order to have finite widths. But for the mass shift one clearly cannot stop there because the real part behaves rather smoothly at the threshold.

If one does not include strange (and charmed) hadrons as intermediate states one breaks flavour symmetry in a very explicit way. Similarly if one does not include mesons of opposite C-parity the OZI-rule will be grossly violated. In our model[8,9] we therefore sum over complete flavour-spin multiplets of intermediate states. This means a very large number (over 20 with charm included) of thresholds. But, this is an unavoidable computational complication if one wants to have a self-consistent scheme.

7. The hadronic shifts to ρ, ω, φ and ψ

The flavour structure of the hadronic shifts due to the PP and PV thresholds are with obvious notation:

$$\sum_{ij} \Delta M^2_{P_i P_j} = -\gamma^2 \left[\begin{pmatrix} 2 & 0 & 0 & 0 \\ 0 & 0 & 0 & 0 \\ 0 & 0 & 0 & 0 \\ 0 & 0 & 0 & 0 \end{pmatrix} \Lambda_{\pi\pi} + \begin{pmatrix} 1 & 0 & 0 & 0 \\ 0 & 1 & -\sqrt{2} & 0 \\ 0 & -\sqrt{2} & 2 & 0 \\ 0 & 0 & 0 & 0 \end{pmatrix} \Lambda_{K\bar{K}} \right.$$

$$\left. + \begin{pmatrix} 1 & 0 & 0 & 0 \\ 0 & 1 & 0 & -\sqrt{2} \\ 0 & 0 & 0 & 0 \\ 0 & -\sqrt{2} & 0 & 2 \end{pmatrix} \Lambda_{D\bar{D}} + \begin{pmatrix} 0 & 0 & 0 & 0 \\ 0 & 0 & 0 & 0 \\ 0 & 0 & 1 & -1 \\ 0 & 0 & -1 & 1 \end{pmatrix} \Lambda_{F\bar{F}} \right] \tag{7}$$

$$\sum_{ij} \Delta M^2_{P_i V_j} = -4\gamma^2 \left[\begin{pmatrix} 0 & 0 & 0 & 0 \\ 0 & 3 & 0 & 0 \\ 0 & 0 & 0 & 0 \\ 0 & 0 & 0 & 0 \end{pmatrix} \Lambda_{\pi\omega} + \begin{pmatrix} 1 & 0 & 0 & 0 \\ 0 & 0 & 0 & 0 \\ 0 & 0 & 0 & 0 \\ 0 & 0 & 0 & 0 \end{pmatrix} (\Lambda_{\pi\omega} + \sin^2\delta_P \Lambda_{\eta\rho} + \cos^2\delta_P \Lambda_{\eta'\rho}) + \right. \tag{8}$$

$$\begin{pmatrix} 1 & 0 & 0 & 0 \\ 0 & 1 & \sqrt{2} & 0 \\ 0 & \sqrt{2} & 2 & 0 \\ 0 & 0 & 0 & 0 \end{pmatrix} \Lambda_{K\bar{K}^*} + \begin{pmatrix} 0 & 0 & 0 & 0 \\ 0 & 1 & 0 & 0 \\ 0 & 0 & 0 & 0 \\ 0 & 0 & 0 & 0 \end{pmatrix} (\sin^2\delta_P \Lambda_{\eta\omega} + \cos^2\delta_{P\eta'\omega}) + \begin{pmatrix} 0 & 0 & 0 & 0 \\ 0 & 0 & 0 & 0 \\ 0 & 0 & 0 & 0 \\ 0 & 0 & 0 & 1 \end{pmatrix} \Lambda_{\eta_c\psi}$$

$$\left. \begin{pmatrix} 0 & 0 & 0 & 0 \\ 0 & 0 & 0 & 0 \\ 0 & 0 & 2 & 0 \\ 0 & 0 & 0 & 0 \end{pmatrix} (\cos^2\delta_P \Lambda_{\eta\phi} + \sin^2\delta_P \Lambda_{\eta'\phi}) + \begin{pmatrix} 1 & 0 & 0 & \sqrt{2} \\ 0 & 0 & 0 & 0 \\ 0 & 0 & 0 & 0 \\ \sqrt{2} & 0 & 0 & 2 \end{pmatrix} \Lambda_{D\bar{D}^*} + \begin{pmatrix} 0 & 0 & 0 & 0 \\ 0 & 0 & 0 & 0 \\ 0 & 0 & 1 & 1 \\ 0 & 0 & 1 & 1 \end{pmatrix} \Lambda_{F\bar{F}^*} \right],$$

The VV thresholds are similar to the PP except for an over all weight factor of 7 in the exact $SU(6)_W$ limit. The function $\Lambda_{ij} = \Lambda(s, m_i^2, m_j^2)$ is an analytic function with correct threshold behaviour (c.f. Fig. 1). The angle δ_P is the deviation from ideal mixing for the P mesons. The corresponding angle δ_V for the vector mesons has in eqs. (7,8) been put equal to zero for simplicity, but not in the numerical calculations. In eqs. (7,8) we have summed over charge states e.g. the $\Lambda_{K\bar{K}}$ term is a sum over K^+K^- and $K^0\bar{K}^0$ putting $m_{K^+} = m_{K^0}$. In general we allow for $m_{K^+} \neq m_{K^0}$ which gives a small but nonvanishing isospin breaking ρ-ω matrix element since the K^+K^- and $K^0\bar{K}^0$ contributions do not cancel exactly.

If one analoguously neglects the flavour SU(3) breaking for the PP and PV thresholds the terms in eqs. (7) and (8) can be summed giving (neglecting charm):

$$\Delta M^2_{PP} = -\gamma^2 \begin{pmatrix} 3 & 0 & 0 \\ 0 & 1 & -\sqrt{2} \\ 0 & -\sqrt{2} & 2 \end{pmatrix} \Lambda_{PP}, \qquad M^2_{PV} = -\gamma^2 \begin{pmatrix} 3 & 0 & 0 \\ 0 & 5 & \sqrt{2} \\ 0 & \sqrt{2} & 4 \end{pmatrix} \Lambda_{PV}, \tag{9,10}$$

which in a frame of pure SU(3) states (ρ,ω_8,ω_1) are diagonal:

$$\Delta M^2_{PP} = -\gamma^2\begin{pmatrix}3&0&0\\0&3&0\\0&0&0\end{pmatrix}\Lambda_{PP}, \qquad M^2_{PV} = -\gamma^2\begin{pmatrix}3&0&0\\0&3&0\\0&0&6\end{pmatrix}\Lambda_{PV}. \tag{11,12}$$

Thus in the exact SU(3) limit, F-coupled states shift the singlet twice as much as the octet. Note the selfconsistency: An SU(3) symmetric input gives an SU(3) symmetric output with a definite singlet-octet splitting. In order to have near octet-singlet degeneracy and good OZI rule in the output, the F and D coupled threshold must contribute nearly equally.

For the vector and heavier mesons this turns out to be consistent with $SU(6)_W$ conditions on the coupling constants VPP, VPV and VVV. For the pseudoscalars on the other hand the F coupled loops $P \to PV \to P$ are dominant giving rise to large η-π splitting and large deviation from ideal mixing.

8. Signs of mass splittings and mixing angles

Assuming that the nearest thresholds are the most important some simple sign rules emerge for the SU(2) singlet-triplet mass difference, for the SU(3) singlet-octet mass splitting, and for the deviation from ideal mixing (δ):

$$\text{sign}\,(m_A^{\text{singlet}} - m_A^{\text{triplet}}) = \text{sign}\,(\delta_A) = -(-)C_AC_BC_C, \tag{13}$$

When applied to the usual meson nonets one gets the predictions of Table 1.

Multiplet	Nearest group of thresholds	$-C_AC_BC_C$	Experimental sign δ	Experimental sign "ω"-"ρ"
0^{-+}	PV	+	+ ($+44^o$)	+ (η-π)
1^{--}	PP	+	+ ($+3^o$)	+ (δ-ρ)
2^{++}	PP	-	- (-10^o)	- (f-A_2)
0^{++}	PP	-	?	? (ε-δ)
1^{++}	PV	+	+ ?	+ (D-A_1)
1^{+-}	PV	-	?	-?(H-B)

Table 1 The sign rules of eq. (13) compared with experiment.

The signs are predicted correctly in all seven cases where the experimental situation is unambiguous. For the scalar mesons the sign rule suggests the low ε mass alternative ($m_\varepsilon < m_{\delta(980)}$). For the 1^{++} nonet a positive δ is predicted agreeing with the analysis of Dionisi et al.[10]. The H-B mass difference is predicted to be negative in agreement with the recent measurement[11] m(H) = 1190 ± 60 MeV. In comparison, if gluon annihilation graphs with transverse gluons are assumed to be dominant all signs of table 1 should be negative.

9. Fits to the vector and pseudoscalar mesons

In the numerical work we compute the mass matrices for the vector and pseudoscalar mesons including all PP, PV and VV thresholds. Taking into account both the charmed states and the non-degeneracy of isospin related thresholds this amount to 34 different thresholds for the ρ^0,ω,ϕ, and ψ and 24 for the other vector meson states. In table 2 below preliminary results for the vector mesons are summarized including charm, but with $m_u=m_d$. (For results without charm and for more details on the model see Ref.[9].)

Quantity	Experiment	Model	Quantity	Experiment	Model
m_ψ	3.097	<u>3.097</u>	Γ_ρ	0.158	<u>0.158</u>
m_{F^*}	2.14	2.137	Γ_{K^*}	0,050	0.051
$m_{D^{*o}}$	2.006	2.073	Γ_ϕ	0.0041	0.0045
m_ϕ	1.0196	<u>1.0196</u>	$\Gamma_{D^{*+}}^{\text{hadronic}}$		16.5 keV
$m_{K^{*+}}$	0.8918	0.8908	$\Gamma_{D^{*0}}^{\text{hadronic}}$		31.5 keV
			Branching ratios:		
m_ρ	0.771	0.768	$\phi \to K^0\bar{K}^0$	37.7 %	35.3 %
m_ω	0.7824	<u>0.7824</u>	$\phi \to K^+K^-$	52.1 %	53.1 %
ϕ-ω		38.5^o	$\phi \to \rho\pi$	6.7 %	6.3 %

<u>Table 2</u> Predictions for the vector mesons. The four underlined numbers essentially fix four of the five parameters of the model. The units are in GeV except when otherwise indicated.

Quantity	Experiment	Model	Quantity	Experiment	Model
m_{η_c}	2.978	2.978	$m_{\eta'}$	0.9576	0.9576
m_F	2.030	2.010	m_η	0.5488	0.5486
m_{D^o}	1.8631	1.874	m_{K^o}	0.4977	0.4988

Table 3 Predictions for pseudoscalar meson masses in units of GeV.

The model has only five free parameters besides the cut off (= 0.6 GeV/c corresponding to a hadron size of 0.8 fm). These are (i) the "bare" ω mass $m_0 + 2m_u = 1.190$ GeV which is essentially fixed by the physical ω mass, (ii) $m_0 + 2m_s = 1.306$ GeV (fixed by m_ϕ), (iii) $m_0 + 2m_c = 3.120$ GeV (fixed by m_ψ), (iv) the over all coupling constant g_{VPP} (fixed by Γ_ρ), (v) a $SU(6)_W$ violating parameter $g^{eff}_{VVV}/g_{VPV} = 0.717$ which by exact $SU(6)_W$ would be 1.

With these parameters altogether 13 data points are fitted well except the D^* mass which comes out a little too high. Although some of the predictions are not independent the over all fit is a success. More significantly when applying the model to the pseudoscalars one finds also a quite good fit for all states except the pion, with parameters close to those for the V-meson fit (m_0+2m_u = 1.145 GeV $m_0+2m_s = 1.323$ GeV, $m_0+2m_c = 3.021$, $g_{PPV} = 0.66\ G_{VPP}$). The results are shown in Table 3 above.

I would like to thank Lucien Montanet and Tran Thanh Vanh for a most enjoyable and enlightening conference.

References

1) T. DeGrand, R.L. Jaffe, K. Johnson and J. Kiskis, Phys. Rev. D10 (1974) 2599 and D12 (1975) 2060.
2) N. Isgur and G. Karl, Phys. Lett. 72B (1977) 109
N. Isgur, lecture notes of Erice School of Subnuclear Physics 1978.
3) G.E. Brown and M. Rho, Phys. Lett. B82 (1979) 177.
G.E. Brown, M. Rho and V. Vento, Phys. Lett. B84 (1979) 383.
4) W.N. Nottingham, K. Tsu and J.M. Richard, Nucl. Phys. B179 (1981) 541.
5) K.G. Wilson, Phys. Rev. D10 (1974) 2445.
C.G. Callan, R.F. Dashen and D.J. Gross, Phys. Rev. D19 (1979) 1826.
6) R.L. Jaffe and F. Low, Phys. Rev. 19 (1979) 2105.
7) A.K.A. Maciel and J.E. Paton, Nucl. Phys. B181 (1981) 277.
8) N.A. Törnqvist, Ann. of Phys. 123 (1979) 1.
9) M. Roos and N.A. Törnqvist, Zeit. Physik C5 (1980) 205 and to be published.
10) C. Dionisi et al., Nucl. Phys. B169 (1980) 1.
11) J.A. Dankowych et al., "Evidence for I=1 (A_1) and I=0 H axial-vector resonance in charge exchange", preprint DOE/ER/01545-304.

WHAT HAVE WE LEARNED FROM SYMMETRIES AND/OR THE QUARK MODEL

Patrick J. O'Donnell
Dept. of Physics and Scarborough College
University of Toronto
West Hill, Ontario M1C 1A4
Canada

ABSTRACT

The ideas of vector dominance, SU(3) symmetry and the quark model which have evolved over the past twenty-four years are reviewed in the light of new data on the radiative decays of mesons. It is emphasized that new experimental measurements of the decays $\omega \to \pi\gamma$ and $K^{*0} \to K^0\gamma$ take on an added importance.

The vector dominance model was invented twenty-four years ago.[1] Within the next few years many applications of vector dominance and SU(3) symmetry were given,[2,3] details of which can now be found in many books and review articles. By the end of 1965 the quark model had been used to estimate some of the decays of vector mesons in a non-relativistic approach based on the analogy with M1 transitions in hydrogen-like atoms. Within the past six years or so much new experimental data have appeared on radiative decays, the most recent of which is discussed by Ferbel in his talk and which has just been published.[4] Due to the amount and accuracy of much of these new data it is now possible to take a critical look at the predictions of symmetries and the quark model.

Vector Dominance. We begin by examining the vector dominance model.[3] The electromagnetic current $j_\mu(x)$ is written in terms of the ρ,ω and ϕ field operators in the following definition.

$$j_\mu = \frac{em_\rho^2}{2\gamma_\rho}\rho_\mu + \frac{em_\omega^2 \sin\theta_V}{2\sqrt{3}\gamma_Y}\omega_\mu + \frac{em_\phi^2\cos\theta_V}{2\sqrt{3}\gamma_Y}\phi_\mu \ . \tag{1}$$

In the limit of SU(3) symmetry $\gamma_Y = \gamma_\rho$. The angle θ_V is the usual vector meson mixing angle by which the physical ω and ϕ states are defined in terms of the octet ω_8 and singlet ω_1 states as follows:

$$\phi = \omega_8\cos\theta_V - \omega_1\sin\theta_V \tag{2a}$$

$$\omega = \omega_8\sin\theta_V + \omega_1\cos\theta_V. \tag{2b}$$

From Eqs. (1) and (2) we can immediately obtain a formula for the width of the decay of a vector meson into e^+e^- pairs,

$$\Gamma(V\to e^+e^-) \simeq (\pi\alpha^2/3)m_V g_{V\gamma}^2 \tag{3}$$

where $g_{\rho\gamma}\equiv\gamma_\rho^{-1}$, $g_{\omega\gamma}\equiv\sin\theta_V/(\sqrt{3}\gamma_Y)$ and $g_{\phi\gamma}\equiv\cos\theta_V/(\sqrt{3}\gamma_Y)$. When θ_V has the value $\tan^{-1}(1/\sqrt{2})$ (ideal mixing) the SU(3) relation is $g_{\rho\gamma}^2 : g_{\omega\gamma}^2 : g_{\phi\gamma}^2 = 9:1:2$ is obtained. In Fig. 1 we show the results of such a condition in the case where $\Gamma(\phi\to e^+e^-)$ has been arbitrarily set to a value of 2. The definition, Eq. (1), is only one among many ways of defining the coupling of the ρ,ω and ϕ mesons to the electromagnetic current. Following the conventional wisdom SU(3) symmetry has been applied to obtain the ratio 9:1:2 but in the phase space calculations the physical masses have been used. Other choices can be made and again, in Fig. 1, the quantity $m_V\Gamma(V\to e^+e^-)$ has also been compared to the SU(3) ratio. From this example we can see that deviations from SU(3) symmetry

are, to some extent, a matter of definition!

In the quark model the mesons are formed, of course, from $q\bar{q}$ states. It turns out to be more convenient to measure the difference of the mixing angles from the ideal mixing angle $\hat{\theta}=\tan^{-1}(1/\sqrt{2})$. We define $\alpha_V=\theta_V-\hat{\theta}$ and $\alpha_p=\theta_p-\hat{\theta}$ for the vector- and pseudoscalar-mesons, respectively. The physical states are then given by

$$\phi = \cos\alpha_V(-s\bar{s}) - \sin\alpha_V(u\bar{u}+d\bar{d})/\sqrt{2} \tag{4a}$$

$$\omega = \sin\alpha_V(-s\bar{s}) + \cos\alpha_V(u\bar{u}+d\bar{d})/\sqrt{2}$$

for the vector mesons and by

$$\eta = \cos\alpha_p(-s\bar{s}) - \sin\alpha_p(u\bar{u}+d\bar{d})/\sqrt{2}$$

$$X = \sin\alpha_p(-s\bar{s}) + \cos\alpha_p(u\bar{u}+d\bar{d})/\sqrt{2}$$

for the pseudoscalars. Recent values[5] for the widths of decays $\eta\to\gamma\gamma$ and $\pi\to\gamma\gamma$ are 323±46 eV and 7.86±0.54 eV respectively. In a straightforward application of the quark model the ratio of the widths for these two decays is given by

$$\frac{\Gamma(\eta\to\gamma\gamma)}{\Gamma(\pi\to\gamma\gamma)} \sim 20[1-2\sqrt{2}\tan\theta_p]^2 \ . \tag{5}$$

A value of $\theta_p\sim-10^o$, consistent with a quadratic mass formula, brings this ratio to 41 in agreement with experiment.[3] An example of vector dominance occurs in the relationship between the coupling for the decay $\pi\to\gamma\gamma$ and for $\rho^-\to\pi^-\gamma$, viz.,

$$g_{\pi\gamma\gamma} = \frac{e}{3\gamma_p} g \tag{6}$$

where $g_{\rho\pi\gamma}\equiv g/3$. As we mentioned above such a relationship presupposes a specific prescription on how one extracts mass factors and where SU(3) symmetry breaking is to be imposed. I shall choose to make the couplings dimensionless by removing a common mass factor m_π^{-1} from all couplings and assume physical masses in subsequent phase space calculations. The motivation for such a choice is that when we compare with the quark model the coupling g will be a multiple of the magnetic moments of the quarks in the simplest approximation. We have the ratio of widths under such a prescription given by

$$\frac{\Gamma(\rho^- \to \pi^- \gamma)}{\Gamma(\pi^o \to \gamma\gamma)} = \frac{16}{3\alpha}\left(\frac{k}{m_\pi}\right)^3 (\gamma_p^2/4\pi) \tag{7}$$

and from the reported width[5] $\Gamma(\pi \to \gamma\gamma) = 7.86 \pm 0.54$ eV, a prediction $\Gamma(\rho^- \to \pi^- \gamma) = 58 \pm 8$ keV, to be compared with the recent new evaluation[6] of 67 ± 7 keV. Finally, in this discussion of the vector dominance model we list the various relationships among the coupling constants of interest in meson decays.

$$g_{\rho^o\pi^o\gamma} = g/3 \tag{8a}$$

$$g_{\omega\pi\gamma} = \frac{1}{3}\{\sqrt{2}(g-g_1)\sin\alpha_V + (2g_1+g)\cos\alpha_V\} \tag{8b}$$

$$g_{\phi\pi\gamma} = \frac{1}{3}\{\sqrt{2}(g-g_1)\cos\alpha_V - (2g_1+g)\sin\alpha_V\} \tag{8c}$$

$$g_{K^*K^oK^o\gamma} = -\frac{2}{3}g \tag{8d}$$

$$g_{K^{*\pm}K^\pm\gamma} = g/3 \tag{8e}$$

$$g_{\rho\eta\gamma} = \frac{1}{3}\{\sqrt{2}(g-g_1')\cos\alpha_P - (2g_1'+g)\sin\alpha_P\} \tag{8f}$$

$$g_{X\rho\gamma} = \frac{1}{3}\{\sqrt{2}(g-g_1')\sin\alpha_P + (2g_1'+g)\cos\alpha_P\} \tag{8g}$$

$$\begin{aligned} g_{\omega\eta\gamma} = {} & \frac{1}{9}\cos\alpha_V\sin\alpha_P(g-2g_1'-2g_1) - \frac{2}{9}\sin\alpha_V\cos\alpha_P(g+g_1'+g_1) \\ & + \frac{\sqrt{2}}{9}\sin\alpha_V\sin\alpha_P(g-2g_1'+g_1) + \frac{\sqrt{2}}{9}\cos\alpha_V\cos\alpha_P(-g-g_1'+2g_1) \end{aligned} \tag{8h}$$

$$\begin{aligned} g_{\phi\eta\gamma} = {} & -\frac{1}{9}\sin\alpha_V\sin\alpha_P(g-2g_1'-2g_1) - \frac{2}{9}\cos\alpha_V\cos\alpha_P(g+g_1'+g_1) \\ & + \frac{\sqrt{2}}{9}\cos\alpha_V\sin\alpha_P(g-2g_1'+g_1) - \frac{\sqrt{2}}{9}\cos\alpha_V\cos\alpha_P(-g-g_1'+2g_1) \end{aligned} \tag{8i}$$

$$\begin{aligned} g_{X\omega\gamma} = {} & -\frac{1}{9}\cos\alpha_V\cos\alpha_P(g-2g_1'-2g_1) - \frac{2}{9}\sin\alpha_V\sin\alpha_P(g+g_1'+g_1) \\ & - \frac{\sqrt{2}}{9}\sin\alpha_V\cos\alpha_P(g-2g_1'+g_1) + \frac{\sqrt{2}}{9}\cos\alpha_V\sin\alpha_P(-g-g_1'+2g_1) \end{aligned} \tag{8j}$$

$$\begin{aligned} g_{\phi X\gamma} = {} & \frac{1}{9}\sin\alpha_V\cos\alpha_P(g-2g_1'-2g_1) - \frac{2}{9}\cos\alpha_V\sin\alpha_P(g+g_1'+g_1) \\ & - \frac{\sqrt{2}}{9}\cos\alpha_V\cos\alpha_P(g-2g_1'+g_1) - \frac{\sqrt{2}}{9}\sin\alpha_V\sin\alpha_P(-g-g_1'+2g_1) \end{aligned} \tag{8k}$$

where g, g_1 and g_1' denote the couplings $V_8P_8\gamma$, $V_1P_8\gamma$ and $V_8P_1\gamma$ respectively.

The Quark Model. An early triumph of the quark model was the calculation of M1 transition between $^3S_1$ and $^1S_0$ meson states formed from (non-relativistic) $q\bar{q}$ states. The approach used was obtained by the analogy with similar decays in hydrogen-like atoms.[7,8] The strength of this approach lies in the connection of the decay matrix elements to the static magnetic moments of the baryons. Since Overseth will discuss in a following talk the new measurements of these magnetic moments it will be sufficient to note here that the new measurements appear to force explicit SU(3) symmetry breaking in the static limit. That is we write the magnetic moment operator as

$$\underset{\sim}{M} = (2/3)\mu_u \underset{\sim}{\sigma}_u - (1/3)\mu_d \underset{\sim}{\sigma}_d - (1/3)\mu_s \underset{\sim}{\sigma}_s \qquad (9)$$

where $\mu_q = (2m_q)^{-1}$, for point-like Dirac particles. With the quark masses fixed from the observed magnetic moments of the P,N and Λ the quark masses turn out to be $m_u = 338$ MeV, $m_d = 322$ MeV and $m_s = 606$ MeV. The overall predictions are listed in Table I and the comparison with experiment seems to be fair but not exceptionally good.

Table I. The baryon magnetic moments (in units $e\hbar/2m_p c$) in the simple static quark model with differing quark masses.

Baryon	Prediction	Experiment
P	2.792846	2.7928456(11)
N	-1.913042	-1.91304184(88)
Λ	-0.6138	-0.6138±0.0047
Ξ^-	-0.5	-0.75±0.06
Ξ^o	-1.44	-1.237±0.160
Σ^+	2.26	2.33±0.13
Σ^-	-1.03	-1.48±0.37

Given the static magnetic dipole operator we are now in a position to evaluate the $^3S_1 \to {}^1S_0 + \gamma$ transition matrix elements in the long wavelength approximation[7] (i.e., setting $\exp(i\underset{\sim}{k}\cdot\underset{\sim}{r}) \sim 1$). This approach has been considered[2] to be one of the strengths of the quark model since it seems to permit a prediction of the magnitude of the decay $\omega \to \pi\gamma$, say, whereas previously we could only relate such a decay to others using vector dominance arguments. Alas, a closer look at the approximations involved show that this conclusion does not appear to be warranted. To see why we note[3,8] that in a non relativistic treatment the bound state wave functions are usually normalized in a non-covariant way $\langle f | i \rangle = \delta_{fi}$ and the transition matrix element for the decay

$i \to f + \gamma$ is then regarded[8] as an approximation to the covariant matrix element T_{fi}. Thus we obtain

$$\Gamma(V \to P\gamma) = \frac{e^2}{2\pi} \frac{\omega E_P}{m_V} \int \frac{d\Omega}{4\pi} \sum |M|^2 \tag{10}$$

where $E_P = \sqrt{\omega^2 + m_P^2} = (m_V^2 + m_P^2)/2m_V$ and $\omega = |k| = (m_V^2 - m_P^2)/2m_V$. The matrix element for M1 decays is

$$eM \sim \mu_q e_q \sigma \cdot k \times \varepsilon + \ldots \tag{11}$$

so that, for example,

$$\Gamma(\omega \to \pi\gamma) = \frac{4}{3}\alpha\mu^2\omega^3 \left(\frac{E_\pi}{m_\omega}\right). \tag{12}$$

In the original calculations the factor (E_π/m_ω) was set equal to one, the justification being that it arises from non-relativistic phase space and in such a case we should assume that ω is small. Alternatively, comparison may be made with the vector dominance calculations, which are relativistic calculations and do not have such a factor. With $(E_\pi/m_\omega) \approx 1$, Eq. (12) predicts a width of 1.17 MeV to be compared with the 1965 experimental value of 1.2 MeV. If, on the other hand, we use the physical masses (E_π/m_ω) is approximately 1/2, leading to a prediction of about 600 keV instead for this decay. The Particle Data Group[5] give a world average value of 889±57 keV for this decay and a recent re-evaluation[10] of this data suggests that the width may be even lower, at 789±92 keV. The important point from the point of view of the experimental data is that a more careful determination of the neutral decay modes of the ω is needed since a small deviation from the assumption $\omega \to \pi\gamma \equiv \omega \to$ neutrals can lower the width for $\omega \to \pi\gamma$ considerably. From the theoretical point of view it would seem that there remains an important ambiguity in the application of the simple quark model, which has a major effect on the calculation of an absolute rate of decay. It does not appear possible to predict the magnitude of the decay $\omega \to \pi\gamma$, say, but only to evaluate it relative to other decays.[11]

Having given up our attempt to predict an absolute rate we can compare the quark model with the vector dominance model. In the simplest approach, with all quark magnetic moments kept equal, the predictions are exactly equivalent to those following from Eq. (8) with $g = g_1 = g_1'$ (nonet symmetry) and are shown in Fig. 2. The agreement overall is reasonable considering that the results do not represent a fit to the data. The results of two recent attempts to fit the data are given in Table II below.

Table II. In this table we show two recent fits to the experimental data. Also shown are the experimental data of the Particle Data Group[5] (col. 1) and a recent critical re-evaluation of this data[10] (col. 3).

			Ohshima[10]	Geffen and Wilson[12]
$\rho\pi\gamma$	38±11 keV	67±7 keV	67±7 keV	67 keV
$\omega\pi\gamma$	889±56 keV	789±92 keV	789±120 keV	861 keV
$\phi\pi\gamma$	5.7±2.1 keV	6.5±1.9 keV	11.1±14.5 keV	5.9 keV
$K^{*o} \to K^o \gamma$	75±35 keV	75±35 keV	147±16 keV	139 keV
$K^{*-} \to K^- \gamma$	-	62±14 keV	37.5±4 keV	96 KeV
$\rho \to \eta\gamma$	50±13 keV	52.5±13.7 keV	45.6±21.7 keV	57 keV
	76±15 keV	79.8±15.9 keV		
$X \to \rho\gamma$	83±30 keV	93.1±25.1 keV	93.1±24 keV	108 keV
$\omega \to \eta\gamma$	3.0±2.5 keV	3.2±2.6 keV	9±2.5 keV	4.4 keV
	29±7 keV	30.5±7.4 keV		
$\phi \to \eta\gamma$	62±9 keV	67.7±9.5 keV	137±18 keV	57 keV
$X \to \omega\gamma$	7.6±3.1 keV	8.4±2.7 keV	8.4±2.4 keV	8.7 keV

Conclusions: It would appear that the old ideas on symmetries, vector dominance and the quark model do reasonably well in accounting for the radiative decays of the "old" mesons, since, with few parameters many decays are related. From the experimental point of view it would be nice to have another determination of the decay $K^{*o} \to K^o \gamma$ and a careful re-evaluation of the $\omega \to \pi\gamma$ width. The future importance of these processes for theory lies in the role they play in determining the properties of the light quark bound states. For example, in a calculation of the meson spectra[13] it turned out that these decays played a crucial part in determining the correct eigenvectors in the mixing problem of radially excited states. With the renewed interest in the possibility of glueball states and the likelihood that there will be important mixing effects among these and the conventional $q\bar{q}$ states the radiative decays will remain a crucial theoretical test.

REFERENCES

1. Y. Nambu, Phys. Rev. 106, 1366 (1957).
2. For example, F.E. Close, An Introduction to Quarks and Partons (Academic Press, 1979).
3. P.J. O'Donnell, Radiative Decays of Mesons, Rev. Mod. Physics (to appear). This article contains many references omitted in this talk.

4. D. Berg et al., Phys. Lett. 98B, 119 (1981).
5. Particle Datas Group, Rev. Mod. Phys. 52, 51 (1980).
6. D. Berg et al., Phys. Rev. Lett. 44, 706 (1980).
7. G. Morpurgo, in "Theory and Phenomenology in Particle Physics" (ed. A. Zichichi, Academic Press 1969) p. 84.
8. A review covering the application of M1 transitions in atomic and particle physics is given by J. Sucher, Rep. Prog. Phys. 41, 1781 (1978).
9. O. Overseth, following talk.
10. T. Ohshima, Phys. Rev. D22, 707 (1980).
11. See P.J. O'Donnell, Can. J. Phys. 55, 1301 (1977) for a fuller treatment of this phase space problem.
12. D.A. Geffen and W. Wilson, Phys. Rev. Lett. 44, 370 (1980).
13. R.H. Graham and P.J. O'Donnell, Phys. Rev. D19, 284/1979).

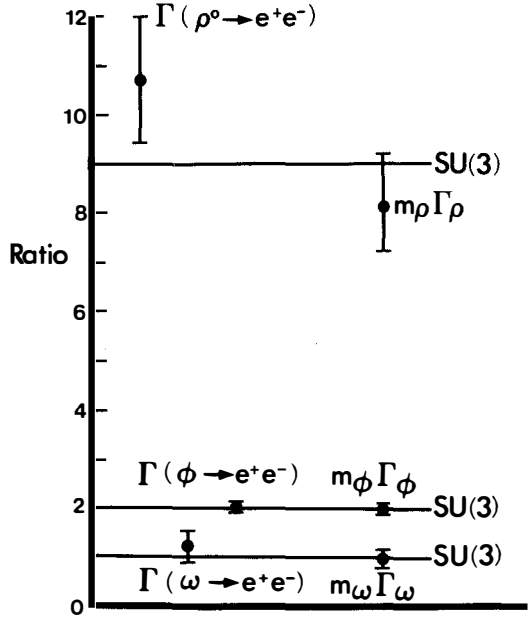

Fig. 1. Ratios of widths and of mass x widths are shown for the leptonic decays of the ρ,ω and φ mesons. Here Γ_ρ denotes the width for $\rho \to e^+e^-$ and similarly Γ_ω,Γ_ϕ denote the widths for $\omega \to e^+e^-$ and $\phi \to e^+e^-$. The data are from the Particle Data Group.[5] The value 2 is arbitrarily given to Γ_ϕ or $m\phi\Gamma\phi$ and the other quantities are shown relative to this.

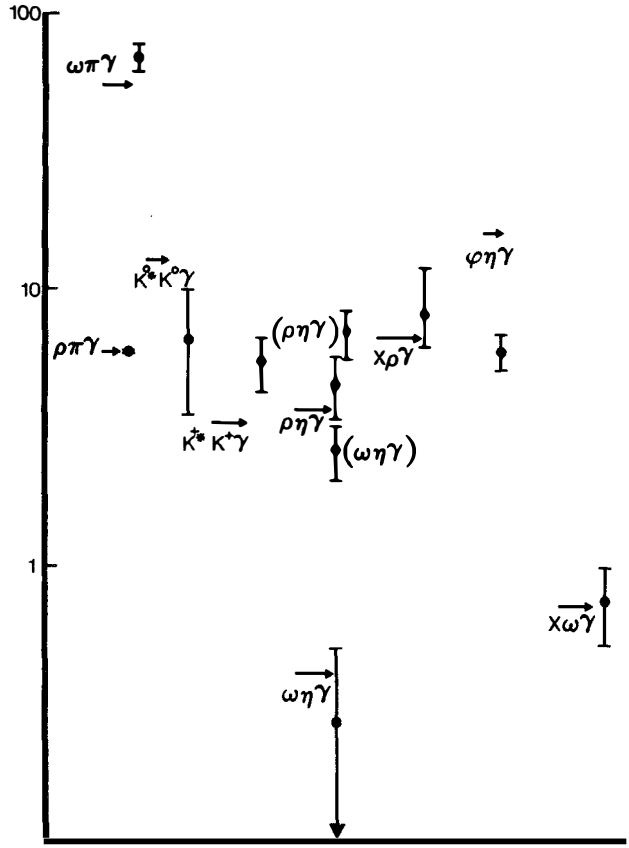

Fig. 2. The arrows show the predicted values of the radiative decay in the simple case as discussed in the text. The mixing angles were chosen to be $\alpha_V=0$ and $\alpha_P=-45^o$. The ambiguous experimental determinations of $\rho\to\eta\gamma$ and $\omega\to\eta\gamma$ are shown with the parenthesis denoting one of the two solution fits.

HEAVY MESONS, HEAVY BARYONS AND HEAVY MULTIQUARKS IN POTENTIAL MODELS

J.M. Richard
Division de Physique Théorique, IPN Orsay, France and CERN, Geneva, Switzerland

ABSTRACT

We review some recent work done on heavy hadron spectroscopy in the framework of potential models. We stress the difficulty of deducing the QQQ or $QQ\bar{Q}\bar{Q}$ potential energy from the $Q\bar{Q}$ potential if the latter is purely empirical. On the other hand, the bag model, although quite involved to handle, provides a unified derivation of the potential governing the quarks inside the mesons, the baryons, and the multiquarks.

RESUME

Nous passons en revue certains travaux récents sur la spectroscopie des hadrons lourds à l'aide de potentiels non relativistes. L'accent est mis sur la difficulté qu'il y a à déduire l'énergie potentielle des systèmes QQQ et $QQ\bar{Q}\bar{Q}$ à partir du potentiel $Q\bar{Q}$ si ce dernier est purement phénoménologique. Le modèle des sacs, quoique un peu compliqué, permet par contre de passer sans ambiguïté du cas des mésons à celui des baryons ou des multiquarks.

1. HEAVY MESONS

The ability of potential models to describe the spectrum of heavy mesons is now well established. Logarithmic or power-law potentials are especially attractive, because of their simplicity and their nice scaling properties[1]. For instance, A. Martin recently proposed a potential[2]

$$V^{I}(r) = A + Br^{\beta} , \qquad \beta = 0.100 . \tag{1}$$

He successfully fitted the T, J/ψ, F($c\bar{s}$), and ϕ families. The ϕ family means the $\phi(1020)$, the DCI $\phi'(1650)$ [3], and the E(1.42), with $J^{PC} = 1^{++}$ interpreted here as an $s\bar{s}$ P-state rather than as a glueball[4]. Moreover, the quark masses used in the fit are compatible with the experimental value of $M_D - M_K$ and $M_B - M_K$.

Simple potentials such as V^{I} can be understood as a parametrization of the intermediate-range part of more traditional potentials, which are of the type "Coulomb-plus-linear"[5]

$$V^{II}(r) = -\frac{4}{3}\frac{\alpha_s}{r} + \lambda r + b , \tag{2}$$

and provide also very good fits[6]. The form of V^{II} has clear theoretical motivations. The Coulomb term comes from one-gluon exchange, and the linear behaviour at large distances is common to strong coupling expansion, and to string or bag models.

The bag model, precisely, provides a continuous interpolation from the Coulomb régime to the vortex limit. This application of the bag model was first presented at Moriond in 1975 by Hasenfratz, Kuti and Szalay[7] and has recently been developed in more detail[8-10]. The bag model for heavy quarks is basically the same as the one for light quarks. It is, however, handled differently. In the latter case, the MIT group assumed that highly relativistic quarks oscillate freely inside a fixed spherical cavity. The mass of the hadrons was obtained by minimization on the radius[11]. The case of heavy quarks, on the other hand, is treated in an adiabatic approximation similar to the Born-Oppenheimer treatment of the molecular spectrum. For a given interquark separation, the bag energy is minimized with respect to the size and the shape of the bag. The minimum is then plugged into the Schrödinger equation as the $Q\bar{Q}$ potential. In other words, this picture means that the bag re-adjusts itself almost immediately to an optimal configuration when the quarks move. With only two parameters -- the QCD coupling constant α_s and the bag pressure B -- the $Q\bar{Q}$ potential obtained in the bag model describes the spectrum of the J/ψ and T families[8] very well.

2. HEAVY BARYONS

Starting from a phenomenological $Q\bar{Q}$ potential such as V^I, the simplest and most commonly adopted strategy[12] for computing the baryon spectrum consists in adding QQ potentials given by

$$V_{QQ}(r) = \frac{1}{2} V_{Q\bar{Q}}(r) \ . \tag{3}$$

This is a special case of the "additive" model, in which the potential energy of a colour singlet $(Q_1 Q_2 \ldots Q_n)$ made of n quarks or antiquarks is

$$V(Q_1 Q_2 \ldots Q_n) = \sum_{i<j} \lambda_i \cdot \lambda_j \, V_8(r_{ij}) \ . \tag{4}$$

If one uses the Martin potential V^I and the rule (3), one gets[13] for the Ω^-(sss) the very satisfactory value $M(\Omega^-) = 1.662$ GeV (after spin corrections), to be compared with the experimental one $M(\Omega^-) = 1.672$ GeV. Note that, in Ref. 13, the three-body problem is treated carefully by the method of the hyperspherical expansion[14], which turns out to be very well suited to the study of baryons in the quark model.

This success in reproducing the mass of the Ω^-, as well as other successes in describing the properties of light baryons[12], must not overshadow the theoretical questions concerning prescriptions (3) or (4)[15]. For two-body forces, dominance of colour-octet exchanges seem reasonable, unless there would be confining forces between hadrons. A small amount of non-confining colour-singlet exchange cannot, however, be excluded. Moreover, three-body forces can very well be present. In perturbation theory, the three-gluon vertex induces three-body forces at the order α_s^2. Considerations of lattice gauge theories or of string models also suggest that the linear potential $V^L_{Q\bar{Q}} = \lambda r_{Q\bar{Q}}$ has to be generalized into

$$V^L_{QQQ} = \lambda \ \mathrm{Min} \ (d_1 + d_2 + d_3) \ , \tag{5}$$

where d_i is the distance between the quark i and a "junction" point chosen such that the sum of the d_i's is minimal[16]. Such a behaviour is recovered in a bag model calculation of the QQQ potential[17]. Asymptotically, this generalized linear term V^L_{QQQ} corresponds to a "Y-shape" (three-arm star) for the bag. However, as for the $Q\bar{Q}$ case, we have the property of "precocious linearity", i.e. when the interquark separations increase, the asymptotic régime is obtained much earlier for the potential than for the shape of the bag. For instance, the linear potential V^L_{QQQ} plays an important role in binding the ccc ground state (charm = 3), but the corresponding bag remains always almost spherical.

The potential V^L_{QQQ} in Eq. (5) is manifestly of the three-body type. Unfortunately, it is rather well approximated numerically by $\sum_{i<j} 0.5\ \lambda\ r_{ij}$ [16], which is exactly what would give the application of rule (4) to $V^L_{Q\bar{Q}}$. So the study of baryon spectroscopy would hardly distinguish between simple additive models of type (4) and more complicated models involving three-body forces. On the other hand, the above remark implies that the extrapolation from the mesonic to the baryonic sector is quite safe for phenomenological applications, since different approaches lead to the same effective interaction.

3. MULTIQUARKS

Going from n = 3 to n = 4 quarks (or antiquarks) does not only mean more technical difficulties. In fact, this raises a fundamental question: Do we have narrow hadronic "molecules", i.e. in more precise terms, stable or metastable multiquark hadrons which do not split spontaneously into smaller colour singlets by simple quark rearrangement? For n = 4, the question is whether or not a $Q\bar{Q}Q\bar{Q}$ composite lies below the threshold made of two quarkonia.

The literature on multiquarks already contains a great variety of papers[18]. Most of them concern light quarks, for which the chromomagnetic forces play the most crucial role. Recently we have studied the problem for heavy quarks[19], where the spin-independent potential is presumably dominant. Some of our preliminary results are presented below.

First we considered additive potentials of type (4). For n = 2 ($Q\bar{Q}$) or n = 3 (QQQ), the operators $\lambda_i \cdot \lambda_j$ have a well-defined value, $-16/3$ and $-8/3$, respectively, and the colour wave function is factorized. For $n \geq 4$, there are different ways of building a colour singlet. The wave function thus has several components and the potential (4) is a matrix in the colour space. We have assumed that the colour wave function is still factorized, i.e. that we have only one spatial wave function. This is largely justified in the case of identical quarks, where the constraints due to the Pauli principle reduce considerably the possibility of colour mixing. In our approximation, we are dealing with a single-channel potential

$$V(Q_1 Q_2 \ldots Q_n) = \sum_{i<j} a_{ij}\ V_8(r_{ij}) \ , \qquad (6)$$

with $a_{ij} = \langle \lambda_i \cdot \lambda_j \rangle$, $\sum_{i<j} a_{ij} = -8/3\, n = C_n^2 \bar{a}$. Such an interaction has the following properties:

i) If we denote by $M_n^{(S)}$ the mass of the ground state for a symmetric potential ($a_{ij} = \bar{a}$ $\forall$ i,j), then

$$\frac{M_2^{(S)}}{2} \leq \frac{M_3^{(S)}}{3} \leq \ldots \leq \frac{M_n^{(S)}}{n} \ . \tag{7}$$

This means, for instance, that with an additive potential of type (4), we have $M(\Omega^-) > {}^3/_2\, M(\phi)$ [including the spin-spin corrections if we consider V_8 as being the spin-triplet potential].

ii) For n fixed, if we compare several (a_{ij}) distributions with a given total strength $\sum_{i<j} a_{ij}$, the symmetric case always gives the heaviest mass for the ground state:

$$M_n(a_{ij}) \leq M_n^{(S)} \ . \tag{8}$$

iii) For n = 4, the "true" diquonium with colour wave function $|QQ - \bar{Q}\bar{Q}\rangle = |\bar{3} - 3\rangle_1$ is always above the threshold:

$$2M(Q\bar{Q}) < M(\bar{3} - 3) \ . \tag{9}$$

The results (7), (8), and (9) are rigorous and independent of the confining potential V_8.

iv) For a "mock" baryonium of colour structure $|QQ - \bar{Q}\bar{Q}\rangle = |6 - \bar{6}\rangle_1$, there are compelling reasons for believing that it satisfies for most potentials V_8:

$$2M(Q\bar{Q}) < M(6 - \bar{6}) < M(\bar{3} - 3) \ . \tag{10}$$

This means that there is no narrow $QQ\bar{Q}\bar{Q}$ state within the additive model (6).

So far, however, we considered only quarks with equal masses. We also studied the effect of the potential (6) on some configurations involving two different masses m and m′. We assumed that the static potential V_8 is mass (or flavour) independent, as suggested by QCD and by the ability of $Q\bar{Q}$ potentials to describe different quarkonium families simultaneously ($s\bar{s}$, $c\bar{c}$, $b\bar{b}$, $c\bar{s}$ ...).

a) The crypto-exotic (in flavour) state $X = QQ'\bar{Q}\bar{Q}'$ has two thresholds: $T_1 = Q\bar{Q} + \bar{Q}'\bar{Q}'$ and $T_2 = Q\bar{Q}' + Q'\bar{Q}'$. Within our assumptions, we can prove that $T_1 \leq T_2$, and it seems almost sure that we have always $T_1 \leq X_1$, i.e. X is very broad and never shows up as a structure in the spectrum.

b) The genuine exotic $Y = QQ\bar{Q}'\bar{Q}'$ may become stable in additive potential models (6) if the ratio of masses m/m′ is large enough. This property and, eventually, the critical value of m/m′ depends upon the specific potential V_8 that we consider. With the model V^I [Eq. (1)] and the prescription (4), a state such as $tt\bar{s}\bar{s}$ would be bound provided m(t) $\gtrsim$ 10 GeV. With the model V^{II} [Eq. (2)], the state $tt\bar{c}\bar{c}$ also has a chance if m(t) $\gtrsim$ 15 GeV.

The estimate of the $QQ\bar{Q}\bar{Q}$ masses can also be done with the bag model. As already stressed, in this framework there is no extra parameter, nor is there any extra parameter when going from the $Q\bar{Q}$ to the $QQ\bar{Q}\bar{Q}$ case. We have estimated the potential within the approximation of a spherical bag centred at the centre of mass of the four quarks. The resulting $QQ\bar{Q}\bar{Q}$ potential has multibody components and is more attractive at short distances than one would expect from the additive rule (3). When this potential is plugged into the Schrödinger equation, narrow multiquarks do not, however, proliferate. In fact, we very often obtain states at the edge of the threshold, and so to arrive at conclusions regarding their stability would require some refinements in our calculation. This could concern the effect of surface tension, of higher order terms in α_s inside the bag, of non-spherical deformations, etc.

To conclude, we wish to underline the following points:

1) The potential models work very well for mesons.

2) They can safely be extended to the sector of baryons.

3) The existence of narrow heavy multiquarks could be a good test of the nature of interquark forces. For instance, a model with pairwise forces and colour-octet exchange dominance provides less attraction than the more collective interaction arising from the bag model.

4) In any case, from our preliminary calculations, there is no tendency to a proliferation of heavy multiquarks. If any, they would more likely appear in flavour-exotic configurations such as $tt\bar{s}\bar{s}$ involving very different masses rather than in crypto-exotic configurations with nearly equal masses such as $b\bar{b}c\bar{c}$.

Acknowledgements

I would like to thank L. Montanet and J. Trân Thanh Van for the organization of this meeting. I enjoyed the collaboration of J.P. Ader, P. Hasenfratz, R. Horgan, J. Kuti and J.P. Taxil. We benefitted from several discussions with A. Martin.

REFERENCES

1) C. Quigg and J.L. Rosner, Phys. Rep. 56 (1979) 167.

2) A. Martin, Phys. Lett. 100B (1981) 511.

3) J.C. Bizot, Recent results at DCI, Contribution to this conference.

4) C.E. Carlson, J.J. Cogne, P.M. Fishbane, F. Gross and S. Meshkov, Phys. Lett. 98B (1981) 110.

5) E. Eichten, K. Gottfried, T. Kinoshita, J. Kogut, K.D. Lane and T.M. Yan, Phys. Rev. Lett. 34 (1975) 369.

6) R.K. Badhuri, L.E. Cohler and Y. Nogami, Phys. Rev. Lett. 44 (1980) 1369.

7) P. Hasenfratz, J. Kuti and A.S. Szalay *in* Proc. 10th Rencontre de Moriond (Meribel, 1975) (ed. J. Trân Thanh Van), p. 209.
P. Hasenfratz and J. Kuti, Phys. Rep. 40 (1978) 75.

8) P. Hasenfratz, R.R. Horgan, J. Kuti and J.M. Richard, Phys. Lett. 95B (1980) 299.

9) L. Heller and K. Johnson, Phys. Lett. 84B (1979) 501.
W.C. Haxton and L. Heller, Phys. Rev. D 22 (1980) 1198.
A.T. Aerts and L. Heller, Phys. Rev. D 23 (1981) 185.
For a review, see, for example, R.H. Dalitz, Nucl. Phys. A353 (1981) 215.

10) A different approach has been developed by J. Baacke and G. Kasperidus, Z. Phys. C5 (1980) 259. See also J. Baacke, Y. Igarashi and G. Kasperidus, Dortmund preprint DO.TH 81/01 (1981).

11) T. DeGrand, R.L. Jaffe, K. Johnson and J. Kiskis, Phys. Rev. D 12 (1975) 2060.

12) I. Cohen and H.J. Lipkin, Phys. Lett. 93B (1980) 56, and references therein.
N. Isgur, Light quark spectroscopy, Contribution to this conference.

13) J.M. Richard, Phys. Lett. 100B (1981) 515.

14) For a detailed review see, for example, M. Fabre de la Ripelle, Weizman preprint WIS 80/11/Mar-ph. (1980).

15) For recent discussions, see G. Feinberg and J. Sucher, Phys. Rev. D 20 (1979) 1717.
D.P. Stanley and D. Robson, Phys. Rev. Lett. 45 (1980) 235.
T. Bender and H.G. Dosch, Heidelberg preprint HD.THEP. 81-3 (1981).

16) H.G. Dosch and V.F. Muller, Nucl. Phys. B116 (1976) 470.

17) P. Hasenfratz, R.R. Horgan, J. Kuti and J.M. Richard, Phys. Lett. 94B (1980) 401.

18) R.J. Jaffe, Phys. Rev. D 15 (1977) 267 and 281 and D 17 (1978) 1444.
H.M. Chan, M. Fukugita, T.H. Hansson, H.J. Hoffman, K. Konishi, H. Høgaasen and S.T. Tsou, Phys. Lett. 76B (1978) 634.
L. Montanet, G.C. Rossi and G. Veneziano, Phys. Rep. 63 (1980) 149.
N. Isgur and H.J. Lipkin, Phys. Lett. 99B (1981) 151.

19) J.P. Ader, J.M. Richard and P. Taxil, Do narrow heavy multiquark states exist? preprint CERN TH (in preparation).

RECENT RESULTS ON SCALAR MESONS

A. B. Wicklund
Argonne National Laboratory
9700 S. Cass Avenue
Argonne, IL 60439

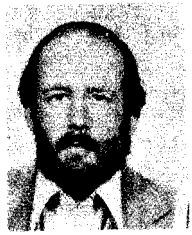

ABSTRACT

We review recent analyses of $J^{PC} = 0^{++}$ mesons in the $\pi\pi$, $\bar{K}K$ and πK channels. These analyses point to the existence of a $Q\bar{Q}$ nonet in the mass range 1300-1600 MeV with fairly well established members, which we denote as $\varepsilon(1425)$ and $\kappa(1450)$. Other S-wave effects, which we label by $\varepsilon(800)$ and $\kappa(800)$, occur as backgrounds in $\pi\pi$ and $K\pi$ scattering. The S*(980) effect is shown to be inconsistent with a normal width hadron, and is probably a bound state of the $\bar{K}K$ system.

Our discussion of light quark scalar mesons may be regarded as an update of Martin's review at the 1978 Rencontre de Moriond.[1] At that time the most interesting issue relating to $J^{PC} = 0^{++}$ states was Jaffe's hypothesis, namely that the "established" low-lying S^*, δ, ε, and κ mesons comprise a nonet of 4-quark states.[2] Jaffe's hypothesis had neatly explained both the mass degeneracy of the $S^*(980)$ and $\delta(980)$, and also the apparently large widths associated with the ε and the κ. It had also rendered unnecessary any explanation for the large deviation from magic mixing, which Morgan[3] had required in order to fit these states into a conventional $Q\bar{Q}$ nonet. Martin noted that there was evidence for I=0 and I=1 states in the $\bar{K}K$ S wave around 1300 MeV, and that these effects might be associated with the real 0^{++} $Q\bar{Q}$ nonet. Since Martin's 1978 review, the nature of the $\bar{K}K$ S wave has been clarified, and also a companion I=1/2 $Q\bar{Q}$ candidate has been clearly seen in $K\pi$ scattering with mass around 1450 MeV.[4] In addition, there is new information on the other P-wave $Q\bar{Q}$ states, and this may be regarded as a guide in looking for the $^3P_0$ levels.

Our purpose in this discussion is to focus on some basic physics issues; for details on the analyses of the experiments, we refer to the published literature. To give a brief summary of the experimental situation, we note that amplitude analyses have been performed on the charge-exchange reactions $\pi^-p \to K^-K^+n$,[5,6,7] $\pi^+n \to K^-K^+p$ (by isospin invariance this is equivalent to $\pi^-p \to \bar{K}^0K^0n$),[5] and $\pi^-p \to K_sK_sn$.[8,9,10] Cohen *et al.*[5] showed that these data are consistent with a unique solution for the I=0 and I=1 S,P, and D waves in the $\bar{K}K$ system. In this solution the P waves can be identified with the high mass tails of $\rho^0 \to \bar{K}K$ and $\omega \to \bar{K}K$; The D wave is dominated by the f(1280) for small momentum transfers; the I=0 S wave is produced by π exchange and exhibits considerable mass-dependent structure; the I=1 S wave has a t dependence consistent with B-exchange and is featureless in both phase and magnitude. The more recent high-statistics analyses of $\pi^-p \to K^-K^+n$[6,7] are consistent with the solution of Cohen *et al.*, provided similar assumptions are made on production mechanisms. Finally, the pure I=1 $\bar{K}K$ system was studied by Martin *et al.* using the reaction $\pi^-p \to K^-K_sp$.[11] This analysis suggested an S-wave bump around 1300 MeV, as noted in Martin's 1978 Review. The apparent absence of this effect in charge-exchange production[5] might be explained by postulating a pure Z-exchange (no-B-exchange) production mechanism.[19] All that we can assert now with any confidence is that very high statistics on the reactions $\pi^-p \to K^-K_sp$ or $\pi^-p \to \pi^-\eta p$ would be helpful in clarifying the I=1 0^{++} spectrum.

We now turn to the physics results, first the I=0 $\pi\pi$ and $\bar{K}K$ S waves. We note first that in a two-channel analysis there are only three parameters, namely the elastic $\pi\pi$ and $\bar{K}K$ phase shifts, δ_π and δ_K, and the elasticity, η. The $\pi\pi$ phase shift has been determined, albeit with ambiguities, in dipion production reactions.[12] The parameters δ_K and η can be deduced from the reaction $\pi\pi \to \bar{K}K$; the phase of this off-diagonal matrix element is simply related to the elastic phase shifts by $\phi(\pi\pi \to \bar{K}K) = \delta_\pi + \delta_K$. The range of solutions for δ_π is shown in Fig. (1a); $\phi(\pi\pi \to \bar{K}K)$ obtained by Cohen et al. is shown in Fig. (1b); δ_K obtained from $\phi(\pi\pi \to \bar{K}K) - \delta_\pi$ for the various $\pi\pi$ solutions is shown in Fig. (1c). From these phases alone, the following three effects can be disentangled: (1) "$\epsilon(800)$" is an essentially constant ($\delta_\pi \sim 60°$) background in $\pi\pi \to \pi\pi$; (2) S*(980) causes a 180° advance in δ_π at $\bar{K}K$ threshold, and also a ~ 90° retreat in δ_K just above threshold; (3) $\epsilon(1425)$ is a relatively narrow resonance ($\Gamma \sim 160$ MeV) that accounts for the phase advance in δ_π and $\phi(\pi\pi \to \bar{K}K)$ above 1300 MeV. Cohen et al. showed that the $\epsilon(1425)$, superposed on the background due to S*(980) and $\epsilon(800)$, is responsible for the bump at 1300 MeV originally seen in the $\pi\pi \to \bar{K}K$ S wave. The $\pi\pi \to \bar{K}K$ Argand plot shown in Fig. 2 illustrates the effect of the $\epsilon(1425)$ on the $\pi\pi \to \bar{K}K$ intensity and phase. The measured $\pi\pi$ phase shifts for solution β, which are favored by the dipion analysis of Becker et al.,[13] are roughly consistent with Cohen et al.'s parametrization of $\phi(\pi\pi \to \bar{K}K)$ in terms of $\epsilon(800)$, S*(980), and $\epsilon(1425)$ (these are the dashed and solid curves respectively in Figs. (1a) and (1b).) It is important to note that the $\epsilon(1425)$ must couple mainly to $\pi\pi$, with $\Gamma_{\bar{K}K}/\Gamma_{\pi\pi}$ in the range 0.1 to 0.25; conversely the S*(980) effect couples mainly to $\bar{K}K$ above $\bar{K}K$ threshold.

The $K\pi$ S wave from the SLAC experiment[4] behaves similarly to δ_π and could be characterized as a superposition of "$\kappa(800)$" (a slowly varying background phase that approaches ~ 70° at 1300 MeV), plus a relatively narrow "$\kappa(1450)$"; using the same criteria as for the $\epsilon(1425)$, the latter would have a mass in the range 1430-1500 MeV and width 100 to 180 MeV.

Thus, we would be tempted to label the $\kappa(1450)$ and the $\epsilon(1425)$ as the I=1/2 ($s\bar{u}$) and the I=0 ($u\bar{u} - d\bar{d}$) members of the 0^{++} nonet, and relegate the "$\epsilon(800)$", "$\kappa(800)$", and "S*(980)" effects into the multiquark category. The measured coupling, $\Gamma_{\bar{K}K}/\Gamma_{\pi\pi}$, for the $\epsilon(1425)$ implies a mixing angle in the range 35° to 50° (35° would be "magic"),[20] and in turn, a ratio $\Gamma[\epsilon(1425) \to \pi\pi]/\Gamma[\kappa(1450) \to \kappa\pi]$ in the range 2.0 to 1.4, which is not in gross disagreement with the observed widths. The masses of these states would seem to be rather high if only L.S splittings were hypothesized for the ^3P ($Q\bar{Q}$) states.

Comparing the 1^{++} and 2^{++} nonets, we find the experimental mass splittings $M(A_2(1310) - (A_1(1240)) \sim +70$ MeV, and $M(K^*(1430)-Q_A(1340)) \sim +90$ MeV;[14] thus for pure L.S splittings we would expect an I=1 $\delta(\sim 1200)$ and $\kappa(\sim 1300)$, and presumably an $\epsilon(\sim 1300)$, depending on the mixing angle. On the other hand, for pure tensor force splittings we would anticipate 0^{++} states $\kappa(\sim 1550)$ and $\delta(\sim 1430)$, the sign of the splitting being opposite to that observed for $c\bar{c}$ states. However, it is worth noting that the 0^{++} states are unique among the ^3P $(Q\bar{Q})$ levels in that they are accompanied by their "$\epsilon(800)$", "$\kappa(800)$" and "S*(980)" relatives; whatever the nature of the latter states, mixing between them and the genuine $Q\bar{Q}$ scalar mesons could alter the masses and widths of the physically observed $\epsilon(1425)$ and $\kappa(1450)$ states.

The coupled-channel analysis of Cohen et al., and more recently of Irving, Martin and Done,[15] sheds further light on the nature of the S*(980). As noted originally by Flatté,[16] because the S* occurs close to $\bar{K}K$ threshold, the sharp structure caused by the S* is mainly a reflection of the behavior of the ratio $\Gamma(S^* \to \bar{K}K)/\Gamma(S^* \to \pi\pi)$, rather than the Breit-Wigner denominator, $m_{S^*} - m - i\Gamma_{S^*}$. Consider a simple Breit-Wigner form for the S* contribution in the coupled-channel $\pi\pi$ and $\bar{K}K$ T matrix: (we ignore background for the sake of this discussion):

$$T_{ij}^{S^*} = \frac{\sqrt{\Gamma_i \Gamma_j}/2}{m_{S^*} - m - i\,(\Gamma_1 + \Gamma_2)/2}$$

Below $\bar{K}K$ threshold, the $\pi\pi \to \pi\pi$ amplitude will exhibit a loop in the Argand plot, provided Γ_π ($\sim$ 200 MeV) is not too large. Now suppose that above $\bar{K}K$ threshold, Γ_K increases rapidly so that $\Gamma_K >> \Gamma_\pi$; in that case both the $\pi\pi \to S^* \to \pi\pi$ amplitude, and also the $\pi\pi \to S^* \to \bar{K}K$ intensity, will fall like $\sim 1/\Gamma_K$ (e.g. $\sim 1/Q_K$). The only observable that can discriminate between a very broad ($\Gamma_K \to \infty$) and a "narrow" (Γ_K, $\Gamma_\pi \sim$ 200 MeV) S* is the phase $\phi(\pi\pi \to \bar{K}K)$. At $\bar{K}K$ threshold this phase is constrained by unitarity to be equal to the measured $\pi\pi$ phase shift, that is $\phi(\pi\pi \to \bar{K}K) \approx 180°$. (Both δ_π and $\phi(\pi\pi \to \bar{K}K)$ include a background phase of $\sim 70°$ due to the $\epsilon(800)$.) From Fig. (1b) we see that $\phi(\pi\pi \to \bar{K}K)$ remains constant at $\sim 180°$ above $\bar{K}K$ threshold. The associated behavior of δ_K (Fig. (1c)) shows that the $\bar{K}K$ elastic amplitude simply moves to the top of the Argand plot (to the left of center, hence to $-90°$) and stays there; a narrow S* would result in δ_K returning rapidly from $-90°$ to $0°$. Quantitatively, it can be shown that a coupled-channel Breit-Wigner resonance, irrespective of the channel coupling strengths and nonresonant backgrounds, must exhibit a Breit-Wigner phase advance in the 1-2

amplitude; in our case $\phi(\pi\pi \to \bar{K}K) = \delta_\pi^B + \delta_K^B + \delta^R$, where δ^B are (smooth) background phase shifts and $\delta^R = \arg(m_R - m + i\Gamma/2)$.[5] Such a phase advance is seen in Fig. (1b) above 1300 MeV due to the $\epsilon(1425)$, but is absent in the S* region.

A simpler description of the S* is that it is a virtual bound state of $\bar{K}K$. Recall that in K-matrix formalism, a Breit-Wigner resonance coupled to N open channels can be parametrized with an N + 1 dimensional constant K matrix, the N + 1'th channel being closed (for example a $Q\bar{Q}$ channel); above threshold, the amplitudes involving the N + 1'th channel do not show Breit-Wigner phase advance. Similarly, a $\bar{K}K$ bound state would explain the Argand loop in $\pi\pi \to \pi\pi$ below 1000 MeV, and the constant phase of $\phi(\pi\pi \to \bar{K}K)$, above 1000 MeV. In practice, the virtual-bound state parametrization is probably indistinguishable from the infinite-width Breit-Wigner discussed above. It is amusing to note that the I=1 $\bar{K}K$ S wave behaves similarly to the S* and shows no phase advance above $\bar{K}K$ threshold;[5] this wave is probably the tail of the $\delta(980)$. Thus, the $\delta(980)$ is consistent with being also a $\bar{K}K$ bound state.

Are there other ways to establish the S* properties? Consider the following reactions: (1) $K^-p \to \pi^+\pi^-\Lambda$,[17] (2) $\gamma\gamma \to \pi^+\pi^-$, $\gamma\gamma \to K^+K^-$,[18] and (3) $\psi \to \phi\,\pi^+\pi^-$.[15] The intensities expected from a Breit-Wigner parametrization of the S* contribution would be proportional to $1/\Gamma_K^2$ $(1/\Gamma_K)$ for the $\pi^+\pi^-(K^+K^-)$ final states above $\bar{K}K$ threshold; below threshold the $\pi^+\pi^-$ final states would show peaks characterized by $\Gamma_\pi^{S*}(\sim 200$ MeV). Thus, Flatté's argument can be extended to these reactions. Intensity peaks are expected due to the rapid increase of Γ_K^{S*} above $\bar{K}K$ threshold; if the phases could be measured, we would expect no phase advance in the K^+K^- channels above threshold.

We conclude that, where the $\epsilon(1425)$ and $\kappa(1450)$ are reasonable candidates for being "normal" (e.g. $Q\bar{Q}$) hadrons, the S*(980) behaves more like a $\bar{K}K$ bound state. We can say little about the nature of the "$\epsilon(800)$", "$\kappa(800)$" backgrounds, except that they are needed to fit the $\pi\pi$ and $K\pi$ phase shifts; and may, via mixing effects, modify the masses and widths of the physical $Q\bar{Q}$ states.

References

(1) A. D. Martin, Proc. of the 13th Rencontre de Moriond, ed. by J. Tran Thanh Van, 363 (1978).

(2) R. L. Jaffe, Phys. Rev. D15, 267 (1977).

(3) D. Morgan, Phys. Lett. 51B, 71 (1974).

(4) B. N. Ratcliff, Experimental Meson Spectroscopy, ed. by. S. U. Chung and S. J. Lindenbaum, 37 (1980); also B. N. Ratcliff, paper presented at this conference.

(5) D. Cohen et al. Phys. Rev. D22, 2595 (1980).

(6) L. Görlich et al., Nucl. Phys. B174, 16 (1980).

(7) G. Costa et al. Nucl. Phys. B175, 402 (1980).

(8) N. M. Cason et al., Phys. Rev. D19, 1317 (1979).

(9) W. Wetzel et al., Nucl. Phys. B115, 208 (1976).

(10) Loverre et al., Zeit. Phys. C6, 187 (1980).

(11) A. D. Martin et al., Nucl. Phys. B140, 158 (1978).

(12) P. Estabrooks and A. D. Martin, Nucl. Phys. B95, 322 (1975); A. D. Martin and M. R. Pennington, Ann. Phys. 114, 1 (1978).

(13) H. Becker et al., Nucl. Phys. B151, 46 (1979).

(14) R. J. Cashmore, Experimental Meson Spectroscopy, ed. by S. U. Chung and S. J. Linderbaum, 1 (1980).

(15) A. C. Irving, A. D. Martin, and P. J. Done, "On the Nature of the S* and Related Scalar Resonances", Durham Preprint-81-0212 (1980).

(16) S. M. Flatté Phys. Lett. 63B, 228 (1976).

(17) G. W. Brandenburg, et al., Nucl. Phys. B104, 413 (1976).

(18) P. Leu, paper presented at this conference.

(19) The I=1 S wave is detected in the charge-exchange channel by its interference with the π-exchange waves; Z exchange would contribute incoherently to the cross section and would be included in the I=0 intensity (See Ref. (5)).

(20) A mixing angle of ~ 50° would be required for the $^3P_1$ nonet to explain the 1^{++} widths, and the relative production cross sections for D(1280) and E(1420) with pion beams; see Ref. (14).

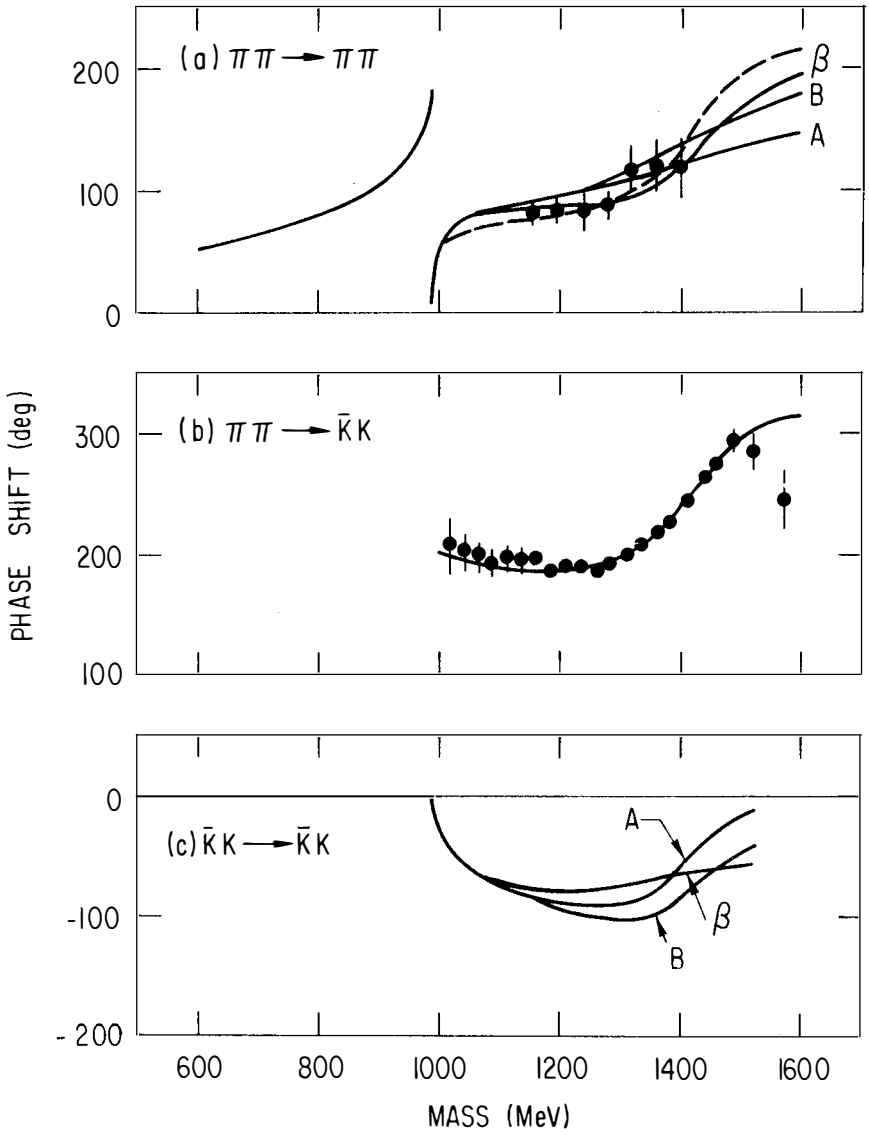

(1) (a) Smooth interpolations of measured $\pi\pi$ elastic phase shift solutions (Ref. 12); the dashed curve shows δ_π as predicted from a fit to $\phi(\pi\pi \to \bar{K}K)$ (Ref. 5). (b) Measured phases for $\phi(\pi\pi \to \bar{K}K)$ with the results of the same fit. (c) Interpolations of the $\bar{K}K$ elastic phase shift obtained from $\phi(\pi\pi \to \bar{K}K)-\delta_\pi$.

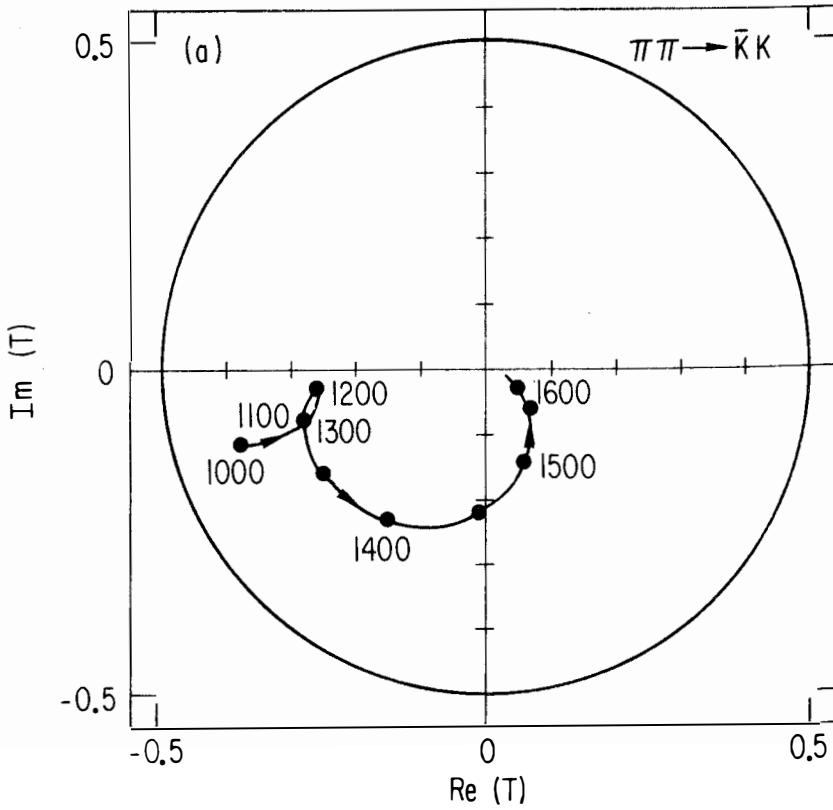

(2) (a) Argand plot representation of $T(\pi\pi \to \bar{K}K)$.

THE POMERON AND HADRONS THROUGH INFRA-RED ANALYSIS OF QCD

Alan R. White
CERN - Geneva

ABSTRACT

Infra-red analysis of QCD in the Regge limit is argued to lead to confinement with chiral symmetry breaking. The resulting Pomeron depends strongly on the centre of the gauge group with SU(3) colour producing uniquely the experimentally observed even signature, factorizing, Pomeron. The critical Pomeron (asymptotic rising cross-sections) occurs when QCD is saturated with quarks.

New calculations are reviewed showing strong evidence for the emergence of the critical Pomeron diffraction peak at present accelerator energies. This leads to exciting predictions for diffraction scattering at $p\bar{p}$ collider energies which could become the most precise experimental confirmation of QCD.

INTRODUCTION

The Pomeron, or diffractive scattering, is the "exchange of vacuum quantum numbers" at high energy as illustrated qualitatively in Fig. 1a. Therefore to understand the Pomeron in QCD will be closely related to *finding the vacuum* and so will inevitably involve *confinement*. Alternatively we can clearly exchange arbitrary numbers of *soft* QCD gluons in the Regge limit ($s \to \infty$, t fixed) as illustrated in Fig. 1b. So the Pomeron in QCD is also formally the sum of infinite numbers of soft gluons. This is, of course, the fundamental "infra-red problem" of QCD whose complexity was originally suggested by Weinberg [1] to be the origin of confinement.

In the last few years it has become accepted [2] as unlikely that the infra-red singularities of (mass-shell) QCD perturbation theory can be directly summed and interpreted as implying confinement. (Although some recent results [3),4)] have perhaps begun to cast doubt on this conventional wisdom.) In fact we shall argue below that *in the Regge limit* a very detailed analysis of the summation of infra-red singularities does lead to confinement with the anticipated spontaneous breaking of chiral symmetry. In addition we shall obtain a very beautiful connection between the nature of the Pomeron and the structure (centre) of the gauge group. The number of fermions is relevant, but turns out to determine only the "fine structure" of the Pomeron - that is the intercept(s) of the Pomeron Regge trajectory(ies).

We should emphasize from the outset that the Regge limit has, as we shall discuss, a special status for analyzing the infra-red problem in that the process of adding a gluon mass (by the Higgs mechanism) and removing it smoothly can be handled *unambiguously*. Away from the Regge limit the infra-red analysis, and hence the connection with confinement, is very likely to be ambiguous.

We shall actually outline a whole programme for studying QCD in the Regge limit which we have described in detail elsewhere [5]. Our intention here will be to provide an easily readable account which avoids the technical complexities of Ref. 5). In addition we shall relate our infra-red analysis more directly to the standard infra-red analysis of QED in the hope of making our arguments accessible to the widest possible audience.

To ensure that they are clearly understood we shall begin by summarizing the results for the Pomeron that we see emerging. Since these results imply that QCD is uniquely related to the well-known Reggeon field theory (RFT) critical Pomeron [6),7)], we shall also present new RFT calculations which suggest that the experimental evidence for the critical Pomeron is *much stronger* than previously

believed. This will allow us to argue that diffraction scattering may in the forseeable future be regarded as the most impressive experimental confirmation of QCD as the strong interaction force between hadrons. This provides a very clear motivation for the programme which we subsequently outline.

EMERGING RESULTS FOR THE POMERON

SU(2) gauge theory

There is no rising cross-section for any number of fermions. (The number of fermions is always restricted by asymptotic freedom in our work. The necessity for this can be seen directly from Regge limit calculations [5] or simply taken as a pre-requisite for a finite short-distance theory.) In an obvious notation

$$\sigma_T \xrightarrow[s\to\infty]{} 0 \qquad \forall\ N_F \tag{1}$$

SU(3) gauge theory

$$\sigma_T \xrightarrow[s\to\infty]{} 0 \qquad N_F < 16 \tag{2}$$

For $N_F = 16$ we obtain the RFT critical Pomeron and so very many predictions follow

$$\forall\ \sigma_T \xrightarrow[s\to\infty]{} \beta_i \beta_j \,[\ln s]^{\eta} \qquad \eta \doteq \frac{1}{3} \quad (= -\gamma) \tag{3}$$

$$\forall\ \frac{d\sigma}{dt} \xrightarrow[s\to\infty]{} \beta_i^2 \beta_j^2 \,[\ln s]^{2\eta}\, f_1\left(t(\ln s)^{\nu}\right) \qquad \nu \doteq \frac{13}{12} \tag{4}$$

$$\forall\ M^2 \frac{d^2\sigma}{dt\,dM^2} \xrightarrow[M^2,\ s/M^2 \to \infty]{} \beta_i^2 \beta_j^2 \beta_k^2 \,(\ln s/M^2)^{\alpha_1} (\ln M^2)^{\alpha_2} \times \times f_2\left(t(\ln s/M^2)^{\gamma}, t(\ln M^2)^{\nu_2}\right) \tag{5}$$

$$\left[\frac{d\sigma}{dt}\right]_{pp} - \left[\frac{d\sigma}{dt}\right]_{p\bar{p}} \longrightarrow 0 \qquad \text{for any particle } p \text{ and its antiparticle } \bar{p} \tag{6}$$

η, ν, α_1, α_2, ν_1, ν_2 are calculable critical exponents, f_1 and f_2 are *calculable scaling functions*.

SU(4) gauge theory

$$\sigma_T \xrightarrow[s\to\infty]{} 0 \qquad N_F < 20 \tag{7}$$

$$\sigma_T \xrightarrow[s\to\infty]{} \infty \qquad \left[\frac{d\sigma}{dt}\right]_{pp} - \left[\frac{d\sigma}{dt}\right]_{p\bar{p}} \not\to 0 \qquad N_F = 21 \tag{8}$$

That is there is an odd signature component of the Pomeron so that probably there is no simple factorization property for differential cross-sections.

SU(N) gauge theory

There is an increasing complexity of the Pomeron with N (that is more Regge trajectories of both signatures). To obtain a rising cross-section requires close to the maximum number of fermions allowed by asymptotic freedom and in general if

$$\sigma_T \xrightarrow[s\to\infty]{} \infty \quad \text{then} \quad \left[\frac{d\sigma}{dt}\right]_{p\bar{p}} - \left[\frac{d\sigma}{dt}\right]_{pp} \not\to 0$$

and there is no factorization.

So QCD with *SU(3) colour* and sixteen flavours (this constraint is deeper than simply saturating asymptotic freedom, as we shall discuss) may be the essentially *unique theory* giving *factorizing, rising cross-sections* asymptotically and equal *particle-antiparticle* differential cross-sections. (We should add that if higher colour representations of quarks are present - as an underlying super-symmetric theory might suggest - then far fewer flavours are required [5] to obtain the critical Pomeron.)

The asymptotic scaling laws for the critical Pomeron are in principle precisely calculable. Recent work by Dash and Grandou [8], and Bourrely and Dash [9] shows that the "$O(\epsilon^2)$" critical Pomeron agrees remarkably well with ISR data.

If the residue functions β_i, β_j in (4) are parametrized as $\beta_{i,j} = e^{At}$ then the best scaling property for $d\sigma/dt$ from the top of the FNAL energy range through the ISR range is obtained with $A \simeq 0.9$ GeV^{-2}. Once this residue function and the explicit energy dependence of (4) is extracted from the differential cross-section the result must be the *parameter-free* scaling function of RFT (the scale in t is, of course, a parameter). The *experimental evidence* for the existence of a scaling property is shown in Fig. 2. Next the *calculated scaling function* is compared in Fig. 3 with the ISR data at a particular energy where the maximum t range is available. The agreement of a parameter-free (but approximate) fundamental calculation with experimental data over eleven orders of magnitude is surely remarkable. I believe it is essential to view this agreement as distinct from many papers on diffraction phenomenology where the dip and the height of the secondary maximum in $d\sigma/dt$ are produced by arbitrary fitting of parameters.

Another recent experimental result of importance here is the $\bar{p}p$ differential cross-section at 50 GeV measured [10] at the CERN SPS. It fits perfectly on top of the ISR pp result as shown in Fig. 4. This result when combined with the FNAL results [11] showing factorization in diffractive processes to within 2% seems to confirm that *all* the essential features of the RFT critical Pomeron are indeed emerging from high-energy diffraction experiments. (Note also the result [8),9)] that the critical Pomeron has Kane's phenomenological Pomeron [12] - fitted to all low-energy data - as a low-energy approximation.)

The emergence of the critical peak already at 50 GeV in the $\bar{p}p$ experiment means that we have the *exciting prospect* of checking the scaling laws (3)-(6) right through the SPS energy range, the ISR, the CERN $\bar{p}p$ collider and finally the FNAL collider range. If the constraints on a gauge theory needed for the theoretical derivation of the critical Pomeron are indeed as we have outlined above then we will truly be able to claim that :

diffraction scattering provides potentially the most detailed experimental verification of QCD.

(Note that if $N_F \lesssim 16$ we anticipate that the critical Pomeron will appear approximately over a large energy range before the cross-section ultimately falls asymptotically.)

We now begin the outline of the arguments leading to the above results. Since the problem of the Pomeron in QCD is, as we implied above, a combination of an infra-red problem and a high-energy problem it will be helpful to first discuss the infra-red problem in QED and its significance in the Regge limit.

THE INFRA-RED PROBLEM OF QED IN THE REGGE LIMIT

The most well-defined way to handle the infra-red divergences of QED is to give the photon a mass M and construct the S matrix $S_F(M^2)$ in the Fock space of massive photons and electrons. We can then write [13]

$$S_F(M^2) = Z(M^2)\,\tilde{S}(M^2)\,Z^+(M^2) \tag{9}$$

where

$$Z = \exp[\,R + i\,\phi\,] \tag{10}$$

R contains the real (radiation) divergences and ϕ is conventionally referred to as the "Coulomb-phase operator". Z contains all the divergences as $M^2 \to 0$ and so it is potentially possible to identify $\tilde{S}(0)$ as the QED "S matrix" between *coherent* asymptotic states [13)-15)] of the form

$$|\,\text{coherent state}\,\rangle = Z^+\,|\,\text{Fock space state}\,\rangle \tag{11}$$

The unitarity property of S_F can then be carried over to $\tilde{S}$ if Z and the coherent state space have suitable properties. (This programme has, however, not yet been carried out to everyone's satisfaction.) The most direct way to obtain asymptotic states of the form (11) seems to be [13),16)] to solve an asymptotic approximation to the QED equations of motion to find appropriate "asymptotic fields" which are, of course, not free electron and photon fields. Recently it has been shown that a surface term in the QED action produces such fields naturally [17].

In perturbation theory, the factorizability of the infra-red divergences as in (9), is well known to be due to the external line rule for soft photons [1),18),19)]. That is all soft photon lines (causing infra-red divergences) are attached only to external (on-mass shell) charged particle lines as illustrated in Fig. 5.

To see how the above analysis carries over to the Regge limit consider elastic scattering of electrons. In fourth order the leading high-energy behaviour comes from the two-photon exchange diagram.

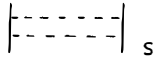

$$\underset{s\to\infty}{\sim}\; s \ln s\; K_{M^2}(q^2) \qquad t = q^2 \tag{12}$$

where $K_{M^2}(q^2)$ is the familiar transverse momentum integral

$$K_{M^2}(q^2) = \int \frac{d^2\underline{k}}{[\underline{k}^2 - M^2]\,[(\underline{q}-\underline{k})^2 - M^2]} \tag{13}$$

$$\xrightarrow[M^2 \to 0]{} \int \frac{d^2\underline{k}}{\underline{k}^2\,(\underline{q}-\underline{k})^2} = \infty \tag{14}$$

Adding the crossed box diagram the real part of (12) cancels, giving

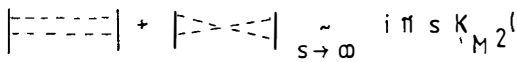

$$\underset{s \to \infty}{\sim} i\pi s K_{M^2}(\underline{q}^2) \tag{15}$$

$$\sim i\infty \equiv \text{infinite Coulomb phase} \tag{16}$$

(That this is indeed the Coulomb phase can be seen by noting that both in its direct evaluation [1] and in the above high-energy limit evaluation the *internal* electron lines are placed on-shell.) So in fourth-order the Regge limit retains only the Coulomb divergence. However, the Coulomb phase can be derived [15] in general by starting in the t channel (annihilation channel), defining coherent state amplitudes by extracting *real* divergences, and analytically continuing to $t < 0$. Consequently the imaginary transverse momentum divergence of the high-energy amplitude corresponds to an analytically continued real divergence of the cross-channel amplitude. Since t channel states are exchanged at high-energy it is not surprising that *Regge limit transverse momentum infra-red divergences carry information only about the need to redefine t channel states*. This is the general conclusion we shall draw from this brief fourth-order discussion [20]. Obtaining the correct states in any channel is, however, sufficient for a complete discussion of external states.

GENERAL DISCUSSION OF INFRA-RED ANALYSIS OF QCD

Before we go into details we first consider in general terms how much of the discussion of QED we can hope to take over to QCD. To find an analogue of (9) we must be able to smoothly add a mass to gluons. If we use the Higgs mechanism lattice results [21),22)] tell us that there is *no phase transition from the confining phase* if the Higgs scalars used are in the *fundamental representation* of the

gauge group. The relevant phase diagram is shown in Fig. 6. As illustrated we can (on the lattice) go analytically from a "Higgs theory" with massive gluons to a confining gauge theory. This is almost certainly not the case for the analogous continuum theories defined by the continuum limits shown. For our purpose, therefore, a lattice or equivalently some form of momentum cut-off is essential. A general momentum cut-off potentially clashes with gauge invariance. However, in the (multi-) Regge limit

a transverse momentum cut-off in the massive S matrix provides a gauge invariant momentum cut-off.

This is the technical point which makes the Regge limit infra-red analysis unambiguous and allows us to hope that for the high-energy S matrix we may be able to write :

$$S_{F\Lambda}(M^2) = Z_{\Lambda}(M^2)\,\tilde{S}_{\Lambda}(M^2)\,Z^{+}_{\Lambda}(M^2) \tag{17}$$

where Λ is the transverse momentum cut-off and $S_{F\Lambda}$ is a Fock space S matrix for massive quarks and gluons.

The possibility of writing an equation of the form of (17) is really the cornerstone of the programme that we wish to outline. This is because we can apply to $S_{F\Lambda}(M^2)$ our general dispersion theory [23] for all multiparticle amplitudes of a *massive unitary S matrix* which is valid in the multi-Regge limit and leads to a comprehensive multi-Regge theory. [The transverse momenta in the relevant dispersion integrals are what we can cut off to define (17) precisely.] Further the states of $S_{F\Lambda}(M^2)$ are massive quarks and gluons lying on Regge trajectories and there exist perturbative high-energy calculations of $S_{F\Lambda}(M^2)$ up to tenth order [24)-26)] (that is *several hundred Feynman diagrams* have been calculated). Thus we can hope to *use the general dispersion and Regge theory to build the perturbative results into a complete description of that part of* $S_{F\Lambda}(M^2)$ *that is well-defined and has a limit into pure QCD.* Hence we can try to identify $Z_{\Lambda}(M^2)$ and see the unitarity of $S_{F\Lambda}$ carry over into that of $\tilde{S}_{\Lambda}(0)$ which we will identify as the S matrix of the confining, "massless", gauge theory. Clearly $Z_{\Lambda}(M^2)$ will have to contain all the necessary information on how infra-red singularities select hadrons as the correct *t channel* external states. [The limit $\Lambda \to \infty$ can presumably be taken on $\tilde{S}_{\Lambda}(0)$ by appealing to asymptotic freedom *after* the limit $M^2 \to 0$ has been taken.]

The importance of the Higgs representations used will, for us, be in the unique way they prescribe how the gauge symmetry is restored. Breaking the symmetry with fundamental representations of scalars and then decoupling them one at a time, as we shall do, implies [27] the gauge symmetry is increased step by step through the sequence

$$\text{“}SU(1)\text{”} \longrightarrow SU(2) \longrightarrow SU(3) \longrightarrow SU(4) \longrightarrow \cdots \tag{18}$$

until the full symmetry is restored. The expected smooth formation of states created by (fixed-time) Wilson loop operators (the gauge theory analogue of closed-string operators) from local states as this symmetry restoration takes place is illustrated in Fig. 7. The topological complexity [28] of the "closed-strings" as the centre of the gauge group increases in size is provided by *adding local singlet vectors* (and open strings) to a basic "non-orientated" SU(2) string. We believe this is the *essential feature* of the symmetry restoration (18) *which allows us to obtain the Pomeron.*

PERTURBATIVE CALCULATIONS

We next review very briefly the existing perturbative calculations and their connection with Reggeon diagrams [29),30)]. Most calculations have been done in SU(2) gauge theory with a complex doublet of Higgs used to break the gauge symmetry down to a global SU(2) "colour" symmetry which we refer to as "isospin" I. (The gluons form a triplet with mass M.) The leading log calculations [24)-26)] of elastic scattering amplitudes give series

$$T_{I=0} = i g^4 \sum_{n=0} a_{0n}(t) [g^2 \ln s]^n \quad - \text{ even signature} \tag{19}$$

$$T_{I=1} = g^2 \sum_{n=0} a_{1n}(t) [g^2 \ln s]^n \quad - \text{ odd signature} \tag{20}$$

$$T_{I=2} = i g^4 \sum_{n=0} a_{2n}(t) [g^2 \ln s] \quad - \text{ even signature} \tag{21}$$

All the series up to tenth order are reproduced [31),26)] by *four* Reggeon diagrams. That is we write :

$$T_i(t=\underline{k}^2, \ln s = y) = \int dE\, e^{-Ey}\, T_i(E, \underline{k}^2) \qquad i = 0,1,2 \tag{22}$$

where

$T_0 =$  (23)

$T_1 =$ 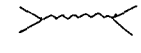 (24)

$T_2 =$ 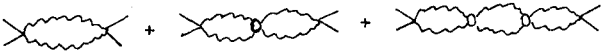 (25)

and in these diagrams the *odd signature* "Reggeized gluons" are represented by the Reggeon propagator

 $= \dfrac{1}{E - \Delta(\underline{k}^2)} \dfrac{1}{\underline{k}^2 - M^2}$ (26)

with $\Delta(\underline{k}^2)$ given by the transverse momentum "bubble"

$\Delta(\underline{k}^2) =$ 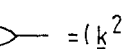 $= (\underline{k}^2 - M^2)\, g^2 \int \dfrac{d^2\underline{q}}{(\underline{q}^2 - M^2)((\underline{k}-\underline{q})^2 - M^2)}$ (27)

There is a four-Reggeon interaction

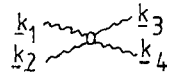

which is a function of all the transverse momenta (which we do not give explicitly for simplicity). The usual Reggeon diagram rules [29),30)] to impose E and $\underline{k}$ conservation at each vertex and write $\int dE d^2\underline{k}$ for each loop are applied. The number of Feynman diagrams involved [24)] in the tenth order calculations is gauge dependent, but "in order of magnitude" we can say

$$500 \text{ Feynman diagrams} \sim 4 \text{ Reggeon diagrams} \tag{28}$$

The power of Reggeon diagrams is therefore apparent.

We note that similar results to (23)-(25) have also been obtained for some multiparticle amplitudes [26]. Also although all the high order results have been obtained in a particular gauge group it is known that a *non-Abelian* gauge symmetry is in general sufficient for the Reggeization of all gauge vectors and fermions in a spontaneously broken theory [32]. The Reggeon diagram results are expected to generalize in the same way.

We now wish to extrapolate the perturbative calculations to obtain the complete set of Reggeon diagrams for an *arbitrary multiparticle amplitude*. Clearly this is a very big step which requires using all the multi-Regge theory we have. We can only possibly give a *very* abbreviated version of this here. For more details we refer the reader to Refs. 5) and 23).

MULTI-DISPERSION AND MULTI-REGGE THEORY (for a massive unitary S matrix)

For a single multiparticle amplitude we can write many dispersion relations which are generalizations of the familiar fixed t dispersion relation for a four-particle amplitude. There is one for each tree diagram that can be drawn with three-point vertices, e.g. :

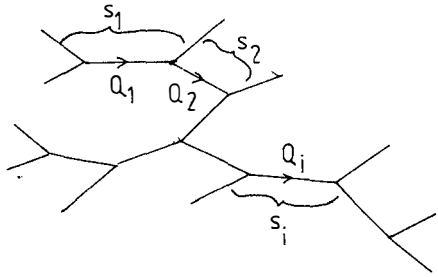

The dispersion relation is written in "sub-energy" variables $S_1, S_2, \ldots, S_i, \ldots$ with transverse momentum variables $t_1 = Q_1^2 \ldots t_i = Q_i^2, \ldots$ kept fixed. There are many spectral functions in each dispersion relation which (asymptotically) can be classified by a set of *hexagraph* diagrams constructed from the original tree diagram, e.g. :

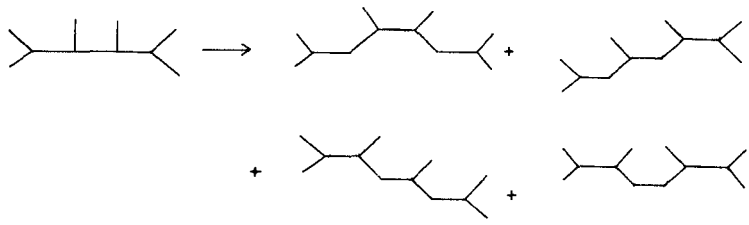

Each hexagraph represents an amplitude with *much simpler* analyticity properties than the complete amplitude. As a consequence an analytically continued (Froissart-Gribov) partial wave amplitude a_H exists which can be used to write a generalized Sommerfeld-Watson representation for each hexagraph amplitude. Writing $y_i = \ell n\, S_i$

$$M_H(y_1,\ldots y_i,\ldots t_1,\ldots,t_i,..) = \int \prod_i dE_i\, e^{-E_i y_i}\ \tau_H(\underset{\sim}{E})\ a_H(\underset{\sim}{E},\underset{\sim}{t}) \tag{29}$$

where $\tau_H(\underset{\sim}{E})$ is a generalized signature factor.

A very technical partial wave analysis of multiparticle t channel unitarity can now be used to show that each a_H satisfies a *Reggeon unitarity* equation in *each* E_i

$$\underset{E_i}{\text{disc}}\ a_H(E_1,\ldots E_i,\ldots) = \sum_i \int d\varrho_i\ \tilde{a}^{+}_{H_R}\tilde{a}^{-}_{H_L} \tag{30}$$

where the sum is over all Regge singularities in the E_i channel. $\tilde{a}^{+}_{H_L}$ and $\tilde{a}^{-}_{H_R}$ are residues of the corresponding Regge poles in hexagraph partial wave amplitudes a_{H_L} and a_{H_R}. Given the Regge poles in the theory, the Reggeon unitarity equations, plus the multiple discontinuity formulae defining the hexagraph amplitudes can be iterated to produce a complete set of Reggeon diagrams for all the a_H. However, the resulting diagrams are really only calculable (or at least controllable) *if the Reggeon interactions are simple* - in particular *non-singular in transverse momentum variables*.

At first sight the Reggeon interactions appearing in gauge theories are singular. The four-Reggeon interaction appearing in (23) and (25) has the decomposition [5),25),30)]

"local" "non local" ≡ transverse momentum pole (31)

Fortunately it can be shown [5] that the singular part of the interaction can be written in terms of triple Reggeon interactions with a (nonsense) zero. That is (23)-(25) can be rewritten in term of diagrams as

$T_0 =$ 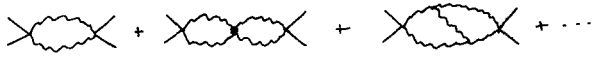 (32)

$T_1 =$ 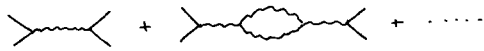 (33)

$T_2 =$ 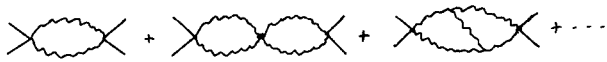 (34)

Although the Reggeon diagram rules in this form are more complicated all the Reggeon interactions and trajectory function(s) are non-singular and the results can be confidently extended to all higher Reggeon diagrams and all multiparticle amplitudes.

* * * * *
* * * *
* * *
* *
*

We now come to the central problem.

THE INFRA-RED LIMIT DEFINING A MASSLESS GAUGE THEORY

It has been well-known for many years that the infra-red problem (mass-shell infra-red singularities) in a non-Abelian gauge theory is very much worse than in QED. The triple gluon coupling allows soft gluons to cascade so that there is no "external-line soft-gluon rule" as there was for photons (except in leading logs [33),34)]). Weinberg [1] has called the task of unravelling such divergences "Herculean". We shall use all the power of our Reggeon diagram analysis to attack the problem, knowing that such diagrams do keep the full infra-red divergence structure for t channel states.

In the infra-red limit Reggeization appears as a simple exponentiation

$$s^{\Delta(t)} = e^{\Delta(t)\ln s} \underset{\tilde{M}^2 \to 0}{\sim} e^{-\ln s\, g^2 \ln[t/M^2]} \longrightarrow 0 \qquad (35)$$

which at first sight sends all Reggeon diagrams to zero as $M^2 \to 0$. (That this exponentiation is controlled by unitarity and analyticity is what gives the Regge limit infra-red analysis its power in contrast to, say, form factor exponentiation [35].) To analyze this situation more carefully [25] we first undo all Reggeization involving those gluons to be made massless. We then write diagrams for "elementary" gluons with a propagator

$$= \frac{1}{E} \cdot \frac{1}{\underline{k}^2} \tag{36}$$

by absorbing the "Reggeization" bubble and all other triple Reggeon interactions into an interaction "kernel" K_I defined for each t *channel* isospin I. [This analysis applies to the restoration of the $SU(2)$ symmetry in (18).] That is

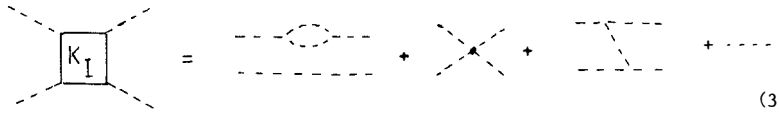

(37)

The first important result for the infra-red analysis is that

$$K_I \underset{M^2 \to 0}{\longrightarrow} \infty \qquad I \neq 0 \tag{38}$$

because the exponentiation of Reggeization dominates. (This is the first indication that only amplitudes with $I = 0$ in each t channel survive as $M^2 \to 0$.) This result generalizes [26),35)] to kernels for arbitrary numbers of gluons. For $I \neq 0$ the Reggeization dominates and only

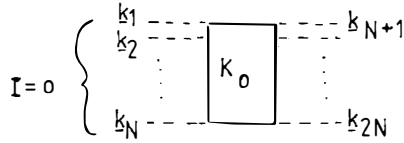

is finite and therefore a *scale-invariant* function of the $\underline{k}$'s. The scale-invariance property also implies that $K_0 \to \infty$ if *any subset* of the gluons involved goes to zero transverse momentum. However, if

$$\underline{k}_1 \sim \cdots \sim \underline{k}_i \sim \cdots \sim \underline{k}_{2N} \to 0 \qquad \underline{K_0 \text{ is finite}} \tag{39}$$

The consequences of the above structure of the gluon kernels are as follows. Firstly for elastic scattering amplitudes (whose external states are quarks and gluons) we have the results, already well-known in leading logs [32),33)],

$I \neq 0$ internal soft gluons exponentiate the amplitudes to zero

$I = 0$ internal soft gluons again exponentiate but give finite amplitudes (singularities remain at $t = 0$).

The really important consequence is, however, that the more complicated signature properties of multiparticle amplitudes *combined* with the scale-invariance of the kernels K_o produce a new class of infra-red singularities which *cannot exponentiate* to "screen" themselves.

There are two further properties of a gauge theory which also play a central rôle at this point. The first is a generalized *charge conjugation operation* which can be defined directly from the global "isospin" symmetry I. [This global symmetry always remains when the gauge symmetry is sequentially broken by fundamental representations, provided the initial gauge symmetry is an SU(N) symmetry.] When the gauge symmetry is unbroken the charge conjugation can equally well be defined by projecting the gluon field on to colour generators and writing

$$C\, A^{i}_{\alpha\beta}\, C^{-1} = - A^{i}_{\beta\alpha} \qquad (40)$$

where i labels a colour generator and α,β are the (colour) spinor matrix indices. (For quarks C includes the usual charge conjugation.)

The second property needed is helicity conservation at zero transverse momentum. This implies that signature and *charge parity* coincide in elastic amplitudes as in (19)-(21). More importantly it implies that Reggeized gluons (or quarks) cannot have a local (Reggeon) interaction at zero transverse momentum if they have disparate signature τ and charge parity C (which coincides with charge conjugation for $I = 0$ states). Combining this property with the finiteness of the kernels when all gluons have uniformly soft transverse momentum we obtain our *central result* :

an $I = 0$ cloud of uniformly soft gluons with $\tau \neq C$ accompanies an $I = 0$ combination of massive Reggeized gluons or quarks without screening its own infra-red singularity.

This "flux-tube" of (*uniformly*) soft gluons therefore satisfies something like the external line rule for soft photons in QED. It can therefore potentially be factorized off onto external states which will effectively be defined by this process. It seems that both the hadronic external states and the exchanged Pomeron are produced by the gluon flux-tube. Hadrons appear as $I = 0$ combinations of Reggeized quarks accompagnied by a flux-tube of soft gluons, e.g. :

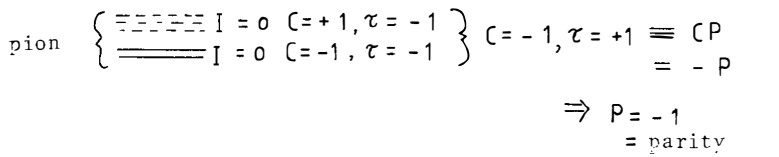

(41)

So the signature rule for Regge cuts (which produces $\tau = -1$ for a pair of Reggeized quarks) when combined with the $C \neq \tau$ rule for the soft gluon flux-tube implies that the *pion is a pseudoscalar*.

A Pomeron (with intercept close to one) appears for the first time when we consider QCD with the full $SU(3)$ gauge symmetry *partially broken* to an $SU(2)$ gauge symmetry [that is only the $SU(2)$ symmetry of (18) is restored]. It appears as an $SU(2)$ singlet accompanied by a flux-tube of soft-gluons, e.g.:

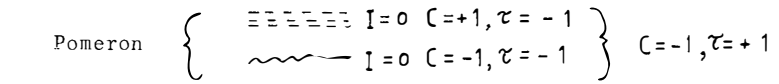

(42)

The triplet of soft gluons is, of course, only the simplest configuration. The complete flux-tube will be an infinite superposition of soft gluons - always with total $I = 0$ and $C = +1$. In general we can say that from the point of view of the Regge limit infra-red analysis confinement appears as the property that *colour zero Regge cut singularities with special combinations of charge parity and signature (or parity)* - which prevent them from appearing in elastic quark or gluon amplitudes - *are superposed and enhanced by the infra-red limit to become the true hadrons and Pomeron, automatically breaking chiral symmetry in the process*.

The promotion to a pole of the Regge cuts forming the Pomeron is straightforward and is described in Ref. 5). The Pomeron simply acquires the trajectory of the $SU(2)$ singlet. We have some idea how the hadronic Regge cuts are enhanced to become Regge poles but we have not yet published it. Here we note only that the trajectory intercept for hadrons formed from N light quarks will be given approximately by the well-known Regge cut formula

$$\alpha_N(0) = N\,\alpha(0) - N + 1 \;\simeq\; N\alpha(m_q^2) - N + 1 = -N/2 + 1 \qquad (43)$$

$$= 0 \text{ for pions} \qquad = -1/2 \text{ for nucleons!!} \qquad (44)$$

We anticipate that hadrons and the Pomeron appear simultaneously (with finite coupling) in multiparticle quark and gluon amplitudes where all t channels are $I = 0$, e.g.:

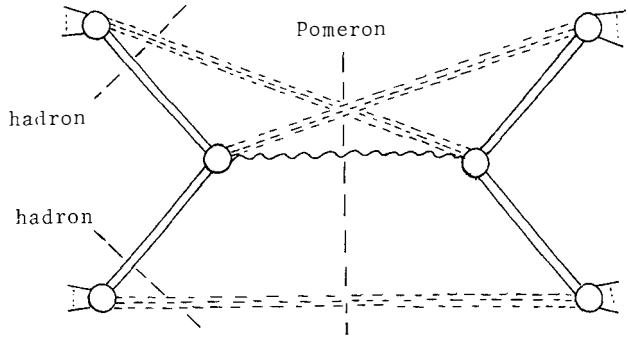

(45)

Such amplitudes are indeed infinite due to the gluon flux-tube infra-red singularities, while other amplitudes are finite. This implies that the hadronic part of the S matrix is dominant in the infra-red limit. However, we still have to understand how to use this explicitly to write an equation of the form of (18) and so determine to what extent the space of states and $\tilde{S}_\Lambda(M^2)$ is completely defined by the formalism. Clearly this is an essential final part of our programme which will require a more complete infra-red analysis than we have so far carried out.

Finally we discuss what controls the Pomeron intercept in QCD. We have analyzed, in outline [5], the full set of infra-red singularities (relevant to the Pomeron) when the gauge symmetry is restored to $SU(2)$ and the Pomeron is formed as in (42). (*One* triplet of Higgs scalars is added to the QCD Lagrangian in this theory.) There is a complicated structure of divergences, e.g. :

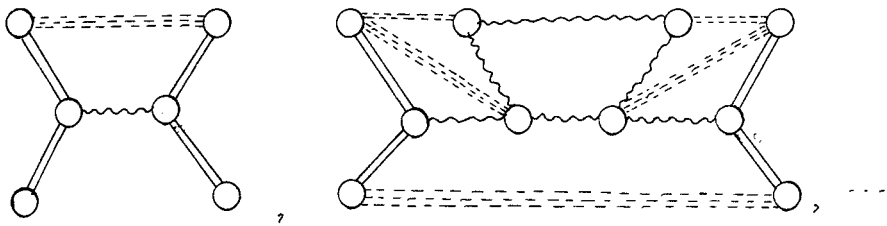

(46)

There are many reasons [5] to believe that the complete structure can be mapped on to the supercritical Pomeron theory [37] [formally $\alpha(0) > 1$] described by Pomeron diagrams

(47)

The supercritical Pomeron is distinguished from the subcritical Pomeron by the presence of "vacuum production and absorption of Pomerons". This, at first sight bizarre, phenomenon is due in partially broken QCD, directly to SU(2) soft gluons.

Assuming that the mapping can be carried out completely we conclude that restoring the gauge symmetry in QCD from SU(2) to SU(3) (by decoupling the scalars) produces the critical Pomeron (that is unit intercept) *provided* that the transverse cut-off can be removed before the symmetry is restored. (Otherwise it can be shown [5] that the intercept will be lowered by the subsequent removal of this cut-off.) This requires asymptotic freedom of the partially broken theory, which in turn requires sixteen flavours of quarks [37),38]. We therefore reach the conclusion stated above :

The critical Pomeron is produced by saturating QCD with quarks.

The analysis of QCD can be extended to higher SU(N) gauge groups by restoring the symmetry as in (18). From Fig. 7 it is clear that for each increase in N a new singlet "Pomeron" trajectory is added to the theory. This leads to the conclusion that producing rising cross-sections in SU(4) or a higher group involves a more complicated critical phenomenon with more "Pomeron" Regge trajectories. The method of calculation makes it clear that there is a correspondence between the structure of Wilson loops in transverse space and the Pomeron spectrum as illustrated

in Fig. 8. Implying that the spectrum of the Pomeron is a direct reflection of the centre of the gauge group. Why this might be anticipated from unitarity is explained in Ref. 5). The need for asymptotic freedom in the relevant partially broken theory again leads to the result [39] that in general a rising cross-section requires close to the maximum number of fermions allowed for asymptotic freedom of the unbroken gauge theory.

We end by noting that in our formalism the QCD triple Pomeron coupling r_o satisfies

$$r_o \sim (m_q)^{-2} \sim (m_{\tilde{\pi}}^2)^{-2} \tag{48}$$

which implies that the "precocious scaling" of the critical Pomeron diffraction peak shown in Figs. 2-4 is due to the small pion mass. It also implies that the chiral limit $m_\pi^2 \to 0$ and the critical Pomeron limit $r_o \to \infty$ are closely related. In fact the existence of the chiral limit may be tied to the criticality of the Pomeron !

REFERENCES

1) S. Weinberg - Phys.Rev. 140B (1965) 516.

2) W. Marciano and H. Pagels - Physics Reports 36C (1978) 137.

3) C.E. Carneiro, M. Day, J. Frenkel, J.C. Taylor and M.T. Thomas - Sao Paulo Preprint IFUSP/P-237 (1980) and references therein.

4) G.F. West - Los Alamos Preprint (1981).

5) A.R. White - CERN Preprint TH. 2976 (1980).

6) A.A. Migdal, A.M. Polyakov and K.A. Ter Martirosyan - Zh.Eksp.Teor.Fiz. 67 (1974) 84.

7) H.D.I. Abarbanel and J.B. Bronzan - Phys.Rev. D9 (1974) 2397.

8) J.W. Dash and T. Grandou - Z.Phys. C3 (1979) 9.

9) J.W. Dash and C. Bourrely - Marseilles Preprint CPT-81/P.1280 (1981).

10) Z. Asad et al. - CERN Preprint (1981).

11) K. Goulianos - These Proceedings (1981).

12) B. Hartley and G. Kane - Nuclear Phys. B57 (1973) 157.

13) L. Faddeev and P. Kulish - TIMF 4 (1970) 153.

14) V. Chung - Phys.Rev. 140B (1965) 1110.

15) J.K. Storrow - Nuovo Cimento 54A (1968) 15 ; 57A (1968) 763.

16) D. Zwanziger - Phys.Rev. D11 (1975) 3481, 3504.

17) J.L. Gervais and D. Zwanziger - Phys.Lett. 94B (1980) 389.

18) D.R. Yennie, S.C. Frautschi and H. Suura - Ann.Phys. 13 (1961) 379.

19) J.S. Ball, D. Horn and F. Zachariasen - Nuclear Phys. B132 (1978) 509.

20) For an analogous derivation of the Coulomb phase from higher order Regge limit calculations, see : S.J. Chang and E. Ma - Phys.Rev. 188 (1969) 2385.

21) E. Fradkin and S.H. Shenker - Phys.Rev. D19 (1979) 3682.

22) T. Banks and E. Rabinovici - Nuclear Phys. B160 (1979) 349.

23) H.P. Stapp and A.R. White - Lectures at the Les Houches Institute (1975).

24) H. Cheng and C.Y. Lo - Phys.Rev. D13 (1976) 1131 ; D15 (1977) 2959 ;
L. Tyburski - Phys.Rev. D13 (1976) 1107 ;
M. McCoy and T.T. Wu - Phys.Rev.Letters 35 (1975) 604.

25) E.A. Kuraev, L.N. Lipatov and V.S. Fadin - Soviet Phys. JETP 44 (1976) 443.

26) J. Bartels - Nucl.Phys. B151 (1979) 293, B175 (1980) 365.

27) L.F. Li - Phys.Rev. D9 (1974) 1723.

28) G. 't Hooft - Nuclear Phys. B138 (1978) 1.

29) V.N. Gribov - Soviet Phys. JETP 26 (1968) 414.

30) H.D.I. Abarbanel, J.B. Bronzan, R.L. Sugar and A.R. White - Physics Reports 21C (1975) 119.

31) J.B. Bronzan and R.L. Sugar - Phys.Rev. D17 (1978) 585.

32) M.T. Grisaru and H.J. Schnitzer - Phys.Rev. D20 (1979) 784.

33) J.M. Cornwall and G. Tiktopoulos - "New Pathways in High-Energy Physics", Plenum, New York (1976).

34) P. Carruthers, P. Fishbane and F. Zachariasen - Phys.Rev. D15 (1977) 3675.

35) J.M. Cornwall and G. Tiktopoulos - D13 (1976) 3370.

36) T. Jaroszewicz - Acta Phys.Polon. B11 (1980) 965 ; Trieste Preprint (1980).

37) A.R. White - Proceedings Marseilles Conference on High-Energy Physics (1978) ; Proceedings 2nd International Symposium on Hadron Structure, Kazimierz, Poland (1973).

38) D.J. Gross and F. Wilczek - Phys.Rev. D8 (1973) 3633.

39) T.P. Cheng, E. Eichten and L.F. Li - Phys.Rev. D9 (1974) 2259.

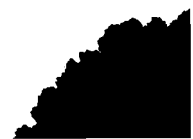

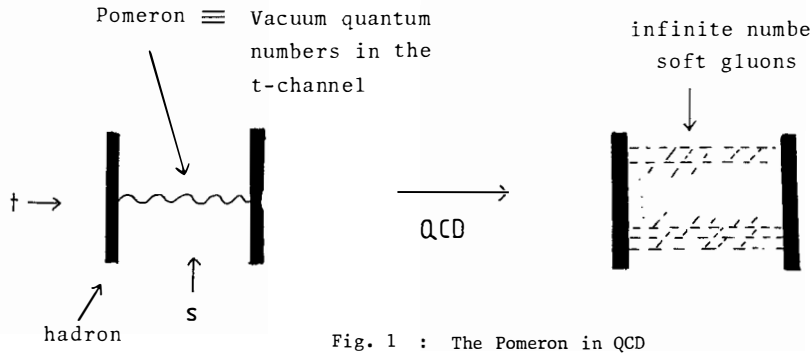

Fig. 1 : The Pomeron in QCD

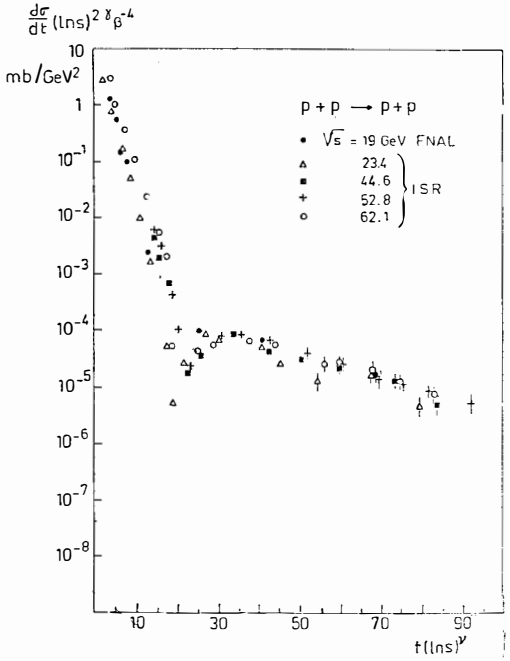

Fig. 2 : Experimental evidence for critical Pomeron scaling

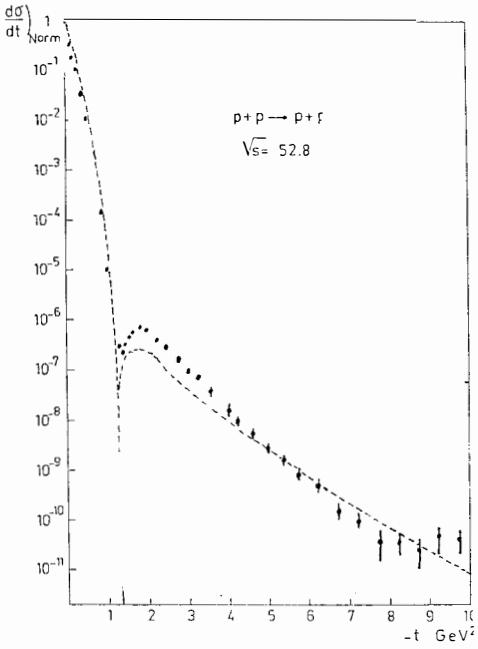

Fig. 3 : Comparison of the critical Pomero scaling function with ISR data

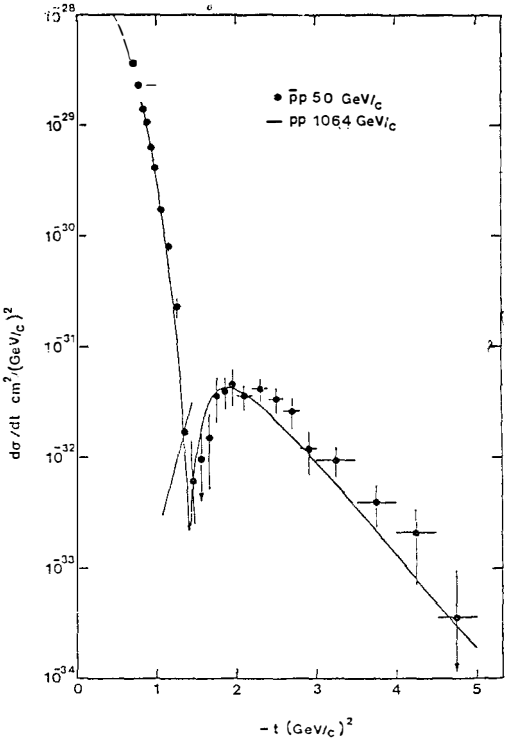

Fig. 4 : Comparison of pp and $\bar{p}p$ experimental diffraction peaks

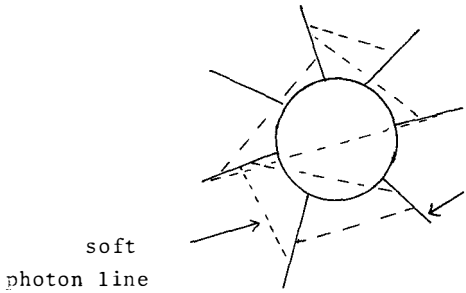

Fig. 5 : The external line rule for soft photons

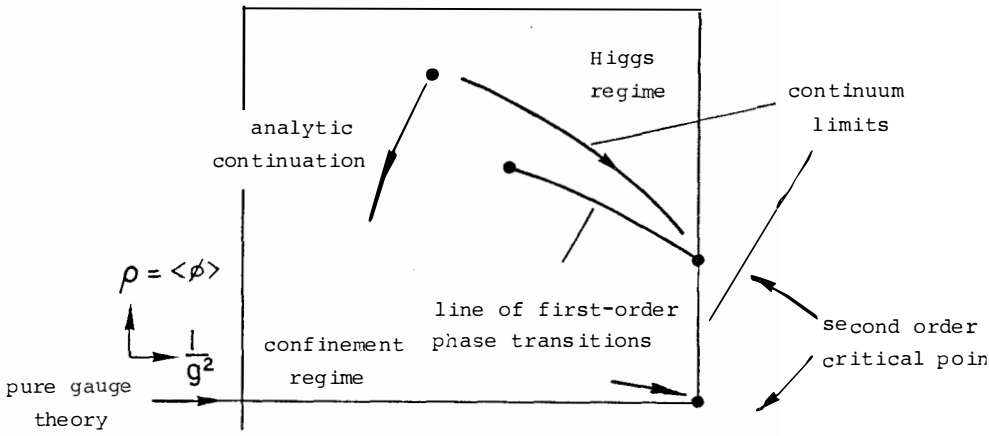

Fig. 6 : The phase diagram for fundamental representation scalars

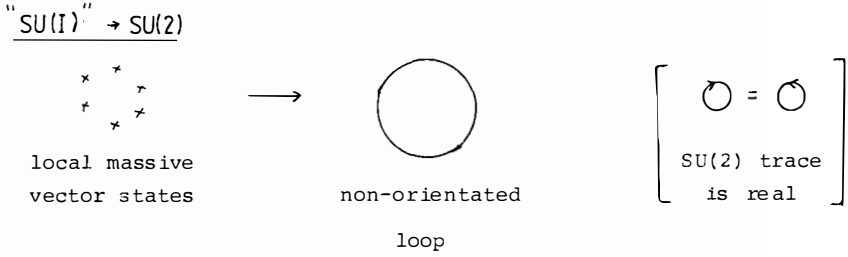

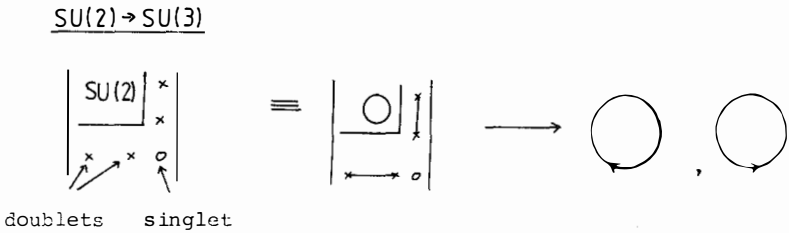

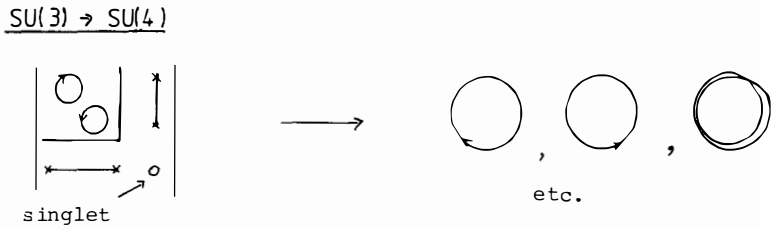

Fig. 7 : Formation of Wilson loops as the gauge symmetry is restored

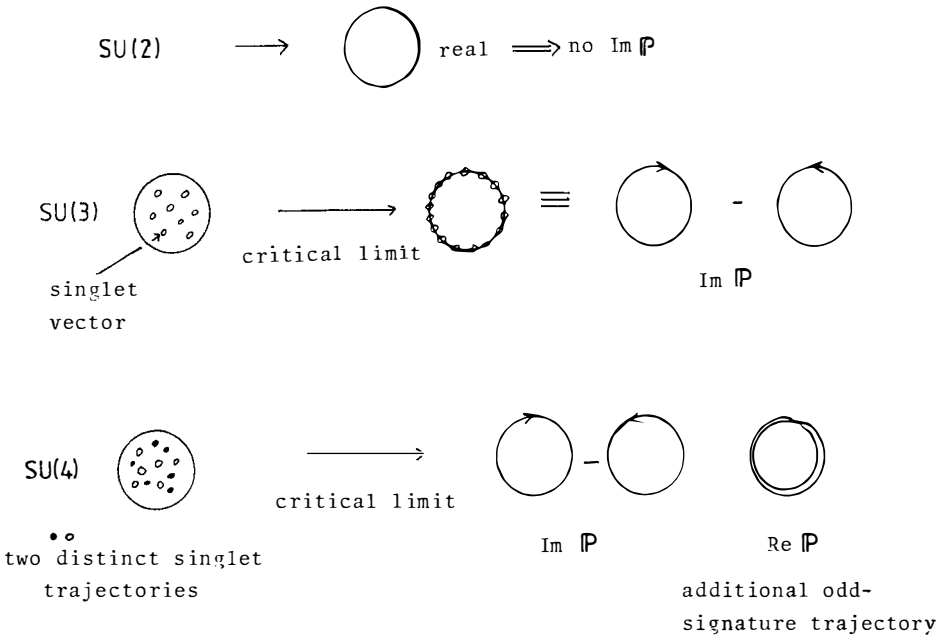

Fig. 8 : The correspondence between Wilson loops and the Pomeron

INTERACTIONS OF MESONS IN THE NUCLEAR COULOMB FIELD AT HIGH ENERGIES

D. Berg, J. Biel, C. Chandlee, S.Cihangir, B. Collick, T. Droege, T. Ferbel, S. Heppelmann, J. Huston, T. Jensen, A. Jonckheere, T. Joyce, P. Koehler, F. Lobkowicz, Y. Makdisi, M. Marshak, M. McLaughlin, C. Nelson, T. Ohshima, E. Peterson , K. Ruddick, M. Shupe, P. Slattery, and P. Thompson.
Fermilab-Minnesota-Rochester Collaboration

Presented by T. Ferbel, E.P. Division CERN and
University of Rochester, Rochester, N.Y. 14627 USA

ABSTRACT:

Using the Primakoff formalism, we have extracted radiative decay widths of vector and tensor mesons produced in interactions of pions and kaons in the nuclear electromagnetic field at beam energies of 150 GeV to 250 GeV. In particular, our recent measurement of the transition $\rho^- \to \pi^-\gamma$ is in good agreement with SU(3) symmetry, while the rate we obtain for $K^{*-} \to K^-\gamma$ suggests the presence of substantial symmetry breaking. In addition to these results, we have studied the characteristics of hitherto unexplored channels such as $\pi\eta'$ and $\pi D(1285)$, produced in the coherent excitation of incident pions on nuclear targets.

INTRODUCTION

We have been investigating the coherent dissociation of pions and kaons on nuclear targets at beam energies of 150 GeV to 250 GeV. A forward spectrometer, with large acceptance, consisting of a drift and proportional-chamber system to measure charged particles, and a finely segmented liquid-argon calorimeter to measure electromagnetic showers, was employed in the experiment [1]. Our main goal was to determine the transition rates for the decays $\rho^- \to \pi^-\gamma$ and $K^*(890)^- \to K^-\gamma$ through the Primakoff effect. The motivation for such measurements, and especially for the remeasurement of the previously established radiative width of the ρ^-, is discussed by P.J. O'Donnell elsewhere in these Proceedings. We will, therefore, only briefly review the essential points.

In simple quark models, the low-lying meson states are thought to be composed of quark-antiquark ($q\bar{q}$) systems. The decay of a vector meson, such as the ρ, into a π meson and a photon can be represented by the magnetic-dipole transition operator:

$$m = \sum_j \mu_j \vec{\sigma}_j \cdot (\vec{k} \times \vec{\varepsilon}) \exp\ (i\vec{k}\cdot\vec{r}_j) \qquad (1)$$

where the summation is over the quarks, with magnetic moments μ_j; $\vec{\varepsilon}$ and $\vec{k}$ are, respectively, the polarization and momentum vector of the emitted photon; $\vec{\sigma}_j$ are the Pauli spin matrices. In the long-wavelength approximation, that is not altogether valid in these decays, exp(ik·r) is set to unity.

The radiative width for the vector-pseudoscalar transition can be written (for non relativistic quarks) in terms of m as:

$$\Gamma\ (V \to P\gamma) \simeq \frac{4k}{3} \left(\frac{E_P}{M_V}\right) \sum_{<i>,\ f} |< P_f \mid m \mid V_i >|^2 \qquad (2)$$

where E_P is the energy of the pseudoscalar decay product, M_V is the mass of the parent vector meson; the sum is over all final states and on average over initial states. The states of interest for the case of the $\rho^- \to \pi^- \gamma$ decay correspond to the $^3S_1$ $d\bar{u}$ quarks that transform into the ^1S_o $d\bar{u}$ singlet combination in spin space; the transition is sketched in Fig. 1.

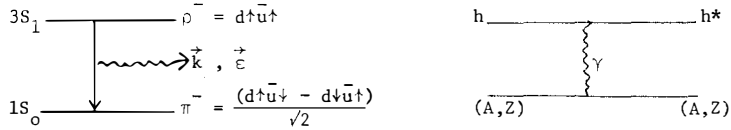

Fig. 1: Quark-antiquark states involved in the transition $\rho^- \to \pi^-\gamma$. On the right is the diagram for the Primakoff production of an excited hadron state (h*) in the Coulomb field of a nucleus of charge Z.

As pointed out by O'Donnell [2], there are several ambiguities in the derivation of Equation (2), which make absolute predictions of these widths somewhat suspect. However, in the case of comparisons of, for example, $\rho^- \to \pi^-\gamma$ and $\omega^o \to \pi\gamma$, where the kinematics are essentially identical, the ratio of the prediction for two widths should be quite reliable. If ideal mixing is assumed for the ω^o $q\bar{q}$ system, then the ratio $\Gamma(\rho^- \to \pi^-\gamma)/\Gamma(\omega \to \pi^o\gamma)$ is expected to be about 0.11. Experimentally, prior to our measurements, this ratio was 0.045 ± 0.013 - a result badly inconsistent with SU(3), and with our notions concerning symmetry properties of the photon. This theoretical difficulty prompted our attempt for a second-generation measurement of $\Gamma(\rho^- \to \pi^-\gamma)$.

RESULTS FOR ρ^- AND $K^*(890)^-$

As in the pioneering work of B. Gobbi et al. [3], we performed the experiment utilizing the nuclear Coulomb field as a source of photons to measure the inverse process $\pi^-\gamma \to \rho^-$ (see Fig. 1). The analysis of our data and the extraction of $\Gamma(\rho \to \pi\gamma)$ was facilitated by the fact that we performed the experiment at high energies where electromagnetic production dominates any strong-exchange contribution (e.g., ω^o or the weaker I = 1 exchanges). Fig. 2 displays several distributions of interest from the recently published data on $\pi^-A \to \pi^-\pi^oA$ and $K^-Pb \to K^*(890)^-$ Pb [4]. The $\pi^-\pi^o$ mass distribution for small values of t is dominated entirely by the ρ^-. The t distributions on Cu and Pb are seen to peak very steeply at t = 0, indicating the presence of electromagnetic production. (In fact, the slope of the t distribution near t = 0 is dominated by the experimental resolution). Similar characteristics are observed for $K^*(890)^-$ production. In this case we have two different topologies ($K^-\pi^o$ and $K^o_s\pi^-$), with totally different systematics, that can be used to crosscheck the extracted values of $\Gamma\gamma$. The radiative widths are obtained by fitting the following expression to the t-spectra:

$$\frac{d\sigma}{dt} = |f_c + \exp(i\phi)\, f_s|^2 \qquad (3)$$

where f_c is the Primakoff amplitude, f_s the contribution from strong-exchange processes, and ϕ is the relative phase between the two amplitudes [1]. The amplitude f_c is linear in $\sqrt{\Gamma_\gamma}$ and in Z, while f_s has a weaker A-dependence. Fits to several nuclear targets and different energies (taking account of resolution) provided a self consistent result for $\rho^- \to \pi^-\gamma$ of $\Gamma\gamma = 67 \pm 7$ KeV. This value of $\Gamma\gamma$ is about a factor of two larger than the previous result and in reasonable agreement with expectations from symmetry arguments.

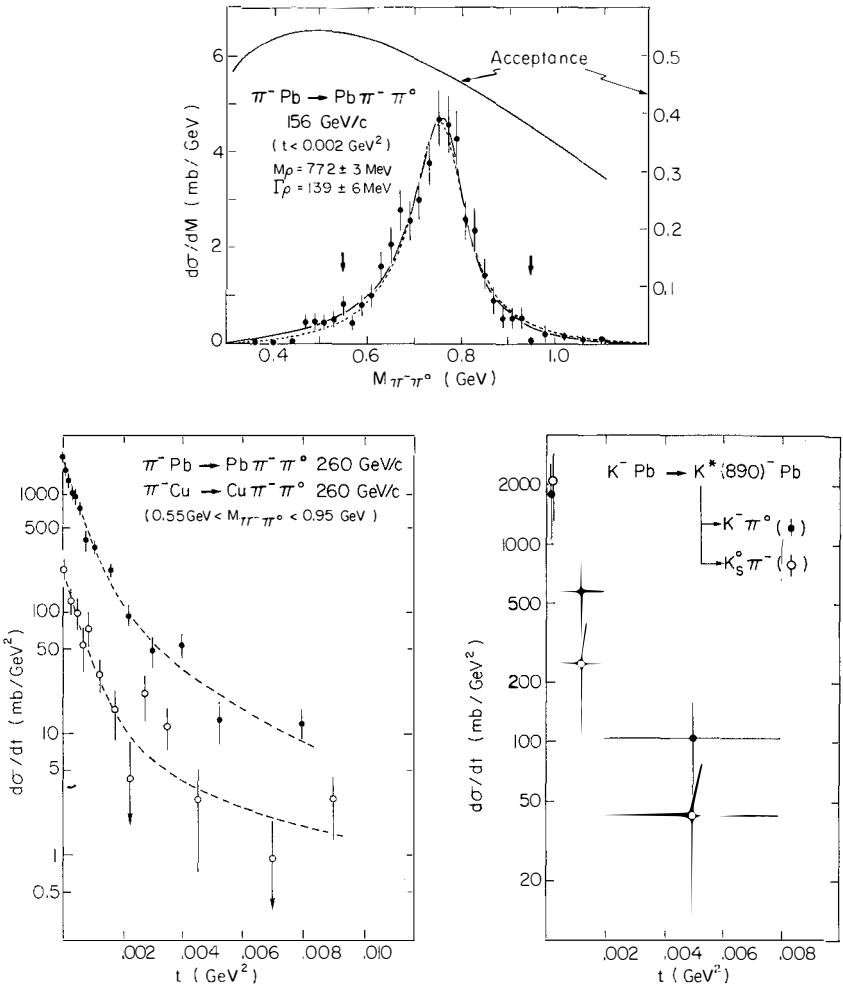

Fig. 2: Mass and t distributions for the reaction $\pi^- A \to \pi^- \pi^0 A$, and for $K^- Pb \to K^*(890)^- Pb$. The smooth curves on the π^- data represent fits used in the extraction of the radiative width of the ρ^-.

The result we obtained for the radiative width of the $K^*(890)^-$ indicates that there is substantial symmetry breaking in these decays but it is similar to that found for the SU(3) breaking observed in the case of the static magnetic moments of the baryons [5].

DATA WITH POSITIVE BEAMS

The results we have described thus far were obtained in our first run at Fermilab. To improve statistics for the K*, we had a more recent second run with a positive, K^+ enhanced, beam at 200 GeV [6]. Figure 3 displays the quality of these preliminary data. The K*(890) is clearly visible in both $K^+\pi^o$ and $K^o_s\pi^+$ final states, as is the K*(1430). The decay of the $K^*(1430)^+$ displays the characteristic form expected for the decay of a $J^P = 2^+$ object produced in a $J_z = \pm 1$ substate via photon exchange. (Acceptance distorts somewhat the $|Y^2_1(\theta,\phi)|^2$ distribution in the Gottfried-Jackson frame).

The new run also has greatly improved the statistics for pion data. A clear signal for the electromagnetic production of the B(1235) meson is displayed in Fig. 4. The steepness of the t-distributions near t = 0, again consistent with our resolution, indicates dominance of the Primakoff process over other contributions. Fig. 5 displays evidence for A_2 production in the $\pi^+\eta$ and in the $K^+K^o_s$ modes. (The t-spectra for these events, again, suggest dominance of photon exchange). The $\pi^+\eta$ mass distribution shows almost a pure A_2^+ signal, whereas the $K^+K^o_s$ distribution indicates the presence of an additional shoulder near 1400 MeV. We are not certain at this time what is the origin of this effect nor, in fact, whether it is due to some subtle background. In principle, this could be very interesting since reactions of the kind we have been discussing, namely $\pi\gamma$ and $K\gamma$ incident channels, have not been studied for masses above the ρ region. This is because it is only at several hundred GeV, and beyond, that investigation of the Primakoff excitation of massive states becomes experimentally feasible. Consequently, this field can be regarded as unchartered territory that could provide surprises. (In this context, it is interesting to note that the $\pi^+\eta'$ mass spectrum (coherently produced) also shows a broad enhancement near $\sim$ 1400 MeV. Evidence for the η' signal is given below).

Fig. 6 shows the $\pi^+\pi^-\eta$ mass distribution in Pb and Cu for coherently produced $\pi^+\pi^+\pi^-\eta$ final states. A clear peak at the η' and at the $D^o(1285)$ is seen in the Fig. Because of poor statistics, it is not completely certain that production is via the Primakoff process. (We should point out that $\pi\eta'$ diffractive production is expected to be greatly suppressed). Independent of whether the mechanism is electromagnetic or hadronic it is nevertheless surprising that we see so much η' and, particularly, so much $D^o(1285)$ production in these data. It is also somewhat

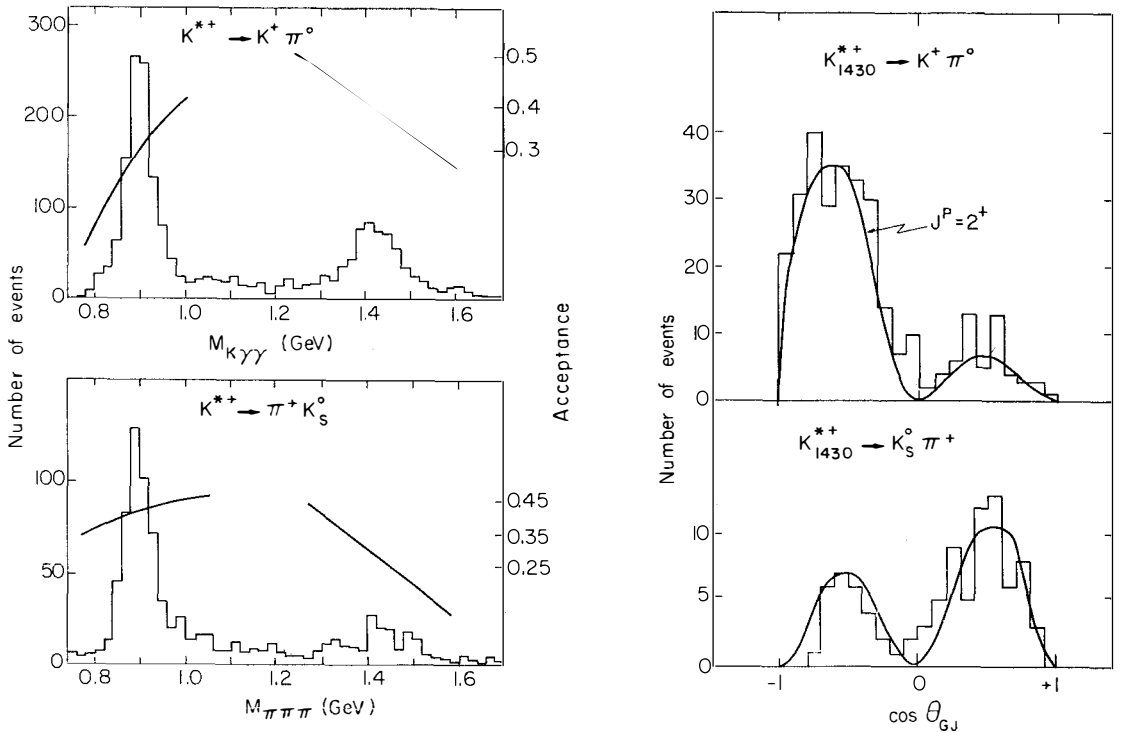

Fig. 3: The $K^+\pi^o$ and $K^o_s\pi^+$ mass spectra for coherent production on a Pb target. The decay of the K*(1430) is observed to display the characteristics expected for the decay of a $J^P = 2^+$ state produced in the nuclear Coulomb field.

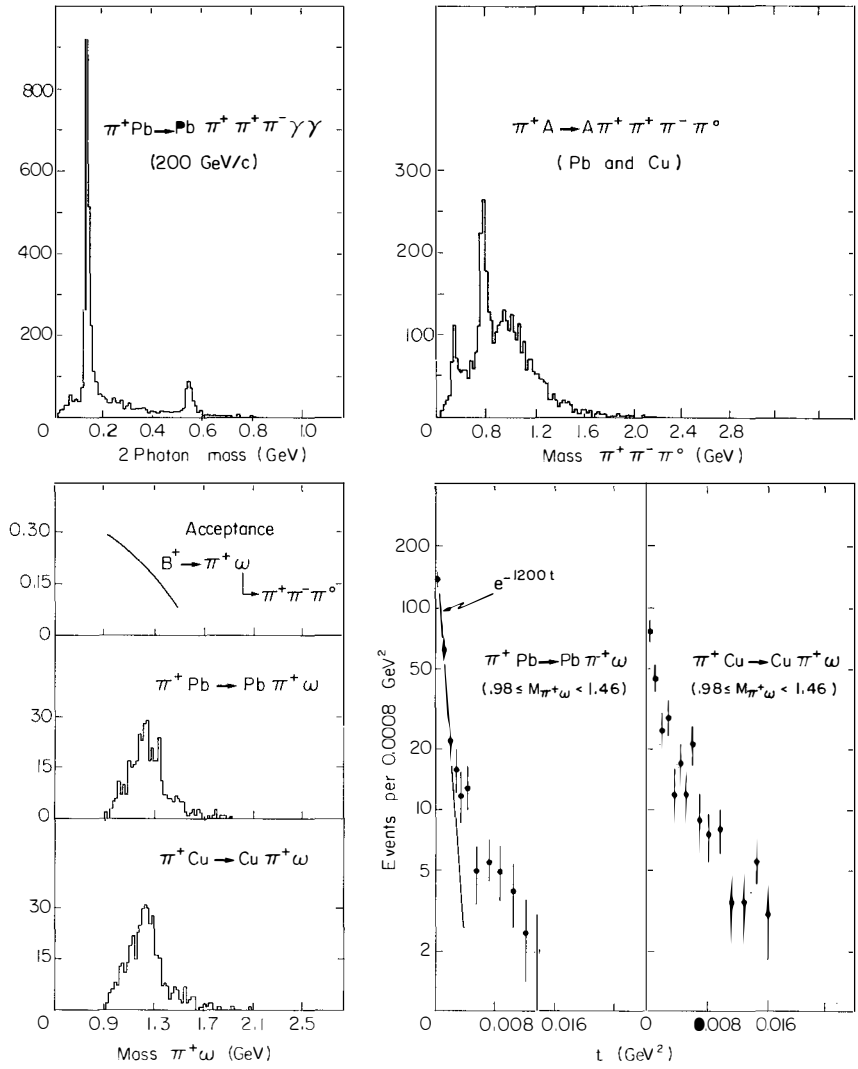

Fig. 4: Evidence for the electromagnetic production of the $B(1235)^+$ meson in the reaction $\pi^+ A \to B^+ A$ at 200 GeV

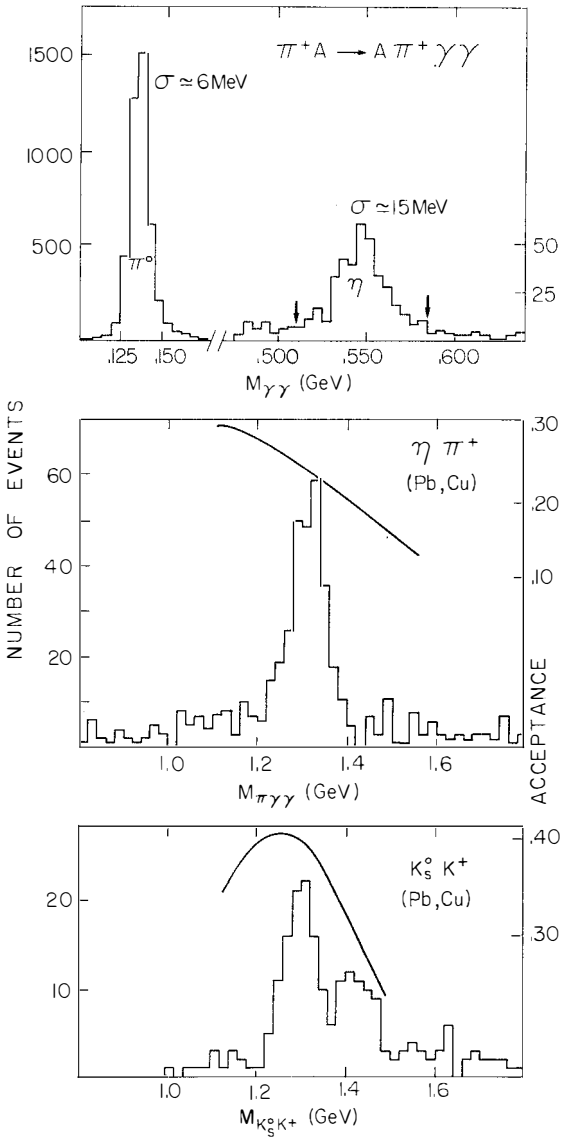

Fig. 5: Coherent A_2^+ production in $\pi^+ A$ collisions at 200 GeV.

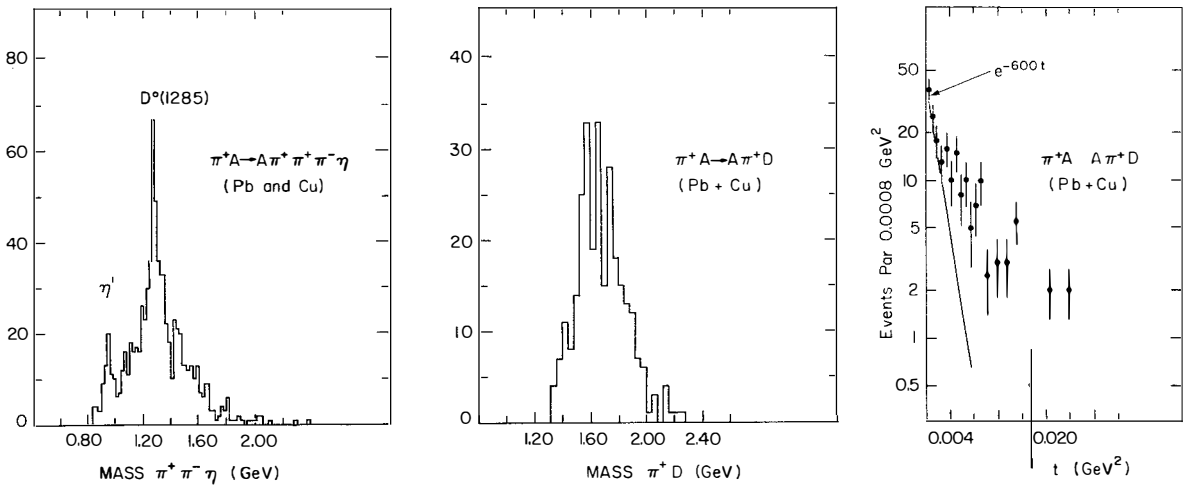

Fig. 6: Characteristics of coherently produced $\pi^+\pi^+\pi^-\eta$ final states at 200 GeV

puzzling that there is no evidence for the E(1430). The π^+D^o mass distribution is broad and appears to peak near the mass value of the A_3 (1660). There is, however, no known decay of the A_3, save into the $\pi^-\pi^+\pi^+$ channel. (Our $\pi^+\pi^+\pi^-$ data do not show a peak in that mass region). Consequently, at this time, we do not understand the nature or origin of the large D^o signal, nor of the connection, if any, of the π^+D^o enhancement to the A_3. Hopefully, once analysis is completed, we will be able to more fully elucidate the nature of these processes.

SUMMARY

Table I summarizes the results we have obtained thus far in our experiment.

Table I: Summary of Results

TRANSITION	Γ(KeV)
$\rho^- \to \pi^-\gamma$ PRL 44, 706 (1980)	67 ± 7
$K^{*-}(890) \to K^-\gamma$ Phys. Lett B98, 119 (1981)	62 ± 14
$\rho^+ \to \pi^+\gamma$ (Preliminary)	Consistent with the above values
$K^{*+}(890) \to K^+\gamma$ (Preliminary)	
$A_2^+ \to \pi^+\gamma$ (Preliminary)	∿ 450
$B^+(1235) \to \pi^+\gamma$ (Preliminary)	A few hundreds
$A_1^+ \to \pi^+\gamma$ (Preliminary)	A few hundreds
$K^{*+}(1430) \to K^+\gamma$ (Preliminary)	350 ± 100

Except for the ρ^-, we have been first to observe clearly the radiative transitions of the states listed in the Table. We anticipate that, in the future, the study of $\pi\gamma$ and $K\gamma$ collisions will contribute not only to the understanding of the properties of the known low-lying states but will also serve as a valuable new tool in meson spectroscopy. Data of the kind we have presented in Fig. 6, suggest that we may now be entering this new phase of investigation of production in the nuclear Coulomb field.

We thank Drs. A. Brenner, J. Peoples, T. Yamanouchi and L. Lederman of Fermi-Lab for their support of our experiment. One of us (T. Ferbel) wishes to thank the EP Division and the Fabjan-Willis group for their hospitality and support, and Drs. L. Montanet and J. Tran Thanh Van for providing him the opportunity of discussing these results at the Rencontre de Moriond. This research was supported by the U.S. Department of Energy and the National Science Foundation.

REFERENCES

1) T. Jensen, PhD thesis, University of Rochester Report 747 (1980).

2) P.J. O'Donnell elsewhere in these Proceedings.

3) B. Gobbi et al., Phys. Rev. Lett 33, 1450 (1974); ibid 37, 1439 (1976).

4) D. Berg et al., Phys. Rev. Lett. 44, 706 (1980);
D. Berg et al., Phys. Lett. B98, 119 (1981).

5) See O. Overseth elsewhere in these Proceedings.

6) A. Jonckheere et al., NIM 180, 25 (1981).

MAGNETIC MOMENTS OF HYPERONS

Oliver E. Overseth
University of Michigan
Ann Arbor, MI 48109

ABSTRACT

The Fermilab Neutral Hyperon Beam Collaboration has measured the magnetic moments of Λ^0, Ξ^0 and $\bar{\Xi}$ hyperons. With a recently published result for the Σ^+ hyperon, we now have precision measurements on the magnetic moments of six baryons. This allows a sensitive test of the quark model. The data are in qualitative agreement with the simple additive static quark model. Quantitatively however the data disagree with theoretical predictions by typically 15%. Several theoretical attempts to understand or remedy this discrepancy will be mentioned.

Knowledge of the magnetic moment of a particle provides information on its internal structure. For a point-like spin 1/2 charged particle the magnetic moment is given by $e\hbar/2mc$ as is known to be the case for electrons and muons. A neutral point-like particle would have no magnetic moment. Departures from these expectations (anomalous moments) imply the particle possesses an internal structure. It hs been known for a long time that the baryons cannot be point-like spin 1/2 particles since the charged baryons have considerable anomalous moments, and the magnetic moments of the neutral baryons are of the same order of magnitude as the charged moments. The baryons must have internal structures. We have, of course, a model, the quark model, for the composition of the baryons. Hence it is to be expected that precise determinations of the magnetic moments of the baryons should provide a good test of this model.

In the simple additive quark model the magnetic moment of a baryon is given by a vector addition of the moments of the three constituent quarks. For example, for the proton composed of 2 up and 1 down quarks with an SU(6) wave function $|p\rangle = \sqrt{2/3}\, u\uparrow u\uparrow d\downarrow - \sqrt{1/6}\,(u\uparrow u\downarrow + u\downarrow u\uparrow)d\uparrow$, $\mu_p = \langle p|\mu_u|p\rangle + \langle p|\mu_d|p\rangle$ results in $\mu_p = 4/3\ \mu_u - 1/3\ \mu_d$. The result for any baryon with two like-quarks can then be given by substitution of symbols. For example, for Ξ° = (ssu) $\mu_{\Xi^\circ} = 4/3\ \mu_s - 1/3\ \mu_u$. On the other hand, the result for Λ = (uds) turns out to be $\mu_\Lambda = \mu_s$. Thus this model predicts all nine baryon magnetic moments in terms of only three parameters μ_u, μ_d and μ_s.[1] These three parameters can be calculated from measured values of the magnetic moments of the proton, neutron and any strange baryon. Accurate measurements of the magnetic moments of the other hyperons thus furnish constraints to test the model.

The model can be pushed one stage further by assuming that the quarks are point-like spin 1/2 particles with a magnetic moment given by $qe\hbar/2mc$ where qe is the charge of the quark and m its mass. Determination of μ_u, μ_d and μ_s then determine the masses of the quarks. Or, conversely, values of quark masses obtained elsewhere can be put in this model and will lead to predictions of the magnetic moments of the baryons[2]. In any event it is clear that precision

measurement of hyperon magnetic moments should provide interesting insights into the quark model.

For 20 years experiments have been done to measure the hyperon magnetic moments but progress has been slow. See Table I. The standard method is to

TABLE I
Pre-hyperon beam magnetic moment determinations

Λ^o	-0.67 ± 0.06 n.m
Σ^+	2.83 ± 0.25
Σ^-	-1.48 ± 0.37
Ξ^o	--------
Ξ^-	-1.85 ± 0.75

produce polarized hyperons and to precess the spin vector in a magnetic field. The magnetic moment is proportional to the angle of precession. In addition to the difficulty of producing polarized hyperons in large numbers, the main problem has been that the short lifetimes of the hyperons limits severely the time spent in the magnetic field and hence limits the angle of precession of the spin vector. For this method to be practical, superconducting magnets have had to be used to provide large precessing fields. Measurements of the magnetic moment of the Σ^- have been made from X-ray studies of fine-structure splitting for transitions in exotic atoms formed with these particles. This is clearly a very difficult experiment also. However with the advent of high energy hyperon beams, and an unexpected gift from nature, we are now in a new era in the measurement of hyperon magnetic moments in which even the first round of experiments provide measurements of a precision of order of 1% or better.

At the Fermilab considerable work has been done in a neutral hyperon beam by a Michigan-Minnesota-Rutgers-Wisconsin collaboration[3]. The apparatus has been described in detail in the literature[4]. Briefly, 400 GeV protons strike a target producing a large number of secondary particles. The target is embedded in a 5 m long 23kG magnet which sweeps charged particles aside and a beam of neutral particles proceeds through a well defined collimator in the magnet to the experimental and detection region. Those that decay in the 12 m decay region are detected and identified by a multiwire proportional chamber

magnetic spectrometer augmented by a lead glass wall for decay modes involving π° mesons. The incident proton beam can be steered onto the target at angles from +10 mrad to -10 mrad with respect to the neutral beam collimator axis so we are not limited to zero-degree production angle. Typical neutral beams consist of 10^4 Λ and 10^2 Ξ° per machine pulse. The mean decay length of a 200 GeV Λ° or Ξ° is 14 meters.

The unexpected gift from nature is that these high energy hyperons are produced with substantial polarization[5] which is revealed by the angular asymmetry in their decay. The magnitude of the polarization increases with the transverse momentum of the hyperon at production and reaches 25% at P_t of 2 GeV/c. This spin vector precesses in the field of the sweeping magnet making possible the measurement of the magnetic moment of the hyperon. The precession angle is large (150° for Λ°, 300° for Ξ°) which allows precision measurements. There is great control over systematic instrumental biases in the apparatus. Bringing the incident proton beam on target from above instead of below reverses the initial direction of hyperon polarization. Reversing the sweeping magnet polarity precesses the spin either clockwise or couterclockwise through an angle of our choice (up to the maximum) by varying the magnitude of the magnetic field. Reversing the field of the spectrometer analyzing magnet cancels left-right biases in the detector. These bias eliminating conditions are crucial to precise determinations.

In this way we have measured the magnetic moment of the Λ to be -0.6138 ± 0.0047 μ_N[6] (proton magnetons) from a sample of 3×10^6 Λ decays. From this same experiment we analyzed 42,000 Ξ° decays and found the magnetic moment to be $-1.20 \pm 0.06 \mu_N$[7]. We have subsequently remeasured this Ξ° moment in an entirely different experiment and from 270,000 decays have determined the magnetic moment to be -1.253 ± 0.014 μ_N[8] for the Ξ° hyperon. Last year we converted the neutral hyperon beam to a charged hyperon beam and took data for the determination of the magnetic moments of the Σ^+, Σ^- and Ξ^- hyperons. For this conference we have a preliminary value for the Ξ^- moment to present, $\mu_{\Xi^-} = -0.75$

$\pm 0.07\mu_N$ (preliminary)[9]. We shall soon have the moments for Σ^+ and Ξ^- to about 1%. We are also working on the Σ^- moment but this is more difficult for us since the asymemtry parameter for this decay is so small.

All the results for baryon magnetic moments are summarized in Table II including a recently published value for the Σ^+ hyperon by the Munich-Vanderbilt HYBUC collaboration[10] at CERN. From a Σ° lifetime determination[11] in a neutral beam at CERN the Σ°-Λ transition moment can be deduced and is relevant as this moment also is predicted by the same model as the static hyperon moments.

We now possess precise determinations of the magnetic moment for six baryons and we can examine the quark model. The Λ hyperon moment is the most precisely known of the strange baryons so we will use it along with μ_p and μ_n as input in the simple static additive quark model. The predictions for this model are compared with experiment in Table II.

TABLE II
Experimental values for the octet baryon magnetic moments

Particle	Experimental	Theoretical
p	2.793	input
n	-1.913	input
Λ	-0.614 $\pm$ 0.005	input
Σ^+	2.33 $\pm$ 0.13	2.67
Σ°		-0.79
Σ^-	-1.48 $\pm$ 0.37	-1.09
Ξ^-	-0.75 $\pm$ 0.07(prelim)	-0.50
Ξ°	-1.25 $\pm$ 0.014	-1.44
$\Sigma^\circ \rightarrow \Lambda$	$1.82^{+.25}_{-.18}$	1.63

Assuming the quarks to be point-like particles and solving for static quark masses gives the mass of up, down, and strange quark, respectively, as 338, 322 and 509 MeV/c^2. These values are in good agreement with the mass ratio[2] and difference[12] obtained from models of hadron mass splittings.

Comparing predictions to experiment we see in the best known cases the data are about 15% below theoretical expectations and many standard deviations away. Although $\mu\Lambda$ has been taken as input in the Table it should be stressed that using instead any of the other hyperon moments as input does not help this

disagreement. The discrepancy is real.

Indeed using the magnetic moment of another hyperon (instead of μ_Λ) to determine the moment of the strange quark will give another value of μ_s other than that of μ_Λ and hence another value for the mass of the strange quark. Taking the model literally these data imply the mass of the strange quark depends on its environment. Or an anomalous magnetic moment of the quark that depends on its environment. Indeed the value of the moment for the Ξ^-, albeit preliminary at this time, has the disagreeable feature of implying that the mass of the strange quark is less than that of the down quark, a point that has not gone unnoticed.[13] Or equally disturbing is our result for the ratio $\mu_{\Xi^0}/\mu_{\Lambda^0} = 2.039 \pm 0.027$, which implies that the mass of the up quark and the strange quark are equal! The extension of the model to determine the magnetic moment of point-like quarks has serious problems with regard to the quark masses.

A number of papers have appeared to examine obvious shortcomings of the static model. Franklin[14] argues relativistic effects are important but orbital contributions probably less so in their effects on magnetic moments. Isgur and Karl[15] also have examined relativistic effects as well as contributions due to configuration mixing. In each of these cases, the corrections discussed have tended to improve agreement of theory with experimental values but discrepancies still remain and the improvements have really not been very satisfactory.

Also arguments have been made that one may consider adjusting the mass scale factor for all the baryons.[16] For example, Tomozawa[17] has argued that theory gives the magnetic moments in hyperon-magnetons (not proton-magnetons). The correction does go in the right direction, i.e. lowers expected moments, but does not solve the problem.

Several authors[18] have attempted to relax the requirements of the static additive quark model to give model independent sum rules between the moments relating the quark contributions. Unfortunately these sum rules almost always include μ_{Σ^-} so the test of their accuracy awaits a precision measurement of this

moment. However recently Lipkin[19] has derived sum rules between the well measured moments which imply a quenching of the contributions of nonstrange quarks in strange baryon magnetic moments, relative to contributions in the nucleon. Possibly this, if true, could be understood in terms of the pion exchange model of Brown, et al[20]. Better measurement of the Σ^- and Σ^+ moments would give additional information on this quenching. We are working hard to analyze our data on both of these moments.

In conclusion, present data indicate a serious disagreement with simple quark models for baryon magnetic moments which it does not appear can be easily fixed up by correcting some obvious shortcomings of the simple theory. Hopefully there is something to be learned from this discrepancy. Better measurements of some of these moments will help. So will some hard thinking.

REFERENCES

1. H.R. Rubinstein, F. Scheck, and R.H. Socolow, Phys. Rev. 154, 1608 (1967); J. Franklin, Phys. Rev. 172, 1807 (1968).
2. A. DeRujula, H. Georgi, and S.L. Glashow, Phys. Rev. D12, 147 (1975); H. Lipkin, Phys. Rev. Letters 41, 1629 (1978).
3. The members of the collaboration whose unpublished results are being presented in this paper are A. Beretvas, G. Bunce, P.T. Cox, L. Deck, T. Devlin, C. Dukes, J. Dworken, R. Grobel, R. Handler, K. Heller, K. Luk, O.E. Overseth, L. Pondrom, R. Rameika, M. Sheaff, and C. Wilkinson.
4. P. Skubic et al., Phys. Rev. D18, 3115 (1978); G. Bunce, et al., Phys. Rev. D18, 633 (1978).
5. K. Heller, et al., Phys. Rev. Letters 41, 607 (1978).
6. L. Schachinger et al., Phys. Rev. Letters 41, 1348 (1978).
7. G. Bunce et al., Phys. Letters 86B, 386 (1979).
8. P.T. Cox, et al., Phys. Rev. Letters. 46, 877 (1981).
9. R. Rameika, private communication.
10. R. Settles, et al., Phys. Rev. D20, 2154 (1979).
11. F. Dydak, et al., Nucl. Phys. B118, 1, (1977).
12. H. Lipkin, Phys. Lett. 74B, 399 (1978).
13. S.L. Glashow; H. Lipkin; private communication.
14. J. Franklin, Phys. Rev. Letters 45, 1607 (1980).
15. N. Isgur and C. Karl, Phys. Rev. D21, 3175 (1980).
16. H. Lipkin, Phys. Lett. 89B, 358 (1980); S. Oneda, T. Tanuma, T. Toiya and M.D. Slaughter, Phys. Rev. D23, 787 (1981).
17. Y. Tomozawa, Phys. Rev. D19, 1626 (1979).
18. J. Franklin, Phys. Rev. D20, 1742 (1979); R.G. Sachs, Phys. Rev. D23, 1148 (1981).
19. H. Lipkin, Argonne preprint ANL-HEP-PR-81-11, 1981.
20. G.E. Brown, M. Rho and V. Vento, Phys. Lett. 97B, 423 (1980).

STRONG INTERACTIONS OF HIGH-ENERGY CHARGED HYPERONS

Pierre Extermann
Université de Genève

ABSTRACT

The charged hyperon beam at the CERN SPS was used to measure the total cross sections of Σ^- and Ξ^- on hydrogen and deuterium between 75 and 135 GeV/c. An overall accuracy of 1% was achieved. The results are compared to various models based on quark additivity. As a by-product, Ω^- and resonance production was observed in Ξ^- p and Ξ^- d interactions. The following states have been identified: $\Sigma^{*-}(1385)$, $\Xi^{*0}(1530)$, $\Xi^{*-}(1700)$ and (1820), and $\Xi^{*0}(1940)$.

1. INTRODUCTION

This experiment was performed by the Bristol-Cambridge-Geneva-Heidelberg-Lausanne-Queen Mary College-Rutherford Lab. Collaboration[1]. It was designed to measure Σ^- and Ξ^- total cross sections on hydrogen and deuterium[2]. As a by-product, the Ξ^-p and Ξ^-d data provided new information on production of strange baryonic resonances and Ω^- [3]. A new experiment dedicated to Ξ^* and Ω^* spectroscopy will start taking data this summer.

2. THE TRANSMISSION EXPERIMENT

The hyperons are produced by 250 GeV/c protons impinging on a BeO target and are selected according to their charge and momentum by a curved magnetic channel about 10 m long. This channel is followed by a differential Cherenkov counter (DISC) that allows triggering either on Σ^- or on Ξ^- over the momentum range 70 to 137 GeV/c.

The experimental arrangement[2] contains the beam telescope, three cryogenic target vessels that are shifted sequentially through the beam, a decay telescope made of 6 clusters of multiwire proportional chambers, and a spectrometer magnet followed by a set of drift chambers.

3. HYPERON-NUCLEON TOTAL CROSS SECTIONS

The total cross section measurement relies on counting the relative number of hyperons that cross the target without interaction and decay in the fiducial decay region. The numbers of incident hyperons N_0^H, N_0^D and N_0^V are determined by the DISC. The superscripts H, D and V correspond to the hydrogen, deuterium and vacuum targets. Outgoing hyperons are identified through the kink in their trajectory corresponding to $\Sigma^- \to n\pi^-$ or $\Xi^- \to \Lambda\pi^-$ decay. The numbers of hyperons that emerge from the target with an apparent scattering angle $\theta < \theta_m$ and decay in the fiducial decay region are denoted N^H, N^D and N^V. The value of the cross sections is obtained from the usual equation

$$\sigma_T^{H,D} = \frac{1}{n\ell} \lim_{\theta_m \to 0} \ln \frac{N^V/N_0^V}{N^{H,D}/N_0^{H,D}} , \qquad (1)$$

where n and ℓ are the target density and length.

The results are presented in Fig. 1 together with p and K^+ cross sections[4]. The statistical errors are $\leq$ 1% and the scale errors are $<<$ 1%. One notices a substantial decrease of σ_T with increasing strangeness which occurs with equal spacing in the hydrogen data but not in the deuterium data. Furthermore, there is a significant rise of σ_T with momentum. The hyperon-neutron cross sections

computed from the deuterium and hydrogen data[5] are shown in Fig. 2. The $\Sigma^- n$ cross sections are found to be smaller than the $\Sigma^- p$ cross sections with a significance of two standard deviations. The opposite effect has been observed for pn and pp cross sections[4].

Various models predict the variation of baryon-baryon total cross sections as a function of projectile strangeness. The Additive Quark Model (AQM)[16] yields the relations

$$\sigma_T(\Sigma^- p) = \sigma_T(pp) - \Delta \tag{2a}$$

and

$$\sigma_T(\Xi^- p) = \sigma_T(pp) - 2\Delta \tag{2b}$$

where

$$\Delta = \sigma_T(\pi^- p) - \sigma_T(K^- p) \tag{3a}$$

$$= 3.55 \pm 0.08 \text{ mb at 102 GeV/c} .$$

The comparison with the hydrogen data presented in Fig. 3 (curve No. 3) shows a discrepancy of 1 to 2 mb. Furthermore, the AQM also predicts

$$\Delta = \frac{2}{3}\sigma_T(pp) - \sigma_T(K^+ p) \tag{3b}$$

$$= 6.76 \pm 0.07 \text{ mb} .$$

This second value which is twice as large as the first one leads to even larger discrepancies with the measured hyperon-proton cross sections.

Lipkin has proposed an empirical model which combines some Regge phenomenology with valence quark counting rules[6]. This model contains a two-component Pomeron and an ordinary Regge component. The momentum dependence of these components is accounted for by power laws. For an incident hadron H on a proton target, one has

$$\sigma_T(Hp) = \mathbb{P}^{(1)} + \mathbb{P}^{(2)} + \mathbb{R} \tag{4a}$$

with

$$\mathbb{P}^{(1)} = \frac{1}{2} N_q^H \sigma_1 \left(\frac{p_L}{20}\right)^{\varepsilon} \tag{4b}$$

$$\mathbb{P}^{(2)} = \frac{1}{2} N_q^H N_{ns}^H \sigma_2 \left(\frac{p_L}{20}\right)^{-\delta} \tag{4c}$$

$$\mathbb{R} = \sigma_R\left(N_d^H + 2N_u^H\right)\left(\frac{p_L}{20}\right)^{-0.5} \tag{4d}$$

where N_q^H, N_{ns}^H, $N_{\bar{d}}^H$ and $N_{\bar{u}}^H$ are respectively the total number of quarks, the number of non-strange quarks, and the number of $\bar{d}$ and $\bar{u}$ quarks in H. The parameters σ_1, σ_2, σ_R, ε and δ are constants to be determined from the data. At a fixed momentum p_L, the following relations result from Eqs. (4a-d):

$$\sigma_T(\Sigma^- p) = \sigma_T(pp) - \Delta^L \tag{5a}$$

$$\sigma_T(\Xi^- p) = \sigma_T(pp) - 2\Delta^L \tag{5b}$$

$$\Delta_1^L = \frac{3}{2}\left[\sigma_T(\pi^- p) - \sigma_T(K^- p)\right] = \frac{3}{2}\,\sigma_2\left(\frac{p_L}{20}\right)^{-\delta} \tag{6a}$$

$$\Delta_2^L = \frac{1}{2}\,\sigma_T(pp) - \frac{3}{4}\,\sigma_T(K^+ p) = \Delta_1^L\ . \tag{6b}$$

Fitting (pp), ($\bar{p}$p), ($\pi^{\pm}$p) and ($K^{\pm}$p) total cross sections, Lipkin obtains σ_1 = 13 mb, σ_2 = 4.4 mb, σ_R = 1.75 mb, ε = 0.13 and δ = 0.2. The resulting hyperon-nucleon total cross sections are in good agreement with our data as shown by curve No. 1 in Fig. 3. The adequacy of this model can be estimated from Fig. 4 where the differences between experimental and predicted hadron-proton cross sections are plotted against momentum. For p_L > 20 GeV/c, the agreement is better than 0.5 mb which is rather good given the small number of free parameters in the model. However, systematic trends appear with increasing momentum: for $\sigma_T(\pi^{\pm}p)$, the predicted values become smaller than the experimental ones whereas for $\sigma_T(K^{\pm}p)$, the effect is reversed. This implies that the discrepancy between Δ_1^L and Δ_2^L increases with momentum as shown in Fig. 5. This means that the quark counting rules in Eq. (4) break down at higher momenta, regardless of the parametrization used for the momentum dependence.

Joynson and Nicolescu[7] have proposed another two-component model. They assume the first component to be constant and SU(3) invariant and the second component to account for both the momentum dependence of the total cross section and the SU(3) breaking. This model provides a reasonable fit to the (pp), ($\bar{p}$p), ($\pi^{\pm}$p) and ($K^{\pm}$p) total cross section data and predicts an equal spacing rule for the hyperon-proton total cross sections similar to Eq. (2) but with a step

$$\Delta^{JN} = \frac{2}{3}\left[\sigma_T(\pi^- p) - \sigma_T(K^- p)\right], \tag{7}$$

which disagrees with our data (see curve No. 2 in Fig. 3).

More recently, Yoshida[8] suggested still another two-component Pomeron scheme that emerges from a model in which all reactions proceed through a two-Reggeon

intermediate state. The $(\Sigma^- p)$ and $(\Xi^- p)$ total cross sections are predicted to be equal, a statement that is clearly not supported by the data.

A different approach to the Pomeron problem was undertaken by Carlitz, Green and Zee[9]. In this model, the Pomeron couples indirectly to the external hadrons through the f and f′ mesons, which carry the vacuum quantum numbers. The f meson is assumed to couple to all quarks in the external hadrons whereas f′ couples only to strange quarks. Two parameters appear in the total cross section estimates:

$$r(t) = \frac{\alpha_P(t) - \alpha_f(t)}{\alpha_P(t) - \alpha_{f'}(t)} \tag{8}$$

where $\alpha_i(t)$ are Regge trajectories, and

$$\varepsilon = D/F \tag{9}$$

where D and F are the spin-nonflip coupling constants of the $\{f, A_2, K^{**}\}$ nonet to the baryon octet. The following total cross section ratios are obtained:

$$R_{K\pi} = \frac{\sigma_T(Kp)}{\sigma_T(\pi p)} \underset{s \to \infty}{=} \frac{1 + r}{2} \tag{10a}$$

$$R_{\Sigma p} = \frac{\sigma_T(\Sigma p)}{\sigma_T(pp)} = \frac{2 + r(1-\varepsilon)}{3 - \varepsilon} \tag{10b}$$

$$R_{\Xi p} = \frac{\sigma_T(\Xi p)}{\sigma_T(pp)} = \frac{1 - \varepsilon + 2r}{3 - \varepsilon} \tag{10c}$$

where $r = r(0)$. With $r = 0.6$ and $\varepsilon = -1/3$ as assumed by Carlitz, good agreement is obtained with our $\sigma_T(\Xi^- p)$ results, but not with the $\sigma_T(\Sigma^- p)$ results (see curve No. 4 in Fig. 3). However, at the time this model was published, the $\pi^{\pm} p$ and $K^{\pm} p$ total cross sections had been measured only up to about 20 GeV/c. If one uses the data obtained up to 300 GeV/c at Fermilab[4], Eq. (10a) yields the values of r plotted in Fig. 6, which are seen to reach an asymptotic value of about 0.73 rather than 0.6. Inserting in Eqs. (10b) and (10c) this new value of r and the cross sections measured at 135 GeV/c, we find $\varepsilon = -0.6 \pm 0.2$ and $\varepsilon = +0.75 \pm 0.10$, respectively. Unless $R_{\pi K}$, $R_{\Sigma p}$ and $R_{\Xi p}$ reach asymptotic values significantly different from the ones used here, this discrepancy between these two values of ε indicate a clear failure of the model.

In conclusion, it appears that none of the existing models provides adequate description of hadron-proton cross sections over the range in momentum and strangeness available today.

4. PRODUCTION OF HYPERON AND HYPERON RESONANCES IN Ξ^-N SCATTERING

The information from the drift chambers downstream of the spectrometer magnet was not used for the computation of total cross sections, but only for finding the beam momentum as well as the contamination in the trigger signal. Nevertheless, this information was recorded for every Ξ^- trigger. Therefore we have re-run the data tapes through a modified version of the reconstruction program with the minimal requirement of one V^0 and at least one additional track reconstructed through the magnet. Since no particle identification is available, we make mass assignments to the reconstructed trajectories and compute effective masses accordingly. Several cuts are applied to the data. (For more details, see Ref. 3.)

The distributions presented in Fig. 7 are obtained from the hydrogen target data at 135 GeV/c. The $(\Lambda\pi^-)$ effective mass distribution is shown in Fig. 7a. In order to suppress transmitted or elastically scattered Ξ^-, we have required i) $x(\Lambda\pi^-) < 0.95$, where $x = p^*_{\parallel}/p^*_{max}$, and ii) that the Λ and π^- trajectories point to the primary vertex. A signal corresponding to $\Sigma^{*-}(1385)$ appears at the right-hand side of the Ξ^- residual peak, over a rather large background. The background subtracted peak shown in the bottom histogram of Fig. 7a is fitted with a p-wave Breit-Wigner curve of fixed mass and width ($M = 1387.5$ MeV/c^2 and $\Gamma = 40$ MeV/c^2). There are 579 ± 145 events in the peak. The (ΛK^-) mass distribution is displayed in Fig. 7b. A minimal distance has been required between primary and secondary vertices and also all events with a $(\Lambda\pi^-)$ effective mass within 20 MeV/c^2 from the Ξ^- mass have been excluded. A clean Ω^- peak containing 245 ± 25 events appears over a rather smooth background. Finally the $\Xi^-\pi^+$ mass distribution appears in Fig. 7c. It is dominated by a peak corresponding to $\Xi^{*0}(1530)$ which contains 456 ± 30 events. In conclusion, we observe the non-diffractive production of three members of the lower mass baryon decuplet. Taking into account the decay branching ratios we obtain production cross sections of the order of 0.3 to 1.6 mb, for $x > 0.5$.

In order to look for less abundantly produced resonances, we have added together the data samples recorded at 102 and 135 GeV/c, with both the hydrogen and the deuterium targets. The (ΛK^-) mass spectrum in Fig. 8a is obtained by demanding i) the (ΛK^-) momentum to be equal to the beam momentum; ii) the Λ and K^- trajectories to point to the primary vertex and iii) the K^- momentum to be greater than 30 (resp. 35) GeV/c. Two peaks appear in the distribution. The first one at 1700 MeV/c^2 may well correspond to the "threshold enhancement" observed in the $\Sigma\bar{K}$ and $\Lambda\bar{K}$ channels by Dionisi et al.[10] thus confirming the resonant nature of

this state. The second peak is likely to be dominated by the well-known $J = {}^3/_2$ $\Xi^*(1820)$ state. The production cross sections times branching ratios for those two states are found to be of the order of 20 to 60 μb. The $(\Xi^-\pi^+)$ mass spectrum is shown in Fig. 8b. A clear enhancement appears at 1937 MeV/c^2 with a width of 40 MeV/c^2. The assignment for this peak is unclear. Several K^-N bubble chamber experiments have obtained indications for a rather broad signal in this mass region and also several states are expected to be there[11-13]. This enhancement is rather wide compared to other Ξ^* and therefore may contain more than one state.

5. HYPERON BEAMS AND STRANGE BARYON SPECTROSCOPY

The pilot search described above demonstrates that hyperon resonances can be produced with appreciable cross sections in Ξ^-N collisions. However, this search is handicapped by the acceptance of the spectrometer which decreases rapidly with increasing resonance mass. A new spectrometer dedicated to Ξ^* and Ω^* spectroscopy is now under installation. It has good mass acceptance up to 3 GeV/c^2 and also incorporates γ and neutron detectors as well as a threshold Cherenkov counter to distinguish kaons from pions.

Until now, almost all information on strange baryon spectroscopy came from K^-p and K^-d scattering experiments. A fair number of Λ^*, Σ^* and Ξ^* resonances have been found either in phase shift analyses or in effective mass distributions. However, many states predicted by SU(6) × O(3) symmetry arguments are still missing even in the $[\underline{70},-1]$ supermultiplet. The most serious problem is the complete lack of Ω^*. Recently, Koniuk and Isgur[12] have provided an explanation for the missing Λ^* and Σ^* resonances by demonstrating that these states have a weak coupling to the K^-N channel. For the missing Ξ^* and Ω^* states, the low cross section for $s\bar{s}$ quark pair production in K^-N collisions is the most likely explanation.

Hyperon beams and especially Ξ^- beams allow resonance production through different mechanisms (e.g. diffractive production) and therefore should enable us to find some of these missing states.

REFERENCES

1) The participants in this experiment were: S.F. Biagi, M. Bourquin, A.J. Britten, R.M. Brown, H. Burckhart, A.A. Carter, J.R. Carter, Ch. Doré, P. Extermann, M. Gailloud, C.N.P. Gee, W.M. Gibson, J.C. Gordon, R.J. Gray, P. Igo-Kemenes, W.C. Louis, T. Modis, P. Mühlemann, J. Perrier, Ph. Rosselet, B.J. Saunders, P. Schirato, H.W. Siebert, V.J. Smith, D.P. Stickland, K.-P. Streit, J.J. Thresher and R. Weill.

2) S.F. Biagi et al., Measurements of the total cross sections of Σ^- and Ξ^- on protons and deuterons between 74 and 137 GeV/c, accepted for publication by Nucl. Phys. B., CERN-EP/80-172.

3) S.F. Biagi et al., Production of hyperons and hyperon resonances in Ξ^-N interactions at 102 and 135 GeV/c, submitted to Z. Phys. C., CERN-EP/81-33.

4) A.S. Carroll et al., Phys. Lett. 61B (1976) 303 and Phys. Lett. 80B (1979) 423.

5) R.J. Glauber, Phys. Rev. 100 (1955) 242. We use $\langle r^{-2} \rangle = 0.035 \pm 0.004$ mb^{-1} as in Ref. 4.

6) H.J. Lipkin, Nucl. Phys. B78 (1974) 381 and Phys. Rev. D 11 (1975) 1827.

7) D. Joynson and B. Nicolescu, Nuovo Cimento 37A (1977) 97.

8) T. Yoshida, Nuovo Cimento 48A (1978) 133.

9) R. Carlitz, M.B. Green and A. Zee, Phys. Rev. D 4 (1971) 3439.

10) C. Dionisi et al., Phys. Lett. 80B (1978) 145.

11) M. Jones, R.H. Dalitz and R.R. Horgan, Nucl. Phys. B129 (1977) 45.

12) R. Koniuk and N. Isgur, Phys. Rev. D 21 (1980) 1868.

13) K.T. Chao, N. Isgur and G. Karl, Phys. Rev. D 23 (1981) 155.

14) J.V. Allaby et al., Phys. Lett. 30B (1969) 500.

15) J. Badier et al., Phys. Lett. 41B (1972) 387.

16) For example, J.J.J. Kokkedee, The quark model (Benjamin, New York, 1969).

17) K.J. Foley et al., Phys. Rev. Lett. 19 (1967) 330.

18) CERN-Pisa-Rome-Stony Brook Collaboration, Phys. Lett. 62B (1976) 460.

19) S.P. Denisov et al., Nucl. Phys. B65 (1971) 1.

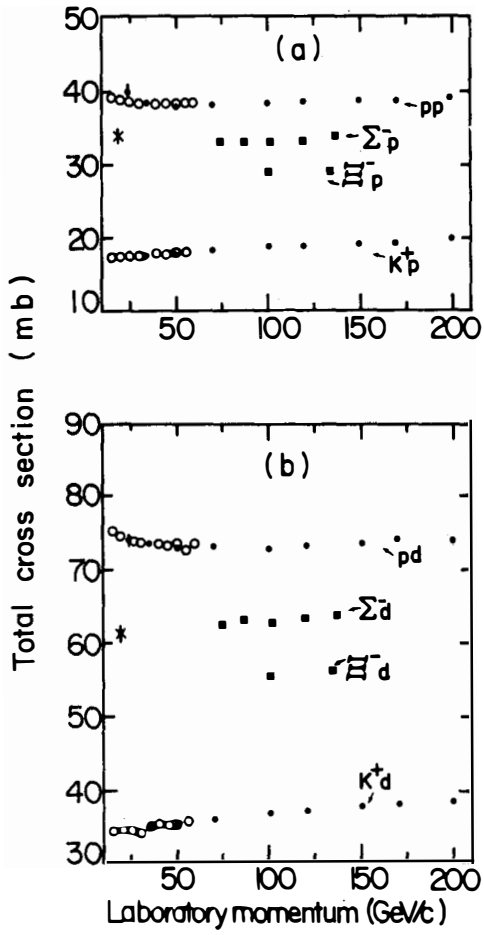

Fig. 1 Hyperon, proton and K^+ total cross sections on hydrogen and deuterium. ■ This experiment; ●Carrol et al.[4]; ○Allaby et. al.[14]; × Badier et al.[15].

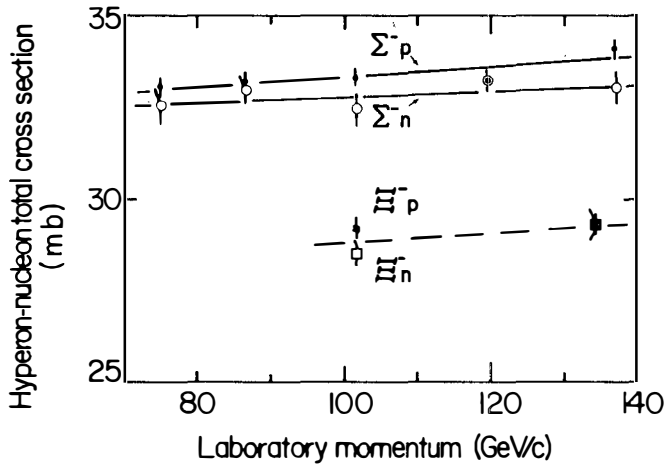

Fig. 2 Comparison of the total cross sections from protons and neutrons. The best straight line fits to the Σ^- data are shown.

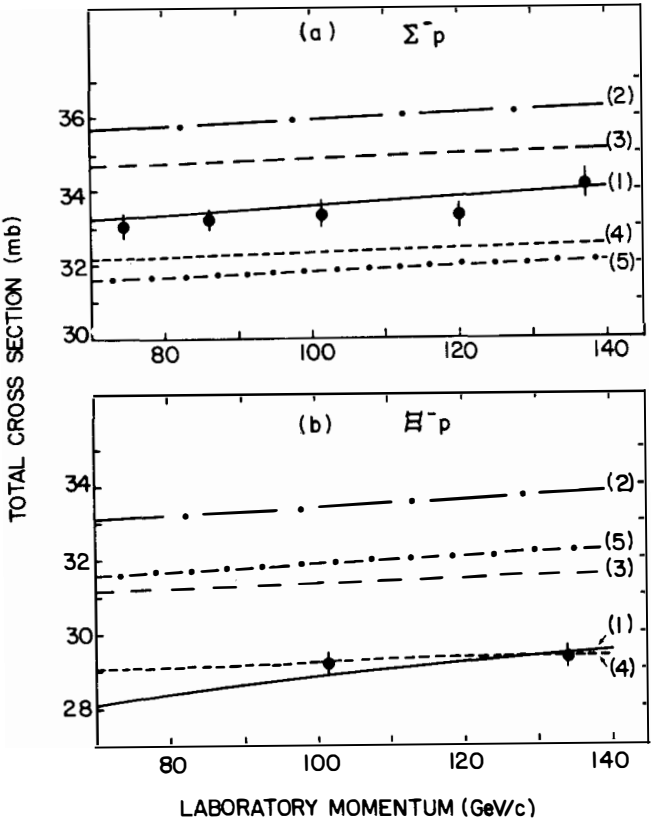

Fig. 3 Comparison of various model predictions with a) Σ^-p, b) Ξ^-p total cross sections. The curves represent the following models: (1) Lipkin[6]; (2) Joynson and Nicolescu[7]; (3) Additive Quark Model[16]; (4) Carlitz, Green and Zee[9]; (5) Yoshida[8].

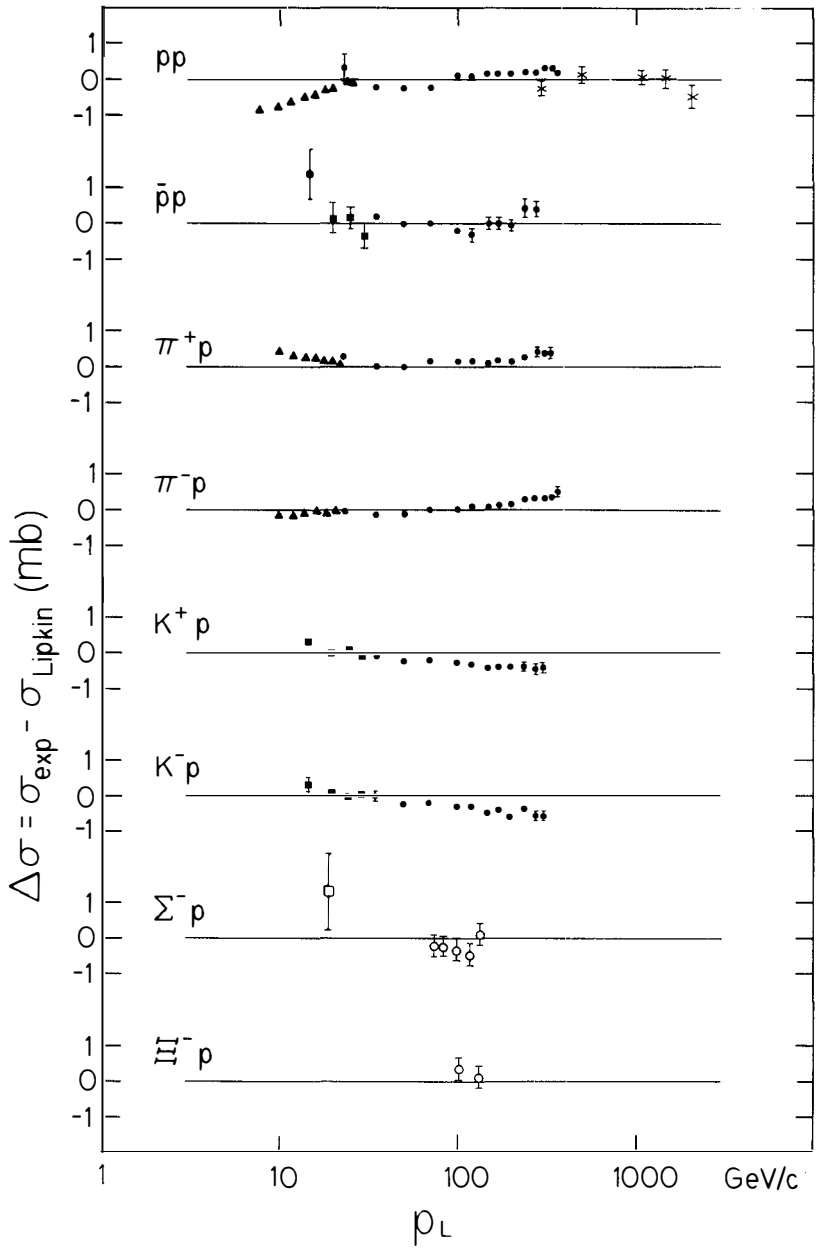

Fig. 4 Differences between experimental hadron-proton total cross sections and Lipkin's predictions. ▲Ref. 17; ● Ref. 4; × Ref. 18; ■ Ref. 19; □ Ref. 15; ○ This experiment.

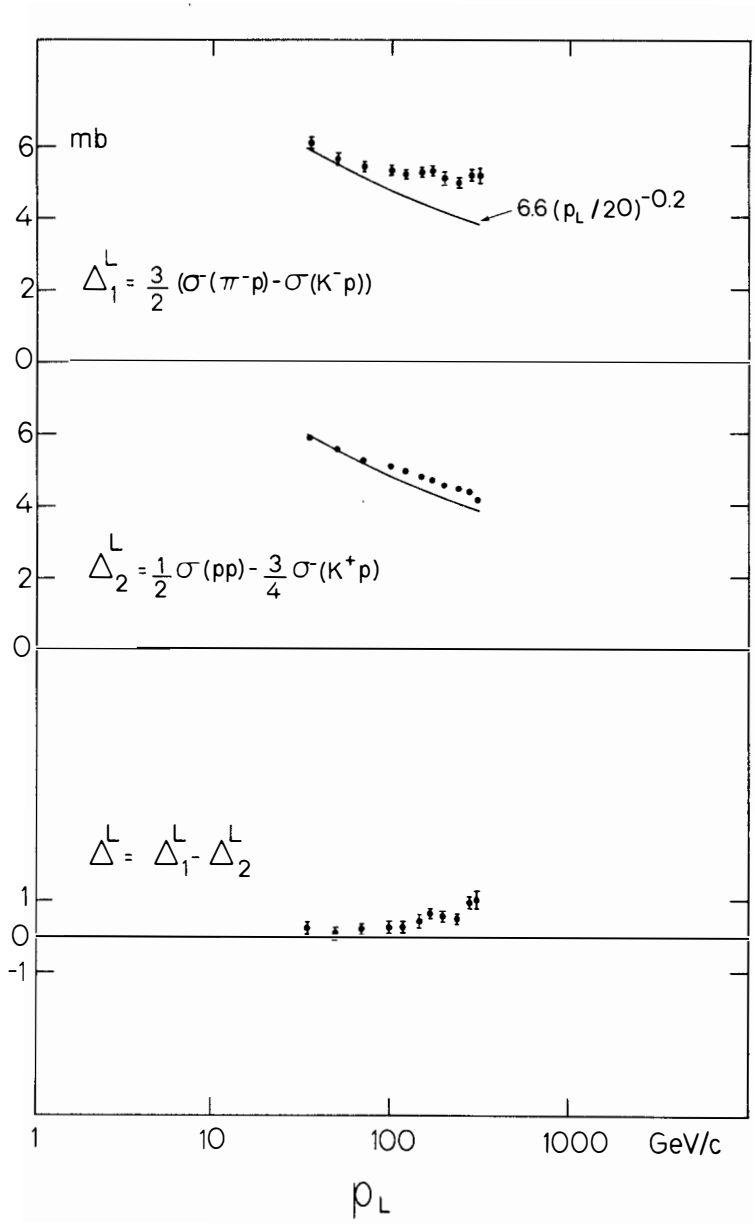

Fig. 5 Cross section spacings Δ_1^L and Δ_2^L (Eq. 6) versus momentum. The dots come from experimental data[4] and the curves from Eq. (6a).

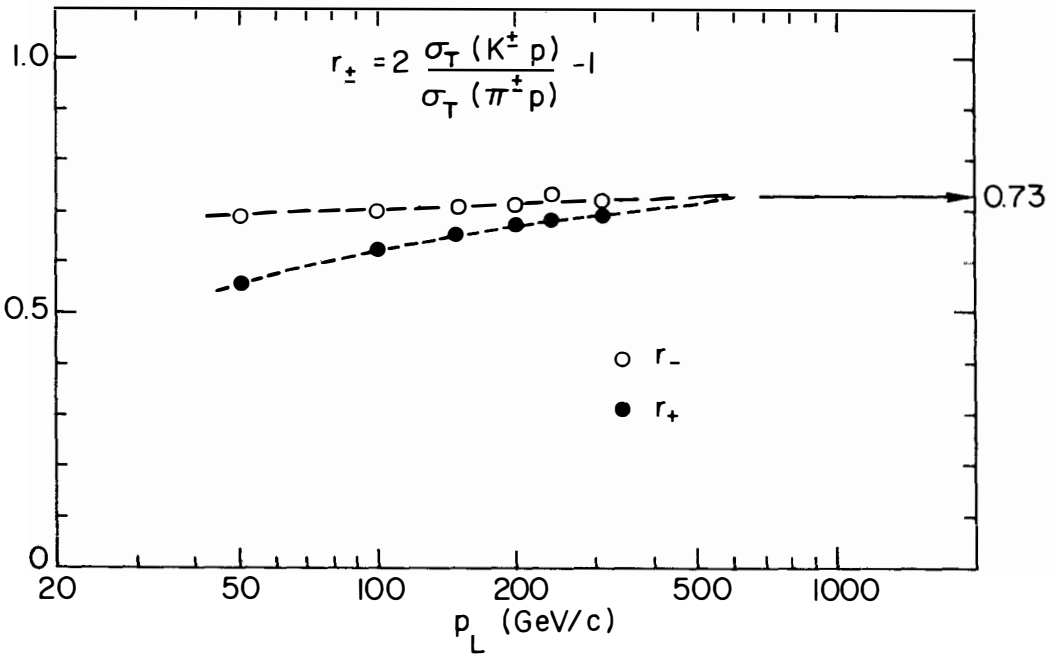

Fig. 6 Parameter r in Carlitz model computed from Eq. (10a).

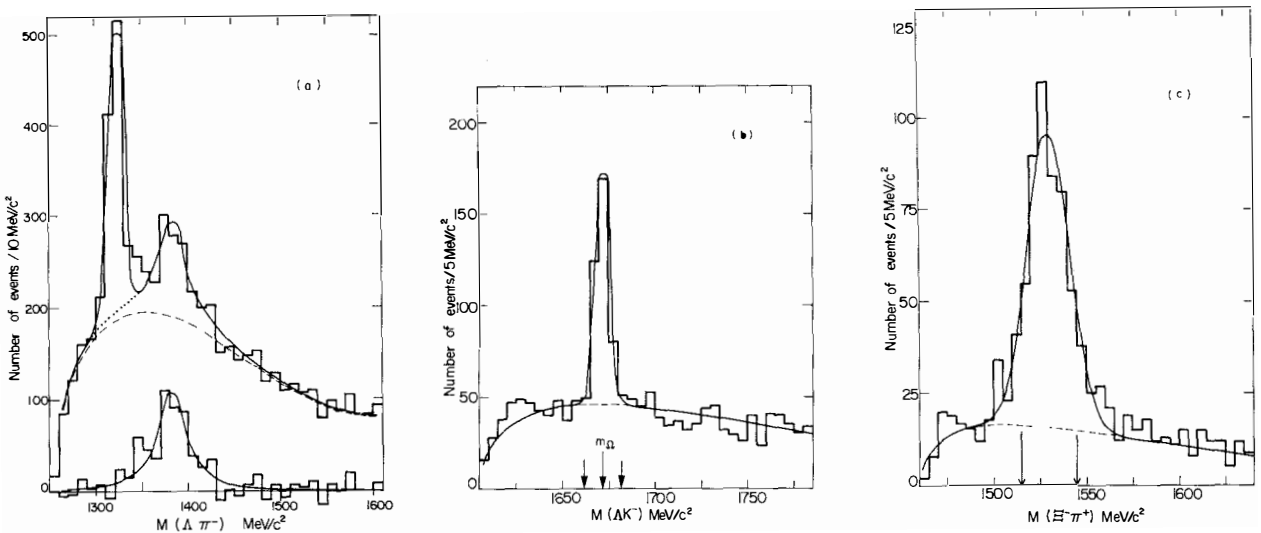

Fig. 7 Effective mass distributions from the 135 GeV/c H_2 target data. (a) ($\Lambda\pi^-$) channel. The dashed line corresponds to the background and the dotted line extends the $\Sigma^{*-}(1385)$ signal across the residual Ξ^- peak. The background subtracted Σ^* signal appears in the bottom histogram. (b) (ΛK^-) channel. The errors define the Ω^- signal. (c) ($\Xi^-\pi^+$) channel. The arrows define the $\Xi^{*0}(1530)$ signal.

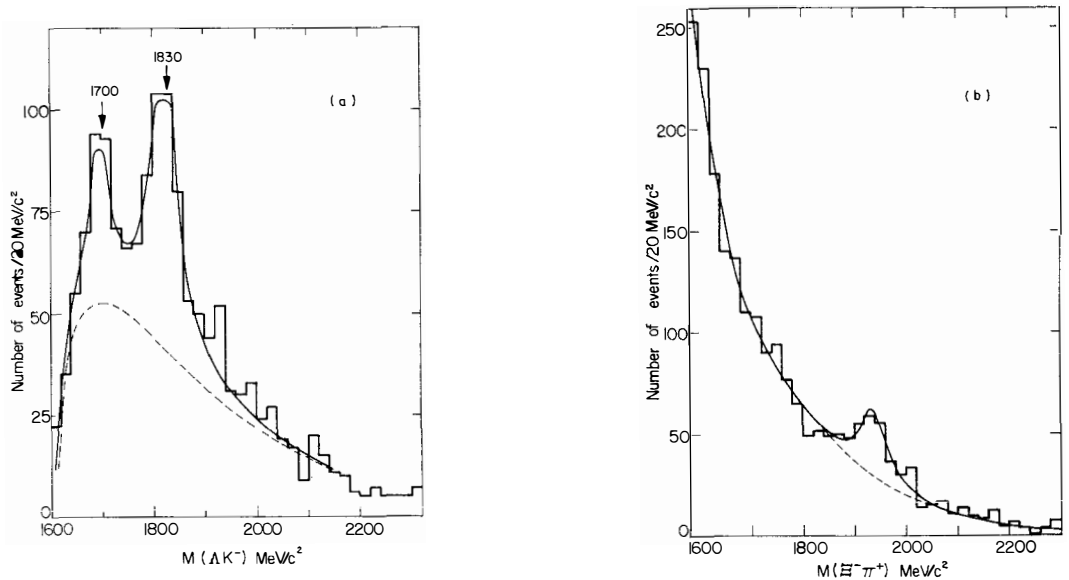

Fig. 8 Effective mass distributions from 102 and 135 GeV/c, H_2 and D_2 data. (a) (ΛK^-) "diffractive channel". (b) ($\Xi^-\pi^+$) channel.

GLUON CONTENT OF THE PROTON AND HYPERON MAGNETIC MOMENTS

Friedrich Wagner
Max-Planck-Institut für Physik und Astrophysik, Munich, Fed.Rep.Germany

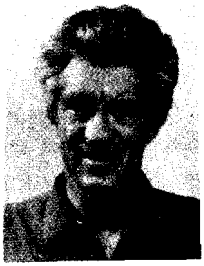

ABSTRACT

It is shown, that a gluon three quark component in the baryon octet and decuplet ground state can be quite large, if it is due to a constant color magnetic field inside the hadron. In the flavor SU(3) limit it reproduces the usual SU(6) quark model prediction except for a reduction of G_A/G_V. Flavor breaking by quark masses improve the agreement of Hyperon magnetic moments with experiment considerably by including such a gluon component.

I. Introduction

The observed hadron spectrum can be explained phenomenologically by a simple model, namely by nonrelativistic massive quarks moving in a potential[1]. Even details of the baryon spectrum can be accounted for by the Isgur-Karl model[2]. It is generally believed that such a model can be finally derived from a more fundamental theory (QCD) where colored light quarks interact via massless vector fields, the gluons. One proposal to solve this confinement problem is made in analogy to superconductivity[3,4] where an electric Meissner effect prevents physical states other than color singlet states to exist. It seems to me unlikely that all long distance QCD effects result in a nonrelativistic potential for quarks, and gluonic degrees of freedom can be discarded all together. One has already some hints that gluon components in the hadron wave function may be important. The hyperfine splitting of hadrons can be understood by a magnetic gluon exchange contribution to the energy[5]. This second order perturbation contribution implies a first order change in the wave-function. Similarily gluon effects have been advocated[6] to explain the mass splitting and decay rates in the charmonium states. Weak decays of D mesons may be affected by gluon effects.[7,8] Especially nonleptonic D (also K°) decays may proceed via annihilation, however the rates are much too small, if the quarks are in a spin singlet state. If gluons are present, the quarks can be also in a triplet state, and annihilation is not suppressed. For quantitative agreement this component must be rather large[8]. In deep inelastic scattering charged constituents carry only half the momentum of the proton. If this effect is due to short distance gluons, these may leave some foot prints also at long distances.

In this paper we want to investigate the effect of color magnetic forces on the hadron wave function. Usually this problem is treated by extrapolation of the short distance perturbation theory. This may be justified for heavy quarks (c,b, ...) but not for light spectrum quarks (u,d,s) whose compton wave length is comparable to the hadronic size. Rather, we will assume that in this case a slowly varying magnetic field induced by the color-magnetic moments of the quarks leads to an adequate description of the gluonic effects. In analogy to problems in solid state physics one can solve the Hamiltonian for the quarks by a semi-classical mean field approximation, which is to be discussed in section II. In presence of a color magnetic field the quarks are no longer in a color singlet state. By the Pauli principle this will change also the spin flavor wave-function and one may worry about the successful SU(6) prediction. In section III it will be demonstrated that in the frame work of the additive quark model the observables essentially do not change by the inclusion of color octet 3q configuration

in addition to the usual color-singlet proton or Δ state. We will not assume any specific potential, but rather fit the free parameters to the observed masses of the octet and decuplet. This fixes the wave-functions, and static properties as G_A/G_V or hyperon magnetic moments can be predicted (section IV).

II. Magneto-static Hamiltonian for quarks

We assume that color-electro-static forces lead to the usual nonrelativistic potential Hamiltonian H_o. To H_o we add the magnetic energy H_m from a constant color magnetic field B_a. Its vector potential reads as

$$\vec{A}_a(r) = \frac{1}{2} \vec{B}_a \times \vec{r} \tag{1}$$

With the conditions

$$\vec{B}_a \times \vec{B}_b \, f_{abc} = 0 \tag{2}$$

the homogeneous Maxwell equation are satisfied. In the nonrelativistic approximation we obtain for H_m in terms of the Pauli quark operator ψ

$$H_m = \frac{1}{2m} \psi^+ \left[\frac{g}{2} \vec{B}_a \lambda^a (\vec{L} + \vec{\sigma}) + \frac{g^2}{12} \vec{A}^2 + \frac{g^2}{4} d_{abc} \vec{A}_b \vec{A}_c \lambda^a \right] \psi \tag{3}$$

The first term describes the interaction of $\vec{B}_a$ with the intrinsic and orbital magnetic moment. Whereas the first two terms are also present in QED, the last term is typical for a SU(n) gauge group with $n \geq 3$. It describes the coupling of the quark charge $\psi^+ \lambda^a \psi$ to the color charge of the magnetic field. In addition to equs. (1-3) there is the constraint from the inhomogeneous Maxwell equation, which we write in analogy to the usual electromagnetic case

$$\vec{B}_a = \chi \, \psi^+ \vec{\sigma} \lambda^a \psi \tag{4}$$

where χ is the susceptibility of the hadronic matter. χ will differ from the diamagnetic value $-\frac{e}{2m}$ due to vacuum polarization effects. If electrical confinement is due to magnetic monopoles in the vacuum[4], they will strongly influence χ. χ will in general depend on B itself. Since we are interested in the effects of a strong B field we assume that χ is such that B saturates, the field strength is independent of the strength of the source. Neglecting the $\vec{L}$ and A^2 terms in H, equations (3)-(4) are nothing else but the Heisenberg ferromagnet. Also the BCS model[9] or the Jona-Lasinio-Nambu model[10] have a similar

mathematical structure. All these models are solved in the mean field approximation by replacing the r.h.s. of equ. (4) by its expectation value. For a classical $\vec{B}_a$ field the Hamiltonian (3) can be solved with eigenstate $|\varphi(B)\rangle$. Then equ. (4) becomes a nonlinear equation for $\vec{B}$

$$\vec{B}_a = \chi < \varphi(\vec{B}) | \psi^+ \lambda^a \sigma \psi | \varphi(\vec{B}) > \qquad (5)$$

the so-called selfconsistency equation (gap equation). In our case $\vec{B}_a$ can be used to describe many gluon effects in the hadron wave function. From equ. (4) we conclude it must transform like spin 1 under rotations and like a color octet representation under color transformations.

III. Baryon States with L = 0

We want to solve the Hamiltonian (3) for the baryon ground state. These are color singlet states containing three quarks with orbital angular momentum L = 0. The most general state reads as

$$|\varphi> = \frac{1}{\sqrt{3!}} \int \sum_{\alpha_i} \psi^+_{\alpha_1} \psi^+_{\alpha_2} \psi^+_{\alpha_3} \psi_{\alpha_1\alpha_2\alpha_3}(r_i) \, |0> \qquad (6)$$

where the wave-functions $\varphi_{\alpha_i}(r_i)$ depends on the spin, color and flavor index α_i and the quark coordinates r_i. The latter requires a specific H_o. We simply assume that this is independent from α_i. Therefore the r_i dependence can be factored out and need not to be considered anymore. φ_{α_i} consists of products of color wave-functions C_i and spin flavor wave-functions F. The antisymmetric color singlet wave-function has to be combined with flavor spin F_{56}

$$\varphi_0 = C_0 F_{56} \psi_0 \qquad (7)$$

For quarks in a color octet state C_8 the flavor spin part must be a $F_{70}^{SS_3}$ with quark spin S = 3/2, 1/2. The quark spin S will be combined with a spin 1 color octet object $\psi^k_a(B)$ to total spin J,M state. This leads to the following wave-functions $\varphi_{1,2}$ (note that $\varphi_2 = 0$ for the flavor decuplet)

$$\varphi_{S+\frac{1}{2}} = C_8^a F_{70}^{SS_3} < SS_3 \, 1 \, k \, | \, JM > \psi^k_a(\vec{B}) \qquad (8)$$

Color decuplet can be neglected since in this case H_o is purely repulsive.

Occurrence of a F_{70} wave-function in the baryon groundstate will in general change the successful predictions of the naive SU(6) model, which are based on the F_{56} assignment. However these predictions are based on the additive quark model, which tests only the single particle density matrix[11] but not the whole wave-function. For the flavor octet this matrix is characterized by two flavor coupling constants F and D. If only φ_o is present one obtains D = 1 and

F/D = 2/3. Almost any quark model prediction for the octet (magnetic moments, pseudoscalar coupling constants ...) depend only on this F/D ratio. Only $G_A/G_V = F+D = 5/3$ depends on the absolute size and disagrees with experiment. For the combination $\varphi_+ = \frac{1}{\sqrt{2}}(\varphi_1 + \varphi_2)$ for the octet one obtains the same F/D ratio as for φ_o. Therefore this combination leads to same quark model predictions as the usual φ_o. Only the absolute size of D for φ_+ is reduced to 2/3. Therefore G_A/G_V will be $\frac{5}{3} \cdot \frac{2}{3}$ for φ_+ alone. Presence of $\varphi_- = \frac{1}{\sqrt{2}}(\varphi_1 - \varphi_2)$ will lead to a different F/D ratio and thereby destroy the naive SU(6) predictions.

The Hamiltonian equ. (3) for the octet (decuplet) will be a 3x3 (2x2) matrix in the space φ_o, φ_+, φ_-. Solving[12] the self-consistency equation (5) together with condition (2) we find that φ_- decouples from the octet ground state. Therefore, the admixture of a 70 wave-function induced by the color magnetic field does not change the usual SU(6) predictions except for G_A/G_V. In order to describe the hadron masses we have to introduce the usual flavor breaking by assuming a heavier s quark mass. By the same time also coupling to the magnetic color field gets reduced for s quarks

$$B\,\psi^+\,\sigma\,\lambda\,\psi \cdot \rightarrow \frac{m_u}{m_s} B\,\psi^+\,\sigma\,\lambda\,\psi$$

This flavor breaking changes the matrix elements and mixes a φ_- component and flavor decuplet (singlet) contributions into the octet wave-functions. Since the matrix elements of H_m will involve integrals over the coordinate r_i, they depend on the specific H_o. If the B saturates the integrals are the same for the octet and decuplet for the similar radial dependence. Instead of assuming a specific H_o, we rather prefer to fit the seven parameters (integrals of the wave-functions involving B and A^2 terms in equ. (3), quark masses and zero point energy from H_o) which enter in the matrix of the Hamiltonian) to the observed octet and decuplet masses. The result of the fit is shown in table I. It reproduces the octet and decuplet masses up to the level of electromagnetic mass splitting.

Octet	Fit	Experim.	Decuplet	Fit	Experim.
m_P	0.939	0.939	m_Δ	1.234	1.232
m_Σ	1.184	1.193	m_{Σ^*}	1.376	1.383
m_Λ	1.112	1.116	m_{Ξ^*}	1.524	1.532
m_Ξ	1.326	1.318	m_{Ω^-}	1.674	1.672

Table 1: Comparison of fitted octet and decuplet masses with experiment[13]

In view of the many parameters this agreement is not too surprising, but it fixes the relative amount of glue 3 quark φ_+ and 3 quark φ_o wave-function. It turns out that φ_+ actually dominates. We arrive at the somewhat paradoxial

situation, that the proton is 75% of the time a flavor 70 plet and nevertheless we have the same mass spectrum and SU(3) prediction as for the usual 56 assignment. Knowing the wave-function we can now predict some static properties as G_A/G_V and hyperon magnetic moments.

III. Predictions

Since φ_+ dominates the proton wave-function, G_A/G_V will be substantially reduced as compared to the SU(6) value. In fact our value $G_A/G_V = 1.26$ is in good agreement with the experimental value 1.254 ± 0.007[13]. The additive quark model[11] reduces all magnetic moments to the quark magnetic moments μ_u, μ_d and μ_s. Adjusting $\mu_u = -2\mu_d$ and μ_s to the empirical values of Λ and P moments one can predict the other moments. In table II the first column gives the experimental value, and the second column the predictions of the usual SU(6) model ($\varphi_+ = 0$).

Hyperon	Experiment[13,14]	No glue component	Present work
Σ^+	2.33 ± 0.13	2.680	2.28
Σ^-	-1.41 ± 0.25	- 1.03	- 0.84
Ξ°	1.253 ± 0.014	1.42	1.24
Ξ^-	-0.75 ± 0.07	- 0.50	- 0.55

Table II: Comparison of Hyperon Magnetic Moments

Column 3 gives the result with φ_o only and column 4 the prediction of the wave functions including magnetic gluons. In both cases P and Λ moments are used to determine the up and strange mass magnetic moment.

They agree qualitatively with the data, although there is a 20% deviation in the case of Σ^+ and Ξ°. Including our glue component the P/N ratio remains unchanged, but Σ^+ and Ξ° are considerably improved. Unfortunately also Σ^- is moved away from the SU(6) prediction and Ξ^- is encreased not enough. Since these differ only from two standard deviations from experiment, we need not to be worried.

Besides the ground state there will be other positive parity states according to equ. (8) which have no color singlet component. They all are much higher in mass (> 1.8 GeV). They will be mixed with radial excitation occuring in the same energy region. This will be discussed elsewhere[12]

Our prediction for G_A/G_V and the magnetic moments should not be taken too seriously. First we used rather drastic assumption about B_a (constant over hadron and it strength independent whether it is in a Δ or P) and secondly other effects as relativistic effects[15], different sizes for proton and the hyperons[16] and configuration mixing[15,16] will affect matrix elements of the quark spin

operator. We only conclude from our findings, that a large color magnetic field and thereby a dominating quark color octet configuration in the proton is not entirely ruled out by experiment and may improve in the cases of G_A/G_V and Σ^+, Ξ° magnetic moments the agreement of theory and experiment.

I would like to thank Prof. Gourdin for the hospitality at Paris VI where part of the work has been done and also my theoretical colleagues at Munich for fruitful discussions.

References

1) O.W. Greenberg, Phys.Rev.Lett. 13 (1964) 598.
M. Jones, R.H. Dalitz and R.R. Horgan, Nucl.Phys. B129 (1977) 45, and references quoted therein.
2) N. Isgur and G. Karl, Phys.Rev. D20 (1975) 768.
See also N. Isgur's talk at this conference.
3) S. Mandelstam, Phys.Reports 23C (1976) 245.
4) G. 't Hooft, in: High Energy Physics, Proc. European Phys.Soc.Int.Conf., ed. A. Zichichi (Editrice Compositori, Bologna, 1976) p. 1225.
5) A. De Rujula, H. Georgi and S.L. Glashow, Phys.Rev. D12 (1975) 147.
6) For example, L. Heller and K. Johnson, Phys.Lett. 84B (1979) 501.
H. Goldberg, Phys.Rev.Lett. 44 (1980) 363.
7) L. Bernreuther et al., Heidelberg preprint 1980.
8) H. Fritzsch and P. Minkowski, Phys.Lett. 90B (1980) 455.
9) J. Bardeen, L.N. Cooper and J.R. Schrieffer, Phys.Rev. 108
10) Y. Nambu and G. Jona-Lasinio, Phys.Rev. 122 (1961) 345.
11) F.E. Close, Quarks and Partons, Academic Press, London 1979.
12) F. Wagner, to be published.
13) Particle Data Group, Rev.Mod.Physics 52 (1980) No. 2
14) G. Bunce et al., Phys.Lett. 86B (1979) 386.
15) Le Yaouanc, L. Oliver, O. Pène and J.C. Raynal, Phys.Rev. 15D (1977) 844.
16) N. Isgur and G. Karl, Phys.Rev. D21 (1980) 3175.
17) H.J. Lipkin, Phys.Lett. 35B (1971) 534.

NEW LIGHT ON DIPOLE SUM RULES

H. Krasemann
CERN - Geneva

ABSTRACT

We discuss the dipole sum rules in the context of the spin independent first order perturbation theory to a Schrödinger potential model. When applied to charmonium, thirty per cent corrections to the bounds on $\psi' \to \gamma P_c/\chi$ emerge. New upper and lower bounds on charmonium photon transitions are given. The same amount of corrections is discovered in a Klein-Gordon potential model which explicitly contains relativistic kinematics. We then predict photon transition rates for upsilons.

INTRODUCTION: THE STATUS OF $c\bar{c}$ E1 TRANSITIONS AND CORRECTIONS

The charmonium system and especially its spectrum can be understood reasonably well in terms of a non-relativistic potential model with the Schrödinger equation[1),2)]. One test for the degree of non-relativity (which, however, will turn out to be misleading except for the spectrum) is usually a calculation of the first order relativistic correction to the kinetic energy of a c quark in the J/ψ [2)], which turns out to be well below 10% [corresponding to $(v/c)^2 < 0.4$]. Nevertheless we observe big discrepancies between theory and experiment for decays, especially lepton pair decays and radiative transitions. Adopting the naïve model, we can fit the one or the other, but not both[2)]. The sensitive parameter here is the quark mass m_c. With low $m_c \approx 1$ GeV we can fit the lepton pair decay to lowest order

$$\Gamma (J/\psi \to \mu^+ \mu^-) = 16 \pi \alpha^2 e_c^2 \, |J/\psi(0)|^2 \, M_{J/\psi}^{-2} \qquad (1)$$

and with high $m_c \approx 3.5$ GeV we can fit the electric dipole (E1) radiation

$$\Gamma_{E1} (\psi' \to \gamma P_c/\chi) = \frac{4}{3} \quad \frac{2j+1}{9} \quad \alpha \, e_c^2 \, K^3 \, |\langle \psi' | r | P_c/\chi \rangle|^2 \qquad (2)$$

where j is the spin of the P_c/χ and e_c the quark charge, J/ψ, P_c/χ and ψ' are Schrödinger model wave functions.

A good value for the constituent c quarks mass lies between one and two GeV, implying that there are substantial corrections to both formulae (1) and (2). The corrections to (1) are widely discussed in the literature and we will not take this up here. Instead we will concentrate on the corrections to (2). What is the status ? Experimentally, all three transitions (2) are measured to be (16±5) keV [3)], while a model calculation with $m_c = 1.6$ GeV gives (36,50,58) keV for $j = (2,1,0)$. Can we tune the model so that it matches experiment ? The answer is "no", because the best quantity to calculate,

$$K \, |\langle \psi' | r | P_c/\chi \rangle|^2 \quad , \qquad (3)$$

is only sensitive to m_c [it is $\sim m_c^{-1}$, therefore a large m_c makes the rates (2) small] and very insensitive to any other parameter of the model. For example, varying the power α of a power potential $V(r) \sim r^\alpha$ between $\alpha = 0$ and $\alpha = \infty$ changes (3) by less than 10% [4)].

Unable to tune (3), we have to ask for corrections to (2) beyond the strictly non-relativistic model. A list of (relativistic) corrections contains

i) finite size effects (= corrections to the long photon wave length approximation),
ii) recoil corrections,
iii) higher multipoles beyond E1,
iv) extra terms in the transition Hamiltonian,
v) admixtures of different radial and orbital eigenstates, and of a $D\bar{D}$ (or $D\bar{D}^*$, etc.) continuum
vi) corrections to the size of the wave functions.

Finite size effects, which have been discussed by Novikov et al.[5], and recoil corrections both show up as an extra factor $\exp(-i\vec{k}\cdot\vec{r}/2) \neq 1$ in the transition matrix element. For processes (2), $(k\,r/2)^2$ lies between 0.04 and 0.25, but a simple calculation[5] shows that there is an extra suppression factor of 10 coming from the three dimensional nature of the problem. Thus corrections i) and ii) will be negligible. Higher multipoles iii) may be controlled by an expansion of the same $\exp(-i\vec{k}\cdot\vec{r}/2)$, again only the even powers are significant (this corresponds to an expansion of either the electric or the magnetic field of the classical photon). For $j = 0$, multipoles higher than E1 are excluded, for the other states they should be a few per cent at most. It is amusing to note that this order of magnitude estimate leads us to expect at most 10% M2 in $\chi_2(3.55) \to \gamma\, J/\psi$. Extra terms in the transition Hamiltonian which appear as higher terms in the non-relativistic reduction iv) were first discussed by Novikov et al.[5]. More recently, this item has been taken up again by Karl, Meshkov and Rosner[6], who essentially show that no big effects appear. An admixture of different radial eigenstates in either ψ' or P_c/χ can be mimicked by tuning the potential. We have seen that this has no big effects. An admixture of different orbital eigenstates generally occurs in a relativistic treatment. It will only be significantly large if the states which mix lie nearby in energy. Therefore a 1^3D_1 admixture to the 2^3S_1 wave in ψ' is much more likely than any $\ell \geq 3$ admixture in the $\ell = 1$ P_c/χ states. But even in this case, the $1^3D_1 - 2^3S_1$ mixture induced by the bound state dynamics is negligibly small[2),5)]. The $\psi' - \psi''$ mixing occurs predominantly via the coupling of both states to $D\bar{D}$: the ψ'' decays Zweig allowed to $D\bar{D}$ and the ψ' are at least very close to threshold with a large virtual coupling to $D\bar{D}$. Radiative decays of the ψ' are mainly affected twofold: the $c\bar{c}$ content becomes renormalized and a strong (positive) interference between the transitions $2S \to 1P$ and $1D \to 1P$ occurs. In the model of Eichten et al.[7] the net effect, however, is only a 14 - 24% reduction of the rates (2). It is amusing to note that a change

of the sign of the D wave admixture in ψ would make the S-D interference in the $\gamma\,\chi(0^+)$ decay negative and would thus help to make the rates more similar. This is because the ratio of the amplitudes,

$$\frac{A(1^3D_1 \to \gamma\ 1^3P_j)}{A(2^3S_1 \to \gamma\ 1^3P_j)} = \left(5, \frac{-5}{4}, \frac{1}{20}\right)^{1/2} \text{ for } j=(0,1,2) \qquad (4)$$

is not uniform for the three P waves. To summarize this point (correction v), mixing effects are very likely to play an important role among the corrections to naïve non-relativistic dipole rates. We will now turn to another very important correction, namely relativistic effects on the size of $c\bar{c}$ wave functions vi). As a first attempt we will concentrate on spin independent effects. Since these will turn out to be quite large we also expect sizeable spin dependent corrections. To some extend these have been discussed by Jackson[8]. The spin independent corrections we study are a consequence of the modification of the non-relativistic equation of motion. A relativistic equation of motion exhibits a different relation between energy level differences and the size of the wave functions as compared to the non-relativistic case: for fixed level differences the relativistic wave functions will occupy less space and therefore dipole moments will be smaller. This can be seen in two ways. First, we discuss the dipole sum rules in the context of a model in first order perturbation theory to the non-relativistic case. There we will find a 30% reduction of the upper bounds on process (2) as given by the dipole sum rules. We then turn to a relativistic model using the Klein-Gordon (KG) equation. For charmonium, the transition rates of this KG model are reduced by the same 30% ÷ 40% as compared to the non-relativistic model.

E1 SUM RULES IN FIRST ORDER PERTURBATION THEORY

The $c\bar{c}$ Hamiltonian is

$$H = H^{(0)} + H^{(1)} \qquad (5)$$

where in the centre of mass system

$$H^{(0)} = \frac{P^2}{2u} + V(r). \qquad (6)$$

Here μ is the reduced mass and $V(r)$ the static part of the potential, while $H^{(1)}$ contains all non-static corrections. To first order perturbation theory all terms in $H^{(1)}$ are known[9),10)]. Even numerical calculations of $H^{(1)}$ for the $c\bar{c}$ system exist[11),12)]. To this first order all spin dependent terms leave the centres of gravity of multiplets invariant, so that it is consistent to consider these centres of gravity and the spin independent corrections alone. The energy difference k in (3) will change from zeroth to first order, while the matrix element of the dipole operator in (3) will not (wave functions are unaffected in first order). With the numerics of Ref. 11)

$$K^{(1)}/K^{(0)} \simeq 0.7 \tag{7}$$

where $m_c = 1.8$ GeV [a smaller quark mass than 1.8 GeV should make the ratio (7) even smaller]. Expression (3) can now be rewritten as

$$\frac{K^{(1)}}{K^{(0)}} \; K^{(0)} \; |\langle\psi'|r|P_c/\chi\rangle|^2 . \tag{8}$$

The important observation is that the dipole sum rules only bound $k^{(0)}|\langle\psi'|r|P_c/\chi\rangle|^2$ but not the whole of (8). To see this, remember that the sum rules are derived from the uncertainty relation $[\vec{x},\vec{p}] \leq 3i$ ($\hbar\equiv 1$) by using the lowest order equation of motion

$$\vec{P} = i\mu \left[H^{(0)}, \vec{x}\right] \tag{9}$$

to replace $\vec{p}$. It follows that

$$\left\langle \left[\vec{x}, \left[H^{(0)}, \vec{x}\right]\right] \right\rangle \leq 3/\mu \tag{10}$$

and with the insertion of a complete set of final states one arrives at

$$\Sigma_f \, K^{(0)}_{fi} \, |\langle f|\vec{x}|\, i\rangle|^2 \leq 3/2\mu \, , \tag{11}$$

where $k^{(0)}_{fi} = \langle f|H^{(0)}|f\rangle - \langle i|H^{(0)}|i\rangle$. The consequence of this is a modification of all E1 sum rules by factors (7). With the numerics of Ref. 11) we have worked out the following Table of new dipole sum rule bounds.

transition	TRK SR	WK SR
$2^3S_1 \to \gamma 1^3P_2$	-	<25
$2^3S_1 \to \gamma 1^3P_1$	-	<35
$2^3S_1 \to \gamma 1^3P_0$	-	<40
$1^3P_2 \to \gamma 1^3S_1$	<410	>135 + 200 ± 80
$1^3P_1 \to \gamma 1^3S_1$	<310	>105 + 105 ± 40
$1^3P_0 \to 1\gamma\ ^3S_1$	<150	>50 + 40 ± 15

Upper and lower limits on $c\bar{c}$ E1 transitions (in keV) using the Thomas-Reiche-Kuhn and Wigner-Kirkwood sum rules to first order perturbation theory with m_c = = 1.8 GeV. We further use $\Gamma(\psi' \to \gamma P_c/\chi) = (16\pm5)$ kev[3]. Where the bound is expressed as two numbers, the second number and the error arise from this experimental measurement.

We note much less discrepancy between the measured rates (2) and the bounds in the Table than in a lowest order treatment[2]. Especially the upper and lower bounds on $P_c/\chi \to \gamma\ J/\psi$ no longer leave a big gap.

THE KLEIN-GORDON MODEL

The author has studied a charmonium potential model using the Klein-Gordon (KG) equation[13]. A considerable reduction of the quantity (3) as compared to the non-relativistic model was found. These findings have been checked by a detailed study of the $c\bar{c}$ system using the Dirac equation. In the introduction we noted that the quantity (3) varies by less than 10% for all confining power potentials. In fact, it never deviates by more than 10% from the sum rule value $3/2\mu$ (11). Consequently, we study the quantities

$$\delta_1 = \mu\, K_{1P,2S}\, |\langle 1P|r|2S\rangle|^2$$

$$\delta_2 = \frac{2}{3}\,\mu\, K_{1S,1P}\, |\langle 1S|r|1P\rangle|^2 \qquad (12)$$

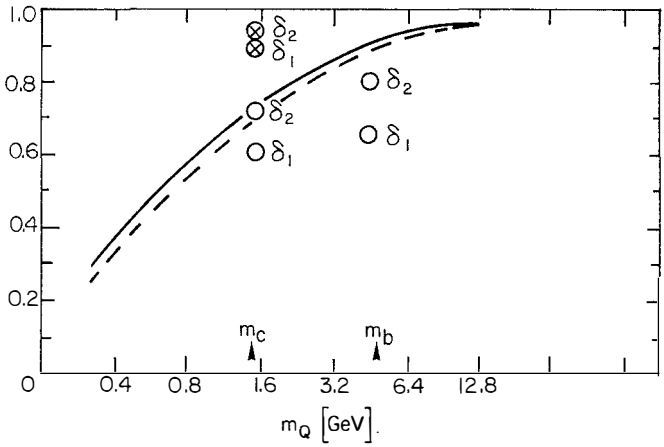

The quantities of (12) as a function of m_Q in a non-relativistic Schrödinger potential model (⊗) and in a KG potential model (○). Both models are of the Coulomb + linear type (standard model) and fit $c\bar{c}$ and $b\bar{b}$ respectively. The solid line shows δ_2 (the broken line δ_1) in a KG model with a pure (scalar) linear potential $V(r) = 0.8$ GeV/fm.

which are one in the non-relativistic harmonic oscillator and ≥ 0.9 in any non-relativistic monominal potential model which confines. The figure shows δ_1 and δ_2 in various models. One readily sees that the non-relativistic limit is not reached before $m_Q \approx 6 \div 10$ GeV. By comparison to the pure linear model it becomes evident that the Coulombic part of the potential plays a role for δ only in $b\bar{b}$, not in $c\bar{c}$. For $c\bar{c}$ the dipole sum rules are quite close to model rates, but for $b\bar{b}$ we need the model. We have done such a model calculation (using the KG equation) and find it most convenient to express the result as a modification of the formulae (6.11) through (6.14) of the second of Ref. 2). The rates are given by those formulae with

$$\bar{K}\,|r_{fi}|^2 = \frac{1}{m_b} \times \begin{matrix} 0.62 \times 4 \\ 0.81 \times 2 \\ 0.66 \times 5 \\ 0.89 \times 5 \\ 0.53 \times 2 \\ 0.73 \times 3 \end{matrix} \text{ for } \begin{matrix} 3S \to 2P \\ 2P \to 1D \\ 2P \to 2S \\ 1D \to 1P \\ 2S \to 1P \\ 1P \to 1S \end{matrix} \qquad (13)$$

where $\bar{k}$ is the average energy difference between the centres of gravity of the spin multiplets. Note that the dipole sum rules would give one for each decimal fraction shown in (13) except for $3S \to 2P$, where no bound exists.

CONCLUSION

We have shown that a good part of the discrepancy between the measured rates $\psi' \to \gamma P_c/\chi$ and their non-relativistic theory can be identified as relativistic size effects on the wave functions. We only discussed spin independent effects but it is conceivable that spin dependent effects may be of similar magnitude at least in charmonium. Such spin dependent effects would also affect ratios of these rates. Another source of this discrepancy is the neglect [with exception of Ref. 1)] of $D\bar{D}$ admixtures in S and P wave functions and of S - D wave mixing. The existing calculation shows relatively few net effects, but this topic certainly remains open. In principle the ratios of our rates are also strongly affected by S - D mixing.

In $b\bar{b}$ transitions relativistic effects are already much smaller, but the dipole sum rules are much less saturated than in $c\bar{c}$ because of the increasing importance of the Coulomb part of the potential. A calculation had to be done.

ACKNOWLEDGEMENTS

It is a pleasure to thank the organizers and especially L. Montanet for the opportunity to participate in such an enjoyable conference and to meet many friends.

REFERENCES

1) E. Eichten, K. Gottfried, T. Kinoshita, K.D. Lane and T.-M. Yan, Phys. Rev. D17 (1978) 3090; ibid. D21 (1980) 203.

2) M. Krammer and H. Krasemann, in "New Phenomena in Lepton-Hadron Physics", eds D.E.C. Fries and J. Wess, Plenum Publ. Corp., New York and London (1980), p. 161 ff., Acta Phys. Austr. Suppl. XXI (1979) 259.

3) Crystal Ball Collaboration, see e.g., C.M. Kiesling in the Proceedings of the 1979 EPS High Energy Physics Conference, Geneva (1979), p. 293 ff.

4) H. Krasemann, Thesis, Hamburg 1978, DESY T 78/01 (1978); compare also A. Martin, in "Quarks and Leptons", eds M. Lévy, J.-L. Basdevant, D. Speiser, J. Weyers, R. Gastmans and M. Jacob, Plenum Publ. Corp., New York and London (1980), p. 549 ff.

5) V.A. Novikov, L.B. Okun, M.A. Shifman, A.I. Vainstein, M.B. Voloshin and V.I. Zakharov, Phys. Rep. 41C (1978) 1.

6) G. Karl, S. Meshkov and J.L. Rosner, Phys. Rev. Lett. 45 (1980) 215.

7) E. Eichten, K. Gottfried, T. Kinoshita, K.D. Lane and T.-M. an, Phys. Rev. Lett. 36 (1976) 500, and Ref. 1).

8) J.D. Jackson, Phys. Lett. 87B (1979) 106.

9) D. Gromes, Nucl. Phys. B131 (1977) 80.

10) W. Celmaster and F.S. Henyey, Phys. Rev. D17 (1978) 3268.

11) D. Beavis, S.Y. Chu, B.R. Desai and P. Kaus, Phys. Rev. D20 (1979) 743.

12) T. Barnes, University of Southampton preprint 79/80-4 (1980), to appear in Z. Physik. Taking the numbers of this paper leads to smaller corrections than the numbers of Ref. 11). In our relativistic model Ref. 13, however, quantity (8) agrees with Ref. 11).

13) H. Krasemann, CERN preprint TH.3011 (1981), to appear in Phys. Lett.

INCLUSIVE $V^{O}V^{O}$ PRODUCTION IN 200 GeV/C $\pi^{-}P$ INTERACTIONS

D. R. Green
Fermilab, P.O. Box 500, Batavia, Ill. 60510

ABSTRACT

Inclusive $V^{O}V^{O}$ production has been studied in 200 GeV/c $\pi^{-}p$ interactions. Preliminary results on 5% of the data are presented. Production characteristics of K_S, Λ, $\bar{\Lambda}$, $K^*(890)$, $\Sigma^*(1380)$, K_SK_S, $K_S\Lambda$, $K_S\bar{\Lambda}$, $\Lambda\bar{\Lambda}$, $\Xi^*(1820)$ and $\Xi^*(2430)$ are discussed.

I. INTRODUCTION

The experiment herein described is Fermilab E580. The collaboration consists of groups from Arizona, Fermilab, Florida State, Notre Dame, Tufts, Vanderbilt and Virginia Tech. The purpose of the experiment is to study inclusively produced two neutral vee events in 200 GeV/c $\pi^- p$ interactions.

$$\pi^- p \to V^o V^o + n\pi^{\pm} \qquad (1)$$

The $K_s K_s$ system is a quantum number filter which allows I=0,1 but J^{pc} must be $(\text{even})^{++}$, i.e., 0^{++}, 2^{++}, ... Known states with $K_s K_s$ decays are $S^*, f, \varepsilon, A_2, f'$ and h. The $K_s \Lambda$ and $K_s \bar{\Lambda}$ systems are required to have I=1/2. One expects strong decays of N* and Ξ^* to have $K_s \Lambda$ decay modes. Finally, the $\bar{\Lambda}\Lambda$ system is required to have I=0. The only established particle with a $\Lambda\bar{\Lambda}$ decay mode is the ψ.

Other data on $V^o V^o$ inclusive production at high energies comes from 250 GeV/c $\pi^- p$ interactions[1] and 100 GeV/c $K^- p$ interactions.[2] Typically about 100 events are reconstructed. In comparison, we expect ultimately to reconstruct 100,000 events in a 400 hour run which yielded 1.5 million triggers.

II. APPARATUS AND TRIGGER

The experiment was run in May of 1980 at the Fermilab Multiparticle Spectrometer (MPS). It consists of 10,000 PWC wires, a spectrometer magnet with $p_\perp$ kick of 700 MeV, two multicell Cerenkov counters, and 24 spark chamber planes. Basically, the trigger consisted of measuring the event multiplicity twice upstream of a 2 m decay volume, and 7 times downstream (3 times behind the analyzing magnet). The multiplicity was required to increase by 3, 4, or 5 in the decay volume. The associated multiplicity n in reaction (1) was required to be ≤ 5 in order to reduce pattern recognition problems.

For diagnostic purposes we also triggered on elastic and 3π diffractive events. The rates for these triggers, and the $V^o V^o$ triggers were consistent with published data and allowed us to use them as normalizing reactions. In addition we took a small sample of events of the type $\pi^- p \to (V^o + \pi^-)\, x > 0$ to use in tuning the pattern recognition program on a single decay V^o with simple topology.

The beam rate was about 8×10^5 π^-/spill. We used a 10 cm active scintillator target. The trigger cross section was 22 μb. Of the 1.5 million triggers, 3×10^5 are diagnostic and 1.2 million are data.

III. PATTERN RECOGNITION AND KINEMATICS

The pattern recognition program used beam track triggers for alignment. Elastic and diffractive triggers were used to check the momentum and mass scale The single V^O triggers were used to study the V^O decay vertex and mass resolutions.

The V^OV^O events typically have an associated multiplicity in the forward hemisphere ($x \gtrsim 0$) of $\langle n \rangle \sim 2.7$. Using simple forms for track parameters, a decay vertex, decay point in the decay volume, V^O pointing at the production target, and V^O mass ~ K_s or Λ mass were required. All events with at least one V^O candidate (40% of all triggers) were selected for further processing.

At present only 5% of the V^OV^O candidates (20% of all triggers) have been further analyzed. First, all tracks were fit to a global 3 dimensional trajectory. This fit improved the track parameters by a factor of 2. Then the same cuts with tighter tolerances were again imposed to define a V^O. Typically, the K_s^O mass had a standard deviation of 5 MeV while the Λ was 2 MeV. Constrained fits were then made for the decay vertex (1-C), V^O mass (1-C) and V_1^O-V_2^O-beam primary vertex (3-C).

IV. SINGLE V^O PRODUCTION

The pions from K_s decays typically had $\langle p_\perp \rangle$ = .3 GeV/c, $\langle \theta \rangle$ = 20 mrad, $\langle p \rangle$ = 20.2 GeV/c, and a uniform azimuthal distribution. Pions from Λ^O decays had $\langle p_\perp \rangle$ = .13 GeV/c, $\langle \theta \rangle$ = 20 mrad, and $\langle p \rangle$ = 8.5 GeV/c. Since the magnet aperture subtended $\theta \sim 80$ mrad, little bias of the V^O decay particles is expected.

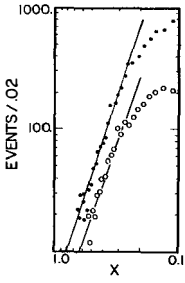

Fig. 1 - x distribution of K_s and Λ or $\bar{\Lambda}$.

The V^O are accepted by the apparatus only if $x \gtrsim 0$. We observe $\langle x \rangle_{K_s} \simeq \langle x \rangle_\Lambda \sim 0.2$ and $\langle p_\perp \rangle_{K_s} \sim \langle p_\perp \rangle_\Lambda \sim 0.5$ GeV/c. The distributions in x and $p_\perp$ are consistent with those of Reference 1, indicating no bias for $x_{VO} \gtrsim .08$. The raw x distributions for K_s and Λ or $\bar{\Lambda}$ are shown in Fig. 1. For $x > .25$ they go as $(1-x)^q$ with $q \sim -4$. It is of interest to compare this shape with dimensional counting predictions.[3] However, at this point we have not corrected

for the V^O detection efficiency.

Also of interest is the question of Λ or $\bar{\Lambda}$ polarization. In pp collisions the Λ is polarized while the $\bar{\Lambda}$ is not.[4] In Fig. 2 is shown the distribution of $\cos\theta_x$, where the x axis is the parity conserving axis, $\vec{p}_{beam} \times \vec{p}_{V^O}$, for Λ and $\bar{\Lambda}$ separately. Clearly, the Λ and $\bar{\Lambda}$ are unpolarized at the $\lesssim$ 10% level (1σ). With the full data set, one may expect to look for a $p_\perp$ dependence of the polarization. Note that the K_s decay angular distribution is uniform, which provides a check on possible systematic errors.

In Fig. 3 is shown the $V^O\pi^\pm$ effective mass distribution for K_s and Λ. A clear indication of K*(890) and Σ*(1385) production is seen. The fact that the trigger is inclusive means that possible states with $V^OV^{*\pm}$ and $V^{*\pm}V^{*\mp}$ decay modes can also be studied when a larger fraction of the data is reconstructed.

V. DOUBLE V^O PRODUCTION

The V^OV^O events accepted by the apparatus have $\langle x\rangle_{VV} \sim 0.4$ and $\langle p_\perp\rangle_{VV} \sim 0.7$ GeV/c. The K_sK_s x distribution goes as $e^{-\alpha x}$ with $\alpha = (6.3 \pm 1.0)$. The shape is distorted by acceptance for $x \lesssim 0.2$ indicating a $\sim$ 15% geometric acceptance for K_sK_s events. This bias represents a compromise between adequate decay length and good geometric acceptance. The x_{VV} distribution for K_sK_s and $K_s\ \Lambda$ or $K_s\ \bar{\Lambda}$ is shown in Fig. 4. For $x_{VV} > 0.5$ they go as $(1-x)^q$ with $q \sim -2$. Again the spectra are not corrected for apparatus bias.

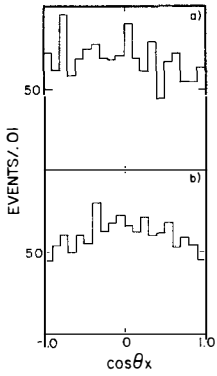

Fig. 2 - $\cos\theta_x$ distribution for a) Λ b) $\bar{\Lambda}$.

The V^OV^O effective mass distributions for K_sK_s, $K_s\Lambda$ or $K_s\bar{\Lambda}$, and $\Lambda\bar{\Lambda}$ are shown in Fig. 5. Typically, they fall as $e^{-\beta m}$ with $\beta \sim 3.1$ GeV^{-1} which is not atypical compared to other dihadron mass spectra at these energies.[5] It is expected that extraction of cross sections of known states will, in general, require the statistics available to the full data set and perhaps complicated subtraction procedures.[6]

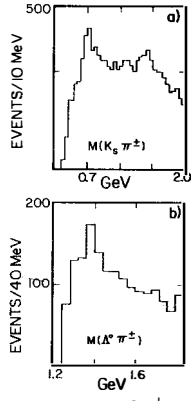

Fig. 3 - $V^O\pi^\pm$ effective mass distributions, a) $K_s\ \pi^\pm$ b) $\Lambda^O\pi^\pm$.

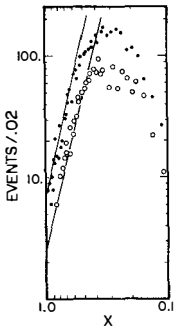

Fig. 4 - x distribution of K_SK_S • $K_S\Lambda$ or $K_S\bar{\Lambda}$ o.

At present, one attempts to extract 2 body decays using the distribution of c.m. decay angle. The $\cos\theta^*$ distribution for $\Lambda\bar{\Lambda}$ is roughly symmetric and forward/backward peaked, but the $\bar{\Lambda}\Lambda$ statistics are inadequate at present. The distribution for $K_S\Lambda$ and $K_S\bar{\Lambda}$ is shown in Fig. 6. Note that the K_S is preferentially emitted forward, while 2 body decays are presumably symmetrically distributed.

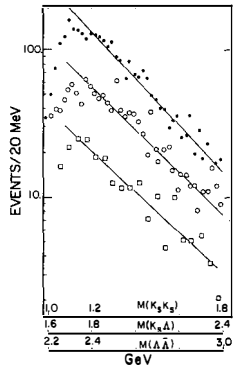

Fig. 5 - V^oV^o mass distributions • K_SK_S, o $K_S\Lambda$ or $K_S\bar{\Lambda}$, □ $\Lambda\bar{\Lambda}$.

The $K_S\Lambda$ or $K_S\bar{\Lambda}$ mass distribution requiring $\cos\theta^*$ ($V^oV^o \to \Lambda$ or $\bar{\Lambda}$) > -0.2 is shown in Fig. 7. The bin size is chosen to be comparable to the resolution. Some weak indications of production of a $\Xi^*(1820)$ and a $\Xi^*(2430)$ are seen.[7] Given the limited statistics, these indications are clearly of a preliminary nature.

VI. CONCLUSIONS

Experiment E580 will yield ~ 10^5 reconstructable V^oV^o events. The single V^o sample yields production characteristics for K_S, Λ, and $\bar{\Lambda}$; $d\sigma/dxdp_\perp$ and $\Lambda(\bar{\Lambda})$ polarization. In addition the production

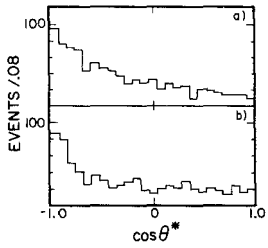

Fig. 6 - Decay angle of Λ ($\bar{\Lambda}$) in V^oV^o c.m. frame for a) $K_S\Lambda$ b) $K_S\bar{\Lambda}$.

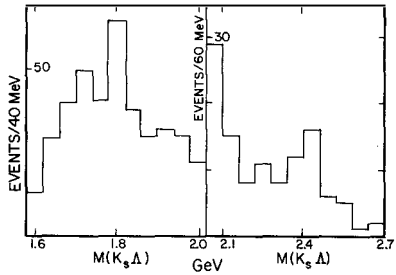

Fig. 7 - Mass distribution for $K_S\bar{\Lambda}$ or $K_S\bar{\Lambda}$ with $\cos\theta^* > -0.2$ a) mass ~ 1.8 GeV b) mass ~ 2.4 GeV.

characteristics for K*(890) and Σ*(1380) can be studied in detail.

The double V^o sample will ultimately yield production characteristics (i.e., $d\sigma/dxdp_\perp$) for: V^oV^o, $V^oV^{*\pm}$, and $V^{*\pm}V^{*\mp}$ with V^o = K_s, Λ or $\bar{\Lambda}$. At present, the statistics are adequate only to look at the dihadron continuum except in the case of $K_s\Lambda$ or $K_s\bar{\Lambda}$ where obvious 2 body cuts exist.

In an attempt to compare with other data on non-leading baryon production, data on $\bar{p}$, $\bar{\Lambda}$, and $\bar{\Xi}^-(1320)$ from the ISR[8] was compared to our data on Σ*(1380), Ξ*(1820), and Ξ*(2430). A distribution $d\sigma/dx = ae^{-bx}$, b = 6.0 was assumed to integrate over all x. Very crudely one finds that $\sigma(m) \sim \sigma_o e^{-\gamma m}$ with $\gamma \sim .25$ GeV^{-1}.

REFERENCES

1) D. Bogert et al., Phys. Rev. D 16, 2098 (1979).
2) P.R.S. Wright et al., CERN/EP, 81-2 (1981).
3) J.F. Gunion, Phys. Lett. 88B, 150 (1979).
4) K. Heller et al., Phys. Rev. Lett. 41, 607 (1978).
5) R.D. Kephart et al., Phys. Rev. Lett, 39, 1440 (1977).
6) A. Böhm et al., Phys. Rev. Lett. 41, 1761 (1978).
7) Particle Data Group, Rev. of Mod. Phys. 52, (1980).
8) S. Erhan et al., Phys. Lett. 85B, 447 (1979).

JET LIKE PROPERTIES OF MULTIPARTICLE SYSTEMS PRODUCED IN K^+p INTERACTIONS AT 70 GeV/c.

Brussels-CERN-Genova-Mons-Nijmegen-Serpukhov Collaboration

F. GRARD

Faculté des Sciences, Université de l'Etat, Mons, Belgique

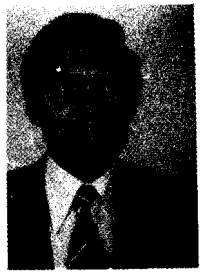

Abstract :

Using a sample of non-diffractive events from K^+p interactions at 70 GeV/c in BEBC, extensive comparisons are made between the hadronic low p_T data and results from hard jet production in e^+e^- annihilations and in deep inelastic ν-N interactions at comparable hadronic energies. Many similarities are found between low-p_T jets in this experiment and jets observed in leptonic interactions. Our data are very well reproduced by the Field and Feynman quark fragmentation parametrisation but equally well by a simple longitudinal phase space model, suggesting that these similarities do not prove or disprove the universal character of the jet fragmentation.

In recent years, hadron production in e^+e^- annihilations and in deep inelastic lepton-nucleon interactions as well as in high transverse momentum hadron-hadron collisions have been successfully interpreted in terms of quark-parton models.

In low p_T hadron-hadron collisions, the bulk of particles are produced in forward-backward jets, aligned along the incident beam direction. Striking similarities have been observed between these jets and those found in the above so-called hard processes. They would suggest that the quark-parton picture could be extended to hadron-hadron collisions at low p_T.

Using data from an exposure of BEBC filled with hydrogen to a RF separated K^+ beam having a nominal momentum of 70 GeV/c [1], corresponding to a c.m. energy of 11.5 GeV, we have made extensive comparisons between the hadronic low p_T data and data from hard-jet production in e^+e^- and neutrino induced reactions at comparable available energies [2].

The analysis is based on a partial sample of 9561 complete well measured events having at least four charged outgoing tracks. All charged particles were assumed to be pions, unless identified as protons by ionization. Neutral particles were identified by kinematical fitting. All measured particles were included in the analysis.

In order to compare our results to leptonic data, the influence of the diffractive component in hadronic interactions has been reduced by removing from the sample the events having at least one leading particle with $|X| > 0.8$. This cut affects 18.3 % of the events, mainly with 4 and 6 prongs.

The data have also been compared to the predictions of two models : a Field and Feynman model (FF) and a simple uncorrelated longitudinal phase space model (LPS). The parameters in these models were adjusted in such a way that the generated events reproduce the multiplicity and P_T distributions observed in our experiment.

In the FF simulation, two back to back quark jets have been generated by allowing only one valence quark from each of the colliding particles to fragment into hadrons. The σ_q parameter which accounts for the quark intrinsic p_T distribution has been extended from its original value of 250 MeV/c to

300 MeV/c[3]. The FF Monte Carlo reproduces quite well the measured charged particle multiplicity.

In the LPS model, n-particle exclusive reactions were generated according to the matrix element

$$|M|^2 = \prod_{i=1}^{n} e^{-B(y_i)m_{Ti}}$$

where m_{Ti} is the transverse mass of particle (i) calculated with respect to the beam direction. $B(y_i)$ are rapidity dependent parameters taken from the experimental inclusive single particle distributions. The various exclusive channels containing $\pi^{\pm}$,p,n,K° and π° particles were properly weighted using the measured average charged and neutral multiplicities.

All generated events were analysed in the same way as the experimental data.

The data have been analysed in terms of the sphericity, thrust and spherocity variables[4]. In principle, the sphericity, thrust and spherocity axes should coincide. In practice, they do not and the average angle between these axes is a measure of the precision with which either of them can be determined experimentally. This average angle is about 10°. It is interesting to note that the average angle between the jet axes and the beam direction has also about the same value. Also of interest is the fact that the above models account quite well for this observed spread in the direction of the jet axes.

In Fig. 1, the normalized sphericity, thrust and spherocity distributions are represented and compared to e^+e^- and ν-N data, as well as with the FF and LPS predictions. In Fig. 2, the average values $\langle S \rangle$, $\langle T \rangle$, $\langle S' \rangle$ are compared with leptonic data plotted over a wide rande range of energy. There is very good agreement between the various sets of data.

The average multiplicity for non diffractive events with $n_c \geqslant 4$ is 7.07 ± 0.03, a value which agrees quite well with leptonic results at the same hadronic energy[2]. In Fig. 3, the multiplicity distribution in a KNO plot is compared to e^+e^- results. We observe a good agreement with these data when the diffractive component is removed, whereas the corresponding distribution for the complete sample exhibits a quite different

shape (full line).

Fig.4 shows the normalized p_T^2 distribution relative to the sphericity axis. It agrees well with the e^+e^- data for $p_T^2<0.5$. At higher p_T^2, the TASSO data are slightly above our data. This effect is most probably due to the higher energy used for the comparison.

The normalized rapidity distribution of the charged particles, in the overall c.m. system, evaluated with respect to the thrust axis, is shown in Fig. 5. To avoid the asymmetry due to the backward identified protons, we use only particles produced forward in the total c.m. The TASSO results at $\sqrt{s}$ = 13 GeV are represented also for comparison. Both distributions are compatible with each other and have a clear plateau practically at the same height at y close to 0. The insert shows that the K^+p data are in agreement with the linear dependance of the height of the plateau on $\ln E_{cm}$ found in e^+e^-.

The average p_T and p_L as well as the average p_L evaluated by considering only secondary particles with $X > 0.1$ to suppress the non scaling part of the single particle distribution are represented on Fig. 6 together with PLUTO data plotted as a function of $\sqrt{s}$. Both sets of data are here also in very good agreement.

In conclusion, we find good agreement between the collective properties of low p_T "jets" in non diffractive K^+p interactions and of jets in leptonic induced reactions at the same available energy. In particular, the average charged particle multiplicity and p_T^2 distributions are very similar.

Furthermore, both Monte-Carlo models (LPS and FF) describle the data equally well and yield very similar predictions. This is not unexpected since the input to the models is essentially the same, namely the average charged particle multiplicity and transverse momentum distribution. We conclude that these two features alone account for many of the similarities observed.

References :

1) Brussels-CERN-Genova-Mons-Nijmegen-Serpukhov Collaboration.

2) ν-N : K.W.J. Barnham et al., Phys. Lett. 85B (1979) 300

e^+e^- : M. Derrick et al., Phys. Lett. 88B (1979) 177
R. Brandelik et al.,(TASSO) Phys. Lett. 86B (1979)243
Ch. Berger et al., (PLUTO) Phys. Lett. 78B (1978) 176
R. Brandelik et al.,(TASSO) Z. Physik C. 4 (1980) 87
R. Brandelik et al.,(TASSO) Phys. Lett. 89B (1980)480
Ch. Berger et al., (PLUTO) Phys. Lett. 81B (1979) 410
G. Hanson et al.,Phys. Rev. Lett. 35 (1975) 196;
SLAC-PUB-1814 (1976)
D.P. Barber et al., (MARKJ) Phys. Rev. Lett. 43
(1979) 830

3) R.D. Field and Feynman, Nucl. Phys. B136 (1978) 1

4) S. Brandt et al., Phys. Lett. 12 (1964) 57.

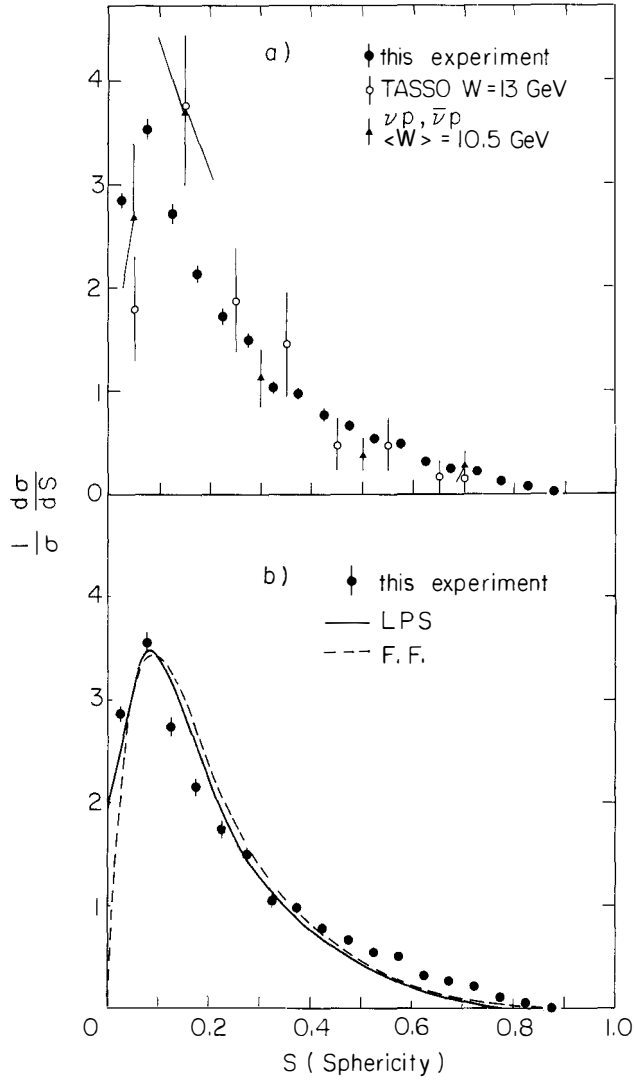
a)
this experiment
TASSO W=13 GeV
νp, ν̄p
<W> = 10.5 GeV
b)
this experiment
LPS
F. F.
1/σ dσ/dS
S (Sphericity)

Fig. 1A

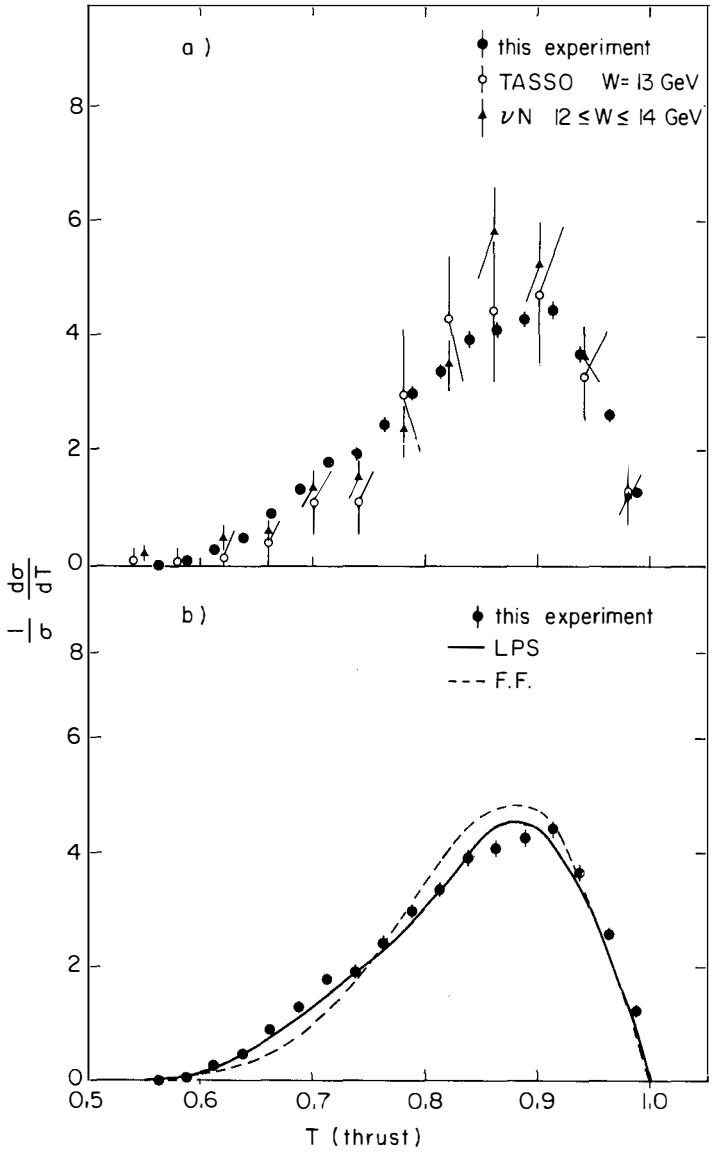
a)
this experiment
TASSO W= 13 GeV
νN 12 ≤ W ≤ 14 GeV
b)
this experiment
LPS
F.F.
1/σ dσ/dT
T (thrust)

Fig. 1B

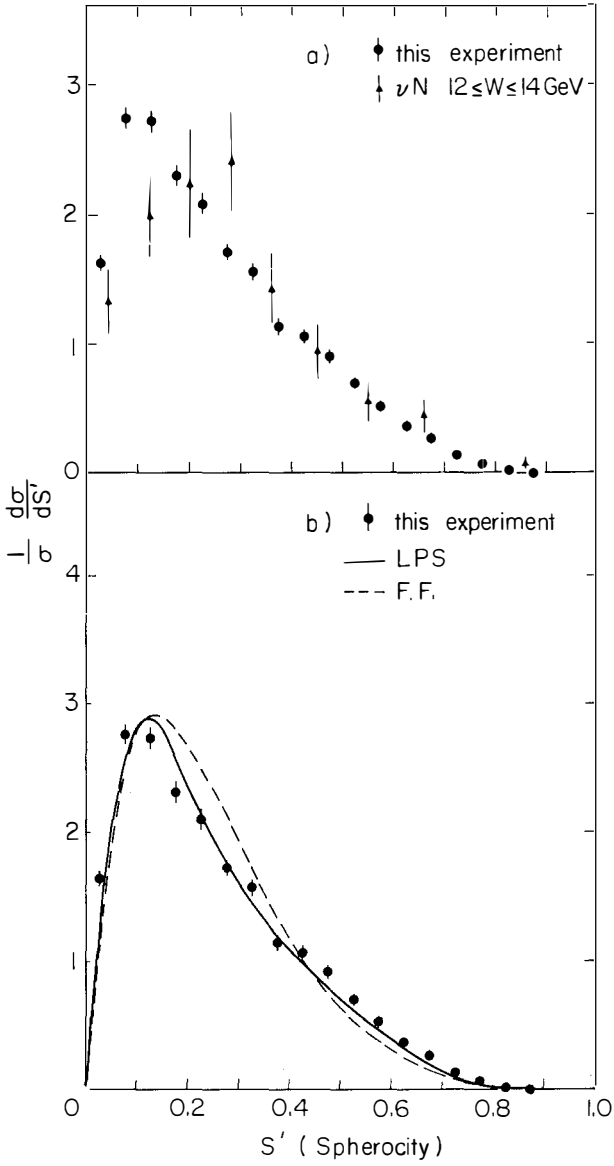
a) this experiment
νN 12≤W≤14 GeV
b) this experiment
LPS
F.F.
$\frac{1}{\sigma}\frac{d\sigma}{dS'}$
S' (Spherocity)
0
0.2
0.4
0.6
0.8
1.0

Fig. 1C

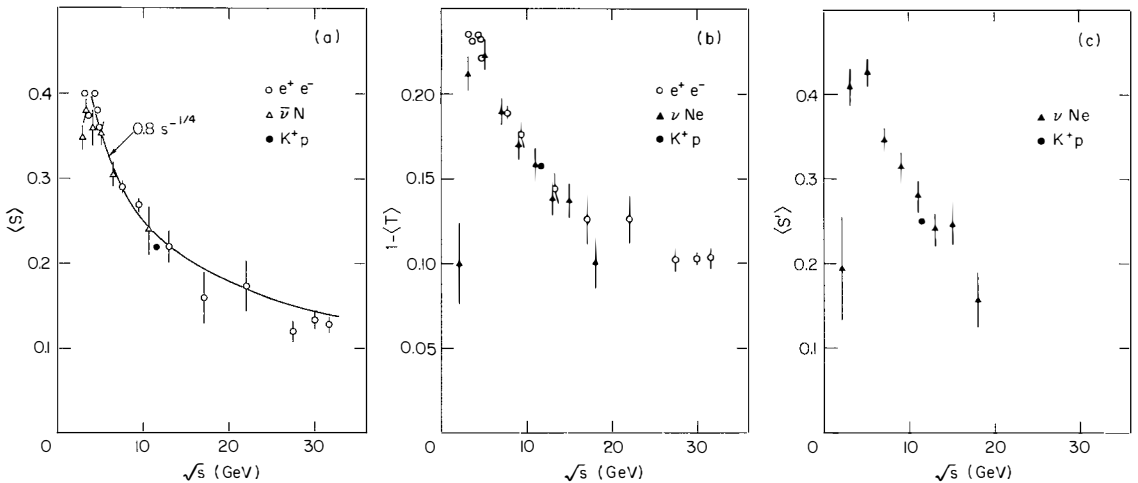

FIG. 2

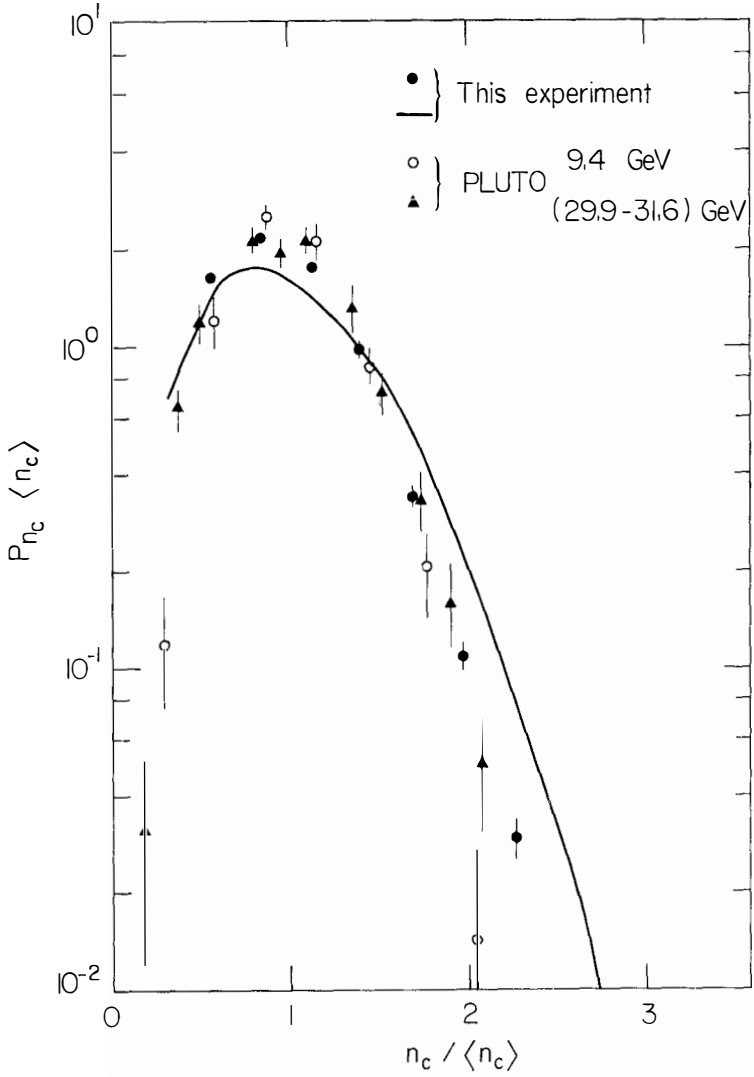
This experiment
PLUTO
9.4 GeV
(29.9 - 31.6) GeV
10^{1}
10^{0}
10^{-1}
10^{-2}
$P_{n_c}\ \langle n_c \rangle$
0
1
2
3
$n_c / \langle n_c \rangle$

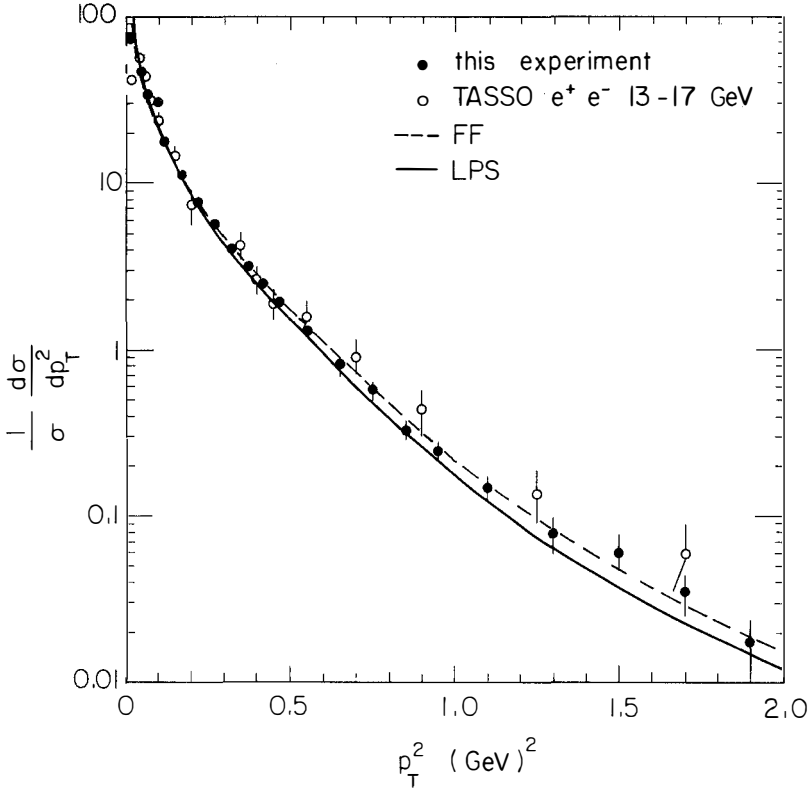
100
10
1
0.1
0.01
0
0.5
1.0
1.5
2.0
this experiment
TASSO e+ e- 13-17 GeV
FF
LPS
1/σ dσ/dp_T^2
p_T^2 (GeV)^2

Fig. 4

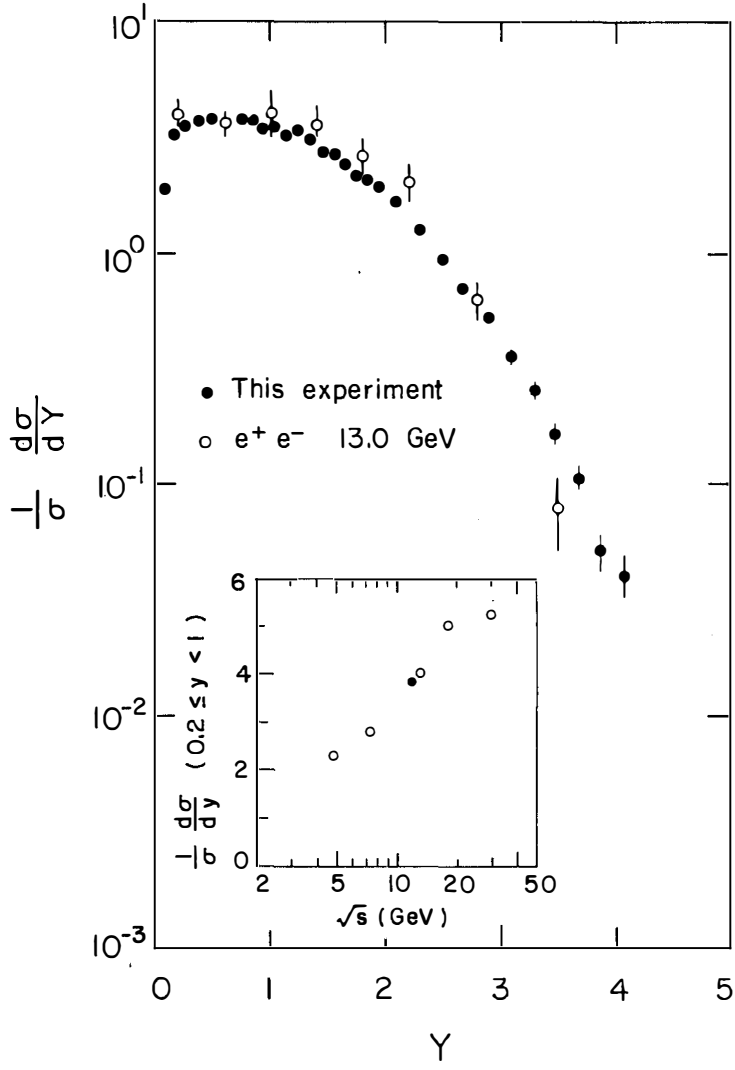
10^1
10^0
10^{-1}
10^{-2}
10^{-3}
$\frac{1}{\sigma}\frac{d\sigma}{dY}$
● This experiment
○ $e^+ e^-$ 13.0 GeV
0
1
2
3
4
5
Y
$\frac{1}{\sigma}\frac{d\sigma}{dy}$ (0.2 ≤ y < 1)
6
4
2
0
2
5
10
20
50
$\sqrt{s}$ (GeV)

Fig. 5

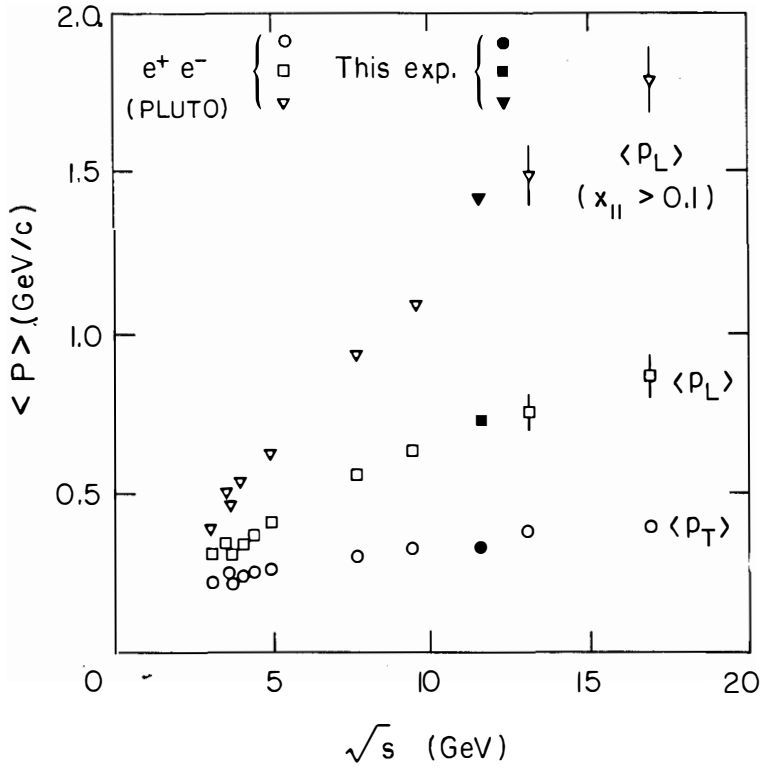
2.0
1.5
1.0
0.5
0
5
10
15
20
< P > (GeV/c)
√s (GeV)
e+ e−
(PLUTO)
This exp.
⟨ p_L ⟩
(x_{11} > 0.1)
⟨ p_L ⟩
⟨ p_T ⟩

Fig. 6

A DIRECT MEASUREMENT OF THE π FORM FACTOR (NA7)*

Francesco FIDECARO
INFN, Sezione di Pisa and Scuola Normale Superiore, Pisa, Italy

ABSTRACT

A π-e elastic scattering experiment is described. $1.2 \cdot 10^4$ events have been collected in a 30 hours test run. We obtain for the r.m.s. radius of the π 0.69 ± 0.09 fm in the range $-0.016 > t > -0.088$ $(GeV/c)^2$.

RESUME

On décrit une expérience de diffusion élastique π-e. Au cours d'un run de test de 30 heures, $1.2 \cdot 10^4$ évènements ont été enregistrés. On obtient pour le rayon du π (r.m.s) 0.69 ± 0.09 fm dans l'intervalle $-0.016 > t > -0.088$ $(GeV/c)^2$.

* NA7: Southampton, Westfield College, FRAMM (Frascati, Milano, Pisa, Torino, Trieste) Collaboration

In the following I report on a direct measurement of the π^- form factor through π-e elastic scattering. A 300 GeV/c π^- beam is steered onto a liquid H_2 target and both the outgoing π and the atomic e^- are measured, together with the incoming particle. The form factor is then deduced from the t-dependence of the cross section. The range in momentum transfer covered by the experiment is shown in Fig. 1.

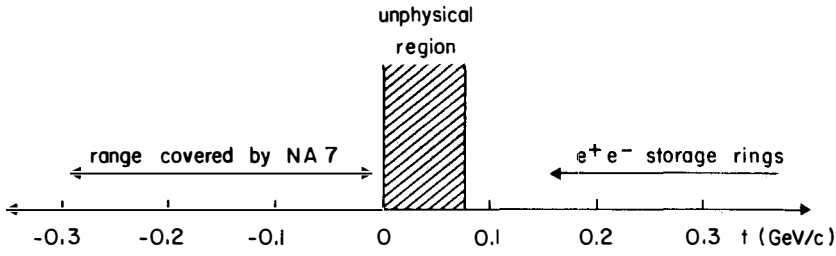

Fig. 1. Range in momentum transfer

The 300 GeV/c π^- beam (E4/H4) in the SPS North Area is tuned to produce a large spot in the vertex region, so that the particle flux per cm² is kept at an acceptable level. The apparatus (Fig. 2) consists of a dedicated vertex detector together with the FRAMM spectrometer. The vertex detector has a high angular accuracy, allowing thus to decouple the measurement of angles from that of momenta. It uses 1 mm pitch staggered MWPC which can stand high rates ($5 \cdot 10^6$ particles/burst). The 30 cm long liquid H_2 target is surrounded by anticoincidences, while scintillator hodoscopes are used to define the ingoing beam and to identify 2-prong events. The spectrometer uses 4 magnets (for a total bending power of up to 6 Tl.m) together with drift chambers to measure momenta, while electromagnetic calorimeters identify the electron in the final state.

Due to the large π-p cross-section ($\sigma_{\pi e}/\sigma_{\pi p} \sim 5 \cdot 10^{-4}$) one has to build a very selective trigger, without loosing any good event. The trigger requirements are as follows :

i) 1 incoming particle

ii) no particle at angles larger than 10 mrad

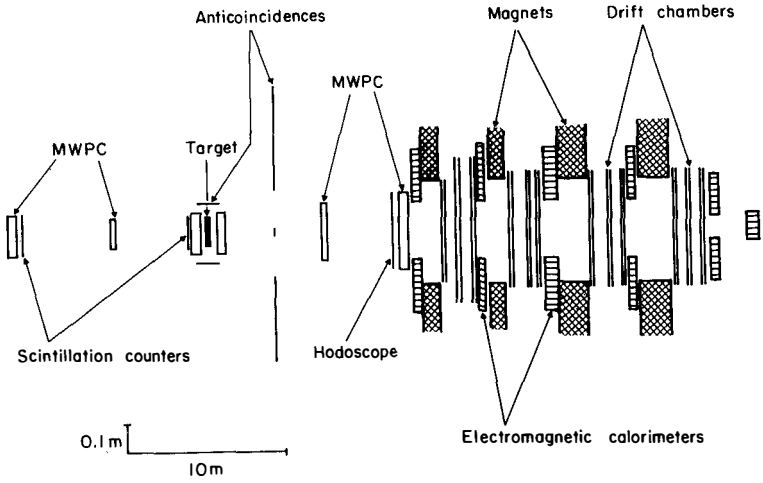

Fig. 2. Experimental apparatus

iii) 2 forward outgoing particles. This is achieved in the following way:

- the multiplicity is checked by counting the fired fingers of the downstream hodoscope.
- the side of FRAMM where positive particles are swept by the magnetic field is used as a veto.

iv) an e^- signal is requested from the e.m. calorimeters.

v) at least 1 particle with a scattering angle larger than 1 mrad is requested (this makes use of the π-e elastic scattering kinematics)

10^6 events were collected in a 30 hours test run in June 1980, out of which $3 \cdot 10^5$ have been reconstructed. The subsequent analysis, based on the vertex information, selects 2-prong events. This rejects 70% of the events, while the requirement of an interaction inside the target reduces the sample to 12.7%. The further request of coplanarity decreases this number to 11.7%, which are good π-e candidates. Kinematics is then checked by requiring that the angles of the outgoing π and of the electron verify the elastic scattering constraint. The scatter plot for the angle of the particle

which goes on the right versus the angle of the particle on the left is shown in Fig. 3. This shows the quality of the selection, while Fig. 4 illustrates the resolution on the constraint and the cuts applied to select the π-e events.

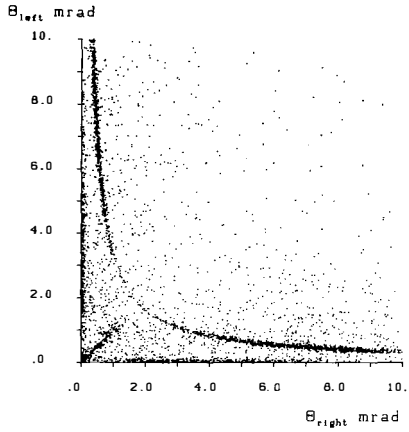

Fig. 3. Angular kinematical constraint for π-e elastic scattering

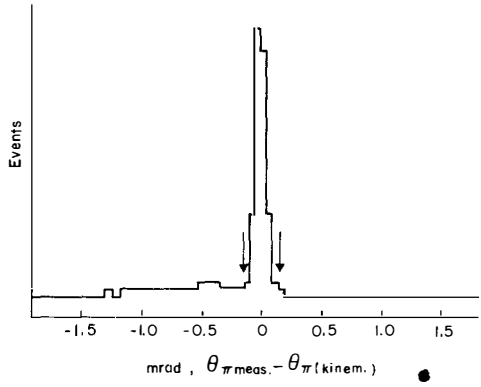

Fig. 4. Resolution on kinematical constraints

To extract the π r.m.s. radius from this first selection we restricted ourselves to the kinematical region:

$$-0.016\ (\mathrm{GeV/c})^2 > t > -0.088\ (\mathrm{GeV/c})^2$$

where the e^- attribution is unambiguous. In addition, since we had a 15% left-right asymmetry due to the geometrical acceptance we selected only the events in which the e^- goes to the right. This was done to avoid corrections at this stage. We ended with $1.2 \cdot 10^4$ π-e events which enter the plot in Fig. 5. This shows the cross-section, scaled to the cross-section for a point-like particle, together with the fit. The absolute rate is off by 20%, explainable by the dead regions on the side of the e.m. calorimeters, and should not be strongly t-dependent. The result of the fit to the data is :

$$\langle r^2 \rangle^{1/2} = 0.69 \pm 0.09 \text{ fm}$$

to be compared with already published results[1),2)].

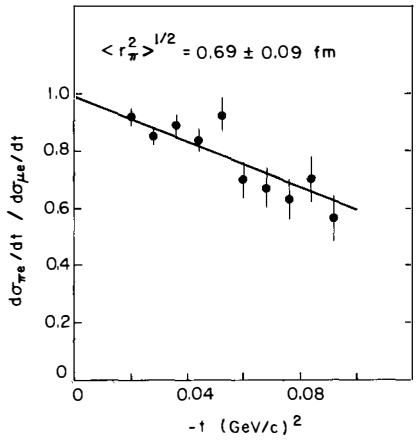

Fig. 5. Cross-section for π-e scattering scaled to μ-e scattering

The analysis is going on and we will be soon in condition of covering the whole kinematical range and the full azimuthal angle.

The experiment will restart at the end of the SPS shut-down and should record $\sim 4 \cdot 10^6$ π-e events, allowing the measurement of the initial slope of the form-factor at a 1% level, while a curvature term can be estimated at a 10% level. Simultaneously, $4 \cdot 10^4$ K-e events will be collected, allowing a measurement of the K meson radius with a precision of 3%.

REFERENCES AND NOTES

[1] G.T. Adylov et al., Nucl. Phys. B128, 461 (1977).

[2] E.B. Dally et al., Phys. Rev Lett. 39, 1176 (1977).

THE ELASTIC FORM FACTORS OF NUCLEONS

B.T. Chertok*)
CERN, Geneva, Switzerland

ABSTRACT

The current state of research on elastic electromagnetic form factors of the proton and neutron at large momentum transfers is presented. Some preliminary conclusions are reached on n/p for $Q^2 > 2$ $(GeV/c)^2$ from a recent SLAC experiment on electron-deuteron quasielastic scattering. Recent theoretical activity in QCD in the study of elastic form factors of hadrons which has been vigorous is documented. Finally, possible future experimental work at larger Q^2 for the pion, proton, and neutron is discussed.

*) On leave from: The American University, Washington, DC, USA.

1. INTRODUCTION

The nucleon is more than just a pole in the complex energy plane with quantum number $J = \frac{1}{2}^+$, $S = 0$, and $B = 1$ [1]. While it has been clear for some time that the nucleon has a rich internal structure and is therefore not elementary, nevertheless the proton and neutron do have a special status -- their existence. This stability has been used with weakly interacting probes to "establish" the quark-parton substructure in deep inelastic scattering investigations, which has in turn led to a standard model of the strong interaction -- quantum chromodynamics (QCD). Furthermore, this remarkable longevity ($> 10^{30}$ years for the proton and 15.3 minutes for the slightly more energetic neutron) is a question that is of great moment in present searches for evidence of proton decay and of the massive $W^{\pm}$ and Z^0 gauge bosons. After this little preamble, let us turn to the subject of this paper.

The elastic form factors of nucleons provide crucial information about the internal structure of matter. One has great confidence in extracting this information, particularly with electromagnetic interactions, as experiments at PETRA have shown the lepton (e,μ) probe to be structureless up to $s = -Q^2 = 1000\ \text{GeV}^2$. We can look forward to enlarging this statement to include the electroweak form factors of hadrons if the SU(2) × U(1) model passes its tests in the coming years. The requirement that the nucleon remains bound after absorbing a massive virtual photon, $Q^2 >> M^2$, places severe constraints on our detailed understanding of structure in a dynamic environment of large Q^2. For the proton these limits have reached $Q^2 = 33\ (\text{GeV/c})^2$ and $-4.5\ (\text{GeV/c})^2$ for the space-like and time-like regions, respectively.

The external electromagnetic interaction is depicted in Fig. 1, where the charge-current density J_μ is described in terms of two scalar form factors, F_1 and F_2 or G_E and G_M for the spin-½ nucleon. The asymptotic nucleon states N and N′ satisfy the Dirac equation for a free particle, and J_μ is constructed according to relativistic covariance and gauge invariance. For the time-like interaction $N\bar{N} \rightleftarrows e\bar{e}$, the N′ arrow would be reversed and the virtual photon γ_v would originate in the annihilation channel. The nucleon form factors are real functions of Q^2 for $Q^2 > 0$, and complex functions for $Q^2 < 0$ beyond ππ threshold.

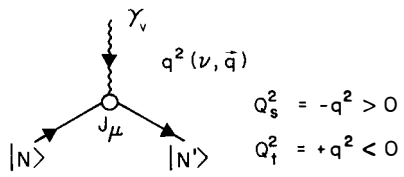

Fig. 1 Diagram for virtual photon-nucleon elastic scattering

With the coming of age of QCD as the standard model of the strong interactions, research into the elastic form factors of hadrons, and of nucleons in particular, should once again be an important frontier area. This standard model must be subject to a variety of experimental constraints.

It was suggested that I present an overview of this field at Moriond. Accordingly, the organization will be a review of previous results in Section 2, presentation of our quasielastic electron-deuteron measurement with elastic n/p results in Section 3, and a brief outline of future plans and possibilities for work in the $Q^2 > 0$ and $Q^2 < 0$ momentum transfer regions in Section 4. Attention is drawn to important possible future work in determining the charged pion form factor at large Q^2. The resurgence of theoretical activity in the last two years will be documented but only a few specific predictions will be mentioned in Sections 3 and 4.

2. PREVIOUS RESULTS

Elastic electron scattering from the proton and neutron was one of the dominant areas of high-energy research during almost two decades, starting in the early 1950's[1]. The principal results were the mapping of the nucleon charge and current distributions for $Q^2 \lesssim 1$ $(GeV/c)^2$, the prediction of vector mesons, and the testing of baryon symmetry models, particularly SU(6). Beyond $Q^2 \simeq M^2$ progress was slow, and the semi-empirical scaling laws for the proton and neutron were known to be, at best, approximate and inconsistent[2]. They are

$$G_M^p = \mu_p/(1 + Q^2/0.71)^2 \tag{1a}$$

$$G_E^p = G_M^p/\mu_p \tag{1b}$$

$$G_M^n = G_M^p\, \mu_n/\mu_p \tag{1c}$$

$$G_E^n = 0\ , \tag{1d}$$

with normalizations at the static limit $Q^2 = 0$ of the magnetic moment $G_M(0) = \mu$ and charge $G_E(0) = Z$. In the time-like region, study of the reaction $\bar{p}p \rightleftarrows \bar{e}e$ for $4M^2 < |Q^2| < 4.5$ GeV^2 has yielded a form factor well above the dipole fit. However, past limitations of low intensity and competing backgrounds have not made this data of comparable quality to space-like e,e′ measurements; no separation of G_E from G_M has been attempted[3]. The experimental situation is summarized in Figs. 2 and 3. In Fig. 2a, G_M^p is extracted from the data for $Q^2 > 3.5$ $(GeV/c)^2$ assuming the validity of Eq. (1b); at $Q^2 \sim 20$ $(GeV/c)^2$ the data are $\sim 20\%$ smaller than the dipole fit, i.e. Eq. (1a)[4]. In Fig. 2b, G_E^p "scales" for $Q^2 < 1$, whereas beyond 1.5 $(GeV/c)^2$ Eq. (1b) may be violated by 50%[5]. For the neutron data,

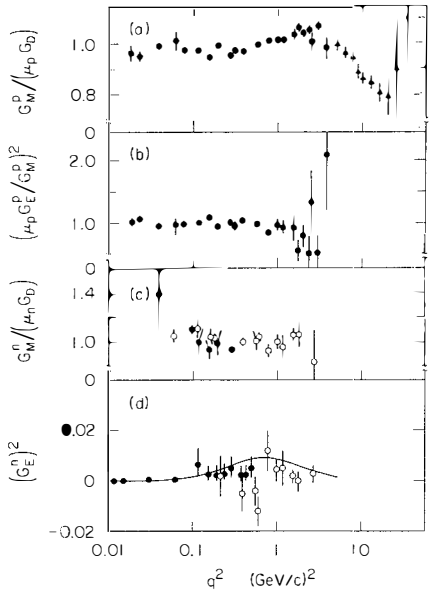

Fig. 2 Existing data for the elastic nucleon form factors. G_D is the dipole form $1/(1 + Q^2/0.71)^2$. a) $G_M^p/(\mu_p G_D)$; b) $(\mu_p G_E^p/G_M^p)^2$; c) $G_M^n/(\mu_n G_D)$; d) $(G_E^n)^2$.

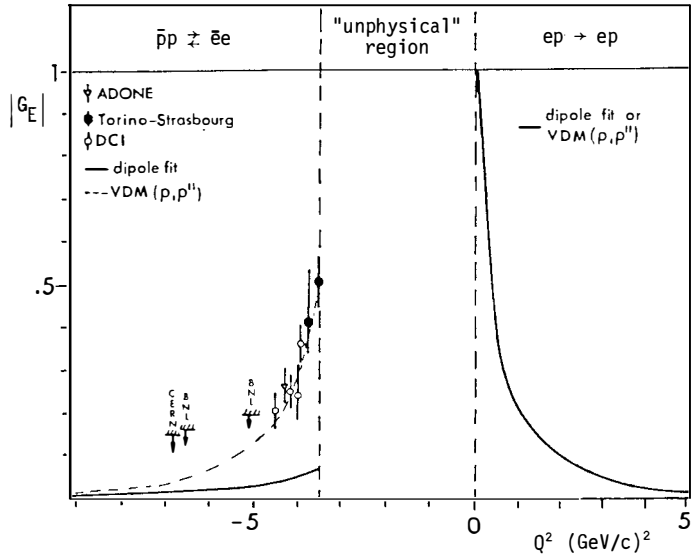

Fig. 3 Proton's form factor G_E for $-10 < Q^2 < 5$ (GeV/c)^2, from Ref. 3

G_M^n follows Eq. (1c) to $Q^2 \sim 2.7$ (GeV/c)^2, whereas $(G_E^n)^2$ is consistent with 0 or slightly positive over the range $0 < Q^2 < 2.7$ (GeV/c)^2 [5,6]. At very low Q^2, 0 to $\sim$ 0.4 (GeV/c)^2, $G_E^n \neq 0$ and is positive[7].

3. QUASIELASTIC e-d SCATTERING

3.1 Motivation

An experiment to measure e + d → e′ + X in the quasielastic region in the interval $2.5 \leq Q^2 \leq 10$ (GeV/c)^2 was performed at SLAC by the American University Group in 1979. Preliminary results have been presented[8]. Our motivation was to provide new information on e-n elastic scattering to extend the Q^2 range for the neutron in Fig. 2. Various theoretical and phenomenological predictions indicated that the ratio of elastic neutron to proton cross-sections (hereafter labelled σ_n/σ_p or n/p) might increase with Q^2, remain constant, or even diminish as $(Q^2)^{-1}$.

It is useful to cast the predictions in terms of two sets of form factors, G_E and G_M of Eq. (1) or the Dirac-F_1 and Pauli-F_2 form factors with the connections

$$G_E = F_1 - \tau F_2 \ , \tag{2a}$$

$$G_M = F_1 + F_2 \ . \tag{2b}$$

where for the neutron, $F_1(0) = 0$ and $F_2(0) = \mu_n$, for the proton $F_1(0) = 1$ and $F_2(0) = \mu_p - 1$, and the dimensionless parameter $\tau = Q^2/M^2$. These original form factors are pertinent when discussing the neutron since, for a particle which is everywhere neutral[9],

$$F_1(Q^2) = 0 \ , \tag{3}$$

and in addition, predictions have been made for F_{1n}/F_{1p} for $Q^2 \gg M^2$. The curve in Fig. 2d satisfies Eq. (3), $G_E^n = -\tau G_M^n$, i.e. $F_{1n} = 0$.

For the conditions of the SLAC experiment, $\theta_e = 10°$, so that the cross-section ratio, to excellent approximation, is

$$\left.\frac{\sigma_n}{\sigma_p}\right|_d = \frac{\left(G_E^n\right)^2 + \tau\left(G_M^n\right)^2}{\left(G_E^p\right)^2 + \tau\left(G_M^p\right)^2} = \frac{F_{1n}^2 + \tau F_{2n}^2}{F_{1p}^2 + \tau F_{2p}^2} \ . \tag{4}$$

Predictions for this ratio as $Q^2 \to \infty$ are:

a) Combining Eqs. (1b), (1c), and (1d),

$$\frac{\sigma_n}{\sigma_p} \to \frac{\mu_n^2}{\mu_p^2} = 0.47 \ ; \tag{5}$$

b) Combining Eqs. (1b), (1c), and (3) ($F_{1n} = 0$) ,

$$\frac{\sigma_n}{\sigma_p} \to \frac{\mu_n^2}{\mu_p^2}(1 + \tau) \; ; \tag{6}$$

c) assuming the asymptotic limits of the dimensional-scaling quark model (DSQM)[10], $Q^4F_1 \to C_1$ and $Q^6F_2 \to C_2$, where C_1 and C_2 are normalization constants, yields

$$\frac{\sigma_n}{\sigma_p} \to \left(\frac{C_{1n}}{C_{1p}}\right)^2 \; ; \tag{7}$$

d) assuming (c) with models for the quark wave functions with dominance of the same spin or flavour, which fit the inelastic structure functions $\nu W_{2n}/\nu W_{2p}$ as $x \to 1$, gives $F_{1n}/F_{1p} = -1/3$ [11] and

$$\frac{\sigma_n}{\sigma_p} \to \frac{1}{9} \; , \tag{8}$$

or $F_{1n}/F_{1p} = -\frac{1}{2}$ [12] and

$$\frac{\sigma_n}{\sigma_p} \to \frac{1}{4} \; ; \tag{9}$$

e) combining (c) with $F_{1n} = 0$

$$\frac{\sigma_n}{\sigma_p} \to \frac{(C_{2n}/C_{2p})^2}{\tau} \; ; \tag{10}$$

f) assuming a VDM model[13], which fits in both the space-like and the time-like region and also satisfies crossing, yields $F_{1n}/F_{1p} = -0.37$, which is between Eqs. (8) and (9).

Recently, perturbative QCD calculations of the elastic form factors of mesons and baryons have been made. (More details will be given in Section 4.) These results appear to confirm the DSQM bounds of item (c) above, and are quite sensitive to the shape of the quark distribution amplitude[14]. In terms of two helicity form factors parallel and antiparallel to the nucleons helicity,

$$\frac{G_M^n}{G_M^p} = -\frac{1}{3}\left[1 - \frac{G_{\overline{\parallel}}}{G_{\parallel}}\right] . \tag{11}$$

If the endpoint region $x \to 1$ dominates, where one valence quark carries essentially all of the momentum[11] rather than the dominant hard-scattering contribution of perturbative QCD, then the prediction is -1/3 for Eq. (11), which is the same result for σ_n/σ_p as in Eq. (8).

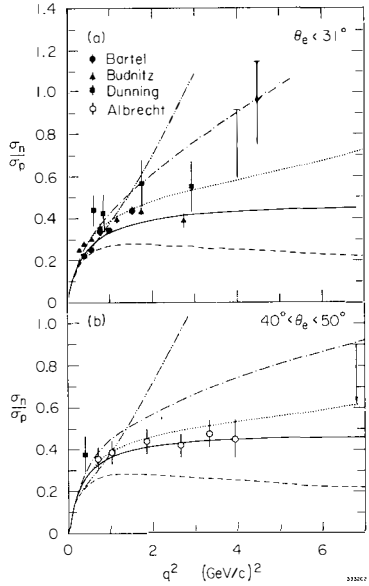

Fig. 4 Existing data and some models for the ratio of elastic neutron and proton cross-sections $\sigma_n^{el}/\sigma_p^{el}$. a) $\theta < 31°$, i.e. $\tan^2 \theta/2 << 1$; b) $40° \leq \theta \leq 50°$. The curves are: ——— Eq. (5), —·—·— Eq. (6), ----- VDM model of Blatnik and Zovko (Ref. 13), —··—··— VDM model of IJL (Iachello et al., Ref. 13), ... Veneziano-type model of Felst (Ref. 13).

Taken together, these predictions in Eqs. (5)-(11), most of which are in reasonable agreement with the data in Fig. 2, yield very different behaviour for σ_n/σ_p at larger Q^2. Some of these predictions are shown in Fig. 4 together with previous small-angle data [Eq. (4)] and for larger-angle data.

3.2 Experiment and preliminary results

A brief report of the experiment together with preliminary results has been given elsewhere[8]. The radiatively corrected quasielastic e-d spectra are presented in Fig. 5. An example of the deuteron to proton ratio is given in Fig. 6, where our measured e-p elastic and inelastic spectra have been smeared with Fermi motion to simulate scattering from a nucleon bound in the deuteron. The ratio of σ_d/σ_p^d is independent of W^2 in the peak region. Further detailed analysis is in progress. As reported, the n/p cross-section is approximately *constant* in the range $2.5 < Q^2 < 8$ (GeV/c)^2, averaging

$$\frac{\sigma_n}{\sigma_p} = 0.3 \pm 0.05 \ . \qquad (12)$$

PRELIMINARY

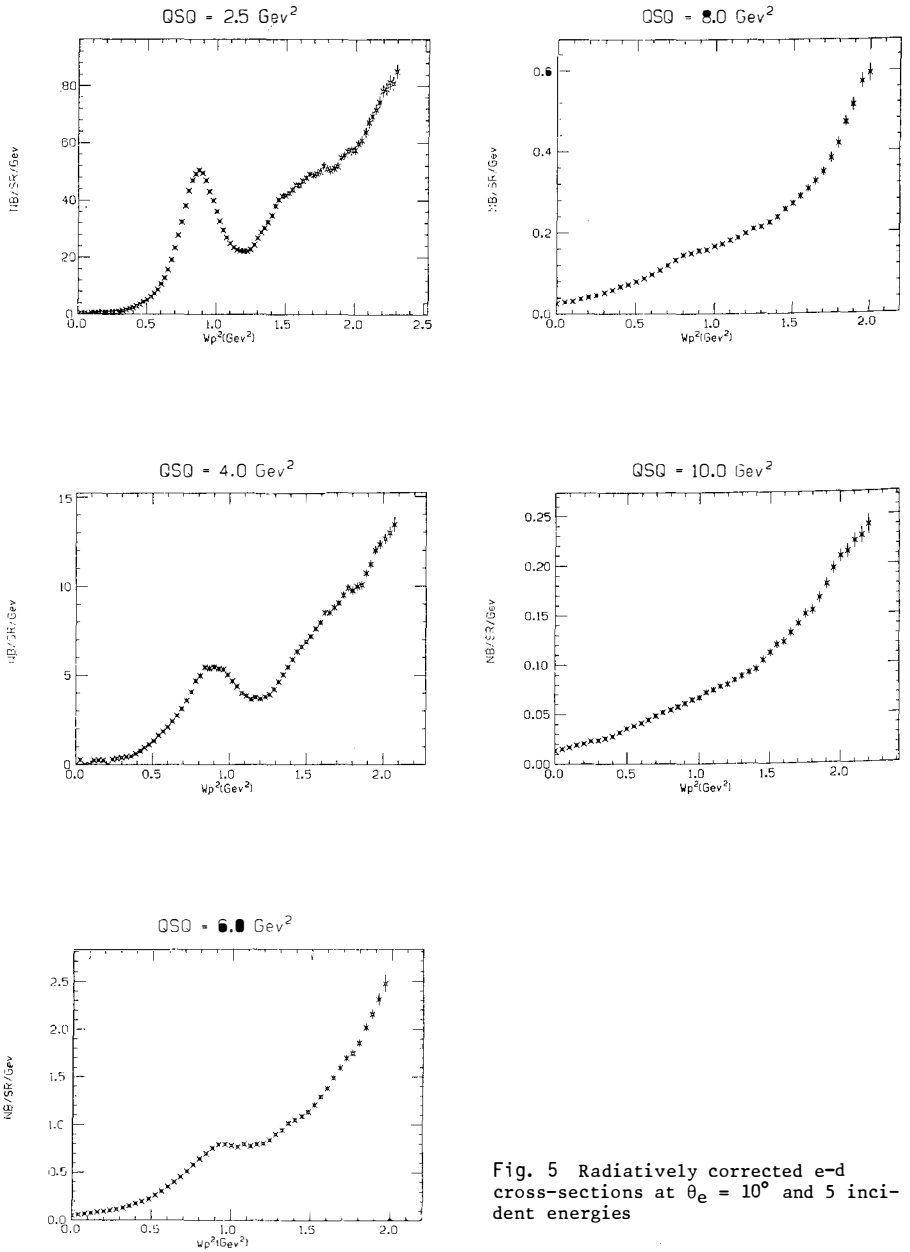

Fig. 5 Radiatively corrected e-d cross-sections at $\theta_e = 10^\circ$ and 5 incident energies

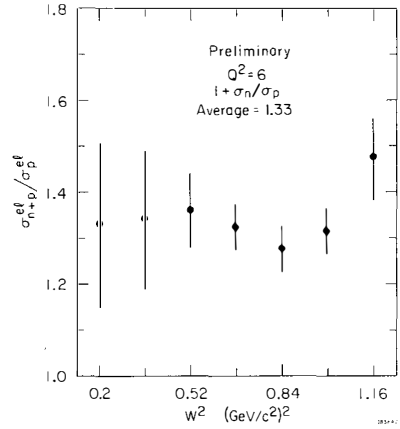

Fig. 6 The ratio of e-d to smeared e-p cross-section at $Q^2 = 6$ $(GeV/c)^2$ near $W^2 = M^2$

Inspection of the e-d spectra in Fig. 5 shows the difficulty in extracting an elastic e-n signal for $Q^2 > 6$ $(GeV/c)^2$. (See Section 4.4 for further remarks.)

These spectra are a beautiful illustration of duality, first noted in e-p inclusive measurements[15], where in the present case the elastic peak and smeared (3,3) resonance rapidly and smoothly disappear with increasing Q^2. Demonstration that this region can be represented by a smooth average of νW_{2d} continued from the deep inelastic scattering region (W > 2 GeV) should be informative[16].

The results of this measurement in Eq. (12) would appear to rule out predictions contained in Eqs. (5), (6), and (8), and most of the predictions shown in Fig. 4. They point to a finite contribution of F_{1n} at least for $Q^2 > M^2$ [17]. [Recall Eq. (3) and earlier work.] The results show the first evidence of dimensional scaling for the elastic neutron form factor $F_n \equiv (\sigma_n/\sigma_{Mott})^{1/2}$, i.e.

$$Q^4 F_n \to \text{const} , \tag{13}$$

with a shape similar to the proton's in the preasymptotic region, $1 < Q^2 < 4$ $(GeV/c)^2$ as displayed in Fig. 7 [12]. In our Q^2 range, the prediction in Eq. (9), $\sigma_n/\sigma_p \to 1/4$, is clearly preferred to that in Eq. (8). It is conceivable that the leading-order QCD Born term, where each valence quark carries momentum (p + q)/3, is subject to strong suppression by the quark distribution amplitudes. Nevertheless, it is certainly premature to argue that σ_n/σ_p has reached an asymptotic value. The VDM prediction of Blatnik and Zovko in Fig. 4 approximately describes the data.

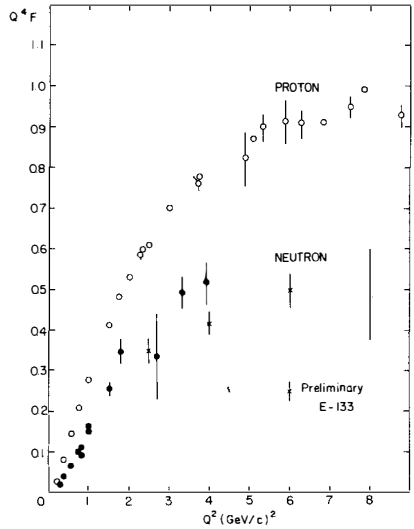

Fig. 7 The approach to the dimensional scaling limit for p and n from data of Refs. 12 and 8

4. FUTURE WORK

4.1 Pions

It may be possible to increase the present Q^2 boundary[18] of 4 $(GeV/c)^2$ for the π^+ elastic form factor by means of, for example, the EMC Forward Spectrometer at CERN using muon-induced scattering from H_2 and D_2 targets. Improvements in small-angle discrimination and in missing-mass resolution would be necessary. In view of the theoretical activity in calculating this form factor within QCD[19], a measurement of F_π to $Q^2 \gtrsim 10$ $(GeV/c)^2$ could be highly significant.

4.2 Protons (space-like)

There is a proposal[20] by our group at SLAC to measure the proton form factor with good statistical precision in the range 10-40 $(GeV/c)^2$. Possible experimental results are displayed in Fig. 8. The highest Q^2 region is now accessible to precise determination with the new high-intensity 30 GeV SLED beam. Coincidence measurements of the e-p final state by the SLAC 8 and 10 GeV/c spectrometers should yield unambiguous results even at the 10^{-39} cm^2/sr cross-section level. Perturbative QCD calculations of G_M of the nucleon have been made[14] and offer the possibility of obtaining important information about the strong coupling constant $\alpha_s(Q^2)$ and the scaling behaviour of the quark-quark interactions. In contrast to inelastic lepton-nucleon scattering, the magnetic form factor is a

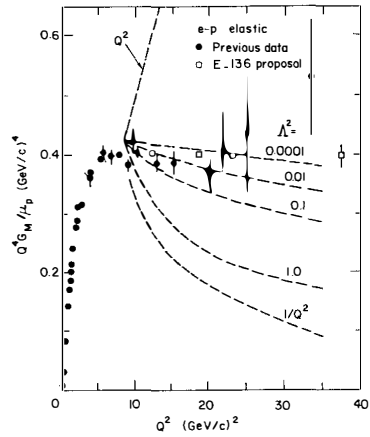

Fig. 8 Comparison from Ref. 14 (Le P and B) extended to 40 $(GeV/c)^2$. The ⊔ are possible precision of a proposed experiment assuming a Q^2-independent value of 0.4. Λ_{QCD} curves for 10 MeV to 1 GeV are shown.

leading-order QCD amplitude proportional to α_s^2, and, in further contrast, higher-order twist terms are expected to be small. (The latter point may be controversial.) These proposed measurements go to larger Q^2 than do other exclusive reactions, in particular pp elastic scattering, and provide a large span in Q^2 from a single experiment.

As always in physics, surprise cannot be ruled out. A speculation on the appearance of structure in the form factor is displayed in Fig. 9 [21].

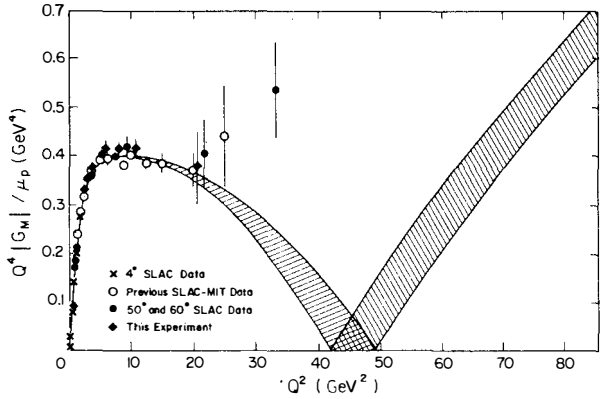

Fig. 9 Fit through existing e-p data of a speculation which allows for new structure inside the nucleon

4.3 Protons (time-like)

There is an approved experiment at LEAR to use the intensive low-energy $\bar{p}$ beam to study the reaction $\bar{p}p \to e^+e^-$ [22]. In the range $0 < p_{\bar{p}} < 2$ GeV/c, this 2×10^6 $\bar{p}$/s beam will permit measurement and possible separation of G_E and G_M for $-6 < Q^2 < -4M^2$. The experimental challenge is to separate electron pairs, with branching ratios of 3×10^{-7} to 4×10^{-9}, from the huge background produced by the hadrons coming from the dominant annihilation final states. The present situation is shown in Fig. 3 where VDM fits both regions, whereas Eqs. (1a) and (1b) fail completely for $Q^2 \leq -4M^2$. Hence the accurate determination of the proton form factors in the time-like region, which is dominated by poles of the vector mesons ρ, ω, ϕ, ρ', ..., J/ψ, should yield significant constraints on hadronic structure.

4.4 Neutrons

The discussion, in Section 3, of the recent quasielastic electron-deuteron experimental results (Fig. 5), makes clear the requirement for deducing the neutron form factor at larger Q^2 -- the recoiling neutron must be measured in coincidence with the scattered electron. To convert a 10 GeV/c neutron in a hadron calorimeter and to time its arrival within a resolution of 500 ps in the environment of an intense electron beam is beyond the state of the art. However, present progress in detector development[23] may make such an e-n elastic scattering experiment possible in the range $8 < Q^2 \lesssim 18$ $(\text{GeV/c})^2$.

Finally, it may be possible to separate the electric from the magnetic nucleon form factors G_E and G_M at moderate Q^2, ~ 1 to 5 $(\text{GeV/c})^2$, using polarization transfer techniques[24]. The development of intensely polarized electron sources makes this possible[25].

5. CONCLUSIONS

Recent theoretical activity, particularly in QCD as the standard model of the strong interactions, has once again emphasized the importance and special role of elastic form factors in elucidating the hadron structure. However, the challenges to both experiment and theory are formidable but this is not a unique situation. The prospects look reasonable -- notwithstanding the prodigious activity in colliding-beam physics -- for maintaining the dialogue between experiment and theory in the fixed-target exploration of elastic form factors at ever-increasing Q^2.

Acknowledgements

Much of the recent research described in this paper has been carried out together with my colleagues, R.G. Arnold, S.E. Rock and Z.M. Szalata at SLAC, and with B.A. Mecking of Bonn. D.J. Sherden of SLAC has made a significant contribution to our investigations. We are indebted to S.J. Brodsky and his collaborators for stimulating and enlightening discussions. I wish to thank J.J. Aubert T. Ekelöf, E. Gabathuler, G. Weber and F. Yndúrain for helpful discussions, and particularly salute J. Tran Thanh Van and L. Montanet for creating the ambiance at the XVI Rencontre de Moriond.

REFERENCES AND FOOTNOTES

For the benefit of younger scientists and others who would like to have the historical perspective, Refs. 1 and 2 should suffice.

1) The early experiments and theory are well summarized in:
R. Hofstadter (ed.), Nuclear and nucleon structure (Benjamin, New York, 1963).
S. Drell and F. Zachariasen, Electromagnetic structure of nucleons (Oxford Univ. Press, Oxford, 1961).
L. Hand, D. Miller and R. Wilson, Rev. Mod. Phys. 35, 335 (1963).
R. Hofstadter and L. Schiff (eds.), Nucleon structure (Stanford Univ. Press, Stanford, 1964).

2) Work in the second decade is summarized by:
W. Panofsky, Proc. 14th Int. Conf. on High-Energy Physics, Vienna, 1968 (eds. J. Prentki and J. Steinberger) (CERN, Geneva, 1968), p. 23.
R. Wilson, Proc. 1971 Symposium on Electron and Photon Interactions at High Energies, Ithaca, NY, 1971 (Cornell Univ., Ithaca, NY, 1972), p. 97.
M. Gourdin, Phys. Rep. 11, 29 (1973).

3) P. Dalpiaz, Proc. 5th European Symposium on Nucleon-Antinucleon Interactions, Bressanone, 1980 (CLEUP, Padua, 1980), p. 711 (quoted *in* U. Gastaldi and R. Klapisch, preprint CERN-EP/81-06, 1980).

4) P. Kirk et al., Phys. Rev. D 8, 63 (1973).

5) W. Bartel et al., Nucl. Phys. B58, 429 (1973).

6) K. Hanson et al., Phys. Rev. D 8, 753 (1973).
J. Tran Thanh Van, an originator of the Rencontres de Moriond, made important contributions. For instance: F. Renard, J. Tran Thanh Van and M. Le Bellac, Nuovo Cimento 38, 552, 565, and 1688 (1965).

7) V. Krohn and G. Ringo, Phys. Rev. D 8, 1305 (1973).
F. Bumiller et al., Phys. Rev. Letters 25, 1774 (1970).
R. Bérard et al., Phys. Letters 47B, 355 (1973).

8) S. Rock et al., Proc. XXth Int. Conf. on High-Energy Physics. Madison, 1980 (eds. L. Durand and L. Pondrom) (AIP, New York, 1981), p. 550.
B. Chertok, same Proc., p. 547.

9) R. Sachs, Phys. Rev. 126, 2256 (1962).
S. Fenster and Y. Nambu, Prog. Theor. Phys. Suppl. 250 (1965); to sample the more recent literature: P. Fishbane et al., Phys. Rev. D 11, 1338 (1975).

10) S. Brodsky and G. Farrar, Phys. Rev. D 11, 1309 (1975).

11) G. Farrar and D. Jackson, Phys. Rev. Letters 35, 1416 (1975).

12) S. Brodsky and B. Chertok, Phys. Rev. D 14, 3003 (1976).

13) S. Blatnik and N. Zovko, Acta Phys. Austriaca 39, 62 (1974).
Bardek and Zovko, see Ref. 8.
F. Iachello, A. Jackson and A. Lande, Phys. Letters 43B, 191 (1973), which predicts $F_{1n}/F_{1p} = 4.75$ for $Q^2 \to \infty$.
F. Felst, preprint DESY 73/56 (1973).
For earlier work, see T. Massam and A. Zichichi, Nuovo Cimento 43, 1137 (1966).

14) G. Lepage and S. Brodsky, Phys. Rev. D 22, 2157 (1980).
G. Lepage, S. Brodsky and S. Zaidi, Phys. Rev. D 23, 1152 (1981).
I. Aznaurian, S. Esaybegyan and N. Ter-Isaakyan, Phys. Letters 90B, 151 (1980).
A.H. Mueller, Columbia Univ. preprint CU-TP-192 (1981).

15) E. Bloom and F. Gilman, Phys. Rev. D 4, 1209 (1971).

16) I. Schmidt and R. Blankenbecler, Phys. Rev. D 16, 1318 (1977).

17) If $F_{1n} = 0$ in $1 < Q^2 < 6$ $(GeV/c)^2$, this would have had a large effect on the relativistic impulse approximation for the elastic deuteron form factor: R. Arnold, C. Carlson and F. Gross, Phys. Rev. C 21, 1426 (1980).

18) C. Bebek et al., Phys. Rev. D 13, 25 (1976).

19) See Ref. 14, and also:
G. Farrar and D. Jackson, Phys. Rev. Letters 43, 246 (1979).
V. Chernyak, A. Zhitnitsy and V. Serbo, JEPT Letters 26, 594 (1977).
R. Coquereaux and E. de Rafael, Phys. Lett. 76B, 475 (1978).
A. Efremov and A. Radyushkin, JINR (Dubna) preprints P2-10717 (1977), E2-11535 and E2-11983 (1978), P2-80687 (1980); Teor. Mat. Fiz. 42, 147 (1980).
S. Brodsky, Y. Frishman, G. Lepage and C. Sachrajda, Phys. Letters 91B, 239 (1980).
A. Duncan and A. Mueller, Phys. Letters 90B, 159 (1980), and Phys. Rev. D 21, 1636 (1980).
K. Tesima, Univ. Tokyo preprint UT-350 (1981).
N. Craigie and H. Dorn, ICTP Trieste preprint IC/80/167 (1980).
This list is certainly not complete. For a review of perturbative QCD, see A.H. Mueller, Columbia Univ. preprint CU-TP-192 (1981).

20) R. Arnold et al., SLAC proposal E-136 (1980).

21) C. Bourrely, J. Soffer and T.T. Wu, Z. Phys. C5, 159 (1980).

22) J. de Brion et al., CERN LEAR proposal, PSCC/80-95, P 25 (1980).

23) See Proc. Int. Conf. on Experimentation at LEP, Uppsala, 1980 [Physica Scripta 23,4:1 (1981)], U. Amaldi, p.409 , A. Astbury, p.397 , P. Carlson, p.393 .

24) R. Arnold, C. Carlson and F. Gross, Phys. Rev. C 23, 363 (1981).

25) C. Sinclair et al,, Symposium on High-Energy Physics with Polarized Beams and Targets, Argonne, 1976 (ed. M. Marshak) (AIP, New York, 1976), p. 424.
C. Prescott et al., Phys. Letters 77B, 347 (1978).

THE INFLUENCE OF PARTONS ON SOFT HADRONIC REACTIONS- A REVIEW

W. Kittel
University of Nijmegen, Nijmegen, The Netherlands

Abstract:
Data on soft hadron-hadron collisions are compared to each other and to deep inelastic lepton-hadron and e^+e^- collisions in the light of quark-parton pictures. Three basic observations are the success of quark statistics to explain different quantum number hadron yields, the reflection of the valence quark distribution in hadronic pion production, and the similarity of jets in hadron-hadron, deep inelastic lepton-hadron and e^+e^- collisions. The models evolving from these observations help to illuminate different aspects of the data. They allow to understand correlations in the proton fragmentation region. Quark and diquark fragmentation functions extracted from hadron-hadron collisions agree with those from neutrino-hadron collisions. Kaon and pion structure functions agree with those obtained from muon-pair production. Hyperon polarization at large energies, not understandable from reggeology, follows naturally from quark-fragmentation-recombination.

I. BASIC OBSERVATIONS

Three observations have recently been drawing increased attention to soft hadronic collisions:

1. Cross sections for resonance and particle production in central and fragmentation regions can be understood from quark statistics.
2. Pion production in the nucleon fragmentation region of soft hadron-hadron collisions seems to reflect the valence quark distribution in the nucleon as observed in moderately deep inelastic lepton-nucleon collisions.
3. Quark fragmentation jets from e^+e^- annihilation and deep inelastic collisions seem to resemble soft hadronic production in longitudinal, transverse and multiplicity behaviour of the produced hadrons.

These observations lead to the expection that the parton structure of hadrons also governs soft hadron-hadron collisions. To test this unifying concept and to use its far-reaching consequences to illuminate not only the complicated hadron-hadron collisions, but the (soft) quark fragmentation in general, is the basis of present experimental and theoretical effort in this field. Before discussing the status of this effort in the later section, we shall first review the three basic observations.

I.1. Quark Statistics

Early data[1] give evidence for a two component picture of inclusive particle and resonance production. The fragmentation component depends on the produced particle or resonance and on the fragmenting incoming particle. The shape of the central component is universal, i.e. does neither depend on the incoming particles nor on the produced particle or resonance.

According to a simple additive quark model[2], one quark of the beam particle reacts with one quark of the target to produce a large quark-antiquark ($q\bar{q}$) sea in the center. One or more quarks (or antiquarks) from the center join respectively the beam spectator and the target spectator quarks to produce hadrons in the fragmentation regions. The remaining quarks and antiquarks join to produce hadrons in the central region. SU(6) symmetry is assumed to be broken only by a relative suppression ($\lambda \approx 1/3$) of strange quark production. The probability of quark production in the sea does not depend on spin projection and charge. Furthermore, due to the large quark multiplicity at high energy, the probability of central quark production does not depend on the nature of the incoming quarks. In meson production in the fragmentation region, on the other hand, one spectator is joined by one quark from the sea, so that there the distribution

depends on the nature of the spectator.

One of the main assumptions is that a "gas" of quarks and antiquarks with non-correlated spin projections is formed. As a consequence, the number of $q\bar{q}$ pairs with total spin s is proportional to the statistical weight 2s + 1. This gives an expected ratio 3:1 for ρ/π or $K^*(890)/K$, more generally for mesons containing the same quarks and belonging to the same SU(6) multiplet. The actually observed ratio depends on the contamination from decays of unobserved resonances. The ratio 3:1 has been verified[3] on K, K^* and K^{**} mesons (which appear in decay processes to a smaller extent and in a better controlled way than π and ρ) from pp and K^-p data.

The probability β for a spectator quark to pick up an antiquark (rather than a quark) from the sea has been estimated[4] to $\beta \approx 30\%$, consistently from $\bar{\Lambda}/K^0_s$ and Λ/K^0_s multiplicity ratios in π^- and K^- fragmentation.

The most detailed application of quark statistics is a systematic study of baryon production in the proton fragmentation region[5]. The data[5a] suggest that antibaryons can be attributed dominantly to the non-fragmentation type $B\bar{B}$ pair production with local compensation of quantum numbers. In that case, each valence quark of the incident proton either recombines with an antiquark to give an outgoing meson or recombines with other quarks, to give an outgoing baryon. From a consistent description of proton, Λ, Σ, Ξ and Ω^- production in proton fragmentation[5b], these two possibilities turn out to occur in an uncorrelated way for each valence quark of the incident proton, with the respective probabilities of about 40% and 60%[5c].

Furthermore, the probabilities a_i (i= 0, ...3) for the produced baryon to contain i valence spectator quarks can be consistently deduced from the same data to be

$$a_0 = 0.05 \pm 0.03 \qquad a_1 = 0.20 \pm 0.04$$
$$a_2 = 0.30 \pm 0.16 \qquad a_3 = 0.45 \pm 0.17$$

We can conclude that pure quark statistics can give a consistent description of relative particle yields in central and fragmentation regions. This description is global, but it can be taken as a first hint that quarks may play a role also in soft hadronic reactions. If we want to know how, we have to go to more differential distributions.

I.2. Reflection of the Valence Quark Distribution

The analysis of lepton induced reactions has shown that only about half of the momentum of the proton is carried by quarks (q) and antiquarks ($\bar{q}$) and a small fraction by antiquarks alone. As $q(x)=\bar{q}(x)$ at x=0, the antiquark distri-

bution is concentrated at small x (say $x \lesssim 0.2$, the "sea" region) and the same is expected for gluons which could dissociate into a $q\bar{q}$ pair. The presence of a $\bar{q}$ component in the proton structure function implies that the proton, which primarily consists of three quarks, has dissociated into a state with many $q\bar{q}$ pairs if hit by the electron.

The suggestion of Ochs[6] is that the same process of dissociation into partons occurs if the proton fragments into hadrons in the field of another hadron at high energies. The longitudinal momenta of partons will be approximately conserved during the interaction and there is a correspondence between the hadron state and the parton state in the following way: A quark in the parton state outside the sea-region ($x \gtrsim 0.3$) is a valence quark of a hadron of the final hadron state, and the momentum of the quark contributes to the momentum of the hadron.

In the fragmentation region of the proton, the π^+ can be assumed to be composed of a u valence and a $\bar{d}$ sea quark. Since the latter carries very little momentum, we expect to find a u quark with similar momentum to that of the $\pi^+ = |u\bar{d}\rangle$. The same holds for a d quark and the $\pi^- = |d\bar{u}\rangle$. As a consequence, the x-distribution of a pion in the fragmentation region of an incident proton is expected to be similar to that of the valence quark which it shares with the proton. Fig.1a-b shows that the x-distribution of π^+ is indeed similar to the u-quark distribution u(x) derived from SLAC data on electron-nucleon deep inelastic scattering[7]. The π^- distribution agrees with d(x) up to $x \sim 0.7$, and is only slightly above d(x) for larger x-values.

We conclude that the quantum numbers and the distribution of the target proton valence quarks can be found back in the particles produced in the target fragmentation region.

What is the role of the beam quantum numbers? Fig.1c gives a comparison of the ratio of the inclusive invariant cross sections for π^+ and π^- production as a function of x in the target fragmentation region for the reactions $\pi^\pm p \rightarrow \pi^\pm X$ at 16 GeV/c to that for $p \rightarrow \pi^\pm X$ (scaling between 19 and 2000 GeV/c). The ratio R is considerably larger for 16 GeV/c π^+p than for pp reactions. On the other hand, R falls below the proton curve for π^-p collisions.

At higher energies, however, the $\pi^\pm$ p ratios tend to converge. The approach of R to a high energy limit is given in fig.2 for $\pi^\pm$ p collisions[9], as a function of $s^{-1/2}$, for several x intervals. The energy dependence agrees with an $s^{-1/2}$ term, the asymptotic limit is consistent with the ratio R for pp reactions. A similar conclusion can be drawn for $K^\pm p$ collisions. This means that at $p_{lab} \gtrsim 200$ GeV/c, the influence of the proton valence quarks alone is observed to govern proton fragmentation in soft hadronic collisions.

This second basic observation supports the quark recombination picture[10]

of hadron production in the fragmentation region. In the framework of this picture a fast meson with small p_t is formed by a two step process:

i) a quark-antiquark pair is picked out from a proton,

ii) this pair recombines to form the meson.

Neglecting many-body recombination the inclusive x distribution of a meson M is therefore given by

$$\frac{x}{\sigma_t}\frac{d\sigma}{dx} = \int f_{v\bar{s}}(x_v,x_s)\, R(x_v,x_s)\, \delta\left(\frac{x_v}{x}+\frac{x_s}{x}-1\right) dx_v dx_s$$

where $f_{v\bar{s}}(x_v,x_s)$ is the probability density of finding simultaneously within the proton two partons v and $\bar{s}$ with respective momentum fractions x_v and x_s (the two-quark structure function) and $R(x_v,x_s)$ is the recombination probability for the v and $\bar{s}$ quarks to form the meson M. The δ-function assures momentum conservation for the process.

Justification[11] for the particular form of $f_{v\bar{s}}$ and $R(x_v,x_s)$ comes from the so-called "valons" (kind of dressed quarks). The distribution of quarks in a valon and of the valons in the proton can be completely determined in shape and normalization by ensuring that they reproduce the quark distribution from low Q^2 lepton-nucleon collisions.

I.3 Jet Universality

The decrease in average sphericity <S>, thrust <1-T> and spherocity <S'> with increasing energy, generally interpreted as evidence for jet production, is not only a feature of reactions in which single quark effects are expected to dominate[12], but also of low p_t hadron-hadron collisions[13]. As is shown in fig.3a-c the average shape of the hadronic system is the same in all three types of collision at given hadronic energy, as is its change with energy.

The energy dependence of the shape of the sphericity distribution itself[13a,c] is shown in fig.3d,e. As for e^+e^- collisions, one observes a change from a dip at S=0 at low energy to a sharp peak at S=0 at higher energies. The shape of the 16 GeV/c K^-p S distribution (E_{cm}=5.6 GeV) is peaked at rather lower S values than the SPEAR data at 6.2 GeV. Very good agreement is observed between the S distribution in K^-p at 110 GeV/c (E_{cm} = 14.8 GeV) with the PLUTO result at 17 GeV, and the h^+p data at 147 GeV/c with the TASSO distribution (the TASSO S distribution at 17 GeV is similar to the PLUTO data). Diffractive events contribute only at the most "jet-like" values, i.e. low S. The agreement between the shape of the K^-p and the leptonic distributions is improved when the diffractive events are removed. The only major difference in

the shapes of S and T distributions in K^-p and in published leptonic data remains the above mentioned peaking at lower S values in the K^-p data at 16 GeV/c, when compared with the SPEAR data. This probably results from the problems in defining the sphericity axis in low E_{cm} e^+e^- events.

The normalized 70 GeV/c K^+p rapidity distribution, evaluated with respect to the thrust axis[13c] is compared to e^+e^- results at 13 GeV/c (TASSO)[14] in fig.4a,b. At similar energy, the two rapidity distributions agree remarkably well and it can be expected from the insert (and from old results on hadronic rapidity plateaus) that hadron-hadron and e^+e^- data show a similar $\ln \sqrt{s}$ increase of the plateau hight and, above all, the same plateau hight at the same energy!

Also the normalized p_t^2 distributions relative to the sphericity axis fig.4c show agreement at 13 GeV/c, even though there may be indication of a larger cross section in the high p_t tail for the e^+e^- results.

The conclusion of jet universality is further supported from a comparison[13] of the energy dependence of $\langle n \rangle$, as well as of $\langle p_t \rangle$ and $\langle p_{/\!/} \rangle$ relative to the thrust axis (not shown). Again, the hp and e^+e^- data have essentially the same values and the same energy behaviour. In particular, the rise in $\langle p_t^2 \rangle$ with E_{cm} felt to be a characteristic feature of single quark jets is in fact also a feature of hadronic low p_t particle production.

At this stage we may ask whether the agreement between the data is accidental, e.g. due to longitudinal phase space, or has any more fundamental dynamical origin. In ref.13c the sphericity, thrust, spherocity and other distributions are compared to mere longitudinal phase space and the Field and Feynman parametrization of quark-parton jets[15]. In all cases, both the FF parametrization as well as LPS more or less describe the data. One may conclude that FF is a somewhat complicated way to parametrize longitudinal phase space. Jet universality may well turn out to reduce to the equal p_t distributions and the equal average multiplicities, the rest may follow from independent emission + conservation laws. But the point is, if this will turn out to be the case, it will hold equally for hadronic, deeply inelastic and e^+e^- hadron production. In all cases the same mechanism is at work, governing multiplicities and transverse momenta in an identical way.

If quark fragmentation is indeed governed by longitudinal phase space, it will be interesting to look for the trivial differences expected from the quantum numbers or excitation modes of the fragmenting quarks, as well as for (non-trivial) flavour correlations within the fragmentation jet.

One difference of the hadron system produced in e^+e^- annihilation and pp collisions is that the baryon number is zero in the first case and two in the second. In other words, there are more interacting valence quarks in pp colli-

sions than in e^+e^- hadron production. A CERN-Bologna-Frascati Collaboration[16] using the CERN Split-Field Magnet at $\sqrt{s}$=62 GeV has attempted to remove the expected effects of baryon-number conservation by selecting events with a leading proton and redefining the fractional variables of the particle after removal of that proton.

The pp data (normalized to the mean charge multiplicity) are compared to (normalized) e^+e^- data from the Tasso Collaboration[17] at three different energies E_{had}. The agreement between the two distributions at all three E_{had} values, both in shape and absolute value (mean charged multiplicity), suggests that the mechanism for transforming energy into particles in these two processes must be the same. This would be surprising if the fragmentation process would not be governed by longitudinal phase space, since excluding the leading proton means excluding the leading parton plus its companion. To be fair, one would have to exclude the leading quark and its companion in e^+e^- annihilation, as well.

The 147 GeV/c h^+p collaboration studied the effect on $\langle S \rangle$ and $\langle T \rangle$ when removing the leading particle. As expected, $\langle S \rangle$ and $1-\langle T \rangle$ increase, but the available hadron energy E_{had} decreases. Both values are compared to the e^+e^- and νN data at the corresponding values of E_{had}. Removing the proton does not improve the agreement. I would suggest to forget this approach and to look for expected differences rather than to exclude them before they are shown to exist.

The better approach seems to me to select certain events where the jet is expected to derive from $q\bar{q}$ separation as in e^+e^- jet production. A possible laboratory for this study is meson or photon diffraction dissociation[18]. The diffractive dissociation can be assumed to be a two-step process. First, the meson dissociates into a $q\bar{q}$ pair, then this $q\bar{q}$ system hadronizes in the same manner as hadronization takes place of neutral quark-antiquark pairs during e^+e^- annihilation to two jets of hadrons. Diffraction dissociation may have the enormous advantage over e^+e^- annihilation that the $q\bar{q}$ pair is known and not a mixture of $u\bar{u}$, $d\bar{d}$, $s\bar{s}$, $c\bar{c}$ or $b\bar{b}$. This may provide the unique opportunity to investigate jets of known flavour!

The fact that jets produced in e^+e^- annihilation and deep inelastic lepto-production are very similar to these produced along the beam direction in ordinary hadron-hadron collisions has led to the assumption of parton fragmentation as a common underlying dynamical mechanism. In the quark fragmentation view[19], inelastic (non diffrative) scattering is dominated by events where one valence quark of the baryon with low momentum interacts with the other hadron and is fixed in the central region. The remaining diquark system will carry almost all the original baryon momentum and subsequently fragment into hadrons in the baryon fragmentation region. The rapidity density of the fragmentation

chain is universal, i.e. it depends only on the nature of the system at the chain end and not on the nature (hard or soft) of the process which produces them. The inclusive one-particle distribution of hadron H in the fragmentation region of hadron h is given by the convolution integral

$$\frac{1}{\sigma}\frac{d\sigma}{dx} = \sum_q \int_x^1 dydz\, f_q^h(y)\, D_q^H(z)\, \delta(yz-x)$$

between the probability distribution $f_q^h(x)$ of the constituents of h to carry momentum fraction x and the fragmentation $D_q^H(z)$ of constituent q into the hadron H, as obtained from leptonic reactions.

The important assumption is that the mechanism responsible for hadronic interactions favours configurations of valence quarks different from those measured in lepto-production. Only configurations in which the diquark carries almost all the momentum are assumed to be responsible for pion production in the proton fragmentation region. This amounts to

$$f_q^h(x) = k_q^h\, \delta(x-x_o)$$

with k being a statistical factor corresponding to the additive quark model and $x_o \simeq 1$. So, hadronic spectra are given by the fragmentation functions $D_q^H(x)$ in a parameter free form.

II. SELECTED APPLICATIONS

The recombination and fragmentation pictures have been designed to describe single particle distributions from a different point of view. Attempts to show the duality or complementarity of the two views have been started[20] and should be continued. Rather than trying to prove one of the pictures and disprove the other, we shall here use their complementarity to illuminate different aspects of the data.

II.1 Target Fragmentation

According to the fragmentation model[19], pion production in the proton fragmentation region can be written in terms of the diquark fragmentation functions D_{qq}^{π} as

$$\frac{1}{\sigma}\frac{d\sigma^{p\to\pi^\pm}}{dx}(x) \simeq \frac{1}{3} D_{uu}^{\pi^\pm}(x) + \frac{2}{3} D_{ud}^{\pi^\pm}(x).$$

From isospin invariance follows $D_{ud}^{\pi^-} = D_{ud}^{\pi^+}$, so that three independent functions remain: $H_1 = D_{uu}^{\pi^+}$, $H_2 = D_{ud}^{\pi^+} = D_{\bar{u}\bar{d}}^{\pi^-}$ and $H_3 = D_{uu}^{\pi^-}$. One can expect $H_1 > H_2 > H_3$ for large x since in H_1 both u-quarks can contribute to the creation of a π^+, while

in H_2 only one quark contributes, and in H_3 none of the two u-quarks contributes to π^- production.

Furthermore, if baryon production is dominant in the diquark fragmentation, the approximate relation $2H_2 \sim H_1 + H_3$ is valid[19]. For the pion cross section in proton fragmentation then follows

$$\frac{1}{\sigma}\frac{d\sigma}{dx}^{p\to\pi^+}(x) \approx \frac{2}{3}H_1(x) + \frac{1}{3}H_3(x) \quad \text{and} \quad \frac{1}{\sigma}\frac{d\sigma}{dx}^{p\to\pi^-}(x) \approx \frac{1}{3}H_1(x) + \frac{2}{3}H_3(x) \ .$$

K^-p data at 70 GeV/c[20] are compared to νp and $\bar{\nu}p$ data[21] in fig.5. The following observations can be made:

- $H_1(x)$ from νp data indeed agrees with $H_1(x)$ from K^-p data.
- $2H_2(x)$ from $\bar{\nu}p$ data agrees with $H_1(x)$, giving support to the above approximation.
- $H_3(x)$ from νp data is much smaller than $H_1(x)$. It is compatible with zero for the K^-p data (not shown).

Of particular interest in connection with the influence of the valence spectators are various types of quantum number correlations between the two different fragmentation regions and within one fragmentation region itself. Long range correlation of pions, each coming from a different one of the two incident protons, has been measured[22] in the form of the two pion correlation function $R(x_1,x_2) = \sigma N(\pi_1\pi_2)/N(\pi_1).N(\pi_2)$ for $pp \to \pi\pi X$ at $\sqrt{s}$ = 62.3 GeV ($0.2<x_1,x_2<0.95$, $0.2<p_{t_1}, p_{t_2}<1.2$ GeV/c). Over most of the x range, the $\pi^+\pi^+$, $\pi^+\pi^-$ and $\pi^-\pi^-$ data are essentially uncorrelated (R≈1), in agreement with factorization of the two fragmentation processes, as is expected for gluon exchange.

For comparison to single particle production in the proton fragmentation region, the ratio R of π^+ to π^- production can be studied in association with various triggers. With a π^+ trigger, the spectator system ($u_v d_v d_s$) should produce equal amounts of π^+'s and π^-'s at fixed $\tilde{x}_\pi = x_\pi/(1-x_{tr})$. This is confirmed by the data[23] in fig.6: Whereas the untriggered π^+/π^- ratio rises with increasing x, the ratio for a π^+ trigger is compatible with unity for $x \geq 0.4$. In comparing this associated ratio to the π^+/π^- ratio measured in charged current $\bar{\nu}p$ collisions where the spectator system is the same, the agreement is indeed striking.

For a π^- trigger, the spectator system is ($u_v u_v u_s$) and a strong increase of the ratio R is expected with increasing x. Also this is indeed observed in fig.6.

We conclude that proton fragmentation is well behaved and understood, so that one can go further and apply the same ideas to extract new information from meson fragmentation.

II.2 Meson Fragmentation

The 70 GeV/c K^-p data were used to extract $D_u^{\pi^+}$ and $D_u^{\pi^-}$ from the π^+, π^- and π^o distribution in the K^- fragmentation region[20] (see fig.7). The contamination from charged kaons has been estimated from K^n production and has been removed. The study of π^- production is restricted to the region $x \leq 0.7$ to avoid contamination from leading K^-. The authors claim rather good agreement with the $\nu(\bar{\nu})p$ data with W>4 GeV and with the Field and Feynman $D_u^{\pi^\pm}$ functions[15]. This is certainly true for the comparison of $D_u^{h^-}$. Note that the difference between νp and hp data for $D_u^{h^-}$ is smaller than between (the isospin symmetric) $D_u^{h^-}$ and $D_d^{h^+}$ from $\nu(\bar{\nu})p$ data. $D_u^{\pi^+}$ seems consistently steeper for hp collisions, but one has to take into account that

- in the $\nu(\bar{\nu})p$ data it is only at high values of z (where the contribution of the sea is negligible) that the functions D^h represent the fragmentation of a pure u(d) quark (in addition they represent production of hadrons $h^\pm$ rather than just $\pi^\pm$);
- it is not clear that diffraction dissociation (Q, L ..) has been sufficiently removed. There may be a contribution $K^- \rightarrow \pi^-$ ...below x=0.7.

With these limitations in mind, one can conclude that one can extract the single quark fragmentation function to a very good approximation from hadronic collisions.

Alternatively, the recombination picture[10,11] can be used to determine[24] the valence quark distribution in mesons, for which there is no direct information from deep inelastic lepton interactions. The results can be given in terms of the power n of the (1-x) distribution of the valence quarks. For a pion it follows from charge conjugation and isospin invariance that the quark distribution function is the same for both valence quarks. For a kaon the situation is expected to be non-symmetric. A value of $n=1.0\pm0.1$ has been obtained for the pion structure function. The power n is indeed larger than unity for the non-strange valence quark in the kaon while it is smaller than unity for the strange valence quark. These results are compatible with those extracted via the Drell-Yan model from μ-pair production[25]. One can conclude that meson valence quarks are harder than those in the nucleon and that strange valence quarks are harder than non-strange ones.

II.3 Meson Resonances

Of particular interest in connection with partons is inclusive production of resonances. One can assume that resonances are more abundantly and more directly produced than pions and kaons, represent a larger variety of quantum

numbers and allow for conclusions about their production from their decay density matrix.

In the quark picture the ϕ is of central interest because of its hidden strangeness quantum numbers. In particular, it has a valence quark in common with an incoming kaon, but not with an incoming pion, proton or antiproton. The x-distribution is therefore flatter for kaon induced production than in the other cases[26].

Furthermore, $K^-p \to \bar{K}^{*0}$, $K^+p \to K^{*+}$ and $Kp \to \phi$ all have the same x dependence[27] and are definitely more forward peaked than $Kp \to \rho^0$. This is a direct consequence of the fact that the strange quark in the incident kaon is harder than the nonstrange quark. The ratio of ϕ and ρ^0 is plotted in fig.8a for K^-p at 32 GeV/c[26b] and compares well to the ratio of s and $\bar{u}$ distribution functions.

Fig.8b gives the forward ρ^0 distribution from $\pi^\pm$ p collisions at 147 GeV/c[28]. The curves shown correspond to a power law fit[29] (DCR), a recombination fit (QRM) and fragmentation predictions (QFM) with Field and Feynman[15] (dashed) and Lund[19] (dot-dashed) parametrizations of the fragmentation functions. The Lund prediction works very well, so do DCR and QRM. In the latter two cases, the distribution function comes out consistently slightly flatter than for pions. This observation does not change after exclusion of diffractive events and should be checked with good statistics.

Fig.9 shows the results for the density matrix for $K^+p \to K^{*+}X$ at 32 and 70 GeV/c[30] as a function of t and M^2/s. Distributions like these should be a challenge to the quark pictures.

II.4 Hyperon Polarization

Non-zero Λ polarization is known since 1976 from pBe collisions at 400 GeV/c[31a] and has been observed in π^-p collisions at NAL[31b] and pp collisions at ISR[31c]. This observation cannot be explained from the Regge model since at these energies RPR terms dominate and these terms do not give rise to polarization. Non-zero polarization has also been observed in ep scattering[32]. In fig.10a the pp and ep points show an increasing polarization for $p_t > 0$. Furthermore, from scattering off deuterium and other nuclei, no difference is found in polarization between proton and neutron targets[33].

The best recent data come from the Michigan-Minnesota-Rutgers-Wisconsin Collaboration[34] (see fig.10b,c). One can conclude that:

- Λ^0's produced in hh, hA and ep scattering are polarized transverse to the production plane, along the $(\vec{p}_\Lambda \times \vec{p}_p)$ axis).

- This polarization is probably independent of the beam energy, the projectile type and largely also of the x value of the Λ^0.
- The polarization increases linearly with the transverse momentum of the Λ^0.
- $\bar{\Lambda}$ and protons are not polarized.
- $\Xi^0, \bar{\Xi}^-$ have the same polarization as the Λ^0.
- Σ^+ has the same polarization as Λ^0 in magnitude but with opposite sign.

A semi-classical model for basically soft Λ^0-production able to explain the observed polarization effect is suggested in the quark fragmentation picture[35]. In this picture, a diquark continues forward as a unit after the collision and a string-shaped colour dipole field is stretched between the diquark and the central collision region. This field can break up by the production of quark-antiquark pairs (as in e^+e^- hadron production). A Λ^0-particle can be formed if an $s\bar{s}$-pair is produced in the field of a (ud)-diquark (of isospin and spin I=S=0), so that the spin of the Λ^0 is determined by the spin of the s-quark.

The transverse momentum p_t of the Λ^0 with respect to the beam direction is made up of two contributions, the transverse momentum $\vec{q}_t$ of the diquark (the direction of the field string) and the (locally conserved) transverse momentum $\vec{k}_t$ of the s quark with respect to the string direction. A pair of massless quark-antiquarks can be produced point-like, but massive quarks have to be produced at a certain distance from each other. Therefore, the pair will obtain an orbital angular momentum perpendicular to the string; this is assumed to be compensated by the spin of the $s\bar{s}$-pair. In a Λ sample of definite p_t, we obtain an enhanced number of events where $\vec{k}_t$ and $\vec{p}_t$ point in the same direction. So the observed effect is explained by a sort of trigger bias. The curves in fig.10a show the model prediction and its upper and lower limits (without inclusion of the effect of Λ production via Σ^0 and Σ^*).

A somewhat similar picture has recently been developed[36] in the framework of the recombination model. Here, the polarization arises via Thomas precession of the quarks' spin in the recombination process. The description accounts for all presently known qualitative features of the baryon and antibaryon polarization as stated above. Also this picture can be extended to e^+e^- annihilation and deep inelastic scattering. Of special interest in this context is further the prediction for polarization of baryons (and vector mesons) in e^+e^- annihilation by Bartl et al.[37]

We conclude that hyperon polarization which cannot be explained by the triple Regge model, may find an explanation from the quark composition of incident and produced particles.

III. CONCLUSION AND OUTLOOK

With the help of quark statistics one can get to a consistent understanding of various particle yields. This first basic observation is taken as a hint that partons may play a role also in soft hadronic reactions.

The similarity of pion production in the nucleon fragmentation region to the valence quark distribution in the nucleon as measured from deep inelastic collisions suggests that valence quarks are governing pion production in proton fragmentation. This observation has led to a recombination and valon picture.

Particle production in soft hadronic collisions shows features very similar to those in e^+e^- and lepton-hadron collisions. This third observation has led to the quark fragmentation picture.

Particle production and correlation in proton fragmentation is well understood in terms of these two pictures. Extracted di-quark fragmentation functions are identical to those from deep inelastic neutrino scattering.

Application of the two pictures to meson fragmentation allows to extract meson structure functions similar to those obtained from μ-pair production on one hand, and quark fragmentation functions similar to those obtained from deep inelastic neutrino scattering on the other.

Differential distribution for resonances start to become available at high energies. They allow to check the results on more directly produced particles, to compare a larger variety of quantum numbers and to challenge models on their decay density matrix.

Hyperon polarization at high energies, not understood from triple Regge exchanges, seems to be explained from both the recombination and fragmentation pictures of hadron production.

We conclude that a new field has evolved in the last 3 years and that partons do play a role in soft hadronic reactions. Work to be done on the theoretical side is on a solid foundation of the two pictures as well as on an explanation of the apparent complementarity of the two views. On the experimental side, high statistics is needed on hydrogen and on higher nuclei at $p_{lab} > 200$ GeV/c in combination with good momentum resolution and particle identification. This will allow to study flavor correlations and resonance production more conclusively than was possible until now and, in particular, to isolate the influence of longitudinal phase space in quark fragmentation.

References

1) K. Böckmann, "Inclusive Vector Meson Production and Hadron Structure", Symp. on Hadron Structure and Multiparticle Production, Kazimierz 1977. W. Kittel, "Inclusive Resonance Production and Fireballs", VIII Int. Symp. on Multiparticle Dynamics, Kaysersberg 1977.

A. Zieminski, "Multiparticle Production", EPS Conf. on Particle Physics, Budapest 1977.
2) H. Satz, Phys.Letters 25B (1967) 220 and Phys.Rev.Letters 19 (1967) 1453.
V.V. Anisovich and V.M. Shekhter, Nucl.Phys. B55 (1973) 455.
J.D. Bjorken and G.R. Farrar, Phys.Rev. D9 (1974) 1449.
3) V.V. Anisovich, M.N. Kobrinsky and J. Nyiri, "A Proof of the Rules of Quark Statistics in Multiparticle Processes", Leningrad 1980.
4) Yu.M. Shabelski, "Production of Projectile Fragments in Additive Quark Model; Inelasticity Coefficients and Probabilities of Inelastic Charge Exchange", Leningrad 1980. Data from R.T. Edwards et al., Phys.Rev. D18 (1978) 76.
5a) J. Kalinowski, S. Pokorski and L. Van Hove, Z. Physik C2 (1979) 85.
b) M. Bourquin et al., Z. Physik C5 (1980) 275.
c) L. Van Hove, "The Role of Valence Quarks in Proton Fragmentation", Ref. TH 2997-CERN, 21 Nov. 1980.
6) W. Ochs, Nucl.Phys. B118 (1977) 397.
7) J. Singh et al., Nucl.Phys. B140 (1978) 189.
8) B. Buschbeck, H. Dibon, H.R. Gerhold and W. Kittel, Z. Physik C3 (1979) 97.
9) M.M. Schouten et al., "Approach to Scaling of π^+/π^- Ratios in Target Fragmentation from $\pi^+/K^+/pp$ Interactions at 147 GeV/c", Nijmegen preprint 1981.
10) K.P. Das and R.C. Hwa, Phys.Letters 68B (1977) 459.
J. Ranft, Phys.Rev. D18 (1978) 1491.
L. Van Hove, Lectures at the XVIII. Int. Universitaetswochen fuer Kernphysik, Schladming, Acta Physica Austriaca, Suppl. XXI (1979) 621.
B. Buschbeck, H. Dibon and H.R. Gerhold, Z. Physik C7 (1980) 73.
11) R.C. Hwa, Phys.Rev. D22 (1980) 759 and 1593.
12) Ch. Berger et al., Phys.Letters 78B (1978) 176 and 81B (1979) 410.
P.C. Bosetti et al., Nucl.Phys. B149 (1979) 13.
K.W.J. Barnham et al., Phys.Letters 85B (1979) 300.
13a) R. Göttgens et al., Nucl.Phys. B178 (1981) 392.
b) Ph. Herquet et al., "Properties of Jet-Like Systems Observed in π^+p, K^+p and pp Interactions", Proc. XVth Renc. de Moriond 1980, Vol. I, edited by J. Tran Than Van, R.M.I.E.M. Orsay, p215.
c) R.T. Ross, "Jet Like Properties in Low p_t Hadronic Interactions", Europhysics Study Conf. Partons in Soft-Hadronic Processes, Erice 1981.
F. Grard, this rencontre.
d) J.M. Laffaille et al., "Energy Dependence of Transverse Momentum Invariant Distribution of Pions and Neutral Kaons in K^-p Interactions between 14.3 and 70 GeV/c", DPh PE 80-16.
14) R. Brandelik et al., Z. Physik C4 (1980) 87.
15) R.D. Field and R.P. Feynman, Nucl.Phys. B136 (1978) 1.
16) M. Basile et al., Phys.Letters 92B (1980) 367, CERN-EP/80-111, 80-205 and 223.
17) R. Brandelik et al., Phys.Letters 83B (1979) 261 and 89B (1980) 418.
18) S.P. Misra, A.R. Panda and B.K. Parida, Phys.Rev. Letters 45 (1980) 322.
J. Randa, "Comparison of Jets in Diffractive Dissociation and e^+e^- Annihilation", Univ. of Colorado preprint COLO-HEP-29 (Okt. 1980) and this rencontre.
J. Gunion, "Unification of Low-p_t Models and their Relation with other Approaches", Europhysics Study Conf. Partons in Soft-Hadronic Processes, Erice 1981.
19) B. Andersson, G. Gustafson and C.P. Peterson, Phys.Letters 69B (1977) 221 and Phys.Letters 71B (1977) 337.
B. Andersson et al., Nucl.Phys. B135 (1978) 273.
A. Capella et al., Phys.Letters 81B (1979) 68.
A. Capella, U. Sukhatme, J. Tran Thanh Van, Z. Physik C3 (1980) 329.
A. Capella and J. Tran Thanh Van, Phys. Letters 93B (1980) 146.

G. Cohen-Tannoudji, A. El Hassouni, J. Kalinowski and R. Peschanski, Phys.Rev. D19 (1979) 3397.
G. Cohen-Tannoudji, A. El Hassouni, J. Kalinowski, O. Napoly and R. Peschanski, Phys.Rev. D21 (1980) 2699.
20) A.M. Touchard et al., Paris-Rutherford-Saclay Collaboration, "Study of the Longitudinal Distribution in the Fragmentation Regions Using the Quark Parton Model in K^-p Interactions at 70 GeV/c", EPS Study Conf., Erice 1981.
R. Göttgens et al., "Fragmentation Spectra in K^-p Interactions at 110 GeV/c", CERN/EP 80-102 ReV.
21) J. Bell et al., Phys.Rev. D19 (1978) 1.
M. Derrick et al., Phys.Rev. D17 (1978) 1.
22) G.J. Bobbink et al., Phys.Rev.Letters 44 (1980) 118.
23a) E.A. De Wolf et al., "Two-Particle Production in K^-p Interactions at 32 GeV/c. Tests of the Quark-Parton Model?" EPS Conf. on High Energy Physics, Geneva 1979.
b) M. Barth et al., Z.Physik C7 (1981) 187.
c) F. Erne, this rencontre.
24) R.C. Hwa and R.G. Roberts, Z.Physik C1 (1979) 81.
Aachen-Berlin-CERN-Cracow-London-Vienna-Warsaw Collaboration, "The Fragmentation Spectra in K^-p Interactions at 10 GeV/c", EPS Conf. 1979.
W. Aitkenhead et al., Phys.Rev.Letters 45 (1980) 157.
D. Denegri et al., Phys.Letters 98B (1981) 127.
M. Barth et al., "Inclusive Neutral Kaon Production in 70 GeV/c K^+p Interactions", Nijmegen preprint 1981.
25) J. Badier et al., "Determination of the π and K Meson Structure Functions from Massive Dimuons Produced at 150 and 200 GeV", CERN/EP 80-148.
F. Vannucci, this rencontre.
26a) D.R.O. Morrison, "Inclusive ϕ-Meson Production-Relation to J/Ψ and T Production", EPS Conf. Geneva 1979.
b) Yu. Arestov et al., Z. Physik 8 (1981).
c) C. Daum et al., "Inclusive ϕ-Meson Production in 93 and 63 GeV Hadron Interaction", Amsterdam preprint NIKHEF-H/81-1.
27) P.V. Chliapnikov, V.G. Kartvelishvili, V.V. Kniazev and A.K. Likhoded, Nucl.Phys. B148 (1979) 400.
C. Cochet et al., Nucl.Phys. B155 (1979) 333.
28) M.M. Schouten et al., International Hybrid Spectrometer Consortium, "Inclusive and Semi-Inclusive ρ^0 Production in $\pi^+/\pi^-/K^+/pp$ Interactions at 147 GeV/c", Nijmegen preprint HEN187, 1981.
29) J.F. Gunion, Phys.Letters 88B (1979) 150.
30a) I.V. Ajinenko et al., Z.Physik C5 (1980) 177.
b) Yu. Arestov et al., Z.Physik C6 (1980) 101.
c) A. Stergiou, "Polarization Measurements on the Inclusive $K^{*+}(890)$ Production in K^+p Interactions at 70 GeV/c", Europhysics Study Conf. Partons in Soft-Hadronic Processes, Erice 1981.
31a) G. Bunce et al., Phys.Rev.Letters 36 (1976) 1113.
b) N.N. Biswas et al., Nucl.Phys. B168 (1980) 4.
c) S. Erhan et al., Phys.Letters 32B (1979) 301.
32) H. Pressner, Proc. Xth Int. Symp. on Multiparticle Dynamics, Goa 1979.
33) K. Raychaudhuri et al., Phys.Letters 90B (1980) 319.
S. Dado et al., Phys.Rev. D22 (1980) 2656.
34) K. Heller et al., Int. Conf. on High Energy Physics, Madison 1980.
C. Wilkinson et al., Phys.Rev.Letters 46 (1981) 803.
O. Overseth, this rencontre.
35) B. Andersson, G. Gustafson and G. Ingelman, Phys.Letters 85B (1979) 417.
36) T.A. De Grand and H.I. Miettinen, "Quark Dynamics of Polarization in Inclusive Hadron Production", HU-TFT 80-47.
37) A. Bartl, A. Fraas and W. Majerotto, Z. Physik C6 (1980) 335.

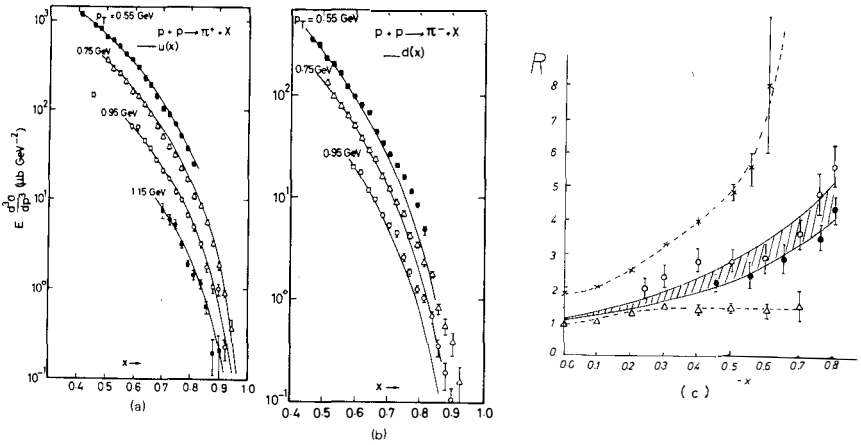

Fig. 1 (a)-(b) Comparison of the invariant π^+ and π^- cross section from pp collisions at $\sqrt{s}$=45 GeV to the u and d quark distribution functions u(x) and d(x), respectively[7],
(c) π^+/π^- ratio[8] in the proton fragmentation region of 16 GeV/c π^+p collisions (crosses) 16 GeV/c π^-p collisions (triangles) and pp collisions (shaded area and circles).

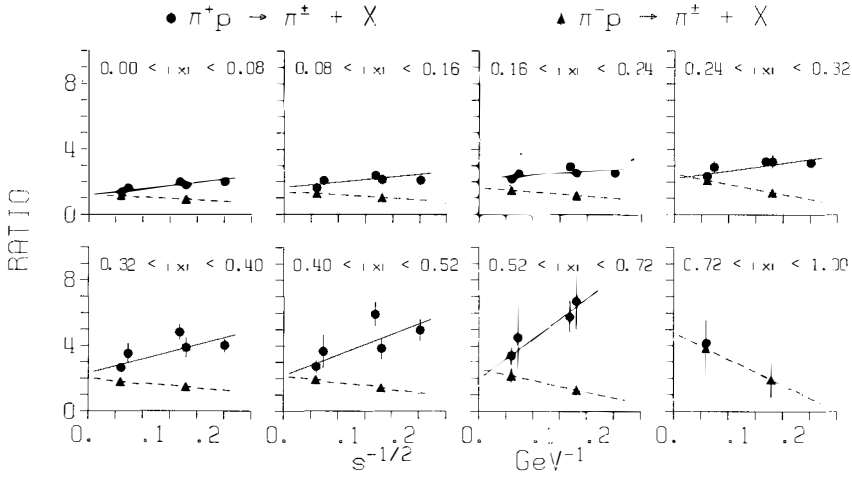

Fig. 2 The π^+/π^- ratio in the proton fragmentation region for $\pi^\pm$p collisions as a function of $s^{-\frac{1}{2}}$, for different x-intervals, as indicated[9].

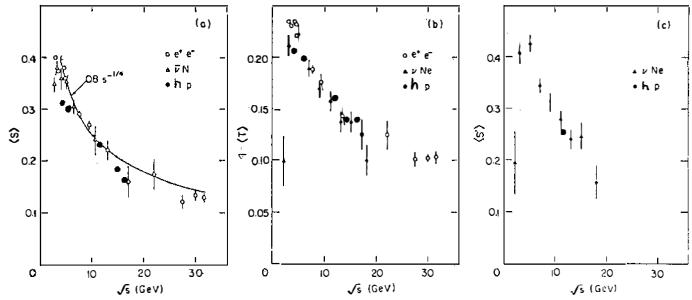

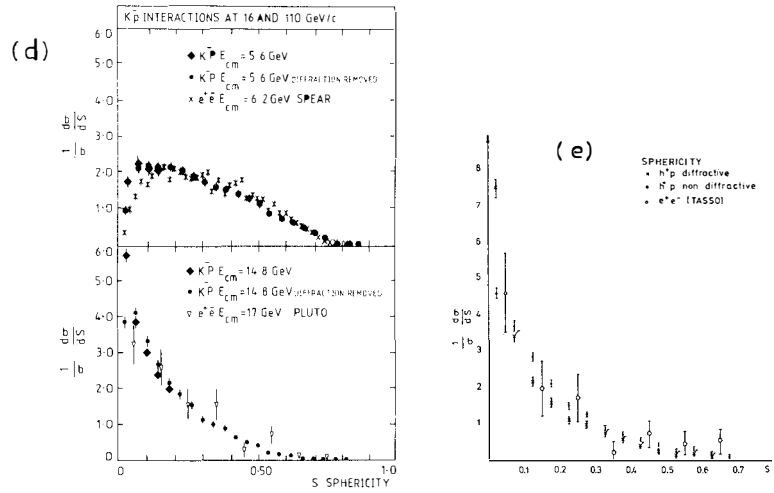

Fig. 3 (a)-(c) Average sphericity, thrust and spherocity as a function of cms energy for e^+e^-, neutrino and hadron-hadron interactions,
(d) sphericity distribution for K^-p at 16 and 110 GeV/c compared to e^+e^- at corresponding energies[13a],
(e) same for h^+p at 147 GeV/c[13b].

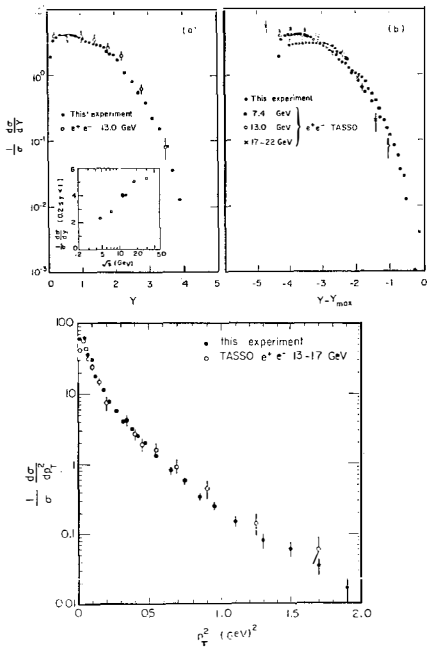

Fig. 4 Rapidity and p_t^2 distributions for 70 GeV/c K^+p collisions, evaluated relative to the thrust axis, compared to e^+e^- collisions at similar and different energies[13c].

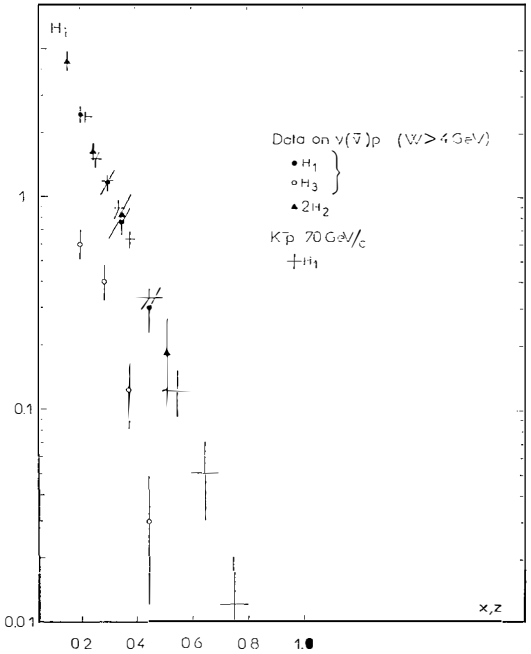

Fig. 5 Diquark fragmentation function $H_1(x)=D_{uu}^{\pi^+}(x)$ obtained in K^-p collisions at 70 GeV/c[20]. Data on $H_1(x)$, $H_2(x)=D_{ud}^{\pi^+}(x)$, $H_3(x)=D_{uu}^{h^-}(x)$ from $\nu(\bar{\nu})p$ experiments are also reported.

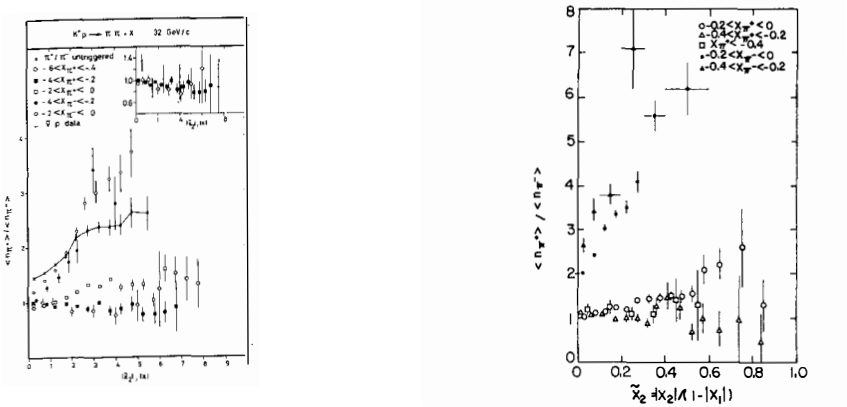

Fig. 6 The π^+/π^- ratio as a function of $\tilde{x}_2$ in the proton fragmentation region of 32 and 70 GeV/c K^+p collisions, associated with a π^- or π^+ trigger, for several trigger momentum intervals[23a,b].

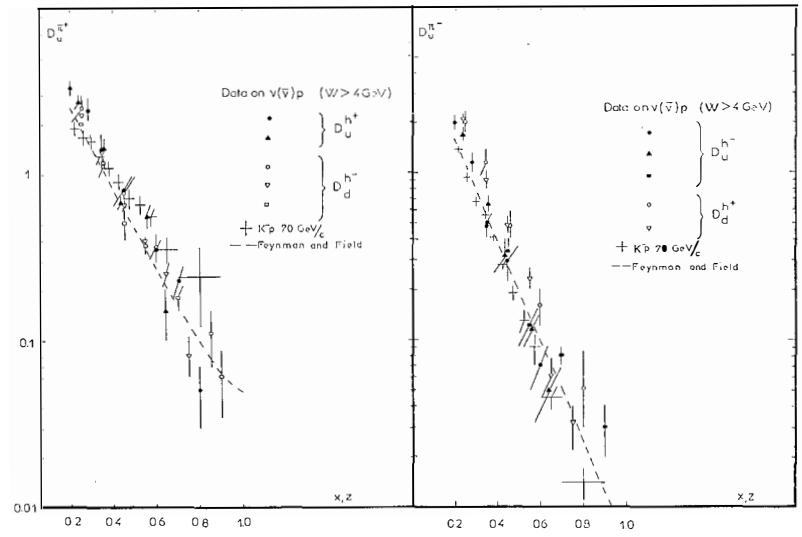

Fig. 7 Quark fragmentation functions $D_u^{\pi^+}(x)$ and $D_u^{\pi^-}(x)$ obtained from K^-p collisions at 70 GeV/c[20]. Data on $D_u^{h^\pm}$ and $D_d^{h^\mp}$ from $\nu(\bar{\nu})p$ experiments are also reported.

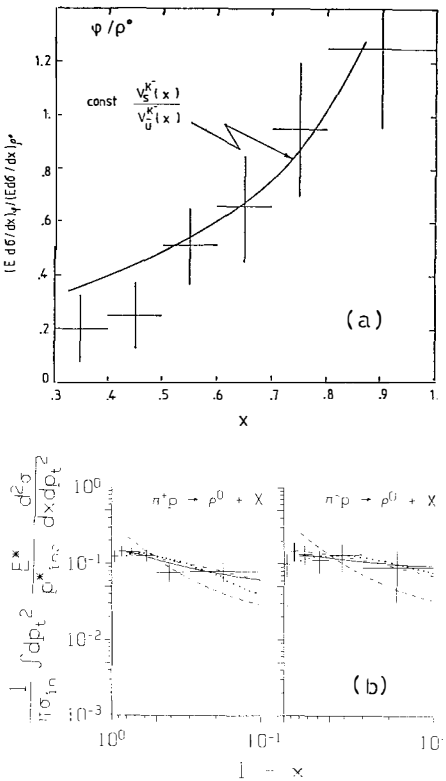

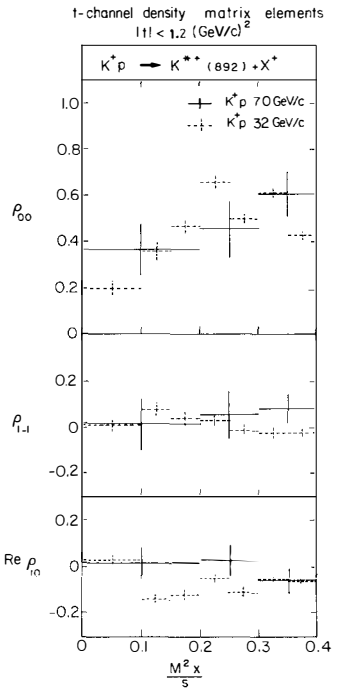

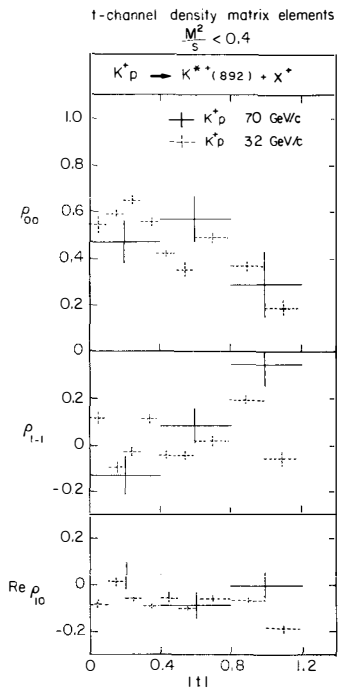

Fig. 9 Density matrix elements in the t-channel for K^{*+} production from K^+p collisions at 32 and 70 GeV/c, as functions of M^2/s and t.[30c]

Fig.8a) The ϕ/ρ^0 ratio as a function of x for K^-p collisions at 32 GeV/c, compared to ratio of the strange to non-strange valence distribution functions,[26b] b) the (1-x) dependence of ρ^0 production in the pion fragmentation region of $\pi^\pm p$ collisions at 147 GeV/c[28]. The curves are explained in the text.

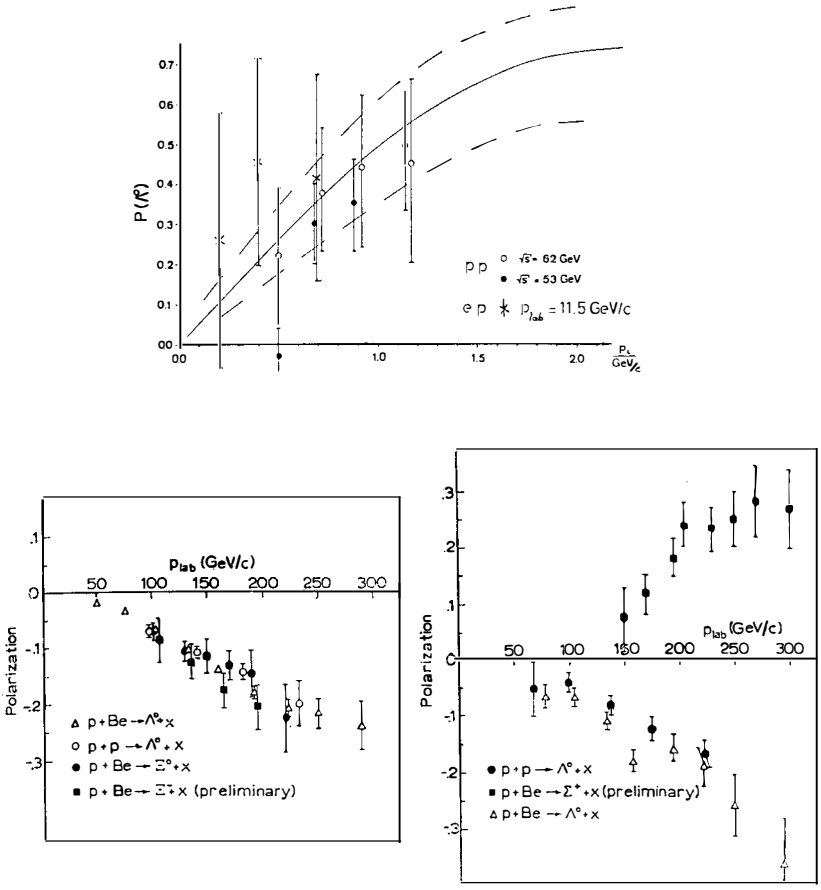

Fig. 10 (a) Λ polarization as a function of p_t for pp collisions at $\sqrt{s}$=53 and 62 GeV[31c] and ep collisions at p_{lab} = 11.5 GeV[32]. The lines are the expectation and its limits from the fragmentation model [35].
(b) Hyperon polarization for pp and pBe collisions at 400 GeV/c, as a function of the hyperon lab momentum[34].

FEYNMAN-X DISTRIBUTIONS OF $\pi^{\pm}$ PRODUCED IN NEUTRINO-PROTON CHARGED-CURRENT INTERACTIONS

Aachen-Bonn-CERN-München(MPI)-Oxford Collaboration

N. SCHMITZ
Max-Planck-Institut für Physik und Astrophysik
München, Germany

ABSTRACT

In an experiment with BEBC the distributions of Feynman-x_F have been measured for positive and negative pions produced in charged current neutrino-proton (νp) reactions with $W > 3$ GeV. In the framework of the quark-parton model the distributions give information about the fragmentation of a forward going u-quark and a backward going uu-diquark. Feynman scaling is observed. Included are preliminary data on negative pions produced in $\bar{\nu}p$ scattering for comparison. The fragmentation of uu and $ud_{\pm}$ diquarks is compared with the fragmentation of protons into $\pi^{\pm}$.

1.) Introduction

In this paper we present the distributions of Feynman-x_F for positive and negative pions produced in the semi-inclusive reaction

$$\nu_\mu p \rightarrow \mu^- \pi^\pm + \text{anything}. \qquad (1)$$

Assuming that according to the quark-parton model (QPM) the reaction takes place on the valence d-quark in the proton (i.e. neglecting the sea), the final state consists on the parton level of a u-quark going forward (i.e. in current direction) and a spectator uu-diquark going backward in the hadronic cm system. Thus, for sufficiently large values of the hadronic effective mass W and not too small $|x_F|$, a forward-going $\pi^\pm$ ($x_F > 0$) comes from the fragmentation of the u-quark (current fragment) and a backward-going $\pi^\pm$ ($x_F < 0$) from the fragmentation of the uu-diquark (target fragment). A measurement of the x_F distributions of $\pi^\pm$ therefore yields information on the fragmentation functions $D_u^{\pi^\pm}(x_F)$ and $D_{uu}^{\pi^\pm}(x_F)$ of the u-quark and uu-diquark, respectively, into $\pi^\pm$. The above restrictions on W and $|x_F|$ are necessary to avoid or at least reduce the kinematical overlap between current and target fragments.

2.) Experimental details

The data were obtained from an exposure of the bubble chamber BEBC, filled with hydrogen, to a wide-band neutrino beam generated by 350 GeV protons from the CERN SPS. The original data sample consists of ~8300 charged-current νp events with a visible energy $E_{vis} > 5$ GeV and a muon momentum $p_{\mu^-} > 3$ GeV/c. The secondary μ^- was identified by a two-plane external muon identifier EMI with a detection efficiency varying from 40% at 3 GeV/c to over 98% above 10 GeV/c.

The unmeasured neutrino energy E_ν in each event was estimated from the momenta of the charged hadrons by a method[1,2] based on transverse-momentum balance. From E_ν the other relevant event and particle variables (W, Q^2, x_F) are then derived. The influence of the uncertainty in estimating E_ν on the x_F distributions was investigated by Monte-Carlo simulations and turned out to be small. Throughout this paper, only events with $W > 3$ GeV were retained leaving a data sample of 5360 CC events. (No Q^2 cut was applied). This W cut is applied to remove the quasi-elastic resonance region, to work in a regime where the QPM is expected to be valid, and to reduce the

overlap of current and target fragments.

Charged hadrons were identified on the basis of bubble density, change of curvature and range in hydrogen, track residuals, break-point probability and kinematic fits. The distinction between a proton and a π^+ for instance was in general possible by ionisation for momenta up to ~1 GeV/c. All unidentified particles were assumed to be pions. Since the bulk of secondary hadrons are pions anyway, this leaves a small fraction of unidentified $K^\pm$ in the pion sample which should not disturb the shape of the x_F distributions noticeably. To remove the unidentified protons from the π^+ sample (~9%) an x_F dependent correction function has been applied to the raw π^+ x_F-distribution. This function was determined from Monte-Carlo simulations which will not be described here. The correction turned out to be largest (~20%) around $x_F \approx 0.15$. It should be noticed that hadrons going into the backward cms hemisphere, in particular those with a large negative x_F, are predominantly slow in the lab system and have thus a sizable chance to be identified.

Further details of the experiment and of the data analysis can be found in previous publications of this collaboration[2,3].

3.) Invariant x_F distributions

After integration over the transverse momentum p_T, the normalized invariant x_F distribution of $\pi^\pm$ is given by

$$F^{\pi^\pm}(x_F) = \frac{1}{\sigma_{ev}} \int E \frac{d\sigma^{\pi^\pm}}{d\vec{p}} dp_T^2 = \frac{1}{N_{ev}} \frac{1}{\pi} \frac{E^*}{p^*_{Lmax}} \frac{dN^{\pi^\pm}}{dx_F} \approx \frac{1}{\pi} x_F D^{\pi^\pm}(x_F) \qquad (2)$$

(≈ for larger $|x_F|$)

with $x_F = \frac{p_L^*}{p^*_{Lmax}}$.

σ_{ev} is the event cross section, $\sigma^{\pi^\pm}$ the inclusive cross section for $\pi^\pm$ production in reaction (1). N_{ev} is the number of events and $N^{\pi^\pm}$ the number of $\pi^\pm$ in these events. E^* and p_L^* are respectively the energy and the longitudinal momentum of the $\pi^\pm$ in the cm system of all secondary hadrons. The maximum value p^*_{Lmax} of p_L^* has been calculated for each event from W, assuming a two-body final state containing a nucleon and a pion.

Fig.1 shows $F^{\pi^\pm}(x_F)$ (before applying the correction function to the π^+ distribution) for two intervals of W, namely $3 < W < 5$ GeV and $5 < W < 10$ GeV. It is seen that apart from the region of small

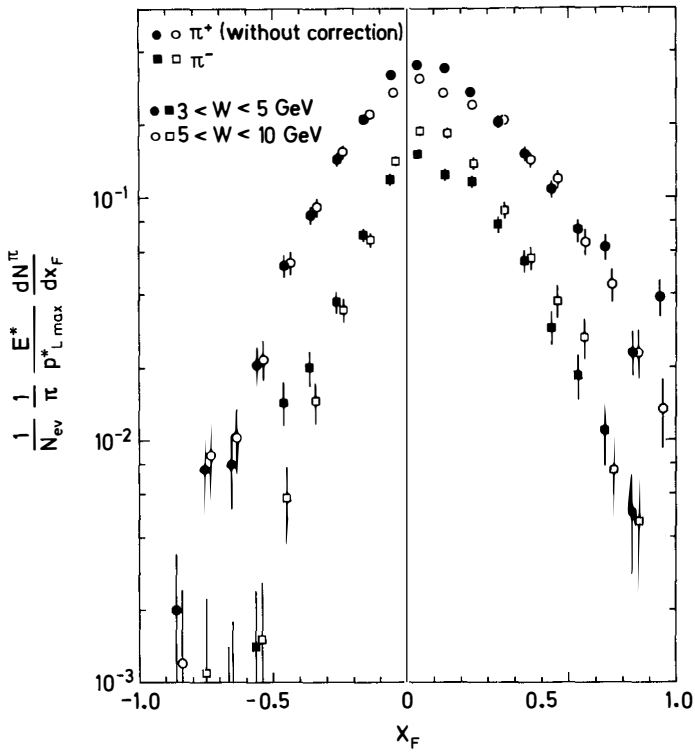

Fig.1 Normalized invariant x_F distributions of π^+ (circles) and π^- (squares) from νp events with $3 < W < 5$ GeV (full symbols) and $5 < W < 10$ GeV (open symbols). The π^+ distributions are without correction for unidentified protons in the π^+ sample. The errors are statistical.

$|x_F|$ the distributions are independent of W, i.e. Feynman scaling is fulfilled. In the subsequent figures all events with $W > 3$ GeV are therefore taken together without any further subdivision into W intervals. It should be pointed out that the distributions of Fig.1 differ, in particular in the backward hemisphere, from the corresponding distributions in Fig.6a,b of ref.4 which were for positive and negative hadrons in the same experiment, whereas here the identified hadrons other than $\pi^\pm$ have been removed.

The dimensional counting rule[5] makes predictions about the x_F dependence of the invariant distributions at larger $|x_F|$ according to the fragmentation processes involved. For a particular quark diagram the prediction is:

$$xD(x) \propto (1-|x|)^n \qquad \text{with} \quad n = 2n_H + n_{PL} - 1 \tag{3}$$

where n_H is the number of hadronic spectator quarks, and n_{PL} is the number of point-like spectator quarks.

The various possibilities for n_H, n_{PL} and n for our cases of $u \to \pi^{\pm}$ and $uu \to \pi^{\pm}$ are compiled in Table 1. They are described in detail in ref.5 where also the various quark diagrams can be found (Fig.18 of ref.5). The predictions of the counting rule in its original form (i.e. with $n_{PL} = 0$) [6] are underlined in Table 1.

Table 1 Predictions of the dimensional counting rule, eq. (3), for n_H, n_{PL} and $n = 2n_H + n_{PL} - 1$.

fragmentation	spectators	n
$u \to \pi^+$	$n_H = 1$, $n_{PL} = 0$	<u>1</u> with spin: 0 and 2
$u \to \pi^-$	$n_H = 0$, $n_{PL} = 3$ $n_H = 3$, $n_{PL} = 0$ via ρ^0	2 <u>5</u> 2
$uu \to \pi^+$	$n_H = 0$, $n_{PL} = 2$ $n_H = 2$, $n_{PL} = 0$ via ρ^0	1 <u>3</u> 2
$uu \to \pi^-$	$n_H = 0$, $n_{PL} = 4$ $n_H = 4$, $n_{PL} = 0$ via ρ^0	3 <u>7</u> 2

The full points in Fig.2 show the normalized invariant x_F distributions of $\pi^{\pm}$ for νp events with W > 3 GeV, <u>after</u> applying the correction function to the observed π^+ distribution. The errors are statistical only and do not include e.g. the uncertainty in the correction function.

Least squares fits of the form $A \cdot (1-|x_F|)^n$ with A and n as free parameters have been carried out to the data points of Fig. 2, separately in each hemisphere. The fits were performed over the whole x_F range and for $|x_F| > 0.2$. The latter cut was applied since the prediction (3) is expected to hold only for larger $|x_F|$ and since the region of small $|x_F|$ is disturbed by an overlap of current and

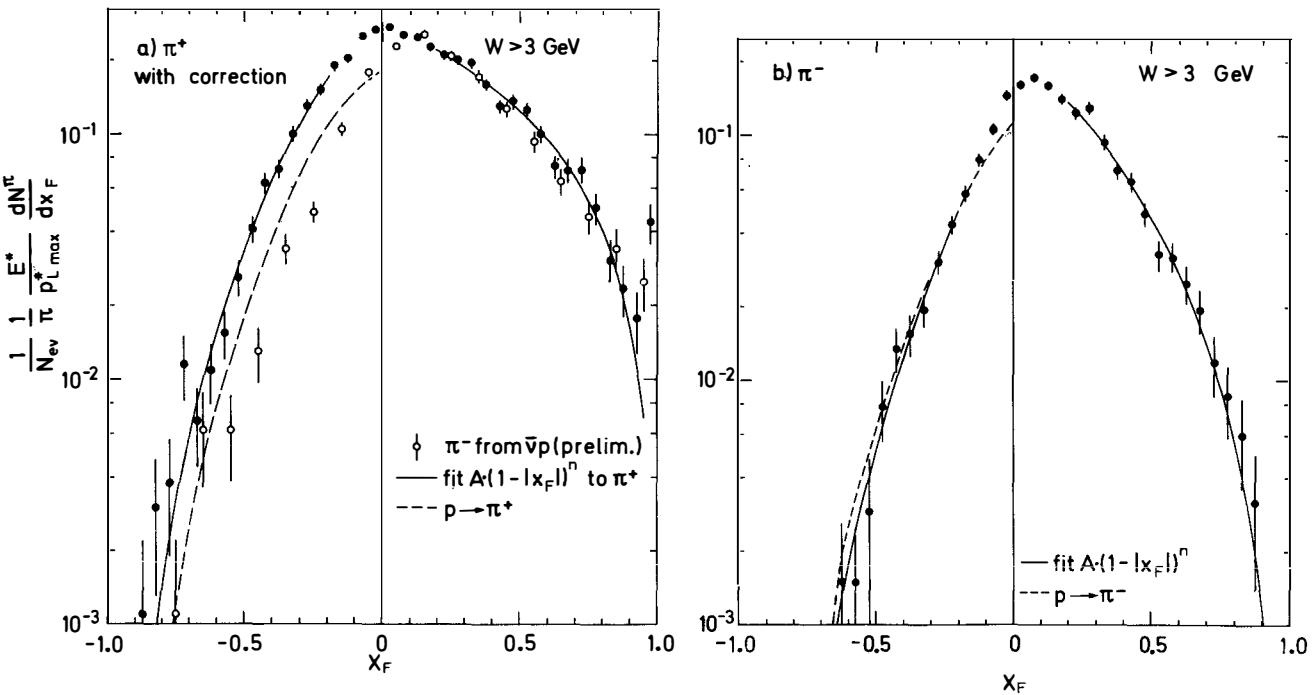

Fig. 2 Normalized invariant x_F distributions of a) π^+ and b) π^- from νp events with W > 3 GeV (full points). The π^+ distribution has been corrected for unidentified protons. The errors are statistical only. The full curves show fits of the form $A\cdot(1-|x_F|)^n$ to the data points for $|x_F| > 0.2$ in each hemisphere (Table 2). The open circles in Fig.2a show the invariant x_F distribution for π^- from $\bar{\nu}p$ events with W > 3 GeV (preliminary). The dashed curves represent one half of the (symmetric) normalized invariant x_F distribution of a) π^+ and b) π^- from a pp experiment[9], averaging the data at 12 and 24 GeV/c.

target fragments at finite W (see Introduction). In the π^+ case, the experimental point in the highest x_F interval (0.95 to 1) has been omitted since it lies outside the general trend by several standard deviations a fact for which we have no simple explanation. Only the statistical errors have been used in the fits.

The results of the fits are summarized in Table 2. For $|x_F| > 0.2$ they are also shown by the full curves in Fig.2. These curves as well as the values of χ^2/NDF in Table 2 show that the data points are well described by the parametrisation $A\cdot(1-|x_F|)^n$. The fitted n values in Table 2 fall in the range predicted by the dimensional counting rule (see Table 1) except for backward-going π^+ where the fitted n exceeds the predicted range of 1 to 3.

The points in Fig.2 and the n values in Table 2 show the following two main features:

- The π^- distribution falls off more steeply than the π^+ distribution in both hemispheres. This is expected from the QPM (and the counting rule, Table 1), since the π^+ can be the leading particle containing for $x_F > 0$ the original u-quark and for $x_F < 0$ a u-quark from the original uu-diquark. The π^- on the other hand contains only quarks created later on in the fragmentation process from the sea.
- The $\pi^\pm$distributions are both steeper in the backward than in the forward hemisphere. This is again expected from the QPM, since a pion from the fragmentation of a single quark gets in the average

Table 2 Results of fitting $A\cdot(1-|x_F|)^n$ to the invariant x_F distributions $F^{\pi^\pm}(x_F)$ for νp events with W > 3 GeV (Fig. 2)

Pion	x_F range	A	n	χ^2/NDF	Predicted n range (Table 1)
π^+	0 to 0.95	0.286±0.004	1.20±0.04	1.11	1 to 2
($u\to\pi^+$)	0.2 to 0.95	0.291±0.010	1.23±0.05	1.31	
π^-	0 to 1.0	0.195±0.004	2.01±0.06	3.09	2 to 5
($u\to\pi^-$)	0.2 to 1.0	0.235±0.014	2.34±0.12	1.20	
π^+	-1.0 to 0	0.308±0.006	3.03±0.07	2.20	1 to 3
($uu\to\pi^+$)	-1.0 to -0.2	0.378±0.025	3.45±0.15	1.05	
π^-	-1.0 to 0	0.163±0.005	5.17±0.19	0.48	2 to 7
($uu\to\pi^-$)	-1.0 to -0.2	0.146±0.024	4.84±0.42	0.51	

a higher momentum fraction than a pion from the fragmentation of a diquark.

The fits to the π^+ distribution were repeated, including a 5% uncertainty in the correction function. The values for A and n remained practically unchanged. Furthermore the analysis was also carried out with the additional requirement that Bjorken-x be > 0.1 in order to remove events where the interaction takes place on a sea quark. Again the values of A and n changed only very little.

Included in Fig.2a are preliminary results (open circles) for the invariant x_F distribution of π^- from the antineutrino part of this experiment. In the forward hemisphere the π^- points from $\bar{\nu}p$ are in good agreement with the π^+ points from νp. This is expected in the QPM from isospin symmetry, which predicts $u \to \pi^+$ and $d \to \pi^-$ to be equal. In the backward hemisphere the two distributions are different as expected since $uu \to \pi^+$ and $ud \to \pi^-$ are not isospin symmetric. The relation $D_{uu}^{\pi^+} \approx 2D_{ud}^{\pi^-}$ suggested by Andersson et al.[7] is only roughly fulfilled. The π^+ distribution from $\bar{\nu}p$ is not yet available since the data analysis of the antineutrino part is not yet completed and the correction for unidentified protons has not yet been performed. $\pi^\pm$ distributions from an $\bar{\nu}p$ experiment have recently been presented by the Argonne, Carnegie-Mellon, Purdue collaboration[8].

Finally we compare the fragmentation of the uu-diquark into $\pi^\pm$ with that of the proton into $\pi^\pm$. Accurate data on $p \to \pi^\pm$ have been obtained by the Bonn-Hamburg-München collaboration[9] in a proton-proton experiment at 12 and 24 GeV/c, corresponding to cms energies of 4.93 and 6.84 GeV respectively. The average W in the present experiment is $\langle W \rangle = 5.57$ GeV for νp events with $W > 3$ GeV. The invariant x_F distributions at 12 and 24 GeV/c (Fig.5 of ref.9 and using $\sigma_{inel} = 29.75$ mb at 12 GeV/c and 30.6 mb at 24 GeV/c for normalisation), which are very close to each other anyway, have therefore been averaged. The averaged pp data are represented by the dashed curves in Fig.2.

From Fig.2a it is seen that the π^+ distributions in νp scattering (backward) and in pp scattering have nearly the same slope. From a naive point of view this is surprising: Comparing $p(=uud) \to \pi^+$ and $uu \to \pi^+$ one would expect, that a π^+, containing one of the original u-quarks, carries in the average a smaller fraction of the total original energy in the first case, where this energy is shared by

three quarks, than in the second case with only two quarks to share the energy. This would lead in the average to a smaller x_F and thus to a steeper x_F distribution for $p \to \pi^+$ than for $uu \to \pi^+$. This expectation is reflected in the predictions of the original counting rule, namely $n = 3$ for $uu \to \pi^+$ and $n = 5$ for $uud \to \pi^\pm$. The dimensional counting rule (3) with the inclusion of point-like emission predicts the leading diagram (Fig.24 of ref.5) to have $n_H = 1$, $n_{PL} = 2$, i.e. $n = 3$ for $p \to \pi^\pm$.

As for the π^- distributions in Fig.2b, there is surprising agreement between $uu \to \pi^-$ and $p \to \pi^-$, in shape as well as in absolute magnitude. Here it is difficult to make a naive qualitative prediction: On the one hand the above energy-sharing argument would lead to smaller x_F values in $p \to \pi^-$ than in $uu \to \pi^-$. On the other hand only in $p \to \pi^-$ can the π^- be the leading particle (containing the original d-quark of the proton), which would yield larger x_F values in $p \to \pi^-$ than in $uu \to \pi^-$. Both effects could cancel each other leading to similar distributions in both cases.

A quantitative prediction for proton fragmentation in proton-hadron collisions is given by the dual model picture[7,10,5]. In this model the interaction takes place on a slow valence quark inside the proton which in the extreme case is stopped by the interaction so that the total proton momentum is carried by the remaining fragmenting diquark. Assuming equal interaction probability for each valence quark one thus obtains in terms of the invariant distributions (2):

$$F_p^{\pi^\pm}(x_F) = \frac{1}{3} F_{uu}^{\pi^\pm}(x_F) + \frac{2}{3} F_{ud}^{\pi^\pm}(x_F). \qquad (4)$$

This prediction is tested in Fig.3 for π^- using the data from νp ($F_{uu}^{\pi^-}$), $\bar{\nu} p$ ($F_{ud}^{\pi^-}$) and pp ($F_p^{\pi^-}$) scattering. It is approximately fulfilled for $|x_F| > 0.2$. If one does not attribute the total proton momentum to the diquark, the right hand side of eq. (4) has to be replaced by a convolution integral; the points in Fig.3 would then move to the right and the agreement can be improved.

4.) x_F distributions

In Fig.4 we show the (unweighted) normalized x_F distributions

$$\frac{1}{N_{ev}} \frac{dN^{\pi^\pm}}{dx_F} = D^{\pi^\pm}(x_F) \qquad (5)$$

for $\pi^\pm$ in νp events with $W > 3$ GeV, after applying the correction

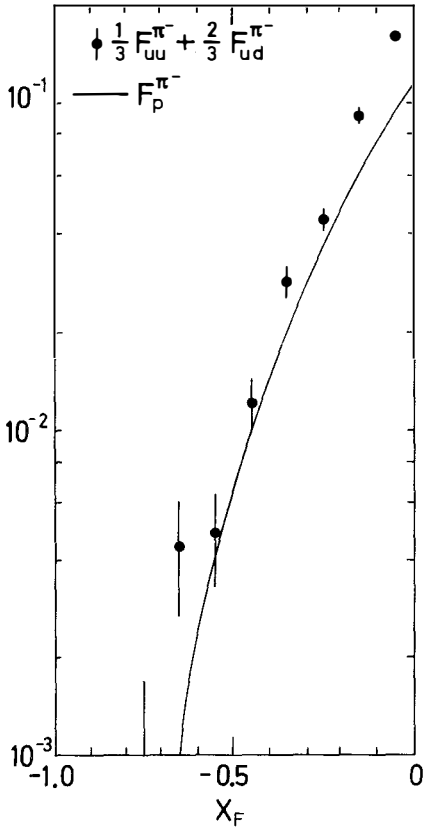

Fig. 3
The points show $\frac{1}{3} F_{uu}^{\pi^-}(x_F) + \frac{2}{3} F_{ud}^{\pi^-}(x_F)$ where $F_{uu}^{\pi^-}$ ($F_{ud}^{\pi^-}$) is the invariant x_F distribution of π^- with $x_F < 0$ from νp ($\bar{\nu} p$) events with $W > 3$ GeV. The curve shows the invariant x_F distribution of π^- in pp scattering[9] (dashed curve in Fig. 2b).

function to the π^+ distribution. It is seen, that in each hemisphere the data points can be approximated rather well by an exponential over the whole x_F range. The straight lines show the results of least squares fits of the form $A \cdot \exp(-B|x_F|)$ to the experimental points. The fitted values for A and B are given in the figure caption.

I would like to thank my colleagues in the WA21 collaboration and W. Ochs for valuable discussions and suggestions. I am grateful to the organizers of the Rencontre de Moriond, in particular to J. Tran Thanh Van and L. Montanet, for the nice and fruitful conference.

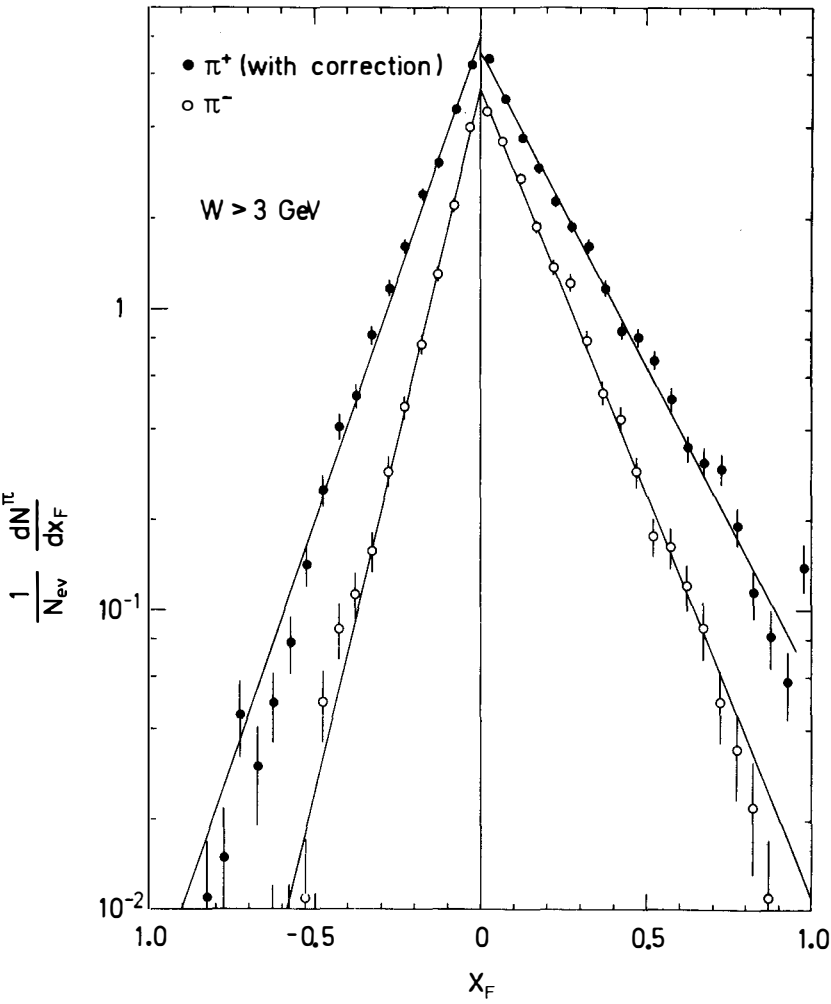

Fig. 4 Normalized x_F distributions of π^+ and π^- from νp events with W > 3 GeV. The π^+ distribution has been corrected for unidentified protons. The errors are statistical only. The straight lines show fits of the form $A \cdot \exp(-B|x_F|)$ to the data points yielding the following values for A and B: π^+: A = 7.14 ± 0.11, B = 4.80 ± 0.06 for $x_F > 0$; A = 8.04 ± 0.14, B = 7.43 ± 0.09 for $x_F < 0$. π^-: A = 5.60 ± 0.11, B = 6.23 ± 0.09 for $x_F > 0$; A = 5.09 ± 0.15, B = 10.64 ± 0.22 for $x_F < 0$.

References

1.) H.G. Heilmann: Bonn Internal Report WA21-int-1 (1978)

2.) J. Blietschau et al.: Phys. Lett. 87B, 281 (1979)

3.) J. Blietschau et al.: Phys. Lett. 86B, 108 (1979); 88B, 381 (1979); P. Allen et al.: Phys. Lett. 96B, 209 (1980); Nucl. Phys. B176, 269 (1980); B176, 333 (1980)

4.) N. Schmitz: Proc. Intern. Symp. on Lepton and Photon Interactions at High Energies, Fermilab, p. 359 (1979)

5.) J.F. Gunion: Proc. XI. Intern. Symp. on Multiparticle Dynamics, Bruges, p. 767 (1980). Here earlier references to the dimensional counting rule can be found.

6.) R. Blankenbecler, S.J. Brodsky: Phys. Rev. D10, 2973 (1974)
J.F. Gunion: Phys. Rev. D10, 242 (1974)
G.R. Farrar: Nucl. Phys. B77, 429 (1974)
D. Sivers, S.J. Brodsky, R. Blankenbecler: Phys.Rep. C23, 1 (1976)

7.) B. Andersson, G. Gustafson, C. Peterson: Phys. Lett. 69B, 221 (1977); 71B, 337 (1977)

8.) M. Derrick et al.: preprint ANL-HEP-PR-80-54

9.) V. Blobel et al.: Nucl. Phys. B69, 454 (1974)

10.) A. Capella, U. Sukhatme, Chung-I Tan, J. Tran Thanh Van: Proc. 14. Rencontre de Moriond, Les Arcs, Vol.1, p. 559 (1979); Phys. Lett. 81B, 68 (1979)
A. Capella, U. Sukhatme, J. Tran Thanh Van: Z. Phys. C3, 329 (1980)
A. El Hassouni, R. Peschanski: Proc. 14. Rencontre de Moriond, Les Arcs, Vol.1, p. 571 (1979)
R. Peschanski: Proc. XI. Intern. Symp. on Multiparticle Dynamics, Bruges, p. 117 (1980)
A. Capella: Talk presented at this meeting.

DIFFRACTION THROUGH PARTIAL IDENTITY *)

W. BLUM

Max-Planck-Institut für Physik und Astrophysik
München, Germany

ABSTRACT

A model of diffraction dissociation is proposed in which the quantum-mechanical interference between the incoming and the outgoing wave determines the cross-section. This interference occurs due to the finite life-time of the excited state.

INTRODUCTION

Diffraction dissociation - the class of exclusive reactions where one of the colliding particles remains the same and the other is excited to a state with similar space-time properties and identical charge-like properties - is similar to elastic scattering because of the large size and the slow energy-variation of the cross-sections. These properties of the cross-section for elastic scattering follow from the optical theorem which states that the imaginary part of the elastic scattering amplitude in the forward direction is equal to a constant times the total cross-section which varies only very slowly with momentum.

ELASTIC SCATTERING

The optical theorem is a consequence of the identity of incoming and outgoing state: Let us consider the scattering of a plane wave on a point target in the stationary state, i.e. with the common time dependence factored out. The intensity at some point (r,θ) behind the target is obtained by first adding and then squaring the amplitudes

$$|\psi|^2 = \left|e^{ikz} + f(\theta)\, e^{ikr}/r\right|^2 \qquad (z = r\cdot\cos\theta) \tag{1}$$

because the corresponding particles are identical (indistinguishable). In the absence of any other amplitudes, the total radial flux through a large sphere around the target (radius r) must vanish and is equal to

$$F = -\int \mathrm{Im}\ \psi \frac{\partial}{\partial r}\psi^* r^2 d\Omega = -4\pi\ \mathrm{Im} f(0) + k\int |f(\theta)|^2 d\Omega = 0 \tag{2}$$

This describes a situation with no inelastic scattering. In this case the total elastic cross section is connected with the imaginary part of the amplitude in the forward direction through the interference term and due to the identity of incoming and outgoing states:

$$\sigma_{el} = \frac{4\pi}{k}\ \mathrm{Im} f(0) \tag{3}$$

DIFFRACTION DISSOCIATION

We propose that for processes of diffraction dissociation [1]

$$A_{in} + B_{in} \to A^*_{out} + B_{out} \qquad (A^*_{out} \approx A_{in},\ B_{out} = B_{in}) \tag{4}$$

$$A^*_{out} \to x + y \ldots \tag{5}$$

there is also a linear relation between the amplitude f' of (4) and

the cross-section σ' for the production of x + y ... . The argument is based on the fact that A^* is unstable and therefore capable of quantum mechanical interference with A, provided A^* is "sufficiently similar to A".

If interference is to occur between A^* and A, account must be taken of the internal structure of A^* and A. If we consider A and A^* as bound states with wave functions $u_1(\vec{x})$, $u_2(\vec{x})$ of a pair of constituents, the interference term will contain the integral over the internal coordinate $\vec{x}$. This is most easily studied in non-relativistic quantum mechanics:

NON-ORTHOGONALITY OF UNSTABLE BOUND STATES

Two states $|1\rangle$ and $|2\rangle$ which are different stationary solutions of the time-independent Schrödinger equation

$$(H-E)|k\rangle = 0 \ , \tag{6}$$

are orthogonal to each other if the Hamiltonian H is hermitian or self-adjoint

$$H = H^+ \tag{7}$$

because

$$\langle 1|H-H^+|2\rangle = (E_2-E_1)\langle 1|2\rangle = 0 \ . \tag{8}$$

For the description of unstable states it is appropriate to consider non-hermitian Hamiltonians

$$H = \bar{H}-iX \ ; \qquad \bar{H} = \bar{H}^+ \ ; \qquad X = X^+ \tag{9}$$

$$H-H^+ = -2iX \tag{10}$$

which allow "eigenstates" with complex energy eigenvalues

$$E_k = \bar{E}_k - \frac{i}{2}\Gamma_k \tag{11}$$

where Γ is given by

$$\Gamma_k = 2\langle k|X|k\rangle \qquad \langle k|k\rangle = 1 \tag{12}$$

In order to derive an expression for the overlap $\langle 1|2\rangle$, the "degree of identity", of two different states where at least one is unstable we consider the generalization of (8) for non-hermitian Hamiltonians

$$\langle 1|H-H^+|2\rangle = -2i\langle 1|X|2\rangle = (E_2-E_1^*)\langle 1|2\rangle \neq 0 \tag{13}$$

from which one derives

$$\langle 1|2\rangle = -\frac{2i}{E_2-E_1^*}\langle 1|X|2\rangle$$
$$\langle 2|1\rangle = \frac{-2i}{E_1-E_2^*}\langle 2|X|1\rangle \tag{14}$$

We will assume the non-hermitian part X of the Hamiltonian and hence also the decay widths Γ to be small in comparison with the hermitian or real parts. Then the states on the r.h.s. can be approximated by their stable standing-wave configurations $|\bar{1}\rangle$ and $|\bar{2}\rangle$ which are real

$$|1\rangle \approx |\bar{1}\rangle = |\bar{1}\rangle^* = \langle\bar{1}|$$
$$|2\rangle \approx |\bar{2}\rangle = |\bar{2}\rangle^* = \langle\bar{2}| \tag{15}$$

In this approximation the overlap of the two states will be purely imaginary

$$\langle 1|2\rangle = -\langle 2|1\rangle = \frac{-2i}{\bar{E}_2-\bar{E}_1}\langle\bar{1}|X|\bar{2}\rangle \tag{16}$$
$$\langle\bar{1}|X|\bar{2}\rangle = \langle\bar{2}|X|\bar{1}\rangle = \text{real}$$

Introducing the total width

$$\Gamma = \Gamma_1+\Gamma_2 = 2[\langle\bar{1}|X|\bar{1}\rangle + \langle\bar{2}|X|\bar{2}\rangle] \tag{17}$$

this can also be written as

$$\langle 1|2\rangle = -i\,\frac{\Gamma/2}{\bar{E}_2-\bar{E}_1}\cdot K = -\langle 2|1\rangle \tag{18}$$

$$K = \frac{\langle\bar{1}|X|\bar{2}\rangle + \langle\bar{2}|X|\bar{1}\rangle}{\langle\bar{1}|X|\bar{1}\rangle + \langle\bar{2}|X|\bar{2}\rangle} = \text{real} \tag{19}$$

$$-1 \leq K \leq +1 \tag{20}$$

We therefore have the important result that the orthogonality of two states where at least one is unstable, gets violated by maximally $\Gamma/2\Delta E$ which is independent of the internal structure and may be referred to as the "external similarity" of the two states. The factor K depends on the particular structure of the states and may be called their "internal similarity".

The situation in which $|1\rangle$ and $|2\rangle$ have different angular momenta will also lead to a nonzero and imaginary overlap, because it can be considered a special case of (16) [2]. The physical interpretation of the possibility of interference between two states with different

angular momenta is as follows: Due to the uncertainty principle which holds between the angular momentum and the angle of rotation, a decaying state cannot have a sharp angular momentum, rather it consists of several different angular momenta, and the interference occurs in the one which is common to both states.

The relativistic generalization of the degree of identity (18), (20) for the case of $|1\rangle$ stable and $|2\rangle$ unstable is, to lowest order of Γ/m,

$$\langle 1|2\rangle = \frac{-im_2\Gamma_2}{m_2^2-m_1^2} \cdot K = -\langle 2|1\rangle \qquad -1 \leq K \leq +1 \quad \text{(real)} . \tag{21}$$

AN OPTICAL THEOREM FOR DIFFRACTION DISSOCIATION

We consider a stationary situation in the C.M. system where there is an incoming plane wave representing the relative motion of particles A_{in} and B_{in} and an outgoing spherical wave representing particles A^*_{out} and B_{out} emerging from a point of interaction. Let B_{out} be the same particle as B_{in}, and let A^*_{out} be an unstable state with mean lifetime of $\tau = 1/\Gamma$ and a squared mass which is higher than the squared mass of A by the amount Δm^2. Then the momentum k' of the spherical wave is smaller than the momentum k of the plane wave and the difference is, to leading order of $\Delta m^2/s$, given by $\Delta k^2 = -\Delta m^2$. The finite lifetime of A^*_{out} causes a damping of the spherical wave which we describe by an imaginary part of the outgoing momentum:

$$k' = k + \Delta k + i\kappa \tag{22}$$

where $1/\kappa$ represents the distance at which the amplitude of the spherical wave has decreased to $e^{-1/2}$.

$$\kappa = \frac{m\Gamma}{2k} \qquad \Delta k = \frac{-\Delta m^2}{2k} \qquad (\Delta k < 0) \tag{23}$$

m is the mass and Γ the width of A^*.

The probability per unit time to find either AB or A^*B at r, θ is

$$|\Psi|^2 = \left| e^{ikz}|A\rangle + f'(\theta)|A^*\rangle\, e^{ik'r}/r \right|^2 \tag{24}$$

$\langle A|A\rangle = 1$ and $\langle A^*|A^*\rangle = 1$; if both $|A\rangle$ and $|A^*\rangle$ were stable states we would have $\langle A^*|A\rangle = 0$, and the interference term would vanish.

In view of the finite overlap which can be attributed in non-

relativistic quantum-mechanics to two states one of which has a non-zero width, we will now study the case of partial identity, i.e. a nonzero value of $q \equiv \langle A|A^*\rangle$. The probability $|\Psi|^2$ then contains a term for which it is not specified whether A^*B or AB is meant to be found at r, θ. As long as A^* has not dissociated and if the charge-like properties of A and A^* are the same, a distinction between AB and A^*B would imply a precise determination of the mass of A^*; this precision and, therefore, the distinguishability between AB and A^*B, are limited through the uncertainty principle by the finite lifetime of A^*.

The probability per unit time to find "the not yet distinguished state" will decrease with increasing r due to the damping of one of the two amplitudes. At every point in space we now identify the probability per unit time to find the not yet distinguished state which is lost with the production probability per unit time of the decay products (x,y..) in the final state. This probability oscillates between positive and negative values as r and θ are varied; this is a consequence of our simplifying picture (point-like scattering centre, sharp momentum). In this picture a local probability has no meaning, only the space integral has a meaning, it is taken to mean the total production rate per unit time of the decay products of A^*.

In order to balance the flux of particles (AB) and (A^*B) that emerges from the target we calculate

$$\vec{F} = -\mathrm{Im}\ (\Psi\vec{\nabla}\Psi^*) \tag{25}$$

which is directed radially away from the scattering centre. To leading order in $\Delta k/k$ and κ/k, the flux through a spherical surface with radius r has the magnitude

$$F(r) = -\mathrm{Im}\int \Psi\frac{\partial}{\partial r}\Psi^* r^2 d\Omega = -4\pi \mathrm{Im}\tilde{f}'\cdot q\cdot e^{i(\Delta k+i\kappa)r}+k\int |f'(\theta)|^2 d\Omega e^{-2\kappa r} \tag{26}$$

$\tilde{f}'$ represents the amplitude $f'(\theta)$ near $\theta = 0$:

$$\int_{-1}^{+1} f'(\theta)e^{ikr(1-\cos\theta)}d\cos\theta = -\tilde{f}'/ikr \tag{27}$$

We identify the flux of the not yet identified state which is lost between r = 0 and r = ∞ due to the instability of A^* with the flux of the inelastic decay channels:

$$k\sigma = F(0) - F(\infty) \tag{28}$$

$$k\sigma' = -4\pi \mathrm{Im}(\tilde{f}'\cdot q) + k\int |f'(\theta)|^2 d\Omega \qquad (29)$$

Using (21)

$$\sigma' = +\frac{4\pi}{k}\,\mathrm{Re}\,\tilde{f}'\cdot\frac{m\Gamma}{\Delta m^2}\cdot K + \int |f'(\theta)|^2 d\Omega$$
$$-1 \leqslant K \leqslant 1\ , \quad \text{real} \qquad (30)$$

We propose that equations (30) relate the cross-section σ' for any diffractive process $AB \to A^*B$, $A^* \to xy..$ to its amplitude $f'(\theta)$ where $\tilde{f}'$ represents $f'(\theta)$ near $\theta = 0$. K is a constant which describes the degree of internal similarity of A and A^*, it is expected to be real in lowest order of $m\Gamma/\Delta m^2$. For the linear term to be positive, $\mathrm{Re}(\tilde{f}'\cdot K) > 0$ has to hold. If A and A^* have different charge-like properties, $K = 0$.

COMPARISON WITH EXPERIMENTAL DATA

The size of the linear term depends on K which we do not know. But we may put $|K| = 1$ and calculate the ratio T_1, of the linear over the quadratic term by assuming a θ-dependence of $|f'(\theta)| \approx |f'(0)| \cdot e^{Bk^2(\cos\theta - 1)}$ and by taking $\mathrm{Re}\,\tilde{f}' \approx |\tilde{f}'| \approx |f(0)|$:

$$T_1 \approx \frac{16\pi B}{\sigma'} \cdot \left(\frac{m\Gamma}{\Delta m^2}\right)^2 \qquad (31)$$

Alternatively we may ask at which value $|K_1|$ the linear term is as large as the quadratic term:

$$\frac{\sigma'}{2} \approx \int |f'(\theta)|^2 d\Omega \approx |f'(0)|^2 \cdot \frac{\pi}{Bk^2} \approx \frac{4\pi}{k}\,|f'(0)| \cdot \frac{m\Gamma}{\Delta m^2} \cdot |K_1|$$

$$|K_1| \approx \sqrt{\frac{\sigma'}{2\pi B}} \cdot \frac{\Delta m^2}{4m\Gamma} \qquad (32)$$

Some examples of T_1 and $|K_1|$ are given in table 1, assuming a range of $B = 5 \div 10\ \mathrm{GeV}^{-2}$.

One observes that the linear term is larger than the quadratic term if $|K_1|$ is larger than the numbers in column 7 which are generally seen to be small compared to unity. In general, if σ' continues to fall fast enough with energy, the linear term will always dominate at high energy.

Table 1

Reaction	Lab mom. (GeV/c)	σ' μb	$\frac{m\Gamma}{\Delta m^2}$	Ref.	T_1 (K=1)	$\lvert K_1 \rvert$ (T=1)
$\pi^- p \to A_1^- p$	63	55	0.24	[3]	260-520	0.05-0.07
$\pi^- p \to A_2^- p$	63	22	0.08		29-58	0.09-0.13
$K^- p \to Qp$	63	70	0.08-0.14	[4]	9-56	0.09-0.23
$pp \to N^*_{1680} p$	1000	170	0.11	[5]	7-14	0.19-0.26

We do not expect $|K|$ to be particularly small if the excited state A^* is very similar to the incoming state A. The case of photoproduction of vector mesons is different from the purely hadronic case because it would require a K which contains a factor of the order of $\sqrt{1/137}$. For the moment we want to leave out photoproduction and study hadronic diffraction dissociation alone for the case that $|K|$ is sufficiently large so that the linear term in (30) dominates.

If this is so, small amplitudes would cause large cross-sections through the enhancement mechanism of interference with the beam. We suggest that large amplitudes are not needed to explain the large cross-sections of diffractive processes.

Dominance of the linear term would also imply an energy variation of the cross-section that is only the square root of the function which describes the energy variation of the quadratic term. The measured energy dependences of some diffractive hadronic processes, parametrized as a power of the beam momentum,

$$\sigma' \sim p_{lab}^{-n} , \tag{33}$$

are given in tables 2 and 3.

Despite the fact that the experimental situation is unresolved for $(N\pi)$ at high energies, most of the exponents are not very far from 0.50. This is interesting because in the Regge theory there is one amplitude with the right quantum numbers which has just this energy behaviour: ω/f-exchange. The behaviour expected from Pomeron-exchange, n = 0, has been reported by refs. [6,7] for the reactions $pp \to N^*_{1680} p$, $np \to (p\pi)p$ in experimental disagreement with ref. [5]. None of the other reactions shows a flattening-off at high energy.

Table 2 Energy dependence of diffraction as compiled by Leith 1975 [1]. Lab momenta from 5 to 20 GeV/c.

Reaction	n
$K^o p \to Q^o p$	0.59 ± 0.16
$K^+ p \to Q^+ p$	0.60 ± 0.05
$K^- p \to Q^- p$	0.30 ± 0.10
$\pi^- p \to A_1^- p$	0.41 ± 0.11
$\pi^- p \to A_3^- p$	0.57 ± 0.2
$Np \to (N\pi)p$	0.5 ± 0.1
$Np \to (N\pi\pi)p$	0.4 ± 0.06

Table 3 Energy dependence of diffraction; some more recent results involving higher energies.

Reaction	Lab momentum range (GeV/c)	Source	n
$\pi^- p \to A_1^- p$	5-94	ACCMOR 1980 [3]	0.42 ± 0.04
$\pi^- p \to A_2^- p$	5-94	ACCMOR 1980 [3]	0.40 ± 0.03
$K^- p \to Q^- p$	14-63	ACCMOR 1981 [4]	0.29 ± 0.09
$Np \to (N\pi)_o p$	≈10-1000	CHOV 1976 [5]	0.30 ± 0.07
$pp \to N^*_{1680} p$	≈10-1000	CHOV 1976 [5]	0.34 ± 0.06
$pp \to N^*_{1680} p$	≈30-1000	Webb 1975 [6]	≈ 0
$np \to (p\pi^-)p$	50-300	Biel 1978 [7]	≈ 0

Another characteristic feature of diffraction dissociation is the presence of a large background under the resonances with low invariant mass. This background, not necessarily resonant, can be imagined as a hadronic state with a life-time in the range corresponding to $\Gamma \approx$ 200-600 MeV (the time in which the size of a nuclear object can be traversed). At low effective mass, the factor $m\Gamma/\Delta m^2$ may typically be as large as 0.2-0.5 (near the maximum of the enhancements). We

propose that these low-mass enhancements are caused by the interference of the production amplitude of the continuum state with the incoming beam due to their partial identity. The enhancement factor T is larger for the background than for the resonances because they have a smaller Γ.

REFERENCES AND FOOTNOTES

*) Work done together with H.-P. Dürr, MPI Munich

[1] There are several extensive reviews on diffraction dissociation. See, e.g., D.W.G.S Leith, SLAC Summer Institute, SLAC Report 179, Volume I (1975) or
U. Amaldi, M. Jacob and G. Matthiae, Ann. Rev. Nucl. Science, Vol. 26 (1976).

[2] For a more detailed discussion, see a forthcoming paper by W. Blum and H.P. Dürr.

[3] C. Daum et al., The ACCMOR collaboration, CERN-EP/80-219 (1980), submitted to Nucl. Phys. B.

[4] C. Daum et al., The ACCMOR collaboration CERN-EP/81-04 (1981), submitted to Nucl. Phys. B.

[5] H. DeKerret et al., CHOV collaboration, Phys. Lett. 63B, 477 (1976).

[6] R. Webb et al., Aachen-UCLA-Riverside-CERN collaboration, Phys. Lett. 55B, 331 (1975).

[7] J. Biel et al., Rochester-Northwestern-FNAL-SLAC collaboration, Phys. Rev. D18, 3079 (1978).

ELASTIC SCATTERING AND DIFFRACTION DISSOCIATION of $\pi^{\pm}$, $K^{\pm}$ and $p^{\pm}$ at 100 and 200 GeV/c

R.L. Cool, K. Goulianos, S.L. Segler, G. Snow,
H. Sticker and S.N. White
The Rockefeller University, New York, NY 10021

Reported by: K. Goulianos

ABSTRACT

We report measurements of the differential cross sections for elastic scattering and diffraction dissociation of $\pi^{\pm}$, $K^{\pm}$ and $p^{\pm}$ on protons at 100 and 200 GeV/c in the range $0.025 < |t| < 0.1$ $(GeV/c)^2$. Both the elastic and the inelastic data display a simple exponential t-dependence. The diffractive cross sections vary mainly as $1/M_X^2$ and scale to the corresponding total cross sections in agreement with Regge theory predictions based on triple pomeron dominance in the amplitude.

We report results on elastic scattering and diffraction dissociation of $\pi^{\pm}$, $K^{\pm}$ and $p^{\pm}$ on protons

$$h + p \to X + p \quad (h = \pi^{\pm}, K^{\pm}, p^{\pm}) \tag{1}$$

at beam momenta of 100 and 200 GeV/c in the range $0.025 < |t| < 0.1$ $(GeV/c)^2$ and $1-x \cong (M_X^2 - M_h^2)/s < 0.1$. These results were obtained in experiment E-396 which was performed in the M6W beam line of the Meson Laboratory at Fermilab. Preliminary results from this experiment were reported at the XIIIth Rencontre de Moriond[1].

The apparatus is shown in Figure 1:

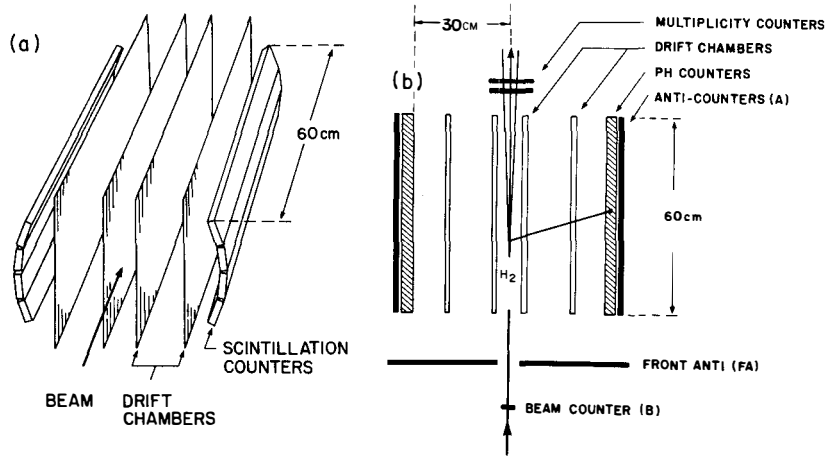

FIG. 1 - APPARATUS

(a) View in Perspective (b) Plan View

Recoil protons from beam interactions in a 1 atm gas hydrogen target were detected on each side of the beam by two drift chambers, measuring the polar angle θ, and by four 2.5cm thick scintillation counters, determining the kinetic energy T_p. Protons were identified by measurement of the time of flight of the recoil particle in combination with T_p.

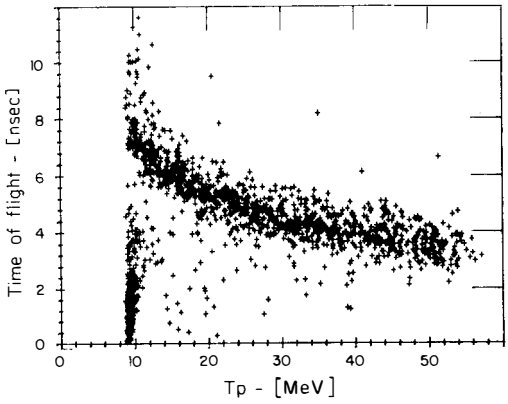

FIG. 2 -

Time of flight versus energy of recoil particles. The horizontal band represents protons. The events in the lower left corner are due to electrons.

The energy and angle of each proton were used to calculate t and M_X^2 or x,

$$|t| = 2M_p T_p \tag{2}$$

$$1 - x = \frac{M_X^2 - M_h^2}{s} = \frac{\sqrt{|t|}}{M_p} \left(\cos\theta - \frac{\sqrt{|t|}}{2M_p}\right) \tag{3}$$

The charged multiplicity of the final state was measured by two 6mm thick scintillation counters located 40cm downstream of the center of the recoil detector. The Landau fluctuations were minimized by always accepting the smaller of the two pulse heights in the calculation of the multiplicities. During part of the running, an array of lead glass blocks was set up 10 meters downstream to measure neutral energy and multiplicity.

Elastic events were separated from inelastic by requiring charged multiplicity of 1 and no neutral energy deposited in the lead glass for runs where such a requirement was applicable.

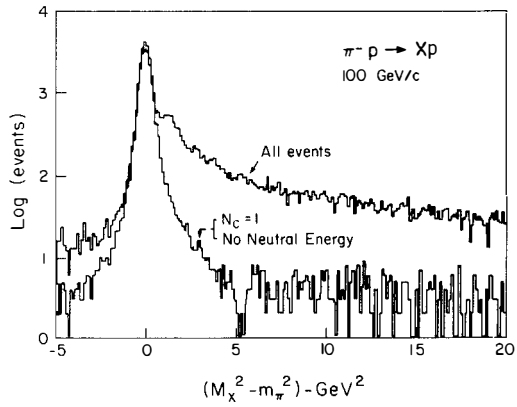

FIG. 3 -

Missing mass distributions for $\pi^- p \rightarrow Xp$ at 100 GeV/c and selection of elastic events.

Final selection was made by a cut in M_x^2 at $\pm 4.5\sigma$ (M_x^2) around $M_x^2 = M_h^2$, where $\sigma(M_x^2) = 0.22\ (p_{beam}/100)$ GeV^2. The events obtained in this manner were corrected for the remaining inelastic contamination (0.3 to 4%), for the geometrical acceptance of the apparatus ($\lesssim$ 4%), for multiple scattering of recoil protons from the DWC field shaping wires ($\lesssim$ 2%) and for nuclear interaction of the protons in the scintillator ($\lesssim$ 2%).

The data were fitted to the function

$$\frac{d\sigma}{dt} = A\, e^{bt} \qquad (4)$$

The normalization was obtained by extrapolating our data from our t region to t=0 and scaling A to the optical point, $\sigma_T^2/16\pi$, using the total cross sections of Carroll et al[2]. Since only the elastic slopes for $\pi^- p$ are determined precisely in this experiment, we used for the extrapolation to t=0 the fitted slopes of Ref. 3 for pp and the measured slopes of Ref. 4 for $\pi^+ p$, $K^{\pm} p$ and $\bar{p}p$.

The normalized differential cross sections and the results of the fits are given in the table which follows.

TABLE I

Elastic hadron-proton cross sections and fits to the form $d\sigma/dt = Ae^{bt}$

BEAM PARTICLE	BEAM ENERGY [GeV]	$d\sigma/dt$ - [mb · (GeV/c)$^{-2}$] t-value							A mb·(GeV/c)$^{-2}$	b (GeV/c)$^{-2}$	χ^2/d.o.f. (5 d.o.f.)
		0.03-0.04	0.04-0.05	0.05-0.06	0.06-0.07	0.07-0.08	0.08-0.09	0.09-0.10			
π^-	100	21.74 ±0.31	19.38 ±0.30	17.91 ±0.29	16.45 ±0.28	15.44 ±0.27	13.89 ±0.25	12.38 ±0.24	29.43 ±0.60	8.92 ± 0.31	0.95
	200	21.57 ±0.37	19.55 ±0.35	18.21 ±0.35	16.27 ±0.33	14.81 ±0.31	13.29 ±0.30	12.22 ±0.28	30.24 ±0.74	9.55 ± 0.38	0.25
K^-	100	14.2 ±1.3	15.3 ±1.3	13.8 ±1.3	13.9 ±1.3	11.6 ±1.1	10.7 ±1.1	08.2 ±1.0	21.4 ±2.6	8.3 ± 1.9	1.2
	200	19.2 ±3.9	11.7 ±3.2	11.4 ±3.1	13.6 ±3.4	08.5 ±2.9	08.3 ±2.8	12.0 ±3.2	22.0 ±6.7	9.0 ± 4.8	0.83
$\bar{p}$	100	57.0 ±3.0	51.1 ±2.8	39.6 ±2.5	42.6 ±2.6	34.4 ±2.3	27.6 ±2.1	26.1 ±2.1	90.6 ±7.0	13.2 ± 1.2	1.3
	200	44.4 ±6.5	41.0 ±6.3	43.6 ±6.4	23.9 ±5.0	19.1 ±4.5	23.3 ±4.8	16.8 ±4.1	87.7 ±19.1	17.0 ± 3.6	1.1
π^+	100	19.97 ±0.84	17.87 ±0.80	16.06 ±0.74	14.12 ±0.72	14.33 ±0.72	11.91 ±0.65	10.95 ±0.63	27.8 ±1.7	9.75 ± 0.93	0.56
	200	22.4 ±1.5	21.5 ±1.5	23.3 ±1.5	19.7 ±1.4	16.4 ±1.3	17.4 ±1.3	16.3 ±1.3	29.0 ±2.6	6.1 ± 1.4	1.2
K^+	100	16.5 ±2.9	11.9 ±2.5	14.0 ±2.7	10.3 ±2.3	08.8 ±2.2	12.1 ±2.5	11.1 ±2.4	18.2 ±4.6	6.2 ± 3.8	0.77
p	100	51.6 ±1.4	44.7 ±1.3	41.3 ±1.2	36.6 ±1.2	32.7 ±1.1	28.1 ±1.0	26.8 ±1.0	75.6 ±2.9	11.20 ± 0.60	0.52
	200	53.16 ±0.93	45.12 ±0.87	40.98 ±0.83	36.30 ±0.78	33.41 ±0.75	27.65 ±0.70	27.22 ±0.67	77.6 ±2.0	11.50 ± 0.40	2.6

It is evident that the simple exponential function (4) provides a satisfactory fit to our data. The slopes obtained are in general agreement with other measurements, as is shown in Figure 4 which presents compilations of slopes from different experiments[4,5,6,7,8,9] for $pp \to pp$ and $\pi^-p \to \pi^-p$ at 100 GeV/c and 200 GeV/c.

For $\pi^-p \to \pi^-p$, the slopes below our t-region are significantly higher than what one might expect from a gentle extrapolation of the slopes at higher t. If the slope increase at $|t| \lesssim 0.04$ (GeV/c)^2 were due to a break in the differential cross section, a unitarity bound derived by Roy[10] would be violated. On the other hand, a reasonably continuous function $b(t)$ would satisfy the Roy bound. As shown in Figure 4, our data, combined with other data, are compatible with a continuous function for $b(t)$.

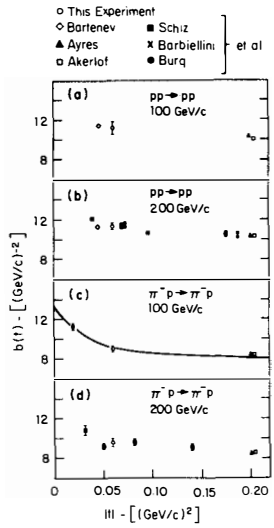

FIG. 4 -
Elastic slope parameters b(t) as a function of t for pp and π^-p at 100 and 200 GeV/c. The line in (c) represents $b(t)=d\ell nF(t)/dt$ where the function $F(t)=N_o(0.065\ e^{39.6t} + 0.649\ e^{5.3t} + 0.286\ e^{2.4t})$ is a good fit to our data along with the data of Burq et al., and Ayres et al.

The normalized hadron dissociation cross sections for $M_X^2 > 4$ GeV^2 were fitted to the form

$$\frac{d^2\sigma}{dtdx} = \left[\frac{A}{1-x} + B\ (1-x)\right]\ e^{b(t+0.05)} \qquad (5)$$

The values for A and B are given in Table II. Selected t distributions are displayed in Figure 5.

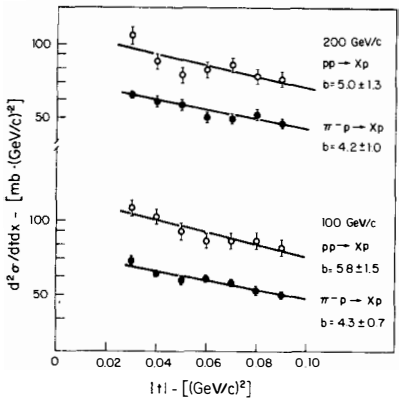

FIG. 5 -
Differential cross sections versus t for pp → Xp and $\pi^-p \to Xp$ at 100 and 200 GeV/c in the region 4 GeV^2/s < 1-x < 0.1 .

TABLE II

Cross Sections for hp → Xp and Fits to the Form

$$\frac{d^2\sigma}{dtdx} = \left[\frac{A}{1-x} + B(1-x)\right] e^{b(t+0.05)}$$

Hadron	p	A	B	χ^2/d.o.f.	$R = A/\sigma_T$
h	GeV/c	mb·(GeV/c)$^{-2}$	mb·(GeV/c)$^{-2}$	(5 d.o.f.)	(GeV/c)$^{-2}$
π^-	100	2.72±0.07	98± 21	1.7	0.113±0.003
K^-	100	2.01±0.33	167±107	1.0	0.098±0.016
$\bar{p}$	100	4.55±0.56	-33±170	2.6	0.108±0.013
π^+	100	2.52±0.18	162± 54	1.6	0.108±0.008
K^+	100	1.80±0.52	-200± 80	0.5	0.095±0.027
p	100	3.80±0.22	306± 70	0.4	0.099±0.006
π^-	200	2.44±0.09	127± 29	0.6	0.100±0.004
π^+	200	2.49±0.30	101± 99	0.8	0.104±0.013
p	200	3.68±0.19	203± 59	0.8	0.094±0.005

In the Regge model, the A term arises from the triple pomeron coupling[11] whereas the B term is due to lower lying trajectories and non-diffractive contributions. The data show that the triple pomeron term dominates hadron dissociation.

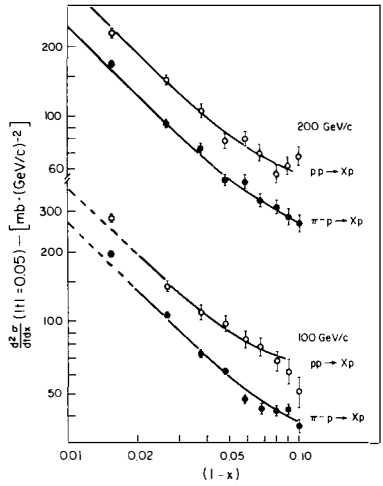

FIG. 6 -

Differential cross sections versus 1-x for pp → Xp and π^-p → Xp at 100 and 200 GeV/c.

The A-term for $pp \to Xp$ is in excellent agreement with that of Ref. 12 but lies about 10% below that of Ref. 4. The difference is not significant as it can be attributed to the different elastic slopes used to normalize the data. The B term, on the other hand, varies significantly from experiment to experiment. This is not surprising since the various experiments have different efficiencies for processes that contribute to B such as target dissociation. Experiments like those performed in the internal target of Fermilab[12] have no bias against any slow recoils. This experiment suppresses events with more than one large angle track which are likely contributors to B. The calculation of the suppression factor is model-dependent and hence the value of the B term cannot be determined accurately. In contrast, the A-term is bias free. Our experiment confirms the $1/M_x^2$ behavior for proton dissociation and establishes it for pion, kaon and antiproton dissociation as well.

In addition to predicitng the correct M_x^2 behavior, the Regge framework provides a way of comparing the absolute values of the diffractive cross sections. Assuming factorization, the triple pomeron term (A-term of Eq. 5) can be written as

$$\frac{d^2\sigma_A^{hp}}{dtdx} = \frac{\beta_{hP}(o)\ \ \beta^2{}_{pP}(t)\ \ G_{PPP}(t)}{16\pi\ \ (1-x)} \tag{6}$$

and the total cross section at high energies as

$$\sigma_T^{hp} = \beta_{hP}\ (o)\ \ \beta_{pP}\ (o) \tag{7}$$

The ratio of diffractive to total cross section

$$\frac{d^2\sigma_A^{hp}/dtdx}{\sigma_T^{hp}} = \frac{\beta^2{}_{pP}(t)}{\beta_{pP}(o)}\ \ \frac{G_{PPP}(t)}{16\pi(1-x)} \tag{8}$$

should be independent of incident particle type.

Our results for $R = A/\sigma_T$, listed in Table II and plotted in Figure 7, show that factorization holds at each beam energy within the experimental uncertainty of a few percent. This remarkable accuracy of the factorization rule which arises naturally in the Regge picture will have to be explained by QCD.

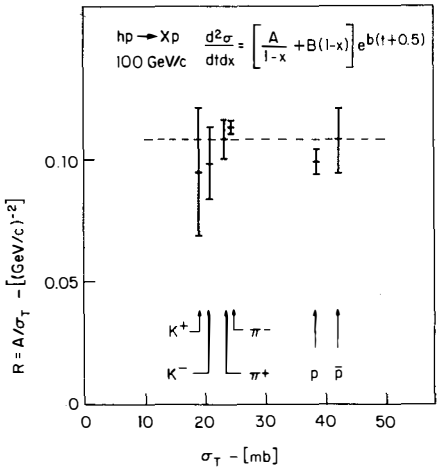

FIG. 7 -
Diffractive to total cross section ratios versus σ_T for $K^{\pm}$, $\pi^{\pm}$ and $p^{\pm}$ at 100 GeV/c.

The triple pomeron coupling constant can be calculated from Eq. (8) by setting $(d^2\sigma^{hp}/dtdx)_A/\sigma_T = R/(1-x)$ and $\beta_{pp}(t) = [16\pi\, d\sigma_{e\ell}^{pp}(t)/dt]^{\frac{1}{2}}$. Using the fitted values of Ref. 3 for the pp elastic scattering cross sections and the weighted average of the values of R in Table II at each of the two beam energies, we obtain $G_{PPP}(t=-0.05) = 0.464 \pm 0.011$ mb$^{\frac{1}{2}}$ at 100 GeV/c and 0.414 ± 0.013 mb$^{\frac{1}{2}}$ at 200 GeV/c. If the energy dependence is parametrized as[1] $A(1+B/p)$, we find $B = 27.3 \pm 11.4$ GeV/c and $G_{PPP}(s \to \infty, t = -0.05) = 0.364 \pm 0.025$ mb$^{\frac{1}{2}}$. The t-dependence of $G_{PPP}(t)$ is given by $\exp(b_D^{hp}\, t - \frac{1}{2} b_{e\ell}^{pp}\, t)$ where b_D^{hp} is the slope parameter for $hp \to Xp$. The pp elastic scattering slope in the energy range of 100 to 200 GeV and at $|t| \cong 0.05$ (GeV/c)^2 is[3] $\cong 11$ (GeV/c)$^{-2}$ or $b_{e\ell}^{pp}/2 \cong 5.5$ (GeV/c)$^{-2}$. Figure 5 shows that the diffraction dissociation slopes are compatible with this value. Thus $G_{PPP}(t)$ is independent of t and our final results is $G_{PPP}(t) = 0.364 \pm 0.025$ mb$^{\frac{1}{2}}$.

REFERENCES

1) K. Goulianos, *Diffractive Hadron Dissociation*, Proceedings XIIIth Rencontre de Moriond, Vol. I, p. 457 (1978).

2) A.S. Carroll et al., Phys. Lett. 61B, 303 (1976).

3) K. Goulianos, Phys. Rev. D14, 1445 (1976).

4) D.S. Ayres et al., Phys. Rev. Lett. 37, 1724 (1976); ibid., Phys. Rev. D15, 3105 (1977); R.L. Anderson et al., Phys. Rev. Lett. 38, 880 (1977).

5) V. Bartenev et al., Phys. Rev. Lett. 31, 1088 (1973).

6) C.W. Akerlof et al., Phys. Rev. D14, 2864 (1976).

7) A. Schiz et al., Fermilab report 79/81, submitted to Phys. Rev.; L.A. Fajardo et al., Fermilab report 80/27, submitted to Phys. Rev.

8) G. Barbiellini et al., Phys. Lett. 39B, 663 (1972).

9) J.P. Burq et al., Phys. Lett. 77B, 438 (1978).

10) S.M. Roy, Phys. Rev. Lett. 43, 19 (1979).

11) A.H. Mueller, Phys. Rev. D2, 2963 (1970).

12) Y. Akimov et al., Phys. Rev. Lett. 39, 1432 (1977).

JET PRODUCTION IN DIFFRACTIVE DISSOCIATION OF MESONS AND PHOTONS

J. Randa
Department of Physics
University of Colorado
Boulder, CO. 80309

I consider the diffractive dissociation of photons and mesons into high-mass subsystems clearly separated in momentum space from fragments of the target proton. Such high-mass $q\bar{q}$ states should exhibit jet behavior. The mass and ("decay") angle dependence of the cross section for production of these jets is predicted. The relative multiplicity of strange and charmed particles is also predicted and compared to that in e^+e^- jet production.

Diffractive dissociation is not a new field, and considerable work has been done on it already. The most developed of the approaches[1] so far have started from the soft (low Q^2) side of the problem, whereas the work on which I am reporting[2-4] approaches from large Q^2, using perturbative QCD. The purpose is twofold: to see what, if anything, QCD and diffractive dissociation say about each other; and to attempt to effect some overlap between the hard and soft regimes, to see whether there is some underlying QCD basis for the success of the soft models.

At the outset we restrict the kind of final state to be considered. In order to distinguish between beam and target fragments we require a clear separation in longitudinal momentum. (This requirement can be replaced by any other which has the property that $p_i \cdot p_j$ is large if i and j are not in the same subsystem.) If such a requirement is not made one cannot tell that a large M^2 was not obtained by including target debris in with the beam fragments. We will concentrate on the case where the target proton recoils elastically, so that in the overall center of mass (CM) the process looks like Fig. 1a), a fast proton alone in one hemisphere and the beam fragments in the other. (Beam fragments can be allowed to spill over into the proton hemisphere, provided they are slow.) Unlike the requirement of a "separable" final state, the limitation to elastic recoil protons is a matter of convenience, not necessity. The beam fragment subsystem X should exhibit two-jet behavior when analyzed in its CM. The angle between the jet axis and the beam direction in the CM of X will be called θ^*, as in Fig. 1b). Note that θ^* is internal to the X subsystem; it is not related to M^2 or t.

The occurence of a large longitudinal momentum gap signals a color singlet exchange, as indicated pictorially in Fig. 2. If net color is exchanged, as in Fig. 2a), then the hadronization will result in a continuous smear of hadrons with no large longitudinal momentum gaps, since the quark and gluon pairs emerging from the sea do so with limited relative momentum $\Delta p \lesssim 1$GeV. For color singlet exchange, Fig. 2b), the hadronization occurs within each final color singlet subsystem, but not between the two since color singlets do not feel the confining force. Consequently large gaps do occur for color singlet exchange.

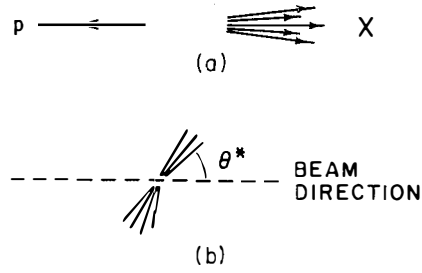

Fig. 1 a) Final configuration in overall center of mass. b) Definition of the angle θ^* in center of mass of X.

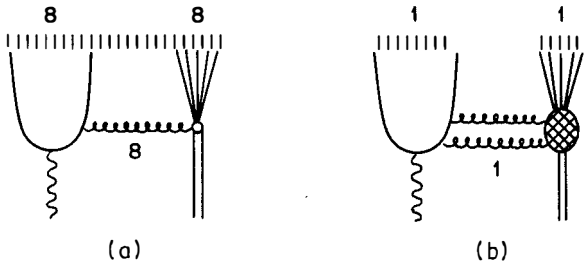

Fig. 2. Final state configuration arising from a) color octet exchange, and b) color singlet exchange.

We must then address the question of whether perturbation theory (PT) can be used. We work in the limit M^2, $s/M^2 \to \infty$ and cos θ^* fixed ($\neq 1$). If $|t|$ is large, PT is on quite a firm footing.[2] Unfortunately, the cross sections will be miniscule at large $|t|$. For small $|t|$, perturbation theory need not be valid, but there are a few hopeful signs. The strongest are that one intermediate particle is highly virtual and that we encounter no divergent integrals, which normally signal the infrared breakdown of PT. In addition, there is a heuristic similarlity to deep inelastic scattering,[2] and there are indications in e^+e^- [5] that large rapidity gaps are amenable to perturbative treatment provided M^2 is large and cos $\theta \neq 1$. Consequently we can adopt the attitude that in this process, PT is justified at large $|t|$ and may well be valid at small $|t|$ as well. If experiment shows that it is, then we shall have learned something nontrivial about diffractive dissociation and about QCD.

The calculation for photoproduction proceeds as follows. The lowest order color singlet exchange which contributes to the leading order in s is two-gluon exchange, as shown in Fig. 3. The quark propagator contains a factor of $(q-\ell)^2 \simeq 2/[M^2(1-\cos\theta^*)]$ which leads to three important features. For large M^2 the quark is highly virtual provided $\cos\theta^* \neq 1$; the cross section peaks near $\theta^* = 0$; and it decreases as M^2 increases. These features are rather general and will be present for almost any exchange.[6] The right hand side of the graph in Fig. 3 is the elastic two-gluon form factor of the proton, which is unknown

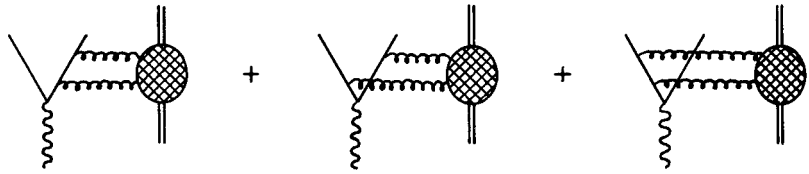

Fig. 3 Leading color singlet exchange diagrams for $\gamma p \to q\bar{q}p$.

at this time. However, ref. 2 found that leading order graphs factorized, so that when the cross section is integrated over t or taken at fixed t it is independent of the right hand side. The cross section was first calculated with the proton replaced by a scalar or pseudoscalar with point-like coupling to quarks. The cross-hatched blob in Fig. 3 was thus a quark loop. The cross section contained no divergences, and when the right hand side was replaced by a phenomenological parameterization the shape of the cross section remained the same (as for the elementary scalar or pseudoscalar case) for a wide variation of the parameters.

The cross section at fixed M^2, cos θ^* is found to be independent of s, as expected for a diffractive process. It is also (for $\cos\theta^* \neq 1$) independent of ϕ^*, the angle between the two planes defined by $\vec{p} \times \vec{p}'$ and by $\vec{\ell} \times \vec{\ell}'$. The dependence on cos θ^* and M^2 at $s = 300\text{GeV}^2$ is shown in Fig. 4 for $(u\bar{u} + d\bar{d})$- and for $c\bar{c}$-initiated jets. Predictions for $s\bar{s}$-initiated jets were also obtained but are not shown. An interesting point is that at large θ^*, where all mass effects have died away, the cross sections for the different flavors are proportional to the charge squared, as in e^+e^-. The normalization[3] is a rather crude estimate, but indicates that the cross section is large enough to observe.

For pion diffractive dissociation the calculation is similar, with the photon in Fig. 3 replaced by a pion.[3] For the pion coupling to $q\bar{q}$ we use a form factor proportional to $\alpha_s(Q^2)/Q^2$, which is valid if one quark is highly virtual[7] ($\cos\theta^* \neq 1$). The results, shown in Fig. 5, are qualitatively similar to those for photoproduction, but the M^2 and cos θ^* dependence is sharper. This is due to the extra $1/Q^2$ in the $\pi q\bar{q}$ coupling.

In comparing these predictions to experiment some care must be exercised. If the data are integrated over all cos θ^*, then cos $\theta^* \simeq 1$ will dominate and our predictions are not applicable. Thus the fact that $d\sigma/dM^2$ falls like M^{-2} for all hadrons[8] is a reflection of the cos $\theta^* \simeq 1$ behavior. For smaller cos θ^*, the cross section will fall faster, and at different rates for different beams (since $F_{\pi,K} \sim 1/Q^2$, $F_\gamma \sim 1$, $F_p \sim 1/Q^4$).

We now turn to details of the final state.[4] The $q\bar{q}$ into which the beam dissociates are a high-mass color singlet as in e^+e^-, and consequently the final state should be the same as in e^+e^- at $s = M^2$. There are, however, two differences. Higher orders in α_s will not be the same, and so there could be ~15% differences. In addition we must take into account the fact that the flavor of the quarks initiating the jets is different in each of the four processes - γ,π, K dissociation, e^+e^-. To the extent that they do not depend on the flavor of the jet, quantities like sphericity, thrust, spherocity, $\langle p_1 \rangle$ will be the same in all four cases. Multiplicity of a given flavor will be different in

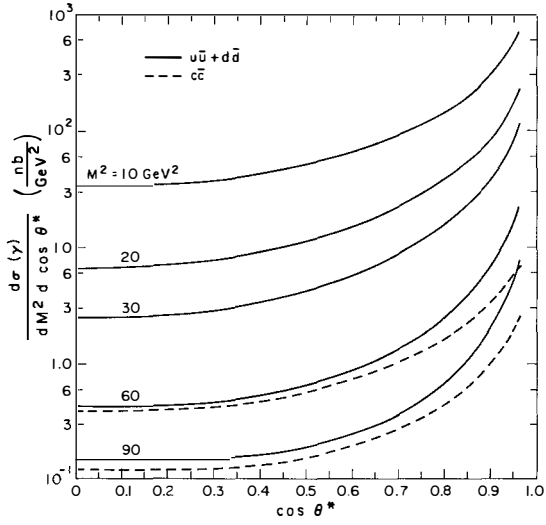

Fig. 4 Cross section predictions for $\gamma p \to q\bar{q}p$ at $s = 300\ GeV^2$.

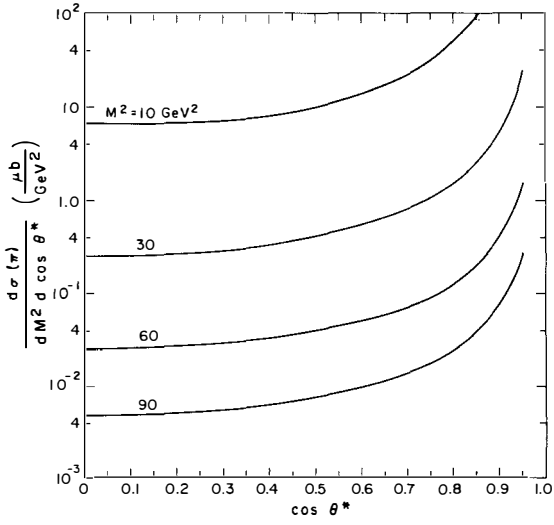

Fig. 5 Predictions for $\pi p \to q\bar{q}p$ at $s = 300\ GeV^2$.

each case and provides interesting predictions. Assuming all final state particles to be $q\bar{q}$ mesons, one can predict the relative multiplicity of a particular flavor in the final state in terms of three quantities: ρ_i, the probability that a given jet was initiated by a quark of flavor i; γ_i, the probability that a $q\bar{q}$ from the sea is $i\bar{i}$; and η_i, the fraction of all i quarks which are hidden in the final state. We know ρ_i for pions and kaons, a point whose utility is emphasized in ref. 9, and we believe we know it in e^+e^- and now, from the predictions outlined above, in photon fragmentation. The strange particle multiplicity $\langle n_S \rangle$ can then be written as

$$\langle n_S \rangle = (1-\eta_s)\langle n_s \rangle,$$

where the strange quark multiplicity $\langle n_s \rangle$ is given by $\langle n_s \rangle = 2\rho_s + (2\langle n \rangle - 2)\gamma_s$. The quantities γ_s and η_s are the same for all four processes; ρ_s is different but known; and $\langle n \rangle$ is the average total multiplicity. Changing s to c and S to C gives the expression for charm multiplicities. (Details can be found in ref. 4.) Here we note that the approximations $\eta_s \simeq 0$, $\gamma_c \simeq 0$ (for $\rho_c \neq 0$) are reasonable. If in addition we use the guess $\gamma_s = 0.2$, the following table is obtained.

	$\langle n_S \rangle$	$\langle n_C \rangle$
γ fragm	$0.4(\langle n \rangle - 0.88)$	0.44 ($M^2 \sim 60$ GeV^2)
π fragm	$0.4(\langle n \rangle - 1)$	$2\gamma_c(1-\eta_c)(\langle n \rangle - 1)$
K fragm	$1 + 0.4(\langle n \rangle - 1)$	$2\gamma_c(1-\eta_c)(\langle n \rangle - 1)$
e^+e^- (W=5-9GeV)	$0.2+0.4(\langle n \rangle - 1)$	0.8

Without the estimate of γ_s, one obtains $\langle n_S \rangle$ in terms of γ_s,[4] which can consequently be measured in four different experiments.

This treatment of the final state relied only on its being a color singlet $q\bar{q}$, not on the exchange mechanism. Consequently, if $\langle n \rangle$ or $\langle p_\perp \rangle$ or other properties of the final state are different (modulo possible higher order effects) then we must discard the assumption that mesons and photons dissociate into $q\bar{q}$ states. A similar comment applies to the flavor multiplicities before the approximations for η and γ are made, although ρ_i in γ fragmentation is actually dependent on the exchange mechanism.

ACKNOWLEDGEMENTS

I am grateful to D. Goulianos for a useful conversation and to L. Montanet and J. Tran Thanh Van for a pleasant and profitable "Recontre".

This work was supported by the U.S. D.O.E. under Grant No. EY-76-C-02-2114.

REFERENCES

1. Chan H. M., J. E. Paton, Tsou S. T., and Ng S. W., Nucl. Phys. B92, 13 (1975); A. Capella, J. Kaplan, and J. Tran Thanh Van, Nucl. Phys. B105,333 (1976); A. Capella, these proceedings.

2. S. F. King, A. Donnachie, and J. Randa, Nucl. Phys. B167, 98 (1980).

3. J. Randa, Phys. Rev. D22, 1583 (1980).

4. J. Randa, Phys. Rev. D23, 1662 (1981).

5. J. Randa, Phys. Rev. D21, 1795 (1980).

6. R. T. Deck, Phys. Rev. Lett. 13, 169 (1964).

7. G. R. Farrar and D. R. Jackson, Phys. Rev. Lett. 43, 246 (1979); S. J. Brodsky and G. P. Lepage, Phys. Lett. 87B, 359 (1979).

8. D. Goulianos, these proceedings.

9. S. P. Misra, A. R. Panda, and B. K. Parida, Phys. Rev. Lett. 45, 322 (1980).

DYNAMICAL MODELS OF HADRON-HADRON AND HADRON-NUCLEUS INTERACTIONS AT LOW P_T

A.Capella
Laboratoire de Physique Théorique et Hautes Energies, Orsay, FRANCE

ABSTRACT

I review some theoretical models which describe the dynamics of low p_T multihadron production in terms of the hadronic constituents.

The aim of the models I am going to review is to describe low p_T physics in terms of the hadronic constituents. The latter have played an important role in the additive quark model and later on in the duality diagrams. Impressive evidence on their importance in low p_T physics came when Ochs and the Lund group discovered two remarkable regularities of the low p_T hadronic spectra at large x[1]. These regularities are at the origin of the recombination and fragmentation models.

1. Recombination models.

Ochs[2] remarked that there is a striking similarity between low p_T hadronic spectra at large x ($x \gtrsim 0.4$) and the structure function of pointlike constituents, namely

$$x \frac{d\sigma}{dx}^{pp \to \pi^+} \propto u(x) \propto (1-x)^3, \tag{1.1}$$

$$x \frac{d\sigma}{dx}^{pp \to \pi^-} \propto d(x) \propto (1-x)^4. \tag{1.2}$$

(Note that the valence quark u is common to p and π^+, whereas the valence quark d is common to p and π^-)

More recently, it has been shown[3] that a similar relationship is also true for $\pi^\pm \to \pi^\mp, K^\pm, \ldots$

Eqs.(1.1) and (1.2) are the basis of the so-called recombination models[4]. In these models one assumes that the glue and sea of the colliding hadrons (which is concentrated at very low x) is responsible for the multihadron production in the central region. The valence quarks, on the contrary, will pick-up (recombine with) a parton from the sea to produce a hadron at large x. Since the sea parton has very small x, the momentum of the hadron will be essentially the same as that of the valence quark, hence eqs.(1.1) and (1.2).

A recent form of the recombination model (valon model) has been introduced by R.Hwa[5]. The word "valon" denotes a constituent quark (of the type the additive quark model deals with) and the word quark always refers to a point-like parton. The starting point of the valon model is the assumption (previously made by several authors[6]) that the quark distribution in a proton p, Fp, can be expressed (see Fig.1) as a convolution of the distribution of a valon in p, $G_{V/p}$, with the quark distribution in a valon, F_v, i.e.*

---

* The impulse approximation is implicitly assumed in eq.(1.3) since each valon in the proton contributes, independently from the other two, to the quark distribution.

$$F_p(x,Q^2) = \sum_{U,U,D} \int_x^1 dy\ G_{V/p}(y)\ F_V(\frac{x}{y}, a^2) \qquad (1.3)$$

Here x and y represent the longitudinal momentum fractions carried out by the quark and the valon, respectively, and the sum is over the three valons in a proton U,U, and D. At high Q^2, F_V can be computed in perturbative QCD at the leading order, whereas F_p is an experimentally measurable quantity (proton structure function). From eq.(1.3) one can then determine $G_{V/p}$ (which is independent of Q^2)*

The generalization to other types of hadrons is straightforward. Since the number of valons in a hadron is known, one can use symmetry considerations and sum rules in order to obtain joint (multi-valon) momentum distributions in a hadron.

A low p_T hadron-hadron collision is then viewed, in the valon model, as a multi-stage process:
initial hadron $\rightarrow^{(1)}$ valons $\rightarrow^{(2)}$ partons $\rightarrow^{(3)}$ valons $\rightarrow^{(4)}$ produced hadrons.
As explained above, stage (1) is given by the valon distribution functions $G_{V/p}$. Stage (4), giving the probability of two (three) valons to recombine into a final meson (baryon), is governed by joint multi-valon distribution functions, and thus is also known. Stage (2) is not known . In the valon model it is parametrized in such a way that the convolution of stages (1) and (2) reproduce the structure functions measured at low Q^2(SLAC data).This is of course in the spirit of eq.(1.3). (Note, however, that one assumes here that the SLAC data are relevant for low p_T hadron-hadron scattering.) The partons resulting from stage (2) just require a few hundred MeV to be put on their mass-shell and can then propagate and interact independently as free partons for a long time. As these partons propagate beyond the interaction region they gradually dress themselves up by virtual interactions and become valons (stage (3)). Each such valon is assumed to have the same momentum as the original bare parton before the dressing process begins . (In this way stage (3) is diposed of.) A pair of these valons, say U and $\bar{D}$, will recombine to produce a π^+. As mentioned above, this stage (4) is described by the joint (multi-valon) momentum distribution functions. These functions change very little the parton momentum distribution(as required in order to reproduce eq. (1.1) and (1.2)). However, with a few assumptions it leads

*An alternative way[5] to determine $G_{V/p}$ from eq.(1.3) is to use experimental data on the charged proton form factors, at low Q^2($Q^2 < 1$ GeV^2). To do so one has to assume that $F_V(z,Q^2) \propto \delta(z-1)$ for $Q^2 < 1$ GeV^2 (the valon structure cannot be resolved at low enough values of Q^2).

to a description of low p_T interactions which is rather constrained, in the sense that, on the one hand, the functions F_V are universal and, on the other hand, the same type of functions govern stages (1) and (4). So far, the model has been successfully applied to $p+p \to \pi^- + X$ inclusive reactions. The results are shown in Fig.2. A check of the overall consistency of the valon approach is not yet available.

2. Dual Fragmentation Models.

The remark of the Lund group[7] is that there is an equally striking similarity (both in shape and absolute normalization) between low p_T hadronic spectra in the fragmentation regions ($|x_F| > 0.2$), and the fragmentation functions measured in hard processes, namely

$$\frac{d\sigma^{\pi^+ p \to \pi^+}}{\sigma dx}(x) \simeq D^{u \to \pi^+}(x) + D^{\bar{d} \to \pi^+}(x) = 2D^{u \to \pi^+}(x) \qquad (2.1)$$

$$\frac{d\sigma^{\pi^+ p \to \pi^-}}{\sigma dx}(x) \simeq D^{u \to \pi^-}(x) + D^{\bar{d} \to \pi^-}(x) = 2D^{u \to \pi^-}(x) \qquad (2.2)$$

Eqs(2.1) and (2.2) suggest that, as a result of the interaction, the q and the $\bar{q}$ in a meson are in a very asymmetric configuration, the q being very slow and the $\bar{q}$ very fast or vice-versa. This is indeed assumed to be the case in the first version of the fragmentation model, proposed by the Lund group. In this model[7], the slow constituent is in fact supposed to be stopped (at x=0) by the effect of the interaction. The hadronization of the fast constituent is governed by the same fragmentation functions measured in hard processes

For proton initiated reactions one has

$$\frac{d\sigma^{pp \to \pi^+}}{\sigma dx} \simeq \frac{1}{3} D^{uu \to \pi^+}(x) + \frac{2}{3} D^{ud \to \pi^+}(x) , \qquad (2.3)$$

$$\frac{d\sigma^{pp \to \pi^-}}{\sigma dx} \simeq \frac{1}{3} D^{uu \to \pi^-}(x) + \frac{2}{3} D^{ud \to \pi^-}(x) . \qquad (2.4)$$

Eqs(2.3) and (2.4) which seem to be true at a $10 \div 20$ % level of accuracy, suggest that a diquark in the proton (acting in a coherent way) carries essentially all the momentum of the hadron -the quark being slowed down by the interaction.

Obviously, if eqs(1.1)-(1.2) and (2.1)-(2.4) (and the corresponding ones for other processes) are well verified, as it seems to be the case, it becomes a challenge to theorists to show why it is so, and, in particular, why the r.h.s. of eqs(1.1)and (2.3) have the same x-dependence at large x.

In this section I am going to show how a fragmentation model can be formulated in an S-matrix framework . The model provides a comprehensive description of

the mechanism of multihadron production, both in the central region and the fragmentation region. Moreover, it can be extended in a rather straightforward way, and without any new concepts or assumptions, to soft high-energy collisions involving nuclei.

The general framework of this model is the topological approach to strong interactions (1/N-expansion). The topological approach is very general. It is based upon the fact that the strong coupling constant is large and therefore one should try and find a new parameter which allows a perturbative treatment (power series expansion). Following t'Hooft[8], Veneziano introduced an expansion in powers of 1/N[9] (N is either the number of colors or the number of flavors; the ratio between the two is kept fixed in this expansion). The physical arguments in favour of the reliability of such an expansion are the following: more than 20 years of experimental and phenomenological work in strong interactions has revealed beyond doubt that the final multi-hadron state is not produced in a random way, but, on the contrary, there is "order" in it. The manifestations of such order are well-known: dominance of short range correlations (short range order), limited p_T, small diffractive dissociation, jet-like final states etc... Moreover, the resonances have rather narrow widths and are located on Regge trajectories which are approximately linear. Also, the O.Z.I. rule is known to be approximately verified. Since order is closely related to topology one gets the idea of the topological approach in which the graphs with the simpler topologies are assumed to dominate. It can, indeed, be shown that graphs with the simplest topology yield the properties of the multi-hadron final state above.

One could ask at this point why these properties are not exact and how one is led to a 1/N expansion. The answer is: because of unitarity. Indeed, once the graphs with the simpler topologies are introduced, more complicated topologies are forced to appear[10] by unitarity. The more the topology of a graph is complicated the more the order of the produced final state is violated. However, it turns out that these more and more complicated topologies are depressed by higher and higher powers of 1/N, hence the relevance of an expansion in power of this parameter.

The graphs with the simplest topologies are:

b = 1, h = 0 : order 1/N corresponds to a planar graph, representing a secondary Regge pole (Fig.3).
The s-channel discontinuity contains one chain or string of produced hadrons (two back-to-back jets).

b = 2, h = 0: order $(1/N)^2$ corresponds to the simplest non-planar topology (sphere or cylinder) and represents a Pomeron pole (Fig.4).
The s-channel discontinuity contains two chains of produced particles.

b = 1, h = 1 : order $(1/N)^3$ represents a R $\otimes$ P cut.

b = 2, h = 2 : order $(1/N)^4$ corresponds to the topology of a cylinder with a handle or tourus and represents a Pomeron-Pomeron ($P \otimes P$) cut. In this case four chains of particles may be produced (Fig.5).

The following remarks are in order:

a) in order to obtain the dominant graphs at high energies one has to take into account both the order in the 1/N expansion and the energy dependence. The reggeon graph corresponds to the lowest order (1/N) but is not dominant because it behaves like $(s)^{-1/2}$.

b) by comparing graphs with the same s-dependence, it can be seen that the true expansion parameter is $(1/N)^2$. For instance $P \otimes P/P \sim (1/N)^2$; $R \otimes P/R \sim (1/N)^2$ etc.

c) the 1/N expansion provides a link between Dual resonance model, Reggeon Field Theory and Gauge Theories.

d) with our present knowledge it is not possible to compute the contributions at the various orders of the 1/N expansion, although interesting attempts are under study by putting the theory on a lattice. Moreover, confinement has to be assumed, even at the planar level. However, we obtain in this way a unified description of lepton and hadron processes. It emerges from it a , QCD inspired, dual string picture of hadrons, satisfying the general requirements of a S-matrix theory. In the case of $e^+e^- \to$ hadrons and $\ell p \to \ell X$ the picture is well-known (Fig.6). However, the corresponding picture for purely hadronic processes, such as $h_1 + h_2 \to h_3 + X$ is rather non trivial. The main contribution at high energy is the Pomeron and one has a two-chain production mechanism as depicted in Fig.4. (for a meson-meson interaction) and Fig.7. Note that the flavor quantum numbers of the projectile are split into the two chains. For this reason all valence quarks of a colliding hadron cannot go into the same produced particle, except in diffractive events which are not included in the Pomeron component. On the other hand, although the diquark belongs to one chain, its two quarks can go into the same or two different produced particles (see Fig.13). Note also that when more than two chains of hadrons are produced, the corresponding contribution is a non-dominant one.

The framework described above is common to the Dual Fragmentation models proposed by the Orsay group[11], Saclay group[12] and Minekata[13] (differences in the detailed formulations of these models are discussed at the end of this section).

In order to have a complete formulation of the Dual Fragmentation model, one has to define the momentum distribution of the valence quarks (border lines of the various chains) and the hadron spectra of each chain.

An important development in the Dual-Parton models occurred when it was realized that the momentum distribution functions of the hadron constituents at the chain ends could be obtained within the Dual model. The main steps of this

important discovery are the following: in 1978, Chiu and Matsuda[14] derived the mass spectrum of the dual loop graph (Pomeron). Simultaneously, Aurenche and Gonzalez-Mestres[15] obtained the same mass spectrum by using only very general features of the Dual-Regge models, namely the dominance of Regge singularities. More than one year later, the Orsay group[11], Saclay group[12] and Minakata[13] realized almost simultaneously that the above mass spectrum yields, in a rather straightforward way, momentum distribution functions of the border lines of the two chains in the Pomeron, which correpond precisely to an asymmetric configuration of the type mentioned at the beginning of this section. In the case of a proton one gets

$$\rho_p(x,y) \propto x^{-0.5}\, y^{1.5}\, \delta(1-x-y) \tag{2.5}$$

Here x(y) denotes the momentum fraction of the quark (diquark). In the case of a pion one gets

$$\rho_\pi(x,y) \propto x^{-0.5}\, y^{-0.5}\, \delta(1-x-y) \tag{2.6}$$

Eq(2.6) is, of course, symmetrical in x and y (the momentum fractions of the quark and the antiquark). From eq(2.5) and (2.6), the momentum distribution function of a valence quark in a proton is given by

$$\rho_{q/p}(x) \propto \frac{1}{\sqrt{x}}\,(1-x)^{1.5}, \tag{2.7}$$

and that of a valence quark or antiquark in a pion by

$$\rho_{q/\pi}(x) \propto \frac{1}{\sqrt{x}}\,(1-x)^{-0.5}\,. \tag{2.8}$$

For a diquark in a proton one has $\rho_{qq/p}(x) = \rho_q(1-x)$ *. The $x \simeq 0$ behaviour in eqs(2.7) and (2.8) is the same as that of the structure functions. However, the powers of 1-x are smaller here (note that in QCD the latter powers depend on Q^2).

Let us now consider the rapidity distribution of particles produced in a chain. The first question one can ask here is: are jets the same in soft and hard processes ? First of all we have seen that the hadronic final state is not the same in the two cases: the dominant contribution to $e^+e^- \to$ hadrons and $\ell_p \to \ell X$ (Fig.6) contains one chain of produced particles, whereas the Pomeron component

---

* The δ-function in eqs(2.5) and (2.6) does not imply that the border lines of the chains are the only constituents of the colliding hadrons carrying energy-momentum. On the contrary, gluons and $q\bar{q}$ pairs are also present (see the last picture in Fig.4). This δ-function expresses the fact that all the energy of the colliding hadrons is given to the particles produced in either chain.

contains two chains (Fig.4). However, the above picture suggests that the single chain spectra of hard processes (Fig.6) is similar to the corresponding one for the Regge component (Fig.3). Positive tests of this idea can be found in refs (17). These tests, together with the fact that the iterative cascade model[18], explains most of the features of e^+e^- → hadron data up to $Q \sim 30$ GeV, suggest that hard hadronic production at present values of Q^2 is mainly dominated by the mechanism of confinement*. In view of that, the hadron spectrum of a chain will be computed in terms of standard quark (diquark) fragmentation functions $D_q(x)$ ($D_{qq}(x)$). For a chain stretched between constituents c (with momentum fraction x) and c' (with momentum fraction x') one has

$$\frac{1}{\sigma}\frac{d\sigma^h}{dy}(y) \equiv N^h(y) = \int dx \int dx' \; \rho^c(x) \; \rho^{c'}(x') \; N_{cc'}[y - \Delta(x,x') \; ; \; P(x,x')] \qquad (2.9)$$

Here $\rho^c(x)$ and $\rho^{c'}(x)$ are the momentum distribution functions of c and c' (the border lines of the chain). These functions are given in eqs (2.7) and (2.8) The other quantities in eq(2.9) are defined as follows:
$P(x,x') \simeq \frac{s}{2}\sqrt{x\,x'}$ is the c. of m. momentum of the chain, $\Delta(x,x') \simeq \frac{1}{2}\ln|x/x'|$ is the distance between the c. of m. of the chain and overall c. of m. and

$$N_{cc'}(y - \Delta \; ; \; P) = \begin{cases} x \; D^{c \to h}(x), & y > \Delta \\ x \; D^{c' \to h}(x), & y < \Delta \end{cases}$$

with $x = m_T^h \sin h\,(y-\Delta)/\,P_{MAX}$ (m_T^h is the transverse mass of h and P_{MAX} its maximum momentum in the chain). As mentioned above the fragmentation functions $D^{c \to h}$ and $D^{c' \to h}$ are obtained from hard scattering data at low or intermediate values of Q^2.

The total inclusive spectrum of particle h is just given[11] by the sum of the hadronic spectra of the two chains. Some results are shown in Figs 8-12. The experimental data, both in the central and fragmentation regions are well reproduced**. Note that, due to the strong peaking of $\rho(x)$ near x=0, the

---

* The pointlike nature of hard processes will probably destroy the above similarity at higher values of Q^2. However, some authors[19] claim that such similarity will be maintained at all q^2.

** In refs (12) and (13) the difference between the c. of m. of each chain and the overall c. of m. is neglected. For this reason the formalism of refs (12) and (13) does not apply to the central region. In the fragmentation regions the three models (11),(12) and (13) are essentially equivalent.

hadronic spectra obtained in the fragmentation regions are very similar both in shape and absolute normalization, to the input fragmentation functions.(See Fig.10). The resulting spectra at large x are thus very close to the ones given by eqs (2.1) to (2.4).

3. Models for quark jets.

So far the quark fragmentation functions are just taken from hard scattering data. Theoretical information on the $x \to 1$ behaviour of these functions can be obtained from dimensional counting rules[20].

The most popular models to determine the fragmentation functions are the so-called iterative cascade models[18]. The parametrizations of these functions obtained by Feynman and Fields and by the Lund group are well-known and I shall not review them here. The latter model describes the fragmentation of quarks, diquarks and gluons. Sukhatme et al.,[21] have introduced a new model for diquark fragmentation which is of the same iterative cascade type. As in the Lund jet model, the two quarks in the diquark can find themselves in the same or in two different produced hadrons (see Fig. 13). The probability for each type of break-up is assumed to depend only on $\delta = |x_1 - x_2|$ (x_1 and x_2 being the fractions of the diquark momentum carried by the two quarks), and is parametrized as $P_B(\delta) = \exp(-a\ \delta^2)$ (probability of baryon formation, Fig.13a) and $P_M(\delta) = 1 - P_B(\delta)$ (probability of meson formation, Fig.13b). In this way, when $\delta \to 0$ only the type of break-up in Fig.13a is possible.

Finally, a complete theoretical determination of the fragmentation functions using, among other ingredients, the information coming from Dual graphs in the triple Regge region, can be found in ref.22.

4. Non-Dual Fragmentation Models.

The Lund group proposes[23] a different interaction mechanism for particle production in the fragmentation region which makes no reference to DTU and uses instead concepts borrowed from classical physics.

In this model a baryon is viewed as an extended object (bag) containing color which is confined by the pressure from the surrounding vacuum. The color is not well localized and a meson (proton) bag contains two (three) color blobs. In a hadron-hadron collision the region where these two (three) color blobs overlap will form a "white" center, whereas the non-overlapping regions will act as color "handles". A color handle of one of the colliding hadrons can connect with a complementary anticolor handle from the other hadron and, in this way, a color flux tube will be stretched between the two hadrons (Fig.14). The resulting extended object will break into pieces (hadrons) in the standard way, via $q\text{-}\bar{q}$

pairs production*. The produced hadron containing the quark labelled J in Fig.14 will be the leading baryon. The Lund jet model is then used to compute the spectra of produced hadrons. Obviously, in order to do so one needs an extra main ingredient, namely the momentum distribution functions of the quarks (I, J and L in Fig.14). A simple parametrization of these functions is extracted from the experimental data for the pion spectra and from simplicity requirements**. The model reproduces well the spectra of various types of produced hadrons (see Fig.15).

The Lund group also proposes an explanation of polarization effects within the framework of fragmentation type models[24]. The idea is the following: in order to give a finite transverse mass to a hadron, a q-$\bar{q}$ pair has to be produced with a finite distance between the q and the $\bar{q}$, the field energy between them can then be transformed into transverse mass. If no transverse degrees of freedom are excited, the two members of the pair will be produced with opposite transverse momentum. The resulting angular momentum of the pair has to be compensated by the spin of the quarks (since no transverse excitation means in particular no net angular momentum). This simple idea leads to a satisfactory description of the polarization of hyperons in the proton fragmentation region[24].

5. Other models.

I should also mention that extensive calculations on the framework of the Geometrodynamic model of G.Preparata are being performed at CERN and interesting results have been obtained[25]. In this model, multiparticle states originate from the decay of two "firesausages" (a "firesausage" is a coherent superposition of physical $q\bar{q}$ states with different angular momentum and approximately degenerate masses). Its decay is described by a sequential process. The model has some similarity with the two-chain dual model, in that a firesausage can be assimilated to a $q\bar{q}$ chain in the Dual model. (In the case of a pp interaction the two chains in the Dual model are quark-diquark chains and the firesausage has to be assimilated to what is left from this chain after removing the leading baryons). It would be interesting to make a detailed comparison

---

*It is easy to show that the bag is stretched to the same length as if all the energy of each colliding hadron were carried by one of its valence quarks.

**It is amazing that these momentum distribution functions are very different from the ones found in the Dual fragmentation models (they vanish both at $x = 0$ and $x = 1$). In spite of that, the resulting spectrum is similar to the one obtained in Dual models.

between the two models.

Finally, J. Gunion [26] has obtained interesting results in a model of the type described in ref (27), using perturbative QCD in the leading log approximation (assuming that this approximation can be used at small p_T).

6. Models of hadron-nucleus interactions.

So far we have briefly reviewed some dynamical models of hadron-hadron interactions . We are going to see next how these models can be generalized to describe hadron-nucleus interactions.

The generalization of the Dual fragmentation model to hadron-nucleus interactions is rather straightforward. Here. multi-chain diagrams, corresponding to higher orders in the 1/N expansion, are enhanced due to combinatorial factors which result from the possibility of linking each chain to different nucleons in the target. The model[28] obtained in this way is of the multiple scattering type[29]. However, the superiority of the dual approach lies in the possibility of determining the energy partition among the various inelastic collisions within the nucleus. For this one needs joint multi-quark momentum distribution functions (see Fig.3). Generalizing the Dual arguments above, one gets for these functions[28]

$$\rho(x_1,x_2,x_3\ldots x_{2n}) = \frac{1}{\sqrt{x_1}}\,\frac{1}{x_2}\,\frac{1}{x_3}\,\ldots\,x_4^{1.5}\;\delta(1-x_1-x_2-x_3-\ldots-x_{2n}) \qquad (6.1)$$

for a proton projectile, and

$$\rho(x_1,x_2,x_3\ldots x_{2n}) = \frac{1}{\sqrt{x_1}}\,\frac{1}{x_2}\,\frac{1}{x_3}\,\ldots\,x_4^{-0.5}\;\delta(1-x_1+x_2-\ldots-x_{2n}) \qquad (6.2)$$

for a pion projectile. The formulae above are quite transparent. There is a x^{-1} factor associated to each sea quark, and the factors $x^{-1/2}$ and $x^{1.5}$ associated to a valence quark and diquark respectively. The probability for having n inelastic collisions within the nucleus is obtained[29] from the standard Glauber-Gribov formulae.

The model describes in a quantitative way the A-dependence in the central and projectile fragmentation regions, with no free parameters. (For a more detailed presentation of this model see the following talk in this meeting by J.Tran Thanh Van.)

A very different model for hadron-nucleus interactions, also based on the two-chain model of hadron-hadron interactions of ref(12), has been introduced by Chao, Chiu, He and Tow, reference (30). The idea is the following. It is well-known from the space-time picture of soft interactions that the (fast) hadrons in the chains of the Dual fragmentation model are produced after

a time which is much longer than the time needed for the projectile to travel from one nucleon of the target to the next one. The authors of ref.(30) assume that the chain which contains the fast projectile fragment (chain II in Fig.16) will act, in a hadron-nucleus interaction, as a newly formed projectile which will interact with another nucleon in the target (see Fig.16). In this way, at each inelastic collision, only chain I is produced, chain I and II being both produced only at the last inelastic collision. Denoting by $N^{I}(y)$ and $N^{II}(y)$ the rapidity distributions of chains I and II respectively, one easily obtains

$$\frac{1}{\sigma^{pA}_{in}}\frac{dN^{pA}}{dy}(y) = \bar{\nu}\, N_{I}(y) + N_{II}(y) \qquad (6.3)$$

where $\bar{\nu} = A\,\sigma^{pp}_{in} / \sigma^{hA}_{in}$ is the average number of inelastic collisions within the target. Formula (6.3) gives a pA charged particle spectrum which is in agreement with the experimental data in the central region (see Fig. 17). An analysis in the projectile fragmentation region is not yet available.

Note that, since $< N_{I} > = < N_{II} > = < N_{pp} >/2$ (where the bracket denotes an integration over y), one gets from (6.3)

$$< N_{pA} > = \left(\frac{\bar{\nu}}{2} + \frac{1}{2} \right) < N_{pp} >$$

A different type of models, of a non multiple scattering nature, are also very popular. All these models[31] are based on the following assumption. One or more quarks* of the incoming hadron interact with target nucleons (wounded quarks) and produce particles which populate mainly the central region. The particles in the projectile fragmentation region come mainly from (spectator) quarks which escape inelastic collisions within the target and go through it retaining their momentum fraction x. These spectator quarks hadronize (either by recombination or fragmentation or both depending on the authors) in a way which is independent of the target** . The probability for a quark to interact or to escape inelastic collisions within the target, can be obtained from the standard Glauber-Gribov formulae together with the additive quark model relations: $\sigma_{\pi p} = 2\sigma_{qp}$ and $\sigma_{pp} = 3\,\sigma_{qp}$. One gets in this way

---

* Most authors working in these models consider these quarks as the constituent quarks of the additive quark model (valon).

**Although the recombination model is only used explicitly by A. Dar and co-workers[31] this model is in the spirit of the recombination model in that the fast particles result from the hadronization of valence constituents which fly undisturbed through the interaction region.

$$R(x) \equiv \left(x\frac{d\sigma}{dx}\right)^{\pi A \to h} \Big/ \left(x\frac{d\sigma}{dx}\right)^{\pi p \to h} = 2\,(\sigma_{\pi A} - \sigma_{qA})/\sigma_{\pi A} \qquad (6.5)$$

The factor in the r.h.s. is just the probability for one of the two quarks in the pion to interact inelastically within the target while the other quark escapes inelastic collisions. Eq (6.5) is valid for $x > 0.4$ and gives the A-dependence of $R(x)$ in this region, with no free parameter. The result, which is independent of the produced hadron, is in agreement with the data. The corresponding ratio for a proton projectile is slightly more complicated since here one or two quarks from the proton can be spectators. However, in this case, the relative normalization of the two contributions cannot be computed from the model. The free parameter depends in general on the type of produced hadron. By adjusting this free parameter one can get a good description of the data. So far for the projectile fragmentation region. In the central region one has to make an extra and, in my opinion, very strong assumption, namely one has to assume that the multiplicity of produced particles is the same in quark-proton and quark-nucleus interactions. I find it very hard to make such an assumption consistent with unitarity for the following reasons. The Glauber-Gribov formulae used in this model were derived by Gribov[32] and Bertochi[33] from Feynman diagrams, which are argued to be dominant at present energies* . Using the unitary condition , the final state obtained when the incoming quark interacts inelastically with two target nucleons, is given by the appropriate discontinuity of these Feynman diagrams. This discontinuity contains a multiplicity equal to twice the multiplicity for a single inelastic collision. One obtains in this way a ratio of average multiplicities $< N >^{qA} / < N >^{qp}$ which is larger than one, and increases with**

7. Recombination versus Fragmentation Models.

The models of the fragmentation and recombination type have both met an undeniable success in describing the fragmentation regions. It becomes a challenge for theorists working in the field, to understand why both are successful

---

* These are the so-called non-enhanced graphs which contain no triple Pomeron coupling. I do not know of any other set of graphs which yields the Glauber formula.

** This criticism also applies to the model of ref(28) where the graphs involved are such that $< N >^{hA}_{\text{double scattering}} / < N >^{hp} \simeq 1.5$ and still use is made of the Glauber-Gribov formula. The same is also true in the model of ref.(34).

and in particular why the r.h.s. sides of eq(1.1) and (2.3) are approximately equal at large x ($x > 0.4$).

At their present stage both models try to make contact with Q.C.D. (the fragmentation Dual model via the 1/N expansion and the valon model via the Q.C.D. evolution equations). Since the confinement problem is not solved, both models have to use (e^+e^- or electro(neutrino)-production) data as an input.

In my opinion there is a formal superiority in the Dual fragmentation model in that it is rooted in the very general S-matrix principles and incorporates the successes of Dual models and Reggeon Field theories. It is remarkable that this model can describe, in a comprehensive way, the central and fragmentation regions both in hadron-hadron and hadron-nucleus interactions with no adjustable parameter.

REFERENCES

1. See also L. Van Hove, The role of valence quarks in proton fragmentation CERN preprint TH 2997 and references therein.
2. W.Ochs, Nucl.Phys.B118, 397 (1977).
3. Brown et al., Phys.Rev.Letters 45 , 157 (1980).
4. For a review see L.Van Hove, Schladming lectures 1979, CERN preprint 2628.
5. R.C.Hwa, Phys.Rev. D22, 759 (1980)
   R.C.Hwa and C.S.Lam preprint 158 (1980).
6. G.Altarelli, N.Cabibbo, L.Maiani and R.Petronzio, Nucl.Phys. B69, 531(1974); N.Cabibbo and R.Petronzio, Nucl.Phys. B137? 395 (1978); V.V.Anisovich, Ya.M. Shabelsky and V.M.Shekhter, Nucl.Phys. B133,447(1978) A.Le Yaouanc, L.Oliver, O.Pène and J.C.Raynal, Phys.Rev.D12, 2137 (1975).
7. B.Andersson,G.Gustafson, and C.Peterson, Phys.Lett.69B, 221(1977).
8. G.t'Hooft, Nucl.Phys.B72, 461 (1974).
9. For non-specialized reviews see G.Veneziano in Proc. XII Rencontre de Moriond 1976, ed.J.Tran Thanh Van and GIF lectures 1977; Girardi GIF lectures, 1976.
10. G.Veneziano, Nucl.Phys.B74, 365(1974) and B117, 519(1976); Chan Hong Mo et al., Nucl.Phys. B86,470 (1975) and B92, 13 (1975); G. Chew and C.Rosenweig, Nucl. Phys. B104, 290(1976) and Phys.Rep 41C, 263(1978).
11. A.Capella, U.Sukhatme, C.I.Tan and J. Tran Thanh Van, Phys.Lett.81B, 68(1979); A.Capella, U.Sukhatme, and J.Tran Thanh Van, Particles and Fields 3 329(1980).
12. G.Cohen-Tannoudji, A.El Hassouni, J.Kalinowski, O.Napoly and R.Peschanski, Phys.Rev. D21, 2689 (1980).
13. H.Minakata, Phys.Rev. D20(1656(1979)
14. C.Chiu and S.Matsuda, Nucl.Phys. B134, 463(1978).

15. P.Aurenche and L.Gonzalez-Mestres, Phys.Rev.D18, 2995 (1978)
16. W.Tomé et al., Nucl.Phys. B129, 365 (1977); W.Tomé , Thesis, III Physikalisches Institut der TH Aachen, Germany.
17. J.Dias de Desu and S.Jadach, Act.Phys.Pol. B9, 249 (1978);
F.Hayot and S.Jadach, Phys.Rev.D17, 2307(1978);
J.Gasser and U.Sukhatme, Cambridge University report DAMTP 76/3(1976) unpublished.
18. A.Krzywicki and B.Petersson, Phys.Rev. D6, 924 (1972)
U. Sukhatme, Phys.Lett.73B, 478 (1978)
R.Field and R.P.Feynman, Nucl.Phys. B136, 1(1978).
19. G.Cohen-Tannoudji and O.Napoly in Proc. XV Rencontre de Moriond, 1980 ed. J.Tran Thanh Van.
20. R.Blankenbecler and S.J.Brodsky, Phys.Rev. D10, 242 (1974);
S.Brodsky, G.Farrar, Phys.Rev.lett.31, 1153 (197);
V.Matveev, R.Muradyan, A.Tavkhelidze, Lett. Nuovo Cim. 7, 719 (1973).
21. U.Sukhatme, K.E.Lassila and R.Oramva, Fermilab-Pub. 81/20-THY.
22. A.El Hassouni, A.Mantrach, E.G.Oudrhiri-Safiani (to be published in Z.Phys.); See also A.El Hassouni and O.Napoly, Phys.Rev.D23, 193(1981).
23. B.Andersson, G.Gustafson and I.Holgersson and O.Mansson, Lund preprint LU TP 80-5.
24. B.Andersson, G.Gustafson, G.Ingelman, I. Holgersson and O.Mansson, Lund preprint
25. G.Preparata and G.Valenti, Nucl.Phys. B183, 53 (1981) and preprint BARI-GT/80-09.
26. F.Low, Phys.Rev. D12, 163 (1975)
S.Nussinov, Phys.Rev. Lett. 34, 1286 (1975).
27. J.Gunion in Proc.of the Europhysics Study Conference on "Partons in Soft Hadronic Processes" edited by R.T.Van de Walle, Erice 1981.
28. A.Capella and J.Tran Thanh Van, Orsay preprint LPTHE 81/2. A simplified version of this model is given in Phys.Lett. 93B, 146 (1980). See also X.Artru, Orsay preprint 79/8.
29. A.Capella and A.Krzywicki, Phys.Rev.D18, 3357 (1978) and Phys.Lett.B67, 84 (1977).
30. W.Q.Chao, C.Chiu, Z.He, D.M.Tow, Phys.Rev.Lett. 44, 518 (1980).
31. For a recent review see A.Dar in Proc. of the Europhysics Study Conference on Partons in Soft Hadronic Processes", Erice 1981, ed. by R.T.Van de Walle.
32. V.N.Gribov, Zh.Eksp. Teor Fiz. 57, 1306(1969) [Sov.Phys. JETP 30, 709 (1970)]
33. L.Bertocchi, Nuovo Cim. 11A, 45 (1972).
34. S.J.Brodsky, J.Gunion and H.Kühn, Phys.Rev.Lett. 44, 518 (1980)

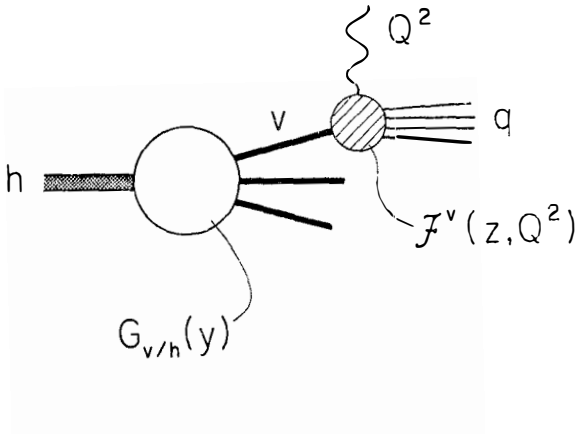

Fig.1: Hadron and valon structure functions (see eq(1.3)

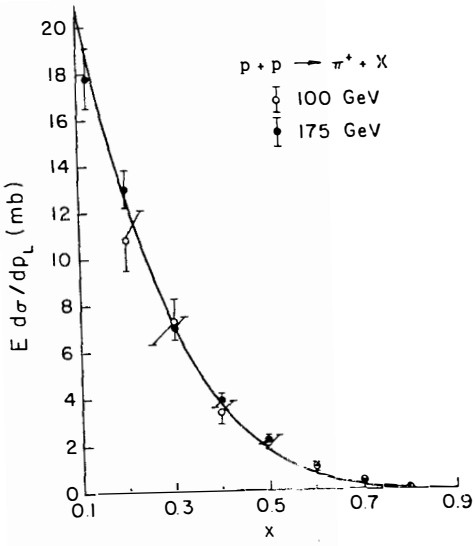

Fig.2: Inclusive π^+ spectrum in pp collisions computed in ref.5

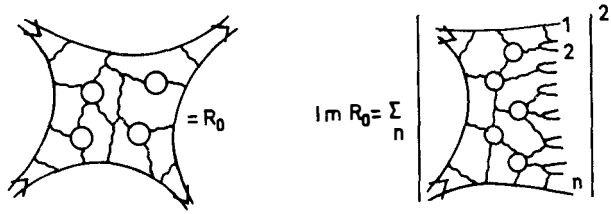

Fig.3: Graphs for a secondary Regge pole and its s-channel discontinuity. The circles represent quark loops and the wavy lines gluons.

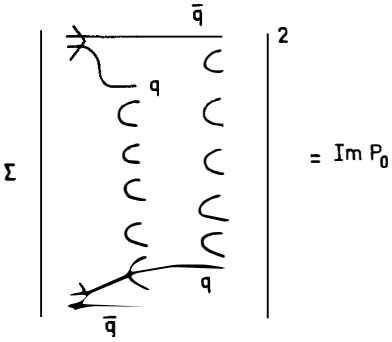

Fig.4: s-channel content of the Pomeron graphs. The summation over quark and gluon lines has been performed.

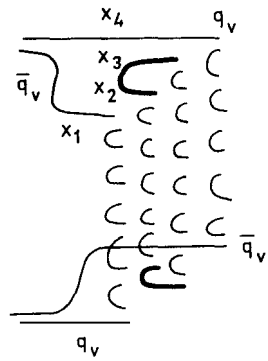

Fig.5: Example of discontinuity of a graph representation a P⊗P cut. Quark loops and gluons have been summed. Two of the chains are stretched between quarks and antiquarks from the sea.

Fig.6: Planar Q.C.D. graphs for $e^+e^- \to$ hadrons and $\ell p \to \ell x$ (in the case where the hard current hits a valence quark of the proton.

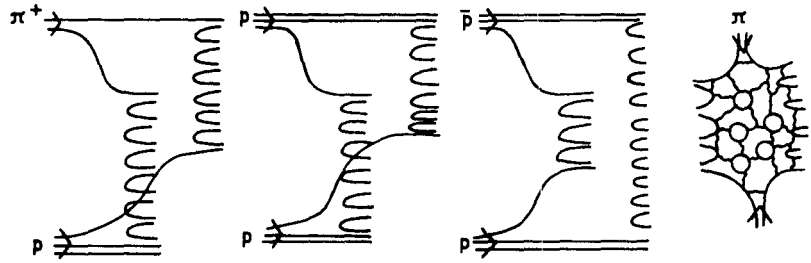

Fig.7: The dominant production graphs for meson-baryon and baryon-baryon interactions. The last graph is identical to the first one except for the fact that quark loops and gluons are displayed.

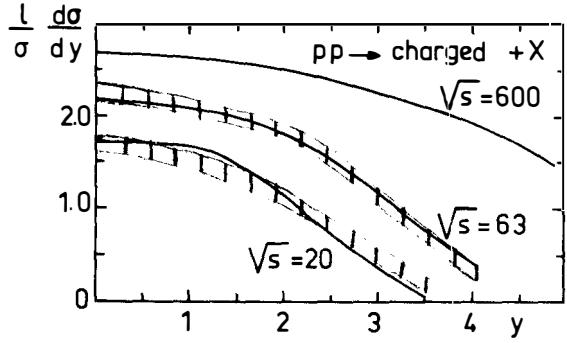

Fig. 8

The calculated rapidity distribution of charged particles in p+p → charged +X at various energies. The dashed area represents the experimental data (16).

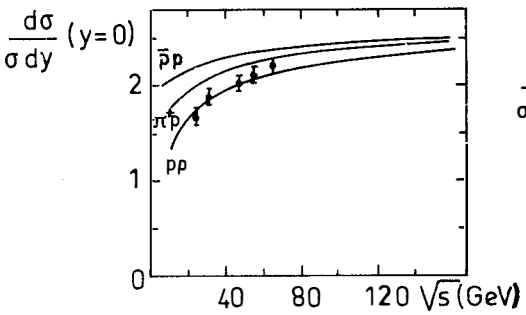

Fig.9: The height of the central plateau as a function of the energy.

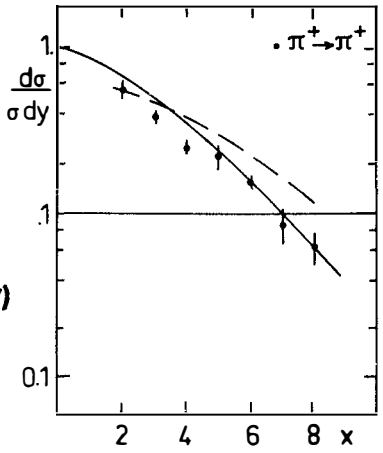

Fig.10: The $\pi^+ \to \pi^+$ inclusive spectrum computed in ref(11). The dashed line shows the input x D (x) .Diffraction has been removed from the data.

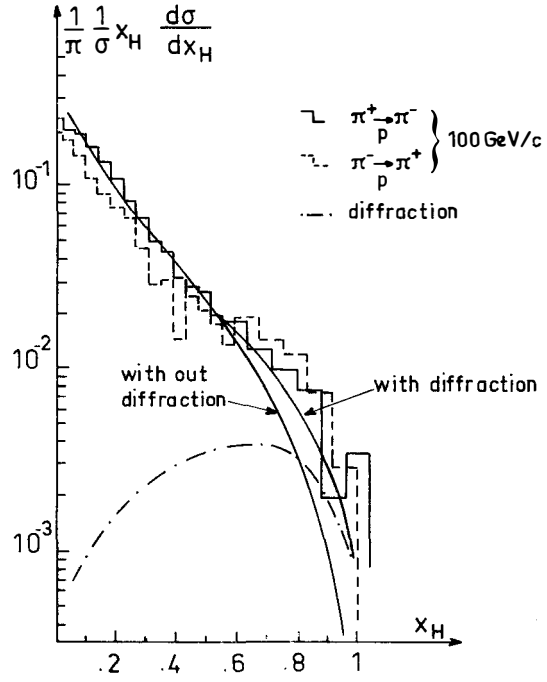

Fig.11: The $\pi^{\pm} \to \pi^{\pm}$ inclusive p spectra computed in ref.(12).

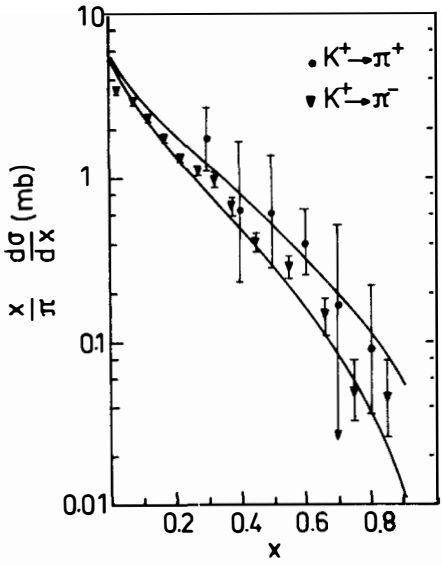

Fig.12: The $K^+ \to \pi^{\pm}$ inclusive spectra computed in ref.(13).

Fig.13: Diquark fragmentation

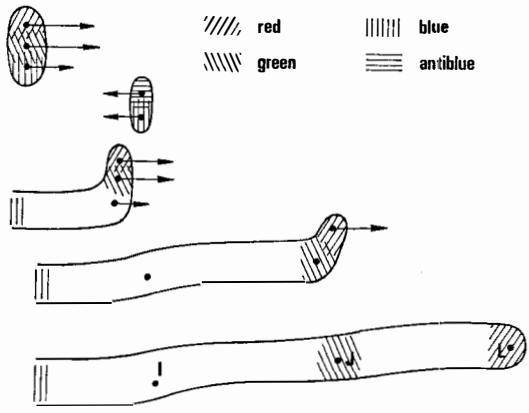

Fig.14: Color flux tube produced in a meson-baryon interaction. Only the baryon fragmentation region is shown.

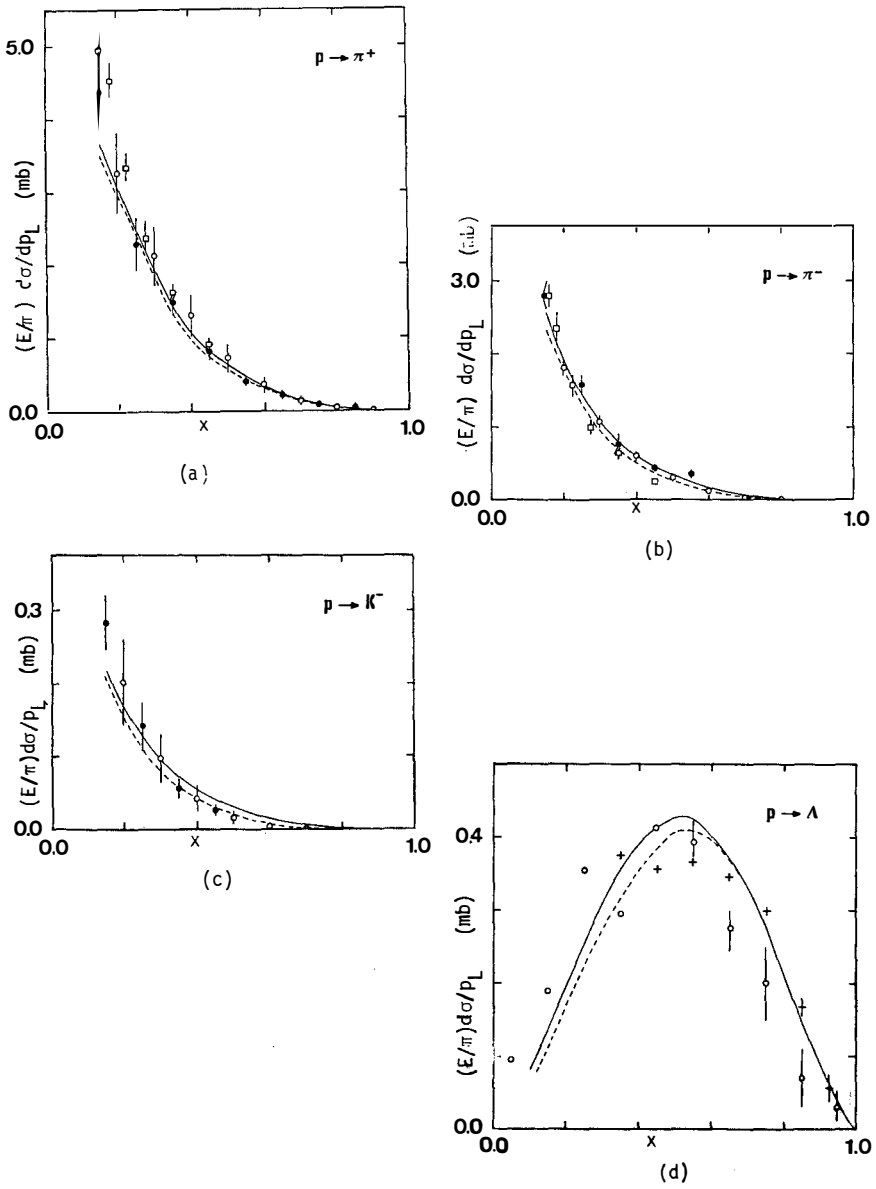

Fig.15: Inclusive π^+, k^+, p and Λ spectra in pp collisions.

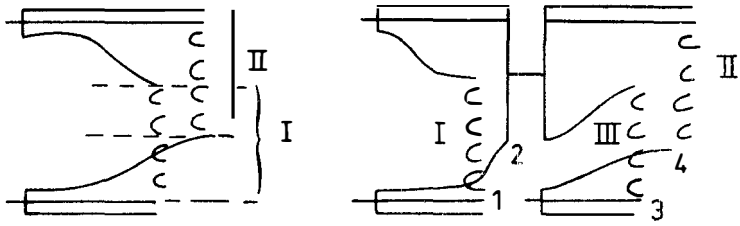

Fig.16: The mechanism of particme production in the model of ref(1). An example of a graph corresponding to two inelastic collisions within the nucleus is shown.

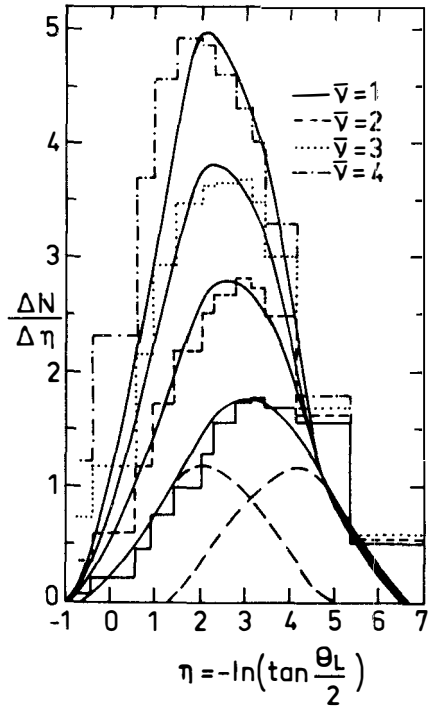

Fig.17: The rapidity distribution of charged particles in p+A → charged + X computed in ref(30).

HADRON NUCLEUS INTERACTIONS IN A DUAL PARTON MODEL

A. Capella and J. Tran Thanh Van
Laboratoire de Physique Théorique et Hautes Energies, Orsay France

presented by J. Tran Thanh Van

ABSTRACT

We describe hadron-nucleus interactions at small p_T in the framework of a dual parton model which is a generalization fo the two-chain dual-parton-model of hadron-hadron interactions introduced recently in the literature.The model (of a multiple scattering type) is formulated in the framework of the 1/N expansion in dual theories. We study the inclusive spectra of various types of secondaries for various projectiles and targets. Particular emphasis is laid on the A-dependence in the projectile fragmentation region. A comparison with available experimental data is presented.

In this short talk I would like to review briefly the main characteristics of the experimental data on high energy hadron nucleus collisions and show how these features can be understood qualitatively and quantitatively in a multiple scattering type model based on dual topological unitarization (D.T.U.) scheme and parton picture.

I. MAIN FEATURES OF THE EXPERIMENTAL DATA.

a) absence of cascading

The main characteristic of hadron nucleus interactions is the absence of intra-nuclear cascade. Indeed, the ratio R_A between the average multiplicities produced on lead (A=208) and on hydrogen is only 2[1] instead of more than an order of magnitude in cascade model. This property, as remarked by K.Gottfried[2], can only be understood if most of the particles are produced long after the projectile interacts with the target, at large distances compared to nuclear sizes (i.e. >> 5-10 fermi).

b) average multiplicities

If we define

$$\bar{\nu}_h = \frac{A\ \sigma_{in}^{hp}}{\sigma_{in}^{h\,A}} \tag{1}$$

then R_A can be parametrized by a simple form

$$R_A^h = \frac{< n >^{hA}}{< n >^{hp}} = 0.5 + 0.5\ \bar{\nu}_h \tag{2}$$

independently of energy and the nature of the incident particle. See Fig.1.

Note that $\bar{\nu}$ can be interpreted as the average number of inelastic collisions of the incident hadron with the nucleons and behaves as $A^{1/3}$ for large A.

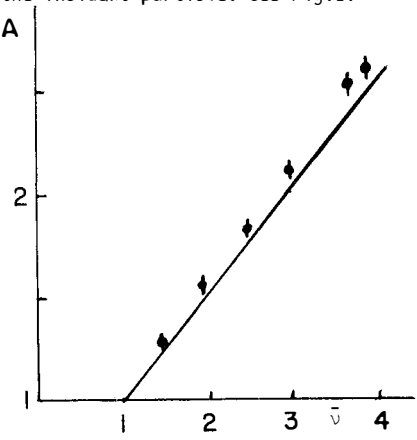

Fig.1

c) density distribution

In the central region the density of produced particles per unit of rapidity

$$\frac{dN}{dy} = \frac{1}{\sigma_{in}^{hA}} \frac{d\sigma^{hA}}{dy}$$

increases as $\bar{\nu}_h$ while it decreases in the projectile fragmentation region when the atomic number A increases. Note that

the depletion (or attenuation effect) in the projectile fragmentation region depends, for a given projectile, on the nature of the produced particle.

II. PHYSICAL BASES OF OUR MODEL.

Let us first summarize briefly the main features of our model. A more detailed description of our model is given in ref.(3).

1. It is a multiple scattering model. In this class of models, many important results such as the A-dependence of the inclusive spectra in the central region have been obtained, using only the basic assumptions of the Reggeon calculus, namely unitarity, analyticity and softness (in the sense of suppression of large p_T). However, in order to obtain a quantitative agreement with the experimental data, energy momentum conservation should be taken into account[4-5]. Indeed, in the case of n inelastic collisions, the secondaries produced in each inelastic interaction do remove energy from the beam and the laboratory energies E_i of each inelastic collision are related through the energy conservation relation

$$\sum_{i=1}^{n} E_i = E \qquad (3)$$

where E is the energy of the projectile.

The results , of course, depend on the partition of beam energy between the various inelastic collisions. Using a naive assumption: the beam energy is equally divided into the various collisions (equipartition), A.Capella and A.Krywicki[5] show that the situation is greatly improved. However, ignoring the hadron constituents, the multiple scattering model does not allow to study the difference between various types of produced particles.

2. It takes into account the nature of hadron constituents. Knowing the hadron constituents it is possible to compute the momentum distributions in terms of dominant Regge singularities[6-7]. These distributions determine completely the way in which the available energy is shared between the various inelastic collisions with the nucleus. The energy partition function is then completely fixed by the nature of the hadron constituents and is no longer arbitrary.

Let us take some examples .

In the case of hadron-hadron scattering[8], each hadron splits into two colored fragments, each of which forms with the complementary colored fragment of the other hadron, a chain or string of particles. See fig.2. The energy partition function is given by the quark momentum distribution which is, in the case of a valence quark,

$$\rho(x) \approx 1/\sqrt{x} \quad \text{for} \quad x \simeq 0 \tag{4}$$

The hadronization of the colored system is described by the fragmentation functions which can be extracted, for example, from e^+e^- annihilation or deep inelastic scattering processes. The produced hadronic spectrum, which is obtained by convoluting the momentum distribution and the fragmentation functions, is completely fixed without any arbitrary parameters.

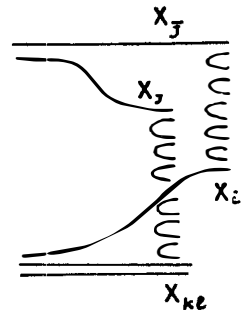

Fig. 2

In the case of hadron-nucleus scattering[9], we still have contributions coming from diagrams of Fig.2. This corresponds to single scattering or impulse approximation . However, due to combinatorial factors, multiple scatterings are enhanced and have to be taken into account. An example with double scattering with four chains is shown in Fig.3. The joint momentum distribution of the four fragments (valence quark at x_1, sea quark and antiquark at x_2 and x_3 and diquark at x_4) in the case of an incident proton is given as follows:

$$\rho(x_1,x_2,x_3,x_4) \simeq \frac{1}{\sqrt{x_1}} \frac{1}{x_2} \frac{1}{x_3} x_4^{1.5} \delta(1-x_1-x_2-x_3-x_4) \tag{5}$$

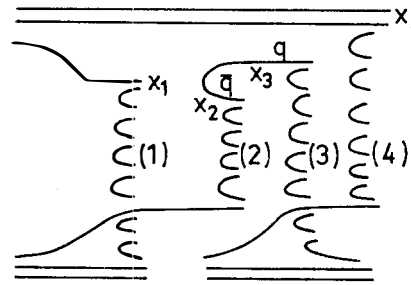

Fig.3

For an n inelastic collisions, the diagram will contain 2n chains which can be classified into four different types. In the case of a proton projectile, chain 1(4) is stretched between a valence quark (diquark) of the proton projectile and a diquark (valence quark) of a nucleon of the target. Chains 2 and 3 involve respectively antiquark (quark) of the projectile sea and valence quark (diquark) of a nucleon of the target. Obviously, in a diagram with n inelastic collisions, chains 1 and 4 appear only once whereas chains 2 and 3 appear n-1 times. Let us denote by $N_\alpha^h(y;n)$, with α = 1,2, 3, 4 the rapidity density of hadrons of type h produced in a chain of type α. The rapidity density distribution of the produced hadron h is given by

$$\frac{dN}{dy}^{pA \to hx}(y) = \frac{1}{\sigma_{in}^{hA}} \frac{d\sigma^{pA \to hx}}{dy} = \sum_{n=1}^{A} \frac{\sigma_n}{\sigma_{in}} \left[N_1^h(y,x) + N_4^h(y,n) + (n-1)\right]$$

$$\left[N_2^h(y,n) + N_3(y,n)\right] \qquad (6)$$

where σ_n is the cross-section for n inelastic collisions with n different nucleons of the target and

$N_i^h(y,n) = \int dx \int dx' \; \rho_n^c(x) \; \rho_n^{c'}(x') \; N_{cc'}[y,x,x']$ $\rho_n^c(x)$ is the momentum distribution of the quark c, obtained by integrating the joint momentum distribution on all x variables except x_c, and $N_{cc'}$ is the density distribution of the chain formed by the system cc'.

III. QUALITATIVE FEATURES OF OUR MODEL.

It can be seen from eq.(6) that the final hadronic spectrum depends on σ_n. However, a numerical computation of $N_\alpha^h(y;n)$ shows that throughout the central region, these functions depend very little on n. Therefore, in this region, the final spectra is essentially independent of σ_n. Indeed, neglecting for a moment the n-dependence of N_α^h one gets:

$$\frac{dN}{dy}^{pA \to hx}(y) = N_1^h(y) + N_4^h(y) + (\bar{\nu} - 1) \left[N_2^h(y) + N_3^h(y)\right] \qquad (7)$$

where $\bar{\nu} = A \, \sigma_{in}^{pp} / \sigma_{in}^{hA}$. In order to obtain the above equation, one has to use the definition of σ_{in}^{hA} ($\sigma_{in}^{hA} = \sum_{n=1}^{A} \sigma_n$), together with the well-known A.K.G. cancellation[13]:

$$\sum_{n=1}^{A} n \, \sigma_n = A \, \sigma_{in}^{pp} \qquad (8)$$

Thus, all sets of σ_n's will yield identical results provided that $\bar{\nu}$ is unchanged.

In order to illustrate the qualitative features of the model let us continue to examine the simple situation in which the N_α^h are independent of n. In this case N_1^h and N_4^h are the same as in a proton-proton collision. If one furthermore makes the very crude assumption that $N_1^h(y) = N_3^h(y)$ (in view of the similarity between chains 1 and 3) and neglects chain 2 (which has at present energies a low average invariant mass), one obtains from eq.(7) (independently of σ_n)

$$R \equiv \left[\int \frac{dN^{hA}}{dy} dy\right] \Big/ \left[\int \frac{dN^{hp}}{dy} dy\right] = \frac{1}{2} + \frac{1}{2} \bar{\nu} \qquad (9)$$

where the integral extends throughout the central region . Eq (9) is in rather good agreement with present experimental data.

Notice that, when the energy increases, all the chains develop energy

independent plateaus of identical height and it is no longer possible to neglect the contributions of chains 2. In this high energy limit, we obtain

$$R = \bar{\nu}$$

This result is a general consequence of unitarity in multiple scattering models provided the triple Pomeron coupling is neglected.

Let us now discuss the projectile fragmentation region (large x). The only important contribution comes from the chain 4 which contains the fast diquark. Therefore, if $N_4(y;n)$ was independent of n in the projectile fragmentation region, one would get:

$$R(y) = \left(\frac{dN}{dy}\right)^{hA} : \left(\frac{dN}{dy}\right)^{hp} = 1 \qquad (10)$$

Experimentally, this ratio decreases when A or y increases. This effect can be qualitatively understood as due to energy momentum conservation. Indeed, when $n > 1$ more than one inelastic collision occur. The sea quarks which initiate the supplementary chains do remove energy from the fastest particle in chain 4. As n increases, the length of the chain becomes shorter and $N_4(y,n)$ decreases. This depletion or attenuation effect [$R(y) < 1$] with increasing A at fixed y is larger for larger y . This feature agrees qualitatively with the experimental data. At a quantitative level, the distribution of energy among the various inelastic collisions within the target, which results from the joint momentum distribution function, is, in our approach, very different from the equipartition ansazt of ref(3).Indeed, in the equipartition case, the average laboratory energy of each inelastic collision is E_{lab}/n where n is the number of inelastic collisions. In the present model, the constituents at the projectile ends of chains 2 and 3 (sea quarks) have, in average, very small values of x. Therefore, each inelastic collision (producing chains 2 and 3) removes very little energy from the fast constituents in chain 4. As a result, the attenuation obtained in the present model, in the projectile fragmentation region, is much smaller than in the equipartition case. Such a behaviour seems to be in better agreement with experiment.

IV. COMPARISON WITH EXPERIMENTAL DATA.

In this section we compare the results of our calculation to the experimental data. The A-dependence of the data is correctly described throughout the central and the projectile fragmentation region. In the target fragmentation region, the theoretical A-dependence is not large enough compared with the experimental data, since we do not incorporate in our model the effect of slow secondaries, which is particularly important in this region.

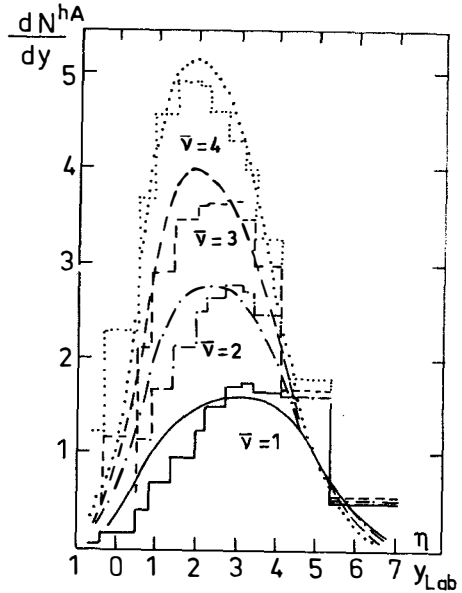

Fig.4: Charged differential multiplicities in proton nucleus collisions at $\sqrt{s}$ = 200 GeV.

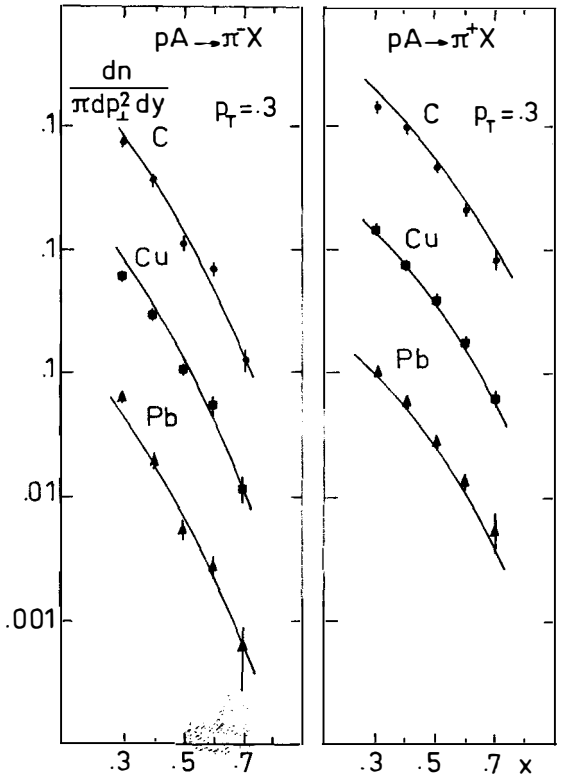

Figs: 5-6: Pion production differential multiplicities in proton nucleus collisions at p_L=100 GeV.

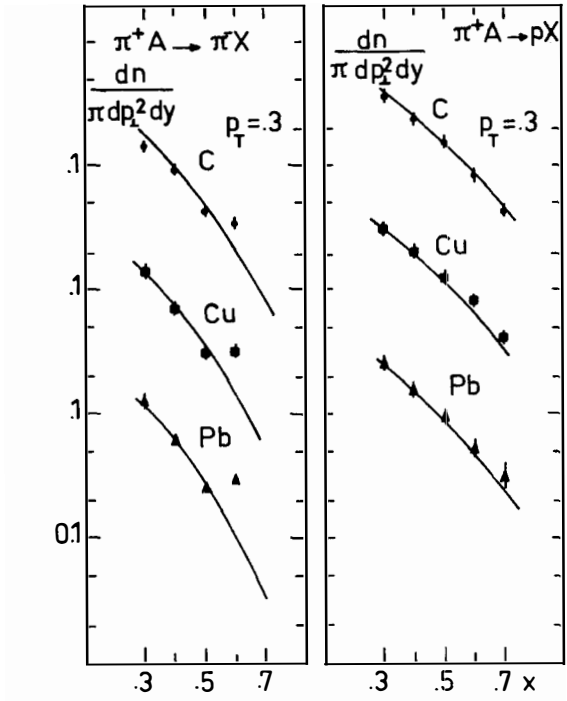

Fig.7

Fig.8

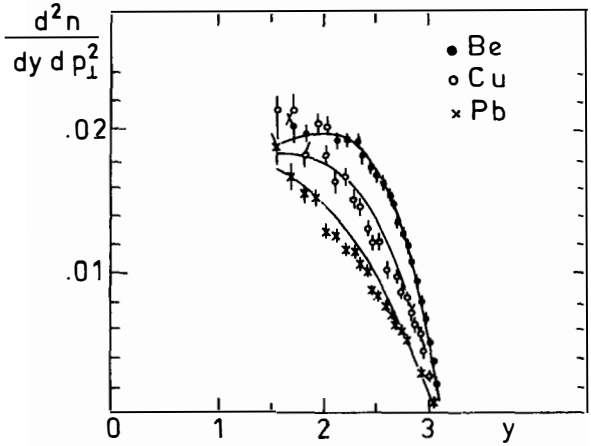

Fig.9: Differential multiplicities at p_L=300 GeV for Λ^0 production at p_T=0.

- A dependence

As stated before, we need to know the fragmentation functions of quarks and diquarks into hadrons.

For pion production, fragmentation functions can be extracted either from e^+e^- collisions or deep inelastic lepton scattering. Thus, our calculation involves only well-known quantities and does not have any free parameter. Comparison with data[10] on $p + A \rightarrow$ charged particles + X, $p + A \rightarrow \pi^+ + X$, $\pi^+ + A \rightarrow \pi^- + X$ in Figs 4 to 7 show that the agreement is excellent.

In the other cases (p,Λ, $\bar{\Lambda}$, K production) fragmentation functions are not known. However, they can be determined in a phenomenological way by fitting the inclusive spectra of the produced hadron in a collision on hydrogen or on a specific nuclear target. The model will then determine the corresponding spectra for a collision on any nucleus. Results are compared with data[10-11] in Figs 8 to 11 for $\pi^+ A \rightarrow p\,X$, $p\,A \rightarrow K^o_s X$, $p\,A \rightarrow \bar{\Lambda} X$ and $p\,A \rightarrow \Lambda X$

As we have seen, the A dependence of hadronic spectra obtained in our model is in good agreement with the experimental data. In what follows we will show that our results are good not only for large nuclei (where summing on all possible inelastic interactions can hide the defects of the model) but also for small nuclei such as deuteron where separation between single scattering and double scattering have been made experimentally.

- Double scattering in π^- d interactions .

Recently, H.Lubatti and co-workers[12] have been able to separate the double scattering cross-section of π^- on deuteron from the single scattering. It is particularly interesting as it allows us to compare with experimental data the n dependence of the rapidity density distribution $N^h_\alpha(y,n)$. In Fig 12 the experimental values for the following ratio are shown:

$$S = \frac{1}{\sigma(DS)} \frac{d\sigma\,(DS)}{dy_{lab}} \Big/ \frac{1}{\sigma(\pi p)} \frac{d\sigma(\pi\, p)}{dy_{lab}}$$

where DS means double scattering.
Using the AGK cutting rules, the amount of double scattering resulting from the four chain diagrams is given by $2\,\delta\sigma$ where $\delta\sigma = \sigma_n + \sigma_p - \sigma_d$, and the rest of double scattering is expected to give rapidity distributions similar to single scattering[12]. Therefore, one has:

$$\frac{dN(DS)}{dy} = \frac{2\,\delta\sigma}{\sigma(DS)} \left[N_1+N_2+N_3+N_4\right]^{n=2} + \left(1 - \frac{2\,\delta s}{\sigma(DS)}\right) \left[N_1+N_2\right]^{n=1}$$

and

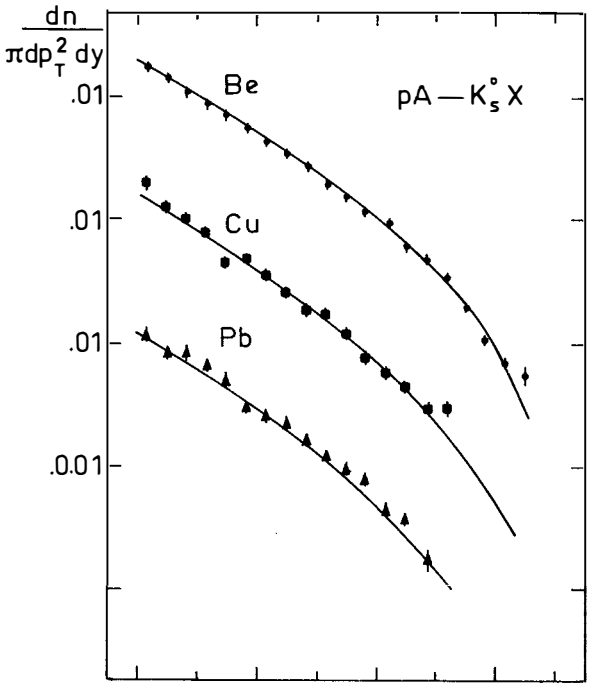

Fig.10

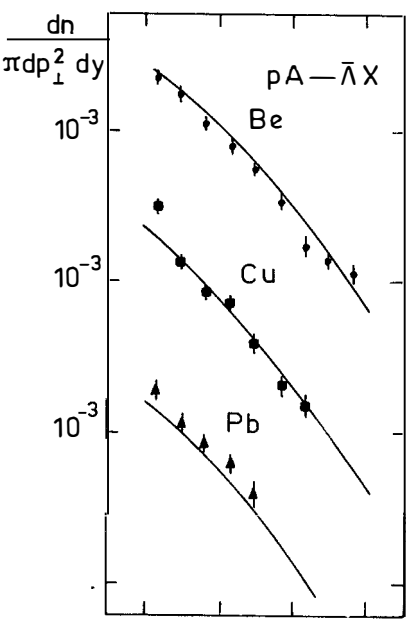

Fig.11

Differential multiplicities at p_L=300 GeV for k_s^o and $\bar{\Lambda}$ production at p_T = 0

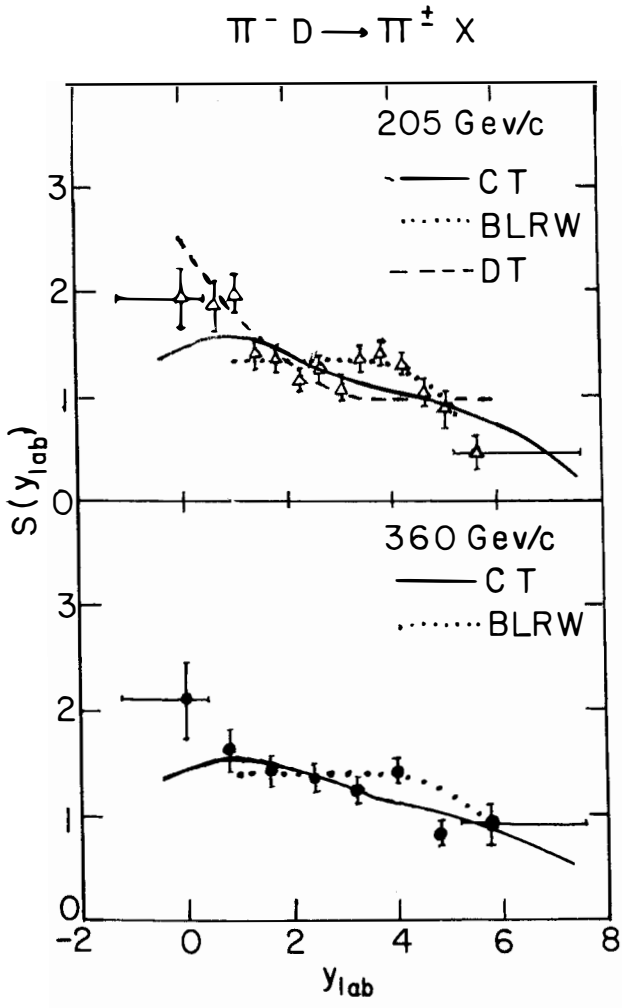

Fig. 12 : Ratio (y_{lab}) of the double scattering to single scattering rapidity distribution of $\pi^- d \rightarrow \pi^{\pm} X$ and comparison with theoretical predictions. Full lines are our predictions (CT), dotted lines are from Baker et al (Nuclear Physics B181, 365, 1981) and dashed lines are from A. Dar and J. Tran Thanh Van (Phys. Lett. 65B, 455 (1976).

$$S = 1 - \frac{2\,\delta s}{\sigma(DS)} + \frac{2\,\delta s}{\sigma(DS)} \left[N_1+N_2+N_3+N_4\right]^{n=2} \Big/ \left[N_1+N_2\right]^{n=1}$$

Using $\delta s = 1,83$ mb $\quad \sigma(DS) = 5,48$ mb at 205 GeV

and $\delta s = 1,81$ mb $\quad \sigma(DS) = 5,89$ mb at 360 GeV

we obtain an excellent agreement with experiments as shown in Fig.12.

REFERENCES

1. W.Busza, Proceedings of the XIIth Rencontre de Moriond (1977) vol.II, p.129.
2. K.Gottfried, Phys.Rev.Lett.32, 957 (1974).
3. A.Capella and J.Tran Thanh Van, Particles and Field (in press).
4. A.Capella and A.Kaidalov, Nucl.Phys. B11 (1976), 477.
5. A.Capella and A.Krzywicki, Phys.Lett.67B (1977), 84; and Phys.Rev. D18 (1977) 3357.
6. P.Aurenche, L.Gonzalez-Mestres, Phys.Rev.D18(1978) 2995.
   C.Chiu and S.Matsuda, Nucl.Phys. B134(1978)463.
7. A.Capella, U.Sukhatme and J.Tran Thanh Van in Proc. of the XIIth Rencontre de Moriond (1979), ed. J.Tran Thanh Van.
   H. Minekata, Phys.Rev. D20(1979) 1656.
   G.Cohen-Tannoudji, A.El Hassouni, J.Kalinowski, O.Napoly and R.Peschanski, Phys.Rev. D21 (1980) 2689.
   A.El Hassouni and O.Napoly, to be published in Phys.Rev.
8. A.Capella, U.Sukhatme, Chung-I Tan and J.Tran Thanh Van Phys.Lett. 81B (1979) 68 and A.Capella, U.Sukhatme and J.Tran Thanh Van, Particles and Fields 3 (1980)68.
9. A.Capella and J.Tran Thanh Van, Phys.Lett. 93B (1980) 146.
10. C.Hallewell et al., Phys.Rev.Lett. 39 (1977)1499.
    A.E.Brenner et al., "A-dependence of Inclusive Hadron Scattering at 100 GeV", Madison, Wisconsin, July 1980.
11. K.Heller et al., Phys.Rev. D16 (1978) 2737 and P.Skubic, Phys.Rev. D18(1978) 3115.
12. H.Abramowicz et al., Nuclear Phys. B181(1981) 365.

CORRELATIONS BETWEEN FRAGMENTATION BARYONS AND MESONS PRODUCED IN HIGH-ENERGY pp INTERACTIONS

F. C. Erné
NIKHEF, Amsterdam*

ABSTRACT

Data from the Amsterdam-Louvain-Northwestern collaboration at the CERN ISR are presented. Inclusive production of baryon-meson and meson-meson pairs in the proton fragmentation region has been measured. Production of resonances is important at high-x. The data are compared with predictions from current fragmentation models.

Résumé:

Nous présentons des résultats de l'experience R607 par la collaboration Amsterdam-Louvain-Northwestern. Nous avons étudié la production inclusive de pairs de baryon-meson et meson-meson dans la région de fragmentation. La production de résonances est importante à haute x. Nous faisons une comparison avec quelques modèles de fragmentation courantes.

* Present address: SLAC, Bin #57, P. O. Box 4349, Stanford, CA 94305.

The idea that x-distributions of fragmentation products may reveal something on the quark-structure of the colliding particles and on the nature of the collision process has some history already. Interpretation of spectra in terms of Triple-Regge amplitudes, quark-fragmentation, quark recombination and counting rules have spurred interest in the measurement of simple production spectra of the type $pp \to {}^{B}_{m} + X$, of spectra of particle pairs, etc.

We will present here new data on particle pairs with both particles in the same fragmentation region, and examine whether these are consistent with one or more of the current pictures for particle production.

The data have been obtained in the R607 ISR experiment by the Amsterdam-Louvain-Northwestern collaboration with two forward spectrometers of modest angular aperture between 17 and 38 mrad wrt the ISR beams, but with good momentum resolution (a few % $\Delta p/p$, depending on the field integral and the momentum) and particle identification by three threshold Cerenkov counters, two of which were split into two halves. A sketch of the layout is presented in Fig. 1. The device has been described in a paper on opposite side $\pi\pi$ correlations.[1] Most of the data to be described here, have been collected with just one of the two spectrometers. A hardware coincidence then required at least two particles to enter the spectrometer aperture. Unambiguous π/K separation was obtained for meson momenta above 3-5 GeV, depending on the Cerenkov gases (FC 114 or CO_2), by requiring consistency with measured Cerenkov counter pulse heights, for the following particle pairs: $\pi^{\pm}\pi^{\pm}$, $\pi^{+}\pi^{-}$, $p\pi^{\pm}$, $\Lambda\pi^{\pm}$, $\Lambda K^{\pm}$, and $\Delta^{++}\pi^{\pm}$.

The $p\pi$ and $\pi\pi$ data have been taken at the highest ISR energy, $\sqrt{s}$ = 62 GeV, the other data were collected also at two lower energies, $\sqrt{s}$ = 53 and 45 GeV. The Λ and Δ^{++} were identified by their mass peaks in $p\pi$ spectra. Subtraction of background is necessary. It is a minor problem for Λ's and introduces a larger uncertainty in $\Delta\pi$ spectra. In total 2700 Λ-meson pairs have been analyzed, 1300 $\Delta\pi$ pairs and 4000 $\pi\pi$ pairs.

The invariant masses accepted in the spectrometer aperture are small. The mass of the $\pi\pi$-pairs remains below the ρ-mass, for example. Nevertheless,

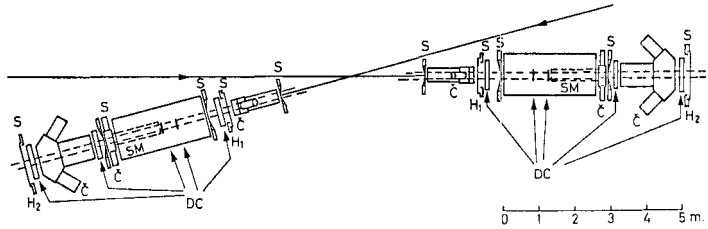

Fig. 1. Schematic top view of the R607 double spectrometer.

surprisingly large contributions were measured from resonances as Λ_{1520}, Σ^{+}_{1385}, and Δ^{++}_{1232}. Their cross sections will be subject of another communication.[2] The data presented here, have been evaluated in the form of particle-pair ratios. The transverse momentum of particles detected in the spectrometer on the average increases with x and ISR energy. Particle ratio's are notoriously insensitive to changes in transverse momentum, as we have shown in previous work.[3] We consequently ignore this variable.

The invariant mass spectra for $\Delta^{++}\pi^{\pm}$ and $\Lambda K^{\pm}$ reveal no outstanding features. The $\Lambda\pi^{\pm}$ spectra are shown in Fig. 2. The data have not been divided by the spectrometer acceptance. The $\Lambda\pi^{+}$ spectrum is dominated by Σ^{+}_{1385} production. The $\Lambda\pi^{-}$ spectrum contains at best a weak Σ^{-}_{1385}. If we do a background subtraction with events around the Σ-peaks we arrive at

$$R\left(\Sigma^{-}_{1385}/\Sigma^{+}_{1385}\right) = 0.07 \pm 0.05 \quad \text{at} \quad x = 0.73 \quad .$$

This value is compatible with earlier measurements at the ISR.[4] We will ignore a possible mass-dependence in the $\Lambda\pi^{-}/\Lambda\pi^{+}$ ratio.

Fialkowski[5] has argued that in the quark recombination model at high-x, the Σ^{+} resonance itself would be suppressed wrt the $\Lambda\pi^{+}$ continuum, because it contains one valence-quark less. The present data are at high-x, $\langle x \rangle = 0.76$, and show no especially weak Σ^{+}_{1385}. The clarity with which the resonance peak stands out might be attributed to a reduction of the combinatorial background at high-x and thus be unrelated to quark recombination arguments.

In Fig. 3 we show the x-distributions of the ratio's $\Lambda K^{+}/\Lambda\pi^{+}$ and $\Lambda K^{-}/\Lambda\pi^{-}$. They are nearly equal at medium-x. At high-x the $\Lambda K^{-}/\Lambda\pi^{-}$ ratio is suppressed (ΛK^{-} requires double strange production) where as the $\Lambda K^{+}/\Lambda\pi^{+}$ ratio rises, presumably because of the $p \to \Lambda K^{+}$ fragmentation channel.

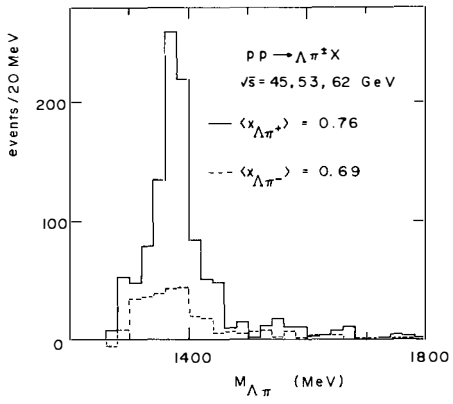

Fig. 2. Invariant mass spectrum of $\Lambda\pi^{\pm}$.

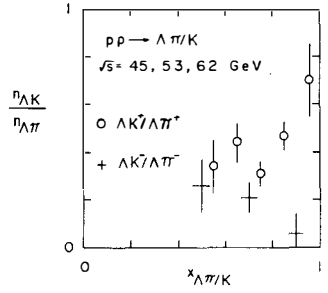

Fig. 3. Ratios $\Lambda K^{+}/\Lambda\pi^{+}$ and $\Lambda K^{-}/\Lambda\pi^{-}$ vs x. The data have been corrected for meson decay in the spectrometer.

Figure 4 shows the ratio's $\Lambda\pi^-/\Lambda\pi^+$, $\Lambda K^-/\Lambda K^+$, and $\Delta^{++}\pi^+/\Delta^{++}\pi^-$. All these ratio's drop to a small value near x = 1. Fits to the x-dependence with $(1-x)^n$ (which assumes that the ratio's are equal at small x) yield values n of the order of 1. These ratio's thus give evidence for symmetry around the proton charge, indicating that fragments from the colliding proton on the average not only account for nearly all of the initial momentum, but also of the charge.

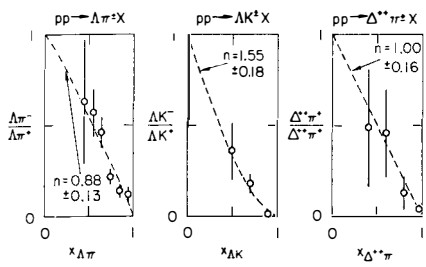

Fig. 4. The ratios $\Lambda\pi^-/\Lambda\pi^+$, $\Lambda K^-/\Lambda K^+$, and $\Delta^{++}\pi^+/\Delta^{++}\pi^-$ vs x.

One can try to derive n from Triple-Regge or quark-counting arguments. In Table I the values of n are compared with the prediction of various current fragmentation models. From that table one concludes that none of these predictions can account for the measured x-dependence. One may argue though, that the x-range over which n is determined extends well outside the region where the Triple-Regge approximation should be valid.

TABLE I

Values of n in $(1-x)^n$, $x = x_1 + x_2$

Pair Ratios	$\Lambda\pi^-/\Lambda\pi^+$	$\Lambda K^-/\Lambda K^+$	$\Delta^{++}\pi^+/\Delta^{++}\pi^-$
Exp R607	0.88 ± 0.13	1.55 ± 0.18	1.00 ± 0.16
Gunion Pointlike Counting Rules[6]	2	4	4
Valence Counting Rules[1]	2	2	2
Triple-Regge Model (exotic/nonexotic exchange)	≥ 2	≥ 4	≥ 4

Charge symmetry in production spectra around the proton charge can be further tested in $p\pi^+$ vs $p\pi^-$ events. We present the $p\pi^+/p\pi^-$ ratio in terms of the reduced x for the pion:

$$\tilde{x}_\pi = x_\pi / (1 - x_p)$$

Figure 5 shows that the ratio is compatible with 1 for $\tilde{x}_\pi > 0.6$. For lower $\tilde{x}_\pi$-values the ratio steeply increases. The reason is easily found if one looks at the $p\pi$ invariant mass spectra. Figure 6 shows that there is considerably more Δ^{++} than Δ^0 production. In fact a calculation of the spectrometer mass-acceptance by combining p and π tracks from different events shows that the data are compatible with the absence of Δ^0 production (dominance of Δ^{++} production in the

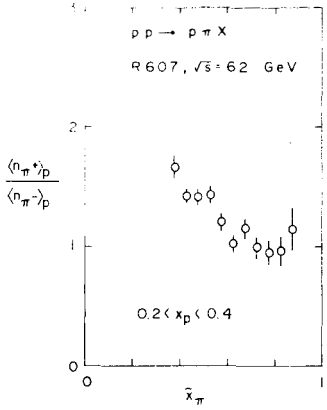

Fig. 5. The π^+p/π^-p ratio vs $\tilde{x}_\pi = x_\pi/(1-x_p)$.

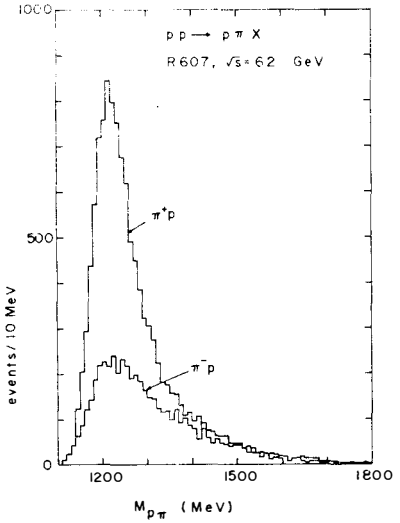

Fig. 6. Invariant mass distributions of identified pπ events. The π^- distribution is compatible with the computed spectrometer mass-acceptance. It therefore shows no evidence for Δ^0 production.

specific $p \to p\pi^+\pi^-$ channel is known from earlier ISR data[7].)

Low values of $\tilde{x}_\pi$ correspond to low values of $M_{p\pi}$, as for the small opening angle of the spectrometer the pπ-mass can be calculated approximately from:

$$M^2_{p\pi} \simeq M^2_p\left(1 + x_\pi/x_p\right) = M^2_p\left[1 + \tilde{x}_\pi(1-x_p)/x_p\right]$$

Abundant Δ^{++} production makes that the π^+/π^- ratio with a proton trigger deviates from the statistical average value 1.

The study of pion production at relatively high values of x in conjunction with other particles appears to provide a good testing ground for fragmentation models. Experimentally there is the severe problem of identifying high-x π^+ in $\pi\pi$ pairs because of the huge p/π^+ ratio at high-x. If another baryon is recorded (Δ^{++}, Λ or p) this problem disappears. In the R607 experiment a pion-pair was required to give signals in agreement with expectation in five Cerenkov counter cells.

In the field of two-pion production there are other data available and we examine first the degree of consistency with our results. Figure 7 shows the π^+/π^- ratio vs x in $pp \to \pi X$ from the present experiment compared with results from a bubble chamber experiment.[8] Note that our ratios are lower, presumably

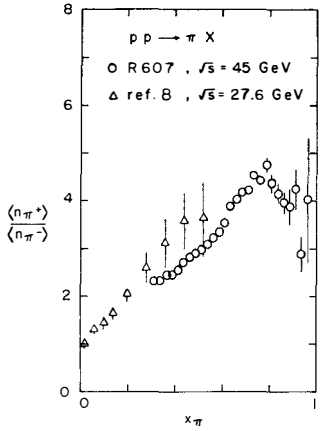

Fig. 7. The π^+/π^- ratio in pp → πX at $\sqrt{s}$ = 45 GeV compared with results from a bubble chamber experiment.

because contamination from K and p has been removed to a larger extent.

Figure 8 shows two-pion ratios compared with the results from the same bubble chamber experiment and also another ISR experiment.[11] Wherever there is disagreement our data have a smaller amount of π^+. This is consistent with the contamination problem we just identified in single-pion production, but there are also differences in the π-π mass range covered.

The x-dependence of single-pion production spectra is similar to the x-dependence of valence quark structure functions derived from deep-inelastic scattering experiments. This has led to the interpretation that fast valence quarks of the proton and slow sea-quarks combine to form pions.[9] The increase with x of the π^+/π^- ratio then would be connected with the ratio of u/d-quark structure functions. The data presented in Fig. 7 extend the x-range covered in an earlier ISR experiment.[10] A speculation by Ochs[9] that the ratio would reach the value of 5 at x = 1 seems no longer tenable.

The trend of the two-pion data is interesting and nontrivial. The $\pi^+\pi^+/\pi^-\pi^-$ and $\pi^+\pi^-/\pi^-\pi^-$ ratios increase rapidly at high-x and the $\pi^+\pi^-/\pi^+\pi^+$ ratio stays constant independent of the discrepancy mentioned. Lockman et al.[11] remarked that these trends would fit in a recombination picture. We will explore this

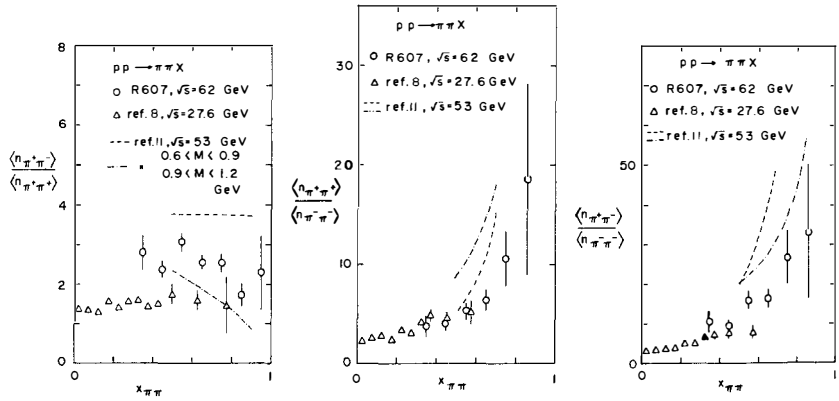

Fig. 8. Two-pion ratios in pp → ππX at $\sqrt{s}$ = 62 GeV compared with results from other experiments.

suggestion a little further. Two-pion spectra from proton fragmentation have been calculated in a recombination model that includes the systematic generation of multiquark structure functions with a modified Kuti-Weisskopf model,[12] as well as in two quark fragmentation models.[13),14] The ideas expressed in these models can be tested most easily on the spectrum of $pp \to \pi^+\pi^-X$.

Following other authors[15] the $pp \to \pi^+\pi^-X$ data can be plotted as

$$\langle n_{\pi_1} \rangle_{\pi_2} \quad \text{vs} \quad \tilde{x}_{\pi_1} = x_{\pi_1} / (1 - x_{\pi_2})$$

with π_2 being the "trigger particle." We have $\pi_1 = \pi^+$, $\pi_2 = \pi^-$ or the other way around. In both cases, we limited x_2 to $0.2 < x_2 < 0.4$ to have an accurate determination of $\tilde{x}_1$. The ratio $\langle n_{\pi^+} \rangle_{\pi^-} / \langle n_{\pi^-} \rangle_{\pi^+}$ should reveal the different quark u/d x-dependence, as for example stated in Ref. 12). Figure 9a shows this ratio together with results from calculations in Refs. 12)-14). The data show no evidence for a dependence on quark structure functions and are in agreement with complete symmetry between π^+ and π^- x-distributions as soon as they are measured in coincidence. One may note that such a symmetry would follow trivially from a statistical model of uncorrelated meson production.

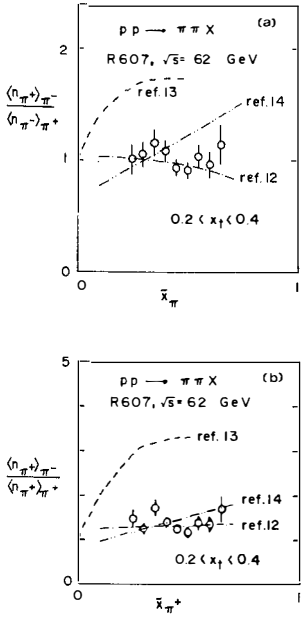

Fig. 9a,b. "Triggered" — pion ratios compared with fragmentation model predictions.

Another ratio, derived from π^+ production, with an π^+ or π^- trigger, $\langle n_{\pi^+} \rangle_{\pi^-} / \langle n_{\pi^+} \rangle_{\pi^+}$, is shown in Fig. 9b, together with predictions by the same authors.[12)-14] Note that for like-charge pairs the trigger can be either of the two pions. This changes the mean value of the pair ratio by a factor 2 wrt the result in Fig. 8.

One can try to use quark-recombination arguments to compare the π^+/π^- ratio with different "triggers." Suzuki et al.[8] compare π^- and Λ triggers. Naively the π^+/π^- ratio with a Λ trigger is expected to be 1/2 of that with a π^- trigger because one valence u-quark is taken away by the Λ-trigger, in addition to the d-quark taken by either π^- or Λ. In Fig. 10 the ratios are compared and the agreement is perfect. However it may be accidental because a similar comparison can be made between the π^+/π^- ratio with a π^+ trigger and this ratio with no trigger. In this case one would expect a factor 2 again because the π^+ trigger takes one of the two valence u-quarks away. The comparison is shown

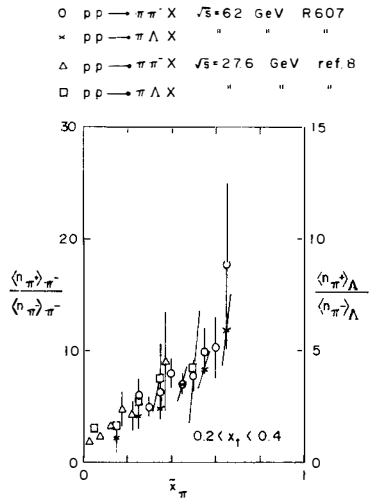

Fig. 10. π^+/π^- ratios with π^- trigger (ℓ.h. scale) and Λ trigger (r.h. scale).

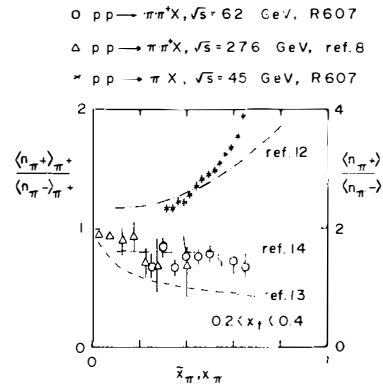

Fig. 11. π^+/π^- ratios with π^+ trigger (ℓ.h. scale) and inclusive (r.h. scale).

in Fig. 11 and this time there is no agreement. The predictions from Refs. 12)-14) for the π^+ triggered ratio are also shown.

From these few examples we learn that naive expectations may not necessarily describe the two-pion data and neither does one of the rather sophisticated models. One is led to ask what is wrong with the simple approach of describing pion production in proton fragmentation as a process in which the proton is excited and subsequently decays with a certain multiplicity distribution. (The present data indicate that one would have to include the production of low-mass baryonic resonances.) After all such a description is likely to apply to diffraction dissociation.

The R607 experiment may provide another clue here. We have taken data with a very high-x proton in one spectrometer and mesons in the spectrometer that covers the opposite fragmentation region. The diffractive particle ratios, from $p_1p_2 \to (\text{high-x p})_1 + \text{meson}_2 + X$, are compared in Fig. 12 with inclusive single particle ratios. One can conclude from the figure that charge ratios and K/π ratios are nearly identical. This is a strong indication that the same fragmentation process is dominant, whether there is single diffraction dissociation or not.

I thank the other members of the R607 collaboration for their cooperation in presenting their data. I thank A. Capella for pointing out the existence of Ref. 12) to me.

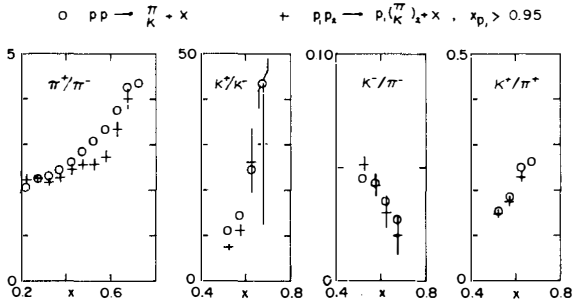

Fig. 12. Comparison of meson ratios for single diffraction dissociation and inclusive particle production at $\sqrt{s}$ = 45 GeV.

REFERENCES

1) G. J. Bobbink et al., Phys. Rev. Lett. 44, 118 (1980), see also Proceedings of the XIVth Rencontre de Moriond - Session I, Les Arcs, Savoie, France, March 11-23, 1979, p. 597.

2) A preliminary account was presented by M. Block et al., Contributed to the International Conference on High Energy Physics, Geneva, Switzerland, June 1979, CERN-EP 79-82, July 1979.

3) M. G. Albrow et al., Nucl. Phys. B73, 40 (1974).

4) S. Erhan et al., Phys. Lett. 85B, 447 (1979).

5) K. Fialkowski, Acta Phys. Pol. B11, 659 (1980).

6) J. F. Gunion, Phys. Lett. 88B, 150 (1979).

7) L. Baksay et al., Phys. Lett. 53B, 484 (1975).

8) A. Suzuki et al., Contributed to the XXth International Conference on High Energy Physics, Madison, Wisconsin, 1980, KEK preprint 80-16, September 1980.

9) W. Ochs, Nucl. Phys. B118, 397 (1977); and K. P. Das and R. Hwa, Phys. Lett. 68B, 459 (1977).

10) J. Singh et al., Nucl. Phys. B140, 189 (1978).

11) W. Lockman et al., Phys. Rev. Lett. 41, 680 (1978).

12) E. Takasugi, Proceedings of the 11th International Symposium on Multiparticle Dynamics, Bruges, Belgium, June 1980, p. 141.

13) B. Andersson et al., Department of Theoretical Physics, Lund University, LU TP 80-5, May 1980.

14) Y. Ishihara and C. Iso, Department of Physics, Tokyo Institute of Technology, TIT/HEP-56, August 1980.

15) E. Lehman et al., Phys. Rev. D18, 3353 (1978); E. de Wolff et al., Contributed to the International Conference on High Energy Physics, Geneva, Switzerland, June 1979.

TOPOLOGICAL SUPERSYMMETRY AND HADRON CROSS SECTIONS

B. Nicolescu
Division de Physique Théorique*, Institut de Physique Nucléaire, 91406 Orsay
and LPTPE, Université Pierre et Marie Curie, Paris, France

ABSTRACT : We show that the Dual Topological Unitarization (DTU) theory of hadron interactions directly leads , at the zeroth order of the topological expansion, to certain relations between hadron cross-sections, in nice agreement with experimental data. A new topological suppression mechanism is shown to play an important dynamical role. We also point out a new topological supersymmetry property, which leads to realistic experimental consequences.

RESUME : Nous montrons que la description topologique des interactions hadroniques à l'aide de deux surfaces bidimensionnelles (une surface "quantique", fermée, et une surface "classique", à bords) conduit, à l'ordre le plus bas, à certaines relations entre les différences des sections efficaces totales et inclusives antihadron-nucléon et hadron-nucléon, en bon accord avec l'expérience.

*Laboratoire associé au C.N.R.S.

I. Introduction

In this talk we will present some recent results obtained in collaboration with P. Gauron and S. Ouvry[1]. We discuss here only the main results. The technical details can be found in Ref.1.

The DTU approach to hadron physics is quite successful in the case of the mesons[2]. However, its extension to the baryons is intrinsically difficult, because of the complex nature of the topological complexity index which governs the topological expansion.

Recently, important progress has been made in this direction.

It has lead to the necessity of considering a new "quantum surface"[3,4] which is conceived as the source of the internal quantum numbers and is responsible for confinement. This new topological variety has to be considered in addition to the "classical surface" which describes the space-time structure of hadron collisions[5]. An important step forward has been the elaboration of a coherent method for incorporating spin into the topological expansion[6].

Finally, a complete topological expansion theory, involving both the "classical" and "quantum" surfaces, has been formulated[7]. An interesting novel feature of the theory of Ref.7 is the explicit embedding of the Landau unitarity graphs on the classical surface, which now appear in addition to the familiar Harari-Rosner graphs[8].

In this talk we want to show that the lowest entropy level of the theory is able to determine a great deal of physics for an important class of phenomena. Namely, we applied the DTU formalism to the study of hadron total and inclusive cross-sections and discovered that many empirical regularities, some of them known for a long time[9], seem to have a general topological foundation.

II. Short description of the general DTU framework

Hadron interactions are described in the theory of Ref.7 by a pair of surfaces, a "quantum" surface and a "classical" surface.

The quantum surface is 2-dimensional, orientable and closed. The last property is related to the conservation of internal quantum numbers. The quantum surface is the space of structures, the space of confined constituents. The classical surface is, like the quantum surface, 2-dimensional and orientable. Its distinctive feature is the fact that it is bounded and

multisheeted. The boundary of the classical surface is obtained via its intersection with the quantum surface. This intersection leads to graphs which are very similar to the familiar Harari-Rosner graphs[8]. However, the quark lines of these new graphs describe neither the flow of the energy-momentum of the quarks nor their flavors, but are consistently associated with ± 1/2 spin indices of the quarks[6]. The space-time aspects of hadron collisions are described by Landau graphs embedded on the classical surface, each Landau arc being associated with the energy-momentum four vector of a particle.

A proper mathematical definition of the overall topological entropy index involves a triangulation of the quantum surface. The triangle -the 2-dimensional simplex- appears naturally as the "basic" object of the present construction.

The fundamental, "primordial" level of the topological expansion is the zero-entropy level, where the nonlinearity of the bootstrap problem is concentrated[7]. The definition of hadrons has to be made at this lowest entropy level. All higher-orders have to be obtained via appropriate connected sums (i.e. unitarity products) of the zero-entropy amplitudes.

At zero entropy the quantum surface is a sphere and the classical surface is a multi-plane surface with a "3-feathered" structure. The Landau graph is a univertex graph and is located on the classical surface.

At the same zero-entropy level, the particles are represented by "discs", i.e. by bounded regions of the quantum sphere without topological singularity points (in simpler words, a "disc" is a region of the sphere whose perimeter touches itself only once). The perimeter of a disc gives the "identity" of a hadron, being a representation of flavor indices. Namely, the hadrons are represented by the "discs" shown in Fig.1(a)-(c). The orientations of the triangles in Fig.1 correspond to an overall patchwise orientation of the quantum sphere[7].

The peripheral triangles describe the topological flavor of the quarks (e.g. by attaching orientations on their edges one obtains eight possible "topological flavors"[7]). The orientations of the interiors of the peripheral triangles distinguish between quarks and antiquarks. The peripheral triangles are not discs -they have incomplete boundaries. Therefore they cannot appear as physical states. The topological quarks are, by construction, confined.

On the classical surface, hadrons are represented by the configurations shown in Fig.1 (d)-(f). By "opening" the vertices of Fig.1 (d)-(f) and by an appropriate projection onto a plane one obtains the meson, baryon and baryonium propagators in their usual Harari-Rosner form (Fig.2 (a)-(c)),

supplemented, of course, with Landau arcs (one per particle) and junctions lines (0 for mesons, 1 for baryons and 2 for baryoniums).

The orientation of the interior of the classical surface can be in agreement or in disagreement with the orientation of its boundary. It is precisely this 2-valued topological degree of freedom which allowed Stapp[6] to include the spin of the quark in the DTU theory.

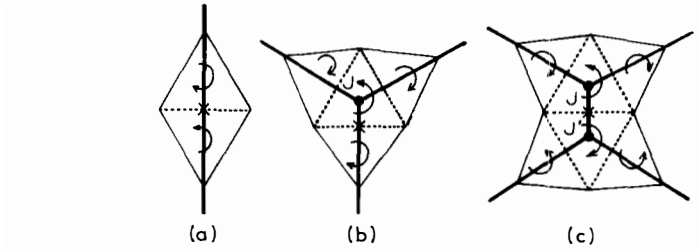

Fig.1 (a)-(c). Meson, baryon and baryonium discs on the quantum surface. The heavy solid lines represent the traces left by the corresponding intersection between the classical surface and the quantum surface. The crosses denote the ends of Landau arcs and the points J denote the ends of junction lines.

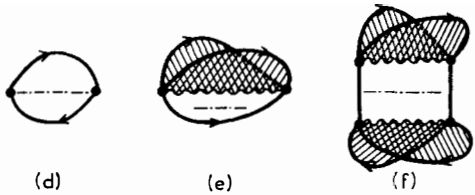

Fig.1 (d)-(f). The classical surfaces corresponding to the propagators of the particles shown in Fig.1 (a)-(c). The dashed-dotted lines denote Landau arcs and the wiggly lines denote junction lines.

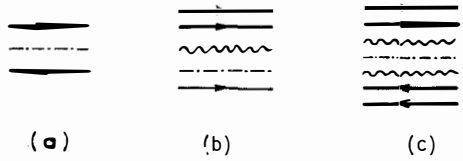

Fig.2 (a)-(c). Hadron propagators in a Harari-Rosner form, obtained by "opening" the vertices in Fig.1 (d)-(f).

III. The supersymmetry property of the topological amplitudes relating bosons to fermions

In the theory of Ref.6 the spectrum of hadrons consists only of ordinary mesons (M_2), ordinary baryons (B_3) and baryoniums (M_4). The four types of zero-entropy 3-particle topological amplitudes ("coupling constants") are shown in Fig.3 (a)-(d) and the six types of zero-entropy 4-particle amplitudes are shown in Fig.4.

In Ref.1 we showed that the zero-entropy bootstrap leads naturally to a topological "supersymmetric" solution at this level of the topological expansion, in which the 3-particle topological amplitudes of Fig.3 are related to each other. Our demonstration is based upon the Stapp's M-function formalism[6].

An M-function is an analytic function of the particle four-momenta characterizing a given process, apart from isolated singularities described by the Landau graphical rules ; it also has a well-defined crossing-principle property. It is not immediately equal to an S-matrix connected part but is related thereto by an explicit momentum-dependent spin-index transformation. Finally it depends on particle spin indices α_k which transform independently of the values of the momenta in changes of Lorentz frames of reference.

For a topological M-function, each α_k is a collection of two-valued indices belonging to (0, 1/2) or (1/2,0) spinor representations of the Lorentz group ; a single such index is attached to each peripheral triangle of the corresponding particle disc. At the zero-entropy level the spin dependence then simply reduces to a product of Kronecker deltas, one for each Harari-Rosner (HR) line joining two mated peripheral triangles (i.e. triangles which share all their vertices). One may then associate a single spin index to each HR line. The momentum dependence of a topological M-function resides in a separate factor F.

The spin dependence of the M-functions has the essential property of transitivity (self-reproducing) in zero-entropy connected sums. In effect, spin and momentum are thus "decoupled" in zero-entropy dynamics.

It is this basic property which enabled us to demonstrate[1] that the zero-entropy bootstrap equations have a unique solution in which the masses of corresponding M_2, B_3 and M_4 states are equal. In particular, we obtain the equalities of Figs. 3 and 4.

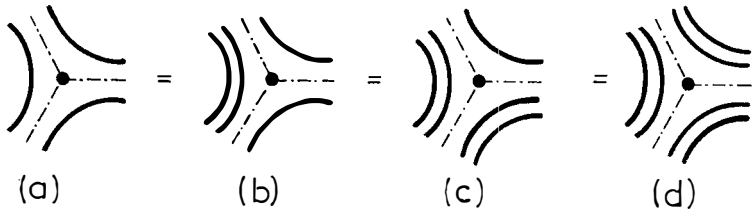

Fig.3. The supersymmetry property for the four possible types of zero-entropy 3-particle amplitudes, as seen on the classical surface. The quark-spin line directions are not indicated. The dashed-dotted lines represent Landau arcs.

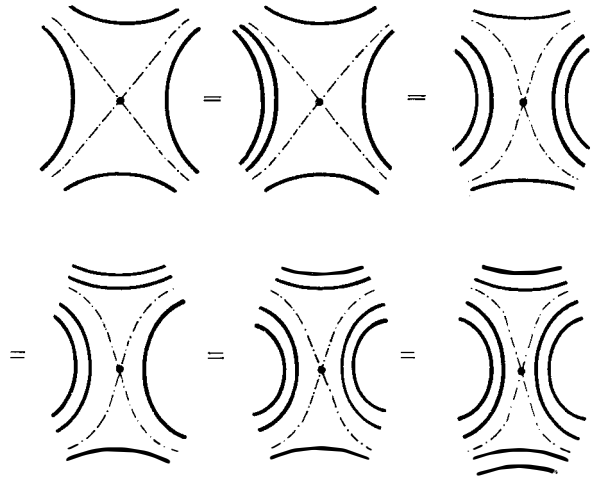

Fig.4. The supersymmetry property for the six possible zero-entropy amplitudes, as seen on the classical surface. As in Fig.3, the quark-spin line directions are not indicated.

One might note that the topological sypersymmetry is a property peculiar to the zero-entropy level of the topological expansion. Supersymmetry must be broken by higher orders of the topological expansion.

IV. Topological supersymmetric structure of hadron cross sections

It is well known that the channels having the quantum numbers of the Pomeron are strongly affected by the higher orders of the topological expansion[2]. Since we want to test the zeroth order of the topological expansion, we choose to deal with the amplitudes which are antisymmetric under crossing, i.e. we study the differences of the antihadron-nucleon and hadron-nucleon total cross-sections

$$\Delta\sigma_{HN}(s) \equiv \sigma_{\bar{H}N}(s) - \sigma_{HN}(s)$$

$$= \frac{1}{2m_N p_L} \text{ Im } F^{(-)}_{HN \to HN}(s,t = 0) \qquad (1)$$

where m_N is the mass of the nucleon.

At zero entropy, the discs which represent the initial particles on the one hand and the final particles on the other are contracted in all possible ways in order to build channel-discs. Then, by unitarity, the amplitudes are obtained by gluing together these channel-discs, so as to cover the quantum sphere. It can happen that different gluing operations lead to the same pair of quantum and classical surfaces. This topological equivalence leads to a well defined topological structure for $\Delta\sigma$. For example, it can be seen from Fig.5 that in the $p\bar{p}$ s-channel there are five possible ways of gluing together a proton p and an antiproton $\bar{p}$ so that we obtain a $p\bar{p}$ channel-disc of the baryonium type. Then there are five connections of one channel-disc with itself (the amplitude in Eq.(1) is elastic) which lead to the same quantum and classical surfaces. (Here u-d symmetry is naturally assumed). Each baryonium channel-disc is dual to a channel-disc of the ordinary meson type in the t-channel.

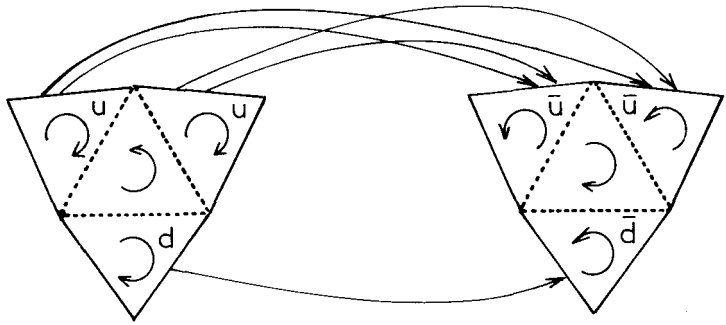

Fig.5. The five possible ways of obtaining the $p\bar{p}$ s-channel baryonium disc by the contraction of a quark-antiquark pair.

One can obviously also form $p\bar{p}$ s-channel discs of the ordinary meson type, which are dual to t-channel baryonium type discs. But we established above that, for the case of baryonium channel-discs, one obtains five identical contributions. The fact that the baryonium is now in the t-channel is irrelevant, the s and t channels being identical in $p\bar{p} \to p\bar{p}$ scattering.

It is clear that no channel-disc can be formed in pp scattering (the gluing is performed only via quark-antiquark pairs). The disc contribution to σ_{pp} is therefore zero.

From the above considerations, we finally obtain

$$\Delta\sigma_{pp} = 5\,\sigma_{M_2}^{(M_4)} + 5\,\sigma_{M_4}^{(M_2)} \tag{2}$$

where σ_{M_2} and σ_{M_4} correspond to quantum spheres whose t-channel discs are of the ordinary meson (M_2) and baryonium (M_4) types ; the upper index of σ refers to the nature of the s-channel discs.

In a similar way, we obtain, for the first generation of quarks (u and d) :

$$\Delta\sigma_{pn} = 4\,\sigma_{M_2}^{(M_4)} + 4\,\sigma_{M_4}^{(M_2)} \tag{3}$$

and

$$\Delta\sigma_{\pi p} = -\,\Delta\sigma_{\pi n} = \sigma_{M_2}^{(B_3)} \tag{4}$$

From Eqs.(2) and (3) we obtain the following relation between $\Delta\sigma_{pp}$ and $\Delta\sigma_{pn}$:

$$\frac{1}{5}\,\Delta\sigma_{pp} = \frac{1}{4}\,\Delta\sigma_{pn} \tag{5}$$

It is important to note the absence of the term σ_{M_4} in $\Delta\sigma_{\pi p}$ and $\Delta\sigma_{\pi n}$ which is a consequence of one of the most remarkable manifestations of the topological selection rules[10] : the non-communication on the sphere between baryonium and ordinary meson channels.

The relation (5) between $\Delta\sigma_{pp}$ and $\Delta\sigma_{pn}$ appears to be in nice agreement with the experimental data (see Fig.6).

We can make a similar analysis of the cross-sections involving s quarks. Namely, we treat s as an index with an unspecified topological form (in other words, we allow for a possible breaking of the SU(3) flavor symmetry at the lowest entropy level) and we assume once again that the hadron interaction proceeds via the minimum possible entropy contribution. We then obtain the relation

$$\frac{1}{2}\,\Delta\sigma_{Kp} = \Delta\sigma_{Kn} \tag{6}$$

The relation (6) between $\Delta\sigma_{Kp}$ and $\Delta\sigma_{Kn}$ is also in nice agreement with the experimental data (see Fig.7).

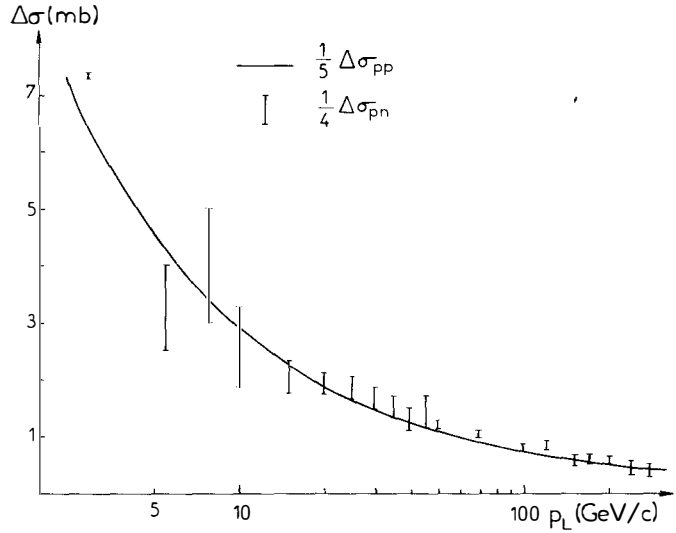

Fig.6. The experimental verification of Eq.(5). The solid curve represents the best fit of $\Delta\sigma_{\bar{p}p}$ obtained via the best fit of the $\bar{p}p$ and pp total cross sections themselves. This curve is subject to an overall $\sim$ 5% error (not shown in the figure). The I represent raw $\Delta\sigma_{\bar{p}n}$ data.

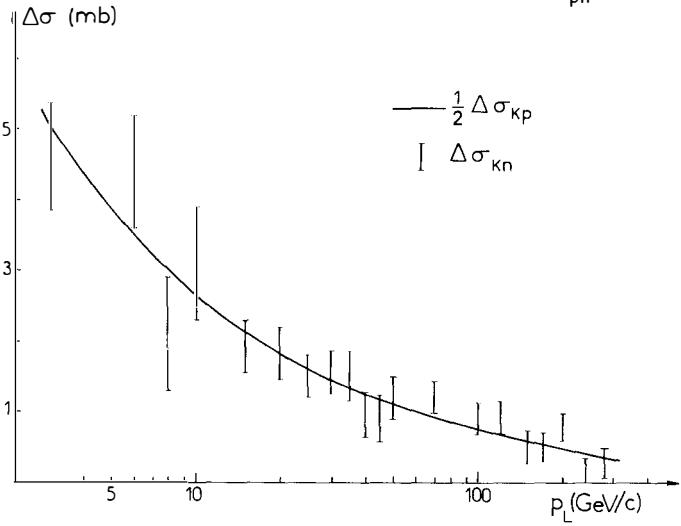

Fig.7. The experimental verification of Eq.(6). The solid curve is affected by an overall $\sim$ 10% error.

Topological supersymmetry has important consequences at the practical level. For example, the second equality belonging to the series of relations shown symbolically in Fig.4 implies that

$$\sigma_{M_2}^{(B_3)} = \sigma_{M_2}^{(M_4)} \equiv \sigma \tag{7}$$

We therefore find, from Eqs.(2),(4) and (7) that

$$\frac{1}{5}\Delta\sigma_{pp} - \Delta\sigma_{\pi p} = \sigma_{M_4}^{(M_2)} > 0 \tag{8}$$

The relation (8) is supported in a spectacular manner by the experimental data (Fig.8). The non-vanishing of the difference of cross sections involved in Eq.(16) can be regarded as one of the most convincing phenomenological proofs of the existence of baryonium (see Ref.1 for a detailed discussion of this fact).

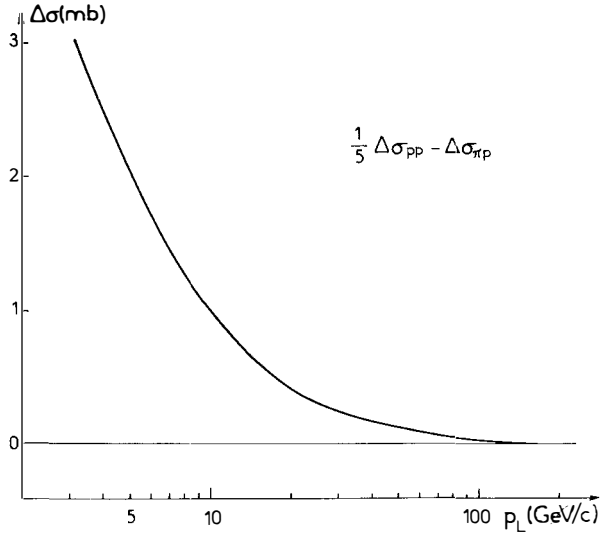

Fig.8. The experimental verification of Eq.(8) as a hint for the existence of baryonium.

By means of the Mueller generalized optical theorem, we can make the same topological analysis in the case of the inclusive reactions $\pi^{\pm}p \to \pi^{\pm}X$ and $p^{\pm}p \to \pi^{\pm}X$ in the fragmentation region of the proton target, where there exists a coherent set of data. From a topological point of view, we will consider the pion to belong to the fragmentation region of the proton when the pion disc shares at least one quark-triangle with the proton discs.

We obtain the following relations[1] :

$$\frac{1}{2}\Delta\sigma_{pp\to\pi^-X} - \Delta\sigma_{\pi p\to\pi^-X} = \frac{1}{2}\sigma_{M_4}^{(M_2)'} > 0 \tag{9}$$

$$\Delta\sigma_{pp\to\pi^-X} + \Delta\sigma_{\pi p\to\pi^+X} = \sigma_{M_4}^{(M_2)'} > 0 \tag{10}$$

$$\frac{1}{2}\Delta\sigma_{pp\to\pi^+X} - \Delta\sigma_{\pi p\to\pi^-X} = 2\sigma_{M_4}^{(M_2)'} > 0 \tag{11}$$

$$\Delta\sigma_{pp\to\pi^+X} + \Delta\sigma_{\pi p\to\pi^+X} = 4\sigma_{M_4}^{(M_2)'} > 0 \tag{12}$$

and, in the case of s quarks,

$$\Delta\sigma_{Kp\to\pi^+X} = 0 \quad . \tag{13}$$

(Here σ'_{M_4} has the same meaning as σ_{M_4}).

These relations are in general agreement with the experimental data[11,12]. As an example, we show in Fig.9 that the vanishing of $\Delta\sigma_{Kp\to\pi^+X}$ predicted by Eq.(13) is compatible with the data for 8 GeV/c $\lesssim p_L \lesssim$ 150 GeV/c.

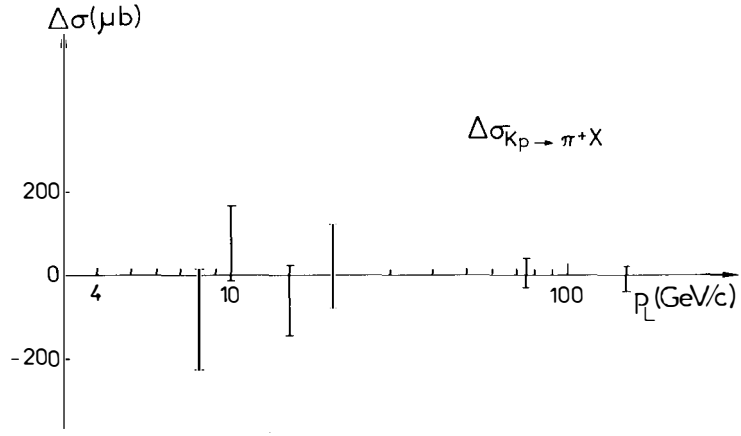

Fig.9. The experimental verification of the vanishing of $\Delta\sigma_{Kp\to\pi^+X}$ predicted by Eq.(13).

An important feature of our analysis has to be stressed here. In the case of the total cross sections, the relations (2)-(6) can also be obtained in models which combine the usual Harari-Rosner duality diagrams (where the flavors are associated with the classical surface) with the additive quark model[13]. However, in the case of the inclusive cross-sections the information coming from the lowest order of the theory of Ref.7 is different from that obtained from the previous models. The difference comes essentially from the explicit consideration of the Landau graphs on the classical surface. The topological mechanism for the suppression of the graphs involving intersections between Landau lines and junction lines was previously ignored. For example, if one ignores these intersections, one obtains a non-vanishing value for the difference between the cross sections for $K^-p \to \pi^+X$ and $K^+p \to \pi^+X$.

V. Conclusions

One can conclude that the recent generalized DTU theory of Chew and Poenaru[7] leads, at its lowest topological entropy level, to a realistic description of an important piece of experimental data : differences of total and inclusive hadron cross-sections.

Of course, we expect higher-order corrections to have important dynamical consequences, via a renormalization of propagators and couplings. However, the overall agreement of our zero-entropy relations with the experimental data suggests that these corrections are such that the "scale" imposed by the topological zero entropy on the amplitudes which are anti-symmetric under crossing has to be globally preserved. The "primordial" world could well be a topological world.

Acknowledgements

I thank Drs. P. Gauron and S. Ouvry for their very pleasant collaboration. I am grateful to Profs. L. Montanet and J. Tran Thanh Van for the kind invitation to give this talk.

References

1) P. Gauron, B. Nicolescu and S. Ouvry, Orsay preprint IPNO/TH 80-58 (1980), submitted to "Physical Review".
2) G.F. Chew and C. Rosenzweig, Phys. Reports 41, 263 (1978).
3) G.F. Chew, Nucl. Phys. B151, 237 (1979) ; Phys. Lett. 82B, 439 (1979).
4) G.F. Chew, B. Nicolescu, J. Uschersohn and R. Vinh Mau, CERN preprint TH-2635 (1979).
5) G. Veneziano, Nucl. Phys. B74, 365 (1974) ; Phys. Lett. 52B, 220 (1974).
6) H.P. Stapp, Lawrence Berkeley Laboratory preprints LBL-10774 (1980) and LBL-11770 (1980).
7) G.F. Chew and V. Poenaru, Phys. Rev. Lett. 45, 229 (1980) ; Lawrence Berkeley Laboratory preprint LBL-11433 (1980) and private communications.
8) H. Harari, Phys. Rev. Lett. 22, 562 (1969) ; J. Rosner, Phys. Rev. Lett. 22, 689 (1969).
9) J.G. Rushbrooke and B.R. Webber, Phys. Reports 44, 1 (1978).
10) B. Nicolescu, "Topological interpretation of multiquark states", Invited talk at the Workshop "From collective states to quarks in nuclei", Bologna, 25-28 November 1980, "Lecture notes in physics", Springer Verlag, Vol. 137, edited by A.M. Saruis and H. Arenhövel.
11) V. Flaminio et al., "Compilation of cross-sections", (I) π^- and π^+ induced reactions, (II) K^- and K^+ induced reactions, (III) p and $\bar{p}$ induced reactions, CERN-HERA 79-01, 79-02 and 79-03.
12) E. Beier et al., Phys. Rev. D17, 2864, 2875 (1978).
13) H.J. Lipkin, Phys. Rev. Lett. 16, 1015 (1966) ; Phys. Reports 8, 175 (1973).

CLASSICAL RADIATION OF GLUON JETS AND HARD DIRECT PHOTONS IN A HADRONIC MEDIUM

I.M. DREMIN

ABSTRACT :

Radiation of gluons by a hadron colliding with another hadron (or with a nucleus) is treated according to the classical radiation theory and compared with radiation of photons by an electron.

It is shown that the observation of jets of secondary particles (in multiple production hadron-hadron processes) copiously produced at the same polar angle would imply both a strong confinement of quarks and Čerenkov-like radiation of gluons by them. There is not such a ring structure for photons.

Some experimental events with emission of groups of pions within narrow rings at large cms angles are presented.

I would like to show that specific multiple production processes may exist with an emission of groups of pions at the same polar angle so that the ring structure reminding of Čerenkov rings of light should be pronounced. In a single event one would observe the hadronic jets correlated in such a way that their centres are distributed on the same circle in the plane perpendicular to the collision axis (i.e. in the target diagram). For different events these circles coincide. Such processes if observed would supply us with knowledge of the confinement mechanism and of some properties of gluons.

Any hadron is a spatially extended object with a radius of the order of the inverse pion mass m_π^{-1}. Therefore the collision of any particle with a hadron can be considered as its passage through such an object. For example, one could ask whether the pointlike electron piercing through hadron emits photons inside this hadron. By analogy, one can consider the problem of emission of gluons by a constituent quark of a hadron colliding with another hadron (or with a nucleus).

I shall treat both problems according to the classical radiation theory restricting myself to the processes with small energy losses (much smaller than the primary energy) but with small enough radiation wavelengths (much smaller than the hadron size). In this case one can consider a hadron as some hadronic medium. The propagation of radiation waves inside this medium can be described by the hadronic index of refraction (analogous to the index of refraction of usual media)[1,2] :

$$n(\omega) \equiv 1 + \Delta n(\omega) = 1 + \frac{2\pi N}{\omega^2} F(\omega) \qquad (1)$$

Here ω is the frequency of the radiation, $N \approx \frac{3m_\pi^3}{4\pi}$ is the density of the scatterers (inhomogeneities) of the medium, $F(\omega)$ is the amplitude of forward elastic scattering of radiation in the medium which is normalized by the optical theorem :

$$\mathrm{Im}\ F(\omega) = \frac{\omega}{4\pi} \sigma(\omega) \qquad (2)$$

where $\sigma(\omega)$ is the total cross-section of the interaction of the radiation with the hadron.

Thus the real part of the refractivity is given by the formula :

$$\mathrm{Re}\ \Delta n(\omega) \equiv \Delta n_R(\omega) = \frac{3m_\pi^3}{8\pi\omega} \sigma(\omega)\ \rho(\omega) \qquad (3)$$

where $\rho(\omega) = \mathrm{Re}\, F(\omega)/\mathrm{Im}\, F(\omega)$.

Let us insert in formula (3) all experimentally known total cross-sections and "real to imaginary ratios" for hadron-hadron collisions. The result is demonstrated in fig. 1. One can see that qualitatively all hadronic reactions give rise

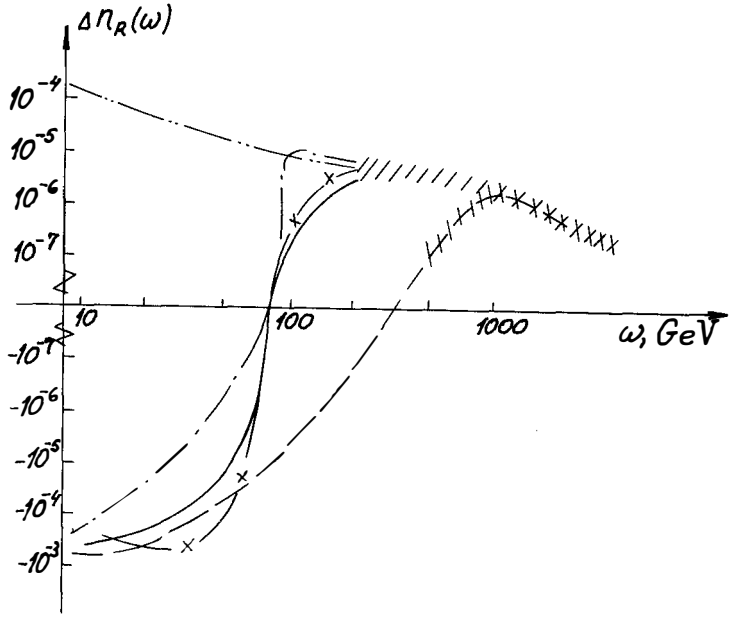

Fig. 1 : The refractivity of the hadronic medium as a function of energy (see (3)). The following experimental results are used : $\pi^{\pm}p$ - full line ; pp - dotted line ; $p\bar{p}$ - crossed line ; $K^{+}p$ - point line ; $K^{-}p$ - double point line. The shaded area indicates the dispersion relations prediction for higher energies.

to a similar behaviour of the refractivity. This statement is true at very high energies where refractivity decreases approximately as ω^{-1} with an increase in ω. At lower energies $K^{-}p$ - reactions differ from others and the zero of refractivity is slightly shifted for pp-reactions to higher energies. Besides the general decrease law there are two other common features of all the curves in fig. 1 : the refractivity is rather small ($\Delta n_R \ll 1$) and it is positive above some threshold. The last feature is an especially important one because it provides the necessary condition for Čerenkov-like radiation in such a medium.

Now let us assume the following picture for the process. The interaction of colliding hadrons is considered as the passage of quarks, carrying colored charge, through a quark-gluon medium. Due to the confinement mechanism and colorless wave-function of a hadron, quarks may not emit gluons before they enter another hadron. But once they penetrate into another hadron, their coherence is violated and each of them can emit gluons independently. Subsequently gluons turn into hadronic jets and quarks can take part in usual violent strong interactions with multiple production of low-P_T secondary particles. These stages of the process are still badly understood but one can try to calculate the properties of gluons emitted by quarks at the previous stage of their almost uniform motion inside a hadronic medium.

Since gluons are vector particles, by ignoring their self-action we can consider the entire process to be approximately analogous to the emission of photons by electrons in an ordinary medium replacing the fine structure constant α by the chromodynamic constant ($\alpha \to \alpha_c C_F$, $C_F = 4/3$). The radiation for uniform motion along a finite segment of length ℓ and with instantaneous acceleration at the beginning and the end of this segment was first calculated in ref. 3. The angular and energy distributions of the number of gluons are given by the formula:

$$\frac{dN_g}{d\omega d\theta^2} = \frac{4\alpha_c C_F}{\pi} \cdot \frac{\theta^2}{\omega} \cdot \frac{\sin^2\left[\frac{\omega\ell}{4}\left(\theta^2 - 2\Delta n_R(\omega)\right)\right]}{\left[\theta^2 - 2\Delta n_R(\omega)\right]^2} \tag{4}$$

if $\theta^2 \ll 1$, $\Delta n_R \ll 1$ and all masses are neglected compared to energies. We have assumed that the quark-gluon medium is described by the common hadronic refractivity with the above-mentioned general features.

According to formula (4) all the gluons are concentrated inside a ring in the plane perpendicular to collision axis. The hadronization of gluons is usually assumed to produce rather narrow jets of pions which will not disturb the ring structure. The ring can be observed very simply in the experiment in terms of the presence of a peak in the pseudorapidity distribution $\eta = -\log \operatorname{tg} \theta_L$ at $\theta_L \sim \sqrt{2\pi/\omega\ell}$.

Surely, a sceptic would object that this radiation is mostly caused by the abrupt start and stop of the quark. Since we know nothing about the release from confinement and the catastrophic collision of the quark at the end we could be wrong in using such stepwise functions. That is why it is desirable to consider that part of the radiation which does not depend on these assumptions and is determined by the uniform motion inside a hadron only. It is easy to treat the case of the infinite medium because for $\ell \to \infty$ one replaces in (4) :

$$\frac{\sin^2\left[\frac{\omega\ell}{4}\left(\theta^2 - 2\Delta n_R(\omega)\right)\right]}{\left[\theta^2 - 2\Delta n_R(\omega)\right]^2} \longrightarrow \frac{\pi\omega\ell}{4}\,\delta(\theta^2 - 2\Delta n_R(\omega))$$

and gets the usual Čerenkov-like contribution which is linear in ℓ and Δn_R (for $\Delta n_R > 0$).

Even though it is not so straightforward for a finite medium, one can argue that the linear in Δn_R term of the series expansion of (4) corresponds to the "faster than light" radiation. Expanding (4) one gets :

$$\frac{dN_g^{\check{c}er}}{d\omega d\theta^2} = \frac{4\alpha_c C_F}{\pi}\,\ell\Delta n_R\, f(Z) \tag{5}$$

where :

$$f(Z) = \frac{\sin Z}{Z}\left[\frac{\sin Z}{Z} - \cos Z\right] \tag{6}$$

$$Z = \frac{\omega\ell\theta^2}{4} = \frac{P_T\ell\theta}{4} = \frac{P_T^2\ell}{4} < \pi \tag{7}$$

The function f(Z) is shown in fig. 2. It displays a similar to (4) maximum at rather large angles. Therefore the ring structure of gluon emission is preserved even though the intensity of the radiation is strongly diminished.

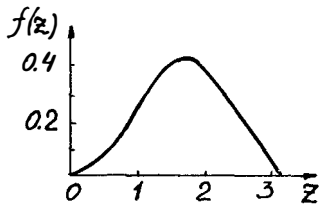

Fig. 2 : The function f(Z) (see (6), (7))

In conclusion, if the above mechanism of hadronic interactions has some rights to exist at all, one must observe the events with densely populated rings

of hadrons in the target diagrams at rather large angles. The intensity of radiation and its specific angular and energy distributions should guide us in the confinement mechanism, the behaviour of the quark-gluon medium and the properties of gluons and gluon jets*.

To elucidate these conclusions let us compare the above model with the radiation of photons by an electron piercing through the nuclear slab of the thickness ℓ. The refractivity is again determined according to formula (3) with the photoproduction amplitude installed there. Thus it behaves similar to the ones in fig. 1 but it is about 200 times smaller.

However, the most drastic difference from the above case comes from the absence of confinement for electrons and photons. If an electron moving uniformly from $-\infty$ crosses the hadronic slab and flies to $+\infty$ it radiates at all the stages and the interference of the successive radiations is very important. It results in the difference of radiation lengths inside and outside the slab which enters now into the formula for the intensity of the radiation of photons[4] :

$$\frac{dN_\gamma}{d\omega d\theta^2} = \frac{4\alpha}{\pi}\frac{\theta^2}{\omega}\sin^2\left[\frac{\omega\ell}{4}\left(\theta^2 + \frac{m^2}{E^2} - 2\Delta n_{R_\gamma}(\omega)\right)\right]\left(\frac{1}{\theta^2 + \frac{m^2}{E^2} - 2\Delta n_{R_\gamma}} - \frac{1}{\theta^2 + \frac{m^2}{E^2}}\right)^2 \quad (8)$$

Besides the trivial changes in formula (4) $\alpha_c C_F \to \alpha$ and $\Delta n_R \to \Delta n_{R_\gamma}$ (where Δn_{R_γ} is the refractivity of the hadronic medium for photons) there is a new term in the parenthesis (the subtrahend) which corresponds to the lengths of the radiation outside the slab. The small terms m^2/E^2 (m, E are the electron mass and its energy) are now taken into account to avoid the singularity of the subtrahend at $\theta^2 \to 0$. Maximum of the radiation lies now at bremsstrahlung angles $\theta \sim m/E$. There is no radiation if $\ell \to 0$ or $\Delta n_{R_\gamma} \to 0$. No ring structure at large angles is now observed and the intensity of the γ radiation is suppressed due to the strong compensation of the terms in the parenthesis.

The compensation is not so strong if the electron undergoes the drastic deflection or the deep inelastic collision inside the slab lest one should consider its path behind the slab. Then the intensity of the radiation can be described by the formula :

---

* Being aware of Sudakov form factors which strongly reduce the probabilities of quanta emission in quantum theory, one would ask whether they destroy the above results. The answer is that we consider such high values of transverse momenta where no exponential suppression exists but power-like dependences play a role. Therefore new mechanisms of particle production can be important.

$$\frac{dN_\gamma}{d\omega d\theta^2} = \frac{4\alpha}{\pi}\frac{\theta^2}{\omega}\left\{\sin^2\left[\frac{\omega\ell}{4}\left(\theta^2 + \frac{m^2}{E^2} - 2\Delta n_{R_\gamma}(\omega)\right)\right]\left(\frac{1}{\theta^2 + \frac{m^2}{E^2} - 2\Delta n_{R_\gamma}} - \frac{1}{2(\theta^2 + \frac{m^2}{E^2})}\right)^2 + \right.$$

$$\left. + \frac{\cos^2\left[\frac{\omega\ell}{4}\left(\theta^2 + \frac{m^2}{E^2} - 2\Delta n_{R_\gamma}(\omega)\right)\right]}{4(\theta^2 + \frac{m^2}{E^2})^2}\right\} \qquad (9)$$

Here ℓ is the path of the electron inside a hadron before its deflection (in the average again $\ell \sim m_\pi^{-1}$). The radiation length outside the hadron is twice smaller now (the factor 1/2 in the parenthesis) and the additional interference term appears. Once again the radiation is strongly peaked at bremsstrahlung angles $\theta \sim m/E$ but the decrease at larger angles becomes flatter because there is no complete compensation of two terms in the parenthesis. Nevertheless, there is still no ring structure at large angles.

The radiation of photons outside the hadron can be suppressed formally if the refractivity of the external medium (which has been put equal to zero in formulae (8), (9)) is infinitely large. For such a situation one obtains instead of (8), (9) formula (4), which corresponds to zero radiation lengths outside the hadronic slab which has been assumed for gluon jets due to confinement. One would get the same formula for the transition radiation in a slab with the refractivity Δn_R immersed in a medium with $n \to \infty$. For quarks immersed in their parent hadron, it means that the bag confining them acts similar to the medium with infinite index of refraction (or to the waveguide).

Therefore, one concludes that the ring structure claimed for gluon jets can appear only as a consequence of confinement.

The intensity of gluonic radiation could provide knowledge about the mechanism of the release from confinement. In any case it can hardly be lower than the intensity of Čerenkov-like radiation expressed by formula (5). The properties of the hadronic medium are represented in formulae (4) and (5) by its refractivity Δn_R.

To be more precise, one should say that the ring structure of gluon emission is determined both by the confinement and by the vector nature of gluons. It is due to the spin of gluons that the factor θ^2 appears in all the formulae. It suppresses the emission of gluons at small angles and strongly influences the position of the maximum of the radiation.

Thus the ring structure of hadronic events, if observed, reveals intriguing

properties of the internal composition of hadrons.

Let us see what indications in that direction can be extracted from available experimental data. The rings could be found at large cms angles about 60-70° for pp-scattering. Really, from (4), (5) one gets for the angles in the lab system $\theta_L \sim \sqrt{2\pi/\omega\ell} \gtrsim \sqrt{2\pi m_\pi / E_L}$, whereas $\theta_L \gtrsim \sqrt{2M/E_L}$ (M and E_L are mass and energy of a proton) corresponds to 90° in cms. In terms of pseudorapidity the peaks at $|\eta|_{cms} < 0.5$ should be observed.

The transition (or the release from confinement) radiation (see (4)) could be visible at any energy while Čerenkov-like radiation (see (5)) is allowed only at very high energies when pions of energy exceeding $\sim$ 100 GeV can be produced.

Some individual multiple production events possess the claimed structure. I have not undertaken a systematic analysis but merely by chance have been shown some target diagrams of events which display the ring structure. One of them is reproduced in fig. 3 from ref. 5 where the ten-prong pp-event at 200 GeV with eight charged particles embedded in the narrow ring at large cms angles is demonstrated. The jets of particles are also well separated. The authors[5] claim that the jet-like structure is far beyond the usual statistical fluctuations but they have not analysed ring-like events separately.

Surely, the above warning about the abrupt release from confinement should be taken seriously because formula (4), if boldly applied, would predict that almost all particles are produced by such a mechanism. Then one-particle inclusive distributions would possess marked peaks at large cms angles and large transverse momenta which is not the case at present accelerator energies*. It means that such transition radiation is diminished by more smooth release and its intensity is lower than it is predicted by (4). It is more reliable to look for Čerenkov-like events at energies higher than 10 TeV. The pseudorapidity plots for three events at energies 10^{13}, 10^{15} and 10^{16} eV from cosmic-ray studies are shown in fig. 4. The most prominent feature of all the three events are dense groups of secondary particles at large angles with almost the same values of cms pseudorapidities. Their target diagrams reveal the ring structure discussed above.

An unambiguous test can be provided by colliding $p\bar{p}$-beams at CERN. The simplest result of the above consideration is flattening and slight increase of one-particle inclusive distribution at high transverse momenta (see fig. 5).

---

* However let us note that one-particle pseudorapidity distributions reveal some substructure over a flat plateau at energies exceeding 200 GeV but this substructure can hardly be connected with the mechanism proposed.

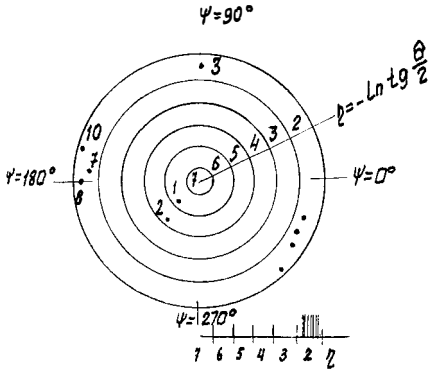

Fig. 3 : The target diagram of a single event[5] of pp-interaction at 200 GeV. Eight particles are imprisoned inside the same ring.

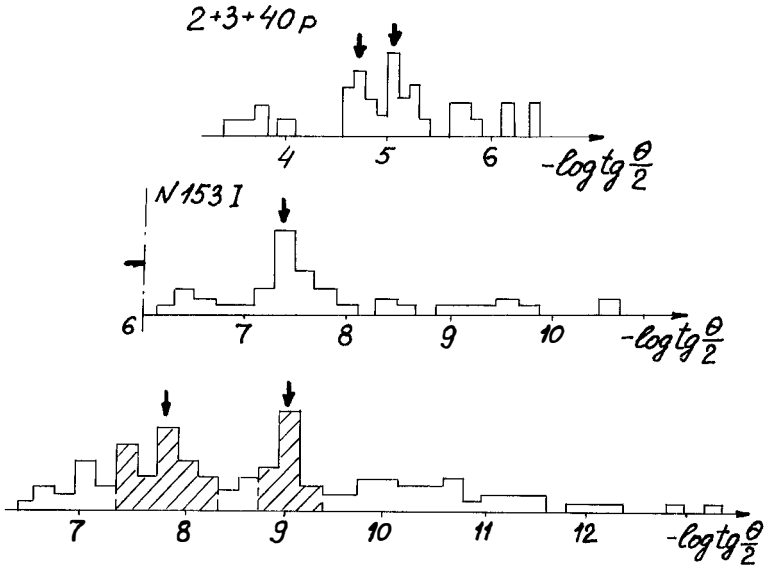

Fig. 4 : The pseudo-rapidity distributions for three cosmic ray events[6,8] at energies 10^{13}, 10^{15}, 10^{16} eV. The peaks at rather large angles are indicated by arrows.
The most completely analysed event at 10^{13} eV (2 + 3 + 40 p) reveals also usual diffraction peaks at small forward and backward angles.

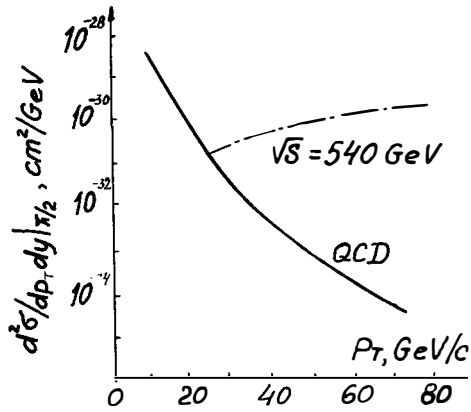

Fig.5

Fig. 5 : Čerenkov-like gluon jets can enlarge the inclusive cross-section at high transverse momenta compared to QCD predictions[9] ($p\bar{p}$ at $\sqrt{s}$ = 540 GeV)

However it would be more conclusive to study dense groups in the pseudorapidity plots of exclusive events. If such groups appear at the same large cms angles, it would be desirable to draw their target diagrams to see whether these events have a jet-like composition.

If experiments verify the proposed mechanism of gluon jet emission, we shall get a new tool for studying the internal structure of hadrons.

REFERENCES

1) Goldberger M., Watson K., Collision Theory, N.Y., 1961.
2) Dremin I.M., 1979, JETP Lett. 30, 140.
3) Tamm I.E, 1939, J. Phys. USSR 1, 439.
4) Paphomov V., 1969, Proceedings of Lebedev Physical Institute, v.44.
5) Marutian N.A. et al., 1979, Jad. Fiz. 29, 1566.
6) Alekseeva K.I. et al., 1962, Journ. Phys. Soc. Japan 17, A-III, 409.
7) Arata N., 1978, Nuovo Cim. 43A, 455.
8) Apanasenko A.V. et al., 1979, JETP Lett. 30, 145.
9) Horgan R., Jacob M., preprint TH-2824 CERN, 1980.

A STUDY OF DEEP INELASTIC HADRON HADRON SCATTERING WITH A 2π CALORIMETER TRIGGER

Bari-Krakow-Liverpool-MPI Munich-Nijmegen Collaboration

K.P. PRETZL
Max-Planck-Institut für Physik und Astrophysik
Munich, Germany

ABSTRACT

Deep inelastic hadron hadron collisions were studied with a large acceptance calorimeter trigger. The cross sections are found to be a factor 5 to 10 times larger than QCD-model predictions. The event structure is predominantly non jet like. Processes other than the scattering of two constituents appear to dominate this deep inelastic hadron hadron scattering process.

Introduction

Previous experiments at the ISR (CERN) and Fermilab[1] have investigated deep inelastic hadron hadron collisions using a single particle trigger at large transverse momenta p_T. It was found that the cross sections decrease not exponentialy with p_T but rather with a power law p_T^{-8}. This was taken as evidence for a hard scattering process. Parton parton scattering models in their original simplest version[2] would have predicted a p_T^{-4} dependence of the invariant cross sections. It was discussed that single particles at large p_T may be rare cases of jet fragmentation and further insight into hard scattering processes could be gained by triggering on particle jets using segmented calorimeters.

Three experiments at Fermilab E236[3], E260[4] and E395[5] have used calorimeters to trigger on particle jets at angles around 90^o in the cms either on one side or on two opposite sides. The solid angle acceptance of each calorimeter arm was about 1-2 sr corresponding to the expected jet size. As expected the cross sections with this so called "jet trigger" were found to be 2 orders of magnitude larger than for the single particle trigger at large p_T. However it may be difficult to verify the existence of jets because the small acceptance of the calorimeter trigger could lead to a trigger bias selecting events which simulate jets due to statistical fluctuations.

In order to circumvent some of these problems we studied deep inelastic hadron-hadron collisions with an "unbiased jet trigger" using a segmented calorimeter with a solid angle acceptance of 2π in the azimuth and 50^o to 130^o in the cms polar angle. With this trigger we selected events in which a large transverse energy $\Sigma|p_T|$ was deposited in the calorimeter. We examined these events for constituent scattering processes leading to two jets at large p_T and two forward/backward spectator jets. Large p_T jets should manifest themselves as energy clusters observed in the segmented calorimeter showing a planar event structure.

Apparatus

The layout of the experiment is shown in Fig. 1. The data presented here were obtained with 150 GeV/c π^- and 300 GeV/c p, π^- beams of $2 \cdot 10^6$ particles/sec incident on a 30 cm liquid hydrogen target using the calorimeters and spark chambers only (magnet off!). The

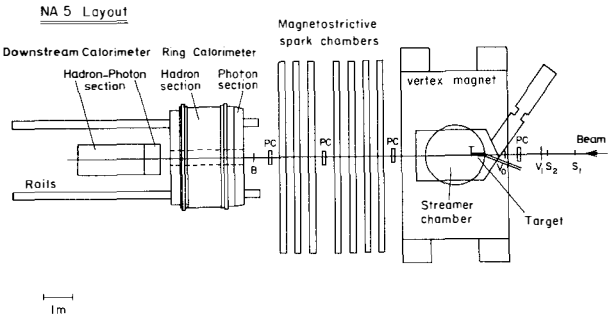

Fig. 1 Layout of the experiment

2 m streamer chamber was employed for part of the data taking to determine the multiplicity of charged particles.

The ring calorimeter, a barrel of 3 m diameter with a 56 cm central hole, has a lead-scintillator sandwich photon section (16 x 0.55 cm Pb-sheets) followed by an iron-scintillator sandwich hadronic section (20 x 5 cm Fe-sheets). Both sections are subdivided into 240 independent cells, each subtending about 9^{o} in the c.m.s. polar angle and 15^{o} in azimuthal angle. Combined wave-length shifting acrylic rods (doped with Yellow 323 and BBQ) were used to draw separated signals from the photon and hardon part of the calorimeter onto 240 pairs of photomultiplier tubes[6]. The principle of the light collection system for a calorimeter cell is shown in Fig. 2.

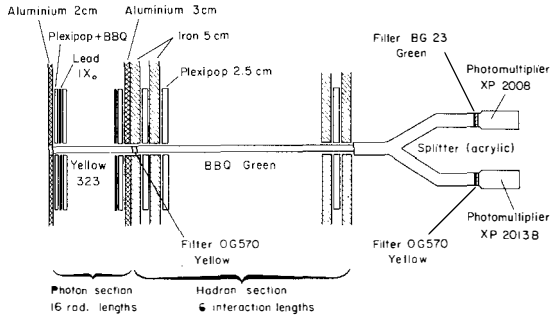

Fig. 2 The principle of the light collection system for a calorimeter cell is shown

The obtained energy resolutions were $\sigma/E = 0.23/\sqrt{E}$ for electrons and $\sigma/E = 0.71/\sqrt{E} + 0.06$ for hadrons. The downstream calorimeter, which covered the central hole of the ring calorimeter, measured the energy flow at small angles. The combined information from both calorimeters was used to reject possible background. Scaling was measured by varying the distance of the calorimeters to the target with the incident beam energy such that the ring calorimeter always covered 50° to 130° in the c.m.s. polar angle. The $\Sigma|p_T|$ trigger was derived from the sum of the analog signals of all or part of the ring calorimeter cells weighted by their radial distance from the beam axis. The shape of the trigger pulses was recorded. Occasional background triggers due to Cerenkov light produced in the acrylic rods was eliminated off-line by pulse shape analysis.

Data were taken with 3 types of trigger:

1. one arm trigger: sector of $\pi/2$ in azimuth;
2. two arm trigger: two opposite sectors each of $\pi/2$ in azimuth;
3. full calorimeter trigger: all sectors of 2π in azimuth.

Triggers similar to 1. and 2. have been used at Fermi Lab. by E236, E260 and E395. The use of trigger 3. allowed us to search for evidence of jets in an unbiased manner.

Preliminary results

The data are still preliminary since no unfolding of the calorimeter resolution has been done. Because of this the $\Sigma|p_T|$ scale uncertainty is estimated to be approximately 10%, but this is not expected to affect our conclusions. All quoted errors are of statistical nature only. Our results show the following features:

1. Cross sections
   a. The invariant trigger 1. cross section for 300 GeV pp collisions shown in Fig. 3 is in reasonable agreement with refs. 4,5 within the above discussed uncertainties. The data were analysed in a similar manner as proposed in ref. 5.

   b. We observe that the cross sections measured with trigger 3. are 10-100 times larger than with trigger 2. (see Fig. 4). If 4 jet events would dominate the trigger 2. data this ratio would be too large when comparing the solid angle acceptance of trigger 2. and 3.. The cross sections measured with trigger 3. are a factor 5-10 times larger than QCD 4-jet model[7)]

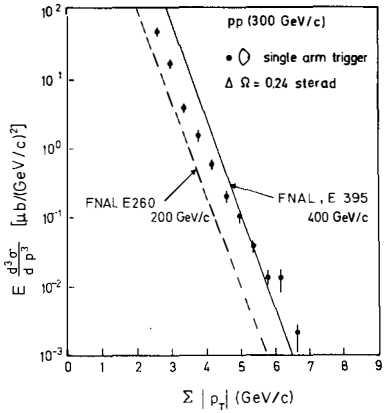

Fig. 3 Invariant cross sections measured with a sector of π/2 of the calorimeter. Results from FNAL experiments E260, E395 are shown for comparison.

predictions. The agreement with a low p_T cluster model[8] seems to be better (Fig. 4).

c. For all triggers the cross sections for pp decrease faster with rising $x_T = 2\,p_T/\sqrt{s}$ than for $\pi^- p$ (see Fig. 5). A similar dependence was observed for jet cross sections as reported by refs. 4, 5, where it has been interpreted as support for constituent scattering, since the partons in the pion contribute on average more energy to the hard scattering process.

d. The scaling parameter n was derived from the energy dependence of the trigger 1. cross section parameterized by $E\frac{d^3\sigma}{dp^3} \sim p_T^{-n}\, f(x_T)$ with $x_T = \frac{2p_T}{\sqrt{s}}$ and of the trigger 3. cross section parameterized by $\frac{d\sigma}{d\Sigma|p_T|} \sim (\Sigma|p_T|)^{-n}\, f(x_T)$ with $x_T = \frac{\Sigma|p_T|}{\sqrt{s}}$. As shown in Fig. 6 n rises from a value of 5 to 8 with increasing x_T. Constituent scattering models predict a constant n = 4 or 3 respectively while the low p_T cluster model predicts an increasing n parameter at large x_T.

2. Event structure

The planarity P of the events has been calculated by performing a principal axis analysis of the transverse momentum distribution for each event as measured by the calorimeter. The planarity was defined as P = (a-b)/(a+b) with a (b) being the sum of the squares of the projected transverse momenta to the maximum

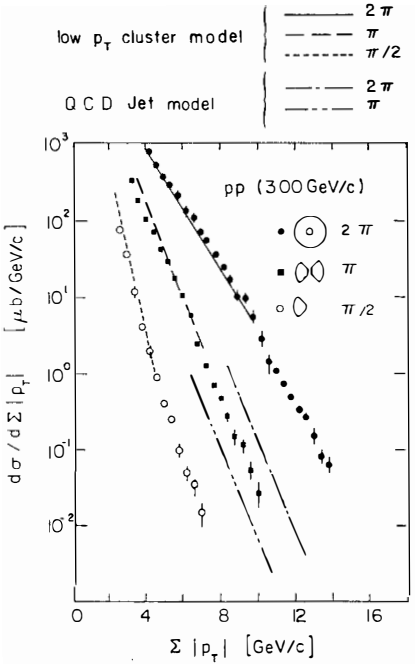

Fig. 4 Cross sections versus transverse energy $\Sigma|p_T|$ measured by the full calorimeter or some sectors of the calorimeter. Low p_T cluster- and QCD 4-jet model predictions are shown.

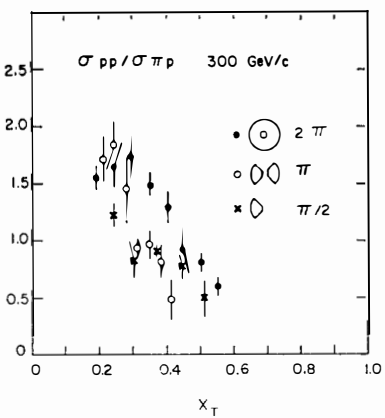

Fig. 5 Ratio of pp to π^-p cross sections as a function of x_T.

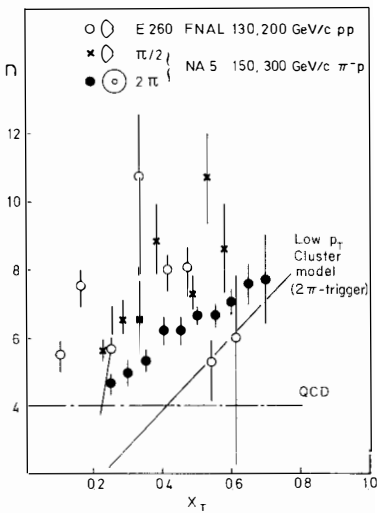

Fig. 6 The scaling behaviour of the full calorimeter and one arm trigger cross sections for π^-p collisions at 300 and 150 GeV/c. Results from FNAL experiment E260 are shown for comparison.

(minimum) principal p_T-axis. For an isotropic event structure we would expect P = 0 and for pencil like jets P = 1. Fig. 7 shows the planarity distributions of events selected by the calorimeter trigger 3. from π^-p and pp collisions at 300 GeV/c for different trigger thresholds. These are compared to the planarity of Monte-Carlo simulated events for pp collisions at 300 GeV/c using a low p_T cluster model and a QCD 4-jet model (Fig.7). For both models the detector resolution and acceptance were simulated.

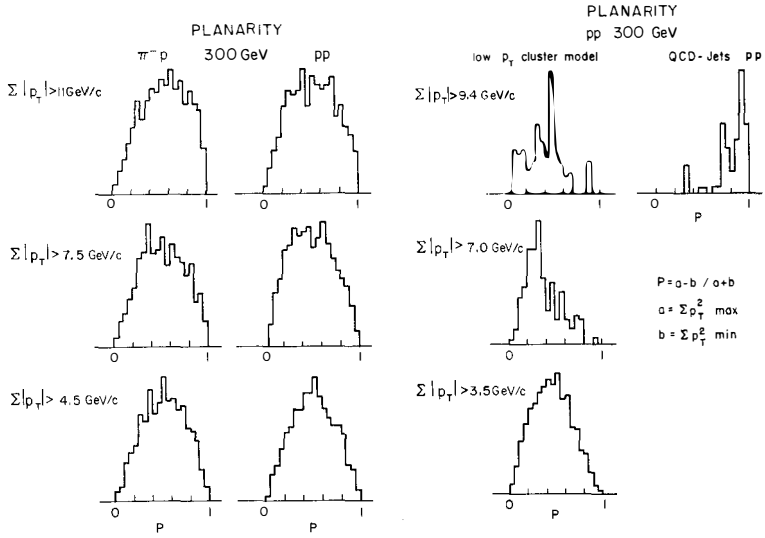

Fig. 7 Planarity distributions of events selected by the full calorimeter trigger from π^-p and pp collisions at 300 GeV/c for different trigger thresholds. Results from a low p_T cluster model and a QCD 4-jet model are shown for comparison.

Planar events do not seem to dominate the trigger 3. data. However the number of events with a planarity close to P = 1 increases with an increasing $\Sigma|p_T|$-trigger threshold. The same conclusions have been drawn from an independently performed "thrust" analysis of the data.

In Fig. 8 the transverse energy deposited in the two arm calorimeter is plotted versus the total transverse energy deposited in the full calorimeter for events selected by the two arm

calorimeter trigger. A clustering of events near the straight line in Fig. 8 is expected if the event structure would be dominated by 2 large p_T jets. The fraction of the transverse energy measured in the two arm calorimeter for events selected with the trigger 2. seems not to favour a dominant jet-like event structure (see Fig.9).

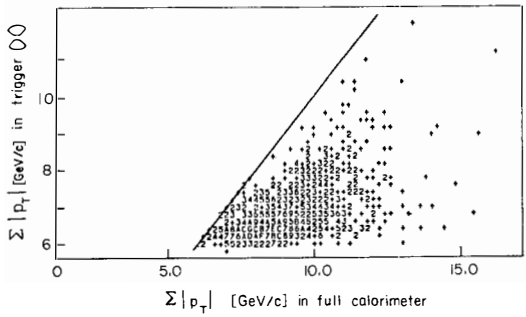

Fig. 8 The transverse energy measured in the two arm calorimeter is plotted versus the total transverse energy measured in the full calorimeter for events selected by the two arm calorimeter trigger in pp collisions at 300 GeV/c.

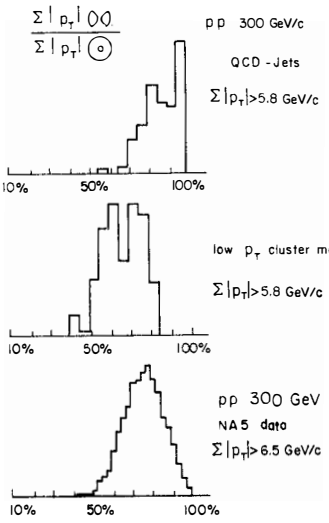

Fig. 9 The fraction of the transverse energy measured in the two arm calorimeter for events selected with the trigger 2. is compared with Monte-Carlo simulated QCD 4-jet- and low p_T cluster model predictions.

3. Multiplicities

The total charged particle multiplicities observed in the streamer chamber using the trigger 3. are rising rapidly with an increasing trigger threshold in $\Sigma|p_T|$ (Fig.10). The low p_T cluster model seems to reproduce the data rather well, while the total charged multiplicity predicted by the QCD 4-jet model is too small.

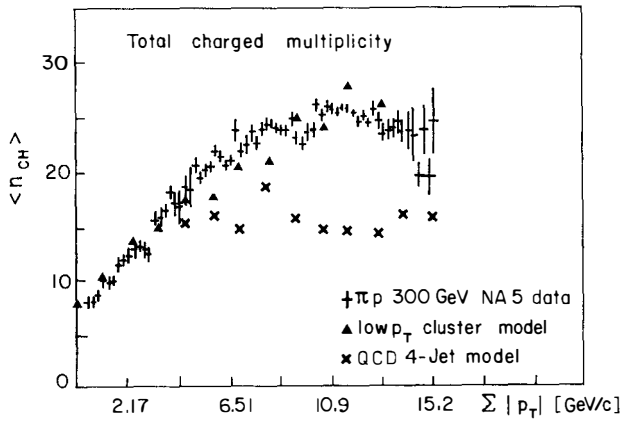

Fig. 10 The total charged multiplicity for πp collisions at 300 GeV/c as a function of the trigger threshold for the full calorimeter trigger

The charged particle multiplicity within the calorimeter acceptance was found to be $<n_{CH}> = 12$ for $\Sigma|p_T| > 10$ GeV/c. This is to be compared to a value of $<n_{CH}> = 17$ and 9 predicted by the cluster- and QCD-model respectively.

Conclusion

The events selected by the full calorimeter trigger show no dominant jet structure. They appear to originate from processes other than two constituent scattering. This observation however does not exclude the existence of jets, but it indicates perhaps that if they exist they are much suppressed in this energy and p_T region. It remains a challenging question: How to trigger on jets ?

References

1.) A summary of large transverse momentum hadronic processes is given by P. Darriulat in Ann. Rev. Nucl. Part. Sci. (1980) 30, 159-210.

2.) S.M. Berman, J.D. Bjorken, J. Kogut: Phys. Rev. D4 (1971) 3388.

3.) V. Cook et al.: Fermilab-Pub-80/91 EXP 7180-236.

4.) C. Bromberg et al.: Preprint CALT-68-738 (1979); Phys. Rev. Lett. 43, 565 (1979).

5.) W. Selove: High p_T jet studies at Fermilab, Proceedings of the 14th Rencontre de Moriond 1979, Vol. I, 401.

6.) V. Eckardt et al.: Nucl. Instr.& Meth. 155, 389 (1978).

7.) In the QCD-model calculations of the cross sections the matrix elements for 2 constituent scattering were used. The quark and gluon distributions were obtained from νN and Drell-Yan experiments. Scale breaking effects were taken into account. A coupling constant $\alpha_s = 12\pi/25 \ln (1+ \frac{Q^2}{\Lambda^2})$ with $\Lambda = 0.5$ GeV and $Q^2 = 4\ p_T^2$ was assumed. The model had 2 large p_T and two forward/backward spectator jets. Each of the two jet systems was made to resemble jets as observed in e^+e^- collisions.

8.) The low p_T cluster model produces clusters with an average mass of $\langle m_c \rangle = 2$ GeV in a cylindrical phase space. The clusters decay isotropically with an average charged multiplicity of $\langle n_{CH} \rangle \sim 2.5$. The resulting p_T-distributions of the final particles have $\langle p_T^2 \rangle^{1/2} = 0.36$ GeV/c. Leading particle effects were taken into account and an overall KNO multiplicity distribution was enforced. The cross sections were normalized to $\sigma_{tot\ inel}$ (pp). The model reproduced well the features of low p_T events observed in bubble chamber experiments.

HOW TO IDENTIFY PARTICLES -- A NEW WAY

T. Ekelöf
CERN, Geneva, Switzerland

ABSTRACT

The use of particle identification in e^+e^- experiments and the various methods available are discussed. The ring-imaging Čerenkov method is described, and some preliminary results obtained by a CERN-Ecole Polytechnique-Uppsala Collaboration using a TPC photon detector with a TEA/CH_4 gas mixture, coupled to a 1 m long argon gas radiator, are reported.

1. INTRODUCTION

One of the dilemmas in particle physics today is the apparent impossibility of observing the quarks directly. This dilemma is theoretical (represented by the confinement problem) and also experimental; when observing the final state in a high-energy collision, we are limited to the study of "quark molecules" rather than the quarks themselves . The point I want to make here is that when trying to carry out the difficult task of disentangling the dynamics and spectroscopy of quarks from this "chemistry", it is quite useful to know not only the energy of the emerging molecules/particles but also their quark content, i.e. the particle identity.

The π, K, and p live long enough for their tracks to be observed over many metres in detectors. The tracks of more short-lived but still weakly decaying particles such as the hyperons and the charmed particles can also be observed if special precautions are taken. In storage ring experiments, however, it has so far only been possible to identify these particles from the invariant mass of their more stable decay products. In the case of particles that decay hadronically, this latter method is the only one available.

In weak decays, the identification of e and μ in the final state is necessary. Gamma identification is needed to detect the electromagnetically decaying π^0 and also, of course, for the detection of direct photons.

There are at least two aspects in which particle identification is important; flavour identification and particle spectroscopy. However, even if one has full γ, e, μ, π, K, and p identification in an experiment, all problems are not solved. To take an example: in a high-energy collision at LEP, the charged plus neutral multiplicity will be of the order of 30. The number of possible ways to combine the observed stable and semistable particles is enormous, leading to a large combinatorial background. Furthermore, a leading K is quite a good signature for a primary $c\bar{c}$ pair. However, for heavier quarks the long decay chain softens the momentum spectrum of the "leading" K, and it will no longer stand out from the other K's that are created in the jet fragmentation.

Particle identification at LEP is no panacea. However, quite clearly particle identification will provide important additional information, in the first instance from inclusive measurements and later on also from exclusive ones. There may in fact be many stimulating surprises awaiting us -- such as, for example, the observed high proton yield recently discovered in e^+e^- collisions.

There is already an established arsenal of detectors for particle identification[1]. One type of such detectors uses the difference in the interaction of the particles with matter, as in electromagnetic shower counters for photons and electrons and in iron filters for muons. This strategy cannot be used to differentiate between the

three hadrons π, K, and p. What remains is then to measure both the velocity γ and the momentum p of the particle and to calculate the particle mass from these quantities. The mass of the π is 28% of that of the K, and the K mass is 53% of the proton mass. To make a π/K and K/p separation at the level of 3 standard deviations, neither γ nor p should have measurement errors exceeding 24% and 16% respectively. The requirement that also the error in the momentum measurement must not exceed a certain limit if particle separation should be possible is not always realized in discussions.

There are a number of methods for determining the particle velocity, such as measuring the time of flight (TOF), the specific ionization (dE/dx), or the threshold for Cerenkov radiation or transition radiation. It turns cut, however, that for storage ring experiments, all these methods have limitations if one wants to identify at particle energies above a few GeV. To cover all directions around the collision point, one is for practical reasons limited to observable track lengths of up to a few metres. As time resolutions of better than 100 ps seem very difficult to obtain over large areas, and since dE/dx needs very long track lengths (cf. the EPI and ISIS detectors) to do particle spearation on the relativistic rise side, it is unclear whether these methods will be of use in the region of many GeV. Čerenkov threshold counters can be used at high energies but have coarse granularity and occupy large volumes. Transition radiation seems to be a promising technique but is only applicable to electron identification at storage rings, as the lowest threshold obtainable seems to be about $\gamma = 500$.

2. THE ČERENKOV RING-IMAGING METHOD

There is also the method that determines the particle velocity from a measurement of the emission angle of the Čerenkov light[2,3]. The nature of Čerenkov radiation has been known and understood since the 1930's, but until now, it has mainly been used for velocity determination in a rather rudimentary way. If a particle of velocity β ($\gamma = 1/\sqrt{1-\beta^2}$) traverses medium of refractive index n, then it will emit a shock wave of light if $\beta > (1/n)$ ($\gamma > 1/\sqrt{1-1/n^2}$). The observation of light or the absence of it will thus allow us to determine whether the velocity is above or below a fixed value. This is the principle of the threshold counter.

However, the angle of emission θ of the Čerenkov light with respect to the particle direction is a direct measure of the velocity β:

$$\cos \theta = 1/\beta n.$$

The angle θ grows from zero at threshold ($\beta = 1/n$) and approaches, from below, an asymptotic value arccos (1/n) at very high energies ($\beta \to 1$). There exists a simple optical arrangement involving a spherical mirror in which the Čerenkov light from particles that emerge from the centre of curvature of the mirror is focused into a ring-image half way between the spherical mirror and its centre of curvature.

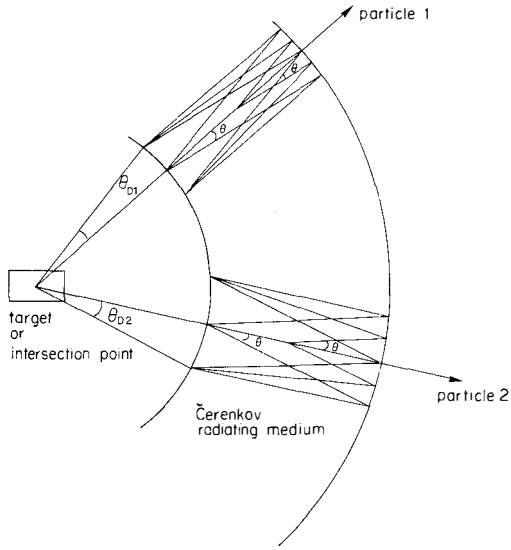

Fig. 1 Optical arrangement to focus the Čerenkov light into circles, using a spherical mirror over a large solid angle.

The ring-image radius r is directly proportional to the Čerenkov emission angle ($r = f \cdot \mathrm{tg}\,\theta$ where f is the focal length of mirror) and its position is a measure of the direction of motion of the radiating particle. The optical arrangement is illustrated in Fig. 1.

This optical scheme is used in, for example, the CEDAR differential Čerenkov counter developed at CERN. However, in this counter the detection of the Čerenkov light image is made by photomultipliers placed behind a fixed annular light collimator. The counter thus gives a signal only if the radius and position of the ring correspond to those of the collimator ring. The counter can therefore only be used to identify particles in a parallel monochromatic beam.

On the other hand, if the light ring could be detected and measured irrespective of its size and its position on the focal surface, then particles in all directions could be detected, and the only condition for obtaining a signal would be that the velocity should be above threshold.

The number of photons emitted by a particle passing through a dielectric medium is

$$N = (\alpha/\hbar c)L \sin^2\theta = 370(E_1-E_2)L \sin^2\theta\ ,$$

where L is the track length in centimetres, θ is the Čerenkov angle, and E_1 and E_2 define the bandwidth of detectable photons in units of electronvolts. To make

measurements in the region of many GeV, a gaseous radiator is needed. In the case of argon gas at NTP with L = 100 cm and $E_1 - E_2$ = 1 eV, 25 photons are emitted by a β = 1 particle.

In order to measure with reasonable efficiency, the position of these photons in the focal surface to a precision of the order of 1 mm, new methods have to be developed. A few different approaches are at present being tried out by different groups. A common feature is the use of a photoionizing vapour such as triethylamine (TEA) to convert the photons into single photoelectrons, which are then detected by gas amplification as in an ordinary particle track detector. One important difference is that there is only one primary electron per coordinate instead of some 10 or 20 as in the case of a typical track detector. The detectors that have been tried out for two-dimensional read-out of Čerenkov photon position are spark chambers[4], multiwire proportional chambers (MWPCs) with cathode read-out[5] Geiger needle counters[6], and time projection chambers (TPCs)[3].

3. NEW RESULTS

I will now turn to some preliminary but very encouraging results[7] recently obtained at CERN by a CERN-Ecole Polytechnique-Uppsala Collaboration using the TPC technique.

The experimental set-up used is shown in Fig. 2. A negative pion beam from the CERN Proton Synchrotron (PS) passes along the axis of a 1 m long, 30 cm diameter, stainless-steel tube filled with argon gas. A spherical mirror with a focal distance of f = 1 m, mounted in the downstream end of the tube, focuses the emitted Čerenkov light into a ring image in the upstream end.

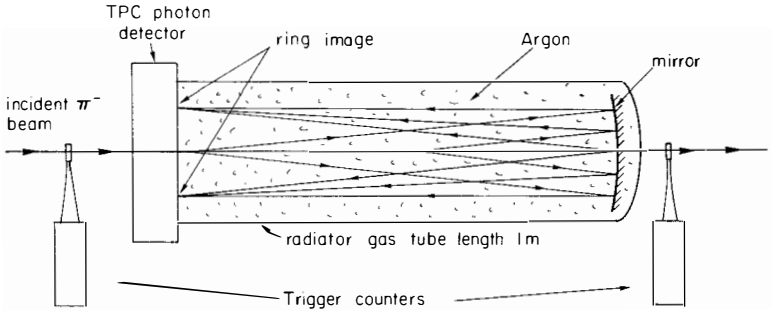

Fig. 2 Experimental set-up showing the radiator gas tube, the mirror, and the photon detector.

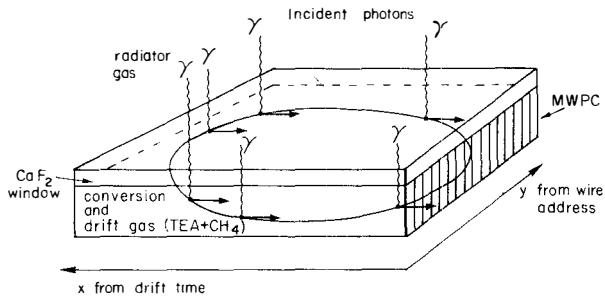

Fig. 3 The photon detector with the CaF_2 window, the conversion and drift region, and the MWPC.

The basic features of the photon detector are shown in Fig. 3. The gaseous volume in which the photons are converted to photoelectrons is separated from the radiator gas volume by a calcium fluoride window. Triethylamine is photoionized only if the incident photon wavelength is shorter than 165 nm ($E \geq 7.5$ eV) and the window, like the radiator gas, must thus be chosen such that both are transparent in the far ultraviolet. A parallel electric field set up across the conversion region makes the photoelectrons drift sideways up to a MWPC which has its wires perpendicular to the electric drift field and to the focal surface. Each photoelectron is multiplied by a factor of about 10^6 in the avalanche around the sense wire it hits, and the resulting signal is fed via a preamplifier and discriminator to a time-to-digital converter (TDC). Thus the drift time and the wire address uniquely determine the position of each photon at the conversion point. The ring image can then be reconstructed provided there are at least three such points.

The wire spacing of the MWPC at present in use is 2.54 mm. The electron drift velocity is about 7 cm/μs and the TDC binning 8 ns. The detector gas is methane with 3.3 Torr triethylamine added, which results in a photon absorption length of 6 mm. The depth of the absorption gap is 15 mm.

The refractive index of argon gas NTP for photons of 8 eV is about 1.00036, and the corresponding maximal ($\beta = 1$) Čerenkov angle is 27 mrad. In argon NTP, the expected ring radius is therefore 27 mm ($f = 1000$ mm).

The first observations of a ring image using this technique were made on 21 February this year, and in Fig. 4 the on-line computer display of this result is shown. At this time, conditions were not optimized. Only one photon per event was recorded, and Fig. 4 shows a large number of triggers superimposed. The width of the circle is determined by the divergence of the π beam used.

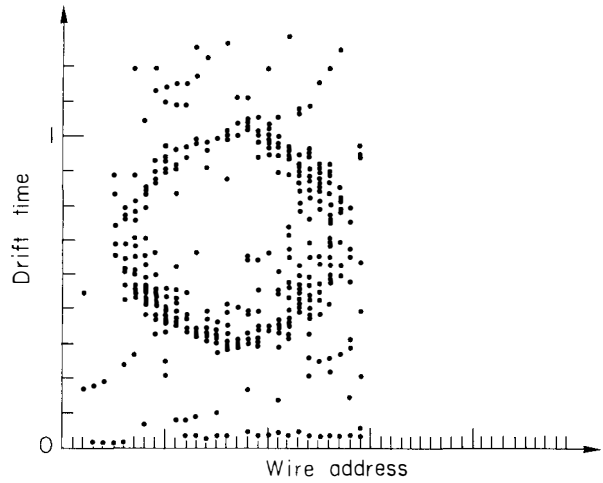

Fig. 4 First electronic observation of a ring-image as seen on the on-line computer display 21 February 1981. Many events have been superimposed in this plot.

Since then, detection conditions have been improved. Furthermore, the radiator gas has been raised to 1.9 bar, and as a consequence we now see on the average four photons per event. Figure 5 shows the on-line display of a single event with as many as seven record photons. The fitted radius of this event is 31.4 mm.

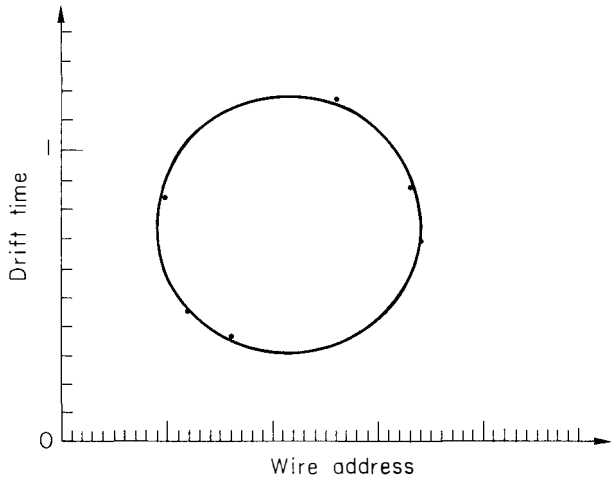

Fig. 5 Single event with seven photons detected and with a circle fitted to the points by the on-line computer.

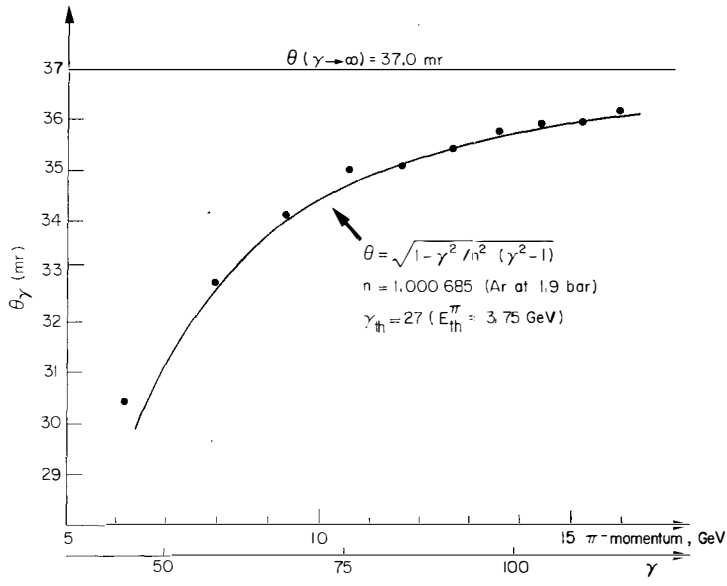

Fig. 6 Preliminary data on Čerenkov angle versus π momentum taken from the logbook. Each point represents the average angle obtained from individual circular fits to about 500 events. The curve is calculated according to the formula in the figure.

Under these conditions a series of runs were made, accumulating data at 10 different energies between 6 and 16 GeV. Each event was fitted individually, and the average radius of about 500 events was computed for each energy. Figure 6 shows a very preliminary plot of these radius averages versus beam momentum. The results are in fact very preliminary; the data points shown have been taken directly from the logbook.

The curve shown is not a fit to the data but a calculation of $\sin\theta = \sqrt{1 - \gamma^2/n^2(\gamma^2-1)}$, with n = 1.000685 (argon at 1.9 bar). The horizontal line represents the asymptotic value of θ when $\gamma \to \infty$.

The fluctuations of the individual points around the curve correspond to the fluctuations of the mean value of 500 events. The resolution in θ of a single event is, in the present situation, on the level of a few percent. After further improvement of the detector, a $\sigma\theta/\theta$ of the order of 1% should be obtainable. This would allow, for example, for e/π separation on the level of 3 standard deviations up to a momentum of about 15 GeV, and π/K separation from 5 GeV to 55 GeV, provided $\sigma p/p$ is much smaller than 24% in the latter case.

4. CONCLUSIONS

From the preliminary data available at this moment one may already conclude that the operation of a Čerenkov ring-imaging counter based on a TPC-type photon detector is feasible. An angular precision of the order of $\sigma\theta/\theta = 1\%$ seems to be within reach.

The average number of photons, which at present is two in 1 m of argon NTP, is still low. However, for trivial technical reasons we are at present using two calcium fluoride windows instead of one. As the transmission of a single window is about 68%, the use of only one window would give three photons. If tetrakis-(dimethylamine)ethylene (TMAE)[8] is used as photoionizing agent, rather than triethylamine (TEA), the threshold for photoionization is lowered from 7.5 eV (165 nm) to 5.4 eV (230 nm) with an expected increase in the number of photons of at least a factor of 2. An average of six photelectrons should be enough for the pattern recognition of a circular image. If a similar detector would be used to study final states with tightly collimated particle jets, one may expect to have several overlapping ring-images. In this case it will be necessary to measure the direction of the particle tracks with external track detectors in order to predict the position of the centre of each ring. If this is done, six photons would probably still be enough, provided that the density of overlapping rings is not overwhelming.

Using this strategy, it would be possible to disentangle overlapping rings which are only a few milliradians apart, from which it follows that the granularity of the described detector is a few milliradians.

Acknowledgements

The technique of Cerenkov ring-imaging discussed here was pioneered several years ago by my collaborators Jacques Séguinot and Tom Ypsilantis[3].

The preliminary results displayed were obtained at CERN by the members of the CERN-Ecole Polytechnique-Uppsala Collaboration:

E. Barrelet, T. Ekelöf, B. Lund-Jensen, J. Séguinot, J. Tocqueville, T. Ypsilantis and M. Urban.

References

1) See, for example, Proc. Int. Conf. on Experimentation at LEP (Session on Particle Identification), Phys. Scripta 23 (1981) 384.

2) J. Séguinot and T. Ypsilantis, Nucl. Instrum. Methods 142 (1977) 377.

3) T. Ekelöf, J. Séguinot, J. Tocqueville and T. Ypsilantis, Proc. Int. Conf. on Experimentation at LEP, Phys. Scripta 23 (1981) 718.

4) G. Charpak, A. Peisert, F. Sauli, A. Cavestro, M. Vascon and G. Zanella, Cerenkov ring-imaging using a television digitizer, preprint CERN-EP/80-179, submitted to Nuclear Instruments and Methods.

5) F. Sauli, private communication.

6) G. Comby, J.F. Chalot, J. Quidort, M. Boussicot and J. Tichit, Le détecteur multipointe dans l'imagerie de l'effet Čerenkov, CEN-Saclay report DET 80.05 PIC (1980).

7) E. Barrelet, T. Ekelöf, B. Lund-Jensen, J. Séguinot, J. Tocqueville, T. Ypsilantis and M. Urban, in preparation.

8) D.F. Anderson, A photoionization detector for the detection of xenon light, Los Alamos report LA-UR-80-3158 (1980).

HOT HADRONIC MATTER

Johann Rafelski
Institut für Theoretische Physik
der Johann Wolfgang Goethe-Universität
Frankfurt am Main, Germany

A description of highly excited hadronic matter is presented. I assume the kinetic and chemical equilibrium and develop a thermodynamic description valid for high temperatures and different chemical hadronic compositions. Two physically different domains are described: firstly the hadronic gas phase in which individual hadrons coexist as separate entities, though sometimes assembled in large hadronic clusters. In the second domain individual hadrons dissolve into one large hadronic cluster consisting of quarks and gluons - this is the quark-gluon phase. Observation of enhancement in the $\bar{\Lambda}$ partial cross-section at subthreshold energies in nuclear collisions is discussed as one of possible characteristic phenomena of this phase.

1. Introduction

A theory of hot hadronic matter is being developed[1] based on the present knowledge about strong interactions. Physically most important is the phase transition in which baryons and mesons are dissolved into the quark-gluon plasma[2]. Essential quantity controlling the occurence of this transition is the energy density of hadronic matter. Hence the heat and pions created in central high energy heavy ion collisions or low energy $\bar{p}$ annihilations on nuclei[3] lower the necessary nuclear density to about 1-3 times normal nucleon density at temperatures of the order of the pion mass. For lack of time and space I can only discuss the nuclear collisions here; for a discussion of $\bar{p}$ annihilations the reader may consult ref. (3).

The theoretical descriptions of both phases are entirely different: In the hadronic gas phase[1] the hadron-nucleon cross section being dominated by the formation of hadronic resonances, the essential physical input is the particle mass spectrum, here derived in the statistical bootstrap model. In the dense domain of the matter it is essential to take into account the finite size and the clustering of individual quark bags. In the quark-gluon plasma, we have to deal with a many body gauge field theory at moderate interaction strength[2]. An insight into the behaviour of the plasma can be gathered studying the Fermi-Bose interacting quantum gases in a large quark bag[4].

In order to test our understanding of hot hadronic matter in kinetic and chemical equilibrium and to show the existence of the plasma phase different experiments are necessary. As an initial step I consider the temperatures of particles emitted in a hypothetical central fireball created in high energy nuclear collisions [1,5]. Suitable care must be taken in an experiment to eliminate the contributions of projectile and target nuclei - here we do not know the model dependent internal excitation. Among the results I discuss here a substantial entropy production in the explosion of the fireball is due primarily to the production of new particles. Under certain conditions I also anticipate that strangeness would equilibrate - the relative yields of (anti) strange particles can be used as a measure of the size of the reaction zone to be confronted with correlation experiments. If the phase transition occurs at moderate energy densities (500 MeV/fm^3), then the relative $\bar{\Lambda}$ to $\bar{p}$

yields can be used as a measure of the relative antistrange quark abundance in the quark phase for heavy ions energies between 2 and 5 GeV/N[7]. Other phenomena will be studied at higher energies: prompt photons, leptons and eventually heavy flavours (charm etc).

It is important to appreciate that all this depends sensitively on the existence of cooperative phenomena in which many nucleons from the projectile and target participate. This behaviour was not so apparent in hadron-nucleus collisions. However, we note that in a first nucleon-nucleon collision the first participants are slowed down and other nucleons can run into the reaction zone. Some of the reaction products acquire significant transverse momenta. Thus the assumption of kinetic equilibrium may be correct in a slightly restricted sense: the center of the energy and momentum distribution will be at a certain mean value - while the low and the important high energy tails will be underpopulated. The chemical equilibrium in which the relative population of different particle states is also governed by the statistical distribution is more difficult to achieve. It is controlled by partial reaction cross sections which are much smaller than total cross sections. Hence for example at low energies (e.g. 1-2 GeV/N kinetic energy) or large impact parameters strangeness may be decoupled from the presumed equilibrium state of hadronic matter.

I would like to emphasize that only in very high energetic central collisions of heavy nuclei we will be able to study the properties of the quark-gluon plasma at high temperatures. Is this worth the effort? Let us consider as an example the production of heavy quark flavours in e^+e^- annihilations and in nuclear collisions: while the first kind of experiment is almost certainly much clearer, a complex state like[8] $cc\bar{s}\bar{s}$ could only be produced when high quark density is reached at high plasma temperature $T \approx 1$ GeV. [This process may be seen as an analogy to the production of $\bar{\alpha}$ in pp-ISR collisions.] Another very fundamental aspect of experiments with high energy nuclei is the exploration of the phase transition between hadron gas and quark plasma states of hadronic matter and the determination of the critical energy density.

2, Hot Hadronic Gas Phase

The basic assumption will be the conceptual validity of the quark bag model[4] - what I propose below is practically thermodynamics of finite size bags[9] interacting through creation or destruction of new bag states. I will neglect quantum statistics - this approxima-

tion turns out to be permissible when the temperatures of individual hadrons are above 40-50 MeV.

From the partition function $Z(V,\mu,T)$ all physically interesting quantities, such as energy, pressure, entropy can be desired as they are simply first derivatives of Z. Here V is the total reaction volume, μ the baryonic chemical potential and $T = 1/\beta$ the temperature. We will also use often the baryon fugacity $\lambda = \exp(\mu/T)$. λ or resp. μ are introduced to allow the conservation of the baryon number. The partition function can be expressed in terms of the hadronic mass - spectrum $\tau(p^2,b)$: $\tau(m^2,b)dm^2$ is the number of hadronic resonances of baryon number b in the mass intervall $(m^2, m^2 + dm^2)$.
We obtain[1]:

$$\ln Z = - \frac{2\Delta}{(2\pi)^3 H} \frac{\partial}{\partial\beta} \Phi(\beta,\lambda) \quad , \tag{1a}$$

$$\Phi(\beta,\lambda) = H \sum_{b=-\infty}^{+\infty} \lambda^b \int e^{-\beta p} \tau(p^2,b) d^4p \quad . \tag{1b}$$

The bootstrap constant H has been introduced here mainly for dimensional convenience: the dimensionless quantity Φ will be derived from the statistical bootstrap model. Δ is the available volume in which hadrons are free to move after subtraction of their proper volumina:

$$\Delta = V - \sum_i V_{h,i} \quad . \tag{2}$$

Here the sum over all individual hadronic volumina $V_{h,i}$ in V is taken. We know that in the bag model of massless relativistic quarks[4] we have

$$V_{h,i} = M_i/4B \tag{3}$$

and hence the sum in Eq. (4) may be easily carried out:

$$\Delta = V - \langle E \rangle/4B \quad , \tag{4}$$

where $\langle E \rangle$ is the statistical average of the total energy. We emphasize that the quantity Δ must always remain positive; hence the total energy (mass) of the hadronic gas phase cannot exceed 4BV. When this limiting value is approached, a tendency of quark bags to cluster together and to form one large bag is found. A necessary condition for this to occur is that the energy density of the (hypothetical) pointlike hadrons

$$\varepsilon_p \equiv - \frac{1}{\Delta} \frac{\partial}{\partial\beta} \ln Z = - \frac{2}{(2\pi)^3 H} \frac{\partial^2}{\partial\beta^2} \Phi(\beta,\lambda) \tag{5}$$

diverges. The energy density $\varepsilon = \langle E \rangle / V$ in terms of ε_p is just $\varepsilon = \Delta / V \varepsilon_p$ and hence with Eq. (4)

$$\varepsilon = \frac{\varepsilon_p}{1+\varepsilon_p/4B} \xrightarrow{\varepsilon_p \to \infty} 4B \qquad (6)$$

The factor $(1+\varepsilon_p/4B)^{-1}$ represents the part of the van der Waals effect introduced by the finite size of individual hadrons.

In order to obtain a complete quantitative description of the hadronic phase we must derive the bootstrap function Φ, Eq. (1b). By requiring that in the limit $\Delta \to 0$ the hadronic state as described by Eq. (1) is again just another state.

In order to obtain a quantitative description of the hadronic phase we must derive an expression for the bootstrap function Φ, Eq. (1b). By requiring that in the limit $\Delta \to 0$ the hadronic state as described by Eq. (1) is again just another particle contained in the mass spectrum τ a nonlinear equation for τ is obtained[10]. In terms of the function Φ it has the convenient form[11]

$$\phi(\beta,\lambda) = 2\Phi - e^{\Phi} + 1 \,. \qquad (7)$$

The input function ϕ is defined in terms of the basic hadronic states [$q\bar{q}$ and qqq] as

$$\phi = 2\pi HT\left[3m_\pi K_1\left(\frac{m_\pi}{T}\right) + 8\cosh(\mu/T) m_N K_1\left(\frac{m_N}{T}\right)\right] . \qquad (8)$$

We recall that Eq. (7) has a real solution $\Phi = G(\phi)$ only for $\phi < \phi_0 = \ln(4/e)$. At this point there is a root singularity. Further study shows that Eq. (1b) then requires an exponential growth of $\tau \sim e^{m/T_0}$. The highest hadronic gas temperature T_0 has the analogous physical meaning as the boiling point of water - for $T > T_0$ the phase containing individual hadrons cannot exist and the constituents - quarks - are liberated [in the sense that they can move within the hadronic volume V_h, Eq. (5)]. In Fig. 1a the dependence $T(\mu)$ is shown following from Eq. (8) at the critical point $\phi = \phi_0$. $T(\mu=0)=T_0$ has been chosen to be 190 MeV ($H = .724\ \mathrm{GeV}^{-2}$). This choice leads to agreement with the slope of inclusive crossections: $6 = 1\mathrm{GeV}/.14\mathrm{GeV}$. The observed low pion temperatures $T_\pi \approx 120\text{-}140$ MeV are so small because pions are emitted mainly from the less dense and cooler domains of hadronic fireballs[5].

We note in Fig. 1a that the maximal temperature of hadronic gas phase decreases with increasing chemical potential - at $\mu = 0$ the

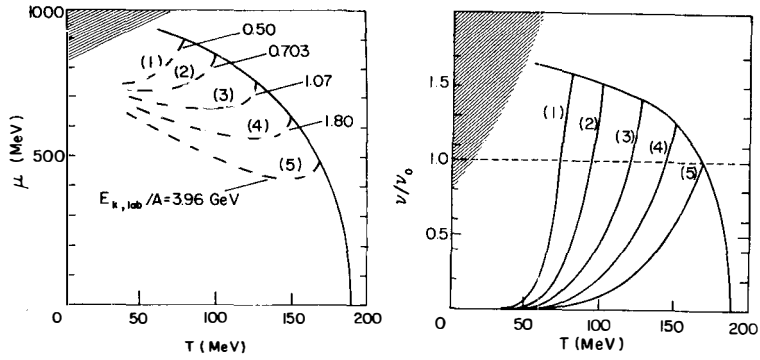

Fig. 1: The critical relationship between temperature T and a) chemical potential μ; b) baryon density ν. Curves 1-5 of constant (shown) projectile kinetic energy per baryon indicate the hypothetical evolution of central fireballs at selected kinetic energies; $\nu_0 = .56\ 4B/m_N$ corresponds to normal nuclear baryon density $\nu_0 = .14/fm^3$ for the old value of the bag constant: $B^{1/4} = 145$ MeV.

large number of mesons generated by high T is sufficient to induce the change to the quark plasma. As a consequence of the Van der Waals effect discussed the energy density along the phase boundary is equal to 4B while pressure vanishes. With $B \approx (170\ \text{MeV})^4 = 110\ \text{MeV/fm}^3$ we expect the phase transition at about 0.5 GeV/fm^3.

To test these ideas about the hadronic gas phase the temperatures (slope parameters) of inclusive particle cross sections expected in relativistic heavy ion collisions have been computed. These calculations require that:

1) small impact parameter collisions are identified,

2) only particles from the central fireball are counted.

Under these circumstances the initial kinetic energy of the projectile nucleus per nucleon, $E_{k,p}$, defines the available excitation energy per participating baryon in the fireball

$$E/b = m_N \sqrt{1 + E_{k,p}/2m_N} \qquad (9)$$

The equations of state distribute this energy among kinetic and chemical degrees of freedom [collective motion and its energy is neglected]. The temperature-density relationship of the exploding fireball is shown for the LBL-DUBNA energies in Fig. 1b. Averaging the temperatures of emitted particles along these cooling curves

gives the results shown in Fig. 2. We record that the nucleon temperature T_N is significantly higher from that of pions. [Hagedorn is presently finetuning the parameters H and B and a ±10 MeV change in shown results is anticipated]. The substantial rise of the temperature with the kinetic energy shown in Fig. 2 is in good agreement with experiment (BEVELAC-ISR)[12].

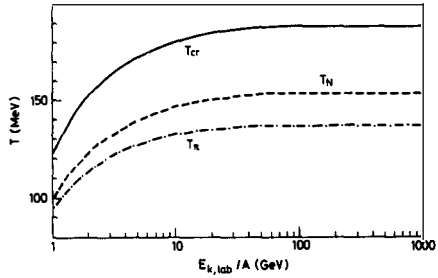

Fig. 2: The dependence of temperatures of nucleons and pions on initial projectile kinetic energy. T_{cr} is the highest temperature of the hadronic gas phase.

In Fig. 3 I show another interesting result: Along the cooling lines of constant energy per baryon, Fig. 1 the (specific) entropy per baryon rises significantly from the (high) value computed at the critical line. This is due to the onset of strong pionization of the available energy. The entropy at the critical line is found recalling that when pressure vanishes

$$(S/b)/_{P=0} = \frac{E/b-\mu}{T}\Big/_{P=0} \xrightarrow[\text{high } E]{} E/bT_0 \qquad (10)$$

We thus keep in mind that hadronic fireballs do not expand adiabatically and that substantial cooperative entropy production is expected. We will return to this point again below.

3. The Quark-Gluon Plasma

When hadrons have coalesced into a large quark bag at the critical curve, we must change the theoretical model underlying the description of hot hadronic matter. The new central assumption, valid strictly only at very high energies, is the weakness of the quark - quark interaction: only in this case a description of interacting quantum Fermi-Bose gases[2] may be successful. The quark masses in the relativistic quark-bag model are small: $m_q \approx$ 10-30 MeV, while

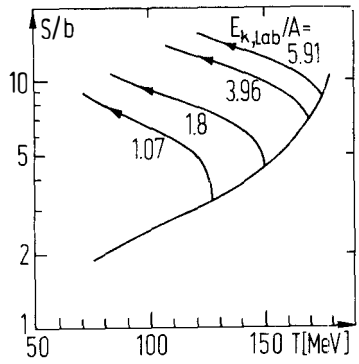

Fig. 3: Specific entropy per baryon along cooling lines for given projectile kinetic energy as function of T. The boundary is the specific entropy at the critical line.

gluons are massless. [These masses should not be confounded with the nonrelativistic quark model masses M_{nr} which correspond to the kinetic energies of the bag model: $M_{nr} \approx 2.04\ \hbar c/R_{bag} \approx 400$ MeV.] Hence in the region of interest to us of μ and T, the quark chemical potential $\mu_q = \frac{1}{3}\mu > m_q$. The factor 1/3 arises in view of the quark baryon number 1/3. As long as this condition is satisfied, the Fermi-Bose gas with interaction $O(\alpha_s)$ can be integrated analytically[13] and we find:

Quarks: (11a)

$$T \ln Z_q = \frac{1}{3}\frac{gV}{2\pi^2}\left[\left(1 - \frac{2}{\pi}\alpha_s\right)\left(\frac{\mu^4}{4\cdot 3^4} + \frac{\mu^2}{2\cdot 3^2}(\pi T)^2\right) + \left(1 - \frac{50}{21\pi}\alpha_s\right)\frac{7}{60}(\pi T)^4\right]$$

Gluons:

$$T \ln Z_g = \frac{8V}{45\pi^2}\left(1 - \frac{15}{4\pi}\alpha_s\right)(\pi T)^4 \qquad (11b)$$

Vacuum:

$$T \ln Z_V = -BV \qquad (11c)$$

where $Z = Z_q\, Z_g\, Z_V$ is the total partition function.
Here $g = 2\cdot 2\cdot 3 = 12$ is the number of distinct quark modes with spin, isospin and colour. α_s is the QCD colour coupling constant [$\alpha_s \approx .5$ for space-like q^2 and $\alpha_s \approx .2$ for time-like q^2 - but we ignored the q^2 dependence of α_s].

In Eq. (11) we show separately the contributions of quarks and gluons; the vacuum term is a phenomenological supplement at this

stage of the discussion and has been chosen so as the bag energy density is B inside the region of the plasma and that an inside pointing pressure P = -B acts on the surface of the bag region. Contributions of heavy and strange quark flavours have been neglected.

The vacuum contribution, Eq. (11c) is as postulated in the quark bag model. However, at finite temperatures additional difficulty arises not shown by the perturbative expression, Eq. (11). We recall that the vacuum structure term originates presumably in the absence of the true vacuum gluonic structure from the region of space containing quarks. Therefore B should be calculated non-perturbatively together with the glue term, Eq. (11b) to yield some T-dependent quantity. In particular, this gauge pressure should vanish at some high temperature $T_{cr} \approx 1.5 B^{1/4}$, when the structure of the true vacuum is destroyed[14]. Only above T_{cr} the expression (11b) is valid - while Eq. (11c) is only correct for $T \to 0$. For $T < T_{cr}$ there is only a partial restoration of symmetry and not all $8 \cdot 2$ gluonic degrees of freedom can be excited. Another aspect of this point is that gluons may not be able to exist as independent particles in the plasma region and are rapidly absorbed on the surface by the true vacuum. This glue dissipation may be the origin of a high instability of gluonic states[15].

In order to estimate the boundary of the quark-gluon plasma phase in the μ-T plane, c.f. Fig. 1a we search for the line of zero pressure PV = T ln Z, as given by Eq. (11), though omitting the little important, but obscure glue term at relatively small temperatures. The result is very similar to the bootstrap line, Fig. 1a, with $T_0 \approx B^{1/4}$ at $\mu = 0$: now it is the quark-antiquark pair pressure that balances the vacuum pressure. This perhaps <u>not</u> accidental coincidence of the critical lines leads to the conclusion that both phases described here are directly adjacent to each other. Adjustung slightly H, B <u>and</u> $\alpha(T)$ we can achieve exact coincidence of the critical lines along which in both phases the energy density is 4 B and pressure vanishes. However, we can have a discontinuity of the baryon density: As in nuclear collisions baryon number should be conserved, the hadronic volume would be discontinuous. Of course this will not be the case - instead we have a Van der Waals transition shown schematically in Fig. 4: On the hadronic gas side we have to construct a new state consisting of a mixture between plasma and hadronic cluster. We will not enter here further into the discussion of this subject.

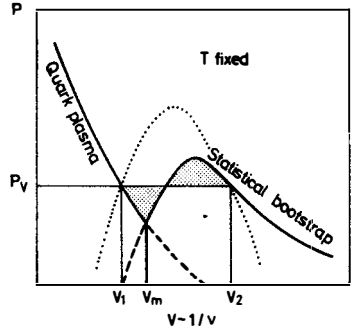

Fig. 4: Pressure vs Volume ($1/\nu$), qualitatively with the Maxwell construction

Finally let us note that as in the hadronic gas phase we can construct in the μ-T plane curves of given available energy per baryon. In a qualitative picture, Fig. 5, the most important aspects are illustrated: there is a highest temperature that can be reached: $T_{max} \sim \sqrt{s}/A$. Furthermore, at hadronization we have very small chemical potentials for ISR energies - hence we find from Eq. (10) that the expected specific entropy in a nucleus-nucleus collision at ISR could reach ~100. In other words, following Boltzmann, we find that there are 2^{100} different final states available to each 15 GeV baryon. We conclude that this enormous amount of entropy must be produced in the nonadiabatic explosions of highly compressed quark plasma.

4. Strangeness in Nuclear Collisions

Unlike p-p collisions, strangeness may be close to kinetic equilibrium in nuclear collisions: it is the large reaction volume with typical lengths exceeding the Compton wavelength of the strange mass that is of great importance here[6]. Let me explain why we should not expect the usual kinetic equilibrium result in p-p collisions: in general when strangeness-antistrangeness pair is mode in hadronic reactions at given temperature T, the expected number of pairs is

$$\langle n \rangle_{pair} \sim e^{-2m_s/T} \qquad (12a)$$

where $m_s \approx 280$ MeV is the relativistic strange quark mass. Instead, when we consider production of particles in a hot star we find

$$\langle n \rangle_{pair} \sim e^{-m_s/T} \qquad (12b)$$

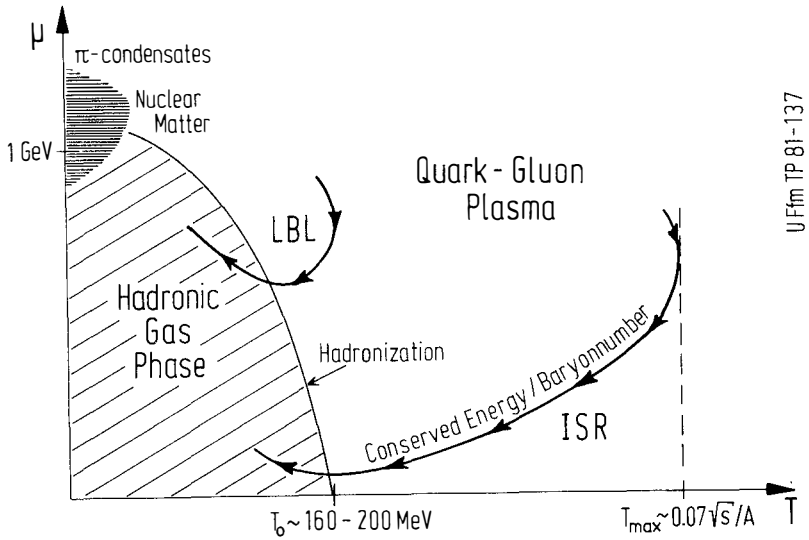

Fig. 5: Cooling lines in the μ-T plane in the quark-gluon plasma (qualitatively)

The fact that a pair is produced seems not to matter here. The crucial question is where the transition from case a) to b) occurs. The quantitative result is that in the hadronic volume $V_h = 4\pi/3\ (1\ fm)^3$ the pair mass matters, case a), while already for $V \approx 6\text{-}8\ V_h$ we are in the limit b) - assuming a typical $T \approx 150$ MeV. The suppression of the kaon yield in p-p collisions as compared with thermodynamic models has so found an explanation. It is expected that in nuclear collisions sufficiently large hadronic volumes are found. Furthermore, I have found from this study[6] that there is no information about the hadronic aggregate state that can be extracted from the total strangeness yields.

However, it is the antistrangeness that may be very usefull in the search for quark matter: below the $\Lambda\bar{\Lambda}$ threshold [at 4-5 GeV taking account of Fermi-motion in both nuclei] the antistrangeness that must balance the strangeness produced in hadronic reactions will generally be found only in kaons, except if quark plasma state were formed. In that case the kinematic limit is of no importance and it is the relative abundance of antiquarks in the plasma that will control the antibaryon yields. Consider for example the $\bar{\Lambda}/\bar{N}$ ratio as a measure of the relative $\bar{s}$ and $\bar{u}$ or $\bar{d}$ abundances: on theoretical grounds I expect $\bar{s}$ to be as abundant as $\bar{u}$ and $\bar{d}$ taken together, supposing the typical T and μ values at 4-5 GeV/N. Hence if quark

plasma is formed at these energies, $\bar{\Lambda}/\bar{N}$ ratio could become an important observable.

A preliminary search for $\bar{\Lambda}$ at 2.1 GeV/N has been negative[16]. As the energy density reached at 2.1 GeV/N - projectile kinetic energy is perhaps only 250 MeV/fm , this result fulfills expectations and sets a lower limit on the value of the critical energy density. It is quite conceivable [say 50%-50%] that at 4-5 GeV/N in some collisions the quark plasma state is formed. With direct $\bar{\Lambda}$ production still strongly suppressed I am awaiting impatiently future results on $\bar{\Lambda}/\bar{N}$ ratios at these energies.

5. Conclusions

In order to obtain a theoretical description of the hadronic gas and quark plasma phases I have used some 'common' knowledge and plausible interpretations of the currently available experimental observations. In particular, the strongly attractive hadronic interactions are included through the rich, exponentially growing hadronic mass spectrum $\tau(m^2,b)$ while the introduction of the finite volume of each hadron is responsible for an effective shortrange repulsion. Aside from these manifestations of strong interactions, I only satisfy the usual conservation laws of energy, momentum and baryon number. I neglect quantum statistics since quantitative study has revealed that this is allowed above T = 50 MeV. But particle production is allowed, which introduces a quantum physical aspect into the otherwise 'classical' theory of Boltzmann particles.

The study of the properties of hadronic matter has just begun and it is too early to say if the features of strong interactions that have been included in these considerations are the most relevant ones. It is important to observe that the currently predicted pion and nucleon mean transverse momenta and temperatures show the required substantial rise, see Fig. 2, as required by the experimental results available[13] at $E_{k,lab}/A$ = 2 GeV [BEVALAC] and at 1000 GeV [ISR]. Further comparisons involving, in particular, particle multiplicities and strangeness production discussed above are under consideration.

I wish to emphasize the internal consistency of the two-fold approach. With the proper interpretation the description of hot hadronic matter leads us, in a straight forward fashion, to the postulate of a phase transition to the quark-gluon plasma. This new phase is treated by a quite different method; in addition to the standard many-body theory of weakly interacting particles at finite temperature and density, we also introduce the phenomenological vacuum pressure

and energy density B.

Perhaps the most interesting and far reaching aspect of this work is the realization that the transition to quark matter will occur at much lower baryon density for highly excited hadronic matter in the ground state (T = 0). The precise baryon density of the phase transition depends somewhat on the phenomenological value of the bag constant; we estimate it to be at about 2-4 ν_0 at T = 150 MeV. The detailed study of the different aspects of this phase transition, as well as of possible characteristic signatures of quark matter, must still be carried out. I have given here only a very preliminary report on the status of my present understanding.

The occurence of the quark plasma phase will certainly be an oberservable phenomenon. Here I have discussed a measurement of the $\bar{\Lambda}/\bar{p}$ relative yield at about 4-5 GeV/N kinetic energy nuclear collisions. In the quark plasma phase we expect a significant enhancement of $\bar{\Lambda}$ production which will be most likely visible in the $\bar{\Lambda}/\bar{p}$ relative rate. Thinking ahead a decade from now, I can foresee colliding nuclear beams with energies of the order of 100 GeV/N: The anticipated temperatures of several GeV in the quark plasma may lead to the formation of very exotic heavy flavour states involving c and b quarks at the same time.

Many fruitful discussions with the GSI/LBL Relativistic Heavy Ion group stimulated many of the ideas presented here. I would like to thank R. Bock and R. Stock for their hospitality at GSI. Parts of this work were performed in collaboration with R. Hagedorn, B. Müller, H.-Th. Elze, and M. Danos. I thank also the organizers of the Rencontre de Moriond for the opportunity to present these ideas and for the fine organization of the meeting.

References

1) R. Hagedorn and J. Rafelski, manuscript in preparation for Physics Reports. See also 'From Hadron Gas to Quark Matter', CERN preprints TH 2947 and TH 2969, to appear in the Proceedings of the 'International Symposium on Statistical Mechanics of Quarks and Hadrons', Bielefeld, Germany, August 1980, H. Satz, editor, North Holland Publishing Company.

2) The many-body theory for QCD at finite temperatures has been discussed by:
B.A. Freedman and L.D. McLerran, Phys. Rev. D16 (1977) 1169;
S.A. Chin, Phys. Lett. 78B (1978) 552;
P.D. Morley and M.B. Kislinger, Phys. Rep. 51 (1979) 63;
J.I. Kapusta, Nucl. Phys. B148 (1979) 461;
E.V. Shuryak, Phys. Lett. 81B (1979) 65 and Phys.Lett.C61 (1980)71;

O.K. Kalashnikov and V.V. Klimov, Phys. Lett. 88B (1979) 328

3) J. Rafelski, H.-Th. Elze, and R. Hagedorn, 'Hot Hadronic Matter in $\bar{p}$-Annihilation on Nuclei', CERN preprint TH 2912, in Proceedings of the 5th European $\bar{p}$-Symposium, June 1980, Bressanone, Italy. CLEUP, Edts., Padova 1980. See also J. Rafelski, Phys. Lett. 91B (1980) 28

4) For review see, for example, K. Johnson, 'The MIT Bag Model', Acta Phys. Polon. B6 (1975) 865

5) R. Hagedorn and J. Rafelski, Phys. Lett. 97B (1980) 136

6) J. Rafelski and M. Danos, Phys. Lett. 97B (1980) 279

7) J. Rafelski, 'Extreme States of Nuclear Matter', Frankfurt Preprint UFTP 52 (1981) in Proceedings of the Workshop on 'Future Relativistic Heavy Ion Experiments', R. Bock and R. Stock, eds. Darmstadt 1981.

8) It has been suggested in the lecture by P. Richard at this conference that this would be a stable state.

9) We record the first attempt by J. Baacke, Acta Phys. Pol B8 (1977) 625 to develop a thermodynamic description of a gas of quark bags.

10) R. Hagedorn, I. Montvay, and J. Rafelski, 'Hadronic Matter at Extreme Energy Density', Proceedings of Erice Workshop, eds. N. Cabibbo and L. Sertorio, Plenum Press (New York 1980), p. 49

11) J. Yellin, Nucl. Phys. B52 (1973) 583; see also E. Schröder, Zs. für Math. und Physik 15 (1870) 361

12) For LBL experiments see e.g. S. Nagamiya, 'Heavy Ion Collisions at Relativistic Energies', LBL preprint 9494 (1979) in Proceedings of the Symposium on Heavy-Ion Physics, Brookhaven National Laboratory, Upton, N.Y., July 15-20, 1979.
The ISR inclusive pp results are summarized in G. Giacomelli and M. Jacob, Phys. Lett. C55 (1979) 1

13) H.-Th. Elze, W. Greiner, and J. Rafelski, J. Phys. G6 (1980) L149 and in Ref. 3 above, H.-Th. Elze et al., to be published.

14) In the model of magnetic Savvidy vacuum the restoration of the perturbative vacuum has first been shown by B. Müller and J. Rafelski, 'Temperature Dependence of the Bag Constant and the Effective Lagrangian for Gauge Fields at Finite Temperatures', CERN preprint TH 2928, Phys. Lett. B in print. See also J. Kapusta, Phys. Rev. D in print and W. Dittrich and V. Schanbacher, Phys. Lett. B in print.

15) This view is at odds with the one presented by S. Lindenbaum at this conference.

16) R. Stock, private communication.

QCD SUM RULES FOR LIGHT QUARKS

Stephan NARISON
ICTP, Trieste (Italy)
and
Centre de Physique Théorique, CNRS, Marseille (France)

I. SUMMARY OF THE TALK

QCD sum rules of the Laplace transform type applied to the two-point functions of the divergence of the axial-vector current are presented. It is shown that the sum of the running up and down quark masses to two-loops within the framework of the $\overline{MS}$ dimensional renormalization scheme is :

$$\bar{m}_u(M_\varrho^2) + \bar{m}_d(M_\varrho^2) \gtrsim \begin{matrix}(30 \pm 7)\ \text{MeV} \\ (13 \pm 3)\ \text{MeV}\end{matrix} \quad \text{for } \Lambda_{\overline{MS}} \simeq \begin{matrix}70\ \text{MeV} \\ 210\ \text{MeV}\end{matrix}$$

at the ϱ-meson mass. Using the $SU(6)_W$ asymptotic symmetry, we equate the isovector two-point functions sum rule and the divergence of the axial vector two-point functions sum rule at the same $M^2 \simeq M_\varrho^2$ where they are both optimized. Then, we derive to leading order of QCD :

$$\frac{1}{2}\left[\bar{m}_u(M_\varrho^2) + \bar{m}_d(M_\varrho^2)\right] \simeq \sqrt{\frac{2e}{3}}\, f_\pi \frac{m_\pi^2}{m_\varrho^2}\, \gamma_\varrho \left[1 - \frac{8\pi^2}{M_\varrho^4} f_\pi^2 m_\pi^2\right]$$

Where $e \simeq 2.72...$ $f_\pi \simeq 93.3$ MeV, γ_ϱ is the ϱ-meson photon coupling normalized as : $\Gamma_{\varrho \to e^+e^-} \simeq \frac{1}{3}\ \alpha^2\ \pi\ M_\varrho^2/\gamma_\varrho^2$. This result differs by a factor $2 \sim 3$ to the Leutwyler current algebra mass :

$$\frac{1}{2}\ (\bar{m}_u^c + m_d^c) \simeq \frac{2}{3}\ f_\pi (m_\pi^2/M_\varrho^2)\gamma_\varrho \simeq 5\ \text{MeV}$$

The details of the above discussion are in S. Narison and E. de Rafael, Phys. Lett. B (to appear).

II. SOME GUIDE REFERENCES TO QCD SUM RULES OF LIGHT QUARKS

Applications of the Laplace transform sum rules to other types of currents are discussed by :

- M.A. Shifman, A.I. Vainshtein and V.I. Zakharov, Nucl. Phys. B147, 385, 448 (1979).
- S.I. Eidelman, L.M. Kurdadze and A.I. Vainshtein, Phys. Lett. 82B, 278, (1979).
- S. Narison, Trieste preprint IC/81/1 (1981), ibid IC/81/56 (1981).

QCD sum rules of the finite energy type are discussed by :

- R. Shankar, Phys. Rev. D15, 755 (1977).
- E.G. Floratos, S.Narison, E. de Rafael, Nucl. Phys. B155, 155 (1979).
- S. Narison, E. de Rafael, Nucl. Phys. B169, 253 (1980).

QCD sum rules based on finite number of derivatives of the two-point functions are discussed by :

- F.J. Yndurain, Phys. Lett. 63B, 211 (1976).
- C. Becchi, S. Narison, E. de Rafael and F.J. Yndurain (to appear in Z-für Physik C).
- S. Narison, Nucl. Phys. B182, 59 (1981).

III. ACKNOWLEDGEMENTS

I wish to thank the organizers of the Moriond Conference especially Tran Tan Van and L. Montanet for the invitation. I am also grateful to the Centre de Physique Théorique of Marseille for partial financial support.

EXPERIMENTAL SUMMARY

Klaus R. Schubert
Institut für Hochenergiephysik
Universität Heidelberg

During this second week of the 16th Rencontre de Moriond we have discussed a large number of new experimental results in "low q^2" hadron physics:

- hadrons with beauty, hidden and open, are becoming objects of detailed studies,
- some open questions in the charm sector have been settled,
- though no evidence for top has been observed, some classes of topless models are now ruled out by CESR results on missing neutral current decays of B mesons,
- only weak hints on the existence of glue balls have been reported so far,
- and "old" hadrons are still being studied extensively.

Let me try to summarize here briefly what has been discussed in these fields of hadron spectroscopy. "Low q^2" is of course more than spectroscopy, and I apologize for not covering the beautiful results on particle production, on electromagnetic form factors, and on parton fragmentation aspects in soft hadronic reactions. Charm production[1] and parton fragmentation[2] were covered by two excellent reviews during this week.

Old-Flavour Hadrons

Several new powerful tools for the spectroscopy of old hadrons have been presented, let me start with $\gamma\gamma$ scattering. Following last year's success of the MARK II group[3] in observing the $\eta'(958)$ in this reaction and determining its radiative width $\Gamma_{\gamma\gamma}$, two PETRA groups reported new results on $\gamma\gamma \to \pi^+\pi^-$ which show clear f(1270) and $S^*(980)$ mass peaks[4]. The channel $\gamma\gamma \to \rho^o\rho^o$ shows a strong threshold enhancement.

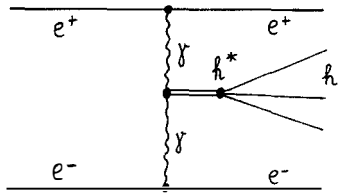

A series of experiments utilizing the nuclear Coulomb field to measure radiative widths for $\rho \to \pi\gamma$, $K^* \to K\gamma$, $A_2 \to \pi\gamma$ ... was reported by T. Ferbel.

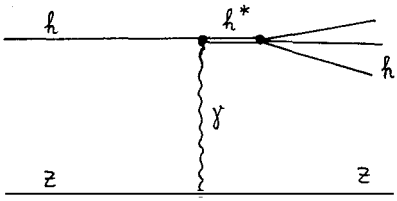

With t cuts less than 0.002 GeV^2 at the nuclear vertex, this is the lowest q^2 physics which was discussed here. Impressively clean resonance peaks[5] can be obtained in submasses of h^*, e.g. $D^0(1285)$ in the $\eta\pi^+\pi^-$ invariant mass.

Experiments with electron-positron annihilation and photoproduction show a new resonance near 1650 MeV. The DCI group[6] observes it in the channel $K^0_S K^\pm\pi^\mp$ and assigns it to a $\Phi' = s\bar{s}$ state.

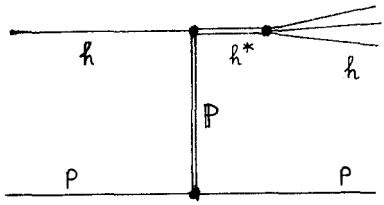

The best tool for high statistics spectroscopy of old hadrons is still provided by the Pomeron.

The ACCMOR group[7] presented a partial wave analysis with 600 000 $\pi^\pm p \to (\pi^\pm\pi^+\pi^-)p$ and 50 000 $\pi^- p \to (\pi^- K^+ K^-)p$ events[8]. The A_3(M = 1660 MeV, Γ = 200 MeV, $J^{Pc} = 2^{-+}$) resonates in $f\pi$, $\rho\pi$ and K^* K channels, while the A_1(1280 ± 30 MeV, 300 ± 20 MeV, 1^{++}) resonates only in $\rho\pi$.

c-Flavour Hadrons

The production of charmed particles[1] and their spectroscopy[9] have been covered in review contributions during this week, therefore I should like to concentrate on the lifetime measurements.

Charm spectroscopy is still mainly the domain of e^+e^- annihilation. The only active detector during the last year has been the Crystal Ball[10] at SPEAR, since MARK II and DELCO are moving to PEP, MARK III is still under construction, and the DESY detectors are tasting the new flavour at DORIS. The Crystal Ball group has confirmed the three χ states (3415, 3503, and 3551 MeV) and established the η_c state with a mass of (2978 ± 9) MeV. Their inclusive η signal, though statistically compatible with the old DASP result[11], does not confirm the DASP conclusions on the production of $F^\pm$ mesons. There remains, however, the evidence for $F^\pm$ in photo- and neutrino production.

The Ω group[12] sees photoproduced $F^\pm$ in the channels $\eta\pi$, $\eta 3\pi$ and $\eta 5\pi$, and

two emulsion groups[13, 14] found four events in neutrino production. Two of these are $K\bar{K}\pi\pi$ decays and the two others decay into 4π with no possible η combination; on the basis of this weak statistics one could conclude that the ratio of cs decay to $c\bar{s}$ annihilation is 1:1 in F decays.

Lifetime measurements of charmed particles were discussed at length during this week because of their fundamental importance and because of the experimental challenge to measure lifetimes in the 10^{-13} sec region. The c-quark lifetime had been estimated long ago[15]:

$$\Gamma(c \to s l^+ \nu) = \cos^2\theta_c \cdot \frac{G_F^2}{192\,\pi^2} \cdot m_c^5 \cdot \text{phasespace} \cdot \text{QCD} \simeq 1.4 \cdot 10^{11}/\text{sec}, \qquad (1)$$

$$\Gamma_{tot}(c) = 1/\tau = \Gamma(e^+\nu_e) + \Gamma(\mu^+\nu_\mu) + N_C \cdot \Gamma(u\bar{d}) \simeq 5 \cdot \Gamma(e^+\nu_e) \simeq 7 \cdot 10^{11}/\text{sec}, \qquad (2)$$

$$BR(c \to s e^+ \nu_e / c \to \text{all}) \simeq 20\ \%\ , \qquad (3)$$

with the Cabibbo angle θ_c and the colour factor $N_C = 3$. If the quark decay mechanism dominates all decays of D^o, $D^\pm$, $F^\pm$, and Λ_c^+ (with the other constituent quarks as spectators), the four hadron lifetimes would be equal and have values around 10^{-12} sec. Contributions of other mechanisms like annihilation of constituent quarks into $W^\pm$ or $W^\pm$ exchange between constituent quarks would diminish the hadron lifetimes (2) and the semileptonic branching ratios (3), but would not change the semileptonic widths (1):

$$\Gamma(D^o \to e^+ X) = \Gamma(D^+ \to e^+ X) \simeq 1.4 \cdot 10^{11}/\text{sec}. \qquad (1')$$

MARK II[9] and DELCO[16] have determined semileptonic branching ratios of D^o and D^+ and find

	Mark II (ref. 9)	DELCO (ref. 16)
$BR^+(D^+ \to e^+ X)$	$(16.8 \pm 6.4)\%$	$(22.0^{+4.4}_{-2.2})\%$
$BR^o(D^o \to e^+ X)$	$(5.5 \pm 3.7)\%$	$< 4\ \%$ (95 % conf.)
$BR^+/BR^o = \tau^+/\tau^o$	$3.1^{+4.6}_{-1.4}$	> 4.3

The first information of the lifetimes τ^+ and τ^o of $D^\pm$ and D^o mesons was deduced from these results: BR^+ is near to 20 % as expected by the dominance of quark decay (3), suggesting that τ^+ is near to 10^{-12} sec (2). However, BR^o

and τ^{o} are 3 to 8 times smaller, suggesting that annihilation/exchange mechanisms dominate in D^{o} decay.

Four different techniques have been discussed this week for measuring directly the lifetimes of charmed particles:

- emulsion plus bubble chamber [EB] [13]
- emulsion plus spectrometer [ES] [14, 17]
- high resolution bubble chamber plus spectrometer [BS] [18, 19]
- surface barrier detector set plus spectrometer [SS] [20].

In all these techniques, the distances between production vertex and decay vertex of charmed particles are directly measured, and, with beams in the 100 GeV region, the sensitivity reaches down to the 10^{-13} sec region.

A key problem, besides limited statistics, is the precise knowledge of the efficiency for finding charm decays as a function of the flight distance. For emulsions, this efficiency is decreasing for large distances because of the "large" volumes which have to be scanned by microscope. An uncorrected average of measured flight times would therefore be lower than the true mean life. For the "high" resolution bubble chambers, the efficiency decrease is more serious towards small distances because of the still limited resolution. Here, an uncorrected average would yield too high values for the mean life. For the surface barrier detector set I cannot judge the bias problems.

The results discussed this week are summarized in the table below:

Experiment	Technique	Beam	Target	Reconstr. Events	Mean Life (10^{-13} sec)
ref. 13	EB	ν	Emulsion	1 F^{+}	—
ref. 14	ES	ν	Emulsion	3 $F^{\pm}$	2.0+1.8-0.8
				18 D^{o}	3.1+1.1-0.7
				6 $D^{\pm}$	9.5+6.5-3.3
				6 Λ_c^{+}	1.7+0.9-0.5
ref. 17	ES	γ	Emulsion	3 D^{o}	0.6+0.8-0.2
				8 $D^{\pm}$	$\approx$ 4.4
ref. 18	BS	π^{-},P	H_2	2 D^{o}	xxx)
ref. 19	BS	γ	H_2	2 D^{o}, 1 D^{+}	xx)
ref. 20	SS	γ	Si	20 $D^{\pm}$	x)

x) The analysis is in progress. The lifetime distribution as shown this week contained about 80 decays with 20 identified $D^{\pm}$ and a small but, up to now, unknown fraction of D^{o}.

xx) The analysis is in progress, more events are expected.

xxx) The analysis has just started. Only one charm event has been fully reconstructed so far and has been published this week[18]. It contains a $\overline{D^{o}} \to K^{-}\pi^{+}\pi^{-}\pi^{-}$ decay with $t = 5.9\ 10^{-13}$ sec and a $D^{o} \to K^{-}\pi^{+}\pi^{o}\pi^{o}$ decay with $t = 2.1\ 10^{-13}$ sec where the two π^{o} mesons are well reconstructed in the EHS gamma detector.

The few new events reported here have changed the value for τ^{+}/τ^{o} in direct lifetime measurements from about 10 last year to 3^{+3}_{-1}. With five or ten times more events next year[18, 19] we may hope to settle this question.

b-Flavour Hadrons

The discussion included properties of the Y family with results from LENA[21], DASP-2[22], CLEO[23], and CUSB[24], and first hints on B mesons from CLEO and CUSB.

The ground state of the Y family has a mass of (9460 ± 10) MeV; its leptonic width has been determined by five groups:

(1.33 ± 0.14) KeV (PLUTO), (1.02 ± 0.17) KeV (CLEO),
(1.23 ± 0.17) KeV (LENA), (1.07 ± 0.17) KeV (CUSB),
(1.35 ± 0.20) KeV (DASP2),

where I have combined statistical and systematic errors. There is a surprising clustering within laboratories, but all values are compatible with their common mean value:

$$\Gamma_{ee}(Y) = (1.20 \pm 0.08)\ \text{KeV}. \qquad (4)$$

This result allows the conclusion that $Y = b\bar{b}$ and that the charge of the b quark, $|q(b)|$, is $1/3 \cdot e_{o}$.

The leptonic branching ratio has also been measured several times. The CLEO group reported here a new method using data taken on the Y':

$$BR(Y \to ee) = \frac{N(Y' \to \pi^{+}\pi^{-} + e^{+}e^{-} \text{ with inv. mass} = M(Y))}{N(Y' \to \pi^{+}\pi^{-} + \text{missing mass} = M(Y))}\ .$$

See the figure in ref. 23; their preliminary result is $(3.9 \pm 1.1)\%$. Together with the DORIS values $(2.2 \pm 2.0)\%$(PLUTO $\mu^+\mu^-$), $(5.1 \pm 3.0)\%$(PLUTO e^+e^-), $(3.5 \pm 1.5)\%$(LENA $\mu^+\mu^-$) and $(2.9 \pm 1.4)\%$(DASP2 $\mu^+\mu^-$) one obtains a mean value of

$$B_{\mu\mu}(\Upsilon) = BR(\Upsilon \to \mu\mu \text{ or } ee) = (3.3 \pm 0.6)\%. \tag{5}$$

This value of the leptonic branching ratio allows in principle a very precise determination of the strong coupling constant α_s, since $\Gamma(\Upsilon \to \mu\mu)$ is proportional to α^2 and $\Gamma(\Upsilon$ direct $\to$ hadrons) is equal to $\Gamma(\Upsilon$ direct $\to$ 3 gluons) in leading order QCD and proportional to α_s^3. Υ direct means that $\Upsilon \to \gamma^* \to q\bar{q}$ decays are subtracted.
Including higher orders:

$$\Gamma(\Upsilon \text{ direct} \to \text{hadrons}) = \Gamma_{3g} + \Gamma_{4g} + \Gamma_{5g} + \ldots = \Gamma_{3g}\left(1 + C_4 \frac{\alpha_s}{\pi} + \ldots\right),$$

$$\Gamma_{3g}/\Gamma_{ee} = 10(\pi^2 - 9)\,\alpha_s^3 / 9\pi\alpha^2,$$

$$\frac{\Gamma(\Upsilon \text{ direct} \to \text{hadrons})}{\Gamma_{ee}} = \frac{1}{B_{\mu\mu}} - (R + 3) = \frac{10(\pi^2 - 9)}{9\pi\alpha^2} \cdot \alpha_s^3\left(1 + C_4 \frac{\alpha_s}{\pi} + \ldots\right). \tag{6}$$

In this last relation, $(R+3)$ takes into account $\Upsilon \to \gamma^* \to q\bar{q}$, ee, $\mu\mu$, $\tau\tau$; and $R = \sigma_{had}/\sigma_{\mu\mu}$ near the Υ resonance is 3.7 ± 0.3. Neglecting all higher orders, $C_4 = C_5 = \ldots = 0$, one obtains

$$\alpha_s = 0.160^{+0.014}_{-0.011}. \tag{7}$$

Given these small errors, it seems highly desirable to calculate the higher order QCD corrections. In private discussions during this week, I learnt that there are two such calculations under way. Combining the new mean values (4) and (5), we find

$$\Gamma_{tot}(\Upsilon) = \Gamma_{ee}/B_{\mu\mu} = (36^{+9}_{-6})\ \text{KeV}. \tag{8}$$

Note that the errors have now reached the precision of the J/ψ width.

The DASP-2 group[22] has studied decay particle spectra with identified particles on and near the Υ in order to see differences between gluon fragmentation and quark fragmentation. A marked effect is seen in the baryon abundancy: the ratio

$\langle n(p+\bar{p})\rangle/\langle n(\text{charged})\rangle$ with particle momenta above 200 MeV/c is (8 ± 2)% on the Y, which is about 3 standard deviations higher than from quark fragmentation in the continuum. The same effect is seen on the Y'. Unfortunately CLEO, the only other magnetic detector which could confirm the effect, identifies charged particles only above 600 MeV/c up to now.

News on the Y' or Y(2S): Three groups have found the $\pi\pi$ cascade to the ground state; I quote here the branching ratios BR = BR(Y' → Y$\pi\pi$) = 3/2 · BR(Y' → Y$\pi^+\pi^-$). The LENA group[21] finds 7 events of the type $\pi^+\pi^-l^+l^-$, and with additional information from the change in decay multiplicity distributions on Y' and Y they give BR = (31 ± 10)%. The CLEO group[23] reports 840 events of the type Y' → $\pi^+\pi^-$ + (missing mass = M_Y) and finds BR = (29 ± 5)%. The CUSB group[24] has got 23 events Y' → $l^+l^-\pi^\pm(\pi^\mp)$ with BR = (30 ± 11)%. The three results agree very well with each other. They may be used for an indirect determination of the leptonic branching ratio and of the total width of the Y', since both quantities have not yet been measured directly. The underlying assumption is

$$\frac{\Gamma_{3g}(Y')}{\Gamma_{ee}(Y')} = \frac{\Gamma_{3g}(Y)}{\Gamma_{ee}(Y)} \quad , \tag{9}$$

from which one derives easily[21, 23]

$$\Gamma_{tot}(Y') = \frac{\Gamma_{ee}(Y')/B_{\mu\mu}(Y) + 4\ \text{KeV}}{1 - BR(Y' \to Y\pi\pi)} = (31 \pm 9)\ \text{KeV}. \tag{10}$$

The 4 KeV value is an estimate for the width of radiative Y' decays. The absolute width $\Gamma(Y' \to Y\ \pi\pi)$ which follows from this calculation allows the conclusion that the $\pi\pi$ cascade is mediated by <u>vector</u> gluons.

No radiative cascade decays Y' → Y $\gamma\gamma$ have been reported up to now, and no news on the Y'' = Y(3S) was given this week.

The Y(4S) state has a mass of about 10.57 GeV and a natural width of Γ_{tot} = (20 ± 8) MeV. It has been discovered at Cornell, and CESR is still the only machine where it may be studied. The DORIS energy range ends now at about 10.1 GeV, but an improvement program is under way which was reported here by W. Schmidt-Parzefall[22]. A workshop on Y and B physics[25] was held in February 81 at DESY to discuss the importance of the energy range up to 11 GeV. In mid 82, the new magnetic detector ARGUS and a nonmagnetic detector of the LENA or Crystal

Ball type are expected to start with Y(4S) physics at DORIS as well.

Since the 3-gluon width of the Y(4S) meson is estimated to be 20 KeV and its natural width is measured to be a factor 1000 larger, it decays predominantly into $(b\bar{d})(\bar{b}d) = B^0\,\bar{B}^0$ and $(b\bar{u})(\bar{b}u) = B^-\,B^+$ pairs. Up to now, neither a fully reconstructed Y(4S) decay nor a B mass peak have been shown. But there is strong indirect evidance for the existence of B mesons from the kaon, muon, and electron excess on the Y(4S) relative to the nearby continuum[23, 24]. The CUSB group reports

$$\langle n(K^0 + \bar{K}^0)\rangle \text{ per } B\bar{B} \text{ event} = 1.2 \pm 0.5,$$

and the same effect is seen by the CLEO group:

$$1/2 \cdot \langle n\ (K^+ + K^- + K^0 + \bar{K}^0)\rangle \text{ per } B\bar{B} \text{ event} = 1.7 \pm 0.5.$$

A Monte Carlo simulation with $b \to c$ decays predicts a value of 1.6 and with $b \to u$ a value of 0.9 for this average kaon multiplicity.

For the inclusive muon and electron yield with $p > 1$ GeV/c reported by the CLEO group, see the figure in ref. 23. Clear enhancements at the Y(4S) mass allow the determination of a semileptonic branching ratio

$$BR(B^0 \text{ or } B^- \to e^- \text{ or } \mu^-, + X) = (11.1 \pm 2.7)\% .$$

In contrast to the charm case, see eqs. 1 to 3, there is neither a prediction for the absolute semileptonic rate nor for the B lifetime within the standard model of weak interactions because of unknown mixing angles. The standard model couples l^- to $W^-\nu$, d' to W^-u, s' to W^-c and b' to W^-t with equal strength, where d', s', and b' are linear combinations of d, s, and b quarks:

$$\begin{pmatrix} d' \\ s' \\ b' \end{pmatrix} = U_{KM} \begin{pmatrix} d \\ s \\ b \end{pmatrix}, \qquad U_{KM} \simeq \begin{pmatrix} 1 & s_1 & s_1 s_3 \\ -s_1 & 1 & s_3 \pm s_2 \\ \pm s_1 s_2 & -s_3 \mp s_2 & 1 \end{pmatrix}.$$

The matrix U_{KM} with four free parameters θ_1, θ_2, θ_3, and δ has been introduced by Kobayashi and Maskawa, $s_i = \sin\theta_i$, $\cos\theta_i \simeq 1$, and $\pm$ is my shorthand notation for $e^{i\delta}$ since δ is probably near to 0^0 or 180^0. θ_1 is nearly the same as the experimentally well known Cabibbo angle θ_c which enters into eq. 1. θ_2 and θ_3 are essentially unknown; there exist only very loose experimental bounds. $s_1 s_3$ is responsable for $b \to u$ transitions and $s_3 \pm s_2$ for $b \to c$. $s_2 = s_3 = 0$ is

excluded since B mesons are not stable. The JADE group[26] at PETRA has recently measured a new limit for the B lifetime

$$\tau(B) < 10^{-11} \text{ sec}, \tag{12}$$

which is roughly translated into $|s_2 \pm s_3| > 0.02$. The angles θ_2 and θ_3 may still be very small. Information on the ratio $(b \to u)/(b \to c) = |s_1 s_3/(s_2 \pm s_3)|^2$ is soon expected to be available, e.g. from the shape of inclusive $B \to$ lepton spectra.

Additional Y(4S) news from CUSB: No 50-MeV-photons have been observed from $B^* \to B\gamma$ decays. This restricts the mass range for B mesons to be between 5.16 and 5.26 GeV. A fine scan between 10.5 and 11.5 GeV does not show any further resonances comparable to the 4S, see the figure in ref. 24. The average $R = \sigma_{had} / \sigma_{\mu\mu}$ in this range is 0.40 ± 0.13 units larger than below the open b - open $\bar{b}$ threshold, and this increase is well compatible with $3\ q(b)^2$.

t-Flavour Hadrons

Nothing has been discussed on this subject for obvious reasons. The search for $t\bar{t}$ states at PETRA has reached the limit[27]

$$m(t\bar{t}) > 36.72 \text{ GeV}. \tag{13}$$

The CLEO group has looked for neutral current decays of b quarks by searching for $B \to l^+ l^- X$ events. No event was found, and an upper limit of

$$BR(B \to l^+ l^- X)/BR(B \to l^\pm \nu X) < 11.8\ \% \tag{14}$$

is deduced with 90 % confidence. Five-quark models require large neutral current coupling to the partnerless b and are ruled out by this result. See ref. 23 for further references.

Hadrons without Flavour

Do narrow glue balls exist, with a width of 30 MeV or less? Does QCD really need them? What is the experimental signature to search for them? There are no clear answers to these questions. But any flavour-neutral broad mass bump in any hadronic reaction may be interpreted as "stripped-off" glue forming a glue "ball" for a time of, say, 10^{-24} sec. So if QCD is content with broad glueball states, or even with many of them which may overlap[28], there is nothing to discover experimentally.

Two possible candidates for narrow glue ball states have been shown during this week. A BNL/CCNY experiment[29] finds that the OZI-forbidden reaction $\pi^- p \to \Phi\Phi n$ has about the same rate as the OZI-allowed reaction $\pi^- p \to \Phi K^+ K^- n$.

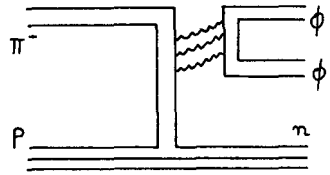

Since OZI-forbidden graphs as shown in the figure are mediated by gluons, the observed enhancement could be interpreted as exchange and decay of a glue ball. The $\Phi\Phi$ mass spectrum, see the figure in ref. 29, has not enough statistics to enable one to decide if there are several narrow peaks between 2.1 and 2.4 GeV/c^2 or one 300 MeV broad bump. The experiment expects to attain 20 times the present number of events.

The other candidate which was discussed is also found in a gluon-rich environment. The J/ψ decays into γ + 2 gluons with about 6% branching ratio. The invariant hadron mass spectrum in $J/\psi \to \gamma$ + hadrons shows three prominent and narrow peaks, $\eta(548)$, $\eta'(958)$, and "E(1420)". The Crystal Ball group[30] sees "E" $\to \eta\pi\pi$; "E" $\to K\bar{K}\pi$ is seen by the Crystal Ball and by MARK II[31]. Both groups are not yet able to determine spin and parity of this "E". I put it into quotation marks because several authors[32] have proposed that it is different from the E(1420) which is seen in hadronic reactions and was determined to have $J^P = 1^+$ in a recent charge exchange experiment[33] $\pi^- p \to En$, $E \to K\bar{K}\pi$. The suspicion that "E" $\neq$ E and J^P("E") $= 0^-$ is based on the observation that the $K\bar{K}\pi$ states of the "E" are mainly $\pi\delta$ and those of the E are mainly $K\bar{K}^*$. If "E" = E, which still seems to be the most likely situation, its spin parity would be 1^+ and it would be the $s\bar{s}$ member of the axial vector nonet instead of a glueball.

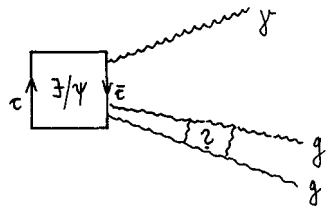

The 1^+ assignment to the E in ref. 33 is based on about 200 $K\bar{K}\pi$ decays. MARK II has about 80 and the Crystal Ball about 100 $K\bar{K}\pi$ decays. I wonder if a combination of the two data sets would allow to settle this burning question. If the "E" turns out to have $J^P = 0^-$, there would be too many pseudoscalars, and either the "E" is a glueball or π^0, η, η', and "E" are mixtures of $u\bar{u}$, $d\bar{d}$, $s\bar{s}$, and gluonium.

A third gluon-rich environment is given in Pomeron-Pomeron collisions, and it has been suggested several times to look for glueball production there. Five years

ago, two ISR groups (CCHK and CHHOV) studied double Pomeron exchange in the exclusive channel $pp \to pp\pi^+\pi^-$. As illustrated in the two diagrams, the kinematical situation is identical to $\pi^+\pi^-$ production in photon-photon collisions where we saw very recent data this week.

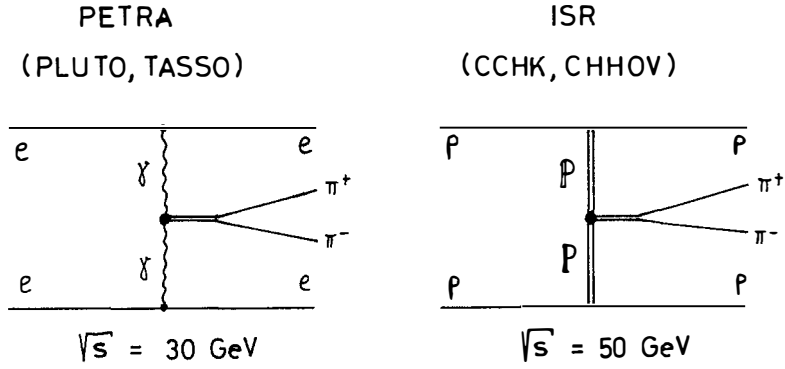

In $\gamma\gamma$ collisions, there is predominantly formation of states with quark content since photons couple to flavour. In Pomeron-Pomeron collisions, however, also states without valence quarks may be formed, if there are any. This expectation is based on the parton picture of the Pomeron as a cloud of hard and soft gluons. As seen in the figure, the data are from ref. 34, there is no indication of narrow resonances in the $\pi\pi$ system - only a broad bump peaking near 600 MeV and a f^0 signal are observed. The f^0 comes out clearer with further cuts; the mass resolution is about ± 50 MeV.

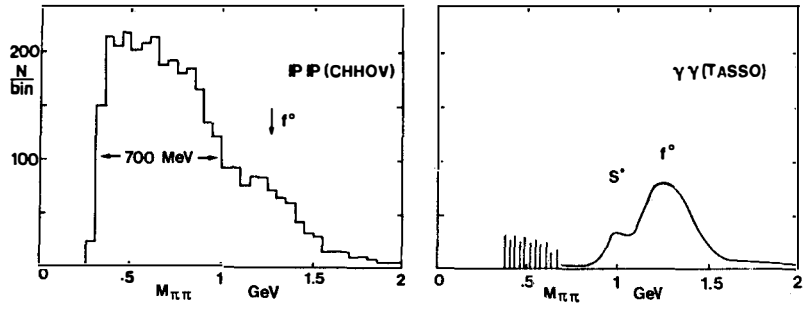

The $\pi\pi$ mass spectrum in $\gamma\gamma$ collisions[4] looks strikingly different[35], I normalize the two spectra arbitrarily to equal f^o peak height.

What message could be learnt from the comparison of the two reactions? The f^o is produced in both reactions since it contains, as all other hadrons, valence quarks and glue. The broad bump around 600 MeV is only produced by glue and not by photons. Let me call it a primitive glue ball[28] or a "glue bump" in contrast to the narrow glue balls which we are still waiting for. If we should wait several more years without success, the message of my comparison would be simple: gg, ggg ... systems are indeed formed - and not only in $\bar{p}p$ collisions -, but their width is broad.

I would like to thank J.Tran Thanh Van and L. Montanet for their invitation to this interesting, pleasant and stimulating meeting. I also thank N. Kwak for a critical reading of this manuscript and Mrs. U. Einecke for typing it in shortest time.

References

1) S. Wojcicki, these proceedings
2) W. Kittel, these proceedings
3) see e.g. R. Hollebeek, proceedings of the 15th Rencontre de Moriond, 1980, Vol. II, p. 107
4) see figure in P. Leu's contribution to these proceedings
5) see figures in T. Ferbel's contribution to these proceedings
6) J. C. Bizot, these proceedings, see figure
7) W. Hoogland, these proceedings and G. Otter, these proceedings
8) with new data from the Ω spectrometer
9) G. Trilling, these proceedings and Physics Reports, to be published
10) R. Partridge et al.,Phys. Rev. Letters 45 (1980) 1150
11) R. Brandelik et al., Phys. Letters 70 B (1977) 132, and Z. Physik C1 (1979) 233
12) D. Aston et al., Phys. Letters 100 B (1981) 91
13) R. Ammar et al., Phys. Letters 94B (1980) 118
14) E 531, J. Prentice, these proceedings
15) N. Cabibbo and L. Maiani, Phys. Letters 79B (1978)109, and references therein.
16) W. Bacino et al., Phys. Rev. Letters 45 (1980) 329
17) M. I. Adamovich et al., Phys. Letters 99B (1981) 271
18) NA 16 (EHS), J. Lemonne, these proceedings, and B. Adeva et al., submitted to Phys. Letters, March 1981
19) SHF, G. Ballam, these proceedings

20) FRAMM, M. Giorgi, these proceedings

21) U. Volland, these proceedings

22) W. Schmidt-Parzefall, these proceedings

23) H. Kagan, these proceedings

24) P. M. Tuts, these proceedings

25) "Workshop on DORIS experiments", a printed set of speakers' transparencies is available from the organizer, H. Schröder, DESY-F15

26) D. Haidt, private communication

27) see e.g. W. Bartel et al., Phys. Letters 100B (1981) 364

28) N. Isgur's "primitive glue balls", these proceedings, and H. Fritzsch's discussion remark in ref. 25

29) S. J. Lindenbaum, these proceedings

30) D. Aschman, proceedings of the 15th Rencontre de Moriond, 1980, vol. II, p. 83

31) D. L. Scharre et al., Phys. Letters 97B (1980) 329

32) During this week S. U. Chung, see these proceedings

33) C. Dionisi et al., Nucl. Phys. B 169 (1980) 1

34) H. de Kerret et al., Phys. Letters 68B (1977) 385, and further CHHOV data, R. Waldi, Diplomarbeit Universität Heidelberg 1979, unpublished

35) This observation and its possible interpretation were pointed out to me by M. Jacob

CONFERENCE SUMMARY TALK
(THEORY)

Howard J. Schnitzer†
Brandeis University
Waltham, Massachusetts 02254
U.S.A.

Abstract

Theoretical highlights of the meeting are discussed, with particular emphasis being given to spectroscopy and the quark model.

I shall present a survey of the work of the meeting very much from the viewpoint of a theorist. In an attempt to give some unity to my report, I shall concentrate on material which has some relation to the quark model and to local gauge theories, with apologies to the authors of several excellent reports that I am unable to review due to limitations of space and/or because of my lack of understanding of a particular area.

I. Spectroscopy

Reports of theorists working in this area were presented by Isgur, Gromes, Barnes, Cho, Krasemann, Michael, Navelet, O'Donnell, Richard, Schnitzer, Tornquist and Wagner. It is the concensus of almost all workers dealing with meson and baryon spectroscopy that a unified approach to the subject has emerged which correlates a great deal of data with very few parameters. A single non-relativistic (N.R.) quark model allows one to discuss the detailed spectroscopy of $(q\bar{q})$, $(Q\bar{Q})$, $(q\bar{Q})$, (qqq), and (qqQ) states with comparable success. [Here q represents a light valence u, d, or s quark and Q a heavy c, b, t, ... quark]. The model is described schematically by the Hamiltonian

$$H = \underbrace{\sum_i (m_i + p_i^2/2m_i) + \sum_{i<j} U^{ij}}_{\text{spin-independent}} + \underbrace{\sum_{i<j} V^{ij}{}_{spin}}_{\text{spin-dependent}} \tag{1.1}$$

The basic assumptions are

1) non-relativistic two-body forces acting between pairs of quarks with constituent masses m_i. Only color singlet hadron states are considered. The [non-relativistic model works well for both ordinary meson and baryon states even though $(v/c)^2$ for these states is uncomfortably large.]

2) $$U^{ij} = (1 \text{ gluon exchange}) + \underbrace{(\text{confining potential})}_{\substack{\text{flavor independent} \\ \text{Lorentz scalar.}}} \tag{1.2}$$

3) $V^{ij}{}_{spin}$ is obtained from U^{ij}, correct to leading order in $(v/c)^2$. This implies that the two-body spin force has the general form

$$V^{ij}_{spin} = \underbrace{\frac{1}{m_1 m_2} V_T(r)\, S_{12}}_{\text{tensor}} + \underbrace{\frac{4}{m_1 m_2} V_S(r)\, \vec{S}_1 \cdot \vec{S}_2}_{\text{spin-spin}}$$

$$+ \Big[\underbrace{\frac{1}{m_1 m_2} V_1(r)}_{\text{spin-orbit}} + \underbrace{1/2 \left(\frac{1}{m_1^2} + \frac{1}{m_2^2} \right) V_2(r)}_{\text{Thomas}} \Big] \vec{L} \cdot \vec{S}$$

$$+ \underbrace{1/2 \left(\frac{1}{m_1^2} - \frac{1}{m_2^2} \right) V_2(r)\, \vec{L} \cdot (\vec{S}_1 - \vec{S}_2)}_{\text{Thomas}} \qquad (1.3)$$

The qualitative behavior of the potentials, as determined from spectroscopic data, is shown in Fig. 1. A large body of empirical data is compatible with the above assumptions and the spin-dependent potentials shown in Fig. 1.

This approach is not without problems, the most serious of which is a lack of understanding why the non-relativistic approximation appears to work so well when $(v/c)^2$ is large. Other questions of detail still open can probably be cured by further experimental and theoretical work, but the successive of the N.R. model itself is embarrasingly good, and may actually be a house of cards. Of course there are some details which require additional attention. For example, both Gromes and Richard emphasize that the omission of either induced or genuine three-body forces in baryon spectroscopy may not be satisfactory. Another issue, which plagues meson spectroscopy, is the status of the $^3P_0$ scalar meson states. The model outlined above clearly predicts that the pure $(q\bar{q})$ $^3P_0$ states lie in the 1.0 to 1.2 Gev region below the corresponding J = 1 P states, although experiment gives little support to this prediction. However the experimentally observed scalar mesons need not be pure $(q\bar{q})$ states. It is possible that the observed scalar mesons contain considerable admixtures of $(q\bar{q})(q\bar{q})$ states as proposed by Jaffe, as well as contributions from gluon continuum and/or discrete states. [In this latter context remember the existence of gluon continuum in the η and η' states]. Further, perhaps not all stationary states of a confining potential are observable in the S-matrix. Possibly one could apply the P-matrix method of Jaffe and Low to treat $(^3P_0)_{\bar{q}q}$ potential model states as primitives, which might then uncouple rrom the S-matrix. Further, Isgur and Karl observed

that not all channels couple to a given baryon state. Perhaps an analogous situation holds for certain of the mesons as well.

It turns out that one may be able to test the validity of the non-relativistic picture itself. As one can observe from Fig. 1, the total spin-orbit potential is attractive at short distances (one gluon exchange is dominant) and repulsive at long-distances (Lorentz scalar confining potential is dominant). The presently known mesons are small enough in spatial extent to be predominately sensitive to the attractive portion of $(V_1 + V_2)\ \vec{L}\cdot\vec{S}$. However, for a meson for which $m_2 \gg m_1$, one has

$$V_{spin} \xrightarrow[m_2 \gg m_1]{} \underbrace{\frac{1}{m_1^2}\, V_2(r)\ \vec{L}\cdot\vec{S}}_{\text{repulsive}} + O(m_1/m_2) \tag{1.4}$$

In this case one predicts (Schnitzer)

$$\underbrace{E(^3P_2) < E(J=1)}_{2\text{ states}} < E(^3P_0) \tag{1.5}$$

which is an inverted multiplet. Presumably this prediction is applicable to the P-wave charmed ($c\bar{u}$), bottom ($b\bar{u}$), and similar mesons. Further, in ordinary ($q\bar{q}$) mesons, for sufficiently large L, the Thomas term also dominates, leading again to a prediction of inverted multiplets. Based on a specific calculation reported at this meeting, Barnes suggests that this phenomenon may occur for L as small as L = 2. For ordinary mesons, the I = 1/2 states are particularly promising candidates for a test of those ideas, as the states in question cannot have any glue admixture. A continuation of the SLAC program reported by Ratcliff may be useful in this context. However, if one is searching for inverted multiplets, one must remember to untangle the tensor mixing which can mix n = 2; $^3S_1$ with n = 1; $^3D_1$ (say), as the unmixed pure ($q\bar{q}$) states are the ones predicted to have inverted multiplets for large enough L.

If the meson multiplets fail to invert, it would be very difficult to save the non-relativistic picture, as the prediction is not sensitive to the details of parameters and wave-functions, and only depends on qualitative features of the model. I believe that very few workers at this stage would be willing to give

up the idea of a Lorentz scalar confining potential. Therefore, a failure of the prediction would appear to be a direct attack on the non-relativistic picture. Hopefully experimentalists will take up the theorists' challenge to test the model.

Both the theoretical and experimental status of multiquark hadron states remains uncertain. In a report to this conference, Richard argued that in a potential model, $E(Q\,\bar{Q}\,Q\,\bar{Q}) > 2E(Q\,\bar{Q})$ which means that the $(Q\,\bar{Q}\,Q\,\bar{Q})$ state is unstable for decay into mesons. For quarks Q and q, with constituent masses M and m respectively, he finds that $(Q\,\bar{Q}\,q\,\bar{q})$ is unstable, while the exotic state $(Q\,Q\,\bar{q}\,\bar{q})$ is stable if (M/m) is sufficiently large.

There is considerable interest in the possible existence of discrete gluon states (glueballs). One expects strongly interacting gluon states because a) asymptotic freedom implies strong-coupling in the infrared region and b) color confinement implies that there must be a mass-gap in the gluon spectrum. That is, there can be no observable zero-mass gluons. These arguments lead one to suspect that the 1 to 3 Gev region would be a profitable mass-domain to search for glueballs. If energies are too high, α_s is too small, and gluons would not be strongly interacting. Of course one could have a strongly interacting gluon continuum as there is no argument that requires discrete gluon states. Many of the theoretical discussions assume the existence of "valence" gluons and gluon counting in order to employ a potential model picture. However, the analogy with valence quarks is far from perfect for strongly interacting self-coupled gluons, and the actual classification of possible gluon states is controversial. If only transverse gluons are permitted (Barnes), then only non-exotic states emerge, which then would be difficult to distinguish from ordinary meson states. On the other hand, if longitudinal states are allowed as well, then exotic gluon states are predicted. Unfortunately there is no general agreement among the workers in the field on these issues, nor on the properties of gluon states.

Some preliminary experimental evidence exists which is suggestive of possible gluon states. There is a peak at 1420 Mev in the decay $\psi \to \gamma + X$ but not at

D(1280). The question is whether the peak is to be identified with the $^3P_1$ E(1420) ($\bar{s}s$) state of the quark model, or is a distinct state. If the bump in $\psi + \gamma + X$ is a 0^{-+} state, then the possibility that it is a gluon state is increased. Navelet reported a calculation which suggests that the bump might in fact be an admixture of 0^{-+} and 0^{++}. Given these indications, a study of D(1280) and E(1420) production mechanisms in hadron collisions may also be helpful in revealing any gluon content of these states. Lindenbaum called attention to the sharp mass peak in the Zweig-rule violating reaction $\pi^- p \to \phi\phi\, n$ as a possible indication of a gluon state, with preliminary data reported in the discussions by Hoogland and by Green tending to confirm the observations of Lindenbaum. However the interpretation of the peak as a gluon state will require further evidence. We heard theoretical discussion of hadron magnetic moments by O'Donnell and by Wagner, while Ferbel and Overseth presented experimental information on meson transition magnetic moments ($V + M + \gamma$), and baryon static moments respectively. Clearly the gross features of these experiments are in agreement with the static quark model. It is particularly interesting that Ferbel does not observe the decay $\rho' \to \pi\gamma$, which in fact is forbidden by the static quark model, just as $\psi' \to \eta_c\gamma$ is forbidden in the absence of relativistic corrections. Here the agreement with the non-relativistic model is embarassingly good, as one would expect relativistic corrections to allow the reaction to proceed. Nevertheless there exist persistent discrepancies with the static model of O(15-20%) if the quarks have $g-2 = 0$. It is my prejudice that one should attempt to organize this entire body of data with a consistent set of $(g-2)$ for the quarks, if possible. One recalls that $(g-2)$ of the muon gives stringent limitations on possible substructure of leptons, and it is possible that $(g-2)$ of the quarks will place useful constraints on possible subconstituents of quarks as well.

II. Production Mechanism

The production of hidden and explicit charm was reviewed by Wojcicki. In that report I was struck by the qualitative success of the gluon fusion picture of charm production. For example, hidden charm seems to proceed predominately by

$$gg \to \chi(^3P:\ I=0) \qquad (2.1)$$
$$\hookrightarrow \psi+\gamma$$

One can explore the possible competition between gluon fusion and quark fusion in various reactions. For example,

$$\begin{aligned} pp &\to gg \\ \bar{p}p &\to q\bar{q} + gg \\ \pi^+p;\ K^-p &\to q\bar{q} + gg \\ K^+p &\to gg \end{aligned} \qquad (2.2)$$

The relevant production mechanisms are shown in Fig. 2. Since gluons are soft, they are expected to be more effective in producing c quarks at higher energies. A Birmingham-CERN-Saclay experiment shows that the ratio $\sigma_p/\sigma_{\bar{p}}$ for production of ψ/J rises from close to zero to nearly one from roughly 50 to 200 Gev. [These data are sketched in Fig. 3]. The energy dependence of the data confirms the anticipated relative importance of quark and gluon fusion at low and high energies as expressed by Eq. (2.2).

Perhaps it is possible to explore the gluon content of E(1420); D(1285); $G(1^{++})$; $\tilde{G}(0^{-+})$, etc. in a similar way. For example

$$\left.\begin{aligned} g\ g &\not\to E(1420);\ D(1285) \\ q\ \bar{q} &\to E(1420);\ D(1285) \end{aligned}\right\} \text{ for } 1^{++}$$
$$g\ g \to G(1420) \text{ for } 0^{-+}$$

Possible production mechanisms for these states are shown in Fig. 4. It would then also be useful to compare the production mechanisms of these states with the production of the I=0, 2^+ states, since $(gg + q\bar{q}) \to f(1270);\ f'(1514)$ is allowed. Hopefully theorists will provide us with models of D(1285), E(1420) and G production, which we suggest may have considerable similarity with χ production of hidden charm. One relevant experiment in the planning stage at BNL was reported by Chung, based on suggestions of Chanowitz. Chanowitz conjectures that there are two states at 1420 Mev, an E(1420) 1^+ $(\bar{s}s)$ state and a G(1420) 0^{-+} state, and he proposes a study of $\bar{p}p$ reactions to reveal them. Also recall the presentation of Navelet, which suggests that G(1420) would be 0^{-+} and 0^{++}.

Other topics dealing with production mechanisms were presented. Vanucci reviewed the Drell-Yan mechanism, while Capella discussed the relative status of the recombination vs. fragmentation model. Tran Than Van, Nicolescu, and Balazs reported on related topics. In more specialized discussions, Rafelski considered the transition from hadronic matter to quark matter, while Dremin presented a model for Cherenkov emission of gluon jets from hadronic matter.

III. Decays

Non-leptonic and semi-leptonic decays were reviewed by Trilling. The principal issue appears to be the relative importance of spectator (1 quark) versus non-spectator (2 quark) weak transitions in Cabibbo allowed and suppressed decays, with the relative significance of the two classes of diagrams still uncertain. Typical diagrams are shown in Fig. 5. One difficulty is that the pure quark diagrams are dressed with an arbitrary number of soft gluons, which then undermines rate and ratio predictions. Unfortunately there is no theorem which factorizes soft from hard physics in non-leptonic decays, contrary to the situation in hard processes such as deep inelastic scattering. Schmid described an attempt to bypass some of these difficulties by concentrating on the flavor topologies of decay processes, which describes the flow of quark flavor through a diagram independent of corrections due to gluons.

The experimental situation on charm particle lifetimes is changing. The lifetime ratio $\tau(D^+)/\tau(D^o)$ is now reported to be roughly 3 to 10, with recent data favoring the smaller value. This ratio provides information on the relative importance of 1 and 2 quark weak transitions so that a definitive experimental result is important. More data is required on Cabibbo suppressed decays as well. It is possible that the study of rare decays of strange particles may also be helpful in understanding one and two quark weak transitions. For example, the experimental branching fractions of radiative weak baryon decays are

	B exp.
$\Sigma^+ \to p\gamma$	$[0.93 \pm 0.10] \times 10^{-3}$
$\Xi^0 \to \Sigma^0\gamma$	$< 7 \times 10^{-2}$
$\to \Lambda^0\gamma$	$[0.5 \pm 0.5] \times 10^{-2}$
$\Xi^- \to \Sigma^-\gamma$	$< 1.2 \times 10^{-3}$

consistent with the theoretical estimate $B \sim O(\alpha/\pi R_{NL}) \sim 10^{-3}$. Gilman and Wise have shown that a 1 quark transition, combined with a conserved vector current, fails to describe these data, and that 2 quark transitions are important. Further, precise experiments examining both charmed and rare strange particle decays would be useful in understanding the relative importance of 1 quark and 2 quark transitions.

In the absence of decisive predictions from the quark model, workers have returned to the older methods of group theory and current algebra which were useful in classifying strange particle decays. Here the status of 20 dominance in non-leptonic decays is still uncertain. Further, current algebra is far less useful for charmed mesons decays than K-meson physics. Although the relation of $D \to K(7\pi)$ to $D \to K(6\pi)$ can be described by soft pion methods, the more interesting relation of $D \to K(2\pi)$ to $D \to K\pi$ does not involve soft pions, and hard pion methods are required. In all these charmed particle decays, final state interactions are expected to be important, as already anticipated by the relevance of soft gluons in the quark model description.

Indirect evidence for B meson production at T''' has been seen at CESR. The observed single lepton decays seem to support the standard model, with $b \to c$ apparently dominating $b \to u$, as expected from the KM 6 quark model, with mixing angles favoring neighboring quark transitions. The experimental results indicate

$$B_r(b \to \mu\nu X) \simeq B_r(b \to e\nu X)$$

$= 11 \pm 2.7\%$ (avg. μ+e) CLEO

$= 15 \pm 4\%$ [e; prelim.] CUSB

with $B_r \sim 17\%$ in a theoretical model which counts degrees of freedom. An upper

limit of 1.7% for dileptons at the T''' was reported, consistent with the absence of flavor changing neutral currents (FCNC). FCNC are heavily suppressed by the generalized GIM mechanism in the standard model, while known topless models permit FCNC for b decays. Therefore the absence of dileptons also appears to favor the standard 6-quark model. [See Fig. 6]

We also heard reports of $T' \to T\,2\pi$ from the DASP 2, LENA, CLEO, and CUSB groups. Roughly speaking the ratios $(T' \to T\,2\pi)/(T' \to \text{hadrons}) \simeq 20\%$ and $(T' \to T\,2\pi)/(\psi' \to \psi\,2\pi) \simeq 1/10$ are consistent with the multipole expansion in QCD, with the $\pi\pi$ distribution in these decays also consistent with the multipole expansion. The multipole expansion was first developed by Gottfried and applied to the $\pi\pi$ distribution by Yan, as well as the Saclay group. Related work using a 2 gluon final state had been carried out by H. Goldberg and by Billoire, et al., although in my opinion the multipole expansion is a more reliable technique when gluons are soft.

IV. Fundamentals

During the meeting Alessandrini, Kovacs, and Sugar provided a review of several aspects of lattice gauge theory. It was emphasized that confinement is a straightforward property of lattice gauge theories in the strong-coupling limit. The difficult problem is to demonstrate that this property survives the continuum limit. It has now been established that the β function controlling the renormalization group evolution of the coupling constant undergoes a sharp transition from the weak coupling to the strong coupling domain. It is then argued that in a non-Abelian guage theory there is no phase transition as one goes to the continuum limit. If so, this would mean that the confinement property would also be a property of the continuum theory, which is what one wants to establish.

It is important to compare these results with studies of QED on the lattice. There is confinement in the strong coupling limit here as well. However, in contrast to the non-Abelian theory, there <u>is</u> a phase transition in lattice QED which implies that the weak coupling theory does not confine, and hence there is

no confinement in the continuum limit. This, of course agrees with what one expects of QED, and leads workers to believe that the results found in lattice theory are reliable.

It is now possible to calculate a semi-realistic $Q\bar{Q}$ potential for QCD on the lattice, as we have heard in the report of Kovacs. Such a potential suffers from the absence of light quarks in lattice theories. One of the effects expected of light quarks is a "screening" of the string tension, so that the string tension computed from the experimentally observed Regge trajectories should be smaller than the theoretical string tension of pure QCD without light quarks. An estimate of this screening by Poggio and Schnitzer suggests a reduction of the string tension by approximately a factor of two. There should be other effects of light quarks as well which should be studied. Nevertheless it is an extremely difficult problem to incorporate light fermions in lattice theories. We heard a very interesting review of the progress in this area from Sugar, who gave particular emphasis to the recent developments applying Monte Carlo methods to the problem.

In future investigations it is hoped that lattice gauge theories will provide us with further insights into the nature of gluon states and into the mechanism of chiral symmetry breaking in theories with confinement. An improved understanding of either of these topics would certainly have important implications for spectroscopy and other aspects of low Q^2 physics.

The interplay between confinement and chiral symmetry breaking seems to be an extremely difficult subject. For example, in a bag or potential model, where the ρ-π splitting is a hyperfine interaction, there seems to be little or no remnant of the chiral symmetry that makes soft pion physics so successful. The confinement itself seems to provide an explicit chiral symmetry breaking, and yet chiral symmetry is a good approximate symmetry of nature. White sketched the results of an extremely sophisticated and deep study of the Pomeron, which hopefully will provide us with new insights into both confinement and chiral symmetry breaking. The understanding of chiral symmetry is certainly to be on

the agenda of the physics of the future, with answers hopefully providing improved understanding of confinement, spectroscopy, the sequential breaking of gauge symmetries in grand unified and hypercolor models, and many other related topics.

In conclusion, we have heard about considerable progress in low Q^2 physics. Nevertheless, to a great extent the various descriptions of these phenomena are based on models which cannot yet be derived directly from the underlying gauge theory. Ultimate progress will eventually require us to refine our methods for dealing with gauge theories in the strong-coupling region, so that these models can be based on first principles.

In closing I wish to thank the conference organizers for providing the hard work, careful planning, and good weather which has made this meeting a success. However, the ultimate criterion of a successful meeting is the quality of the physics, which in our case was everything one could hope for.

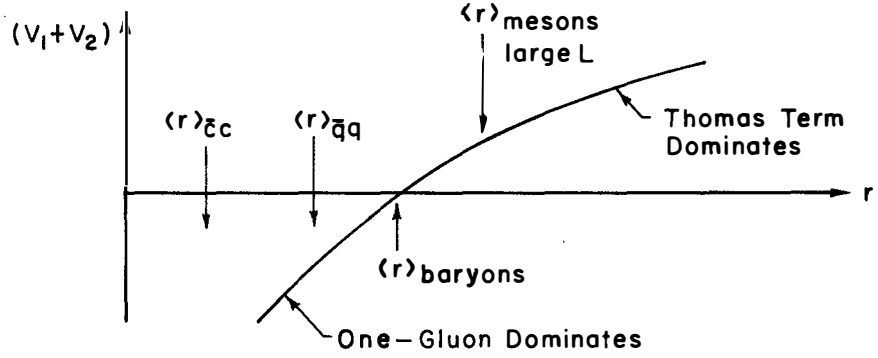

(a) Spin-Orbit Potential

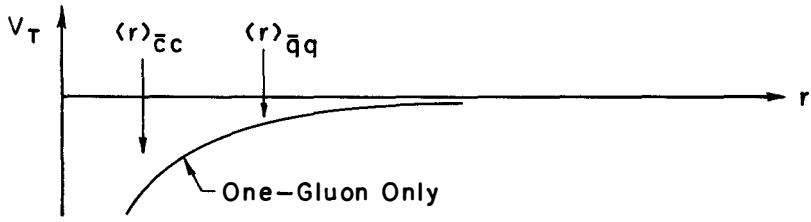

(b) Tensor Potential

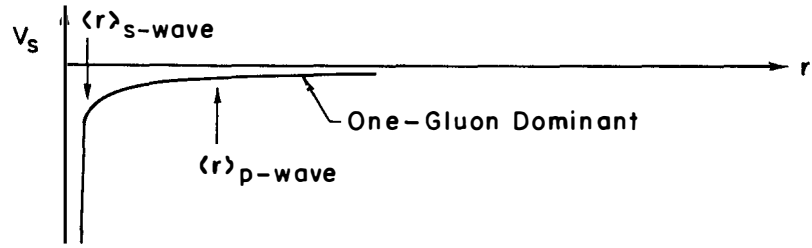

(c) Spin-Spin Potential

FIGURE 1

Qualitative radial dependence of the spin-orbit, tensor, and spin-spin potentials.

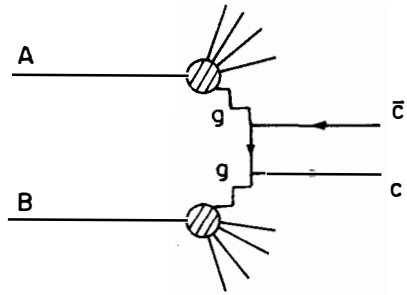

Gluon Fusion

+

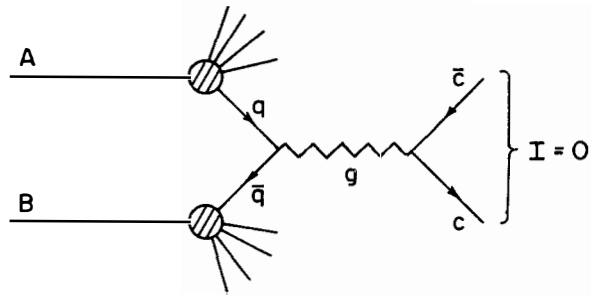

Quark Fusion

FIGURE 2

Production mechanisms for hidden charm.

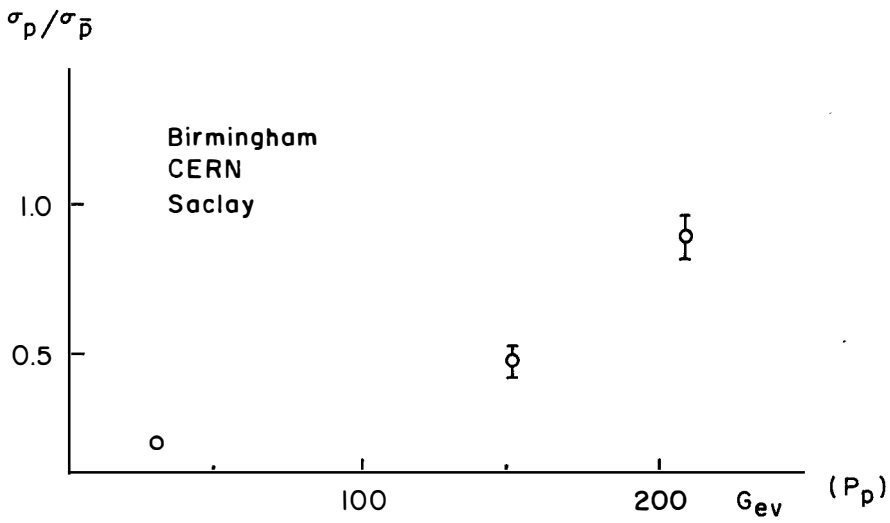

FIGURE 3

Sketch of the ratio of cross-sections for ψ/J production of p and $\bar{p}$.

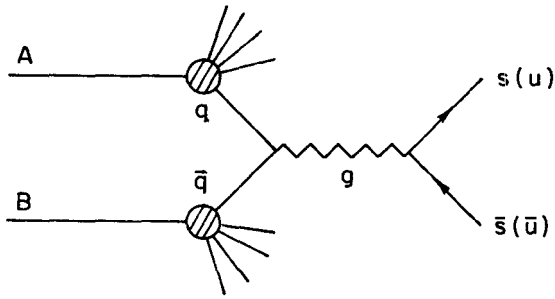

(D) E Production (?)
(1^{++})

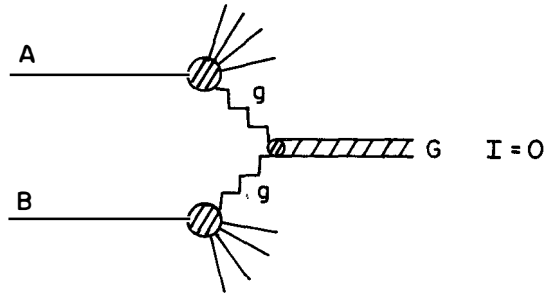

G Production (?)

FIGURE 4
Possible production mechanisms for the D(1285), E(1420) and G.

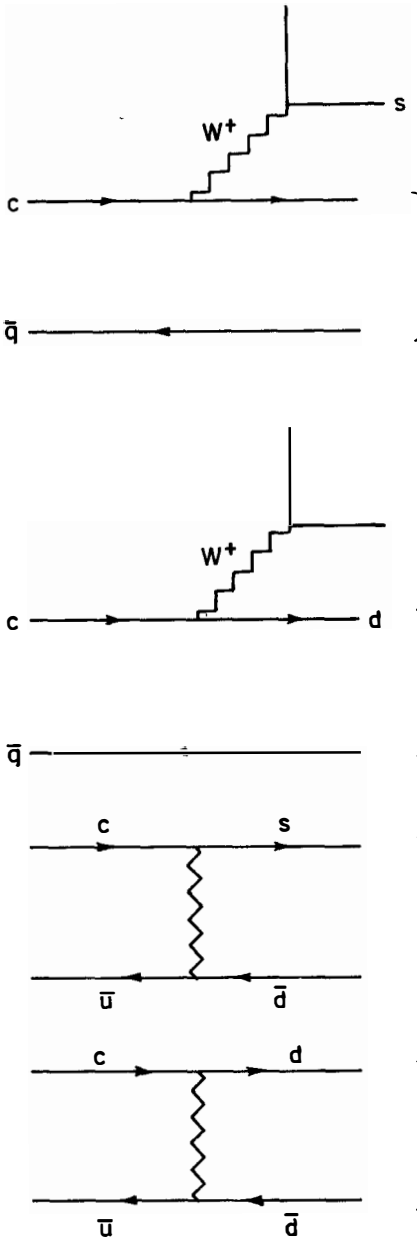

FIGURE 5
Typical non-leptonic decay mechanisms for the c quark.

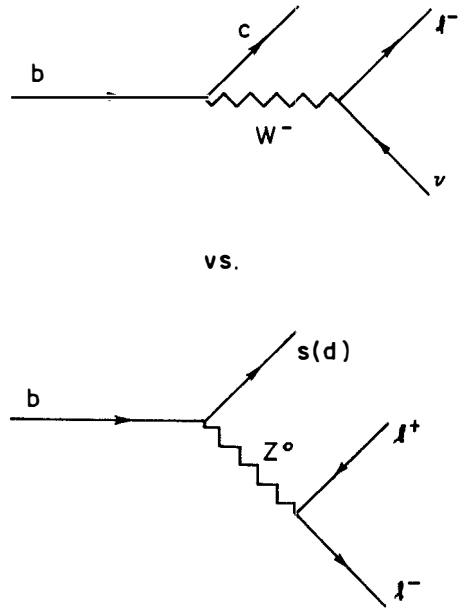

FIGURE 6

Competing mechanisms for dilepton decays of the b-quark.

LIST OF PARTICIPANTS

AGUILAR-BENITEZ Manuel	CERN EP Division 1211 GENEVA 23 Switzerland
ALESSANDRINI Victor	L.P.T.H.E, Bat 211 Université Paris XI 91405 ORSAY Cedex, France
ARTRU Xavier	L.P.T.H.E, Bat 211 Université Paris XI 91405 ORSAY Cedex, France
BAGLIN Christian	LAPP B.P. 909 74019 ANNECY LE VIEUX France
BALAZS Louis A.P.	IPN Orsay LPTPE Univ. Paris XI B.P. 1 91406 ORSAY Cedex France
BALLAM Joseph	SLAC P.O. Box 4349 Stanford, CA 94305 USA
BARNES Ted	Rutherford National Lab. Theor. div. Chilton Didcot OXON OX11 0QX England
BIZOT Jean-Claude	L.A.L. Bat. 200 Univ. Paris Sud 91405 ORSAY Cedex France
BLANKENBECLER Richard	SLAC P.O. Box 4349 Stanford, CA 94305 USA
BLOCH-DEVAUX Brigitte	D.Ph.P.E. CEN Saclay 91191 GIF SUR YVETTE Cedex, France
BLUM Walter	Max-Planck Inst. fur Physik Föhringer Ring 6 8000 MUNCHEN 40 Germany
BOPP F.W.	Fachbereich 7-Physik A. Reichwein Str. 5900 SIEGEN 21, Germany
BOUCHEZ Jacques	D.Ph.P.E. CEN Saclay 91191 GIF SUR YVETTE Cedex, France
CALDWELL David	Dept. of Physics Univ. of California SANTA BARBARA CA 93106 USA
CAPELLA Alfons	L.P.T.P.E, Bat 211 Université Paris XI 91405 ORSAY Cedex, France

CESTER-REGGE Rosana	Ist. di Fisica Via d'Azeglio, 46 10125 TORINO Italy
CHANG Chung-Yun	DESY Notkes. 85 2000 HAMBURG 52 Germany
CHERTOK Benson	American Univ. Dept. of Physics WASHINGTON, DC 20016 USA
CHO Yongmin	L.T.P.H.E. Tour 16 4, Place Jussieu 75230 PARIS France
CHUNG Suh-Urk	Physics Dept. Bldg. 510A Brookhaven Lab. UPTON NY 11973 USA
CLEGG Arthur B	Dept. of Physics Univ. of Lancaster Lancaster, LA 1 47D ENGLAND
COOPER John	Phys. Dept. University of Pensylania PHILADELPHIA 19104 PA USA
DREMIN Igor	P.N. Lebedev Phys. Inst. Leninsky Prospect 53 117 901 MOSCOW A 83 USSR
EKELOF Tord	CERN EP Division 1211 GENEVA 23 Switzerland
EQUER Bernard	Lab. Corpusculaire 11, place Marcelin-Berthelot 75231 PARIS Cedex 05 France
ERNE F.C.	NIKHEF - H Kruislaan 409 1009 DB AMSTERDAM Netherland
EXTERMANN Pierre	Ecole de Physique 25, quai E. Ansermet 1211 GENEVA Switzerland
FERBEL Tom	Physics Dept. University of Rochester ROCHESTER, NY 14627, USA
FIDECARO Francesco	Lab. di San Piero Via Livornese S. PIero a Grado 56010 PISA Italy
GIORGI Marcello-Antonio	Lab. di San Piero Via Livornese S. Piero a Grado 56010 PISA Italy

GORN Martin	Sektion physik Universitat, Theresienstr. 37 8000 MUNCHEN 2, Germany
GOULIANOS Konstantin	The Rockefeller Univ. 1230 York Av. NEW YORK N.Y. 10021 USA
GRARD Fernand	Univ. de l'Etat Av. Maistriau, 19 7000 MONS Belgium
GREEN Daniel	Meson Dept. Fermilab - P.O. Box 500 BATAVIA, IL 60510 USA
GROMES Dieter	Institut fur Theoretische Physik Universitat Heidelberg 6900 HEIDELBERG Germany
HAGUENAUER Maurice	CERN EP Division 1211 GENEVA 23 Switzerland
HARTILL Donald	Physics Dept. Cornell University ITHACA, NY 14853 USA
HAYES Kenneth	CERN EP Division 1211 GENEVA 23 Switzerland
HOOGLAND Walter	NIKHEF - H Krvislaan 409 P.O. Box 41882 1009 BD AMSTERDAM Netherlands
IRVING Alan	D.A.M.T.P. LIVERPOOL L69 3BX England
ISGUR Nathan	Dept. of Physics Univ. of Toronto TORONTO M5S 1A7 Canada
KAGAN Harris	Dept. of Phys. Univ. of Rochester ROCHESTER NY 14627 USA
KARL Gabriel	Dept. of Physics Univ. of Guelph GUELPH, Ont. Canada
KIM Jae Kwan	Korea Advanced Inst. of Science Chong-Ryang-Ri, P.O. Box 150 SEOUL, Korea
KITTEL Wolfram	Physik Laboratorium Toernooiveld NL 6525 ED NIJMEGEN Netherlands

KOVACS Eve	Bin. 81 Slac P.O. Box 4349 STANFORD CA 94305 USA
KRASEMANN Hartmut	CERN-Theor. Division 1211 GENEVA 23 Switzerland
LECOQ Paul	CERN - EP Division 1211 GENEVA 23 Switzerland
LEMONNE Jacques	Universiteit Brussel Pleinlaan,2 1050 BRUXELLES Belgium
LEU Peter	DESY Notkestr. 85 2000 HAMBURG 52 Germany
LINDENBAUM S.J.	Brookhaven Nat. Lab. Upton L.I. NEW YORK 11934 USA
LOUCATOS Sotiris	D.Ph.P.E. CEN Saclay 91191 GIF SUR YVETTE Cedex, France
LUBATTI Henri	Phys. Dept. Univ. of Washington SEATTLE WA 98195 USA
MARTIN Alan D.	Dept. of Physics DURHAM CITY DH1 3LE England
MAY Jorken	CERN-EP Division 1211 GENEVA 23 Switzerland
MICHAEL Christopher	DAMTP Univ. of Liverpool LIVERPOOL L69 3BX England
MILLER Donald	CERN EP Division 1211 GENEVA 23 Switzerland
MONTANET Lucien	CERN-EP Division 1211 GENEVA 23 Switzerland
MOSCOSO Luciano	CEN Saclay Orme les Merisiers 91191 GIF SUR YVETTE CEDEX, France
MUSSET Paul	CERN EP Division 1211 GENEVA 23 Switzerland

Mc INTYRE Peter	Texas A+M University COLLEGE STATION TX 77843 USA
NARISON Stephan	CPT - CNRS U.E.R. de Luminy-Case 907 13288 MARSEILLE CEDEX 2, France
NAVELET Henri	Dept. de Phys. Theo. CEN Saclay 91191 GIF SUR YVETTE Cedex France
NICOLESCU Basarab	Inst. de Phys. Nucleaire Division de Phys. Theo. B.P. 1 91406 ORSAY France
O'DONNELL Patrick	Dept. of Physics Univ. of Toronto TORONTO M5S 1A7 Canada
OLSEN Stephen	Physics. Dept. Univ. of Rochester ROCHESTER NY 14627 USA
OTTER G.	III Physitialishes Inst. Aachen Physiksentrum AACHEN 5100 Germany
OVERSETH Oliver	Physics Dept. University of Michigan ANN ARBOR MI 48109 USA
PEOPLES John	Fermilab P.O. Box 500 BATAVIA IL 60510 USA
PRENTICE James	Dept. of Physics Univ. of Toronto TORONTO M5S 1A7 Canada
RAFELSKI Johann	Inst. Theoretische Physik Robert Mayer Str. 8-10 6000 FRANKFURT MAIN 7 Germany
RANDA James	Physics dept. Univ. of Colorado BOULDER, CO 80309 USA
RATCLIFF Blair	SLAC P.O. Box 4349 Stanford, CA 94305 USA
RICHARD Jean-Marc	CERN Theory Division 1211 GENEVA 23 Switzerland
RITCHIE Jack	Dept. of Phys. Univ. of Rochester ROCHESTER N.Y. 14627 USA

RUNGE Kay	Fakultat fur Physik Hermann Herber str 3 7800 FREIBURG Germany
SASS Jean	D.Ph.P.E. CEN Saclay 91191 GIF SUR YVETTE CEDEX, France
SCHLEIN Peter	CERN EP - Division 1211 GENEVA 23, Switzerland
SCHMIDT-PARZEFALL Walter	DESY Notkes. 85 2000 HAMBURG 52 Germany
SCHMID Christoph	Inst. fur Theor. physik ETH 8093 ZURICH Switzerland
SCHMITZ Norbert	Max Plant Inst. fur Physik Fohringer ring 6 8000 MUNCHEN 40 Germany
SCHNITZER Howard J	Dept. of Physics Brandeis University. WALTHAM MASS 02254 USA
SCHUBERT Klaus	Institut fur Hochenergiphysik Albert Uberle Str. 2 6900 HEIDELBERG Germany
SUGAR Robert	Inst. for Theo. Univ. of California SANTA BARBARA, CA 93166 USA
TAN Chung-I	Physics Dept. Brown University PROVIDENCE, RI 02912, USA
TAUSCHER Ludwig	Inst. fur Physics Ulingelbert str 82 4056 BASEL Switzerland
TORNQVIST Nils A.	Research Inst. Theo. Phys. Siltavuorenpenger 20C 00170 HELSINKI 17 Finland
TRAN THANH VAN Jean	Lab. Phys. Theo. et Haut. Ener. Bat. 211 - Univ. Paris-Sud 91405 ORSAY, France
TRILLING George H.	Lawrence Berkeley Lab. Univ. of Calif. BERKELEY, CA 94720 USA
TUTS Mike	Physics Dept. State University of New York STONY BROOK, N.Y. 11794, USA

VAN DE WALLE Remy	Physics Lab. Toernooiveld 1 6525 ED NIJMEGEN Netherlands
VOLLAND V.	Physikalisches Inst. der Univ. Erwin Rommel, Str. 1 8520 ERLANGERN Germany
WAGNER Friedrich	Max Planck Inst. fur Physik Postfach 40 12 12 8000 MUNCHEN 40 Germany
WAGNER Walter	DESY Notkes. 85 2000 HAMBURG 52 Germany
WHITE Alan	CERN - TH Division 1211 GENEVA 23 Switzerland
WICKLUND Arthur B.	Argonne Nat. Lab. ARGONNE, IL 60439 USA
WOJCICKI Stanley	CERN EP Division 1211 GENEVA 23 Switzerland
WUTHRICK Jean-Pierre	L.P.N.H.E. Ecole Polytechnique 91128 PALAISEAU Cedex France

24 QUARKS GLUONS AND JETS

CONTENTS

25 CURRENT HADRON INTERACTIONS

CONTENTS

26 ELEMENTARY CONSTITUENTS AND HADRONIC STRUCTURE

CONTENTS

27 ELECTROWEAK INTERACTIONS AND UNIFIED THEORIES

CONTENTS

I – ELECTRON-POSITRON PHYSICS

Gittelman B. and *Skubic P.*, First physics results from the CLEO detector at CESR; *Herb S.*, First results from the CUSB detector at CESR; *Bienlein J.K.*, The hadronic width of the Υ (9.46) resonance; *Schubert K. R.*, New upsilon results from DASP-2; *Martin A.*, Heavy quark systems; *Qreglia M.*, Charmonium studies with the crystal ball; *Aschman D.*, Radiative decays of the ψ and ψ'; *Feldman G. J.*, ψ Radiative decays; *Hollebeek R.*, Two-photon interactions from MARK II at SPEAR; *Fritzsch H.*, A new look at the weak decays of charmed particles; *Marshall R.*, Experimental limits on the strength of neutral currents at PETRA energies; *Bartel W.*, Recent results from the JADE Collaboration on a search for new flaver production and for free quarks; *Spitzer H.*, Results from PLUTO: *Vannucci F.*, Leptonic physics with the MARK-J detector at PETRA; *Saxon D. H.*, Lepton and hadron production in e^+ e^- annihilations results from TASSO; *Cordier A.*, New results from DCI: Discovery of A ϕ' (1.64); *Hollebeek R.*, The SLAC linear collider.

II – MUON AND NEUTRINO PHYSICS

Paschos E. A.. Status of the SU(2) X U(1) theory; *MO L. W.*, Neutrino-electron scattering; *Trischuk J.*, Measurement of charmed particle lifetimes; *Meyer J.*, Experimental study of inverse muon decay; *Cronin J. W.*, New initiatives in CP violation; *Duong-Van M.*, Rare muon decays; *Rander J. S.*, High statistics neutrino dimuon production; *Davies J. K.*, Multimuon production results from the European muon collaboration experiment; *Strovlnk M.*, Review of new results on multilepton production by muons; *Kozanecki W.*, Experimental study of prompt neutrino production in 400 GeV proton-nucleus collisions; *Hulth P.O.*, Study of prompt neutrino production from proton copper interactions using BEBC; *Steinberger J.*, Neutrinos produced in the vicinity of hadronic collisions; *Lanou R. E.*, A new neutrino detector at B.N.L.; *Matteuzzi C.*, Study of quark fragmentation functions in neutrino interactions.

III – GRAND UNIFIED THEORIES AND NUCLEON INSTABILITY

Kang K., Introduction to grand unification theories; *Nanopoulos D. V.*, Grand unified models; *Lane K. D.* and *Peskin M. E.*, An introduction to weak interaction theories with dynamical symmetry breaking; *Gavela M. B.*, Non relativistic predictions for proton decay; *Kusmin V. A.* and *Shaposhnikov M. E.*, Baryon asymmetry of the universe versus left-right symmetry; *Barbiellini G.* and *Barloutaud R.*, Experimental projects on nucleon instability; *Lande K.*, The homestake mine nucleon decay experiment.

IV – CONCLUSIONS

Kane G. L., Theoretical conference summary; *Berkelman K.*, Experimental summary.